EXPERIMENTAL AND THEORETICAL ANALYSIS OF BOLTLESS SEMI-RIGID CONNECTORS

BY

FARID DAVAEE-MARKAZI

This programme was carried out under the
sponsorship of
PSS Ltd & Hi-Lo Manufacturing

A thesis submitted in partial fulfilment of the requirements of Oxford Brookes University for the degree of Doctor of Philosophy

September 1999

SOME PARTS EXCLUDED UNDER INSTRUCTION FROM THE UNIVERSITY

To my family

ABSTRACT

Author: Farid Davaee-Markazi

Title: Experimental And Theoretical Analysis Of Boltless Semi-Rigid Connectors

The aim of this research was to investigate the behaviour of the semi-rigid boltless connectors used in cold formed thin walled rack structures. A typical beam end connector consists of an end plate welded to the end of a beam and an interlocking arrangement that engages with perforated columns at optional heights; hence supporting the beam and restraining the column. There are a variety of types and designs of connectors in use, characteristic of different rack manufacturers. In general beam end connectors of this type are produced as the result of processes such as forming and punching. These methods produce the interlocking features, "tabs" or "studs" which perform the same role as that of bolts in conventional structural joints.

In the experimental part of the work an appraisal of commercially available beam end connectors was undertaken classifying them based on their special features. A selected number of connectors were tested and their moment-rotation characteristics were determined. The results were then compared in conjunction with the deformation modes observed. Stress-sensitive lacquer was used to establish an indication of the stress distributions involved. The outcome of this exercise enabled determination of the parameters governing efficient beam end connector design including the effects of dimensional changes of the accompanying members as well as variation in welding arrangements. Corrections were made to the experimental results to allow for flexibility of beam and upright.

Finite Element techniques were used to model the behavior of a boltless semi-rigid beam end connector. The work was carried out in four stages. An elastic global model was set up to investigate the overall deformation of a beam connector using absolute restraints to simulate the resistance to the rotation of the beam end connector. The global model also determined the stress distribution in the critical regions. A number of elasto-plastic sub-models were produced with the aim of obtaining the resistance to rotation offered by the accompanying upright. The global model was later modified to incorporate spring stiffness values.

Two global models were used to investigate the effect of variation in the number and direction of restraints and the incorporated springs. For every case the beam end connector stiffness value was evaluated and was compared against experimental results. The models were also used to examine the test methods recommended in the current and the forthcoming codes of practice for the industry. The models were used to determine the load distribution in the tabs. This later formed the basis of a design approach capable of estimating the bending carrying capacity of a semi-rigid beam end connector.

ACKNOWLEDEMENTS

This thesis has come to fruition under the supervision of:

Mr RG Beale (First Supervisor)
Senior Lecturer in Mathematics & Director of Studies

And

Dr MHR Godley
Principal Lecturer in Structures & Senior Research Fellow

of the Centre for Civil Engineering, School of Architecture, Oxford Brookes University. The author is extremely grateful to these gentlemen for their valuable instructions and guidance throughout the work.

The author also wishes to express his gratitude to the original sponsor of the project, PSS Ltd and subsequently Hi-Lo manufacturing Ltd.

Special thanks are also due to Mr RT Salter, a structural laboratory technician for his assistance during the preparation and execution of the experimental part of the programme.

CONTENTS

CHAPTER 3

Classification of beam end connectors and Experimentation

CHAPTER 5

Elasto-Plastic Sub-Model Of Upright's Web

CHAPTER 6

Global Modelling Of Beam End Connectors In Up Welded & Down Welded Arrangements

CHAPTER 7

Estimating The Ultimate Bending Carrying Capacity Of The Beam End Connector

LIST OF FIGURES

CHAPTER 4

CHAPTER 5

CHAPTER 6

CHAPTER 7

NOMENCLATURE

Symbol	Description
a	Depth of beam
C	Number of levels
c_1, c_2, c_3	Ratio of applied load to the attracted loads at tabs
E	Modulus of elasticity
$F-x$	Horizontal forces at tabs
$F-y$	Vertical forces at tabs
F_{x1}	Horizontal force at top tab
F_{x2}	Horizontal force at middle tab
F_{x3}	Horizontal force at bottom tab
F_{y1}	Vertical force at top tab
F_{y2}	Vertical force at middle tab
F_{y3}	Vertical force at bottom tab
f_a	Applied load to beam end connector
H	Horizontal force-portal frame base
h	System height
I_h	Second moment of area (upright)
I_b	Second moment of area (beam)
KU	Stiffness of the vertical member
K_B	Stiffness of the horizontal member
K_{TL}	Stiffness of the horizontal member (top, left)
K_{TR}	Stiffness of the horizontal member (top, right)
K_{BL}	Stiffness of the horizontal member (bottom, left)
K_{BR}	Stiffness of the horizontal member (bottom, right)
K_C	Stiffness of the vertical member (being designed)
K_L	Stiffness of the vertical member (lower)

k_1	Joint restraint coefficient (node 1)
k_2	Joint restraint coefficient (node 2)
k	Beam end connector stiffness
k_e	Effective beam end connector stiffness
k_E	Stiffness of the connector (experimental)
k_T	Stiffness of the connector (true)
k_W	Combined stiffness (stub column & angle stub beam)
k_{BW}	Angle-stub beam stiffness
k_B	Box beam stiffness
L	Beam Span
L_1	Position of first transducer
L_2	Position of second transducer
L_x	Beam end connector moment arm
L_{x1}, L_{x2}, L_{x3}	Moment arms for horizontal forces at tabs
L_{y1}, L_{y2}, L_{y3}	Moment arms for vertical forces at tabs
$L_{y4}, L_{y5}, \ldots$	Moment arms for reaction forces in compression zone
M_E	Fixed end moment
M_{col}	Bending moment in column being designed
M	Bending moment
M_C	Bending moment at beam centre
M_U	Ultimate moment of a connector (Experimental)
M_u	Ultimate moment of a connector (Theoretical)
$M_{12}, M_{21}..$	Bending moments at nodes
M_a	Applied bending moment to beam end connector
$M_{r1}, M_{r2}, ..$	Moments of resistance
P	Upright axial load
$R_{53}, R_{53}...$	Reaction forces in compression zone
R_1	Shear capacity of a tab (area & yield stress)
R_2	Shear capacity of a tab (outcome of sub model)

R_3	Upright's web strength
U	Strain energy
W	Load per beam
$W_1, W_2..$	Side loads at respective levels
$X_1, X_2..$	Percentage load attracted by each tab
θ_E	Rotation of beam end connector (experimental)
θ_B	Rotation of box beam
θ_U	Rotation of stub column
θ_T	Rotation of beam end connector (true)
θ_W	Combined rotation (stub column & angle stub beam)
θ_{BW}	Rotation of angle-stub beam
θ	Beam end connector looseness
θ_v	Beam end connector rotation measured vertically
θ_{ta}	Beam end connector rotation measured at top of beam (adjacent to bec)
θ_{tr}	Beam end connector rotation measured at top of beam (remote from bec)
θ_{ba}	Beam end connector rotation measured at bottom of beam (adjacent to bec)
θ_{br}	Beam end connector rotation measured at bottom of beam (remote from bec)
α	Deviation from verticality (upright)
ϕ	Deviation from verticality (upright & connector)
δ_1	Deflection at first transducer
δ_2	Deflection at second transducer
σ_{x1}	Yield stress of material

CHAPTER 1

INTRODUCTION

C H A P T E R 1

1.1 Introduction

The connection between a column and a beam can be classified into fixed, pinned or semi-rigid. It is well known that the type of connection affects the buckling load of a column. For example, changing from pinned to fixed ends, for a non-sway column can increase the elastic buckling load fourfold, Jones, Kirby and Nethercot[1]. In practice all connections have some elasticity. A semi-rigid connection possesses intermediate elasticity and the joint is normally formed by use of bolts or welding.

In the storage rack industry boltless semi-rigid connections are used. They are referred to as beam end connectors and use "tabs" as connectors. The tabs are engaged into perforations of cold-formed upright sections at optional heights determined by the perforation pitch. The tabs may be integral parts of the beam end connectors or independent from it, when they are referred to as "studs".

These special connections are developed to take advantage of the thinnest of material from which cold formed perforated columns are produced in racking industry, J Rhodes[2].

The performance of a racking system depends upon the efficiency of the beam end connectors. The beam end connectors provide support to the beams and in unbraced racks are the only source of stiffness required for down-

aisle stability. For practical reasons pallet racks are not braced in down-aisle direction. Therefore, the resulting side sway is governed by the efficiency of the beam end connector, in particular its rotational stiffness, as well as by the behaviour of the floor-upright connection, MHR Godley, RG Beale & X Feng[3]. The degree of side sway determines the strength and stability of the structure, JWB Stark and CJ Tilburgs[4]. This work is concerned with investigating the behaviour of the beam end connector moment-rotation characteristics.

Boltless Semi-rigid beam end connectors can be likened to the bolted end-plated semi-rigid connections used in conventional structural engineering with similar loading conditions.

Analyses of bolted connections have been made by several authors, e.g. Maxwell, Jenkins and Howlett[5], Jenkins[6] and Scholz[7] . However, the author was unable to determine similar work on boltless connections.

Although there are many different designs of beam end connectors, information about the moment-rotation curves which the manufacturers use in the elastic analysis and design of their products is unavailable. In order to obtain an understanding of the complexities involved with boltless connections a selection of the commercially available beam end connectors were tested. These were followed by tests on one type of connector of varying dimensions to fully investigate the parameters involved in the efficient design of beam end connectors.

The experimental work provided an understanding of the parameters and the failure modes involved in the behaviour of the beams end connectors. This then formed the basis of the theoretical work involving the use of Finite Element techniques to model, initially the overall behaviour of the

beam end connector followed by sub modeling exercise whose outcome were used to enhance the global models. The Finite Element work was carried out in five stages:

I. **Global modeling (elastic)-Restraint incorporated-** to determine the overall behavior of the beam end connector absolute restraints were used to simulate resistance to the rotation of the beam end connector which in reality is caused through its interaction with the accompanying upright's web thickness as it interlocks.

II. **Sub-modeling (elasto-plastic)-** to determine the stiffness of an upright's web horizontally. This is a source of resistance to rotation in horizontal direction.

III. **Sub-modeling (elasto-plastic)-** to determine the stiffness of an upright's web vertically. This is a source of resistance to rotation in vertical direction.

IV. **Global modeling (elastic)-Spring incorporated** The stiffness values obtained through the sub-modeling exercises were then used to insert equivalent springs in the global model replacing absolute restraints as the
source of resistance to rotation.

V. **Sub-modeling (elasto-plastic)-** to determine the shear strength of a single tab. This is a source of resistance to rotation in horizontal direction.

The first global model, the model using restraints at the tabs, was used to investigate the effect of varying the number and the direction of the restraints.

The second global model, the model with springs at the tabs, was used to examine the influence of changing the number and the direction of the incorporated springs.

For every case the stiffness value was evaluated for the beam end connector and was compared against experimental results.

Using the models various methods of measuring rotation including those recommended in the current and the forthcoming codes of practice for the industry were investigated and the results were compared.

Finally the global models were used to determine the load distribution in the tabs, which in turn was used to estimate the bending carrying capacity of the connector through a modeling approach.

1.2 Aims of the research

The main aims of the research are:

1. To identify the commercially available beam end connector designs and to classify them.

2. To test the various beam end connectors and compare their performances.

3. To establish an understanding of the parameters responsible for the behaviour of beam end connectors.

4. To determine the influence of upright's flexibility on experimental results.

5. To determine the influence of stub beam flexibility on experimental results.

6. To generate models to elastically determine the overall

behaviour of a beam end connector based on experimental observations and hence determine its deformation modes and stress distribution in the critical regions.

7. To use the models to determine the initial stiffness of a beam end connector.
8. To examine different methods of stiffness value measurement and to compare them with those recommended in the current and the forthcoming code of practice for the industry.

9. To establish the load distribution in the "tabs" for different welding arrangements of stub beam to the beam end connector.

10. To generate an elasto-plastic model to simulate the effect of the accompanying upright as a source of resistance to rotation.

11. To generate an elasto-plastic model to simulate the shear resistance effect of the "tabs" as a source of resistance to rotation.

12. To estimate the ultimate moment carrying capacity of a beam end connector by a design approach.

CHAPTER 2

RESEARCH REVIEWS

C H A P T E R 2

RESEARCH REVIEWS

2.1 Introduction

The role of connections in steelwork structures is to transfer load between members. Steelwork connections influence the way in which a complete structure responds to load. This is through the degree of restraint provided by connectors as well as the ability to transmit load to the adjoining members in frame structures.

In conventional structural engineering, joint behaviour has been represented by idealized joint models. The most commonly used idealized models are the rigid joint model, pinned-joint model and semi-rigid model. These idealized models are categorized by their moment-rotation characteristics. In this regard rigid is classed as possessing high stiffness, pinned as zero stiffness and semi-rigid of intermediate stiffness capacities.

In general in the design of steel structures understanding of joint behaviour has been given secondary importance, J.B.Davison & D.A.Nethercot[8]. Furthermore, historically, the complexities associated with the modeling of semi-rigid connectors and the design analysis methods have discouraged engineers from using semi-rigid connectors.

However with the advent of advances in methods of analysis and computer power driven by economical pressure as well as the emergence of new and sophisticated codes and specification rules, a vast amount of work has been completed on understanding of the behaviour of bolted semi-rigid connections, R Cunningham[9].

The connection under consideration, however, is a semi-rigid one, which derives its properties from "tabs" that result from forming and punching operations. To date manufacturers, as recommended by their codes of practice, namely SEMA[10] in the UK, and AISI[11] in the United States, have resorted to testing such joints to obtain stiffness and strength values. Despite a thorough search the author was not able to obtain much literature directly investigating the performance of such connectors.

However, a cold-formed, boltless, semi-rigid beam end connector may be considered to be analogous to the bolted end-plated semi-rigid connections used in heavy structures. The tabs or studs, which provide the interlocking arrangement, perform the same function as that of bolts in semi-rigid structural joints. The end plates are subjected to the same loading condition as those of other structural joints.

The majority of research carried out on the performance of thin walled cold-formed racking structures has primarily been concerned with the influence of semi-rigid connectors on the performance of the structure. Moment rotation characteristics are used to carry out elastic analysis determining member and overall performances of rack structures, MHR Godley[12] and MHR Godley, RG Beale, X Feng[13].

2.2 Effect of semi-rigid connection to steel column of cold-formed perforated singly symmetric section.

Paul H. Cheng[14]

An early investigation by the above author used full-scale tests of rack structures. The results showed that in every instance torsional flexural buckling caused failure.

To investigate the effect of semi-rigid connections the assembly test results were compared with the outcome of a number of stub column tests. A conclusion was then drawn which implied that column strength was independent of the nature of the beam to upright connection. This is in contradiction with the basic understanding of buckling theories, in that the effect of the end condition was completely dismissed. Furthermore, as shown by many workers in subsequent years and presented in this survey, one explanation for the author's erroneous judgement may be the fact that the connector employed was a highly inefficient one providing negligible stiffness in the down-aisle direction. This coupled with the fact that only one type of connector had been employed in the series of full-scale tests; and therefore the investigation lacked sufficient information on the effect of variation in the degree fixity required for comparison purposes.

The findings of this research later formed the basis of modifications made to the formulae in the 1968 AISI[11] specification as an approximate solution to calculate the carrying capacity of perforated open sections in rack installations.

2.3 Design of cold-formed steel storage racks

Teoman Pekoz[15,16,17]

The author carried out a review of the research conducted in the preparation of the industry's specification in the U.S.

Reviewing the work carried out on the role of beam end connectors, it was acknowledged that, as opposed to the assumptions made in a rigid frame analysis, the joints between the uprights and the beams behave differently.

Due to the distortion of the walls of the uprights at the joints as well as the distortion of the beam end connectors' end plates, the angle between the two members changes as the frame deflects.

This peculiarity coupled with the fact that connection details vary widely makes it impossible to establish general procedures for computing joint stiffness and strength.

The research concluded therefore that testing is the only way by which these characteristics can be determined. To this end the moment at the joint between two connecting members were expressed as the product of the change in the angle between the members and a spring constant relating the moment to rotation.

Two types of test set ups were used in the research. One was a cantilever test, a simple way of getting the value of the spring constant with the disadvantage that shear to moment ratio in an actual joint may not be represented, figure 2.1.

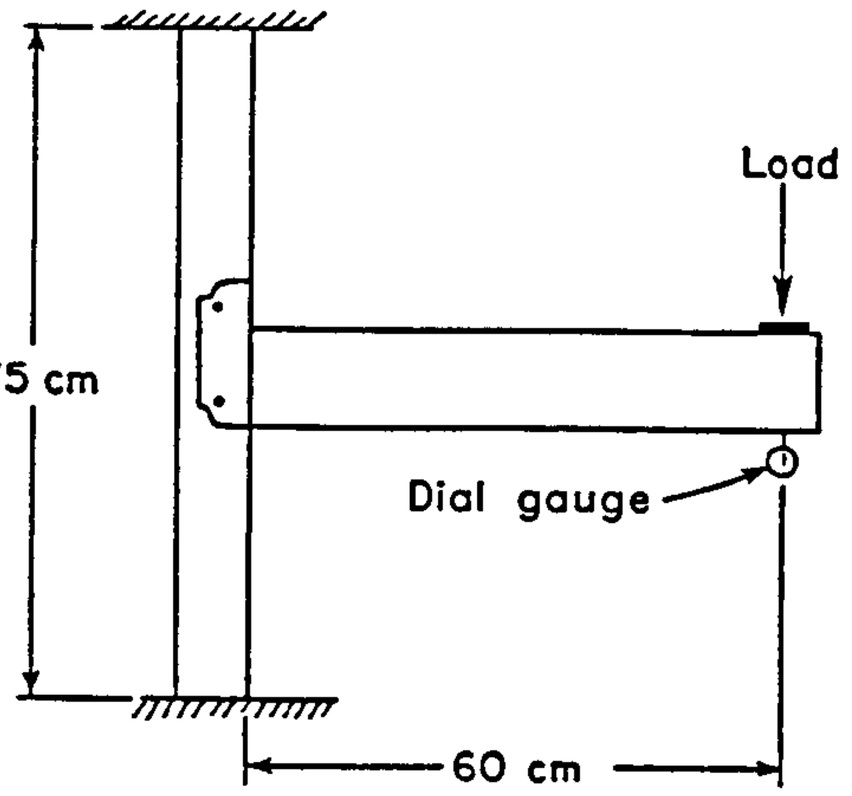

Figure 2.1 Cantilever test

The value of spring constant obtained in such a way was found to be adequate in the design of beams, Teoman Pekoz[16,17]. The report also recommended a portal frame test as being desirable when the value of the spring constant is to be used in a side sway analysis either for lateral deflections or stability, figure 2.2.

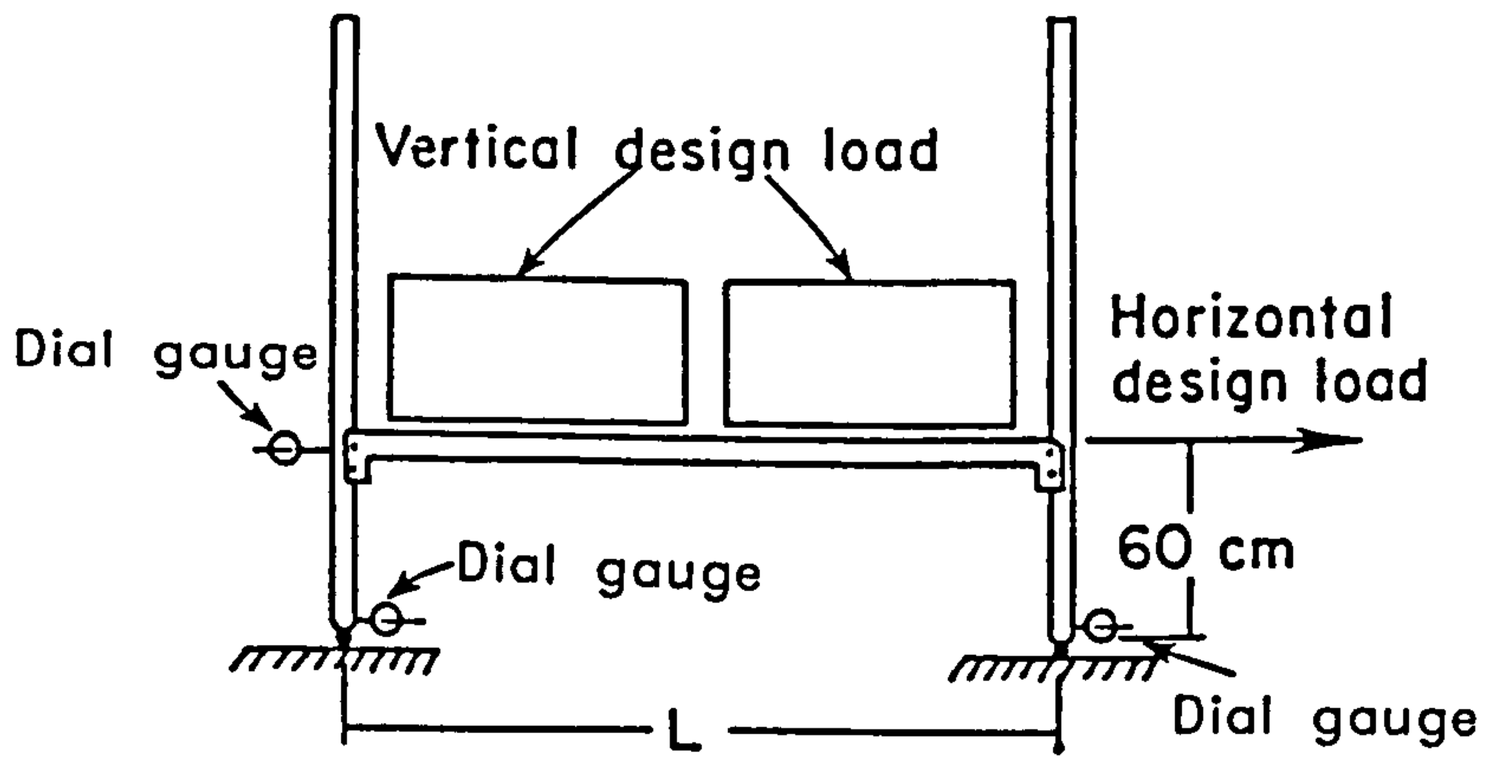

Figure 2.2. Portal test

Under vertical load the connections in general "tighten up". Subsequently, under side sway, the connection at one end of the beam "tightens up" while the connection at the other end "loosens". The portal test gives an approximate

average value of the spring constants involved in this process.

The work further concluded that the outcome of the portal frames test is more appropriate for evaluating side sway behaviour as this has lead to the best correlation between the computed and the observed results, Teoman Pekoz[18].
A further conclusion from both tests was that the relationship between the moment and the angular change at the joint is not linear. Finally the upright design procedure adopted is based on the effective length concept which relies, amongst other parameters, on the rigidity of the beam to upright connection.

2.4 Storage Racking

M.H.R Godley[12]

The article reviewed the past and the present state of racking structures covering all aspects of component design, material, member design, component testing methods as well as the overall structural design of a rack structure. It examined the recommendation of the relevant codes of practice and their base documents.

This was done for both the existing UK trade association, the Storage Equipment Manufacturers' Association, SEMA[10] and the forthcoming continental code, the European trade association, the Federation Europeene de la Manutention, FEM[19].

Finally it proposed assembly design analysis methods taking account of the influence of semi-rigid beam end connector.

The article considered the role of beam end connector, material, design, connector looseness effect, and methods of testing and result analyses.

Characteristics such as inherent connector looseness were considered and their effect on the performance individual members as well as overall stability behaviour of a rack structure was examined.

Some of these issues having direct relevance to this work are considered in more detail below.

2.4.1 Analysis of moment-rotation curves

The article covered the ways in which the stiffness of the beam end connector could be measured. The most convenient was to measure the slope of the initial straight part of the moment-rotation relationship by imposing a best-fit straight line, figure 2.3a. This method however leads to over-optimistic values if the behaviour is not linear for large part of the range.

Godley stated that an alternative to this was the more conservative method which determined the stiffness by taking the slope of the line passing through the origin, figure 2.3b, and the point at which the working moment of half the ultimate bending capacity was reached.

Finally, the curve representing the actual test result could be represented by an idealized characteristic consisting of two straight lines, placed so that the work to failure was the same in the idealized case as in the actual case, figure 2.3c. For this to exist the hatched areas must be equal.

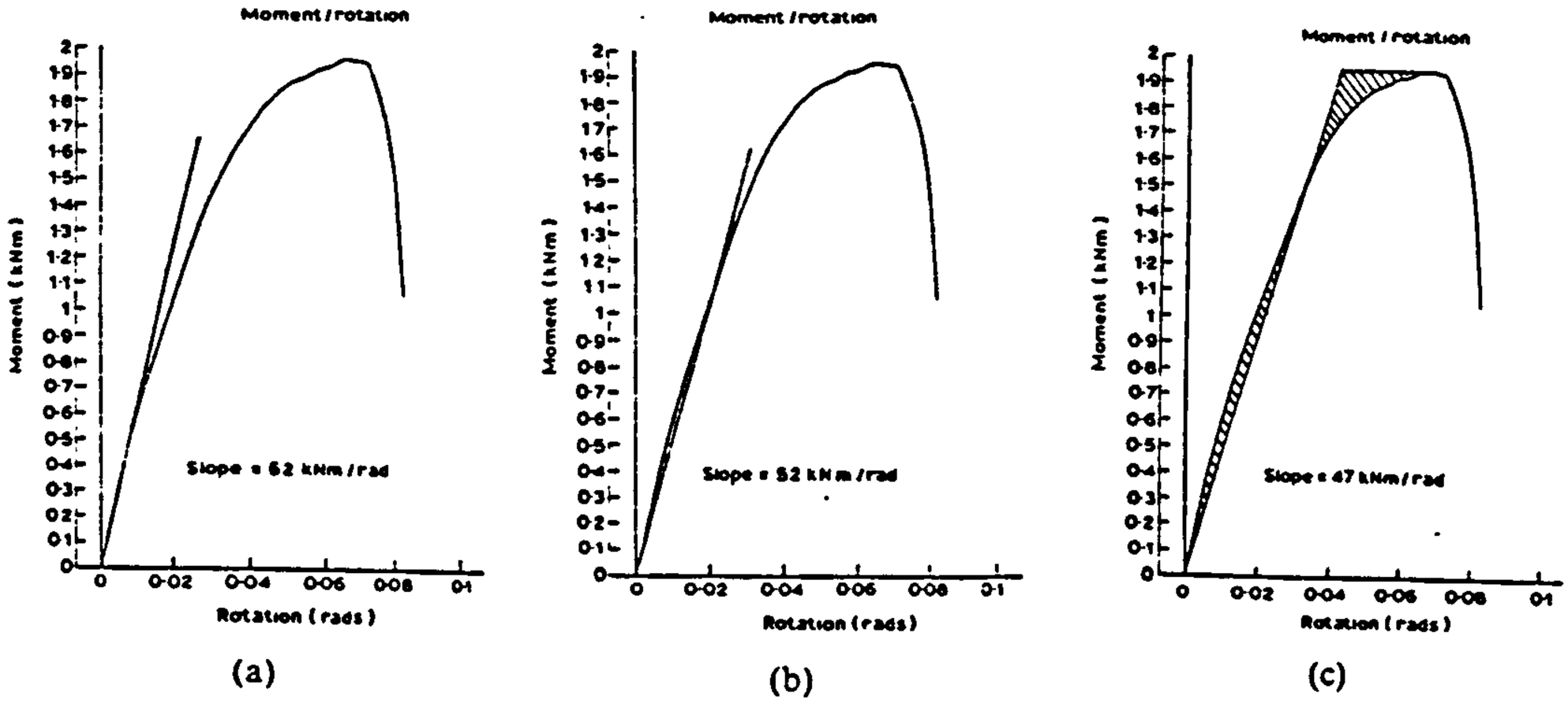

Figure 2.3. Assessment of beam end connector stiffness. (a) initial slope; (b)slope to half ultimate and (c) equal areas.

2.4.2 Connector looseness effect

Another important characteristic of a beam end connector design is resistance to looseness. The looseness of a connector has a significant effect on the load carrying capacity of a structure.

This is particularly important in unbraced racks, as connector stiffness is the only source of stiffness required for down aisle stability, a beam end connector which is loose in the unladen condition allows a degree of rotation before it develops any resistance to bending.

This allows the rack to be assembled out plumb equal to the lack of fit in the beam end connector. The unwanted effect of this is that, when the rack is loaded such imperfection results in bending moments in the structure similar to

those caused by a side load, leading to reduction in load carrying capacity.

2.4.3 Material

Hot rolled alloy steels are used for manufacturing beam end connectors. This selection is based on requirements such as formability and weldability as well as the mechanical properties needed for structural performance.

2.4.4 The role of beam end connector in column design

The load carrying capacity of rack frames and beams depends upon the efficiency of the beam end connectors. The beam end connectors provide support to the beams and in unbraced racks is the only source of stiffness required for down-aisle stability. For practical reasons pallet racks are not braced in the down-aisle direction. Therefore the resulting side sway is governed by the efficiency of the beam end connector, in particular its rotational stiffness.

The fact that beam end connectors are semi-rigid in nature means that when a rack structure is partially laden significant bending moments can be induced in the accompanying upright section by the beam. In the assessment of the load carrying capacity of a rack usually the bottom length of the upright is critical.

Considering a part laden structure, figure 2.4(a), Godley suggests assessment of the load carrying capacity of the structure be carried out by isolating the bottom length of the upright and the adjacent members to create a simplified model for the purpose of calculating bending moments, figure 2.4(b). The model consists of the upright, pinned at the base with the beams connected to it through typical semi-rigid connectors.

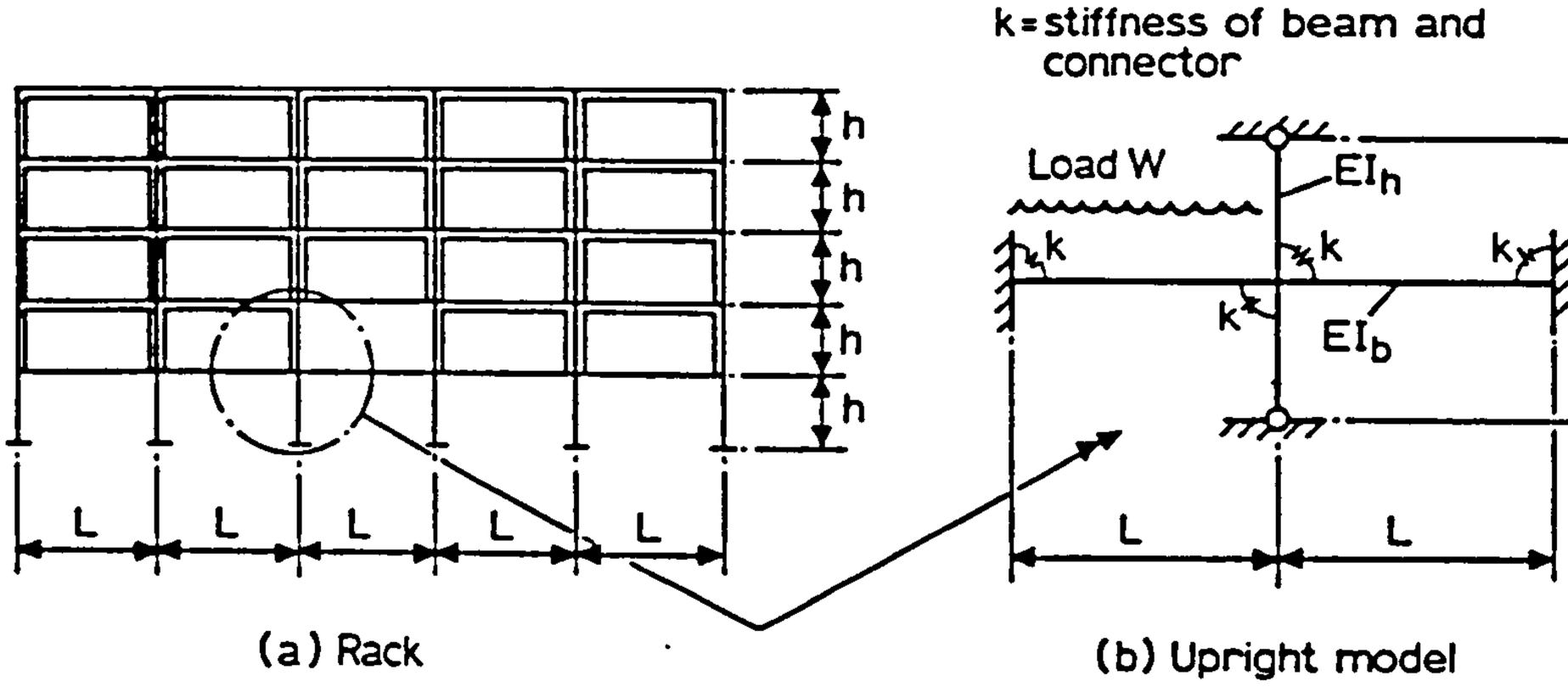

Figure 2.4. Part laden configuration

For a UDL condition the fixed end moments, M_E, takes account of the presence of the semi-rigid connectors to:

$$M_E = \pm\frac{WL}{12}\frac{1}{\left(1+\frac{2EI_b}{kL}\right)} \qquad 2.1$$

The stiffness of the vertical member meeting at the joint is represented by:

$$Ku = \frac{3EI_h}{h} \qquad 2.2$$

The stiffness of the horizontal member however is expressed as a function of geometrical properties and flexural rigidity of the member taking direct effect from the stiffness of the connector in use.

$$K_B = \frac{3EI_b}{L}\left\{\frac{4\left(1+\frac{3EI_b}{kL}\right)}{4\left(1+\frac{3EI_b}{kL}\right)^2-1}\right\} \qquad 2.3$$

Assessment of the above parameters later gives rise to generation of a formula giving the bending moments in the column being designed.

$$Mcol = M_E\left\{\frac{K_U}{2K_U+2K_B}\right\} \qquad 2.4$$

Further influence of beam end connector characteristics are reflected in sway and non-sway analyses.

The sway mode of failure is shown in figure 2.5.

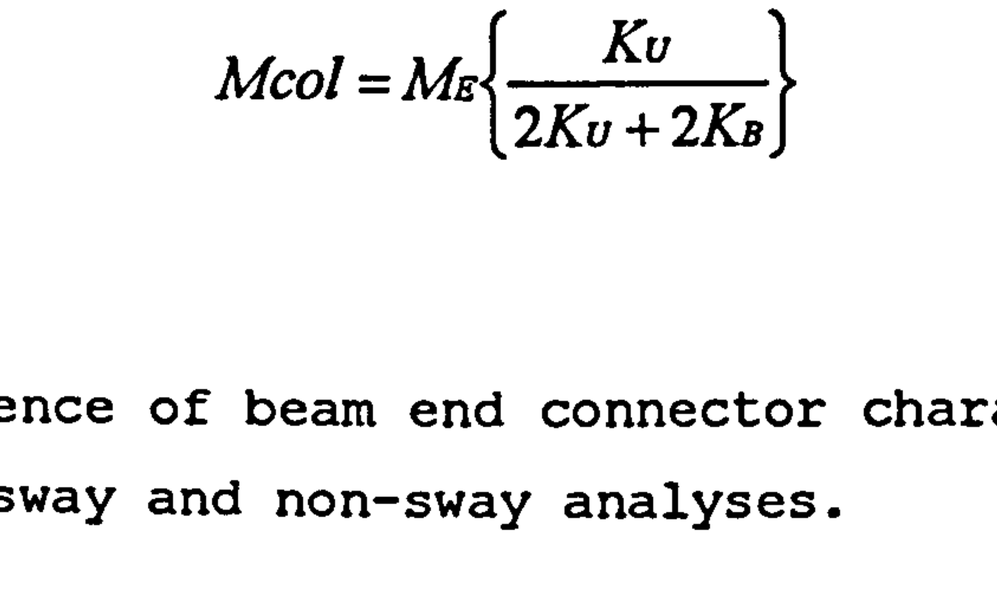

Figure 2.5. Sway modes of failure

This approach relies on both the stiffness of the base and the beam end connector, the stiffness at the first level for the sway condition being dependent on the stiffness of the beam and the connector linking it to the column. This stiffness is obtained by considering the beam end connector assembly shown in figure 2.6,

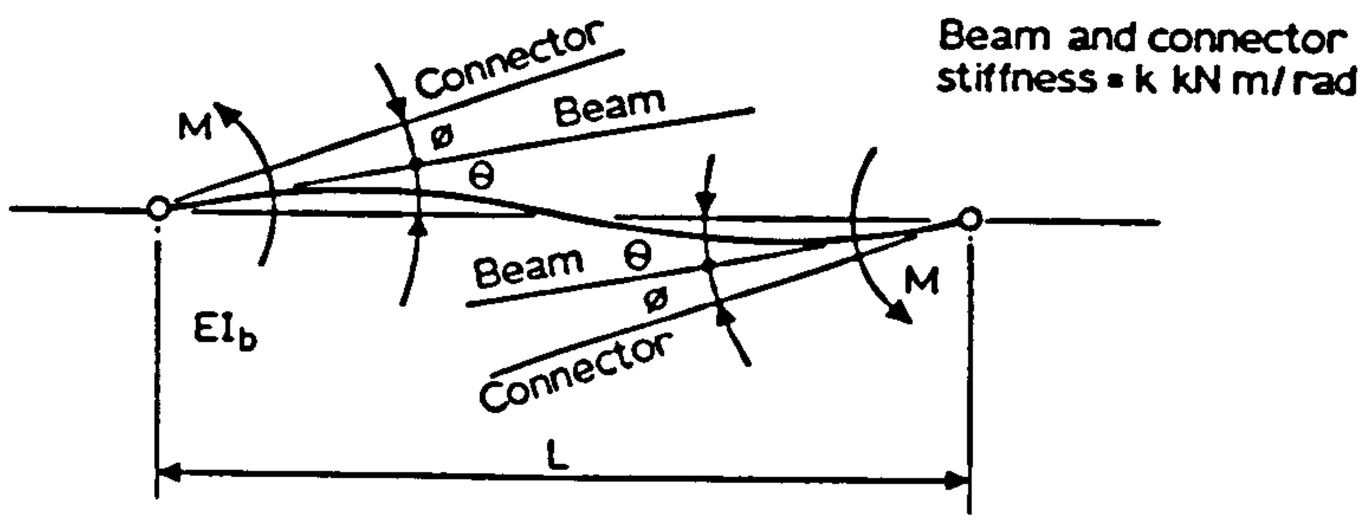

Figure 2.6. Beam in double curvature sway mode.

for which

$$\theta + \varphi = \frac{M}{k} + \frac{ML}{6EI_b} \qquad 2.5$$

Giving the effective stiffness as:

$$\frac{M}{\theta + \varphi} = \frac{\frac{6EI_b}{L}}{\left(1 + \frac{6EI_b}{kL}\right)} \qquad 2.6$$

In instances where spine and plan bracing are fitted to a rack structure, non-sway failure mode, figure 2.7, a similar analysis can be carried out.

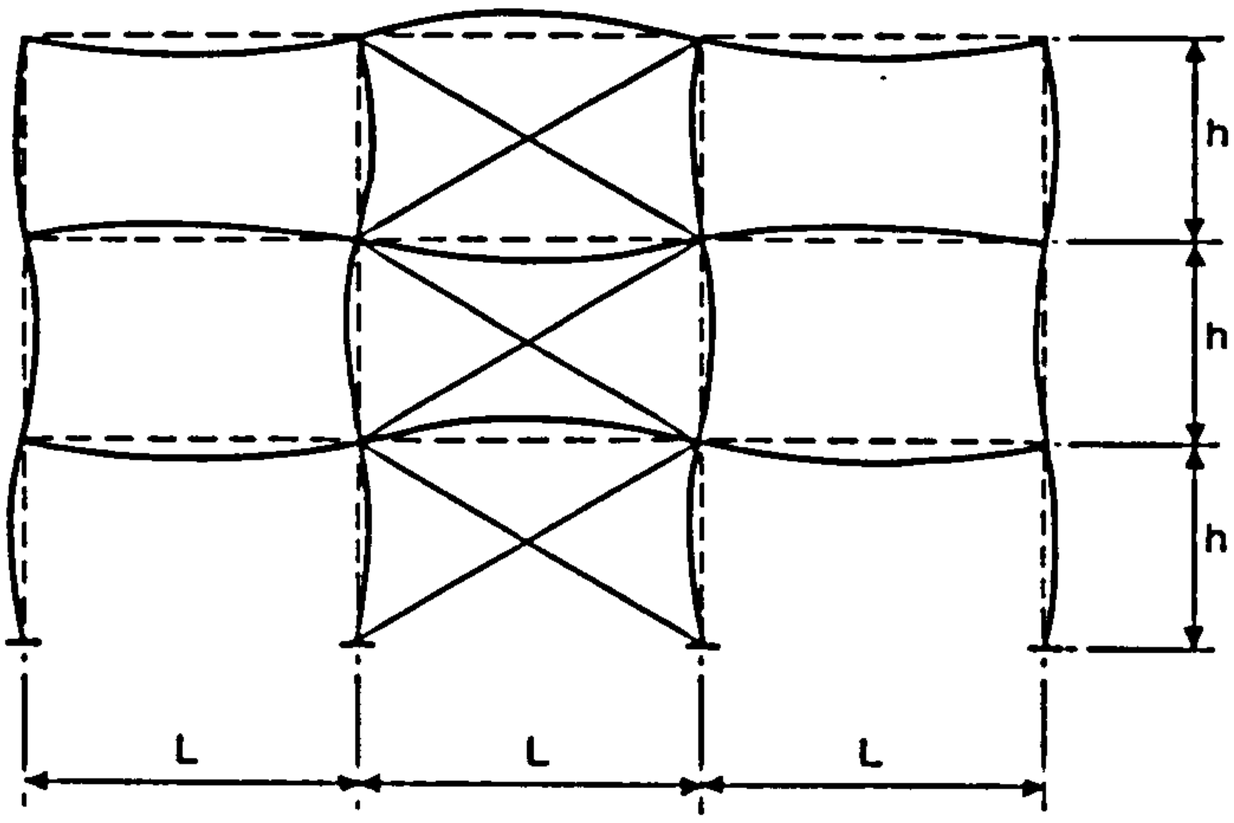

Figure 2.7. Non-sway failure mode

Here it is assumed that the presence of such bracing system provides full positional restraint in the down-aisle direction at the joints, hence resulting in single curvature bending. The effective stiffness for such an arrangement is obtained using figure 2.8, where:

$$\theta + \varphi = \frac{M}{k} + \frac{ML}{2EI_b} \qquad 2.7$$

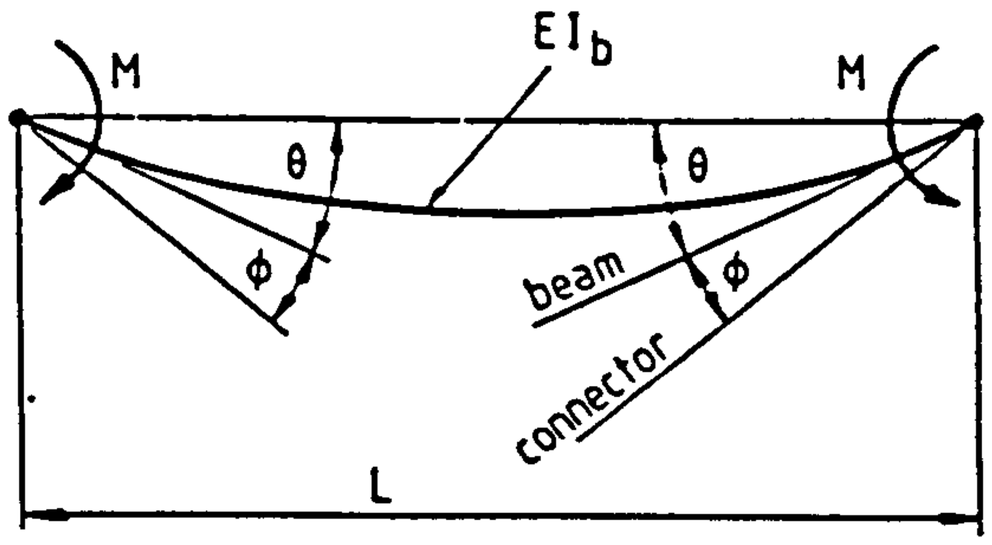

Beam end connection
stiffness = k kNm/rad

Figure 2.8. Beam in single curvature non sway mode.

Giving the effective stiffness as

$$\frac{M}{\theta+\varphi}=\frac{\dfrac{2EI_b}{L}}{\left(1+\dfrac{2EI_b}{kL}\right)} \qquad 2.8$$

With reference to the work by R. H Wood[20] on the derivation of effective length factors and buckling lengths for columns with semi-rigid end connections, joint restraint coefficients were evaluated as a method for column design. This work is incorporated into BS 5950 in the form of graphs relating joint restraint coefficient at each end of the column to the effective length ratio for the column.

Considering figures 2.9, 2.10 and 2.11,for the horizontal member the following formulae are used to determine stiffness for sway and non-sway conditions respectively.

For sway condition where the beam is in double curvature

$$K_{TL}=K_{TR}=K_{BL}=K_{BR}=\frac{1.5\dfrac{I_b}{L}}{\left\{1+\dfrac{6EI_b}{kL}\right\}}=K_B \qquad 2.9$$

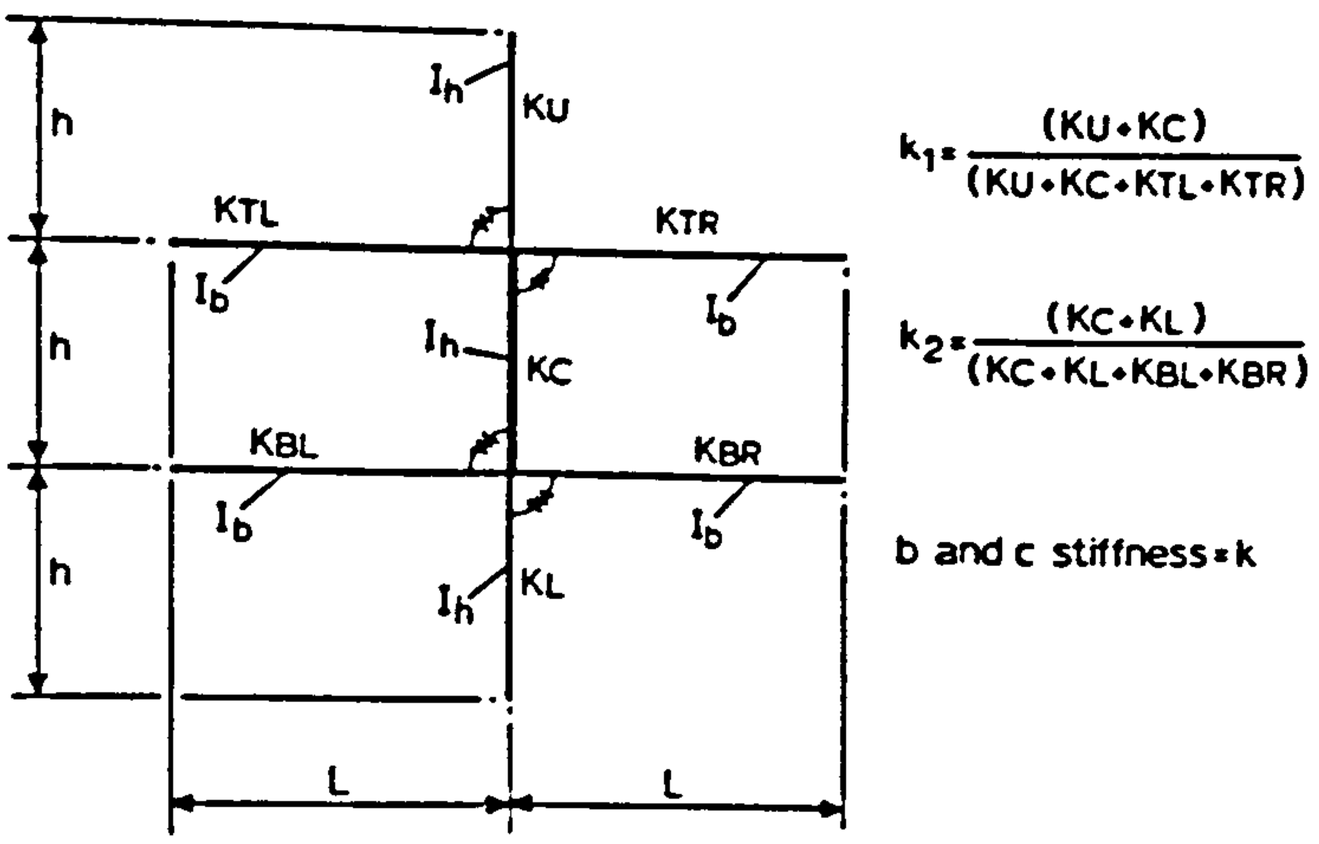

Figure 2.9. Sub frame for column stability

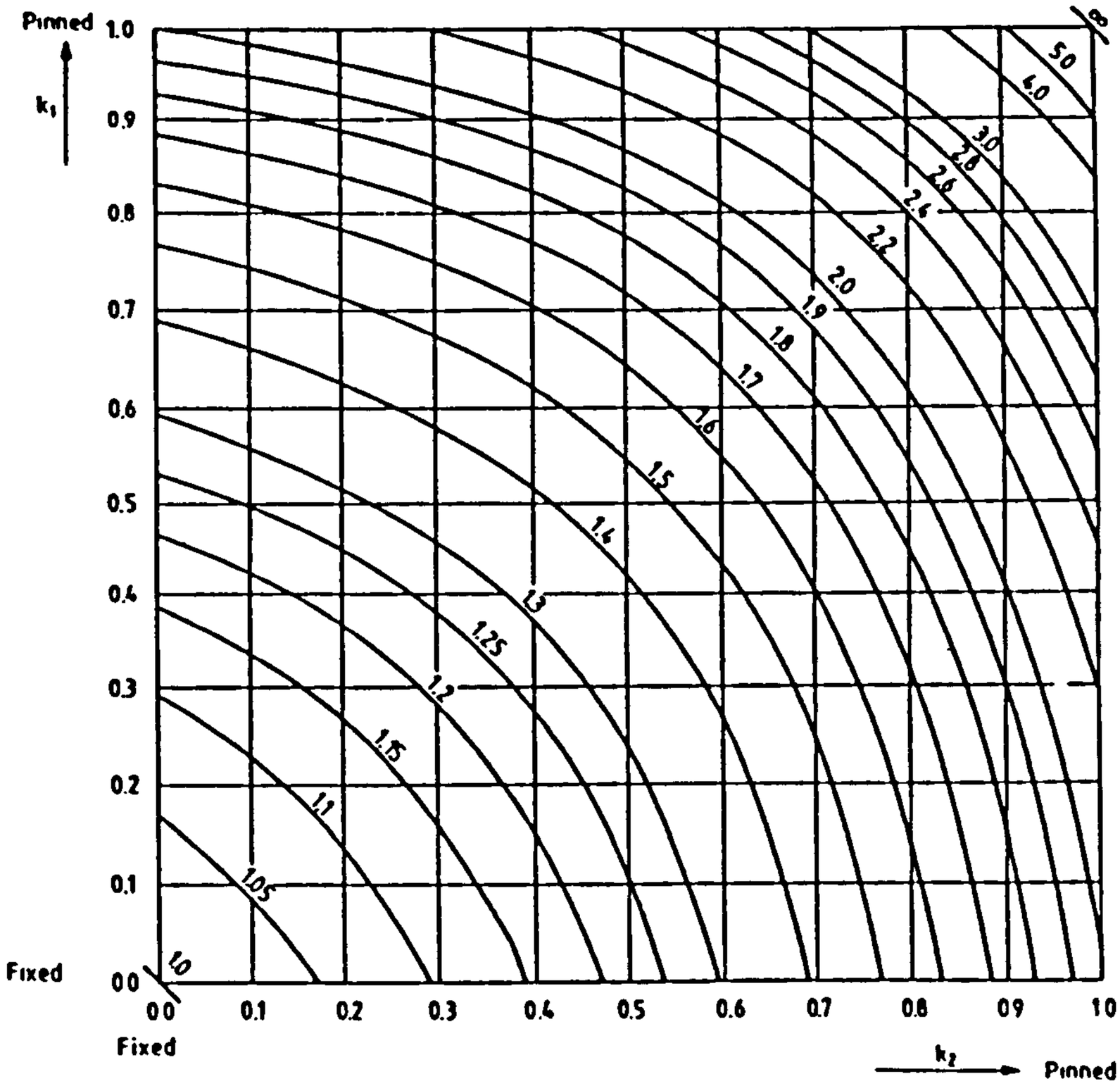

Figure 2.10. Effective length ratio L_E/L for a column free to sway

For non-sway condition where the beam is in single curvature,

$$K_{TL} = K_{TR} = K_{BL} = K_{BR} = \frac{0.5\dfrac{I_b}{L}}{\left\{1+\dfrac{2EI_b}{kL}\right\}} = K_B \qquad 2.10$$

With column stiffness as,

$$Kc = Ku = K_L = \frac{I_h}{h} \qquad 2.11$$

With a rational assumption for the stiffness of the base, 10% of the column stiffness as recommended in BS5950 and

the use of the model, figure (2.9) as well as the graphs in figures 2.10, and 2.11 effective length ratios are determined.

The formulae in this design method are functions of geometrical properties, flexural rigidity as well as the stiffness of the beam end connector in use.

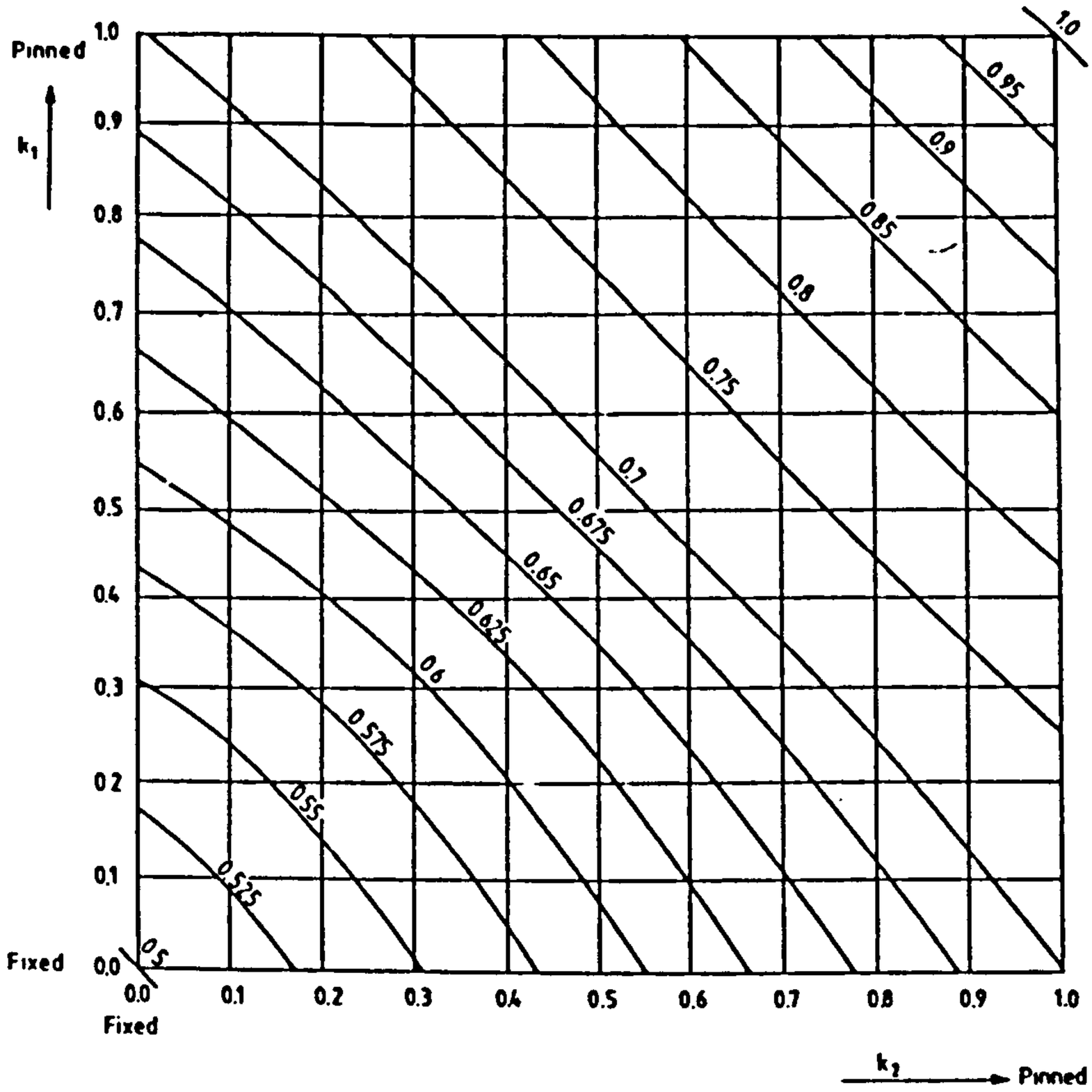

Figure 2.11. Effective length ratio L_E/L for a column with no sway

2.4.5 The role of beam end connector in beam design

Beam design is carried out based on permissible stress approach. Usually in doing so, the beam is checked against the following criteria:

(a) maximum bending moment in the beam

(b) allowable beam deflection

(c) maximum bending moment in the beam end connector

(d) maximum shear in the beam

The performance of the beam is dependent on the make up of the rest of the structure. Depending on the condition being checked, appropriate sub-structures are considered to simulate the effects of the structure.

To estimate the maximum bending moments at mid-span and the largest deflection a sub-structure such as that shown in figure 2.12 is adopted.

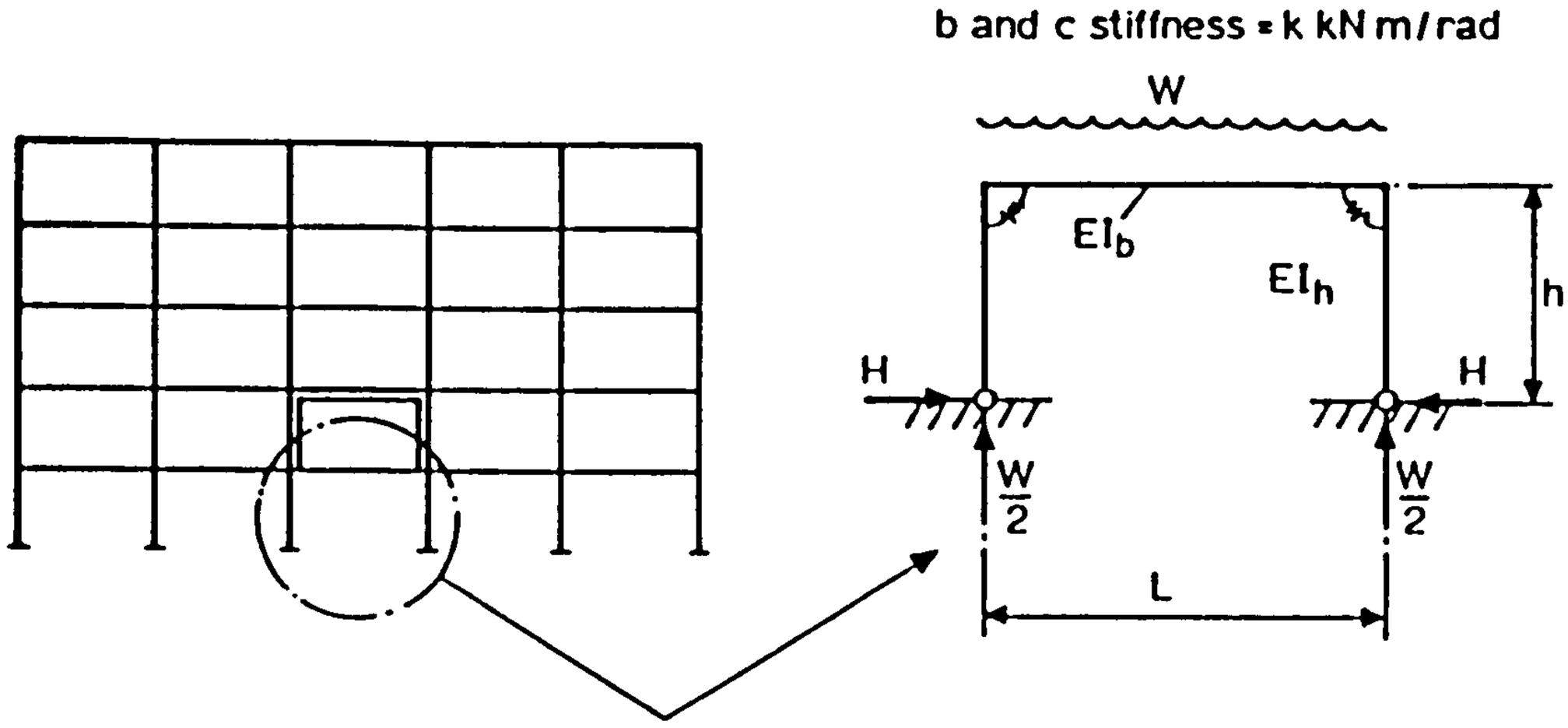

Figure 2.12. Model for beam strength and deflection

Assuming that the beam end connector behaves linearly with a stiffness value, k an elastic analysis is made in that the strain energy stored in the structure is represented by

$$U = 2\int_0^h \frac{(Hx)^2}{2EI_h}dx + \int_0^L \frac{(Wx/2 - Wx^2/2L - Hh)^2}{2EI_b}dx + 2\frac{(Hh)^2}{2k} \qquad 2.12$$

The last term represents the energy stored in the connectors at either ends of the beam.

Assuming

$$\frac{\partial U}{\partial H} = 0 \qquad 2.13$$

i.e. no spreading of upright bases

Then

$$Hh = \frac{WL}{24}\left\{\frac{2}{1+\frac{EI_b}{k_e L}}\right\} \qquad 2.14$$

Where

$$k_e = \frac{k}{\left(1+\frac{kh}{3EI_h}\right)} \qquad 2.15$$

is the effective stiffness of the connector having been reduced to the flexibility of the upright.

The bending moment at the centre of the beam is given by

$$Mc = \frac{WL}{8} - Hh \qquad 2.16$$

Substituting for Hh

$$Mc = \frac{WL}{24}\left\{3 - \frac{2}{1+\frac{2EI_b}{k_e L}}\right\} \qquad 2.17$$

The deflection at mid-span is given by

$$\Delta c = \frac{\left(5WL^3\right)}{384} - \frac{ML^2}{8EI_b} \qquad 2.18$$

Substituting for M as $M = Hh$

We have

$$\Delta c = \frac{5WL^3}{384EI_b}\left\{1 - \frac{0.8}{\left(1 + \frac{2EI_b}{k_c L}\right)}\right\} \qquad 2.19$$

Assessment of maximum bending moment in the beam end connectors is based on the condition that the beam is the middle of the rack, fully laden with adjacent beams also fully laden, this being represented using figure 2.13.

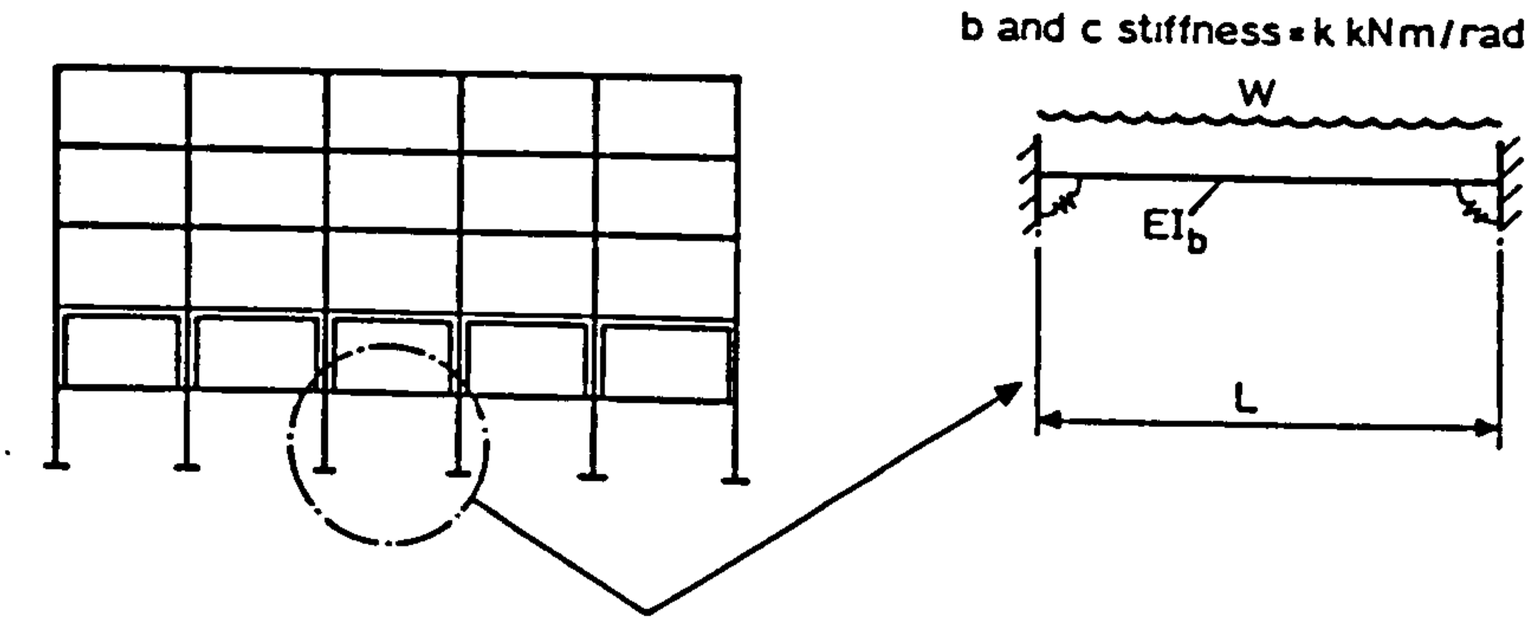

Figure 2.13. Model for beam end connector strength.

The strain energy expression is

$$U = \int_0^L \frac{\left(\frac{Wx}{2} - \frac{Wx^2}{2L} - M\right)^2}{2EI_b} dx + 2\frac{M^2}{2k} \qquad 2.20$$

And

$$\frac{\partial U}{\partial M} = 0 \qquad 2.21$$

Giving

$$M = \frac{WL}{12} \frac{1}{\left\{1 + \frac{2EI_b}{kL}\right\}} \qquad 2.22$$

Using a load factor of 2.0 for the strength of the beam end connector giving a maximum permissible moment of $0.5M_u$ where M_u is the ultimate moment for the connector obtained through tests. The value of the load limited by beam end connector strength is however given by

$$W \leq \frac{6Mu}{L}\left\{1 + \frac{2EI_b}{kL}\right\} \qquad 2.23$$

A further check is to determine the shear capacity of the beam at the connectors. This is usually done through tests but its effect in terms of beam performance is far less critical compared with the conditions discussed earlier.

2.4.6 The role of beam end connector in overall Stability

The restraining effects that the beam provide to the column through the semi-rigid beam end connectors is of great importance as the stiffness of the connector, amongst other factors, influences the strength of the column and its buckling length.

The SEMA code of practice recommends specific effective length factors independent of the stiffness of the beam end connector, however the code includes a check on the overall collapse of the structure using a quasi-rigid plastic mode shown in figure 2.14. The figure shows the structure to be out of plum by an angle φ_o, where

φ_o=beam end connector looseness +0.5%

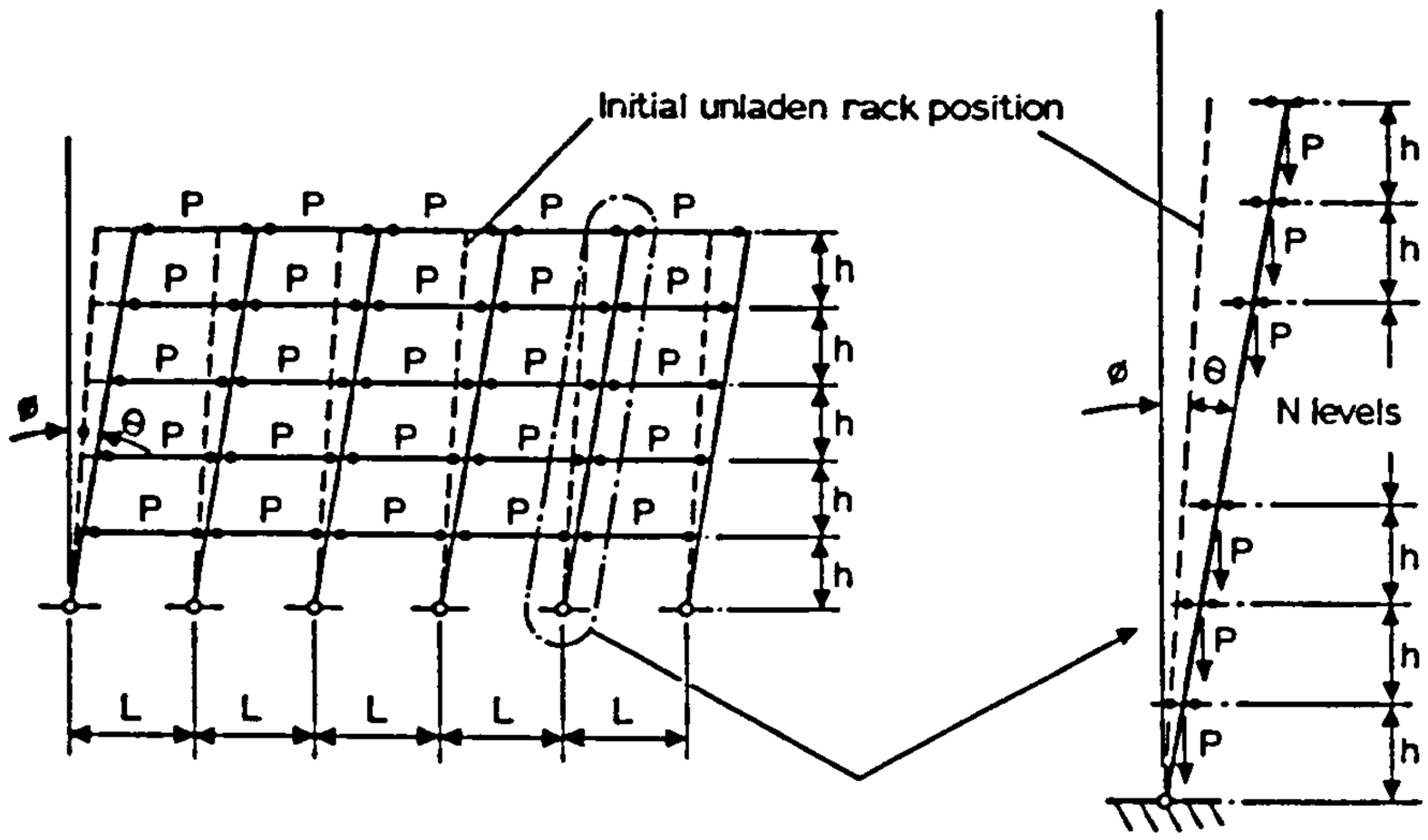

Figure 2.14.Rigid collapse mechanism

Ignoring the P-Δ effects and the additional rotation of the upright, φ the code evaluates the total overturning moment as

$$Ph\frac{n(n+1)}{2}\sin\varphi_o \qquad 2.24$$

and the total resistance moment as $2nMu$

and ultimately proposes the following formulae for the maximum load per upright incorporating a high factor of safety, 8.

$$nP \leq \frac{n}{2h(n+1)}\left(\frac{Mu}{\varphi_o}\right) \qquad 2.25$$

The article rightly emphasizes the need for an analysis including the P- δ effects and proposes a method by which this can be achieved.

2.5 Stability of Rack Structures

G.M. Lewis[21]

A design approach for the stability of pallet rack structures is provided taking into account the effect of the form of moment-rotation characteristic typical of commercial beam end connectors. The analysis is based on establishing an expression for the Total Potential Energy of the system, primarily taking account of the work done by the semi-rigid connectors and regarding the strain energy absorbed by the upright and the beam as being negligible. Figures 2.15 and 2.16 show the idealized loading condition considered for a typical upright and a loading and unloading characteristic respectively.

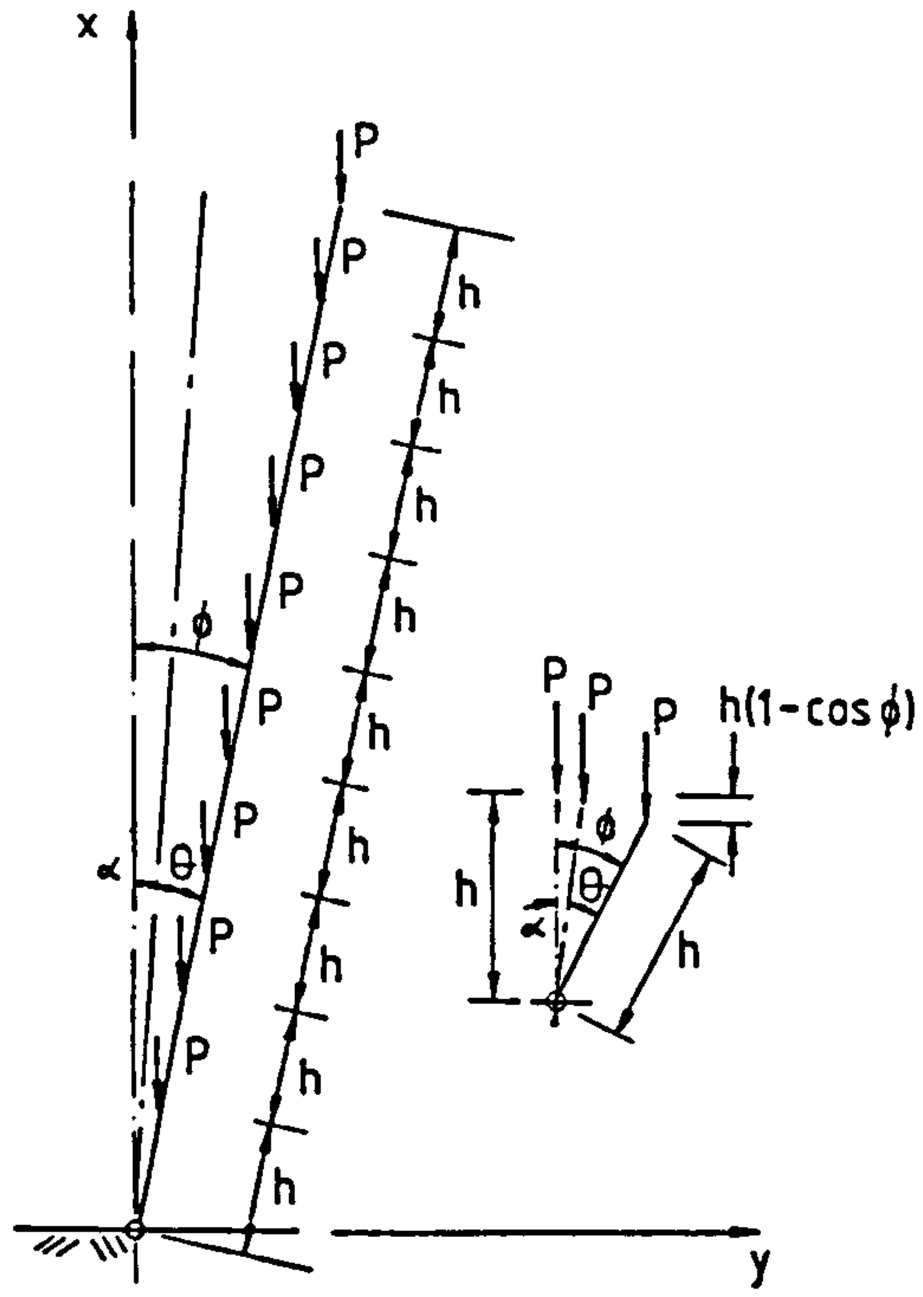

Figure 2.15. Upright in displaced position

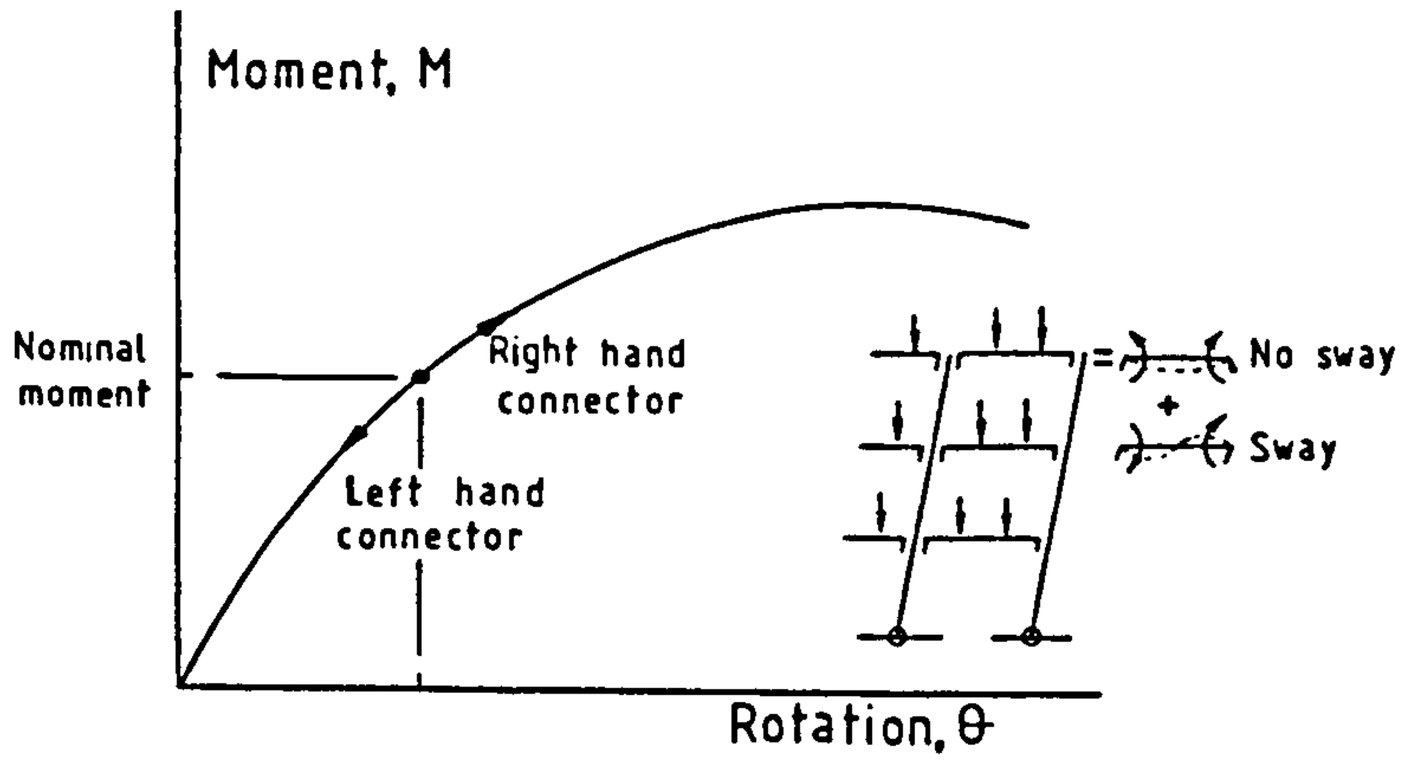

Figure 2.16. Loading and unloading regimes

The work done by the by the semi-rigid beam end connectors are written as.

$$U = \int 2Cf_b(\theta)d\theta \qquad 2.29$$

Where C is the number of levels.

Ignoring the strain energy absorbed by the upright and beams the following expression for potential energy is presented

$$PE = -ph(1-\cos\phi) - p*2h(1-\cos\phi) - \cdots\cdots - p*Ch(1-\cos\phi) \qquad 2.30$$

Where $\phi = \theta + \alpha$

And the total potential Energy of the system is written as

$$U + PE = 2C\int f_b(\theta)d\theta - \frac{phC(C+1)}{2}(1-\cos\phi) \qquad 2.31$$

The work investigated the influence of varying moment-rotation characteristics on the type of stability demonstrated by a racking system, figures 2.17,2.18 and 2.18.

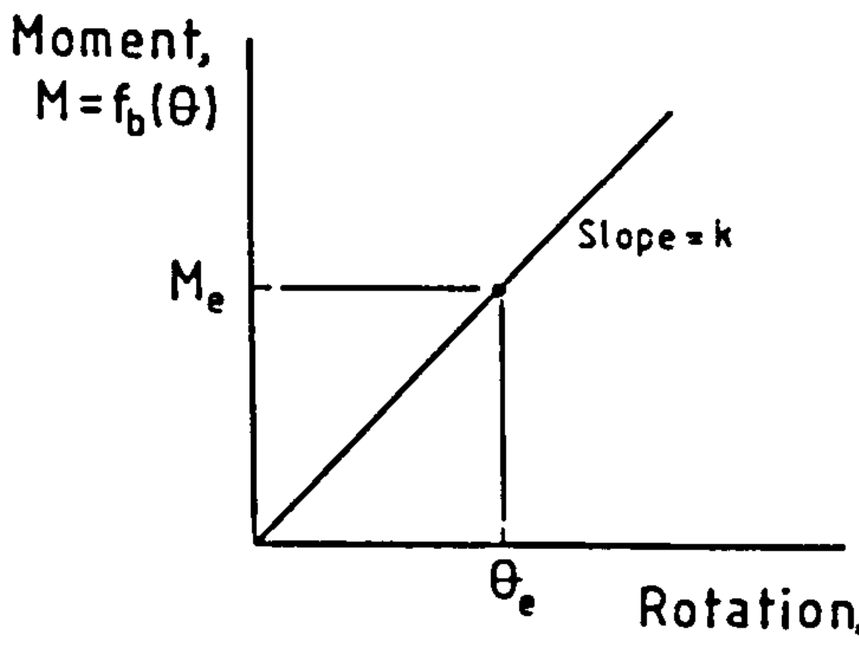

Figure 2.17. Linear characteristic

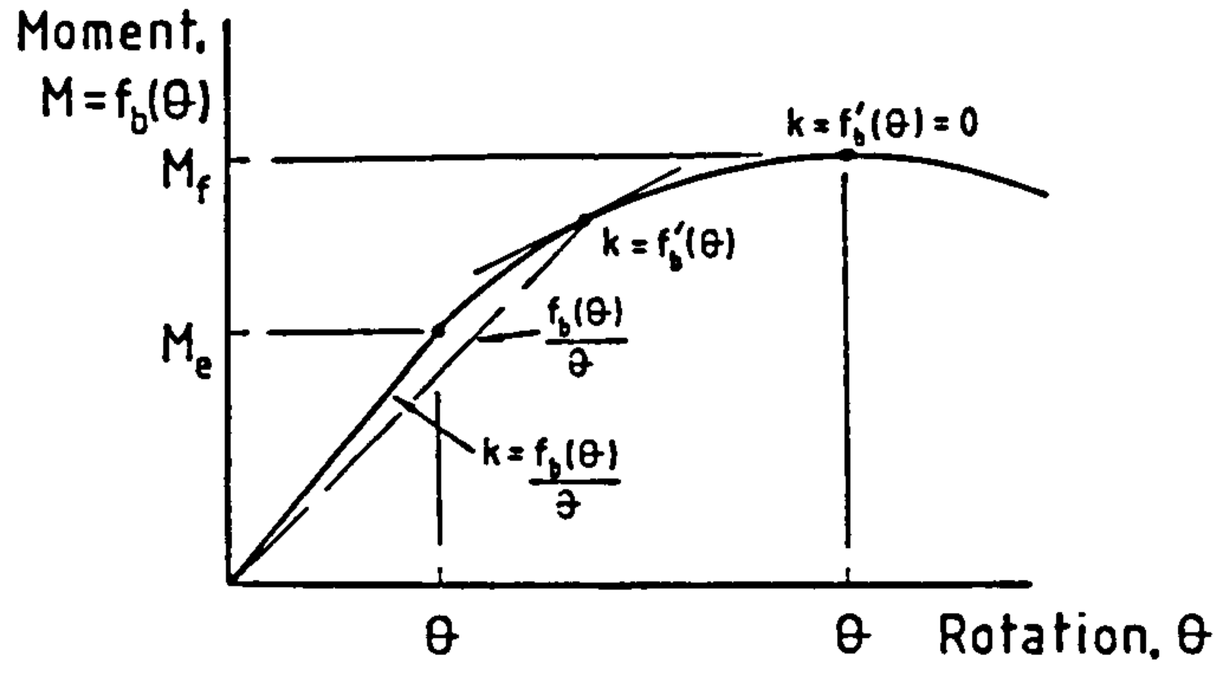

Figure 2.18. Generalized two part characteristic

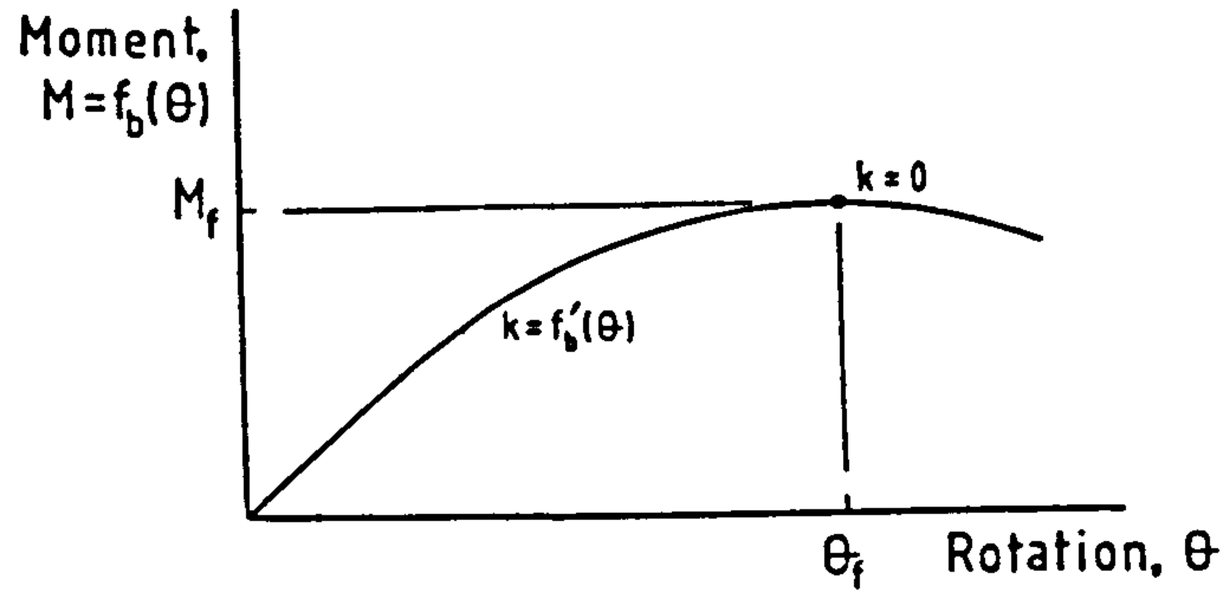

Figure 2.19. Nonlinear characteristic

This is done through expressions representing the total potential Energy of the system both for equilibrium and unstable loading conditions.

The structure was then investigated for the three moment-rotation characteristics of the beam end connectors, linear, generalized two-part linear and non- linear as well as a non-linear case.

The work concluded that the maximum load of pallet rack frameworks could be affected by the beam end connectors characteristics.

This work emphasizes the significance of the overall shapes of moment rotation curves. This is characteristic of the

various beam end connector designs available which will be covered in this work.

2.6 Down-aisle stability of rack structures

J.M Davies[22]

The work presented deals with the concept of effective length factor for unbraced rack structures as a parameter reflecting the behaviour of the complete structure as opposed to it just being the property of individual members and their end conditions. It shows that evaluation of effective length depends on determination of the elastic critical load factor λ_{crit} and this in turn is greatly affected by the properties of the beam end connector. In fact the analysis suggested that as the stiffness of the beam end connector was reduced, the effective length of the uprights in the down-aisle direction of a rack structure tended to infinity.

The work described three methods for the determination of second order behaviour of rack structures. The basis of which is the work carried out by Horne[23] on the procedures for estimating the elastic critical loads of multi-storey frames. The Three models considered are shown in figures 2.20, 2.21 and 2.22.

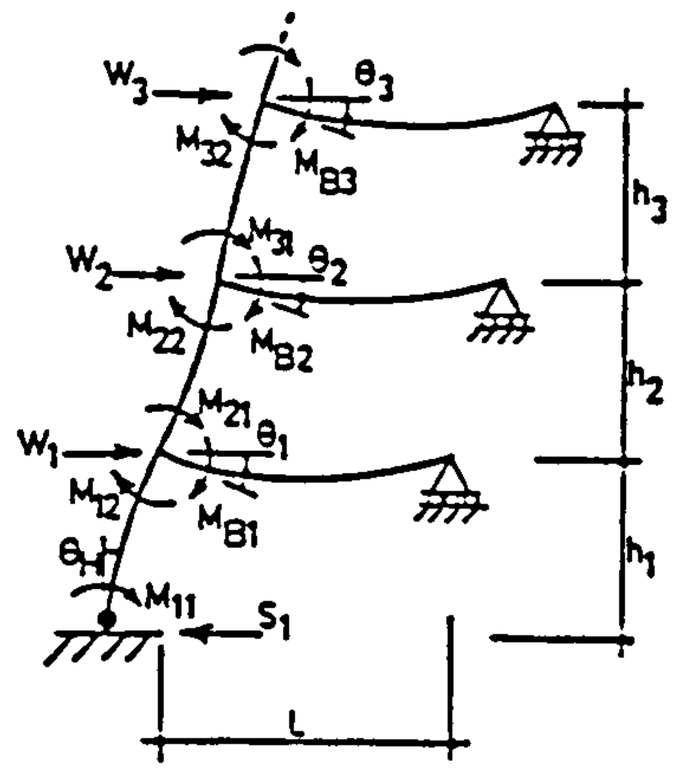

Figure 2.20. Substitute frame

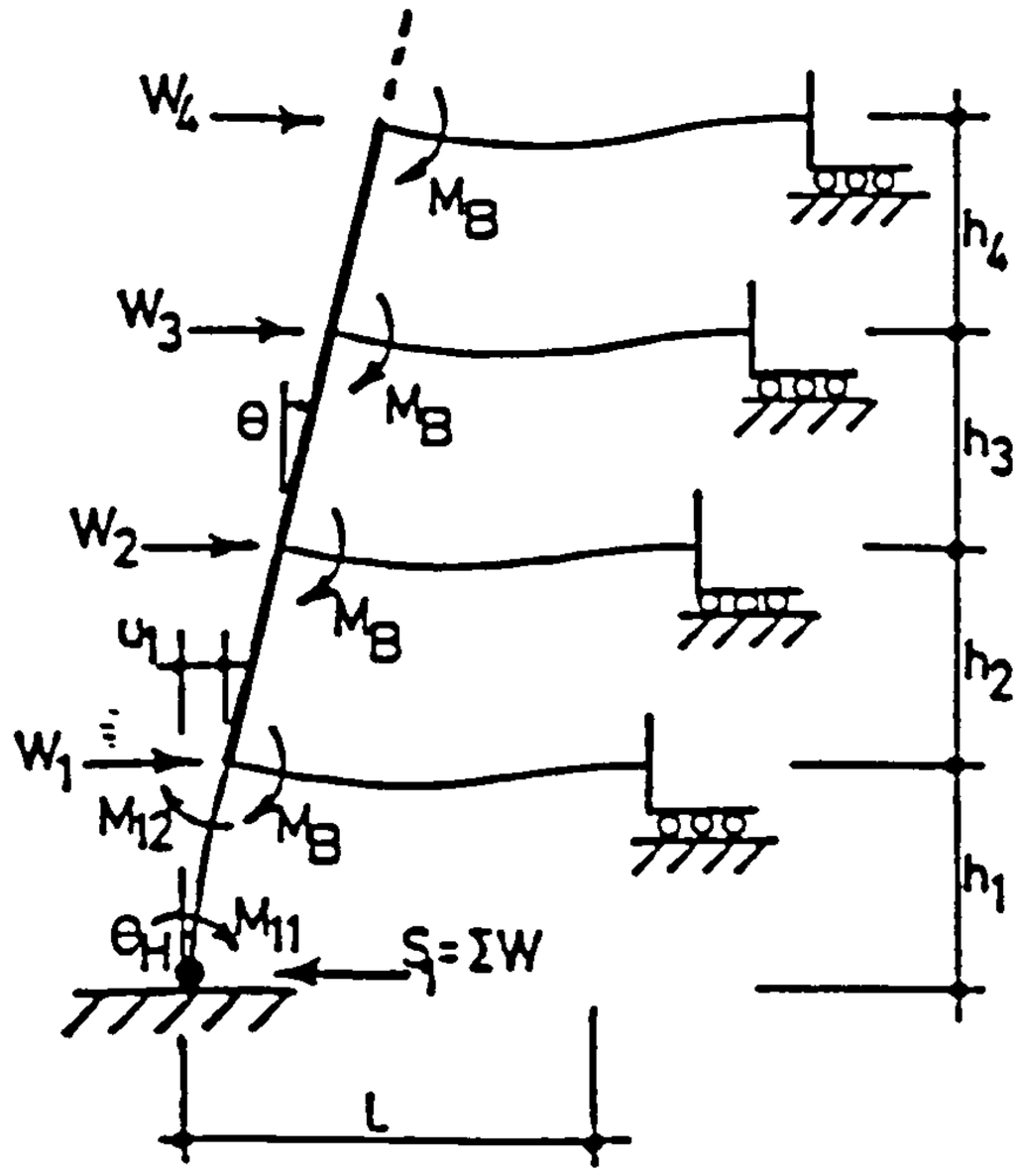

Figure 2.21. Stark and Tilburgs model modified

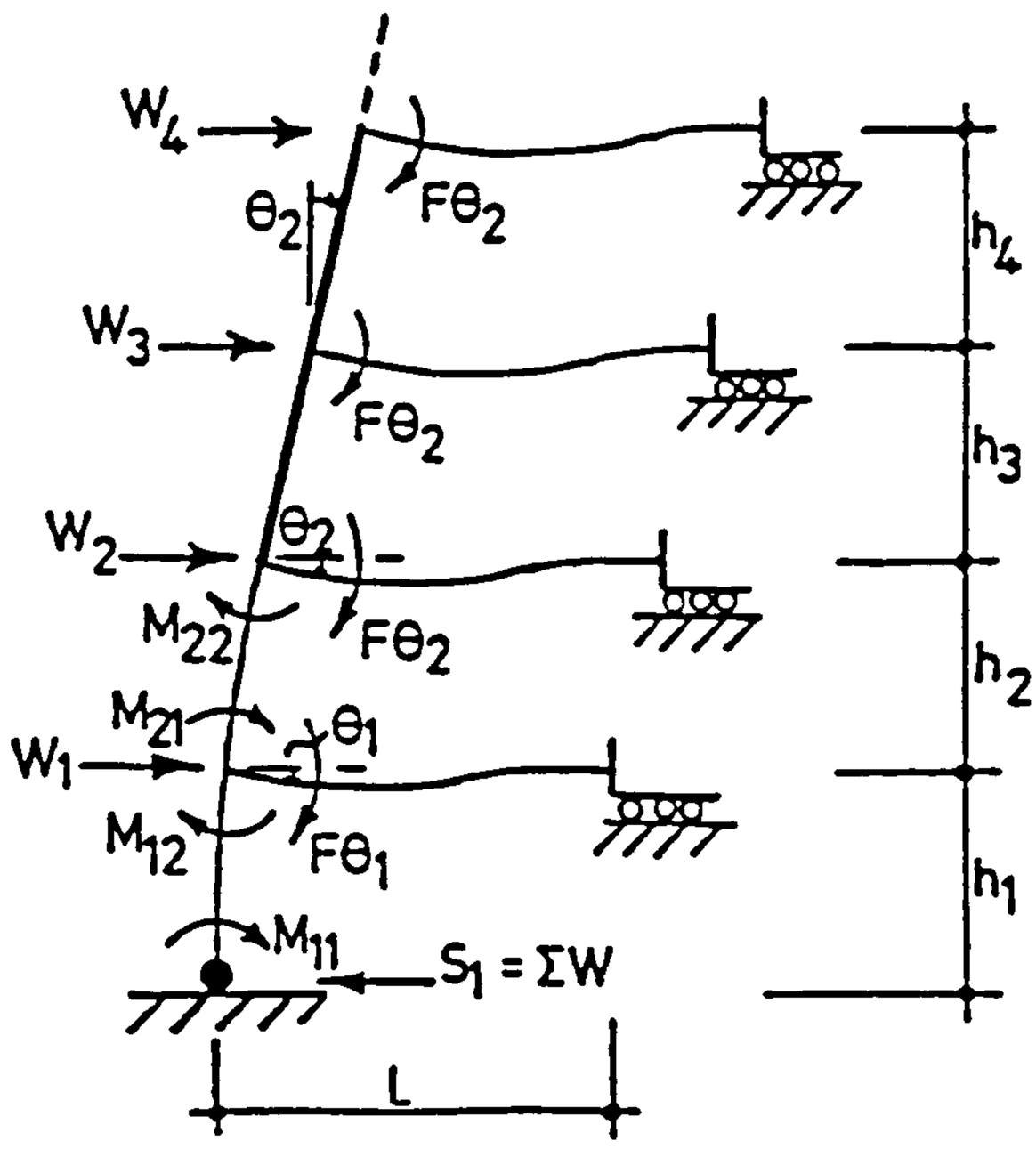

Figure 2.22. Improved model

Figure 2.20 is a substitute frame resulting from modifications made to the model proposed by Horne taking account for the characteristics of a rack structure including modification to the member stiffness to allow for semi-rigid beam end connectors at the ends of the beams and the column bases.

Figure 2.21 shows the Stark and Tilburgs model having been modified according to Horne's work. This the case where the column design was restricted to the height to the first beam and was therefore limited to low-rise applications only as it neglected the flexibility of the upper storey columns.

Figure 2.22 shows the most accurate method where in bending moment distribution in the columns of both first and second storeys are taken account of.

In each case an estimate of the elastic critical load and the bending moment distribution under an appropriate pattern loading condition is carried out.
Undertaking exact analysis verified these methods as being convenient design procedures using explicit equations.

2.7 Imperfection sensitivity of structures with semi-rigid joints

G.M.Lewis[24]

The work demonstrates the imperfection sensitivity that can occur in unbraced pallet rack frames due to the particular characteristics of semi-rigid joints. To achieve this the test result from a pallet rack joint is represented by curve fitting exercises that fitted the test data with a second order regression function and a third order regression polynomial. With an allowable out-of-plum of 0.005 radians, SEMA[10] and the theory, G.M. Lewis[21], it was

demonstrated that for joints that can be represented by a quadratic moment-rotation function the reduction of load conforms to a square root relationship. This leads to reduction in maximum load carrying capacity highlighting the need for accurate site installation tolerances.

2.8 Author's conclusions

As is apparent from the outcome of the literature survey presented above that there has been little or no work carried out to try to investigate the performance of boltless semi-rigid beam end connectors. This has presented no great surprise for a number of reasons. Connectors of this type found in proprietary racking systems greatly vary in design. Their simple method of manufacture allows introduction of a range of features and facets to be included to improve efficiency. These tend to be "intricate" details making it very difficult to establish common characteristics responsible for their behaviour. Added to this is the fact that a beam end connector works as a joint only when it is accompanied by a beam and perforated uprights. The beams and the uprights come in a range of sizes and geometries with direct influence on the performance of the joint. Furthermore, the nature of such members, being thin gauge sections and having their own complicated modes of failure has added to the complexity of the problem. Other factors such as welding arrangement variations greatly affect joint behaviour and therefore have not helped the situation.

All these factors have meant that no modeling approach has been devised which could predict the behaviour of such joints. The only way to determine the performance of such joints has been through testing them individually to gauge the effects of their specific features. However, the author has been unable to access experimental data produced in

such a way as they have never been published by manufacturers.

Furthermore until recent years the amount of research carried out on the overall performance of racking structures itself has been quite limited implying that a lesser attention has been paid to the analysis of the beam end connectors. This has also for years been applicable to the understanding of joints in heavy structural engineering, R. Cunningham[9].

In previous decades simple assumptions were made regarding the behaviour of joints. Amongst other reasons including economy driven causes, the modern development of tall buildings and the use of light cladding with less inbuilt strength has led to the need for joints to be justified in terms of self strength.

In short understanding of mechanical and structural joints have historically taken second place in engineering practices throughout the world. In fact in the design of steel structures it has been common practice to consider the main members first and to relegate connection design to a secondary role to be tackled at a later stage, often with rather less attention being given to the task, J.B Davison & D.A.Nethercot[8].

The present work, however, may well be the first step towards attempts to understand and classify the governing parameters affecting the behaviour of such connectors; as well as measures to devise an effective modelling approach, and to propose a method by which the ultimate bending carrying capacity of a beam end connector can be estimated.

To achieve this a large number of different beam end connector tests were carried out, the results were

analyzed, compared and any commonality in behaviour recorded. The information obtained would form the bases of the theoretical work. This would be to model the beam end connector behaviour globally using finite element techniques.

CHAPTER 3

CLASSIFICATION OF BEAM END CONNECTORS AND EXPERIMENTATION

C H A P T E R 3

CLASSIFICATION OF BEAM END CONNECTORS AND EXPERIMENTATION

3.1 Introduction

There are a variety of types and designs of semi-rigid beam end connectors in use representative of a large number of different rack manufacturers.

In general a semi-rigid beam end connector comprises two plates at right angles to each other. One plate contains a set of tabs which act as an interlocking mechanism and hence the source of resistance to rotation as they are engaged with perforated uprights. The second plate at right angles to this acts as an end plate facilitating various welding arrangements of beam to the beam end connector, figures 3.1 and 3.2.

The tabs that provide the interlocking arrangement perform the same function as those of bolts in semi-rigid structural joints. The end plates are subjected to the same loading conditions as those of other structural joints. Beam end connectors of this type are produced from strips of steel 3 to 5mm thick through a number of operations usually using presses with multi stage tools. The operations involved may be shearing, bending, blanking, piercing and forming. Any combination of these may be employed in the production of a given beam end connector design.

Commercially available beam end connectors have a wide range of features and facets. These can be intricate in geometry and at times difficult to identify.

Usually the end plates of beam end connectors are simply plane plates, but some beam end connectors may include intermediate stiffeners in the height of their end plates, figure 3.3. This may not be a prominent feature but its presence will markedly affect the shape of the moment rotation curve. Figure 3.25 shows the moment rotation characteristics obtained for product 1 shown in figure 3.10. This design incorporated a stiffener in its end plate. The double peak in the curves characterized the effect of this feature.

Furthermore the shapes of the tabs may appear to be similar when they actually differ in reality. Some tabs may be more clear cut in geometry giving more direct contact areas with an upright's web, as shown in figures 3.10 and 3.42, product 1. In other designs the tabs may be round in shape, figures 3.11 and 3.43, product 2.

These different features may look apparently insignificant but they affect the behaviour of a joint. For instance a round tab design could lead to a less effective wedging action against the upright's web. This could lead to variations in strength value, stiffness value or the extent of the inherent looseness in a beam end connector.

3.2 Classification of beam end connectors

The commercially available beam end connector designs may be categorized as follows:

Class (A), "tongue and slot design": the term "tongue" refers to a cantilevered tab which is formed and punched

out of the bracket, This design is said to have integral tabs. The beam end connector during use makes contact with the upright's web and flange, figures 3.1 and 3.3.

Class (B), "blanking design": a blanking operation produces tabs which, depending upon the design of the upright, interlocks either parallel or perpendicular to the web of the upright, figures 3.4 and 3.5.

Class (C), "Stud-Incorporated design": the presence of punched holes in the bracket allows press fitting of studs, hence the term "Non-Integral" tabs. The design comprises a single set of studs replacing the tabs in the tongue and slot design, with two planes of contact with the upright's web and flange, figure 3.6.

Class (D)," Dual integrated tab design": the tabs are formed and punched out of the bracket so that they remain joined to the bracket at two points and therefore termed non-cantilevered. This particular type of beam end connector has one set of tabs and makes contact with the upright in two planes. These are the planes of the web and the flange of the upright, figure 3.7.

Features of the different classes may be combined to give composite beam end connector designs. For example, figure 3.8 shows a beam end connector with two sets of tabs, one set produced by punching and forming, and the other by a blanking operation. The beam end connector has three contact planes with the upright, namely the planes of the web, the flange and the intermediate stiffener.

All the beam end connectors use locking devices as guards against accidental raising of the beams. In most cases a pin provides the required resistance against uplift. An alternative to this, in some cases is the use of an

upwardly extended tab. Figures 3.3 and 3.5 show examples of the locking devices used.

Figure 3.9 shows a summary of the general classification of the commercially available beam end connectors.

The geometry of the tabs determines the geometry of the perforations in the accompanying uprights. The slots facilitate the engaging of the beam end connectors through their tabs in the upright within close tolerances, with a view to achieving a wedging action required for good fit when under load. However tight tolerances are a compromise between having as little looseness in the joint as possible whilst enabling quick and easy installation. Beam end connector looseness can result in bending moments similar to those caused by a side load. This, in unbraced racks, has the unwanted effect of increased sway and shear forces upon the load carrying capacity of the whole structure, Godley[12].

3.3 Beam end connector material

See section 2.4.3

3.4 Beam end connector tests

3.4.1 Introduction

To determine the moment-rotation curves of each joint bending tests were carried out. The curves were then analysed to give the stiffness and the strength values of each joint.

Twelve commercially available products were tested. A selection of these is shown in figures 3.10-3.18. Three identical tests were made of each product to determine the spread of the results. Two tests were made on prototypes of

Planned Storage connectors. Further tests were made on variations of the Planned Storage Systems beam end connector to determine the effects of the various parameters affecting beam end connectors.

Table 3.1 and figure 3.9 show the dimensions and classifications of the products tested. Figure 3.20 is a general representation of all the possible dimensions in a beam and beam end connector assembly.

To describe the welding position of beams to beam end connectors the following terms are commonly used:

Symmetrical: this occurs when the horizontal axis of symmetry of the beam coincides with beam end connector at mid height, figure 3.2(a).

Up welded: this occurs when the horizontal axis of symmetry of the beam is off set upwards from the beam end connector's mid height. This often makes the beam top flange almost level with the top of beam end connector, figure 3.2(b). Dimension *f* in figure 3.20 is used to indicate the exact positioning.

Down welded: this occurs when the horizontal axis of symmetry of the beam is off set from the beam end connector's mid-height, either below or just above it, figure 3.2(c). Dimension *f* in figure 3.20 is used to indicate the exact positioning.

Symmetrical and the up-welded positions are the most common welding arrangements.

The ratio a_1/a represents the ratio of the depth of the beam to the length of the beam end connector and distinguishes between shallow and deep connectors. This

ratio is a measure of the stiffening effect of the beam upon the beam end connector.

3.4.2 Specimen preparation

Fabrication work was carried out according to figure 3.21. This facilitated rigid, quick and easy securing of a short length of upright to the test frame standardising the method of mounting on to the test frame. All specimens had a stress sensitive lacquer applied to them to enable positions of high stress to be identified. Prior to this an alkaline solution had been used to remove the paint from the beam end connectors. The lacquer was then applied using a brush, building up in thin coats until a thickness of about 0.10mm was obtained, figures 3.22 and 3.23.

3.4.3 Test procedure

Figure 3.24 shows the general layout of the tests. A stub column section was rigidly bolted into a test frame through the holes in the pair of prefabricated unequal angles, and a short length of beam connected to it through a beam end connector. To prevent lateral movements whilst loading, the free end of the beam was constrained by vertical guides whose inner faces were lubricated to avoid sticking. The load was applied by a 100kN hydraulic jack supported on a load cell. To measure beam-column rotation two displacement transducers were mounted adjacent to the stub column bearing on top of the beam. Figure 3.19 shows a product under test.

In each test the load was applied incrementally until a maximum was reached, allowing the load to drop by about 1 kN before terminating the test. Developments such as beam displacement, distortion of stress lacquer and deformation of the uprights were monitored through the test.

Photographs were taken of various lacquered beam end connectors after the test to observe the distribution of strain in the beam end connector.

3.5 Results of tests on commercial products

The recorded data was used to plot moment-rotation curves. The results of the tests on commercial products are shown in figures 3.25-3.38. Figures 3.39, 3.40 and 3.41 group the curves for class A, class B and A/B, and class C products. Each curve is typical of the group of three results obtained for each product. The results were used to determine the maximum moments of resistance and the stiffness of the beam end connectors. The stiffness was taken as the gradient of a line passing through the point of zero load and a point on the moment rotation curve at half the failure moment, the method recommended in SEMA[10]. Table 3.2 shows a summary of the results.

Figures 3.42- 3.54 show the beam end connectors with Stress-Sensitive Lacquer before and after test. Close examination of these photographs showed the regions of high stress. These regions were highlighted by either flaking of the lacquer, fading of its colour or the presence of striation. Not too surprisingly, in all cases, the tab corners in contact with the uprights, hence load bearing, were the most affected regions. The photographs also showed the varying stress distribution patterns, characteristic of the different designs. The stress distribution established in such a way was later confirmed by theoretical work using Finite Element techniques.

In general, the moment-rotation curves consist of two parts. The first part represents elastic behaviour. It is to be noted that in some cases this may be non-linear. The second part of the curve includes the start of the material

yielding followed by a peak associated with the Ultimate Failure Load of the connection.

3.5.1 Class A, 3-Tab beam end connectors

Product 1: The moment-rotation curve shows a discontinuity in the slope, figure 3.25. This was because an intermediate stiffener in the beam end connector's end plate came into contact with the upright's flange in the compression zone during the early part of loading, causing a sharp change of slope. Once the gap in the compression zone closed, load was then transferred to the top tab, which cut into the upright causing the second peak. The deep beam section with a_1/a = 0.48, down-welded and f=80mm, distributed the load relatively evenly in the short and stubby tabs located centrally. Their interaction with the relatively thin upright section meant that the value of the ultimate failure load was determined by the tearing of the tabs into the upright with the beam end connector almost fully intact.

Product 2: The relatively shallow beam section, a_1/a =0.35 up-welded and f=8mm, distributed the load unevenly in the formed and punched tabs which had rounded interfaces with the upright gauge. This welding arrangement precipitated a premature tension failure in the face of the connector near the exposed edge, whilst the bottom tabs remained almost fully intact leading to a low ultimate failure load. Characteristic of this type of welding arrangement was also a highly non-linear moment-rotation curve, figure 3.26.

Product 3: A beam end connector design having two contact planes with the upright, planes of the web and the flange. The deep beam section, a_1/a =0.48, up-welded with f=9mm, distributed the load unevenly in the formed and punched cantilevered tabs which had flushed interfaces with the

relatively thin upright gauge. This welding arrangement, as in other similar cases, lead to a premature tension failure on the exposed edge of the face containing the tabs. The bottom two tabs away from the stiffening effect of the beam were almost fully intact. The moment-rotation relationship was a smooth curve showing a highly non-linear deformation band typical of this type of welding arrangement, figure 3.27. This was related to tensile failure in the exposed edge and the cutting of the top tab into the upright.

Product 4: This was identical to product 3 except that the beam was down welded with *f*=46mm. This resulted in a more even distribution of the load in the tabs, evident from the relatively equal degree of distortion incurred by them. The consequence of this was an improvement in the moment-rotation values, see Table 3.2 and figure 3.28. The beam end connector exhibited plate bending as well as local distortion around the tabs. The second test result was affected by a malfunction in the transducers' readings. It was not included in figure 3.28.

Product 5: This was again identical to product 3 except that the beam was welded to the beam end connector symmetrically with *f*= 51.5mm. The symmetrical welding position further promoted uniform distribution of the load into the top and bottom tabs. This resulted in a further improvement in the stiffness and strength values of those obtained in product 4. In addition there was an increased distortion in the top and bottom tabs. The moment-rotation curve showing the shortest band of rotation indicative of the highest stiffness value exhibited by the products in the set 3, 4 and 5, figure 3.29.

3.5.2 Class A, 4-Tab beam end connectors

Product 6: A large 4-tab beam end connector up welded to a deep beam section with a_1/a =0.44 and f=9mm. The resulting moment-rotation curve showed a double arch, figure 3.30. The first peak was associated with the engagement of the two top tabs against the upright, and the start of tensile failure of the beam end connector's exposed edge. This was due to the stiffening effect of the beam section at the top half of the beam end connector. As loading continued, the gap between the end plate and the upright's flange in the compression zone closed and partial engagement of the bottom two tabs took place resulting in the second peak followed by tensile failure of the exposed edge, see figure 3.46.

Product 7: This was identical to product 6 except the beam end connector was down welded with f=46mm. This resulted in a better distribution of the load into the tabs and lead to improved moment-rotation characteristics, figure 3.31. The failure was initially caused by the top tab engaging against the upright and subsequently cutting into it. This was closely followed by distortion caused by the tab immediately below it. The effect of these two developments resulted in the first peak of the curve. Closing the gap between the end plate and the upright's flange followed by a more complete engagement of the bottom two tabs were responsible for the second peak. The failure of the joint was concluded by the top tab completing its tearing process into the upright wall. Associated with this was a drop in load signifying a lack of resistance to rotation.

Product 8: This was again identical to product 6 except that the beam was welded to the beam end connector symmetrically with f=76.5mm. This resulted in further improvements in the moment-rotation values owing to a more

even distribution of the load into the tabs. Also responsible for the improved performance was the fact that unlike product 6 no tension failure was observed with this welding arrangement. The moment-rotation curve was similar in shape to those obtained for products 6 and 7, except that it had the least rotation of the set of products associated with the highest stiffness value, see figure 3.32.

3.5.3 Class B, 3-Tab beam end connectors

Product 9: A radically different design of upright and beam end connector. The beam end connector is the result of a blanking operation. The combination of a thick upright gauge of 2.65mm and large interaction areas at the tabs resulted in significant deformation of the beam end connector, mainly in the form of end-plate bending with distinct signs of hinge formation highlighted by the faded colour of the lacquer, figure 3.49. This effect may have been compounded by the deep beam section with a_1/a = 0.51 having been down-welded excessively and f =72mm. The moment-rotation curve is seen in figure 3.33.

Product 10: A thick gauge, relatively stubby, wrap round design having 63% of the height of its end plate stiffened by the beam section. The accompanying upright, 2.65mm thick, had a 15mm deep intermediate stiffener along its web with rectangular perforations which facilitated the engagement of a single set of tabs of three including an upwardly extended tab as its locking pin. The relatively heavy and compact nature of the members involved resulted in high moment rotation values, sees figure 3.34. The degree of the deformation suffered by the upright in flange crushing was evident, figure 3.50. In comparison, the beam end connector remained undamaged.

3.5.4 Class C, 3-Tab beam end connectors

Product 11: A stud incorporated beam end connector design in conjunction with a large beam section having a ratio of a_1/a =0.60 and up-welded with f = 8mm. The moment-rotation curve showing a comparatively linear behavior, associated, possibly with the large contact area between the studs and the upright, figure 3.35. This effect could have been compounded by the rigidity of the studs, which remained almost fully intact until sudden dislodgment of the bottom stud.

Product 12: The beam end connector was considered as a prototype. It was made of ordinary Carbon Steel and included three 6mm-diameter studs. A beam section was welded to it symmetrically, with f=52mm, a_1/a =0.48 and a 2.7mm thick upright with "tear drop" shape slots accompanied the design. The moment-rotation curve showed a wide band of plastic deformation associated with distinct ductile failure of the beam end connector material, figure 3.36. This was confirmed by the fact that the studs remained firmly fitted to the beam end connector throughout the test, and the upright showed no sign of distortion on test completion, figure 3.52.

Product 13: This product was identical to product 12, but the beam end connector included 10mm diameter studs. This, in comparison with product 12, had larger contact areas at the tabs with the upright, which reduced the stress concentration and consequently delayed the start of plastic deformation. The outcome of this was a higher stiffness value than that obtained for product 12, figure 3.36. The ultimate failure occurred as a result of the beam section tearing off on the top flange near the weld.

3.5.5 Class D, 3-Tab beam end connectors

Although this Class was discovered through Manufacturer's Trade literature it could not be obtained for testing purposes.

3.5.6 Class A/B, composite design

Product 14: This was a wrap round design having three contact planes with the upright. It had two sets of three tabs. The accompanying upright had a deep intermediate stiffener with rectangular perforations designed to receive one set of tabs. The second set of the tabs was engaged into the unstiffened part of the face of the upright. The relatively deep beam section, a_1/a =0.48 was up-welded which limited the otherwise significantly better moment-rotation characteristics observed in figure 3.38. Premature torsion and bending of the beam end connector was the mode of failure, figure 3.54.

3.5.7 Discussion of results of tests on commercial products

The performances of the different beam end connector designs depended on their special features. These apparently insignificant features appeared to affect the shape, strength and stiffness values of the individual beam end connector.

Added to this were the effects of unavoidable variations such as the beam sizes, welding positions of the beam to the beam end connectors, the gauge and the profile of the uprights. This lack of commonality amongst the tested products made the undertaking of a direct comparison not possible.

Visual examination of the beam end connector used in products 3, 4 and 5, during and after test completion showed that ultimate joint failure resulted from the tabs cutting into the upright. An increase in the contact area between the tabs and the relatively thin gauge upright was considered likely to reduce a *"tin opener effect"* responsible for the failure of these designs.

Furthermore, when the beam was up-welded a typical weak point emerged. This was at the exposed edge of the face of the beam end connector containing the tabs. This type of welding arrangement makes the beam end connector vulnerable to tensile failure, hence affecting the value of the ultimate moment carrying capacity.

3.6 Tests to determine the effects of different parameters

Based on the simple observations in 3.5.7, the two dimensions involved were changed, figure 3.20 dimensions d and c. The gauge of the beam end connector material, d, was increased by 30% and the face dimension, *c* by 13%.

To investigate the influence of the parameters identified by testing the Commercial Products an extensive number of tests were devised and carried out. A selected number of these are given here as products 15 to 22. They were all class A. The moment-rotation curves are seen in figures 3.55-3.62.

3.6.1 Effect of beam end connector dimensional changes

Product 15: The modified beam end connector was used in conjunction with the beam section, a_1/a =0.48, up-welded with *f*=9mm. These two changes resulted in moment -rotation curves showing a discontinuity in the slope and offering higher moment-rotation values in comparison with product 3

which, with the exception of the beam end connector, was exactly the same. The moment carrying capacity increased by 8% and the stiffness value by 55%, figure 3.55.

Product 16: The modified beam end connector was used in conjunction with the beam section, a_1/a =0.48, down-welded with f=46mm. These two changes resulted in higher moment-rotation values in comparison with product 4 which, with the exception of the beam end connector was exactly the same. The moment carrying capacity increased by 1.3% and the stiffness value by 54%, figure 3.56.

3.6.2 Effect of upright gauge increase

Product 17: This was identical to product 15, but was tested in conjunction with an upright, which was 28% thicker. The moment carrying capacity increased by 11% and the stiffness value by 25%, showing the effect of upright gauge increase on performance values, figure 3.57.

Product 18: This was identical to product 16, but was tested in conjunction with an upright, which was 28% thicker. The moment carrying capacity increased by 16% and the stiffness value by 29%, demonstrating the gain resulting form the use of a thicker gauge upright, figure 3.58.

3.6.3 Effect of using deeper beam section

Up welded

Product 19: Rather than a_1/a =0.48, as used for product 15, the modified beam end connector was tested in conjunction with a deeper beam section having a_1/a =0.53. The upright gauges were 1.8mm and both products were up-welded. The

moment carrying capacity and the stiffness value remained virtually unchanged.

Down welded

Product 20: Rather than a_1/a =0.48, as used for product 16, the modified beam end connector was tested in conjunction with a deeper beam section having a_1/a =0.53. The upright gauges were 1.8mm and the welding positions were down-welded. The moment carrying capacity increased by 2.8% and the stiffness value by 17%, figure 3.60.

3.6.4 Effect of deeper beam section combined with upright gauge increase

Product 21: Rather than a_1/a =0.48, as used for product 15, the modified beam end connector was tested in conjunction with a deeper beam section having a_1/a =0.53 and an upright which was 28% thicker. The moment carrying capacity increased by 21% and the stiffness value by 37%. This magnitude of gain is also observed when comparing the test results for products 22 and 16 demonstrating a significant gain obtainable by increasing the upright gauge accompanied by deeper beam section, figure 3.61.

3.6.5 Discussion of the effects of the various parameters

Examination of the beam end connectors' faces incorporating tabs, showed the stress patterns extending to the exposed edge of the face making them vulnerable to tension failure. This was typical of the beam end connector designs which had two contact planes with their uprights, and was accentuated when the beam was up-welded to the beam end connector. Welding of the beams to the beam end connectors in such a way was disadvantageous as it resulted in low moment carrying capacity. This was because welding

arrangements of this type did not transmit the load into the tabs evenly.

Considering the modified versions of products 3, 4 and 5, switching from up-weld to down-weld increased the strength from between 10% to 50%. The effects on stiffness were marginal with an increase of between 1% and 5%. When the beam end connector was accompanied by thicker uprights, the switch from up-weld to down weld resulted in better performance values.

A further disadvantage of the up welding option was demonstrated when investigating the effect of switching to deeper beam sections. It appeared that the deeper beam section did not result in better joint performance.

The outcome of the tests on products 15 and 16 confirmed the alleviation of the tin opener effect by extending the contact area between the tabs and the upright.
Symmetrical welding position of the beam to the beam end connector improved the strength and the stiffness values by 32% and 28% respectively as compared to the case where the beam is up-welded. This was because of better distribution of load into the tabs resulting from a more even stiffening effect of beam on beam end connector.

Comparison between the three lug products 3,4, 5 and the corresponding four lug products 6,7, 8 showed an increase in stiffness of up to 280% and strength of up to 36%. This was attributable to larger physical geometry and greater number of tabs. The percentage increase in stiffness value was far greater than that of strength. This implied that enlarging geometrical features had a more direct effect on elastic properties, whereas plastic behavior was always limited by the mechanical properties of the material.

3.7 Corrections to experimental stiffness values

The experimentally measured stiffness values are subjected to errors due to:

(a) the deflection of the stub beam used in recording the rotation between the two points where transducers were placed.

(b) the deflection of the stub column between its supports due to a moment applied at its midpoint.

To determine the effects of these two errors the following corrections were made:

3.7.1 Stub beam rotation

The correction for rotation of the stub beam was applied by considering the differential displacement between the two transducers as shown in figure 3.63. The following relationship, Appendix 3.1, was used to evaluate the true stiffness k_T, which is compared with the experimental stiffness k_E.

$$\frac{1}{k_T} = \frac{1}{k_E} - \frac{1}{6EI}\frac{L_2^2(3L-L_2)-L_1^2(3L-L_1)}{L(L_2-L_1)}$$

Where EI is the flexural rigidity of the beam and L_1 and L_2 are the dimensions that determine the positioning of the transducers according to figure 3.63.

Errors due to beam rotation depend upon the term:

$$\frac{1}{6EI}\frac{L_2^2(3L-L_2)-L_1^2(3L-L_1)}{L(L_2-L_1)}$$

However the value of this term is much smaller in comparison to the value of $1/k_E$ making its effect on experimental test results negligible. As an example, product 3, which from Table 3.2 has a stiffness of 46.35 kNm/radian, was checked.

This was investigated for two extreme locations of displacement transducers with a constant value of $L_2 - L_1$=50mm. In theory, the range of L_1 was from 0mm to 150mm, and the lowest achievable value would have been about 35mm but for the protrusion of the fixing angle, figure 3.24.

However, assuming that L_1 = 0, the first extreme would be L_1 = 0 and L_2 = 50mm.

$$\frac{1}{k_T} = \frac{1}{46.35\times10^6} - \frac{50^2(3\times200-50)}{6\times205000\times838838\times200\times50}$$

i.e. k_T = 46.56 kNm/rad

This produced a correction of 0.6%

The second extreme was taken to be L_1 = 150mm and L_2 = 200mm

$$\frac{1}{k_T} = \frac{1}{46.35\times10^6} - \frac{200^2(3\times200-200)-150^2(3\times200-150)}{6\times205000\times838839\times200(200-150)}$$

i.e. k_T = 47.61 kNm/rad

This produced a correction of 2.7%

In the actual test arrangement the value of L_1 was 85mm giving a stiffness correction of about 2.2%. For a given beam end connector, the deeper the stub beam section, the smaller was the percentage correction. It was felt that this correction was not significant. The finite element work carried out later showed that the initial stiffness of a beam end connector however was sensitive to the position where measurement of deflection was taken.

3.7.2 Stub column rotation

The correction to the stiffness due to the rotation of the upright was appraised by using a short length of 50 x 50 x 5 mm angle section as a stub beam. The beam was welded to the face of a stub column to form a rigid connection. The welding position was at half the height of the stub column as shown in figures 3.64 and 3.65. The beam was then loaded in the same manner as that of a standard test. The data obtained was used to plot a moment rotation curve. Three tests of this type were carried out. The moment-rotation curves are shown in figure 3.66. The mean stiffness value k_W was 114.27 kNm/rad.

The mean rotations of the angle-section stub beam and box section stub beam, θ_B and θ_{BW} respectively were found by the method described above. The value of I for the angle section was taken to be 11cm^4. This was based on the assumption that the vertical guide provided full lateral and torsional restraint without sticking. Also, a loading point was prepared by drilling a countersink whose centre was 10mm from the square edge. The dimensions of the box section-stub beam were a_1 = 95mm, b_1 = 45mm and c_1 =1.5mm.

Appendix 3.2 shows a derivation of the following correction formula:

$$\frac{1}{k_T} = \frac{1}{k_E} - \frac{1}{k_B} - \frac{1}{k_W} + \frac{1}{k_{BW}}$$

Where:

k_T is the true stiffness(corrected)

k_E is the experimental stiffness

k_B is the box beam stiffness

k_W is the combined stiffness of stub column and angle stub beam section(rigid connection)

k_{BW} is the angle stub beam stiffness

Applying this formula to products 3, 4 and 5 produced the improved stiffness values given in Table 3.3. When these are compared to the original values it can be seen that the correction improves stiffness values by up to 44%.

It is to be noted that this correction requires a separate test of a stub column for every different gauge and shape of upright section. As the need for this correction was not determined early in the testing sequence it was only applied to the above products.

3.8 Conclusions

A beam end connector is subjected to a combined shear force and bending moment. Depending on the details of the design, the shear force and the exerted bending moment may result in locally distorting the beam end connector combined with overall bending of the end plate. Observations made during the course of each test revealed a distinct sequence of events in that for the first 0 to 40% of loading the

interaction between the tabs and the upright's web thickness was responsible for resisting any rotation, hence the start of local distortions. It was much later, approaching towards the ultimate loading stage that formation of a compression zone resulted as the lower part of the end plate came into contact with the upright's flange forming a hinge and resulting in bending of the end plate.

The moment-rotation characteristic of a joint however, is determined by not only the design of the beam end connector, but also the efficiency of the accompanying members, in particular the upright.

By examination of joint deformation modes, moment-rotation curves and the ultimate loads given in Table 3.2 the following conclusions about factors affecting efficient beam end connectors can be made:

(a) The number of tabs: Increasing the number of tabs will lead to increases in the stiffness and strength of the beam end connector. Tabs must be arranged so as to resist the loading that may be applied, either collectively or as separate sets.

(b) Detailed geometry of tabs: Stronger tabs incorporate more material in the regions where the load is concentrated, i.e. in the planes of contact with the upright. This applies to all the tab designs, whether they are integral parts of the beam end connector or independent from it.

(c) Design of bracket: The design of the bracket and the tabs must be carried out interactively. A tab design, which fails with its bracket relatively intact, may be too weak and vice-versa.

(d) The gauge of beam end connector and the upright: increasing gauges of beam end connector and upright improve both stiffness and strength of the joint.

(e) The profile of the upright: Changing the profile of the upright to increase its stiffness increases the stiffness of the beam end connector.

(f) The number of contact planes between the beam end connector and upright: Increasing the number of contact planes increases the stiffness of the beam end connector.

The theoretical work established the influence of the flexibility of the upright on the experimental stiffness values.

The use of the brittle lacquer was a qualitative assessment, which enabled identification of the critical regions. The stress distribution established in such a way was later confirmed theoretically by using Finite Element techniques.

Table 3.1 Dimensional and Welding Details of Tested Products

Product Number	Product Class	Beam Dimensions (mm) a1	b1	c1	BEC Dimensions (mm) a	b	c	d	e	Welding Position	Type of weld	Upright length (mm)	Upright gauge (mm)
1 LINK	A	106	50.6	1.85	220	59.5	46.0	4.0	0.0	Down welded f=80mm	Continuous 4 or 5mm fillet, front, rear and top faces	360	1.74
2 DEX	A	79.0	50.0	1.85	225	63.5	49.0	3.57	0.0	Up welded f=8mm	Continuos 3 or 4mm fillet on all faces	360	2.30
3 PSS3	A	95	45	1.5	198	54	39	3.1	0.0	Up welded f=9mm	Continuous 5mm fillet on front face; 25mm stitches top and bottom of rear face	360	1.9
4 PSS3	A	95	45	1.5	198	54	39	3.1	0.0	Down welded f=46.5mm	Continuous 5mm fillet on front face; 25mm stitches top and bottom of rear face	360	1.91
5 PSS3	A	95	45	1.5	198	54	39	3.1	0.0	Symmetrical	Continuous 5mm fillet on front face; 25mm stitches top and bottom of rear face	360	1.91
6 PSS4	A	120	45	1.8	273	77	39.5	3.1	0.0	Up welded f=9mm	Continuous 5mm fillet on front face; 25mm stitches top and bottom of rear face	360	1.8
7 PSS4	A	120	45	1.8	273	77	39.5	3.1	0.0	Down welded f=46.5mm	Continuous 5mm fillet on front face; 25mm stitches top and bottom of rear face	360	1.8
8 PSS4	A	120	45	1.8	273	77	39.5	3.1	0.0	Symmetrical	Continuous 5mm fillet on front face; 25mm stitches top and bottom of rear face	360	1.8
9 APEX	B	101.5	52.5	2.1	200	65.5	40	3.4	0.0	Down welded f=72mm	Continuous 3 or 4mm fillet at front face, top and bottom flanges	360	2.65
10 FINSP	B	103.6	51	1.9	170	74	40.5	4.2	3.5	Down welded f=40mm	Continuous 3 or 4mm fillet at front face, top and bottom flanges	360	2.65
11 POLY	C	119	50.5	1.55	200	56.8	43	4.1	0.0	Up welded f=8mm	Continuous 3 or 4mm fillet on front and rear faces	280	2.15
12 PSS 8- STUDS	C	95	45	1.5	198	55.4	45	4.0	0.0	Symmetrical	Continuous 5mm fillet on front face; 25mm stitches top and bottom of rear face	300	2.7

Note: the dimensions given to be read in conjunction with figure 3.20

Table 3.1 Continued

13 PSS L-STUDS	C	95	45	1.5	198	55.4	45.8	4.0	0.0	Symmetrical	Continuous 5mm fillet on front face; 25mm stitches top and bottom of rear face	300	2.7
	D	NOT AVAILABLE FOR TESTING											
14 REDI	A/B	104	51.5	1.93	215	55	45	3.1	27	Up welded f=0mm	Continuous 3 or 4mm fillet at front and rear faces	355	2.56
15	A	95	45	1.5	198	54	39	4.0	0.0	Up welded f=9mm	Continuous 5mm fillet on front face; 25mm stitches top and bottom of rear face	360	1.8
16	A	95	45	1.5	198	54	39	4.0	0.0	Down welded f=46.5mm	Continuous 5mm fillet on front face; 25mm stitches top and bottom of rear face	360	1.8
17	A	95	45	1.5	198	54	39	4.0	0.0	Up welded f=9mm	Continuous 5mm fillet on front face; 25mm stitches top and bottom of rear face	360	2.3
18	A	95	45	1.5	198	54	39	4.0	0.0	Down welded f=46.5mm	Continuous 5mm fillet on front face; 25mm stitches top and bottom of rear face	360	2.3
19	A	105	45	1.5	198	54	39	4.0	0.0	Up welded f=9mm	Continuous 5mm fillet on front face; 25mm stitches top and bottom of rear face	360	1.8
20	A	105	45	1.5	198	54	39	4.0	0.0	Down welded f=46.5mm	Continuous 5mm fillet on front face; 25mm stitches top and bottom of rear face	360	1.8
21	A	105	45	1.5	198	54	39	4.0	0.0	Up welded f=9mm	Continuous 5mm fillet on front face; 25mm stitches top and bottom of rear face	360	2.3
22	A	105	45	1.5	198	54	39	4.0	0.0	Down welded f=46.5mm	Continuous 5mm fillet on front face; 25mm stitches top and bottom of rear face	360	2.3

Note: the dimensions given to be read in conjunction with figure 3.20

Table 3.2 Beam End Connector Test Results

Product number	Product class	Strength (kNm)	Average (kNm)	Stiffness (kNm/rad)	Average (kNm/rad)	Manufacturer
1	A	2.235	2.171	61.139	67.746	LINK 51
		2.090		71.020		
		2.190		71.08		
2	A	1.811	1.778	73.18	68.193	DEXION
		1.924		72.50		
		1.599		58.90		
3	A	1.500	1.485	48.300	46.35	PSS 3 LUG UP WELDED
		1.485		44.310		
		1.471		46.440		
4	A	2.23	2.16	54.88	49.80	PSS 3 LUG DWN WELDED
		2.09		44.72		
		Unusable Moment-Rotation curve due to transducer fluctuation				
5	A	2.363	2.177	61.139	51.94	PSS 3 LUG SYMMETRICAL
		2.108		42.74		
		2.06		127.1		
6	A	2.037	2.004	112.32	108.63	PSS 4 LUG UP WELDED
		1.980		115.00		
		1.995		98.58		
7	A	2.617	2.574	136.05	143.48	PSS 4 LUG DWN WELDED
		2.589		136.05		
		2.518		158.36		
8	A	3.054	2.964	150.26	146.89	PSS 4 LUG SYMMETRICAL
		3.000		163.33		
		2.84		158.36		
9	B	2.320	2.328	64.400	51.56	APEX
		2.405		44.720		
		2.260		45.560		
10	B	3.815	3.971	71.920	74.88	FINSPA
		4.050		88.170		
		4.050		64.560		
11	C	2.470	2.558	115.00	98.48	POLYPAL
		2.560		105.00		
		2.646		75.46		
12	C	2.957		76.66		PSS 6MM-STUDS
13	C	2.759		127.10		PSS 10MM-STUDS
	D	Not available for testing				
14	Composite design A/B	2.632	2.399	64.40	66.65	REDIRACK
		2.377		58.90		
		2.190		76.66		

Table 3.2 continued

15	A	1.573 1.658 1.592	1.607	73.60 95.40 70.57	72.082	MODIFIED 95BM1.8UP UP WELDED
16	A	2.190 2.155 2.220	2.188	80.10 76.75 73.00	76.617	MODIFIED 95BM1.8UP DWN WELDED
17	A	1.848 1.763 1.734	1.781	89.44 97.05 84.45	90.318	MODIFIED 95BM2.3UP UP WELDED
18	A	2.482 2.516 2.575	2.524	89.44 114.59 92.53	98.852	MODIFIED 95BM2.3UP DWN WELDED
19	A	1.537 1.620 1.620	1.592	73.06 80.50 65.71	73.094	MODIFIED 105B1.8UP UP WELDED
20	A	2.270 2.240 2.239	2.249	89.92 83.23 95.28	89.477	MODIFIED 105B1.8UP DWN WELDED
21	A	1.984 1.910 1.926	1.940	95.68 99.38 100.62	98.563	MODIFIED 105B2.3UP UP WELDED
22	A	2.575 2.701 2.617	2.631	105.00 96.60 113.38	104.993	MODIFIED 105B2.3UP DWN WELDED

Table 3.3 Beam End Connector Test Results With Corrected Stiffness Values

Product number	Product class	Strength (kNm)	Average (kNm)	Stiffness (kNm/rad)	Average (kNm/rad)	Corrected Stiffness (kNm/rad)	Average (kNm/rad)
3	A	1.500	1.485	48.300	46.35	66.26	62.68
		1.485		44.310		58.98	
		1.471		46.440		62.81	
4	A	2.23	2.16	54.88	49.80	79.31	69.51
		2.09		44.72		59.71	
		Unusable Moment-Rotation curve due to transducer fluctuation					
5	A	2.363	2.177	61.139	51.94	93.09	74.66
		2.108		42.74		56.23	
		2.06		127.1			

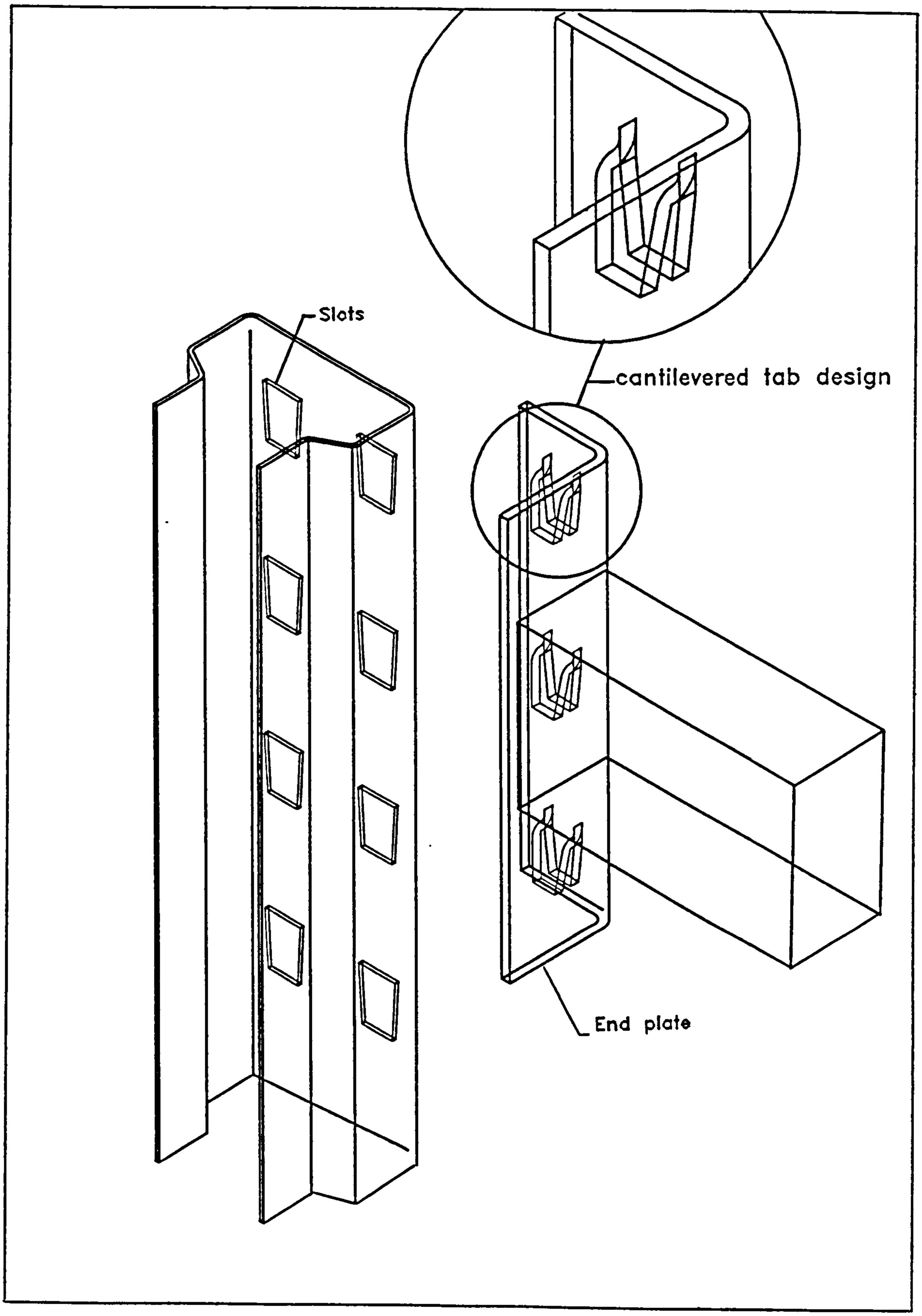

FIGURE 3.1 TYPICAL BEAM END CONNECTOR AND ACCOMPANYING PERFORATED UPRIGHT

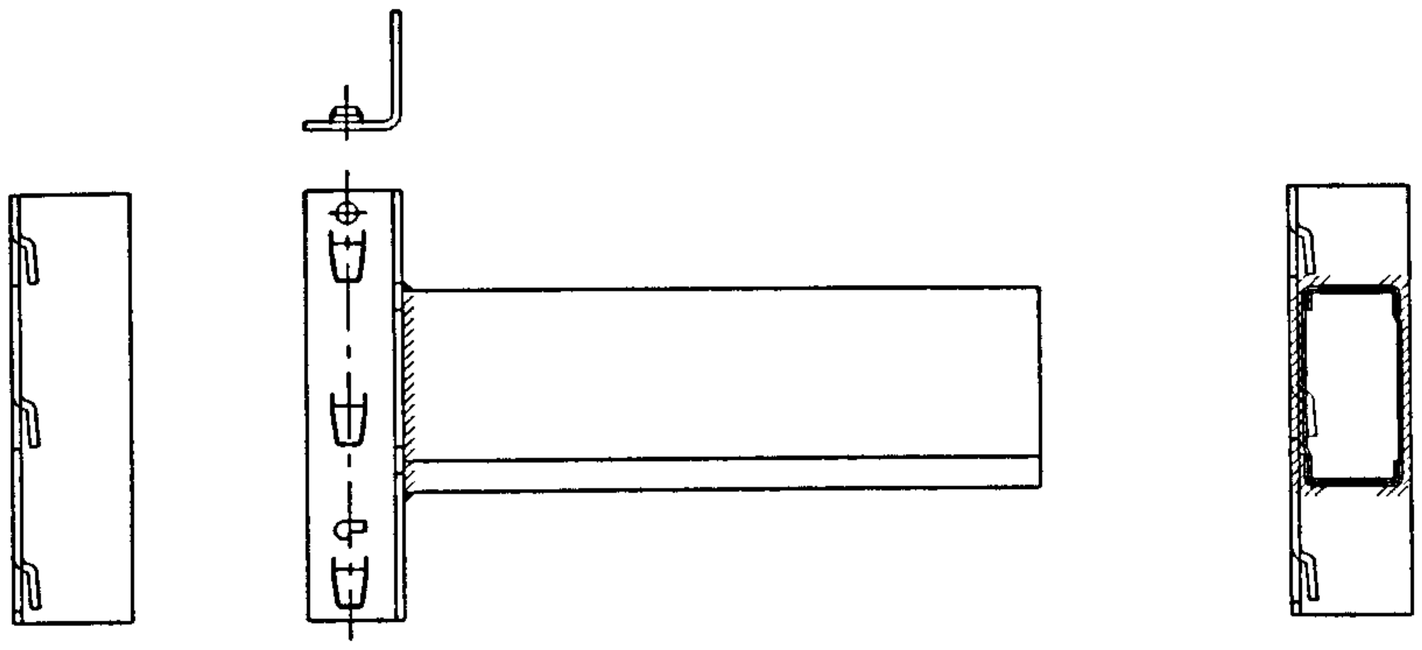

SYMMETRICAL
(a)

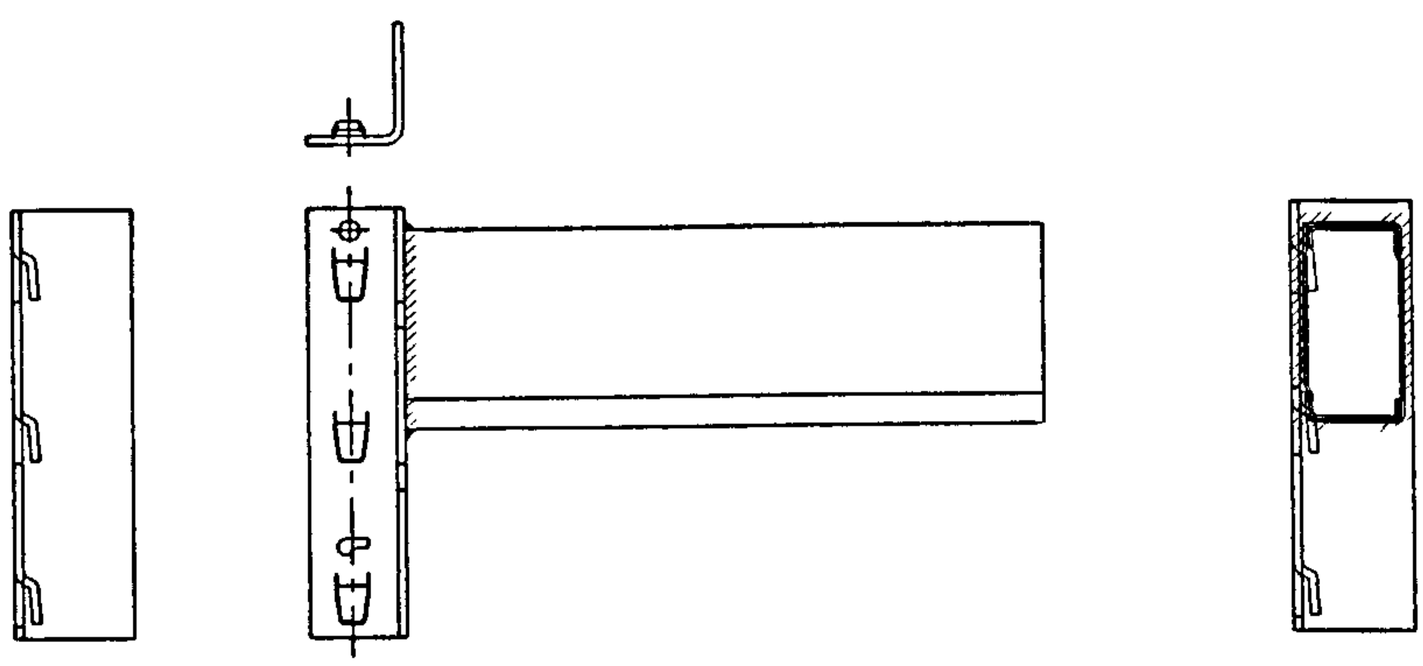

UP-WELD
(b)

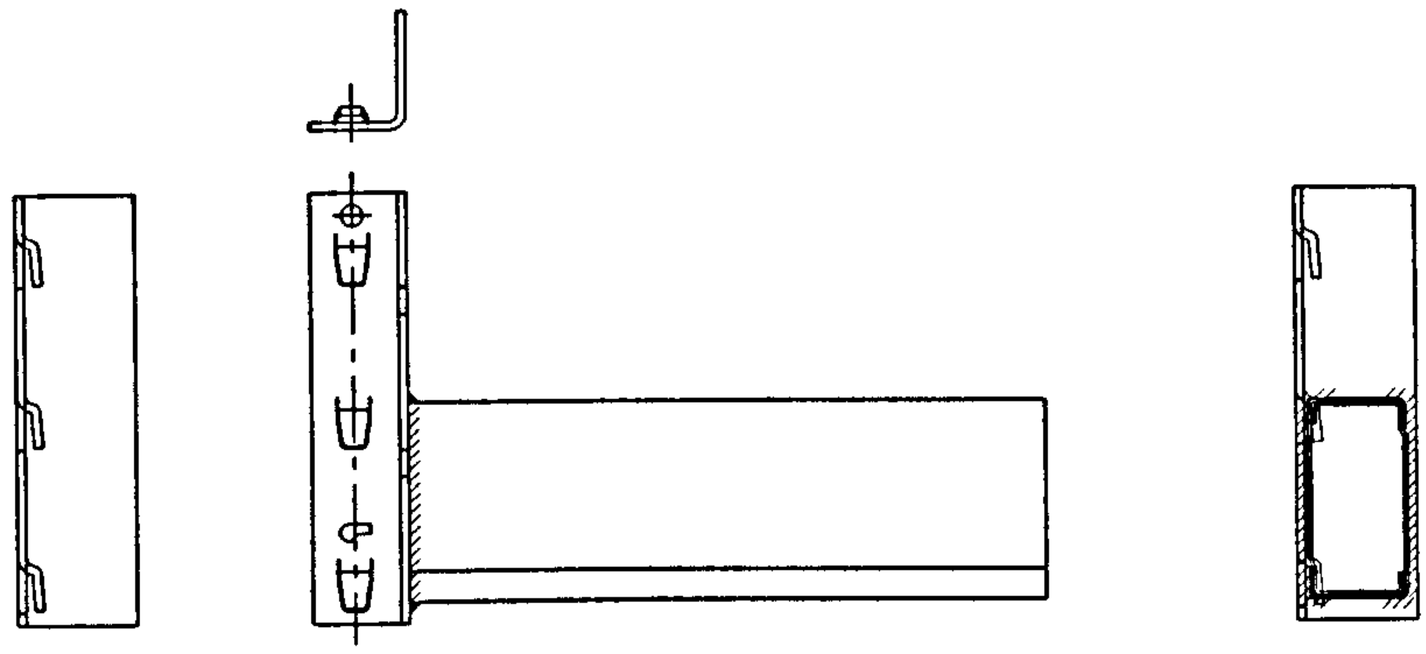

DOWN-WELD
(c)

FIGURE 3.2 THREE WELDING POSITIONS OF BEAM TO BEAM END CONNECTOR

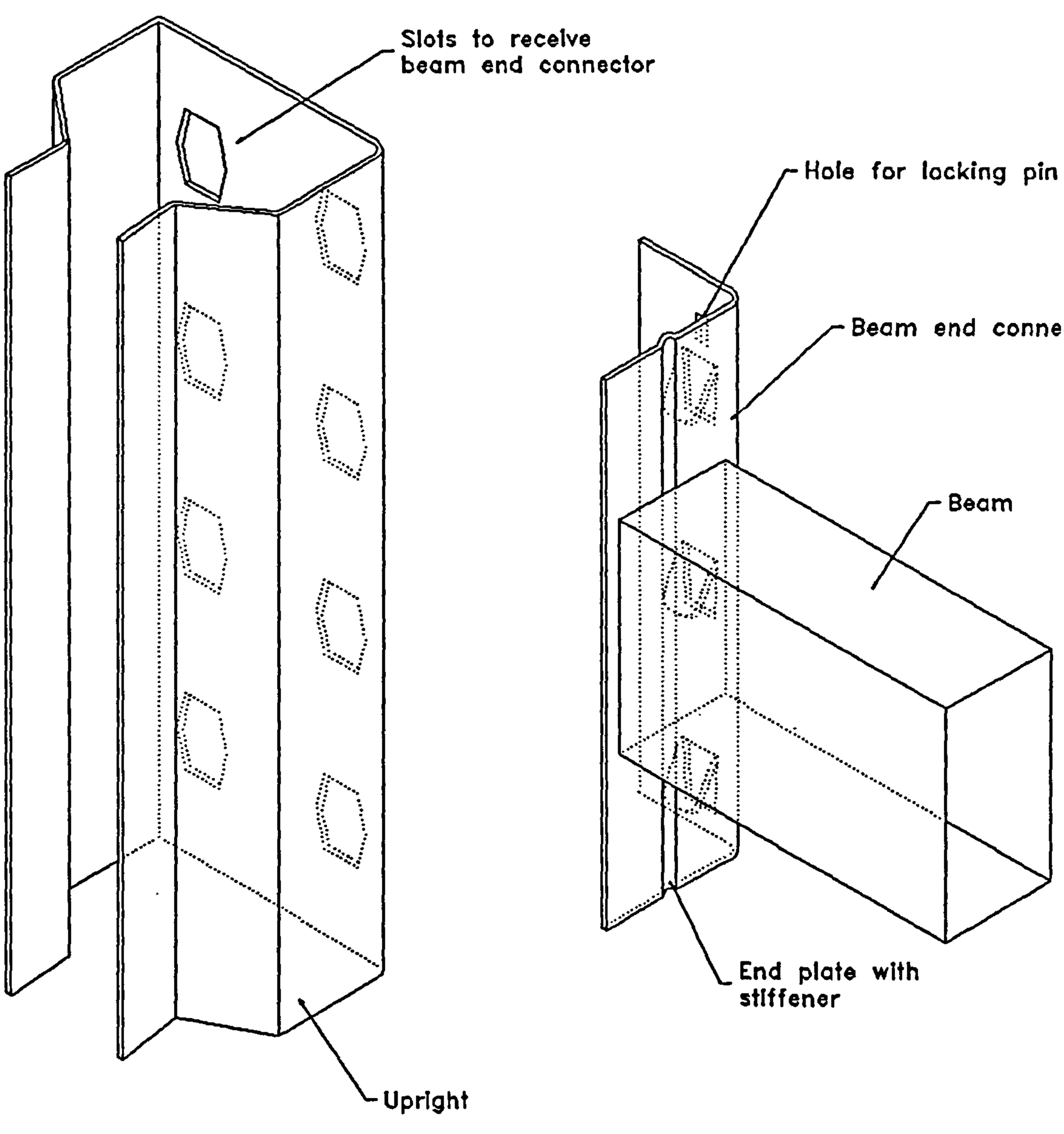

FIGURE 3.3 "Tongue and slot design"

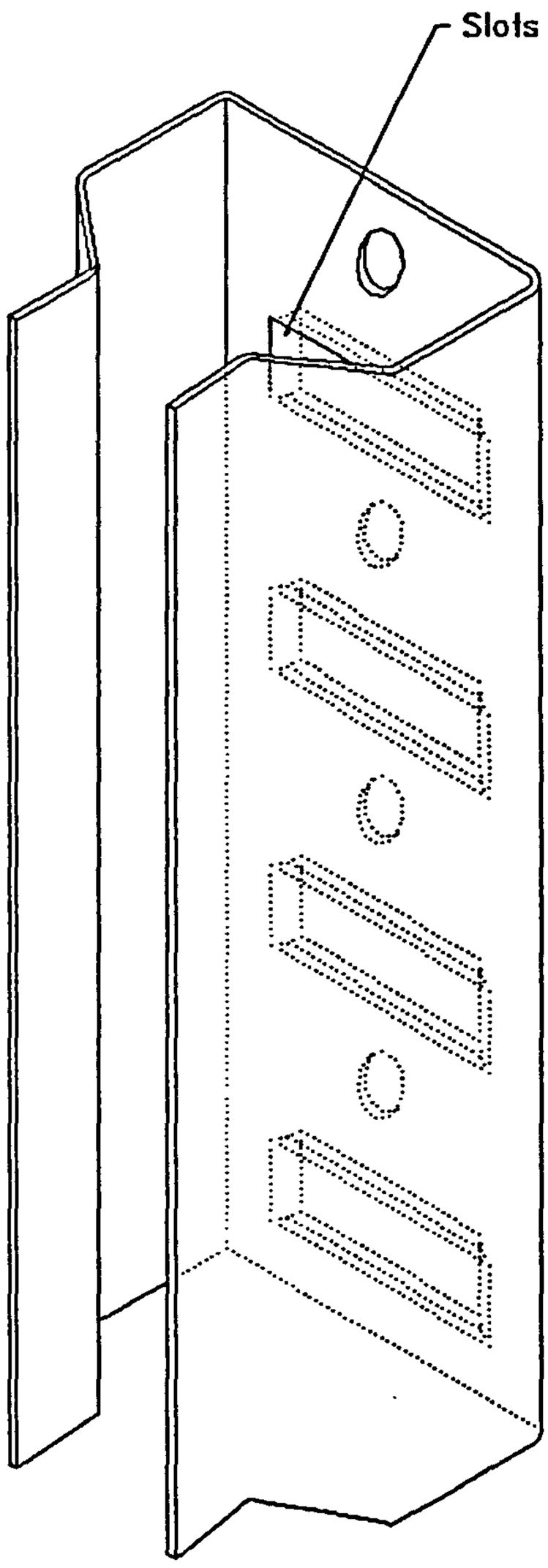

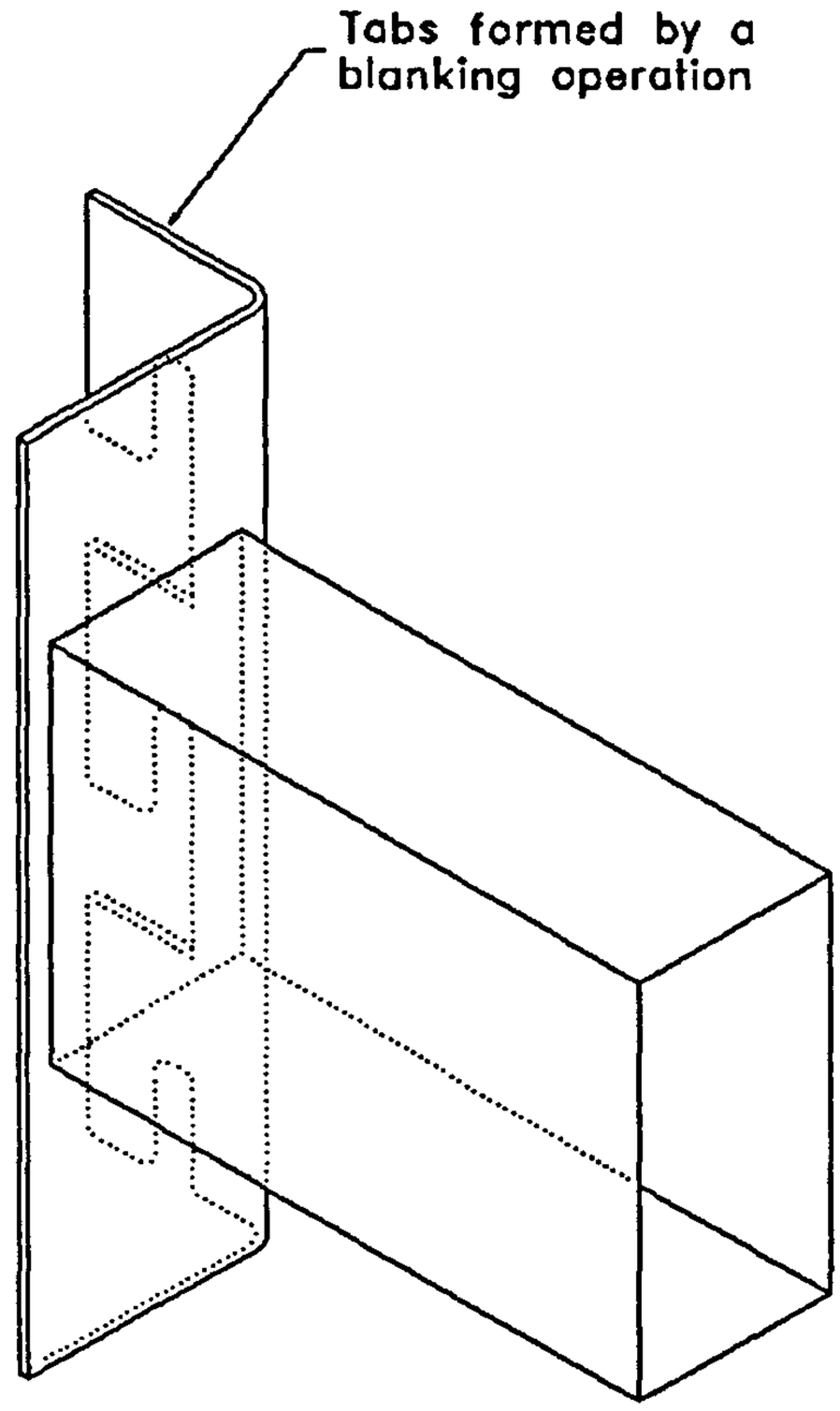

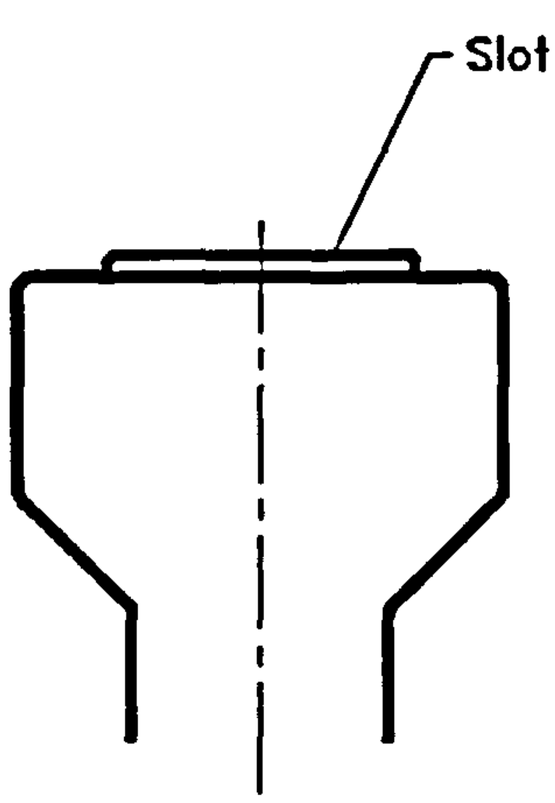

FIGURE 3.4 " Blanking design"

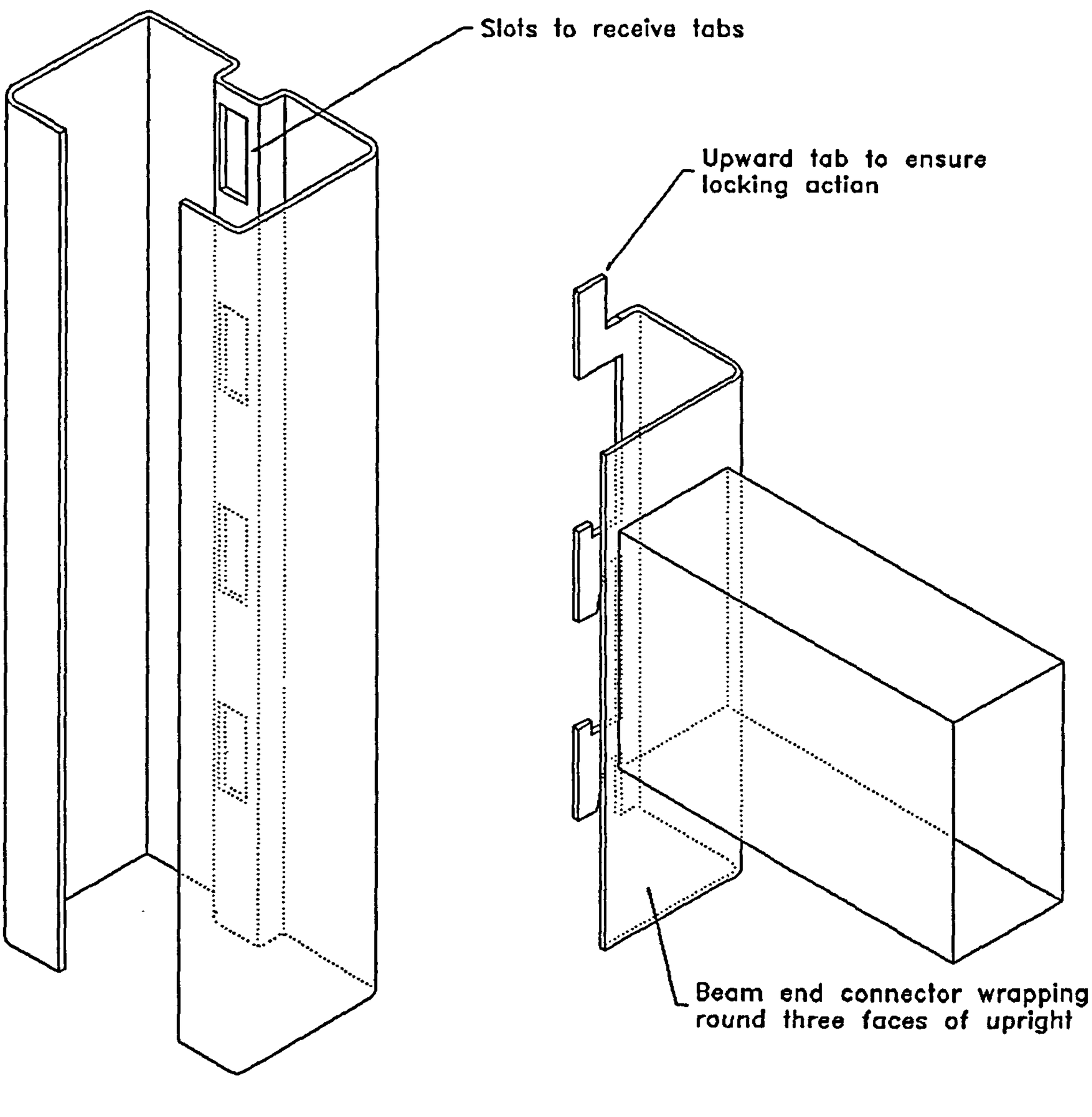

FIGURE 3.5 " Wrapped around blanking design"

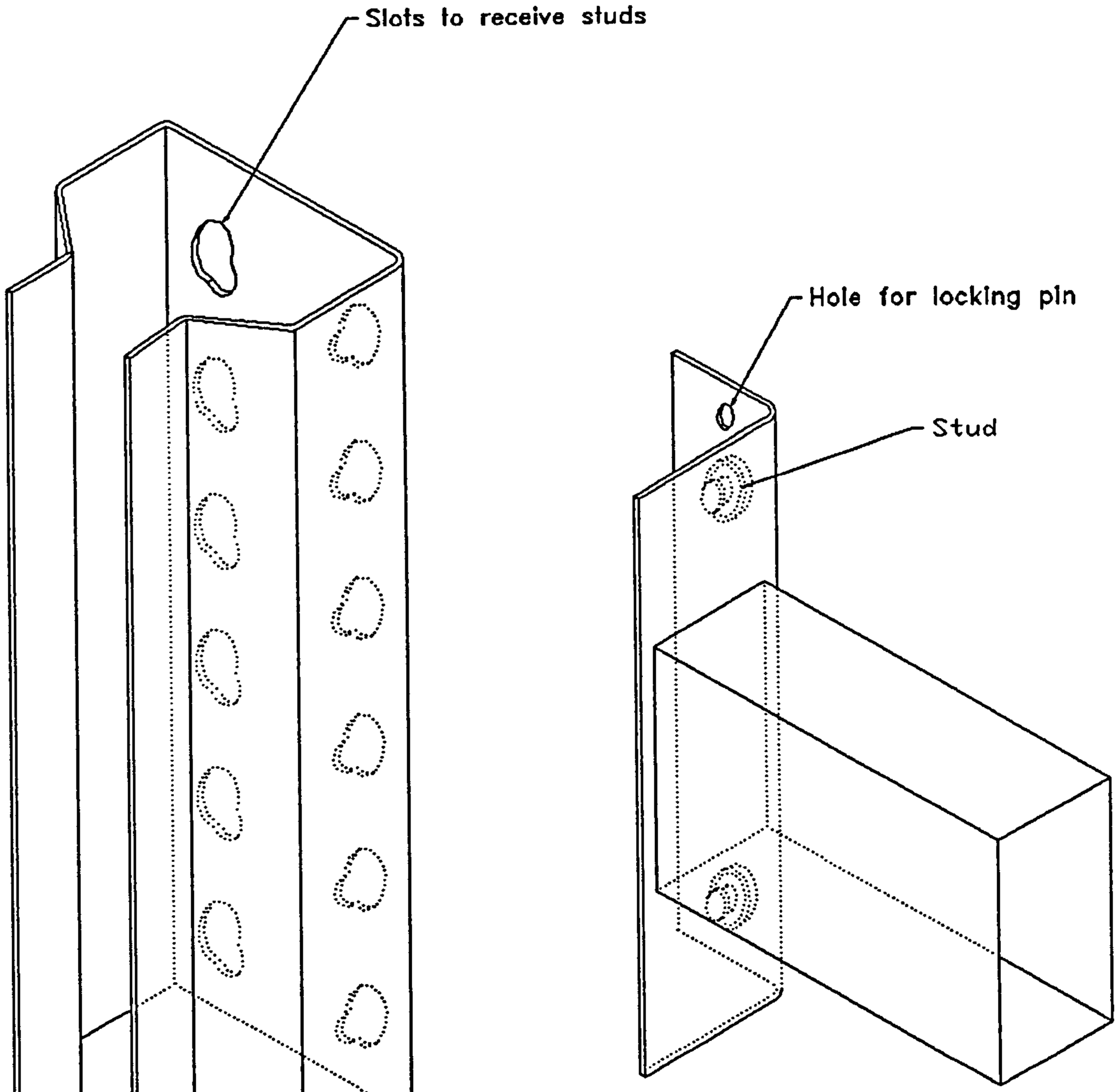

FIGURE 3.6 "Stud incorporated design"

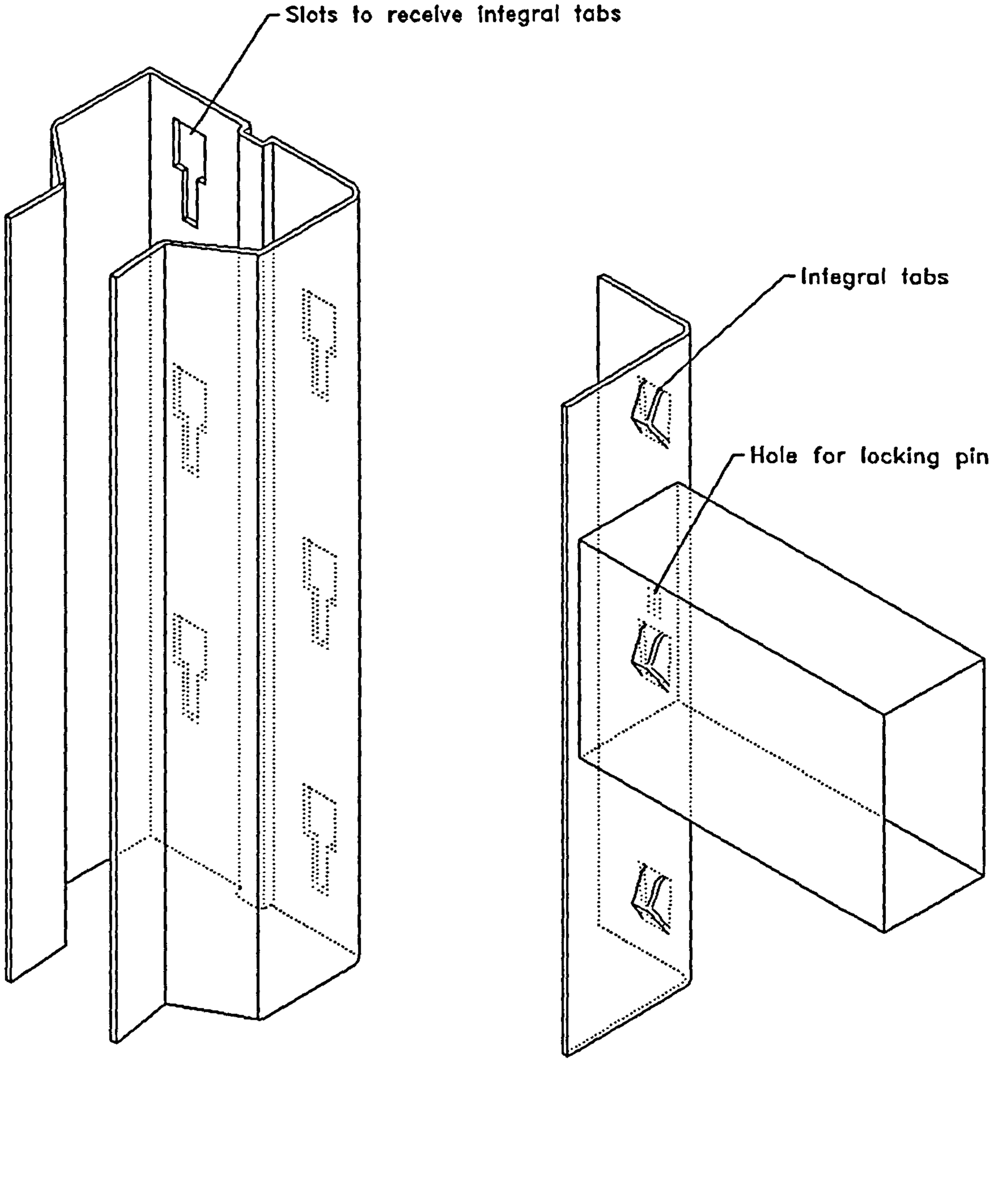

FIGURE 3.7 "Integral non-cantilevered tab design"

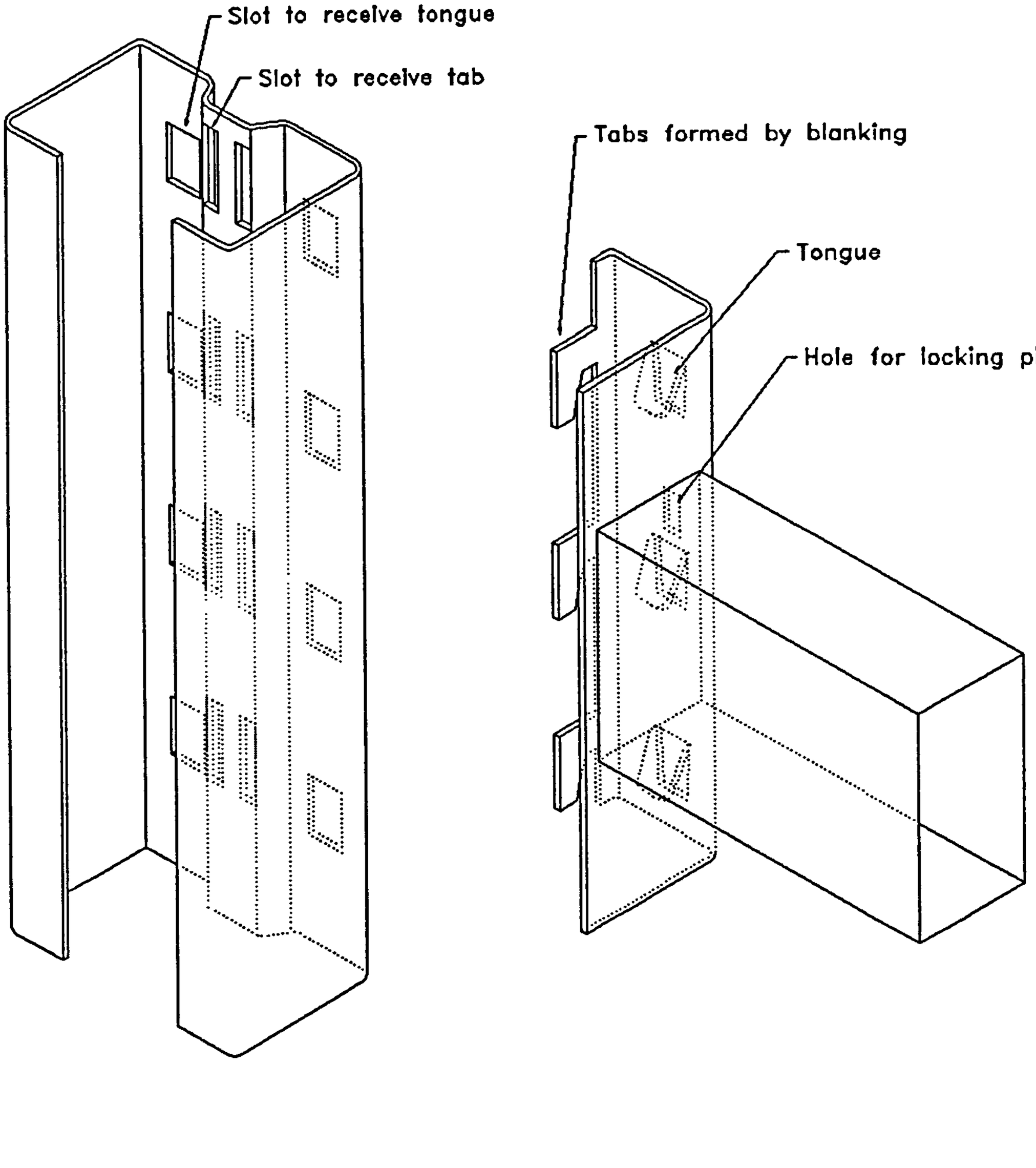

FIGURE 3.8 "Composite class A and class B design"

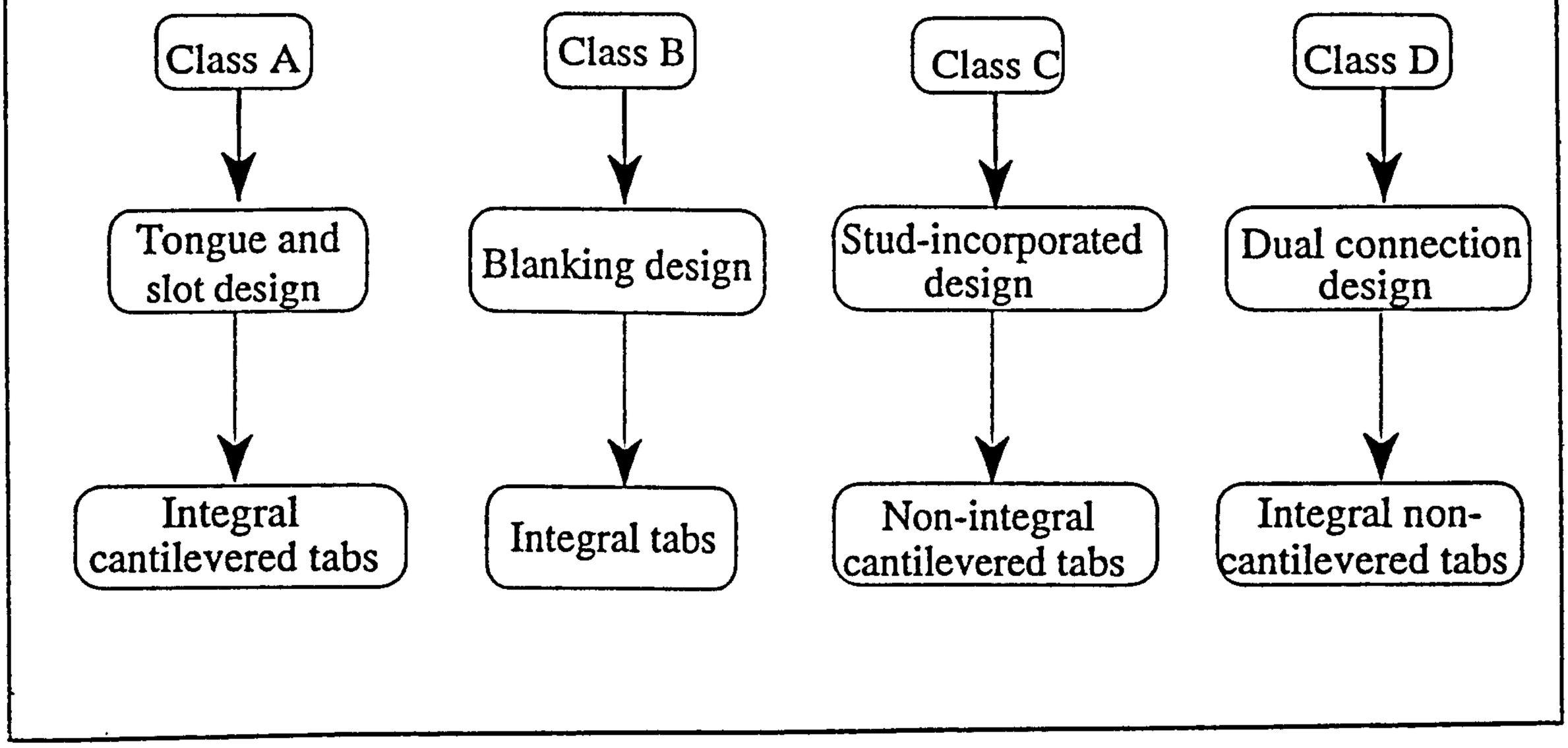

Figure 3.9 General classification of beam end connectors available on the market

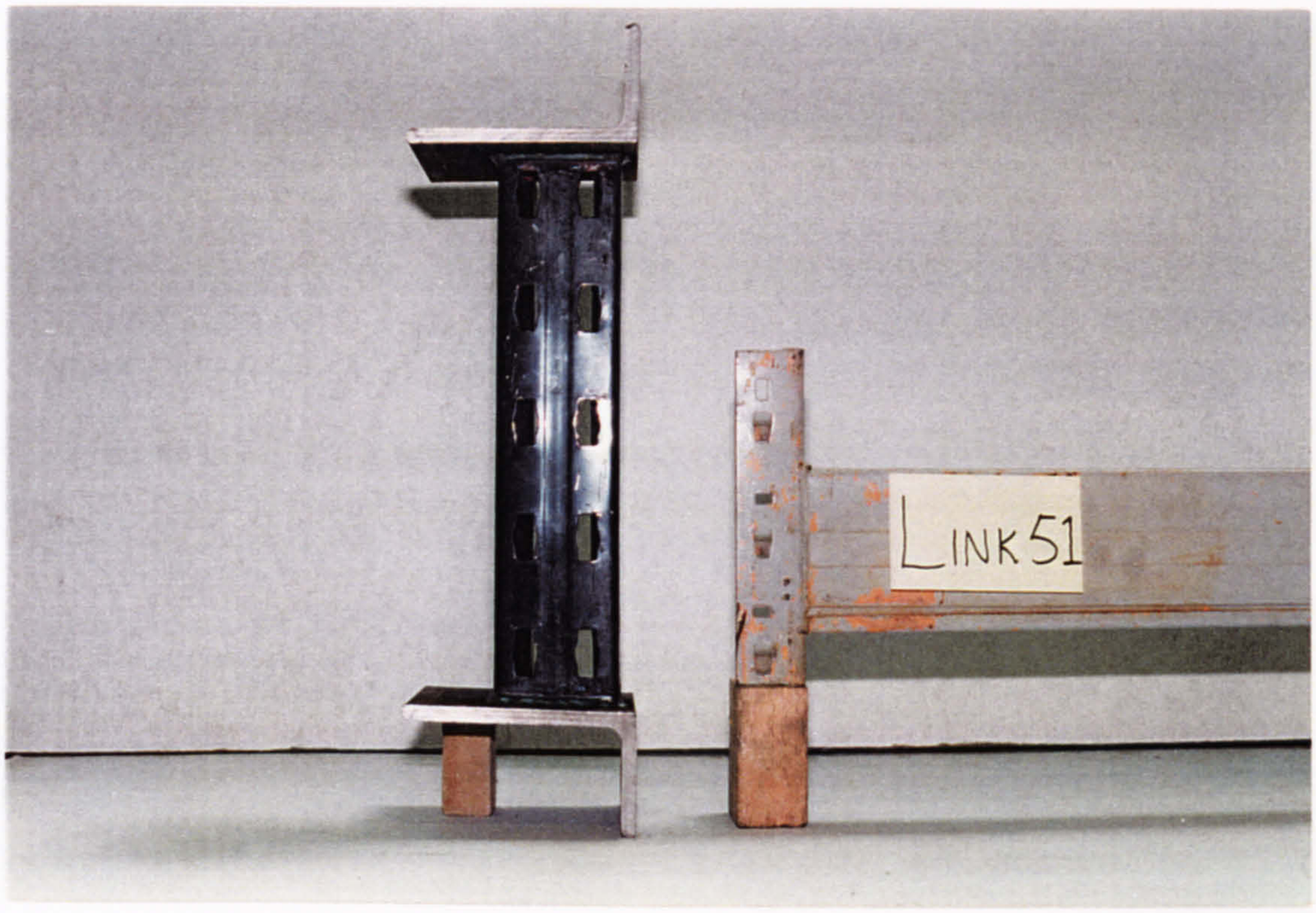

FIGURE 3.10 Product 1

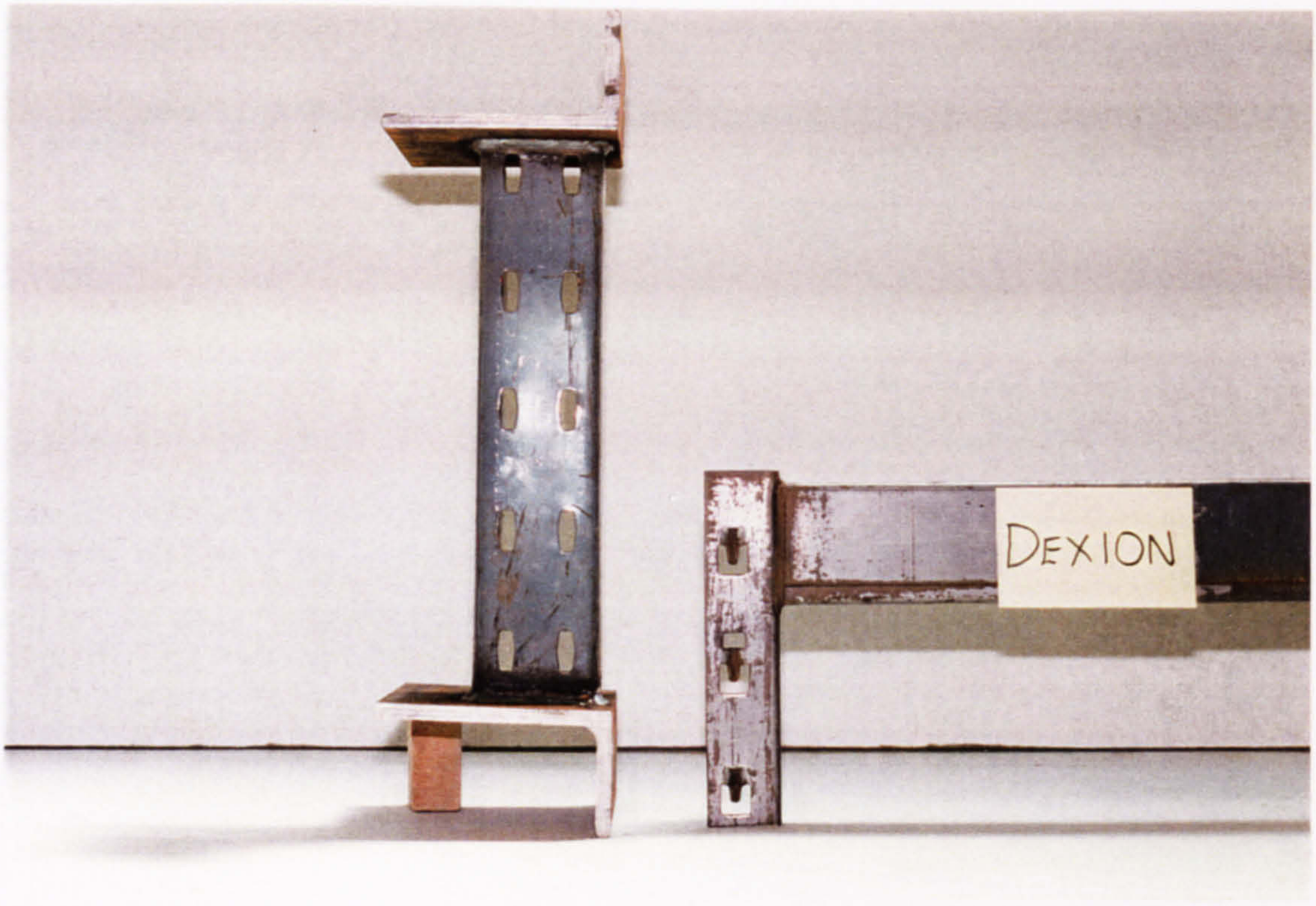

FIGURE 3.11 Product 2

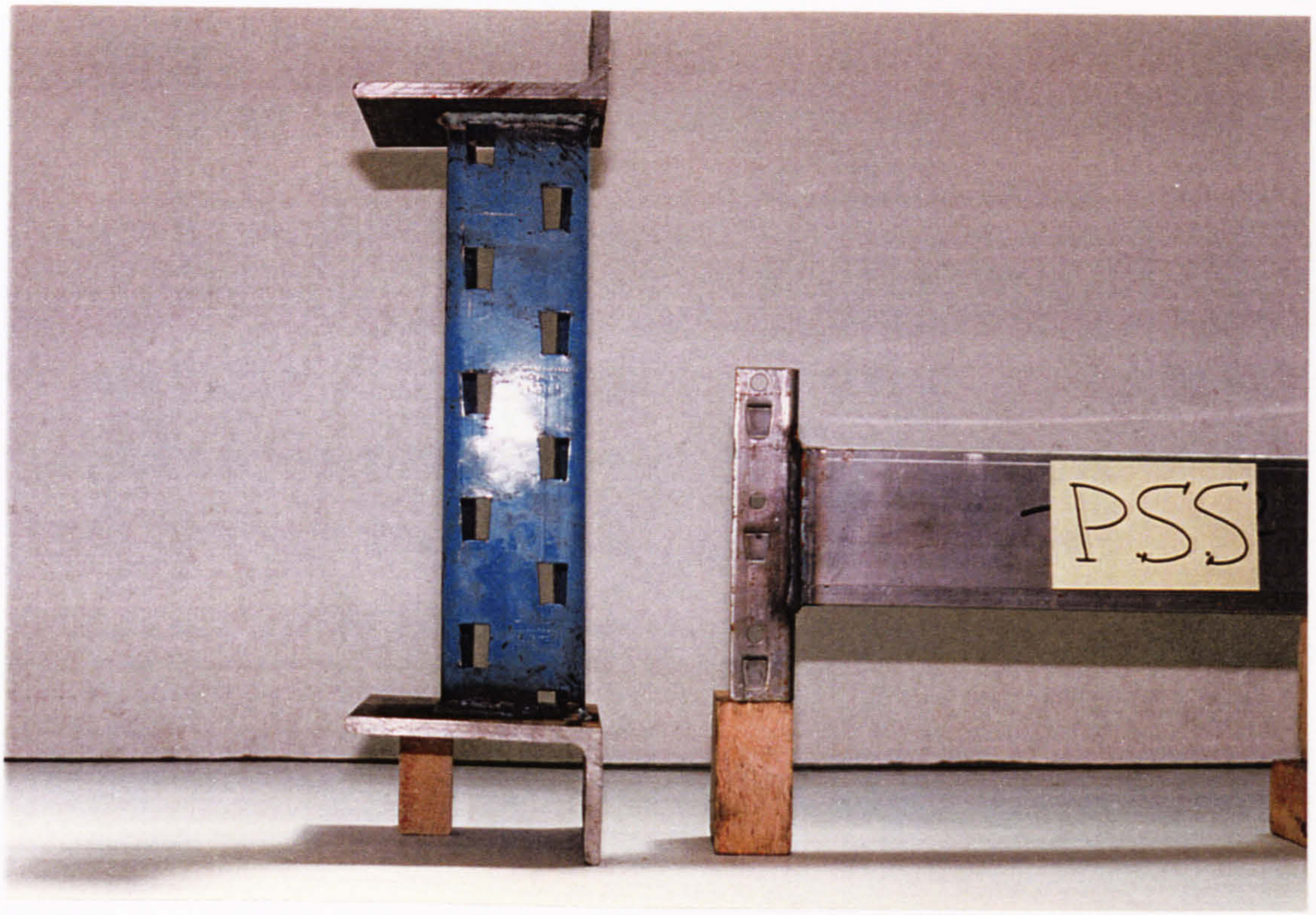

FIGURE 3.12 Product 4

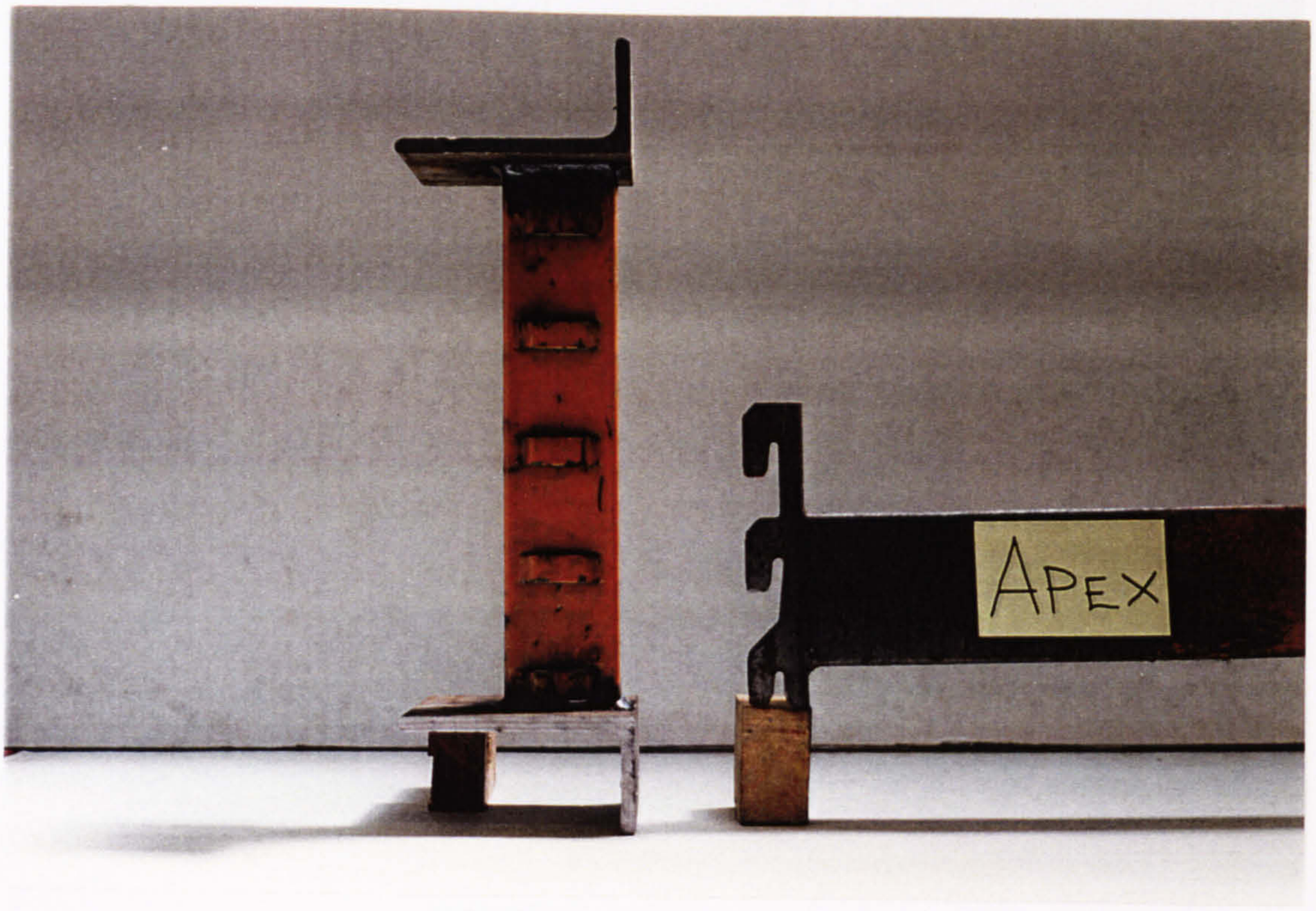

FIGURE 3.13 Product 9

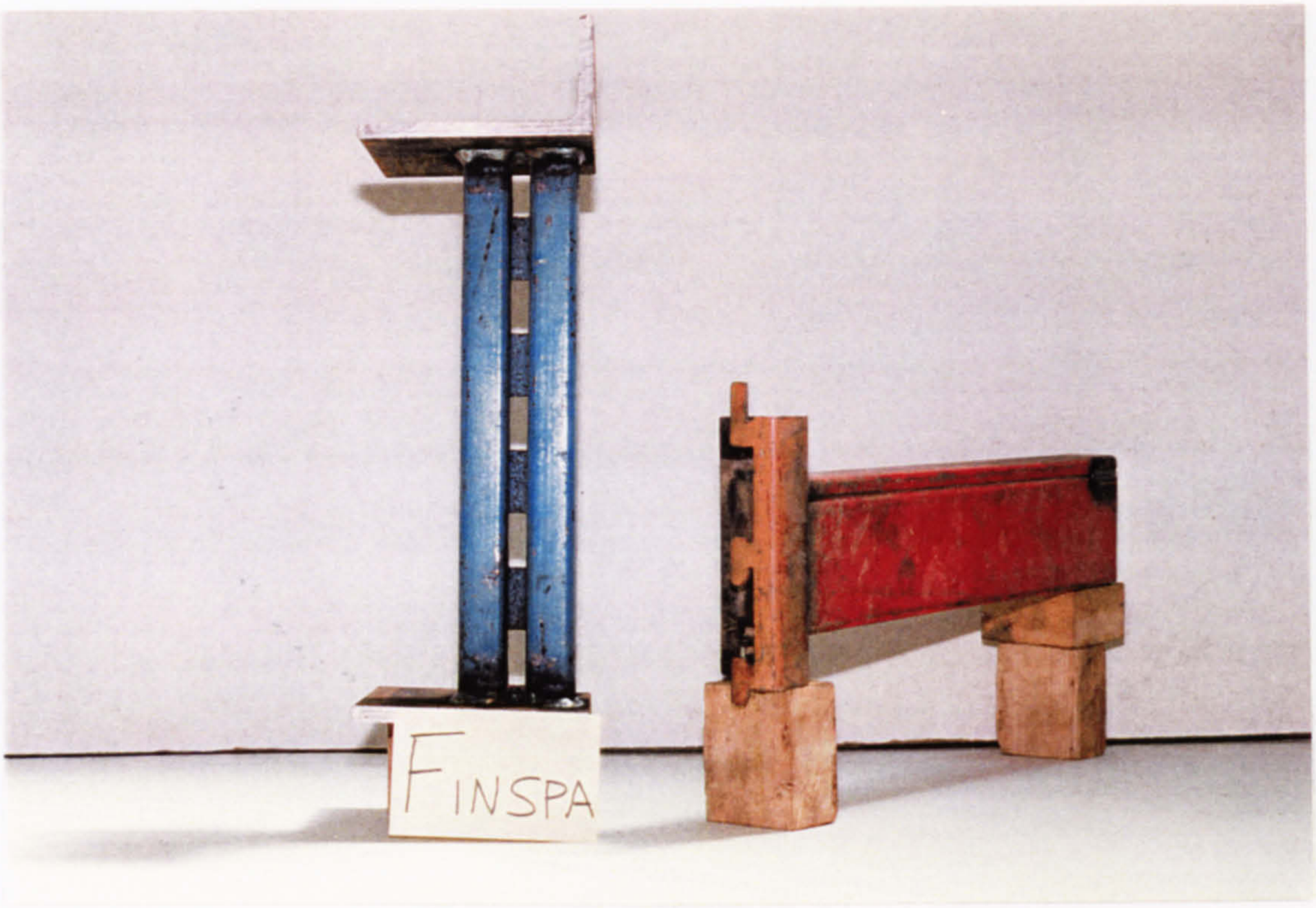

FIGURE 3.14 Product 10

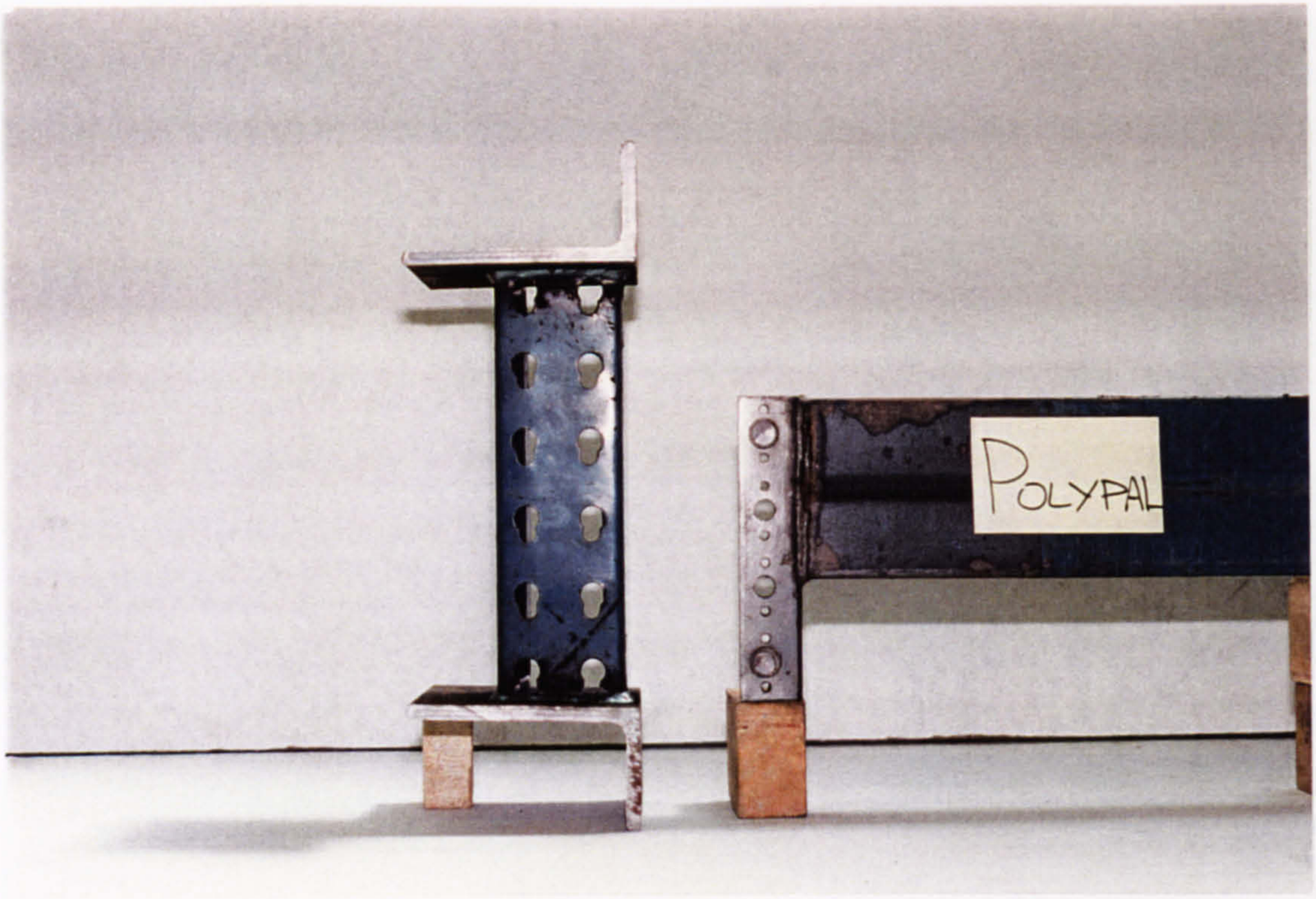

FIGURE 3.15 Product 11

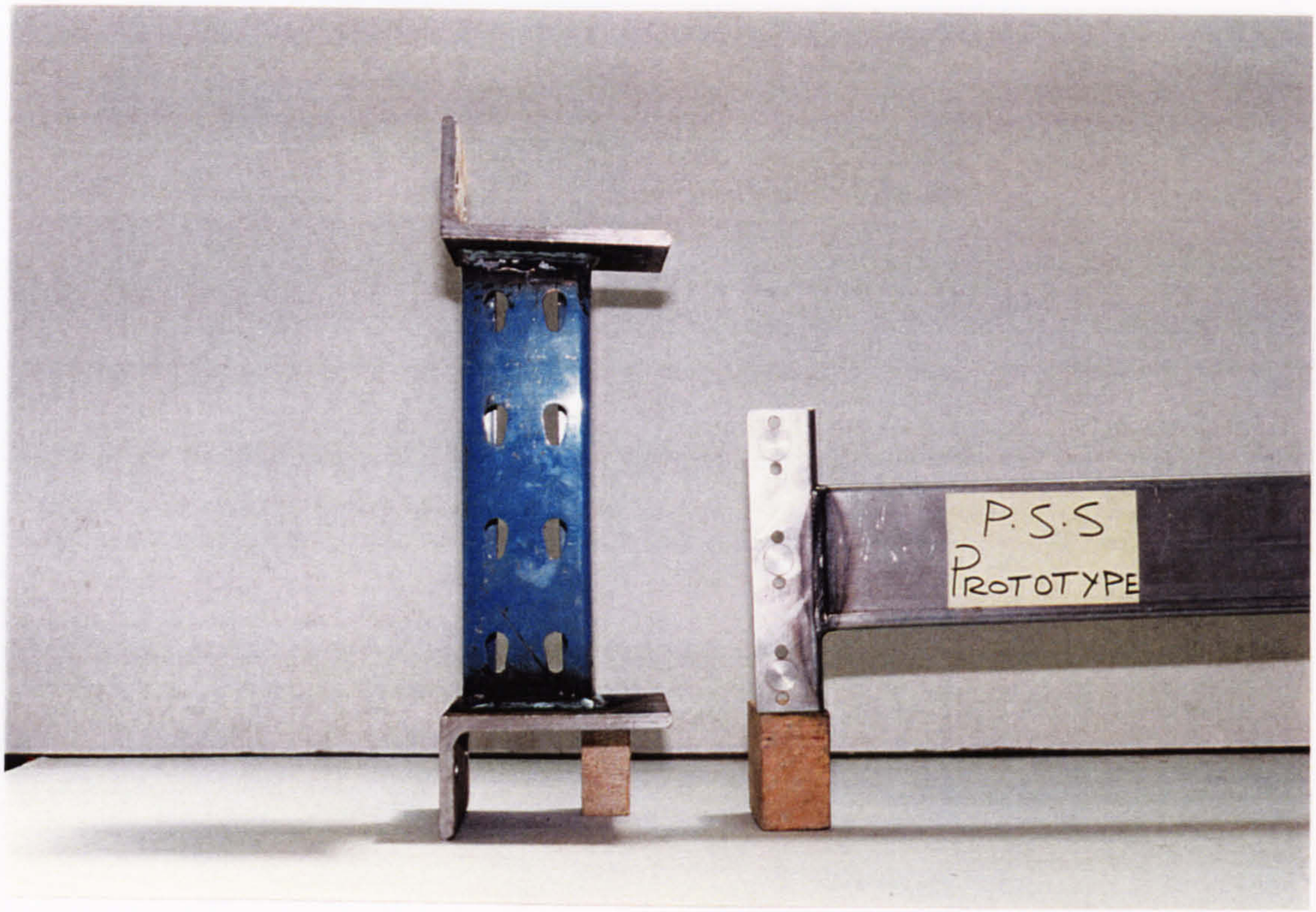

FIGURE 3.16 Product 12

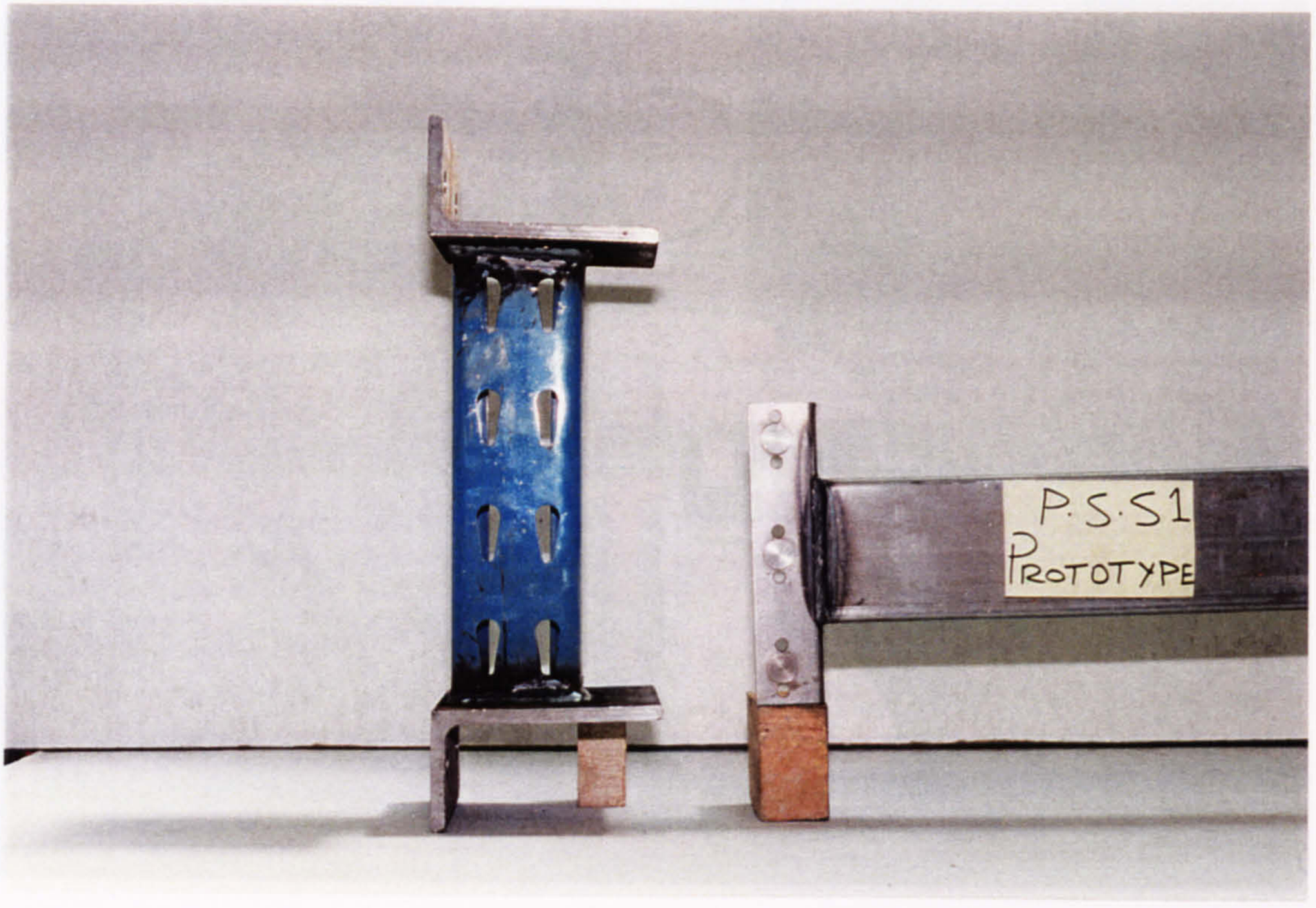

FIGURE 3.17 Product 13

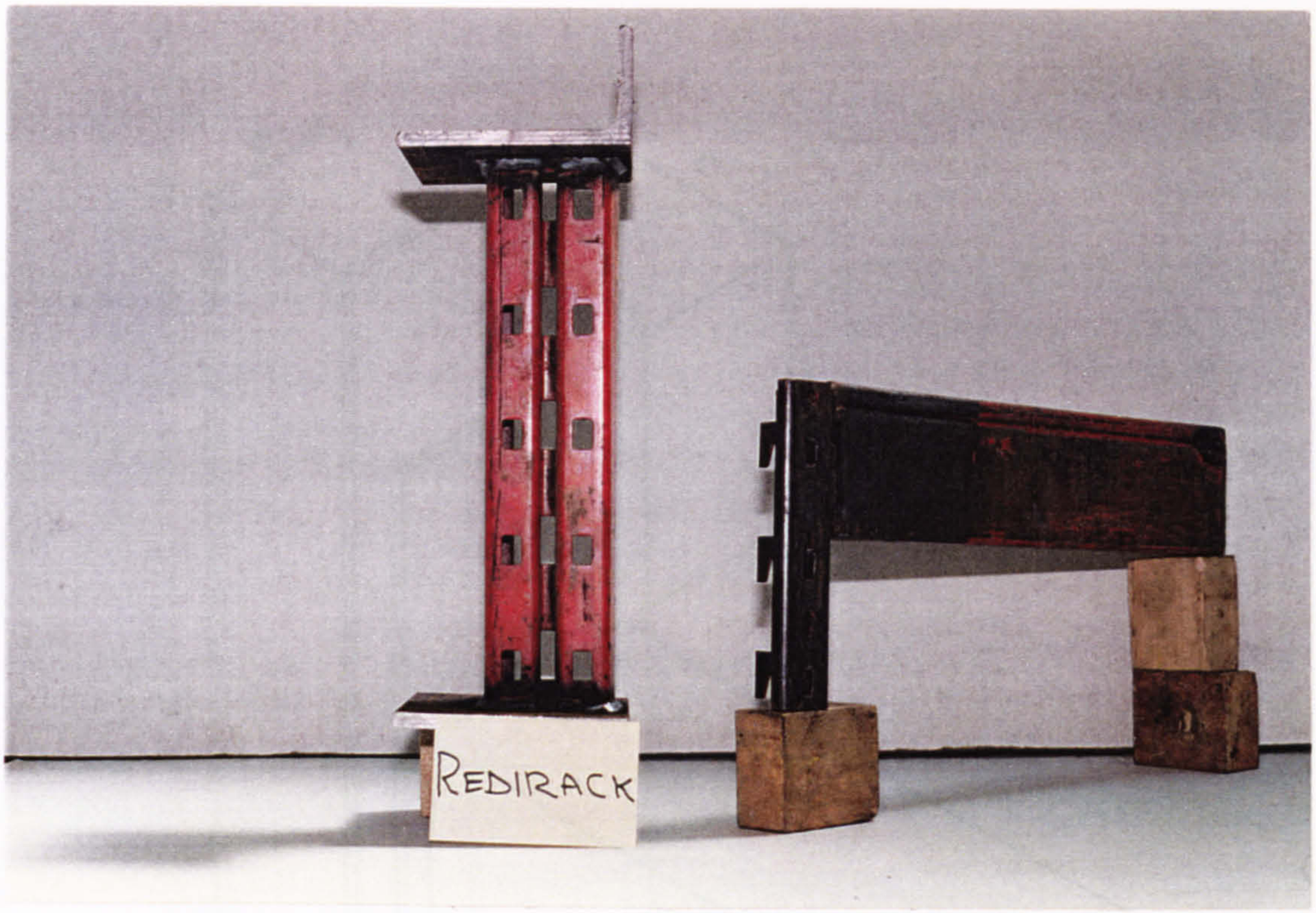

FIGURE 3.18 Product 14

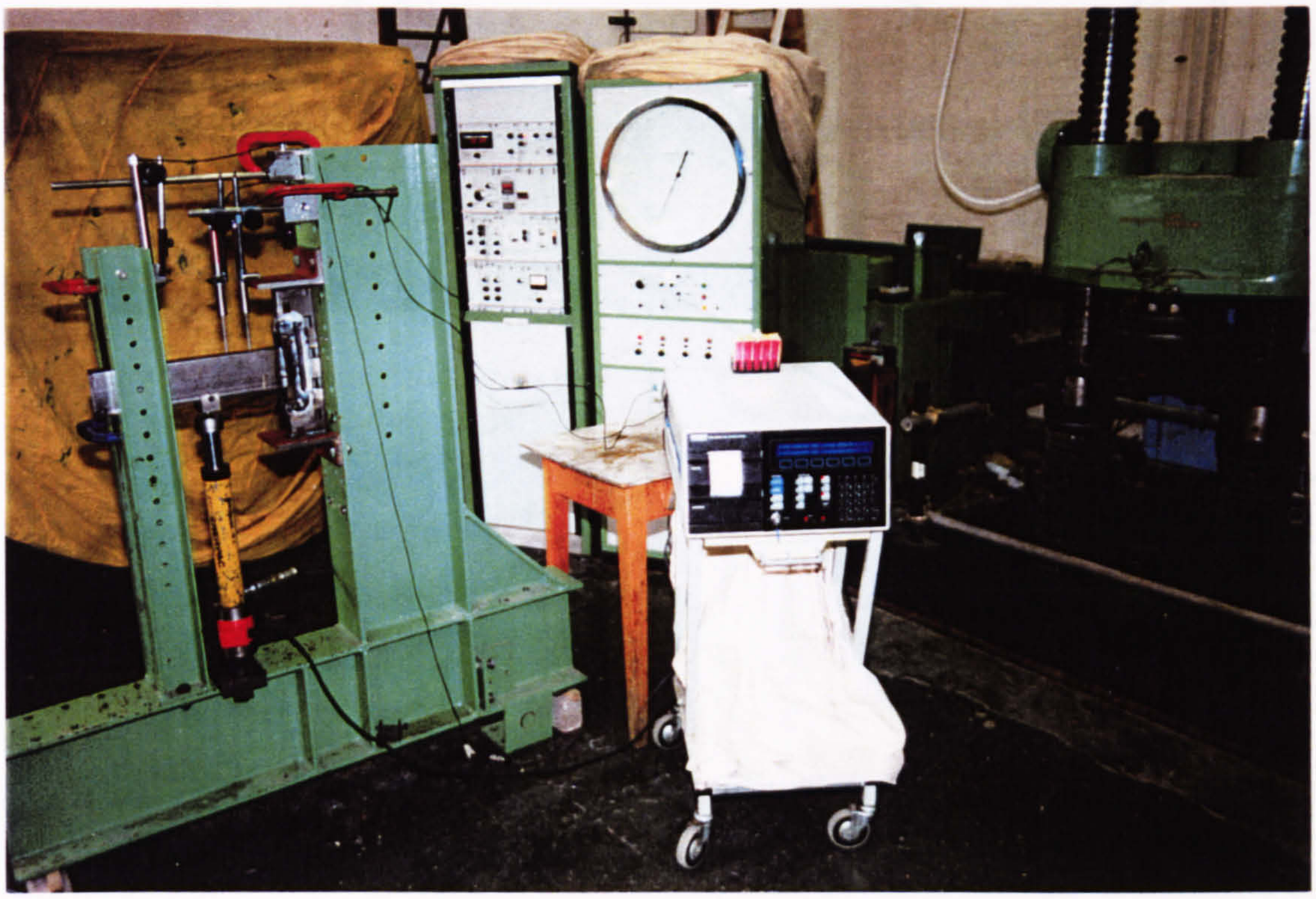

FIGURE 3.19 Test set up

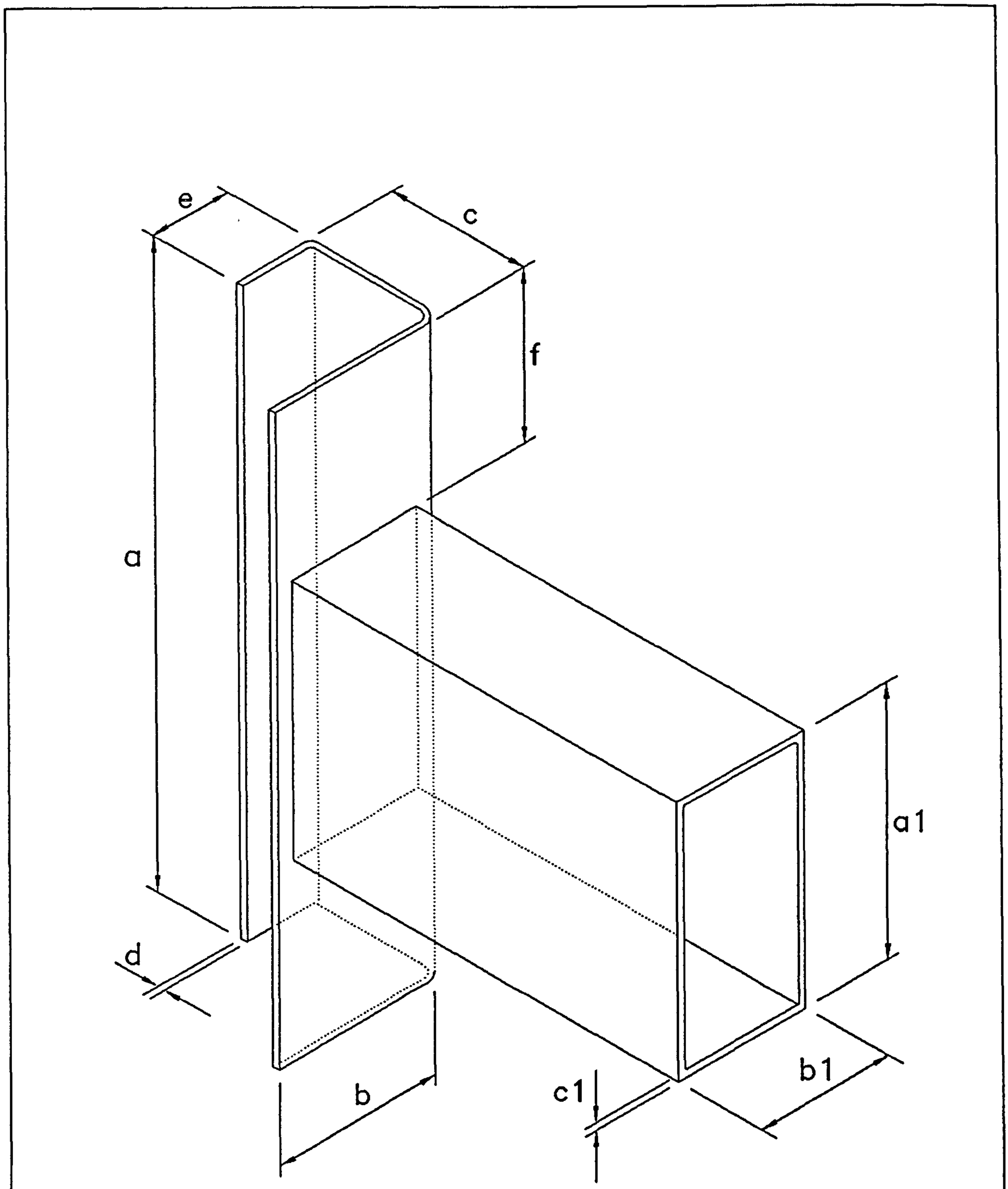

FIGURE 3.20 Dimensions of products tested

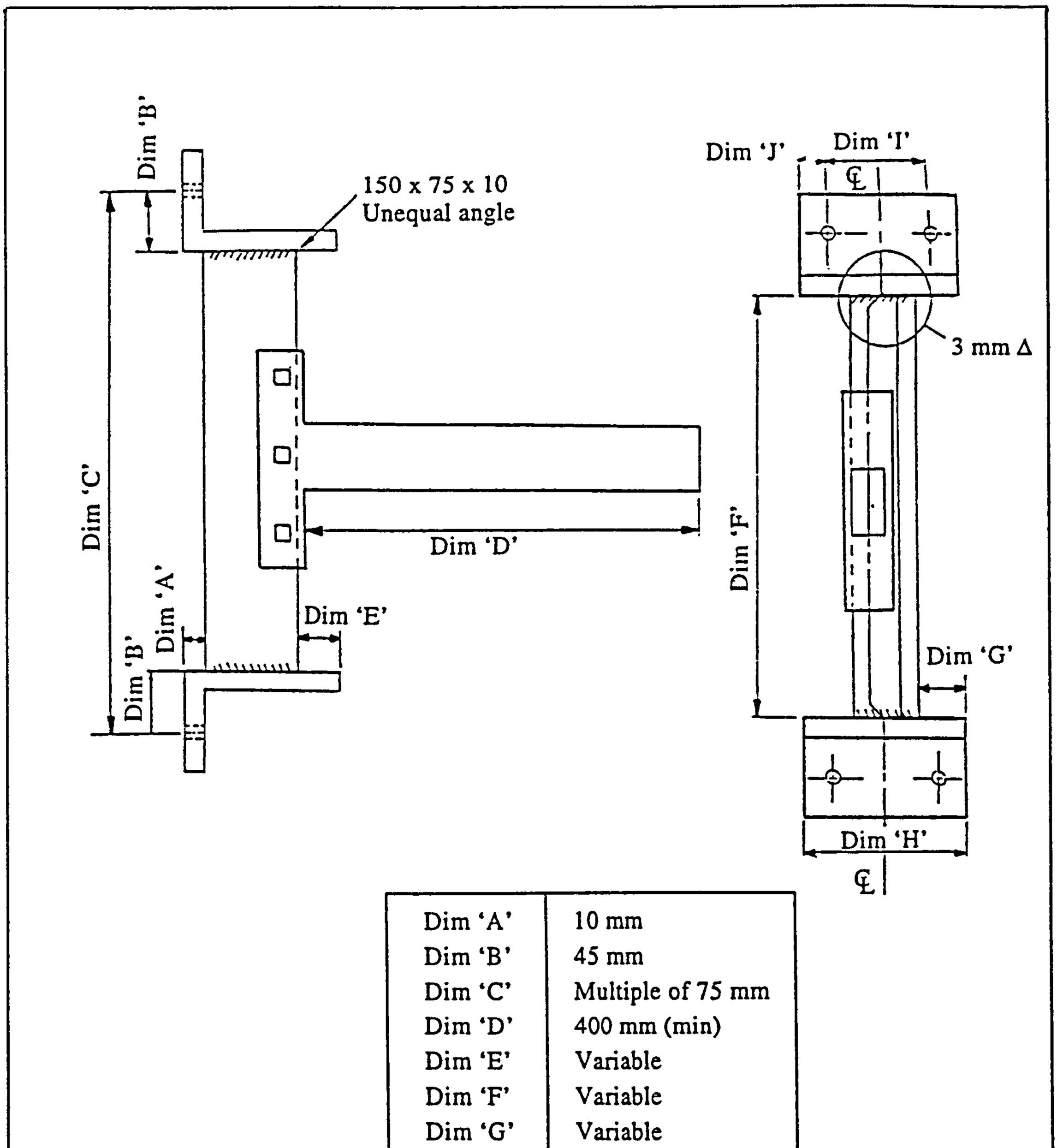

Dim 'A'	10 mm
Dim 'B'	45 mm
Dim 'C'	Multiple of 75 mm
Dim 'D'	400 mm (min)
Dim 'E'	Variable
Dim 'F'	Variable
Dim 'G'	Variable
Dim 'H'	150 mm
Dim 'I'	100 mm
Dim 'J'	25 mm

FIGURE 3.21 FABRICATION SPECIFICATION

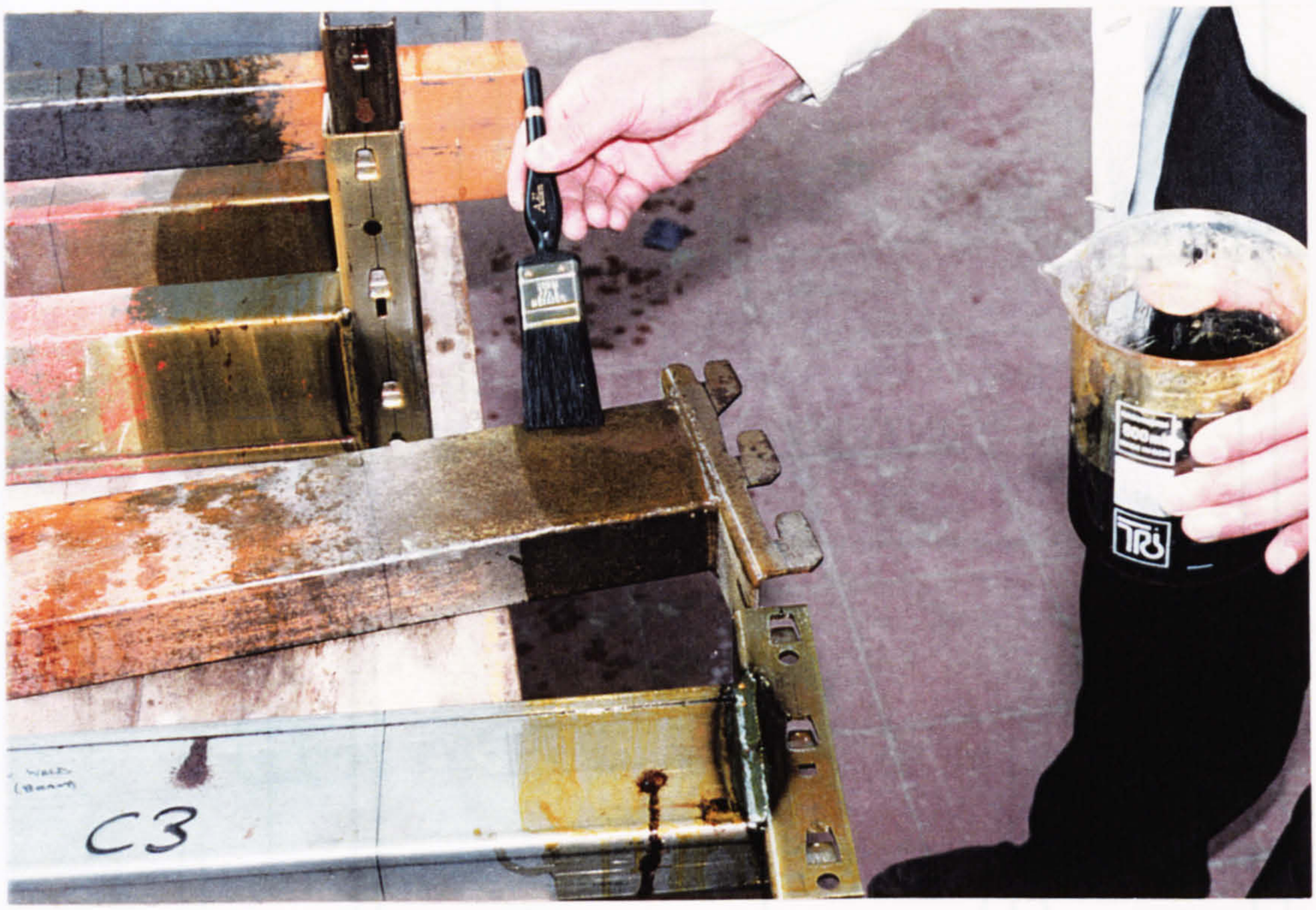

FIGURE 3.22 Applying stress lacquer

FIGURE 3.23 Measuring lacquer thickness

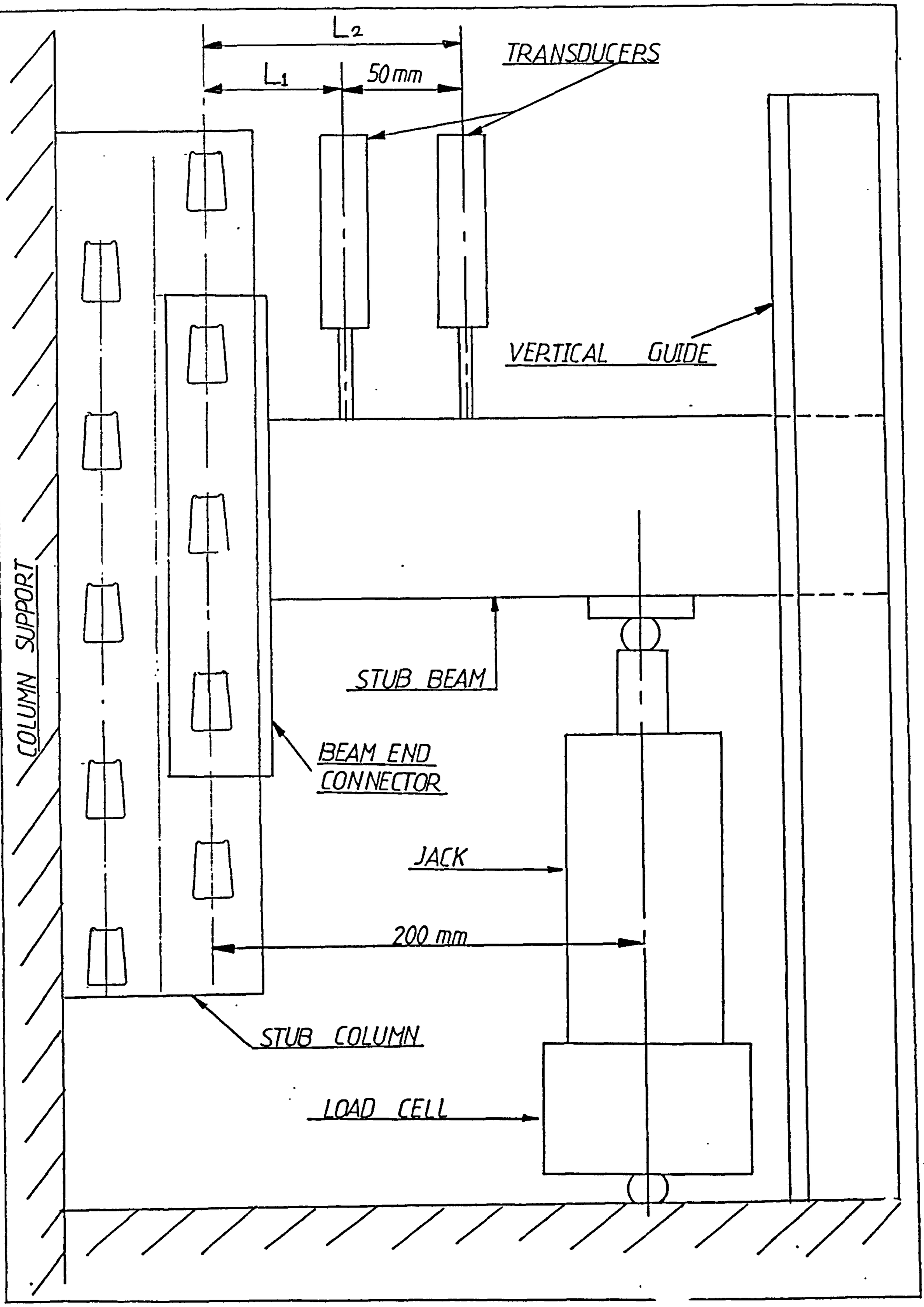

FIGURE 3.24 GENERAL LAYOUT OF TESTS

MOMENT-ROTATION CURVES
LINK51
PRODUCT 1

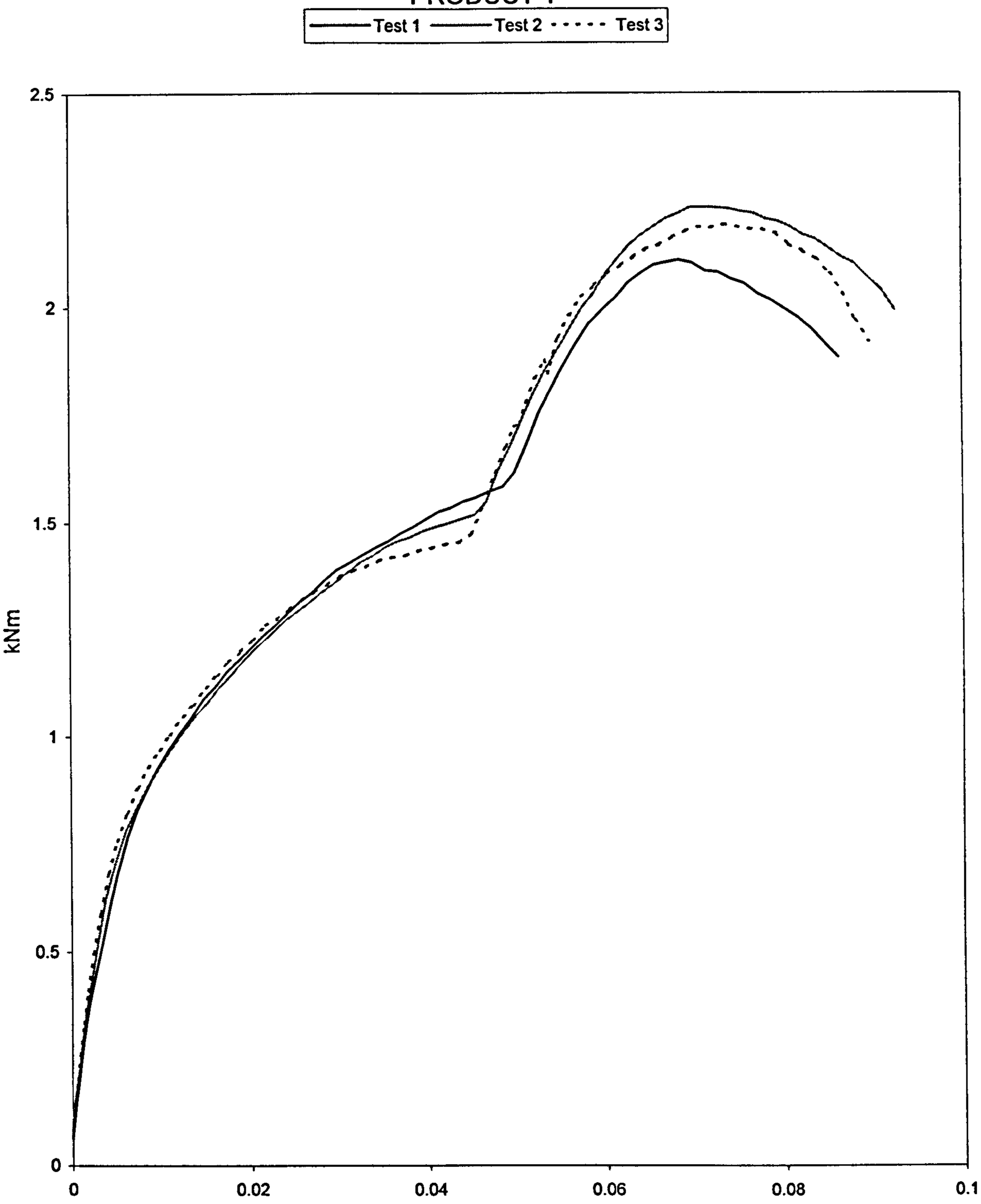

Figure 3.25

MOMENT-ROTATION CURVES
DEXION
PRODUCT 2

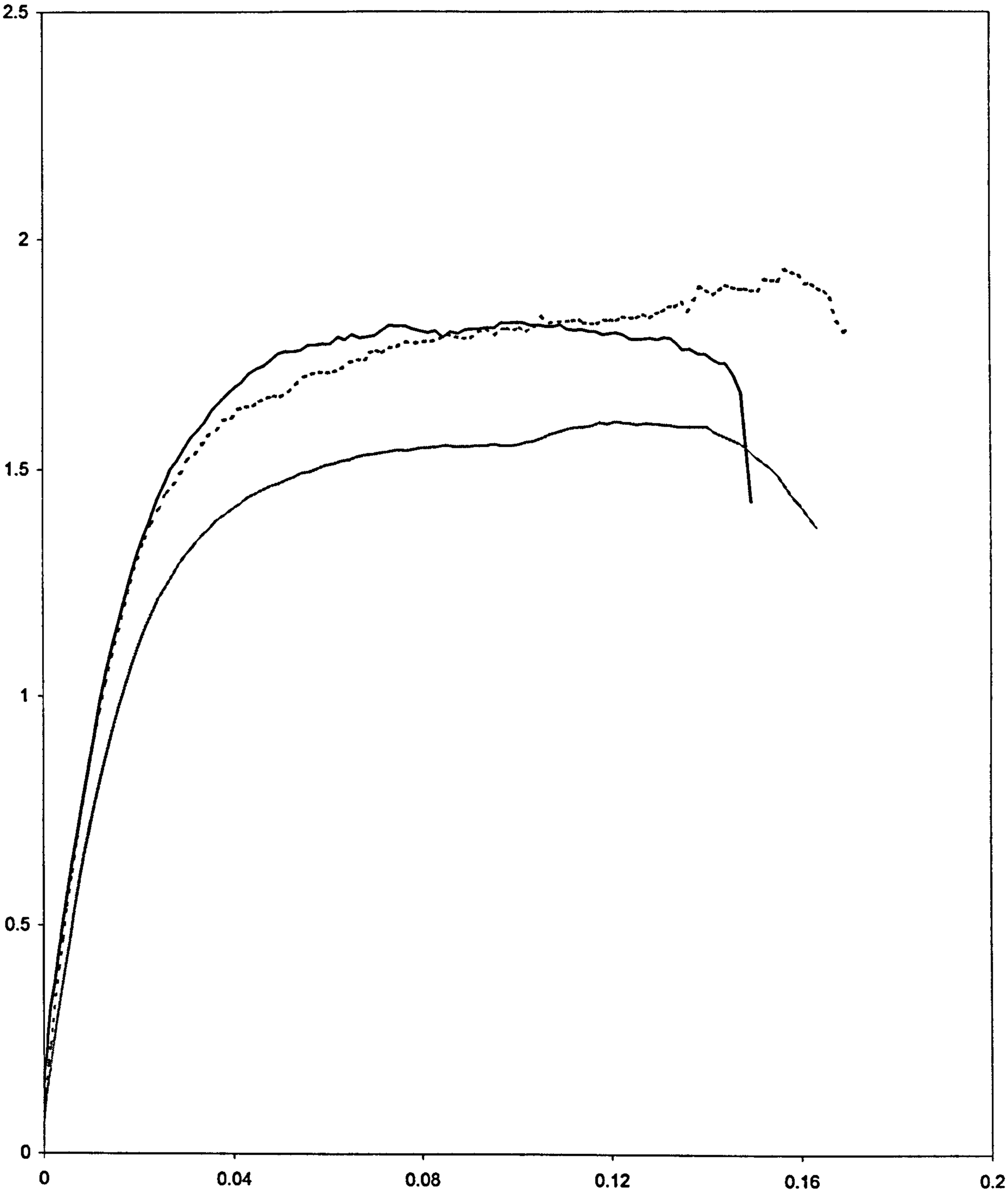

Figure 3.26

MOMENT-ROTATION CURVES
PSS 3 LUG UP WELDED
PRODUCT 3

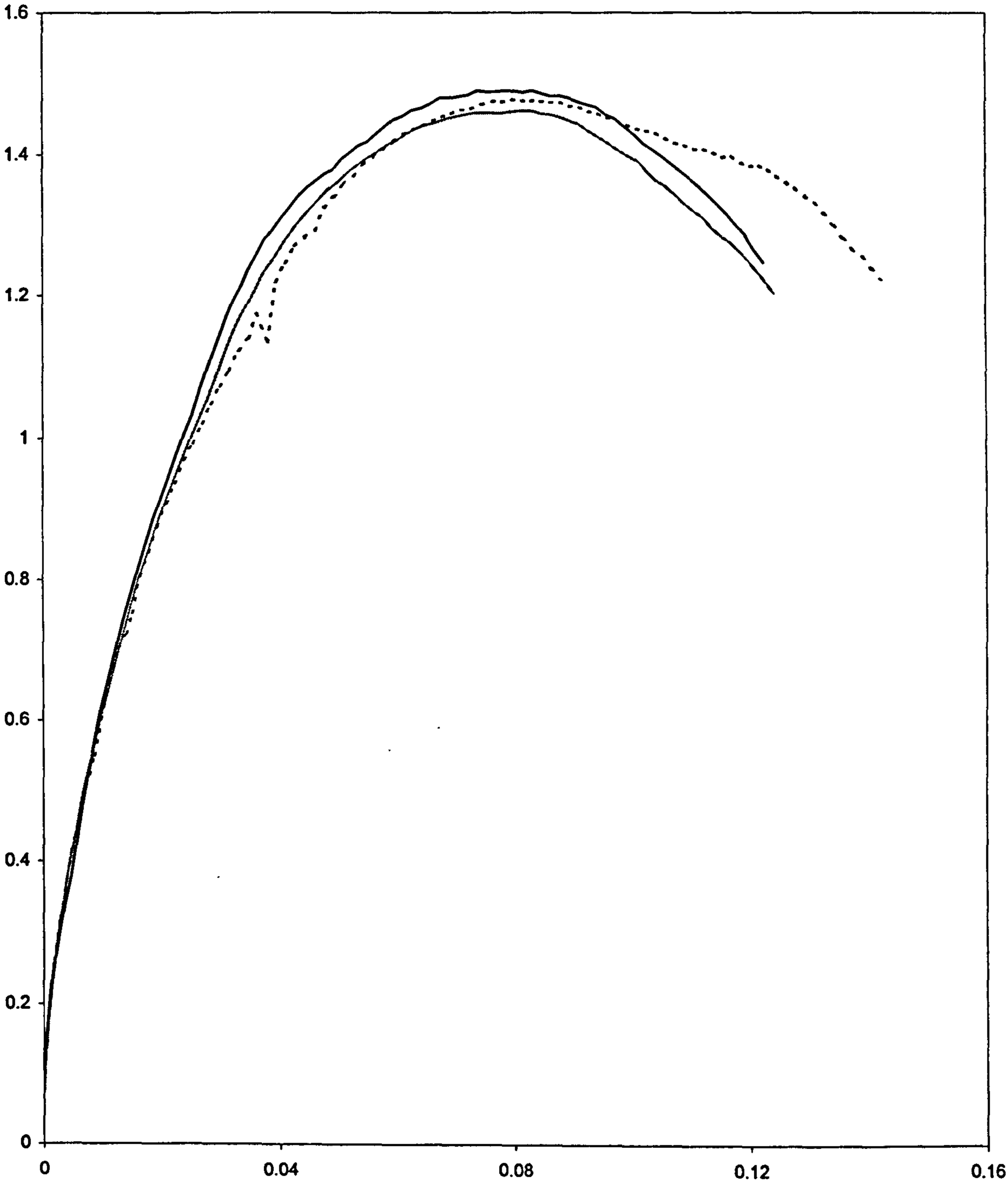

Figure 3.27

MOMENT-ROTATION CURVES
PSS 3 LUG DOWN WELDED
PRODUCT 4

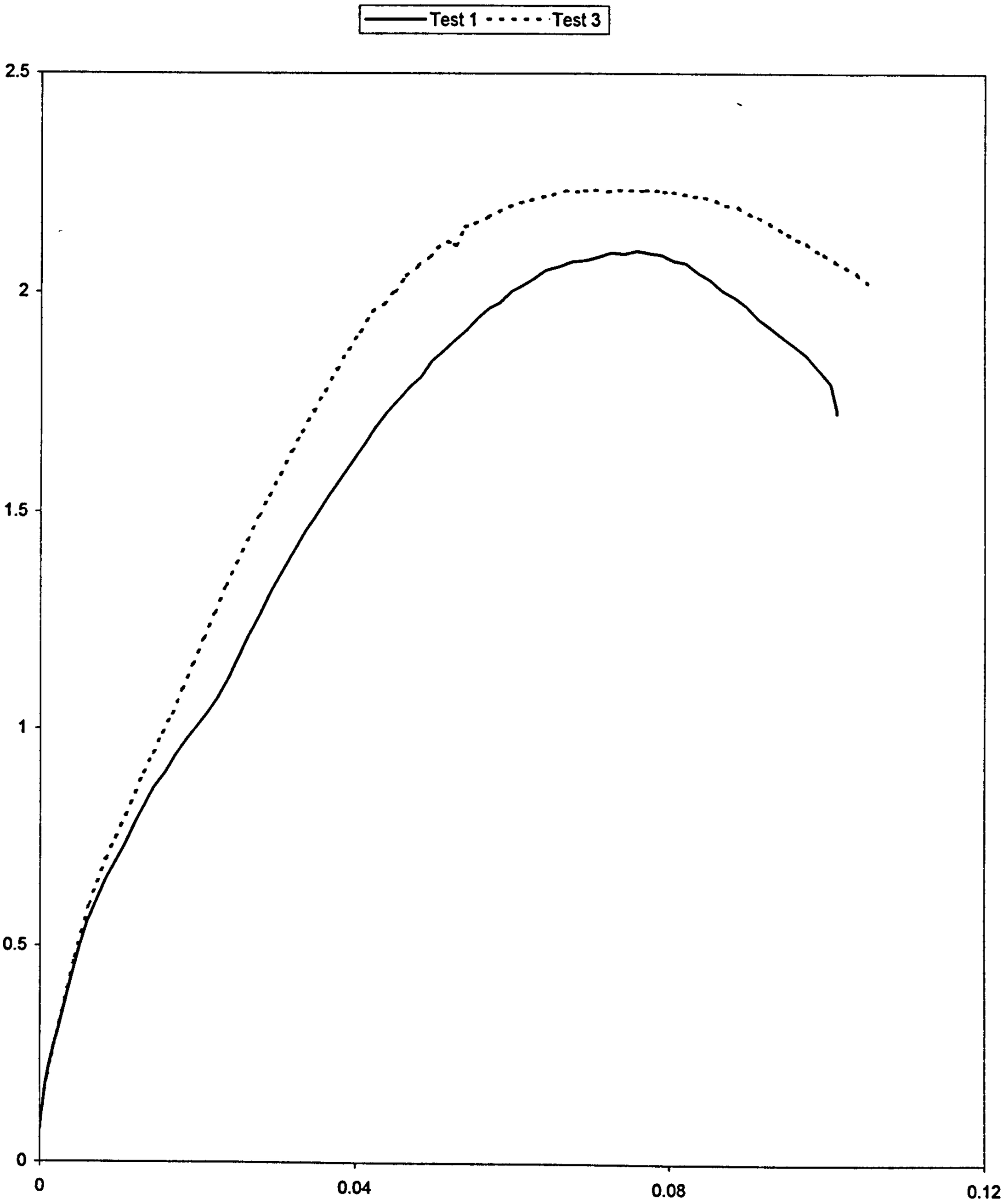

Figure 3.28

MOMENT-ROTATION CURVES
PSS 3 LUG SYMMETRICAL
PRODUCT 5

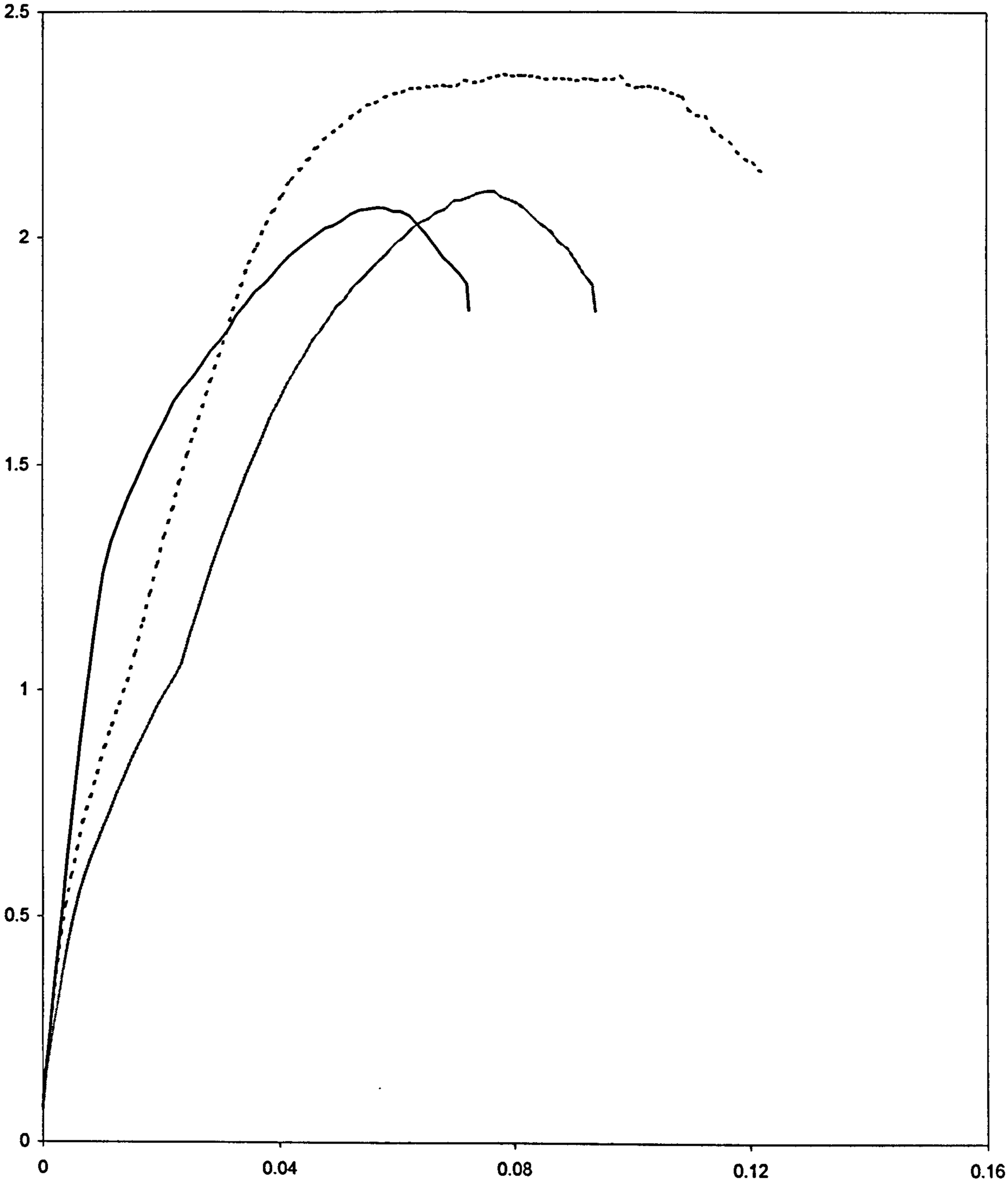

Figure 3.29

MOMENT-ROTATION CUEVES
PSS 4 LUG UP WELDED
PRODUCT 6

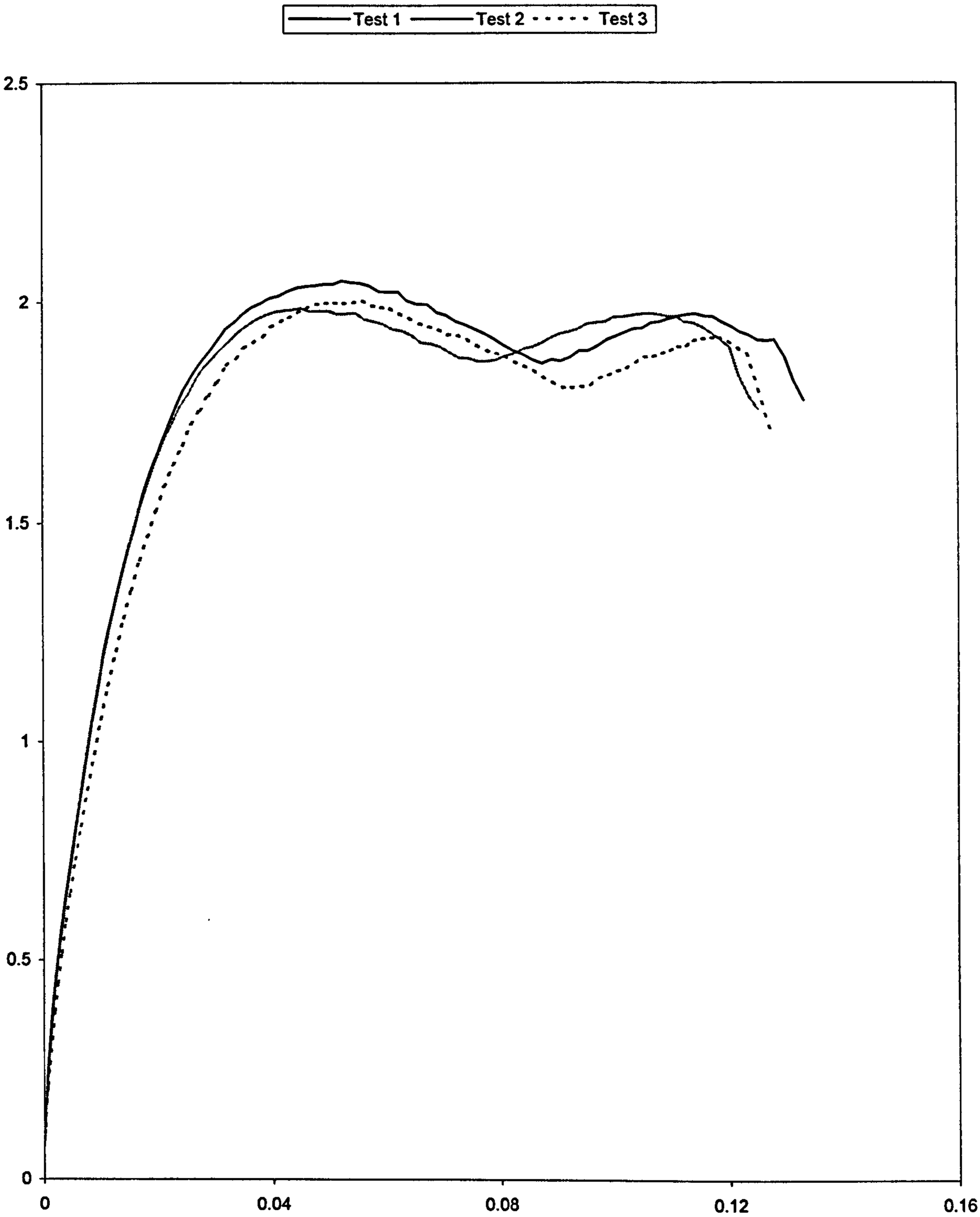

Figure 3.30

MOMENT-ROTATION CURVES
PSS 4 LUG DOWN WELDED
PRODUCT 7

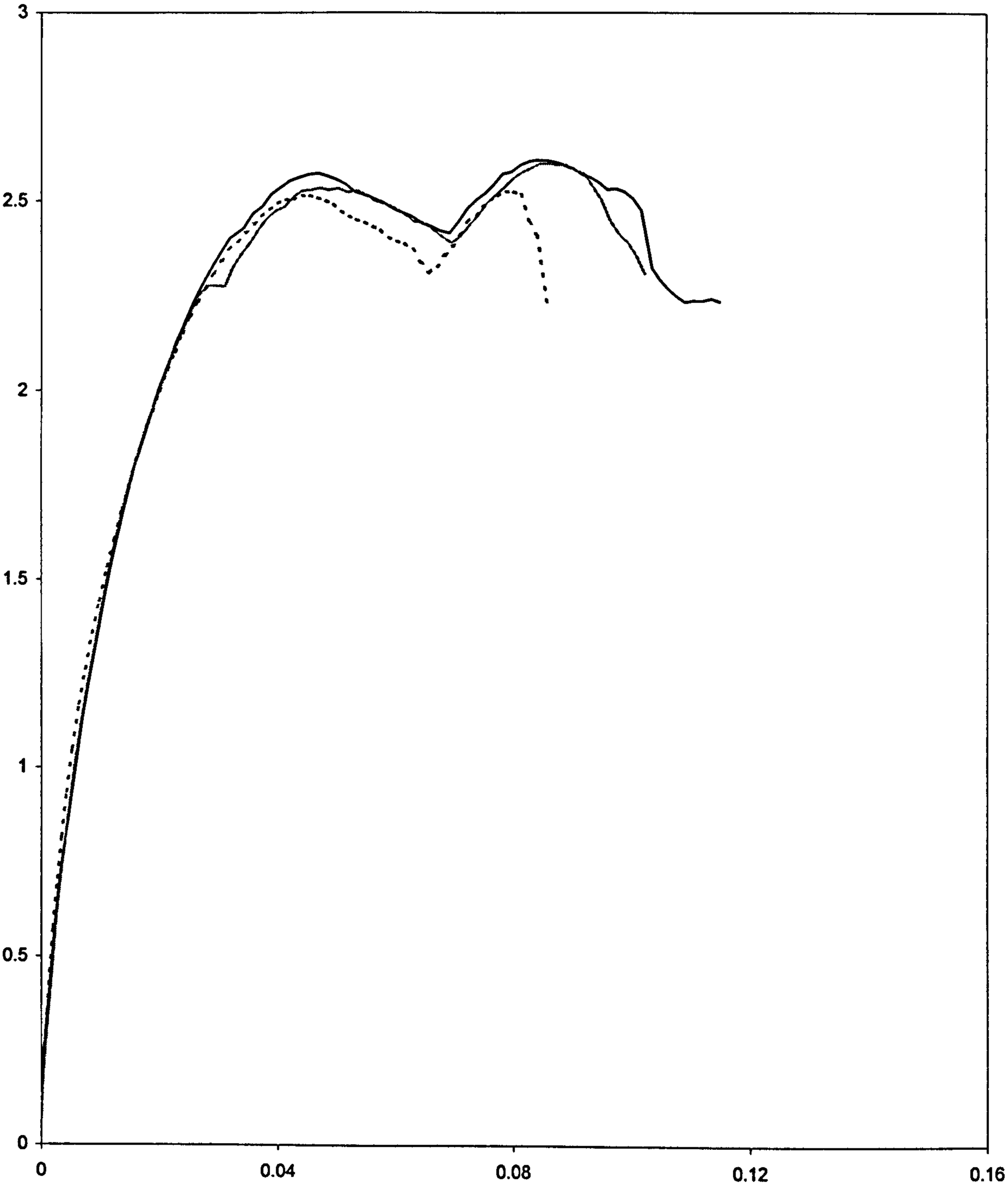

Figure 3.31

MOMENT-ROTATION CURVES
PSS 4 LUG SYMMETRICAL
PRODUCT 8

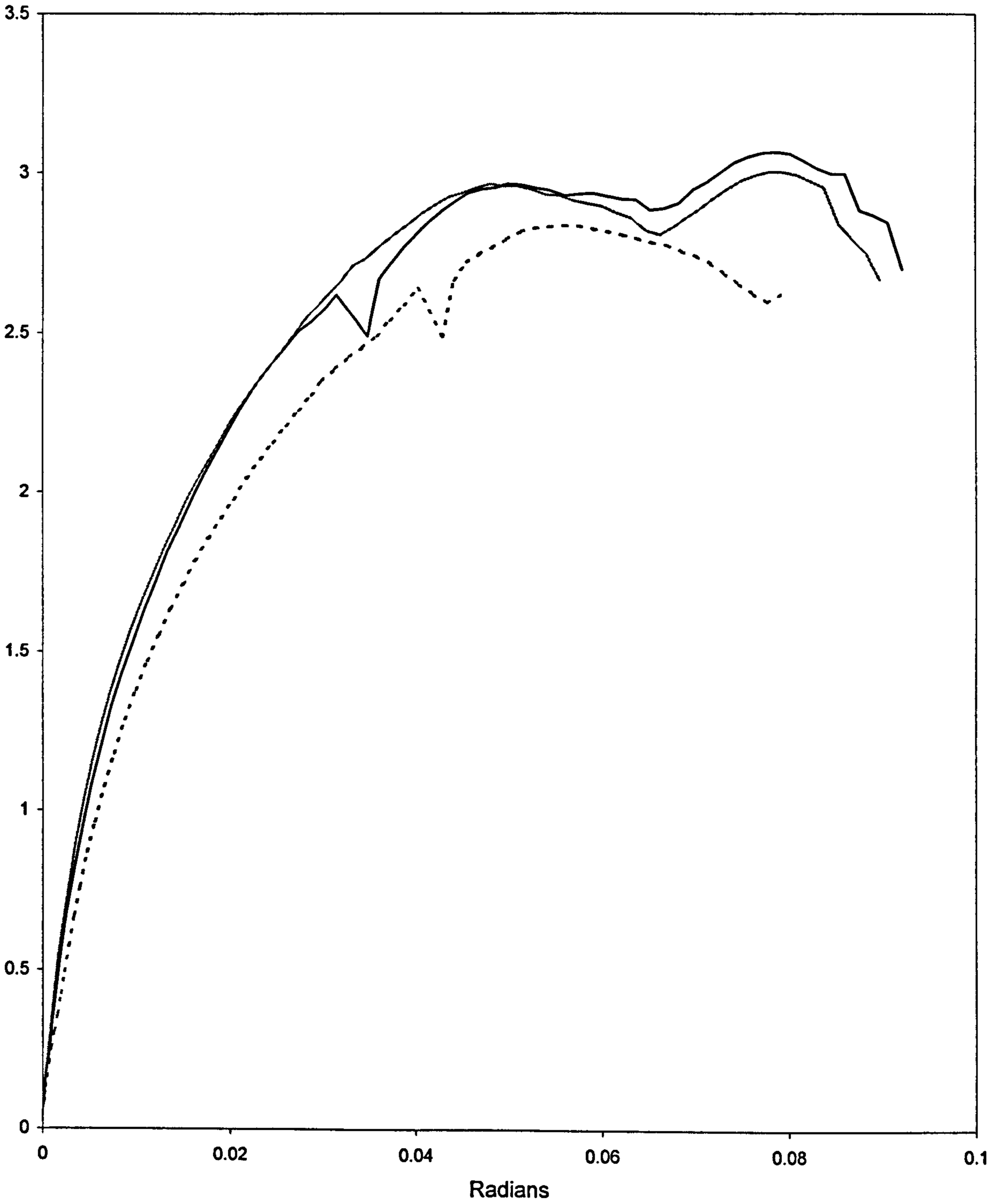

Figure 3.32

MOMENT-ROTATION CURVES
APEX
PRODUCT 9

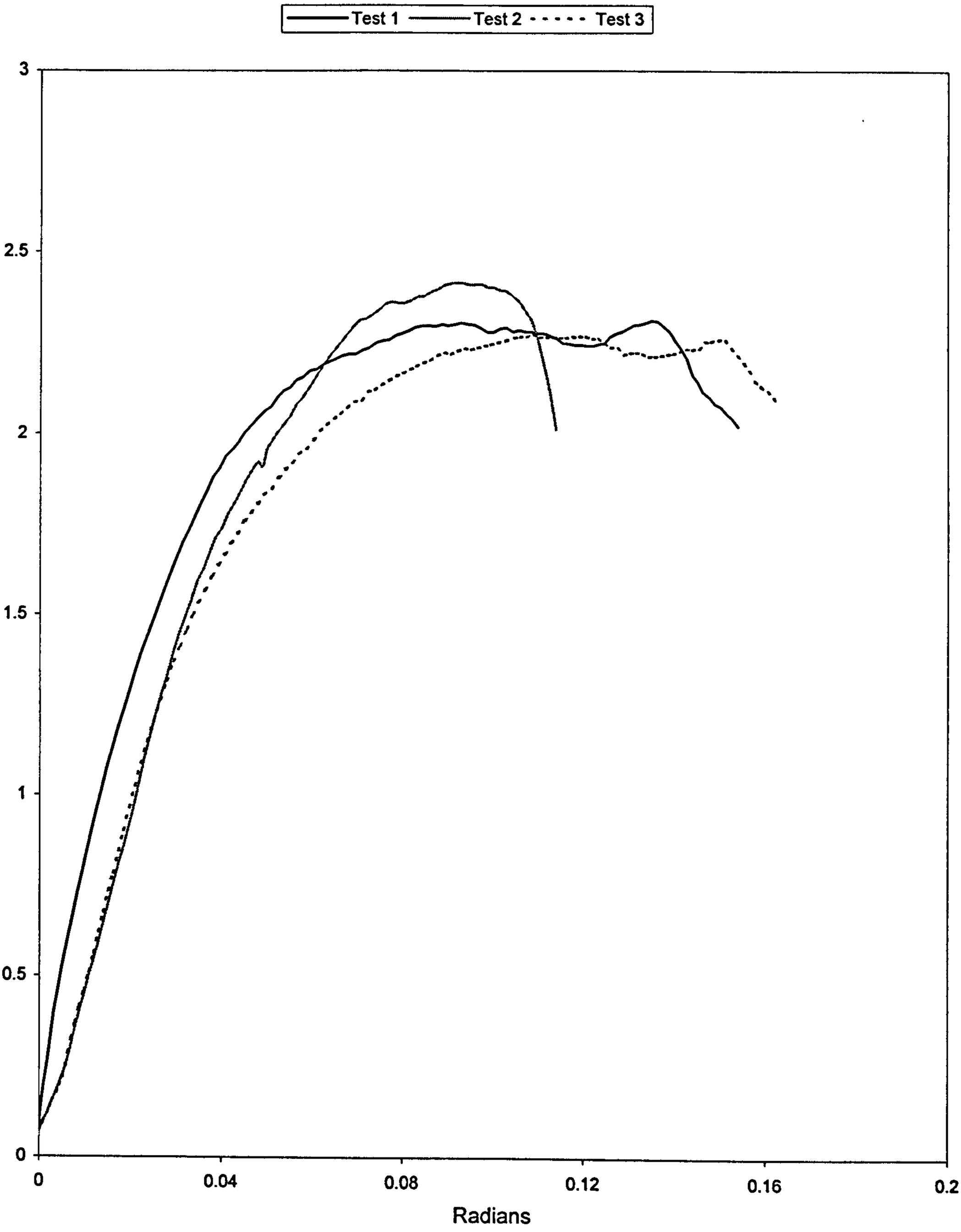

Figure 3.33

MOMENT-ROTATION CURVES
FINSPA
PRODUCT 10

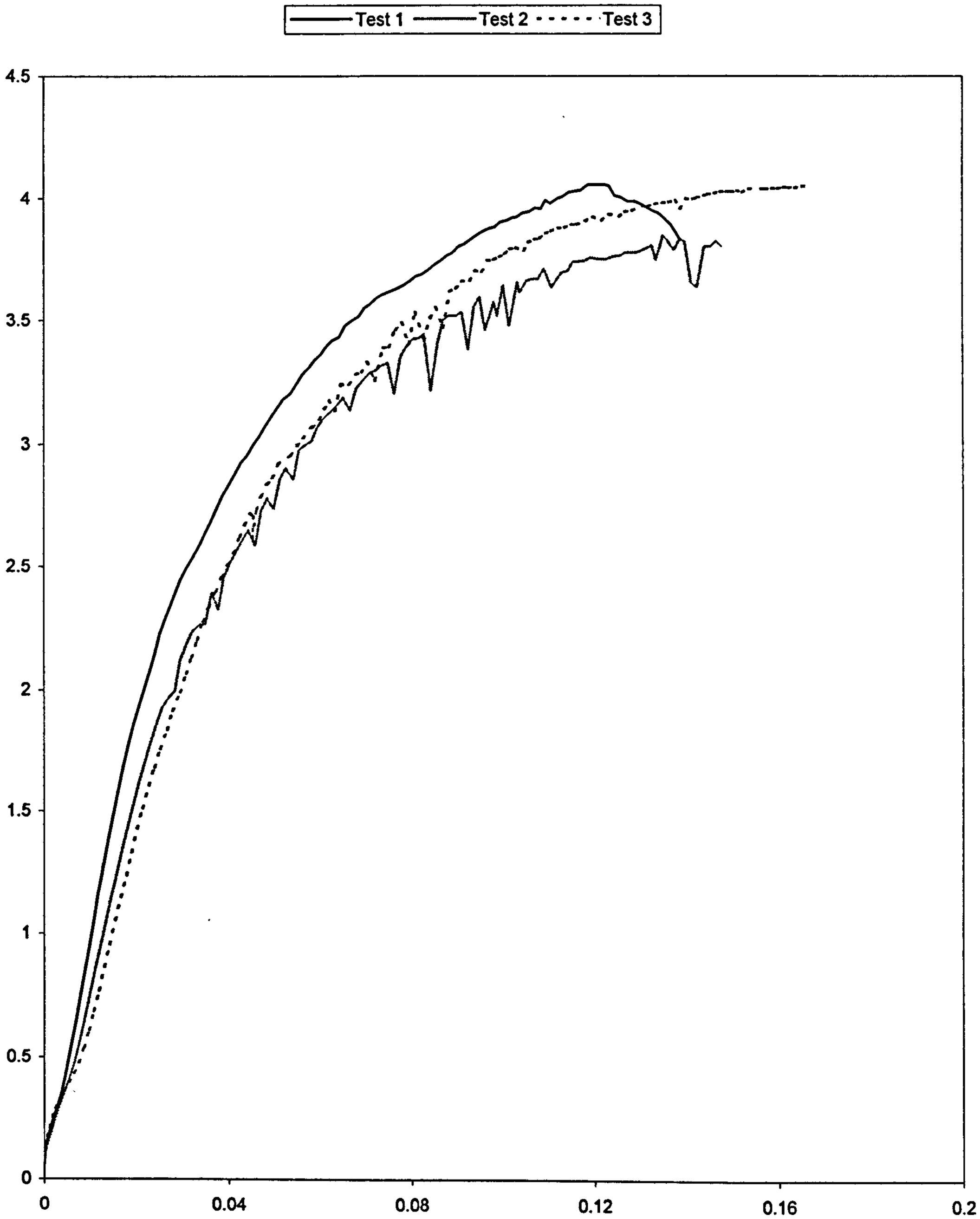

Figure 3.34

MOMENT-ROTATION CURVES
POLYPAL
PRODUCT 11

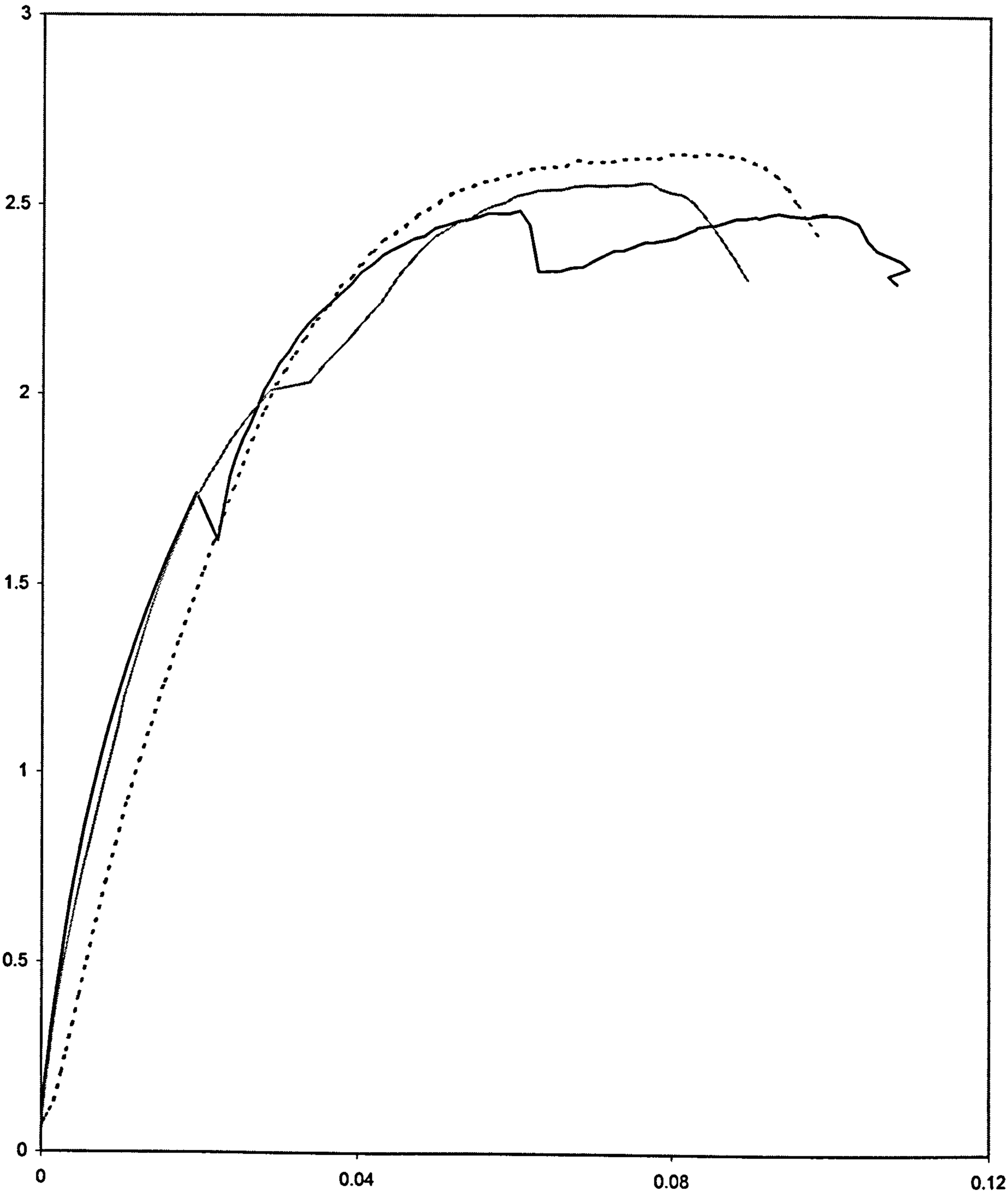

Figure 3.35

MOMENT-ROTATION CURVE
P.S.S (3-Stud, Small, Symmetrical)
PRODUCT 12

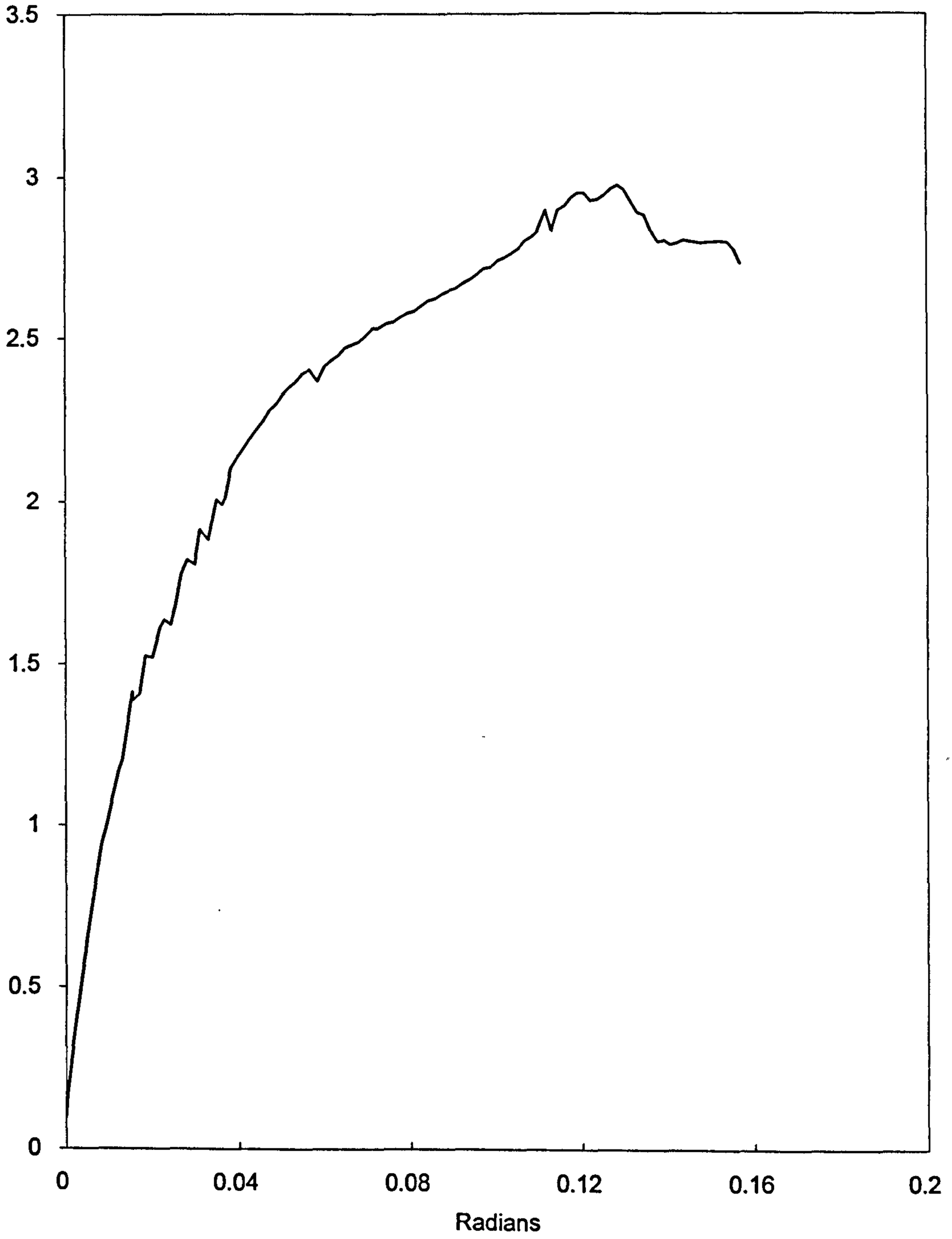

Figure 3.36

MOMENT-ROTATION CURVE
P.S.S (3-Stud, Large, Symmetrical)
PRODUCT 13

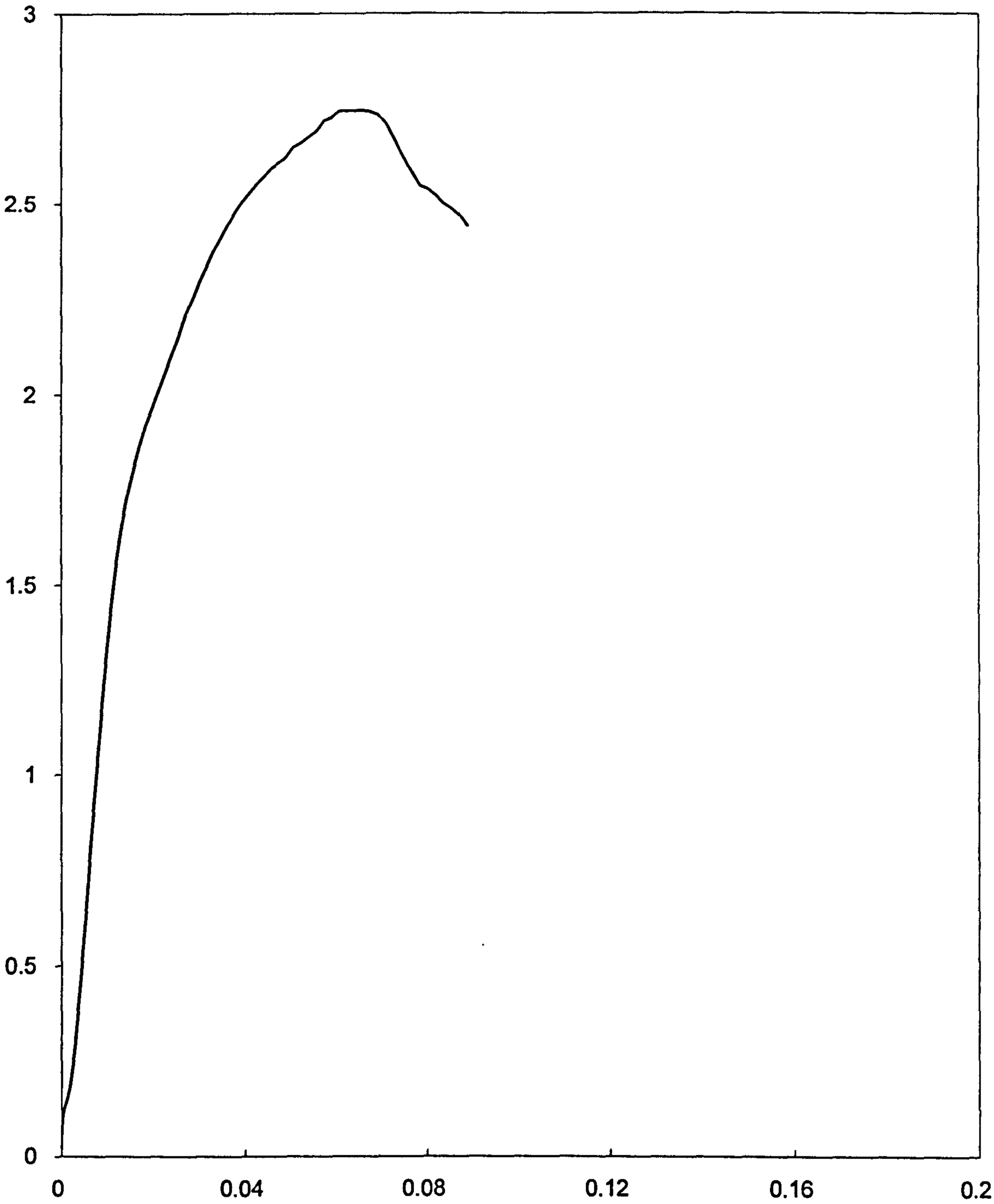

Figure 3.37

MOMENT-ROTATION CURVES
REDIRACK
PRODUCT 14

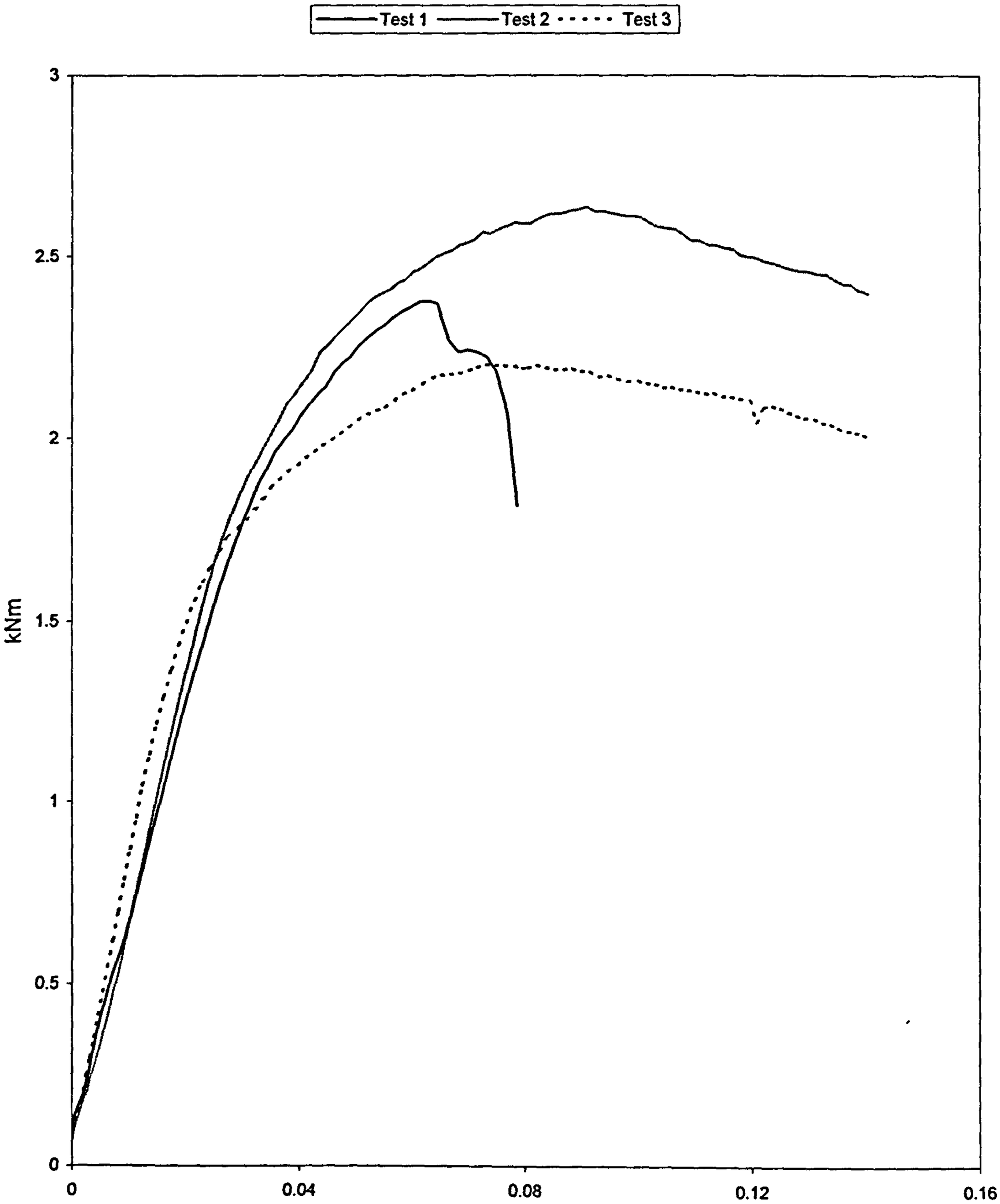

Figure 3.38

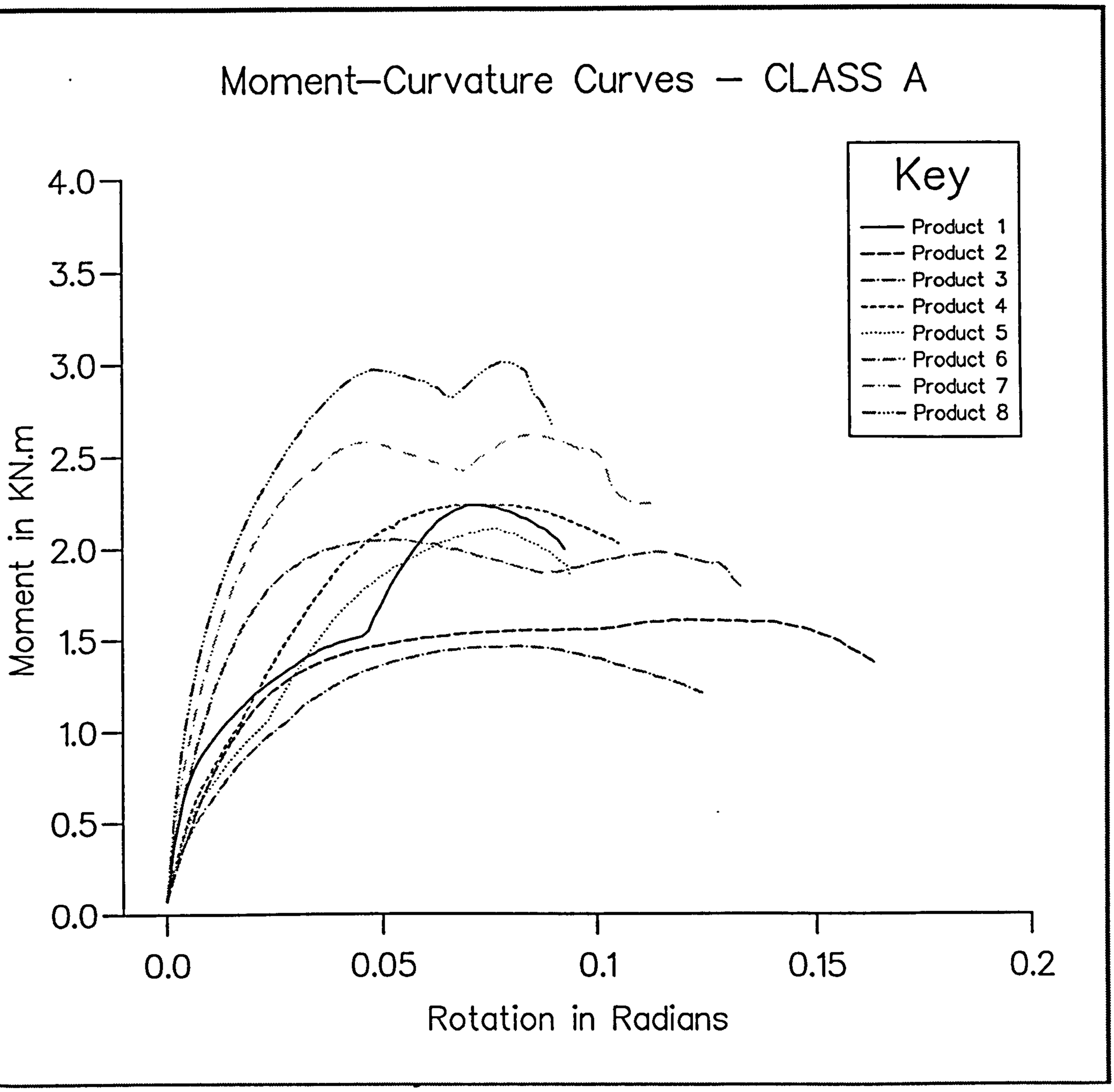

Figure 3.39 Moment-rotation curve, Class A

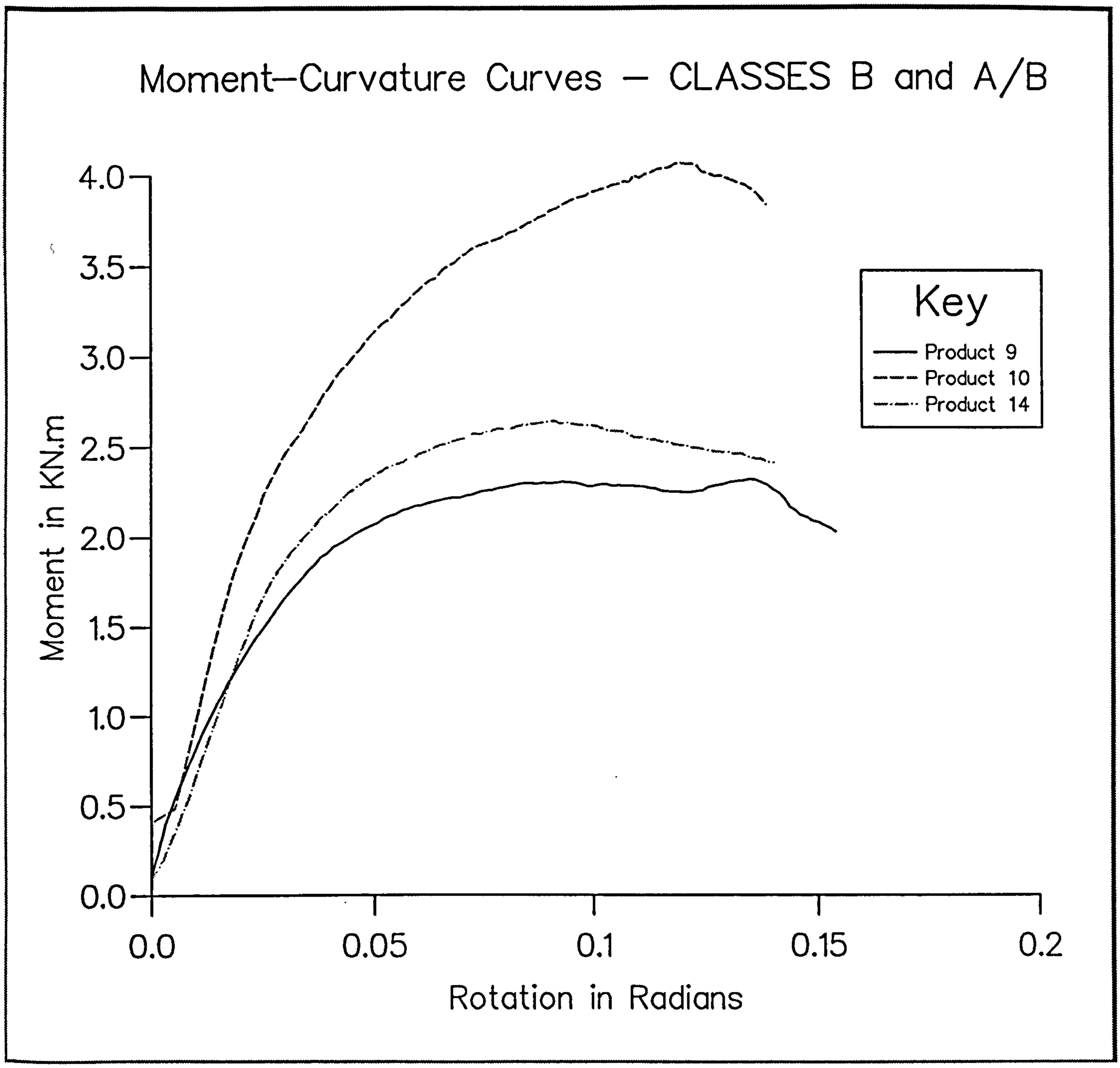

Figure 3.40 Moment-rotation curves, Classes B and A/B

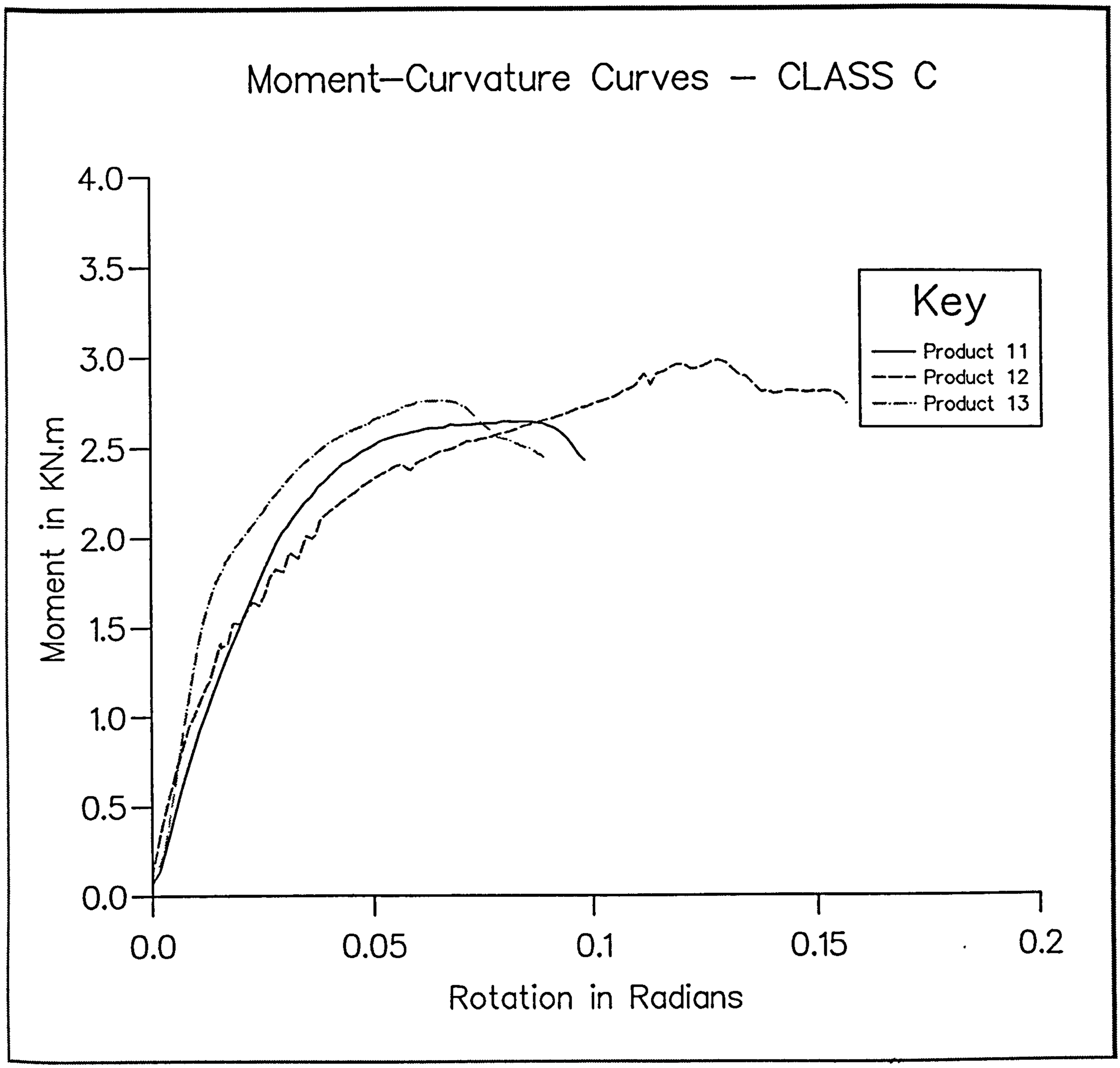

Figure 3.41 Moment-rotation curves, Class C

FIGURE 3.42

(b)

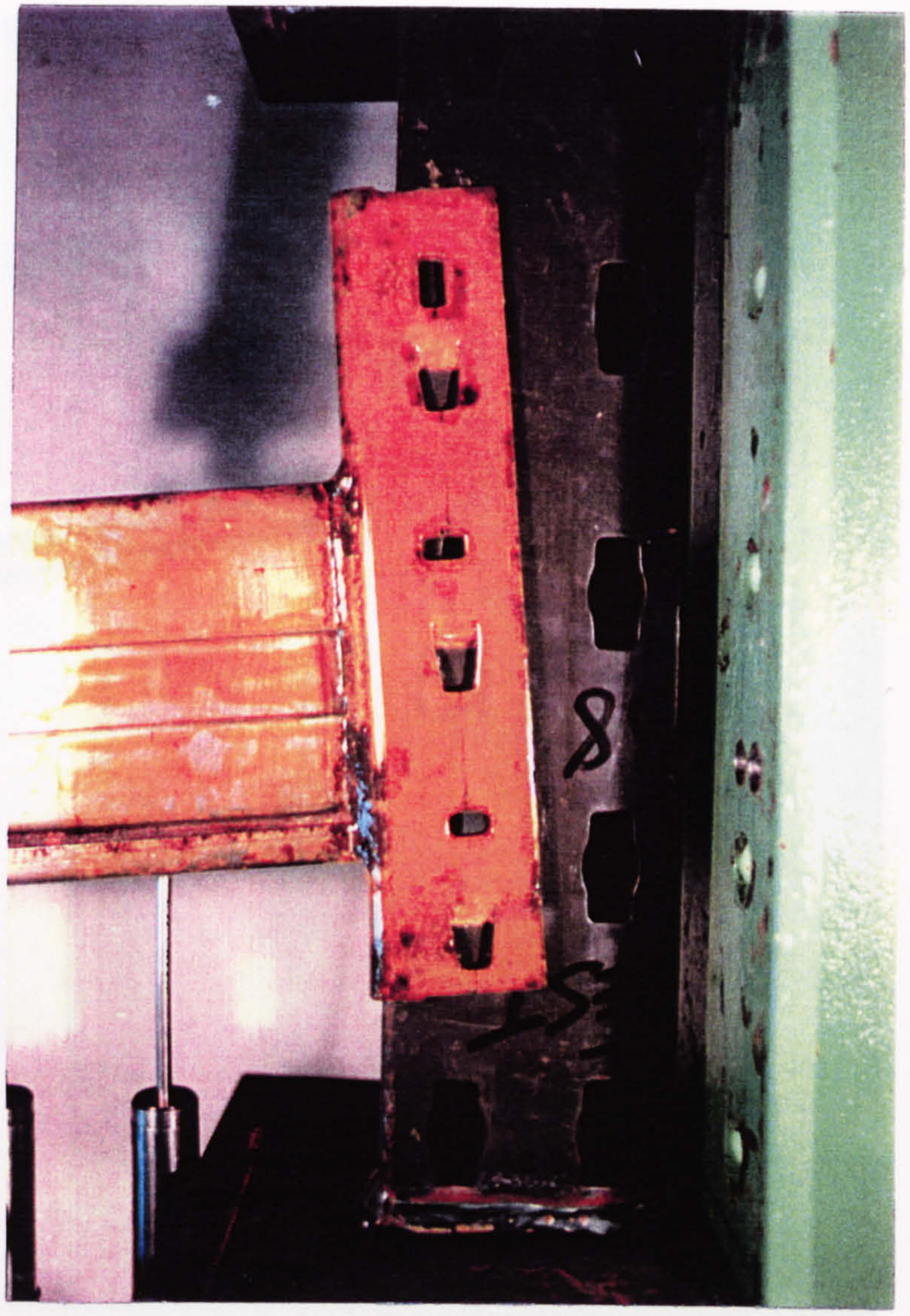

(a)

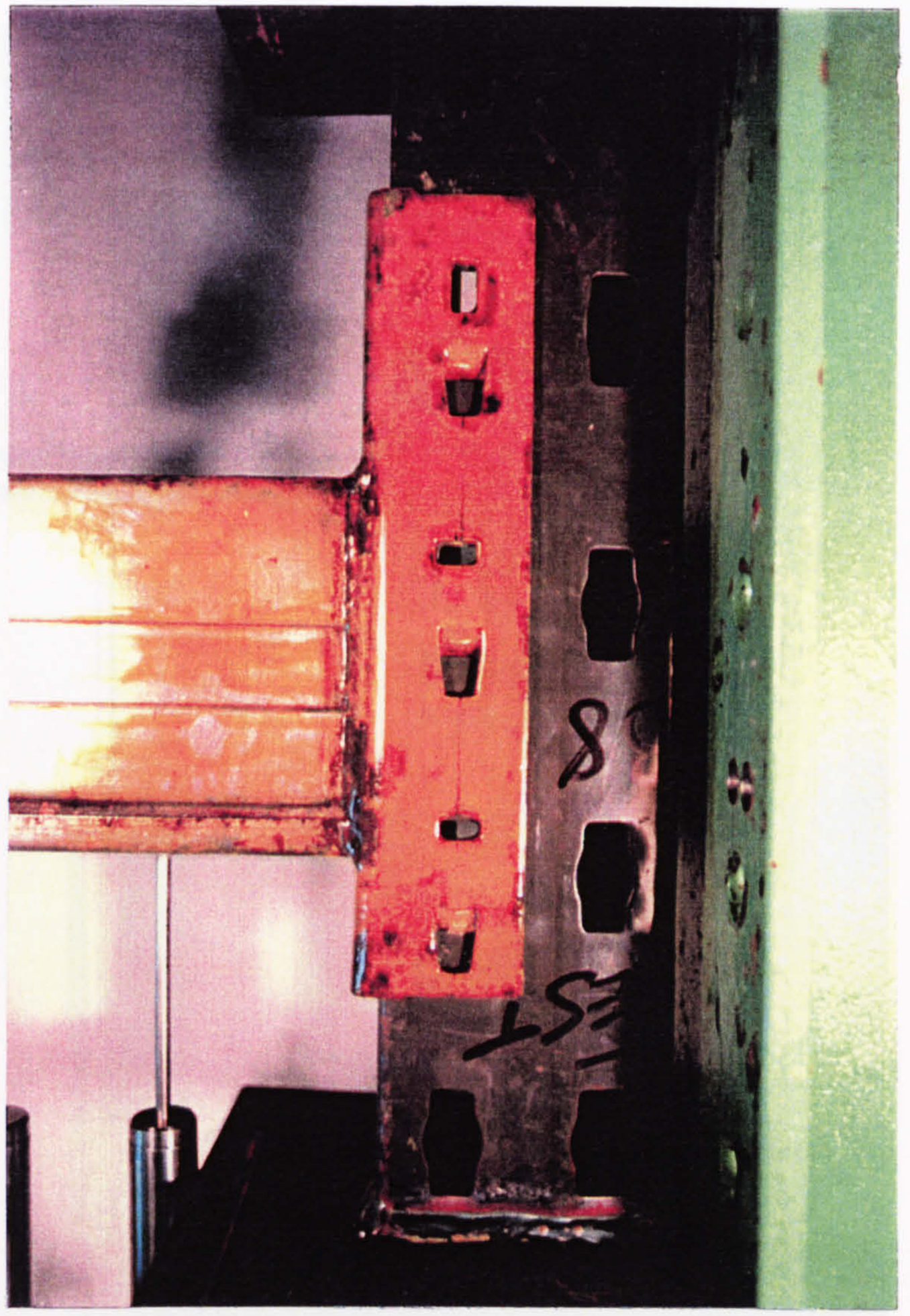

FIGURE 3.43

(b)

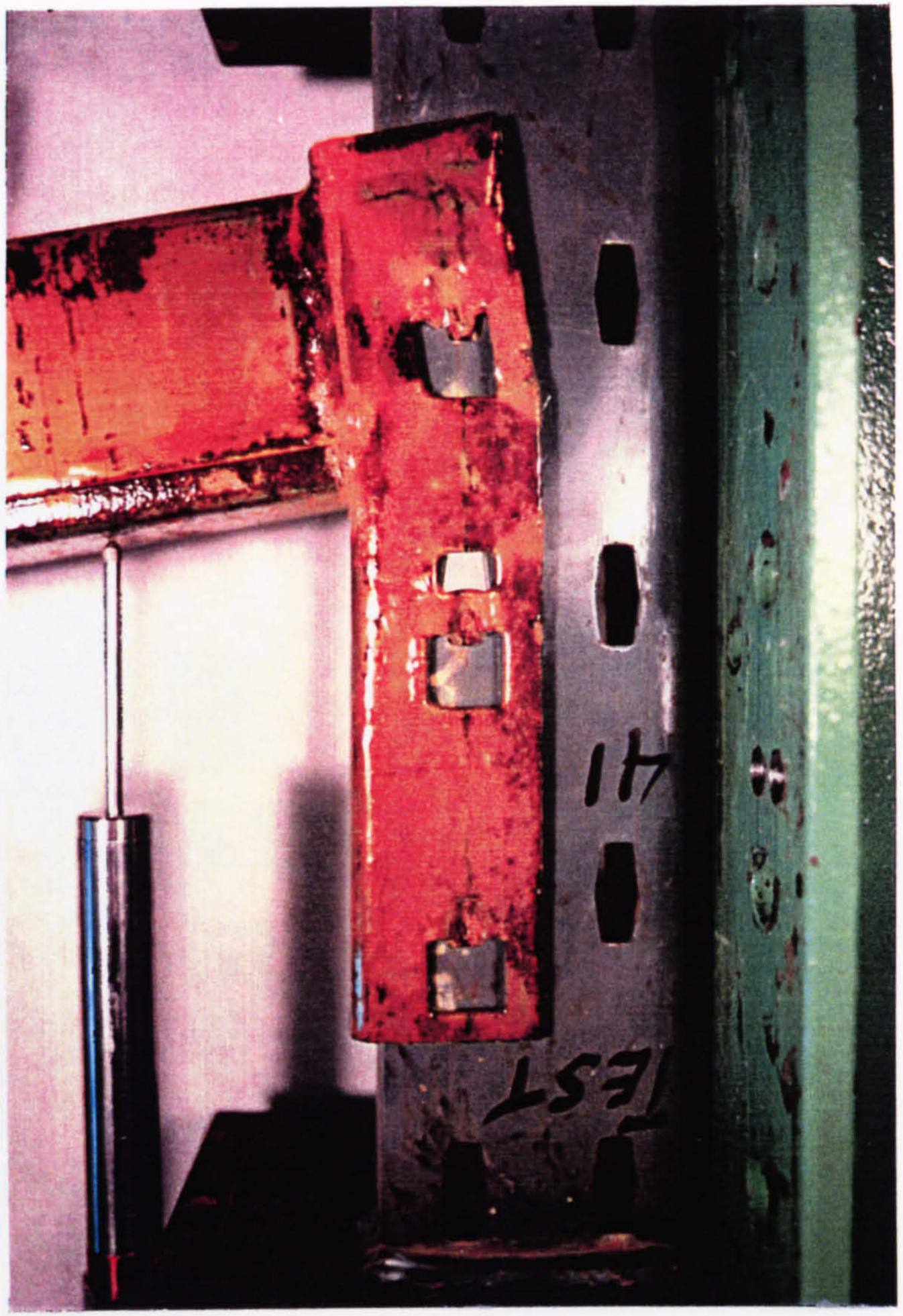

(a)

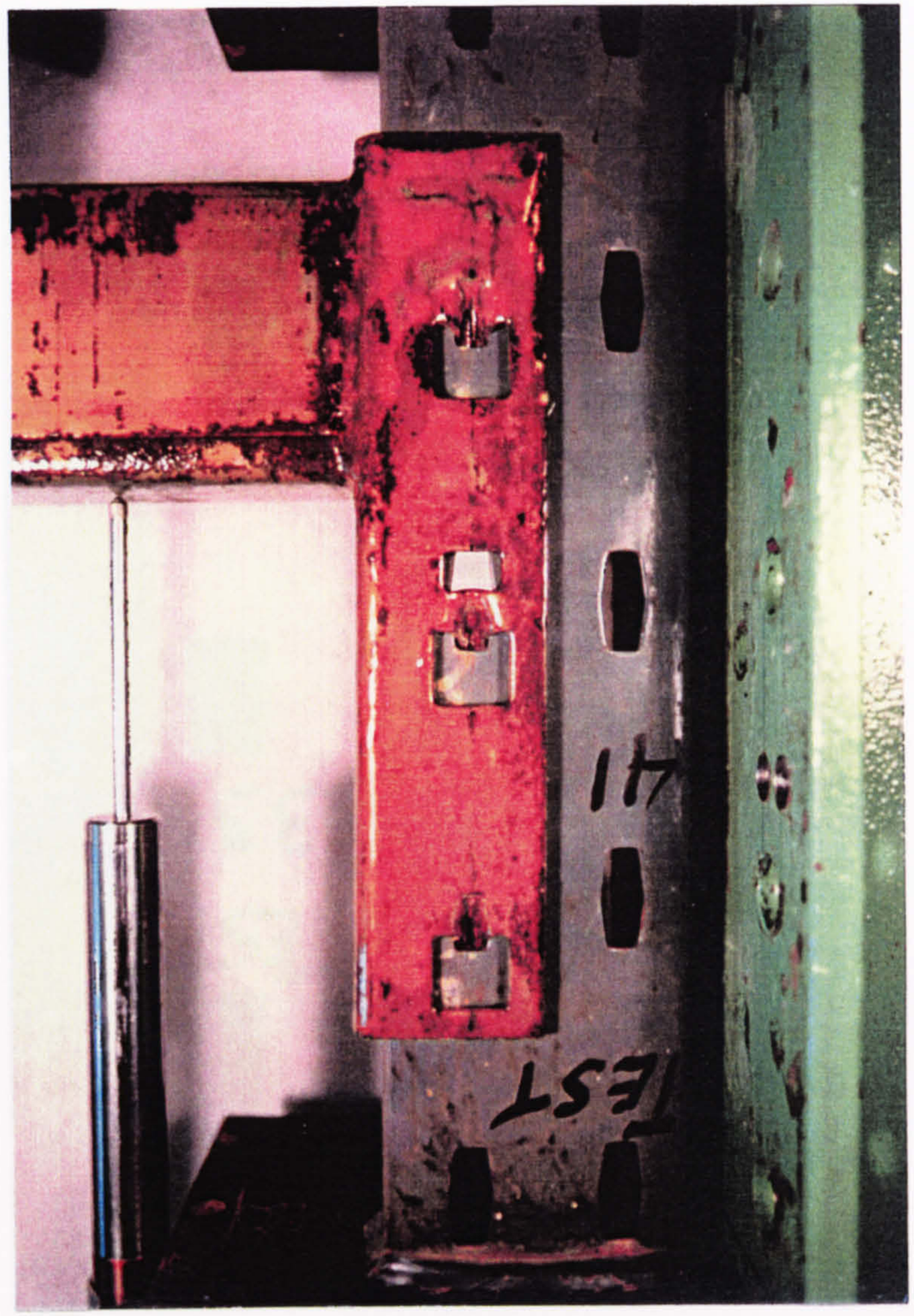

FIGURE 3.44

(b)

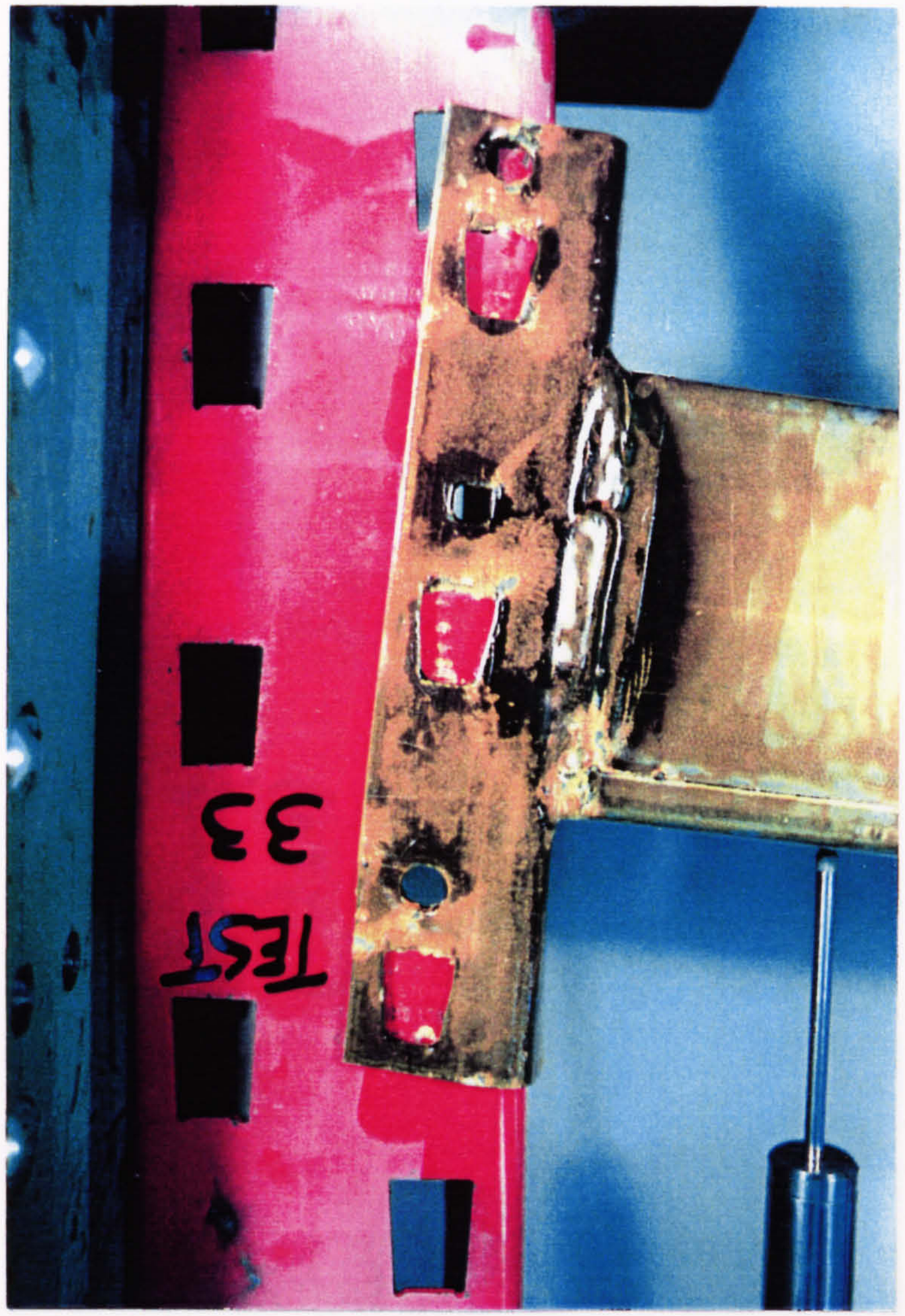

(a)

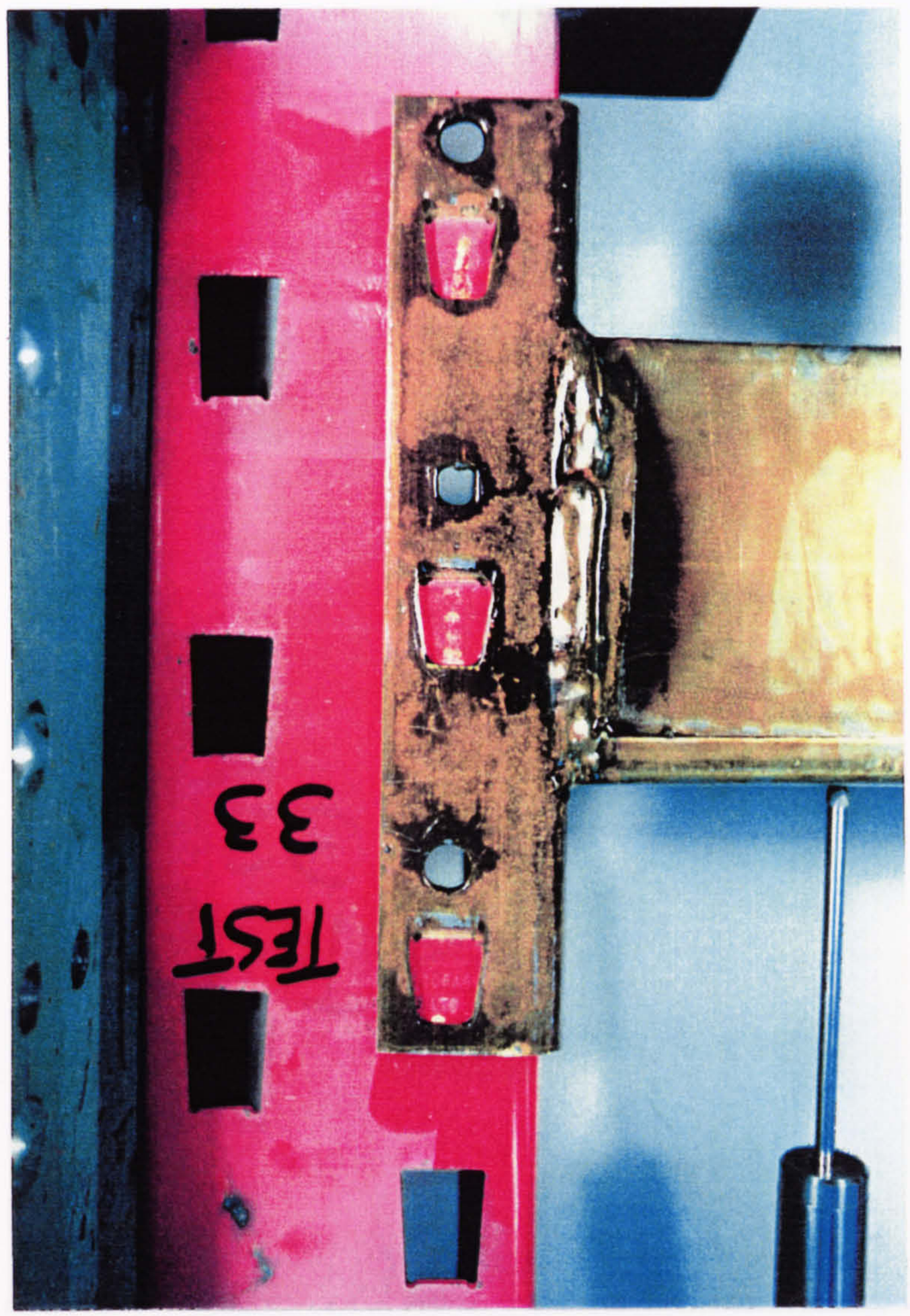

FIGURE 3.45

(b)

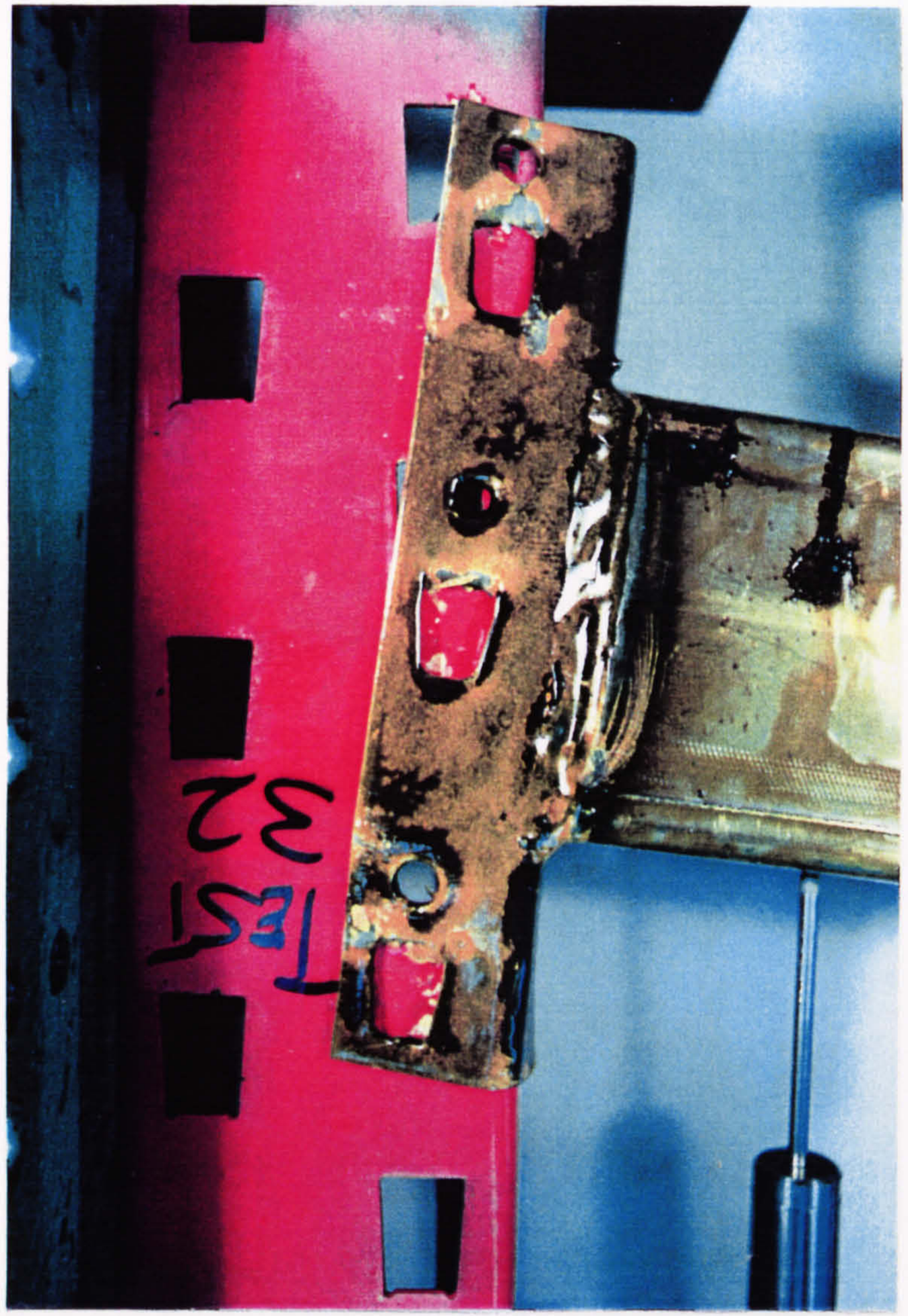

(a)

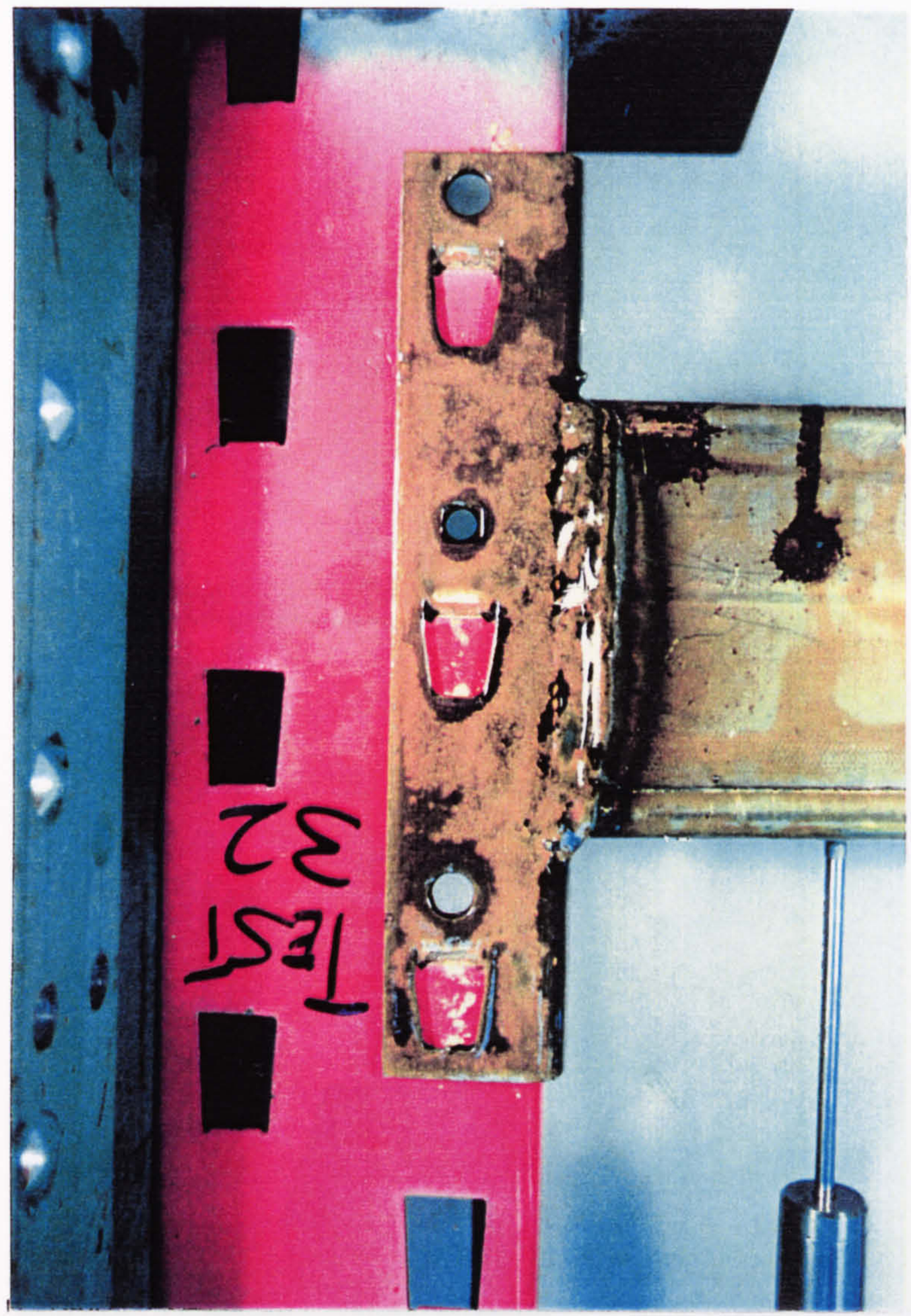

FIGURE 3.46

(b)

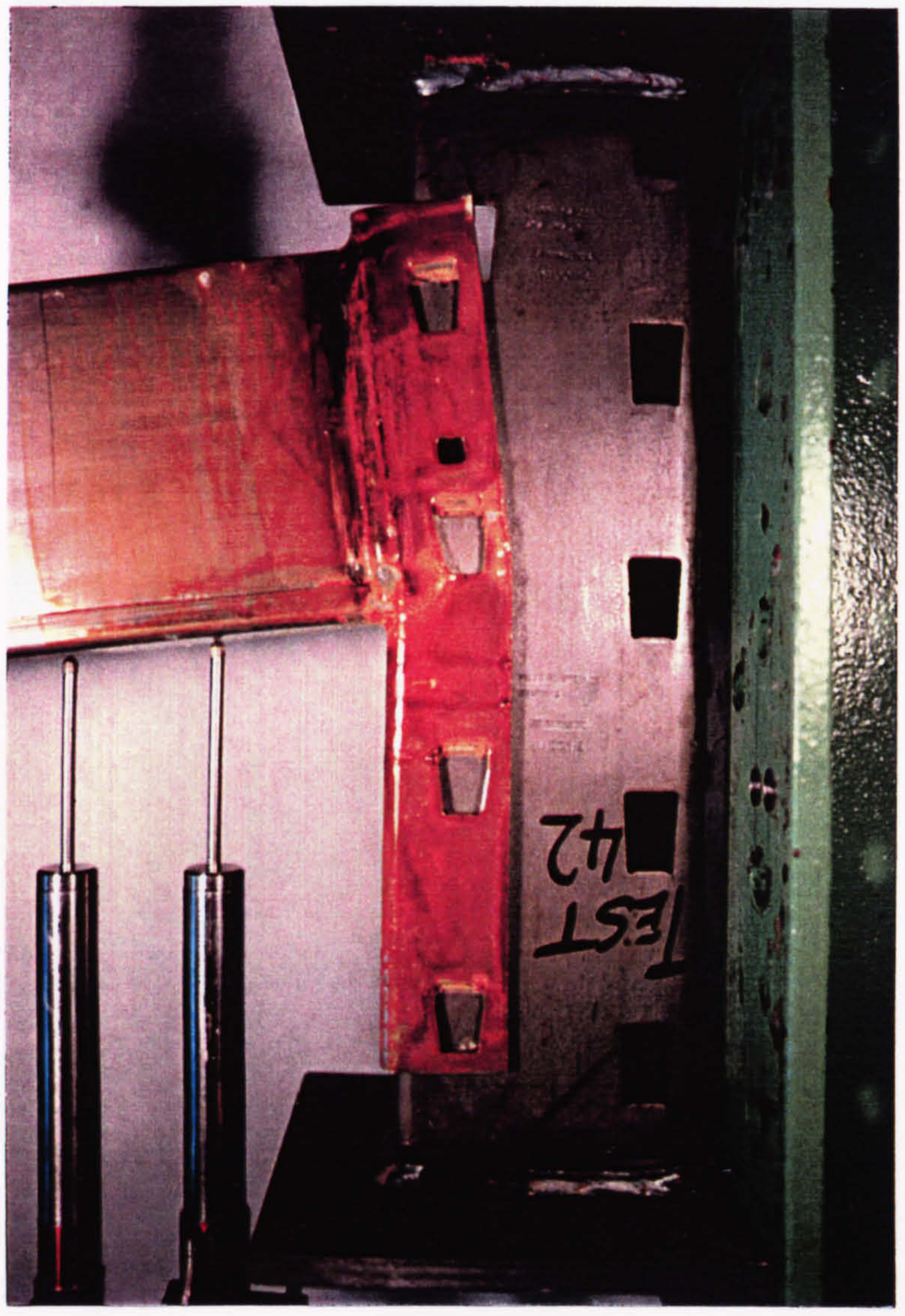

(a)

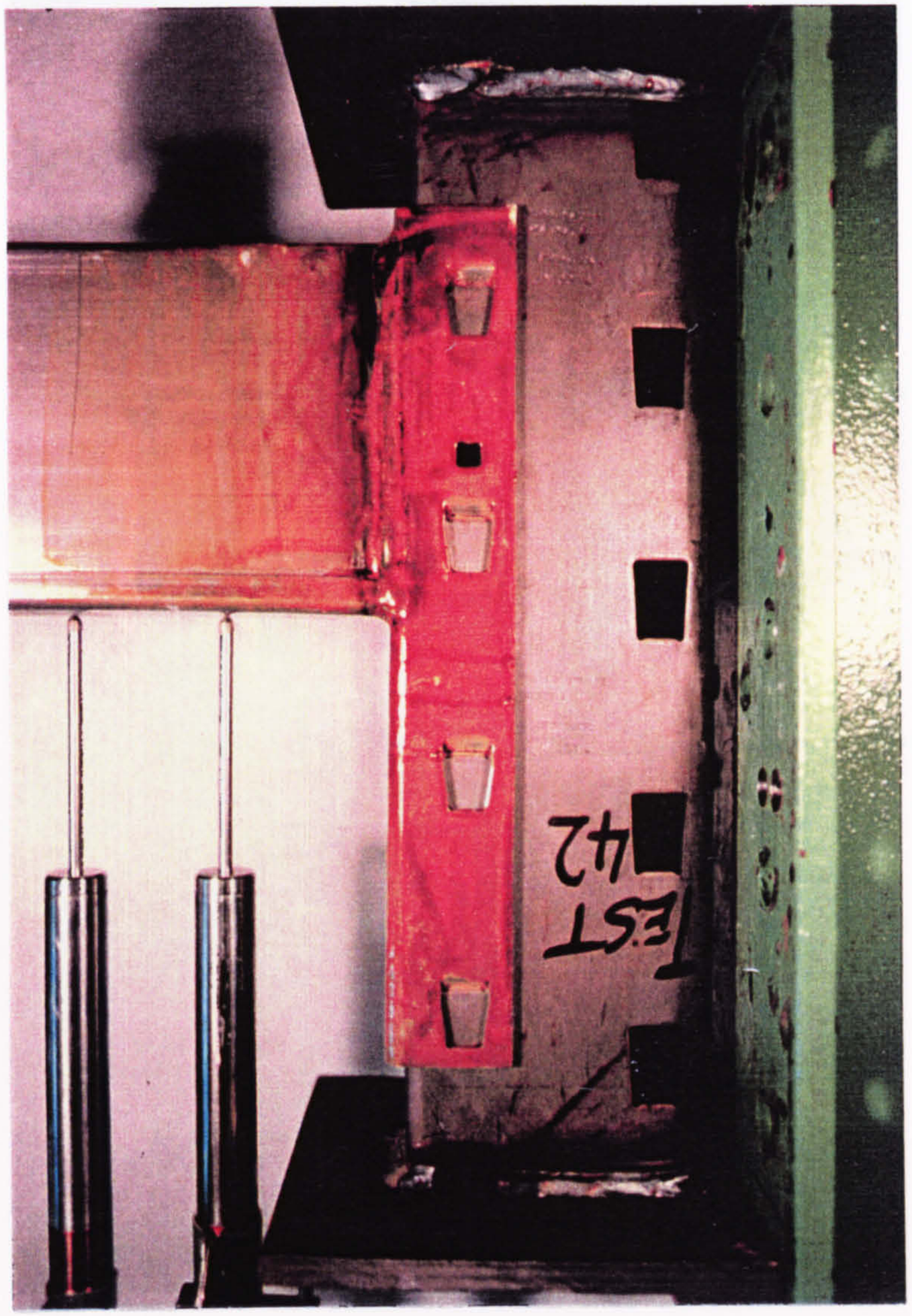

FIGURE 3.47

(b)

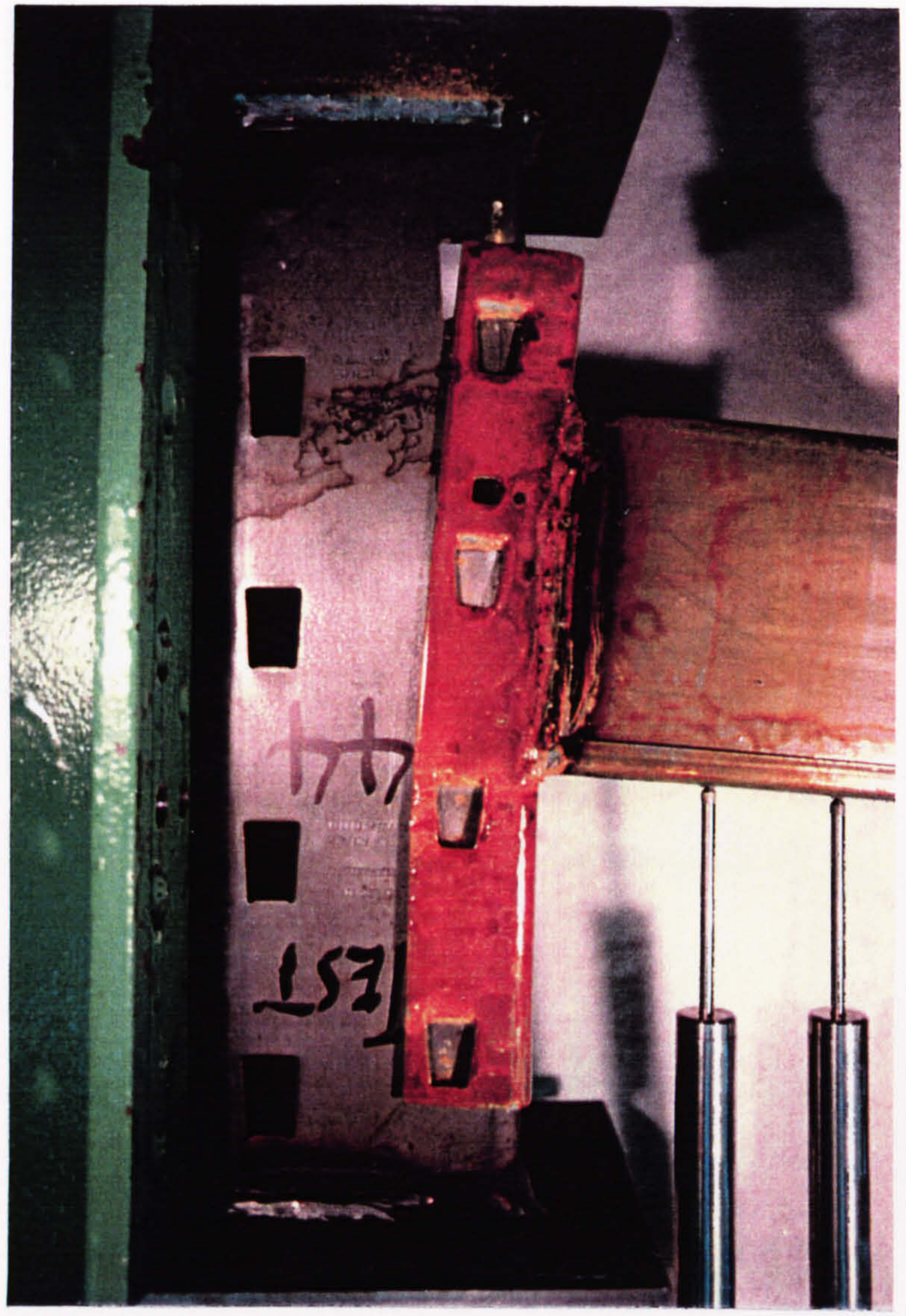

(a)

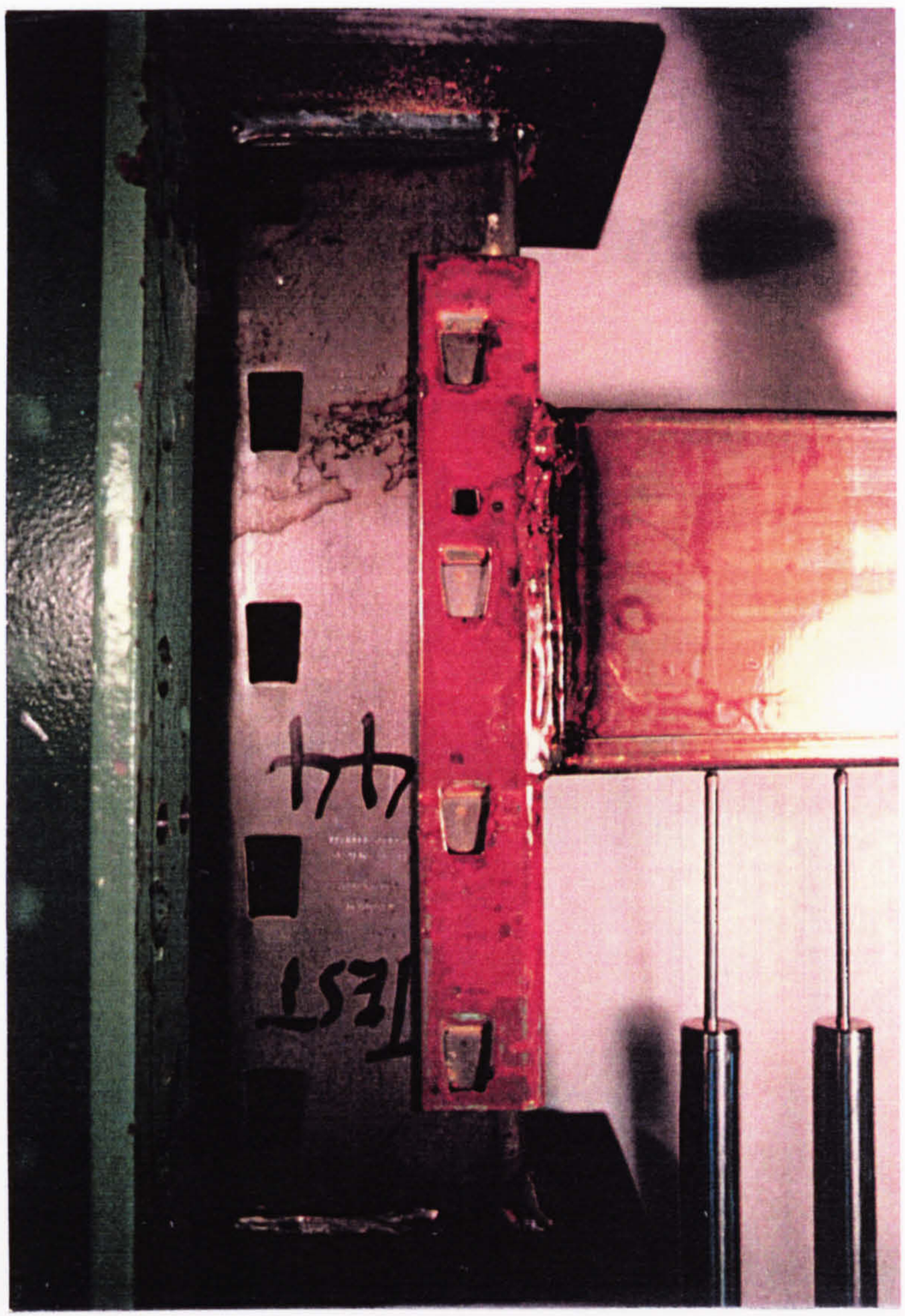

FIGURE 3.48

(b)

(a)

FIGURE 3.49

(b)

(a)

FIGURE 3.50

(b)

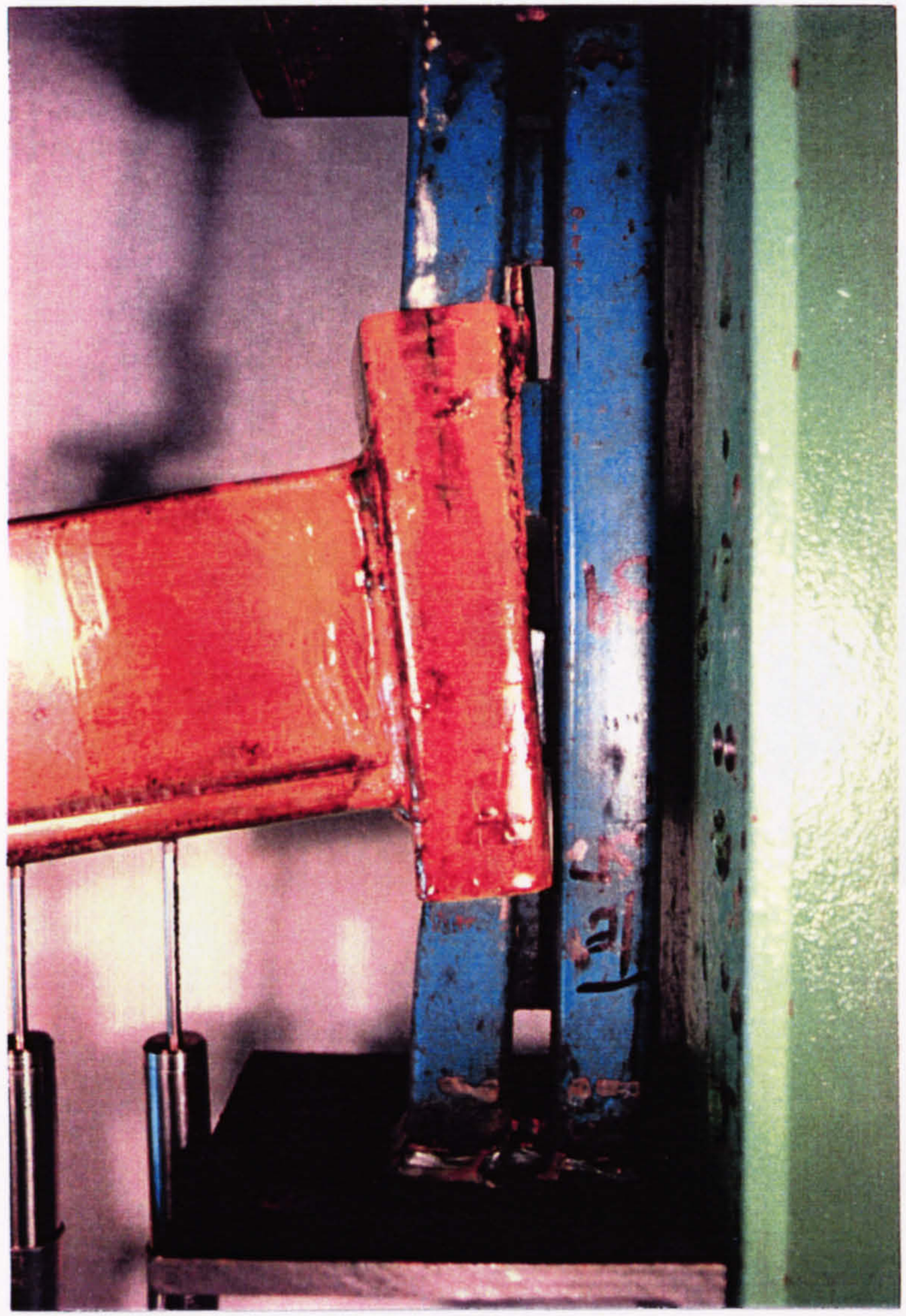

(a)

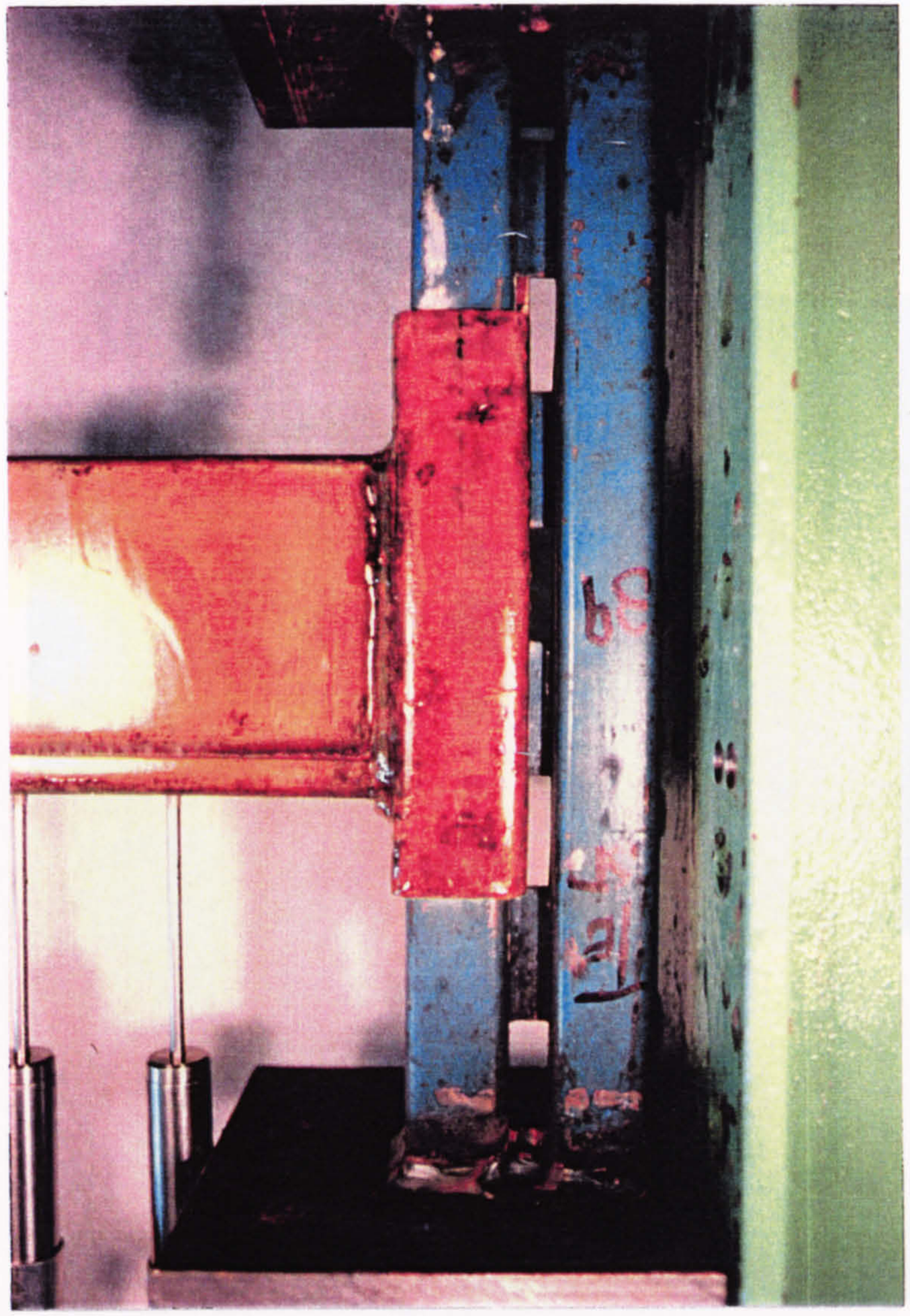

FIGURE 3.51

(b)

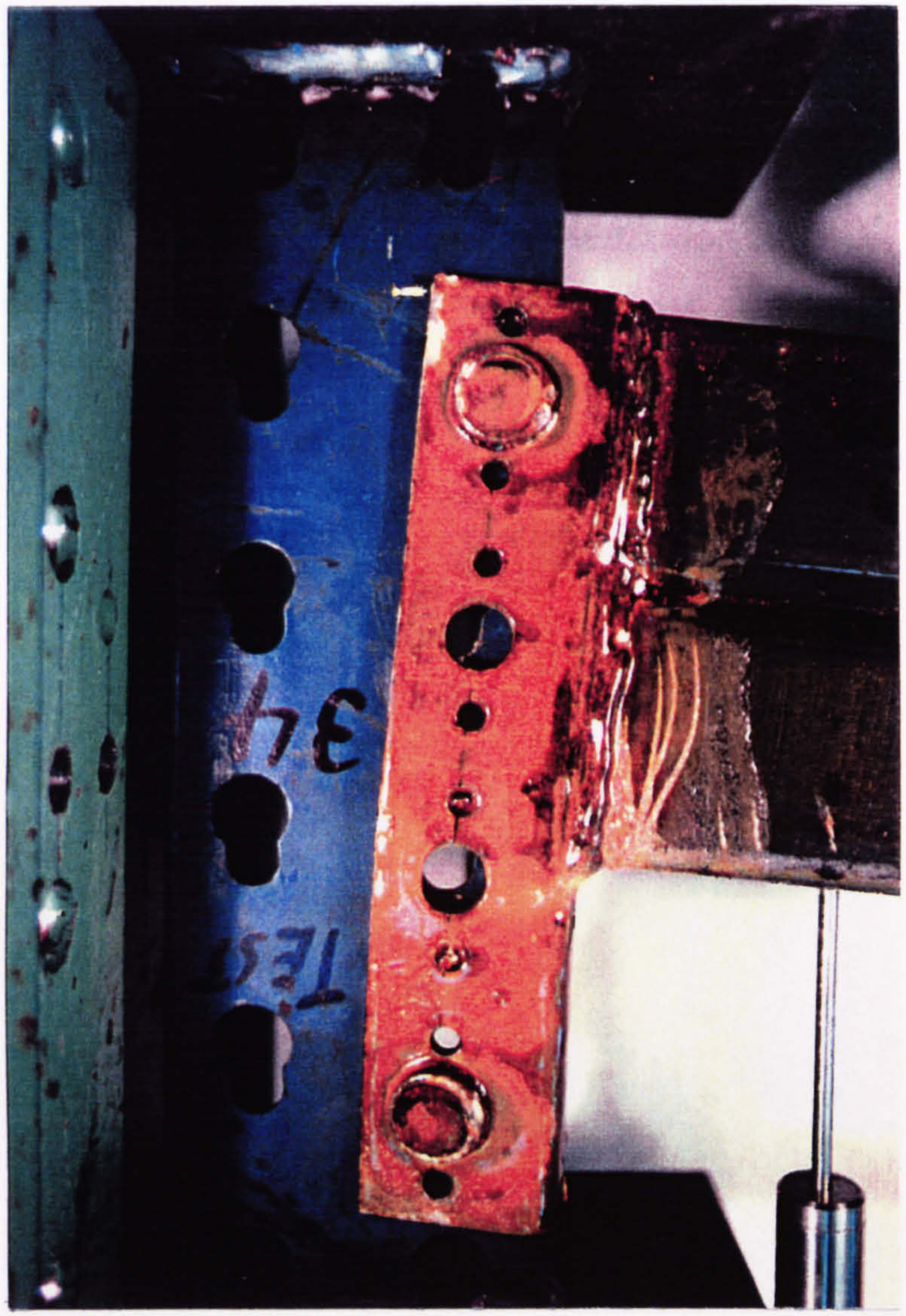

(a)

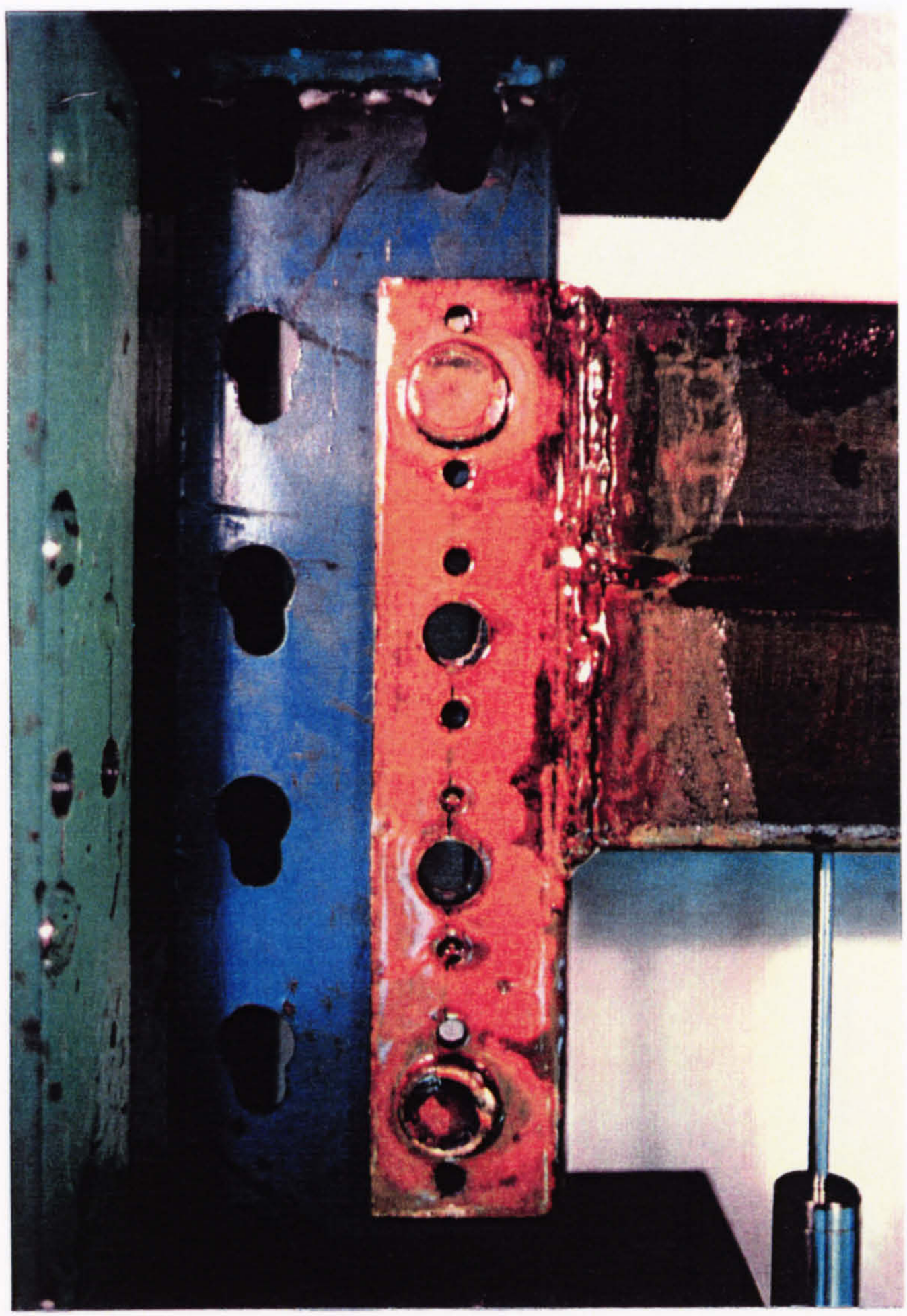

FIGURE 3.52

(b)

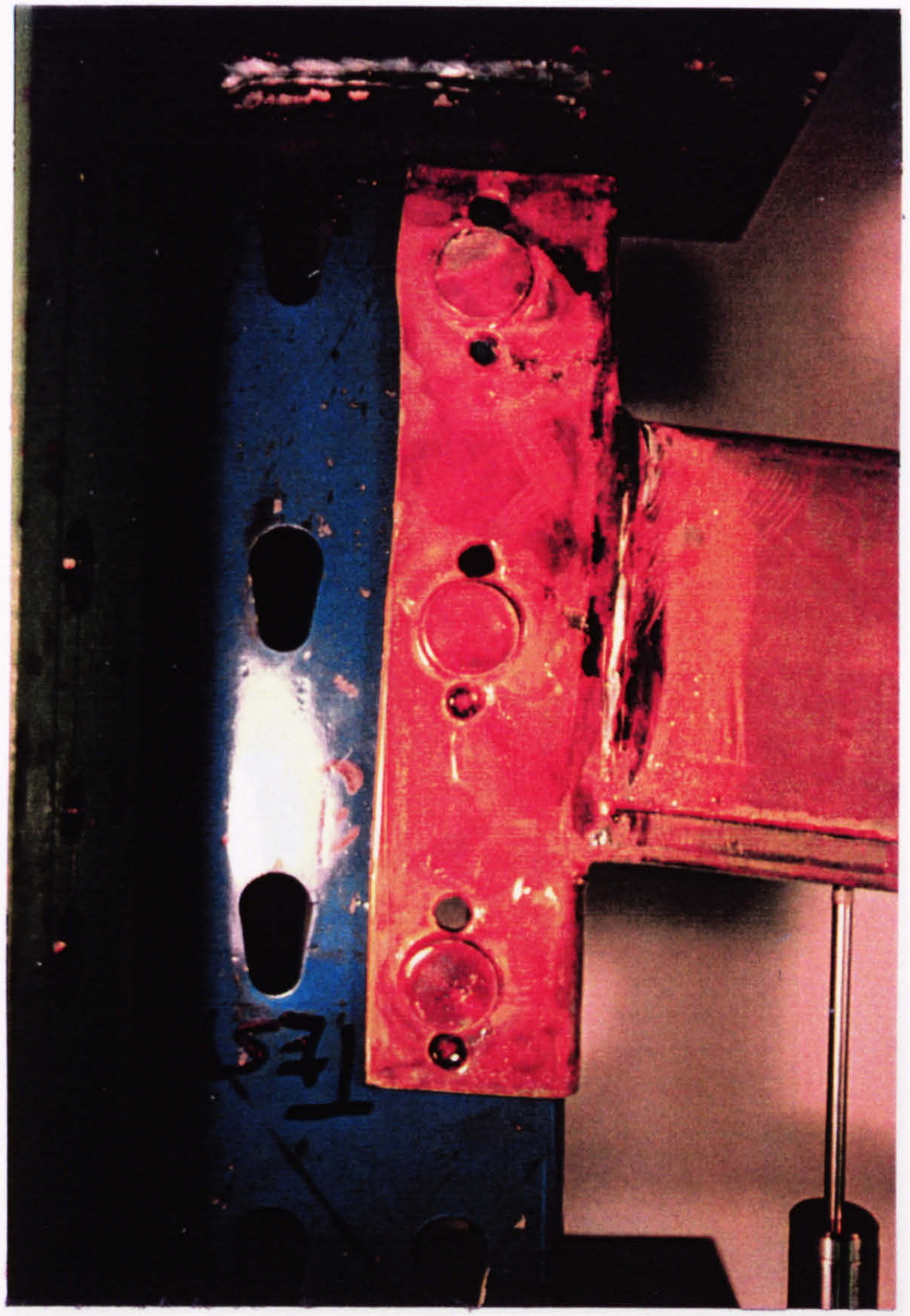

(a)

FIGURE 3.53

(b)

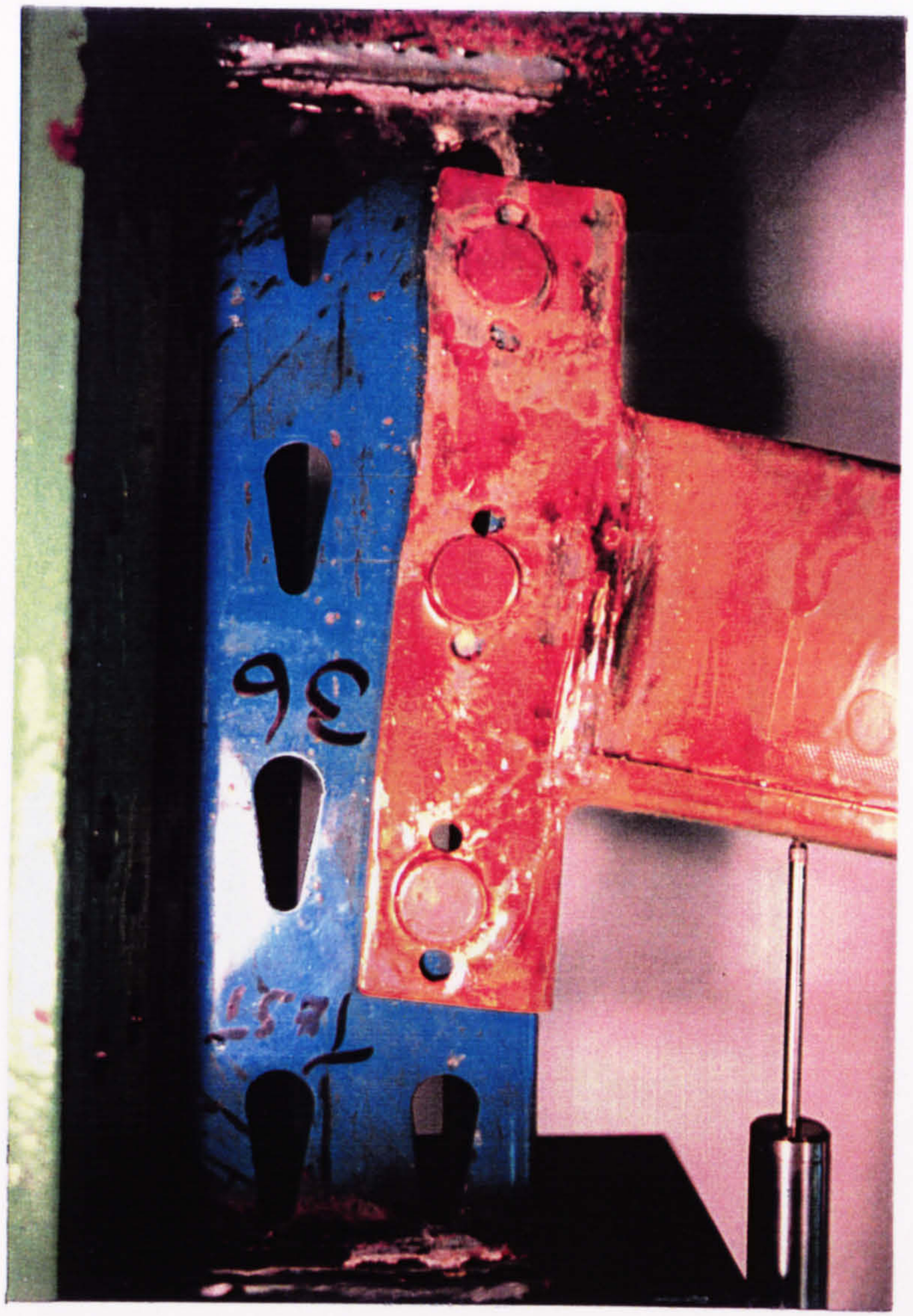

(a)

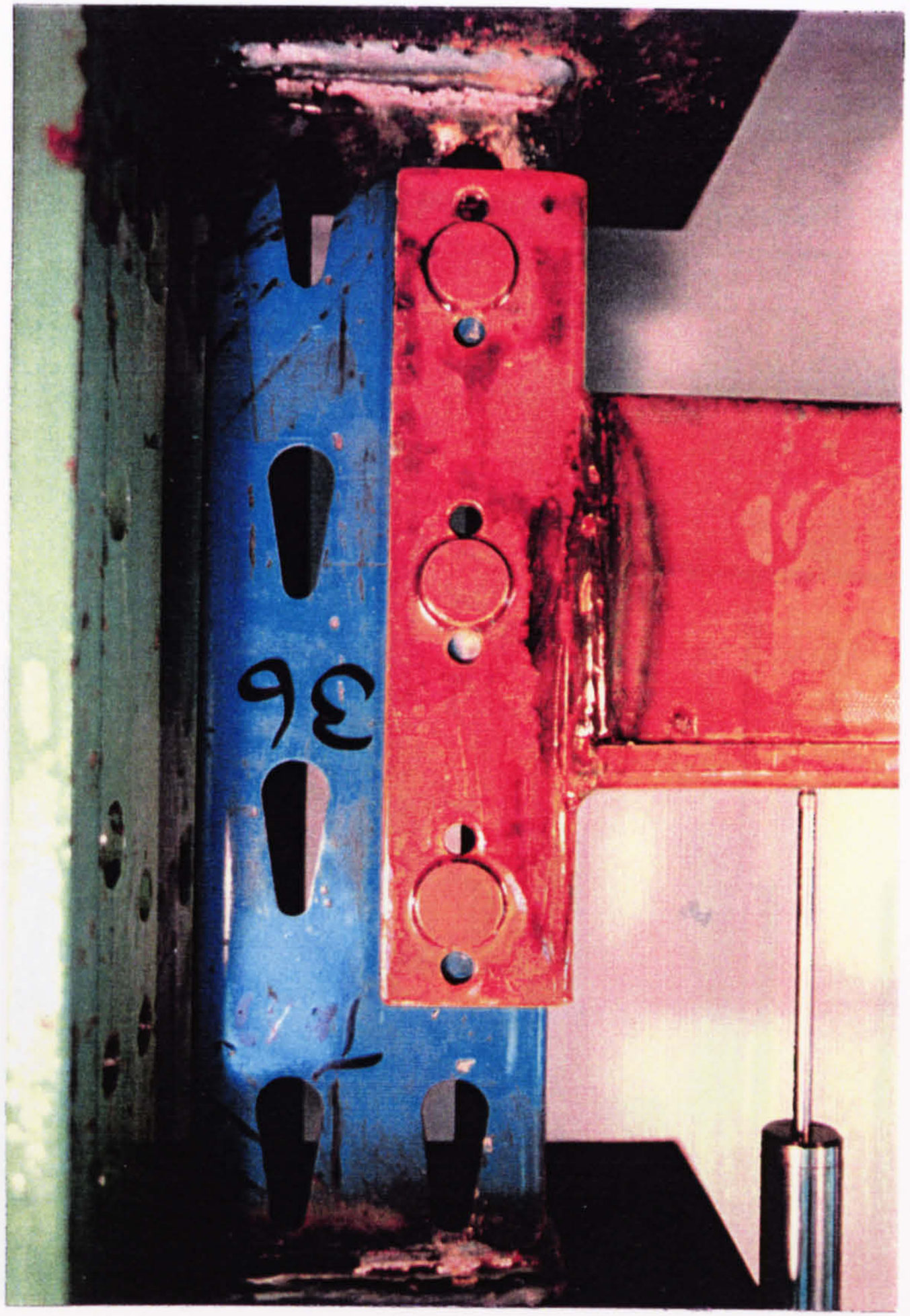

FIGURE 3.54

(b)

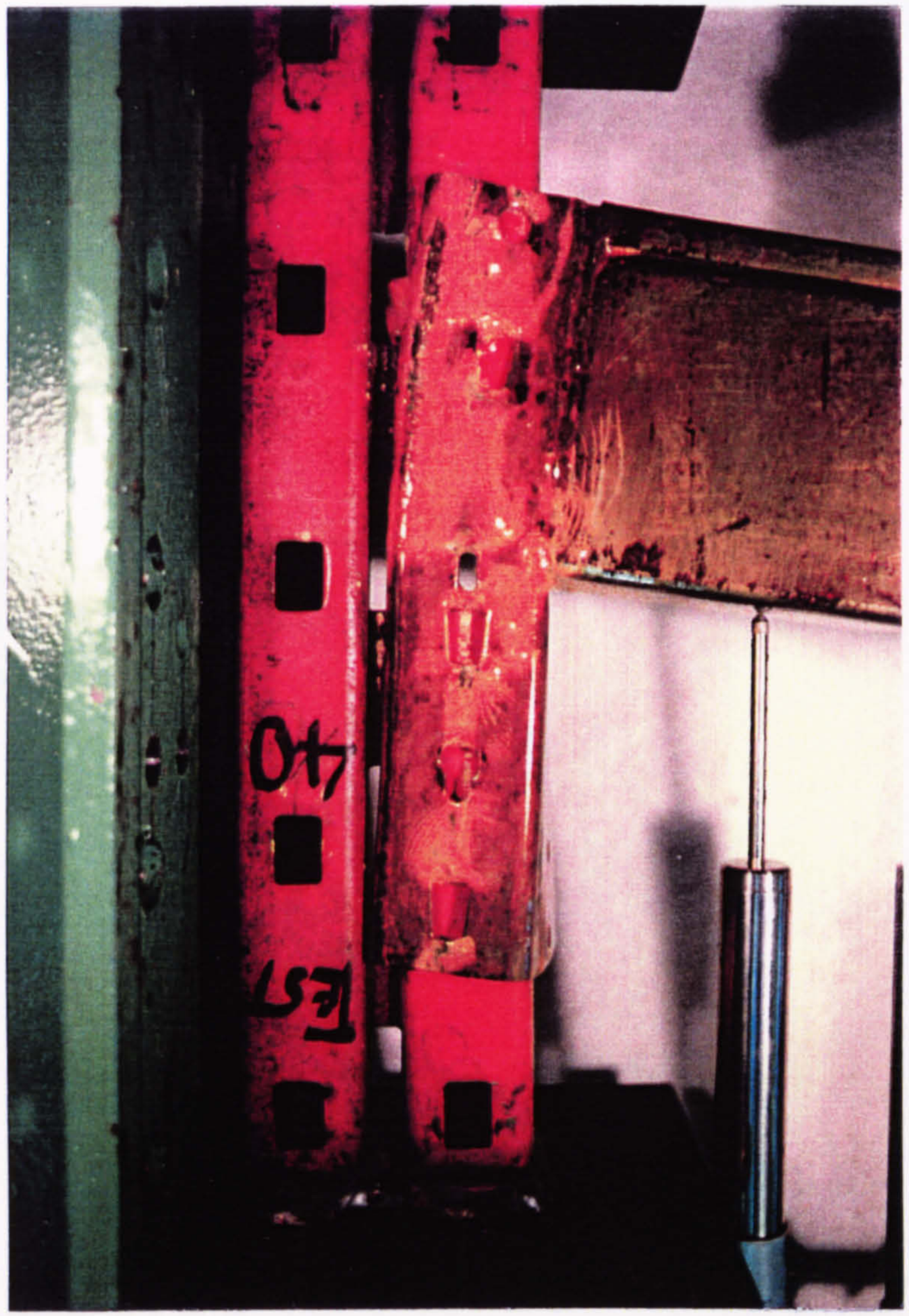

(a)

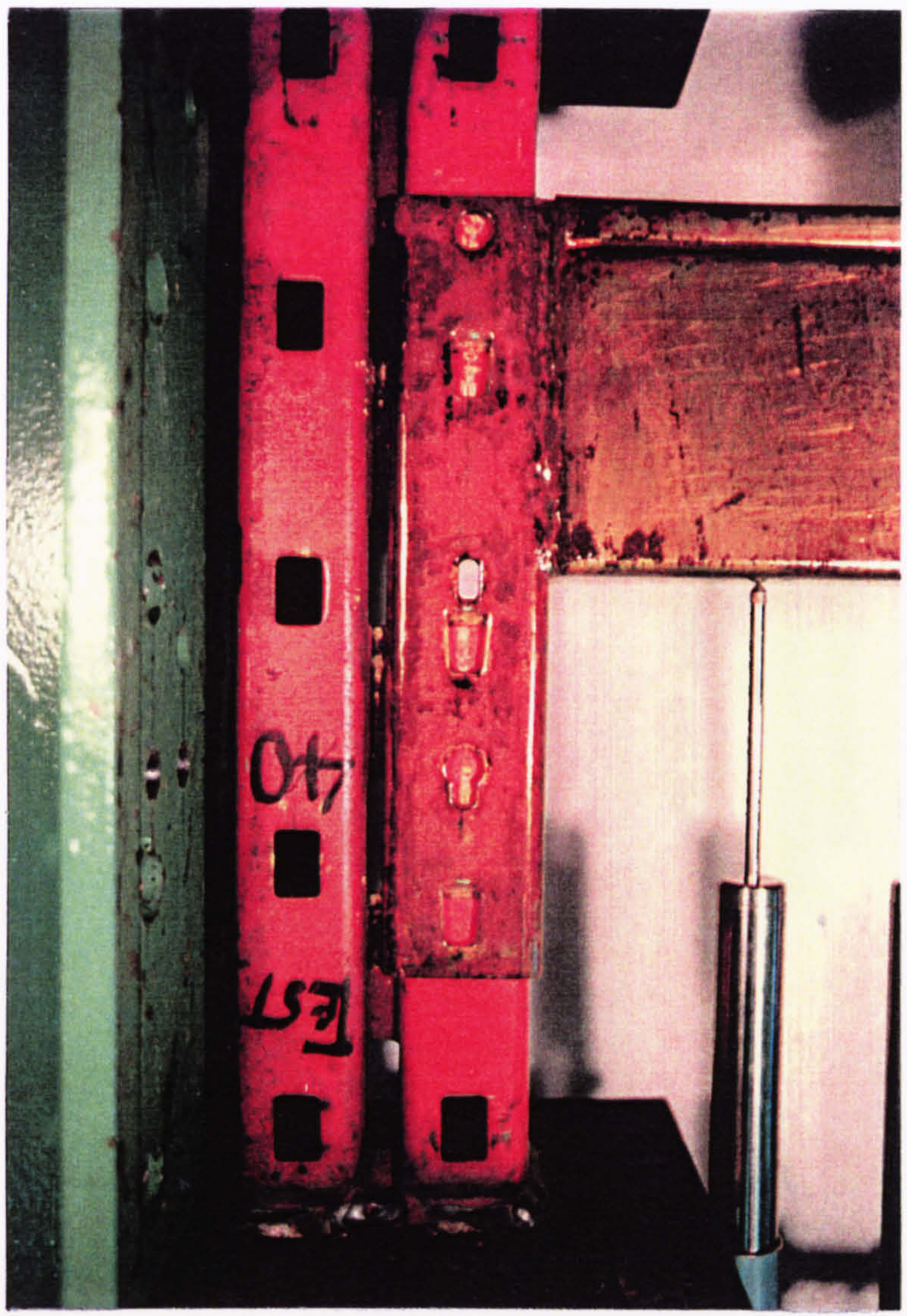

MOMENT-ROTATION CURVES
PSS IMPROVED 3 LUG-UP WELDED
PRODUCT 15

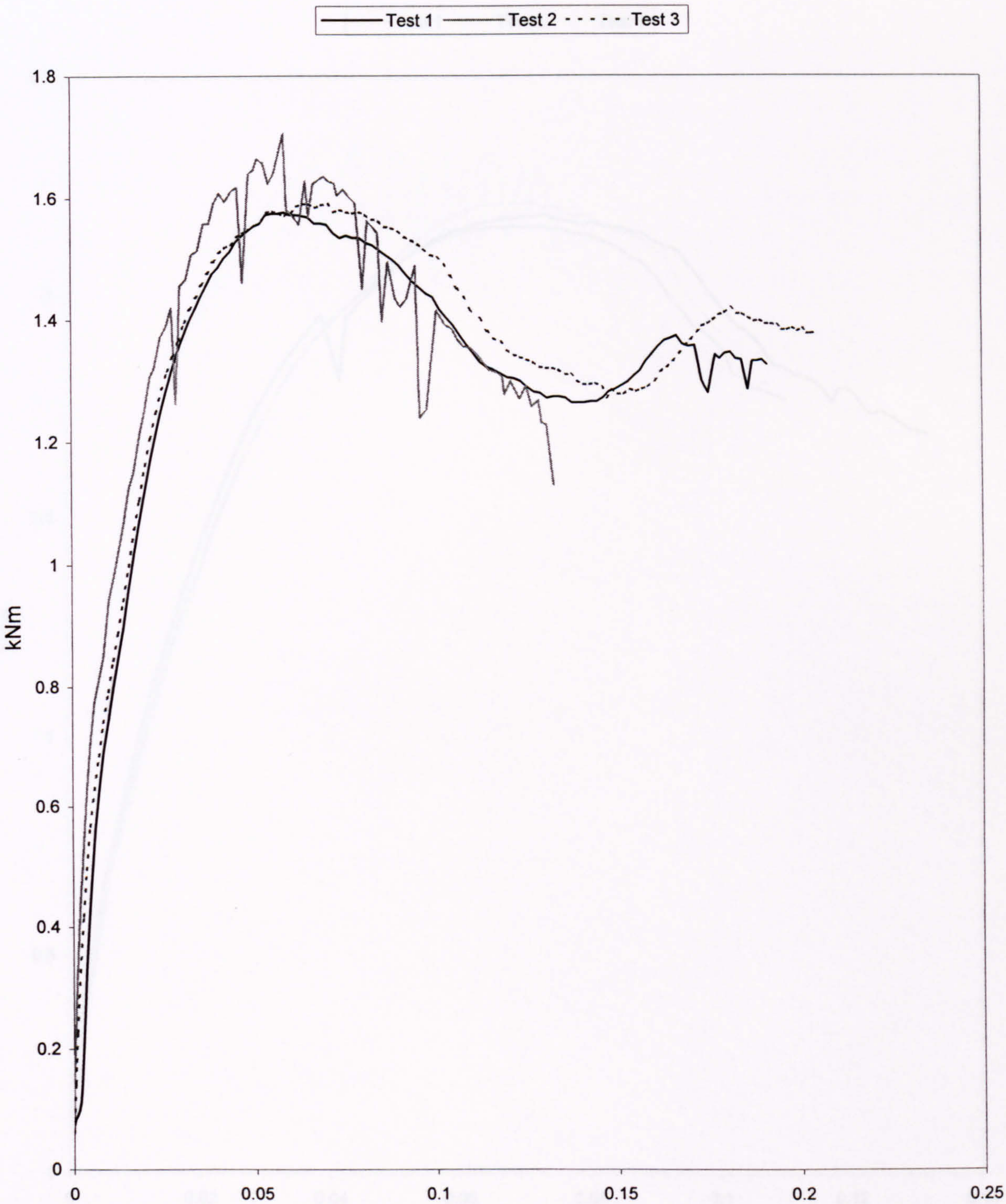

Figure 3.55

MOMENT-ROTATION CURVES
PSS IMPROVED 3 LUG DOWN WELDED
PRODUCT 16

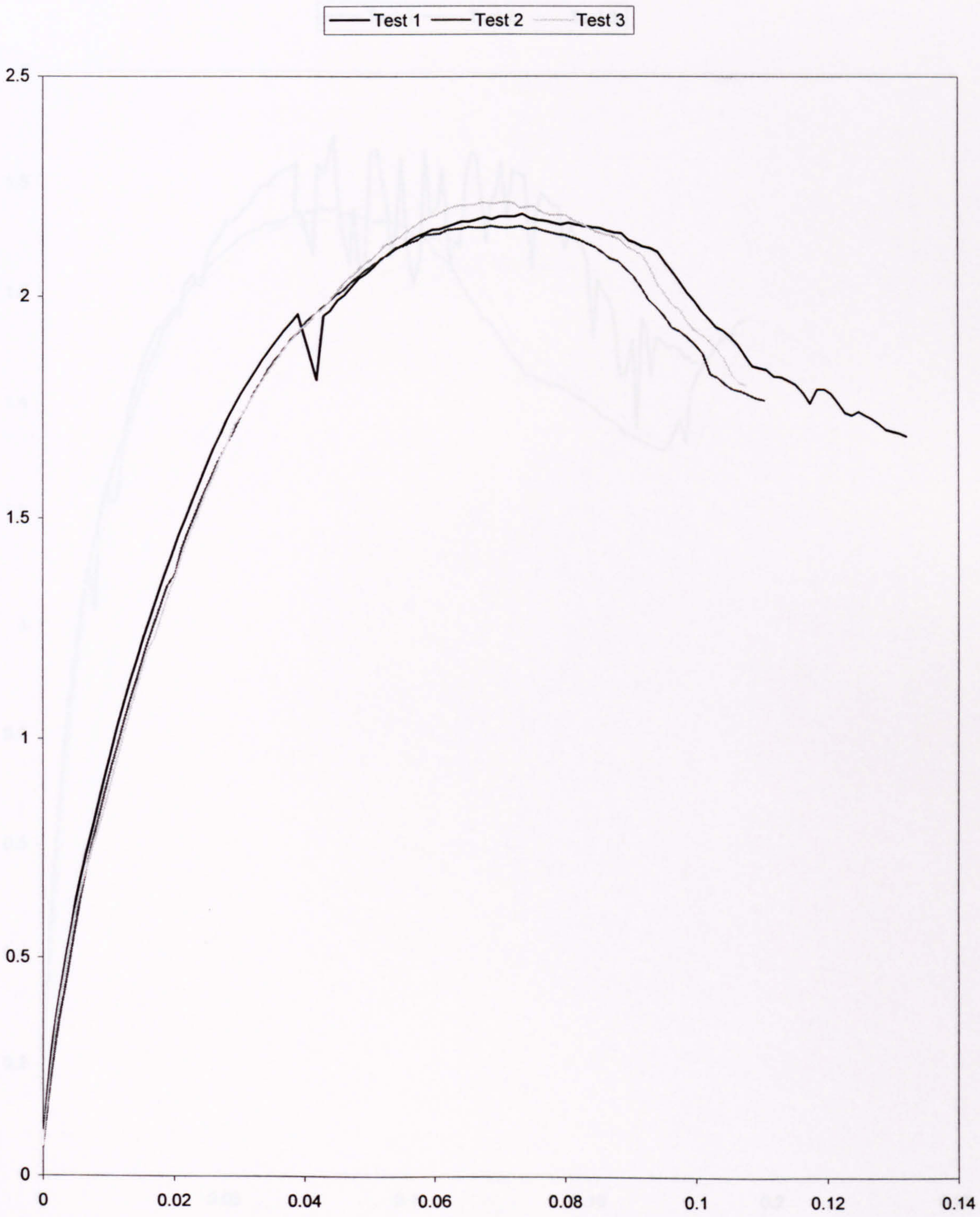

Figure 3.56

MOMENT-ROTATION CURVES
PSS IMPROVED 3 LUG-UP WELDED
PRODUCT 17

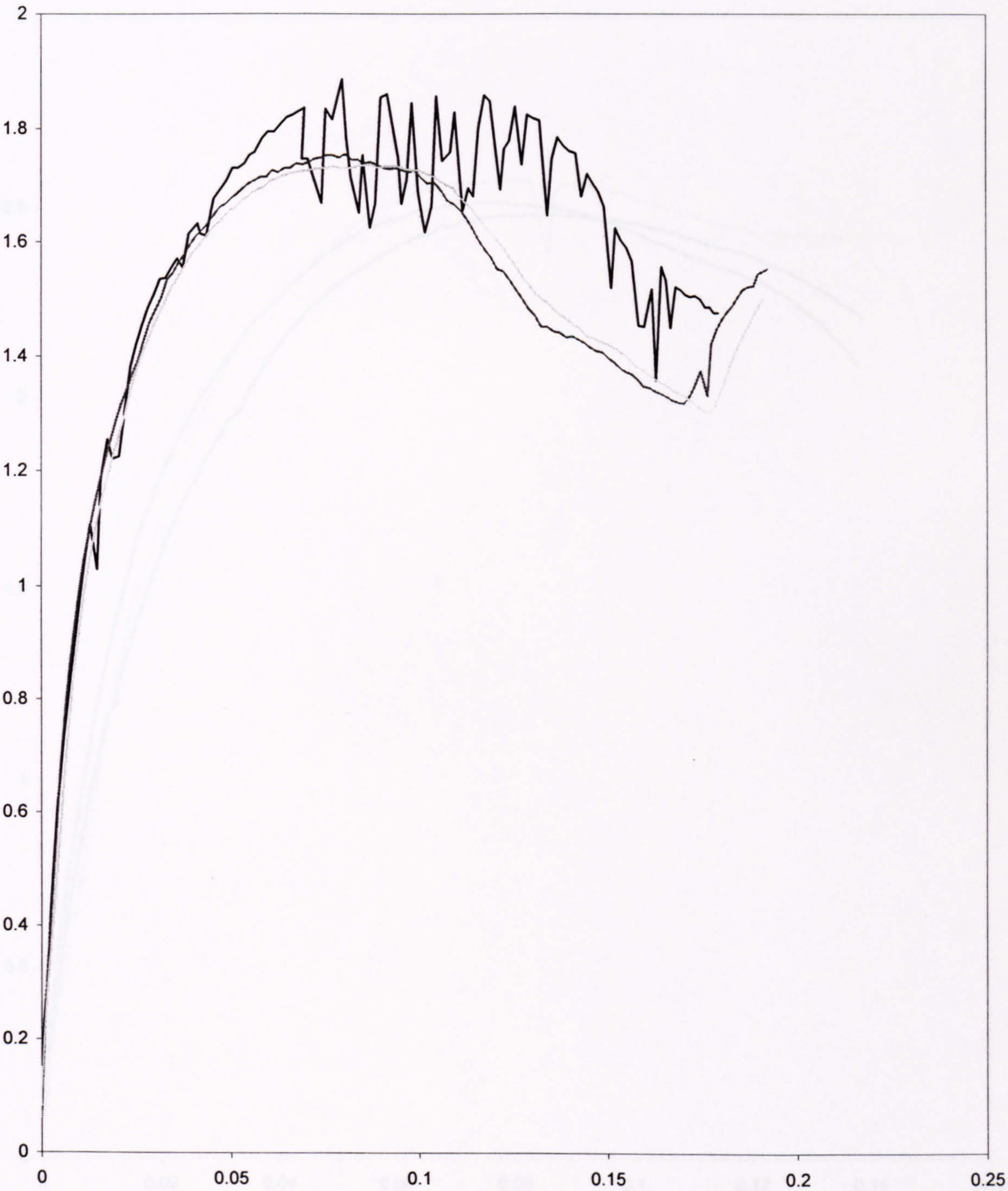

Figure 3.57

MOMENT-ROTATION CURVES
PSS IMPROVED 3 LUG DOWN WELDED
PRODUCT 18

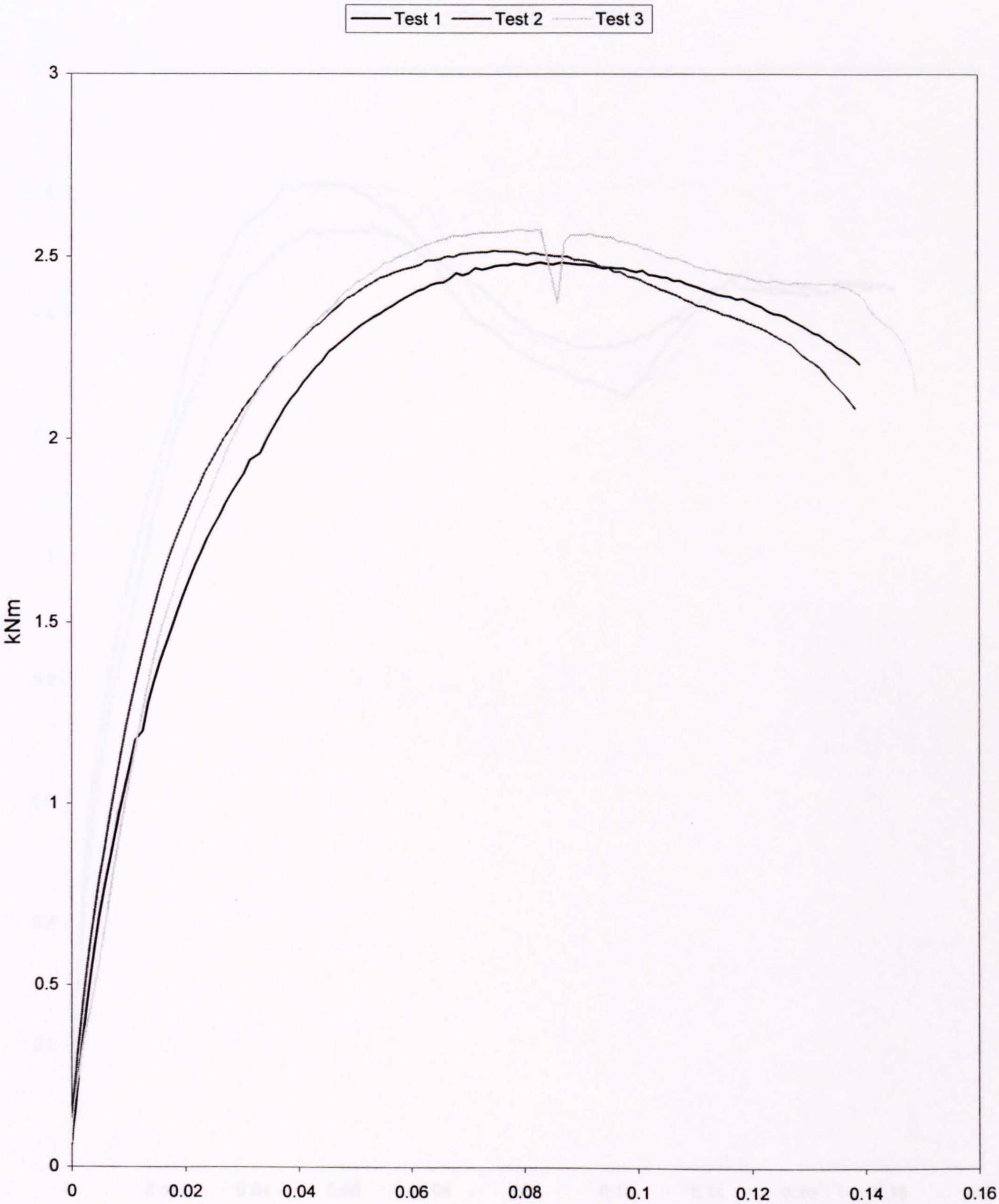

Figure 3.58

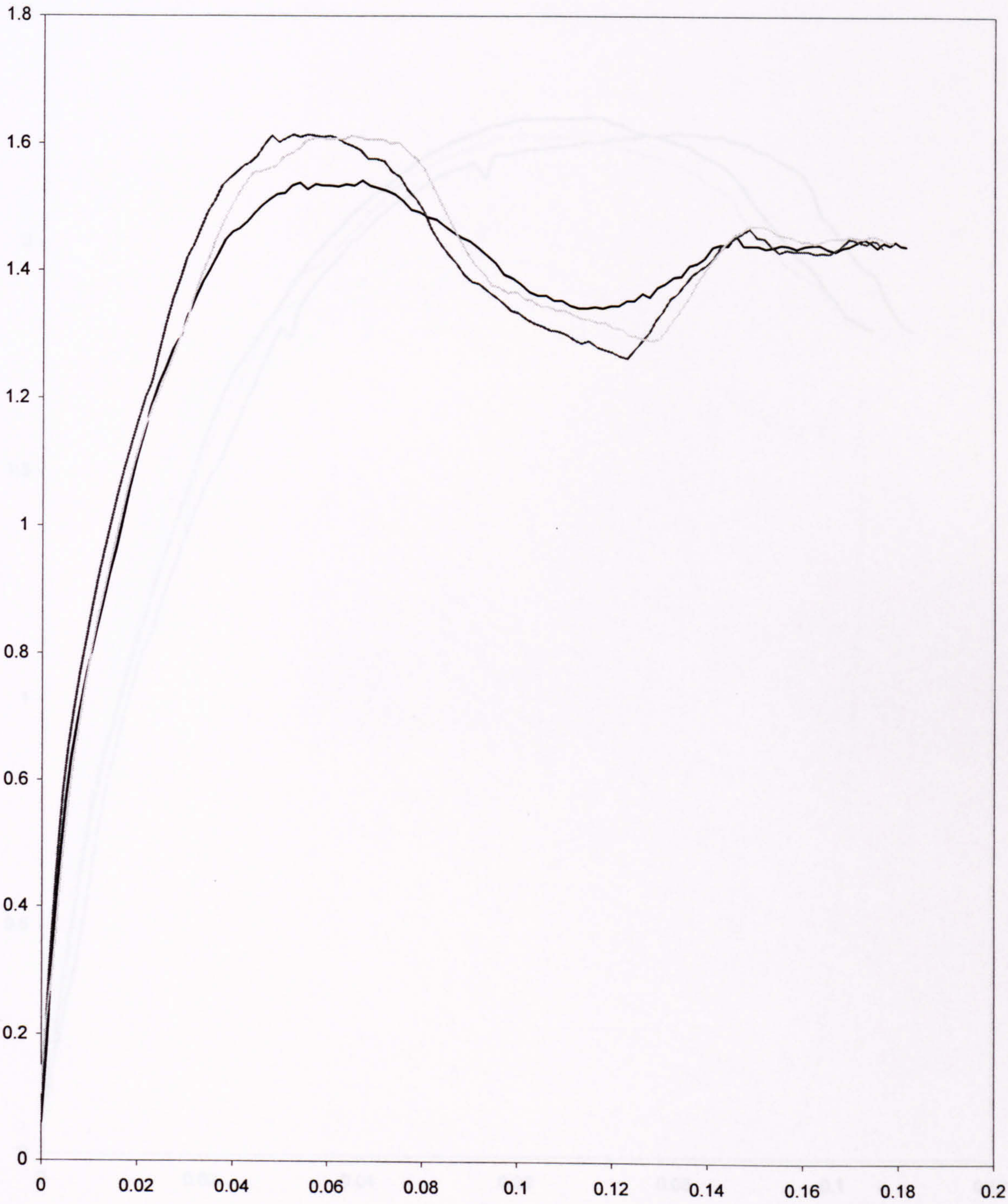
MOMENT-ROTATION CURVES
PSS IMPROVED 3 LUG UP WELDED
PRODUCT 19
Test 1
Test 2
Test 3
KNm
1.8
1.6
1.4
1.2
1
0.8
0.6
0.4
0.2
0
0
0.02
0.04
0.06
0.08
0.1
0.12
0.14
0.16
0.18
0.2
Radians

Figure 3.59

MOMENT-ROTATION CURVES
PSS IMPROVED 3 LUG DOWN WELDED
PRODUCT 20

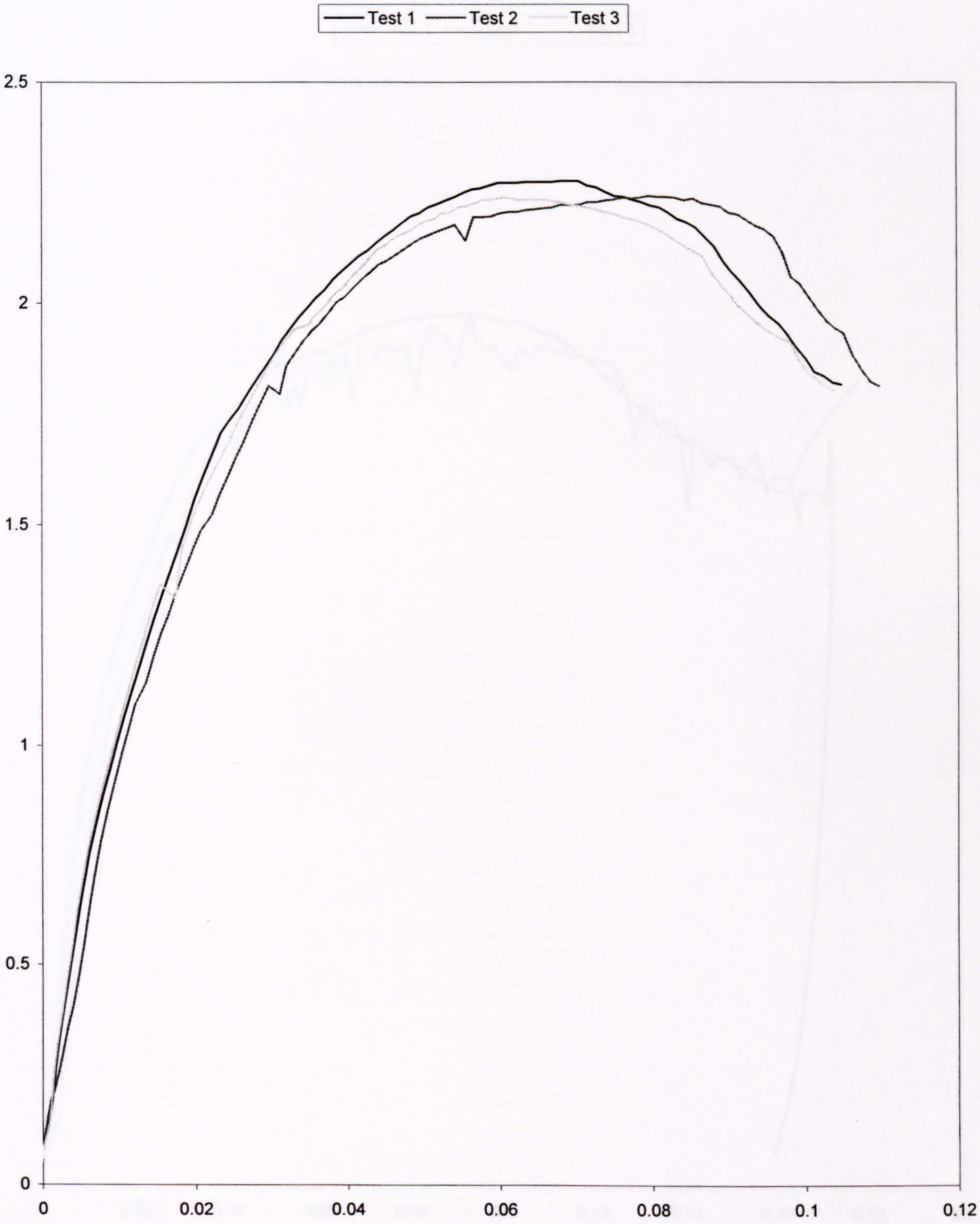

Figure 3.60

MOMENT-ROTATION CURVES
PSS IMPROVED 3 LUG UP WELDED
PRODUCT 21

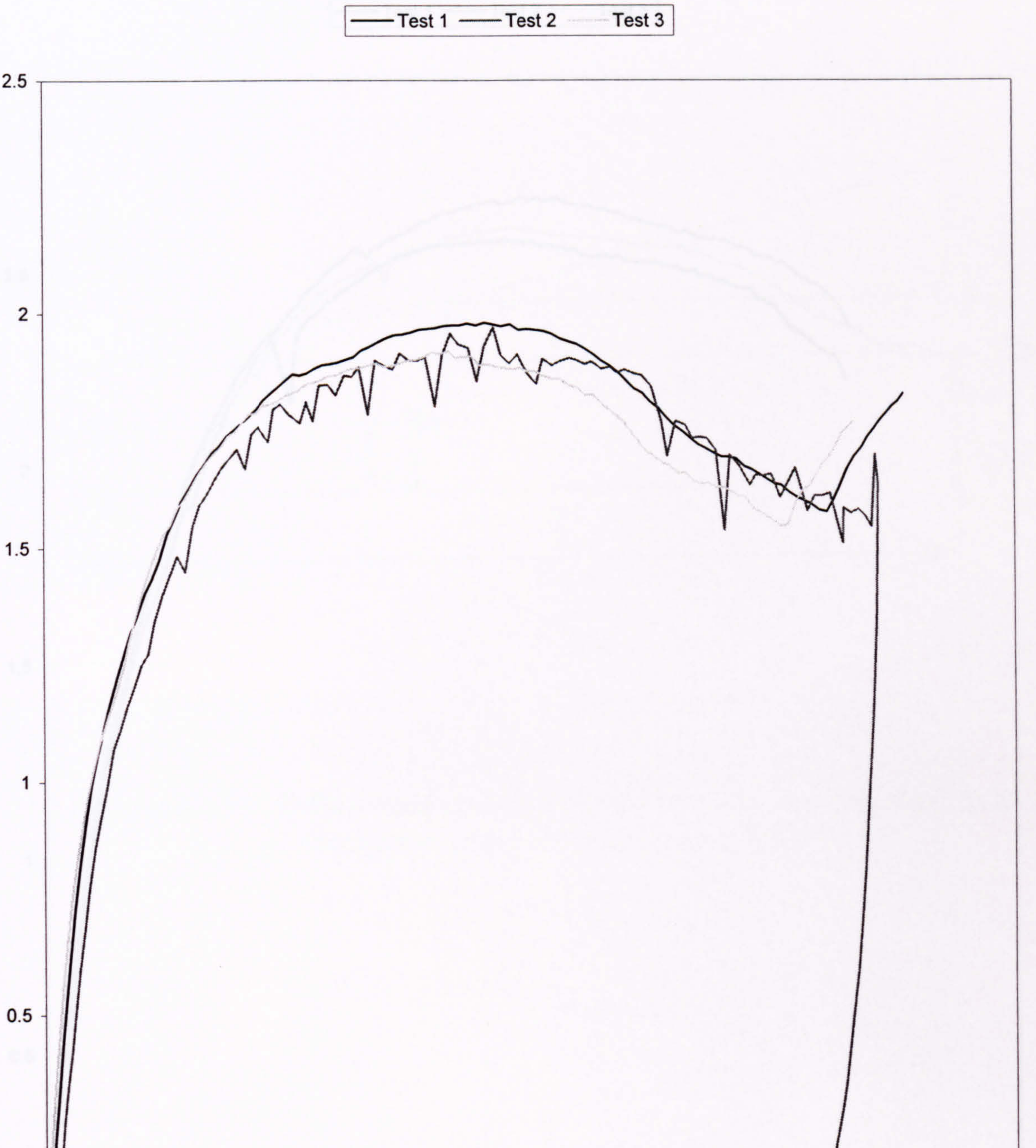

Figure 3.61

MOMENT-ROTATION CURVES
PSS IMPROVED 3 LUG DOWN WELDED
PRODUCT 22

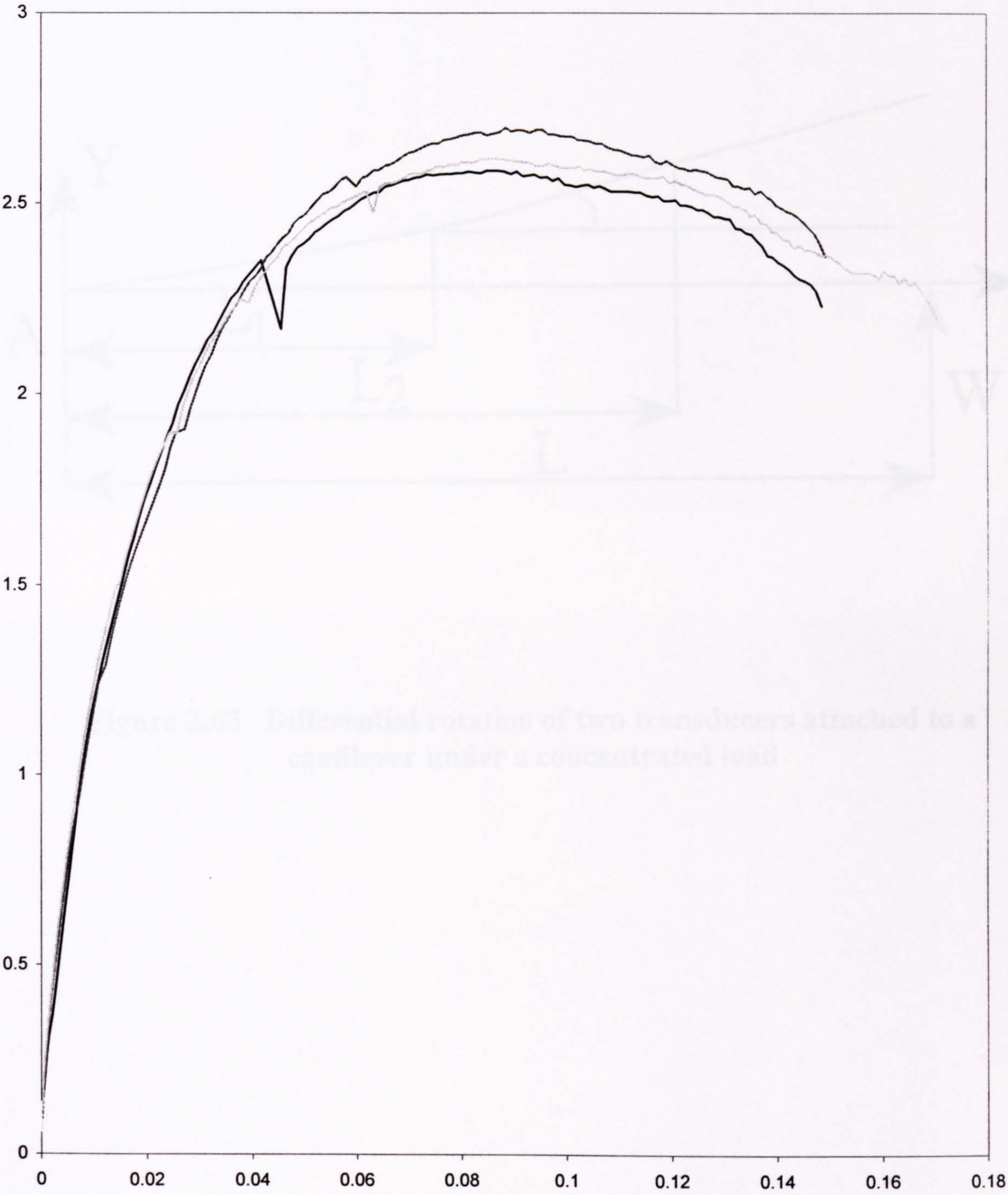

Figure 3.62

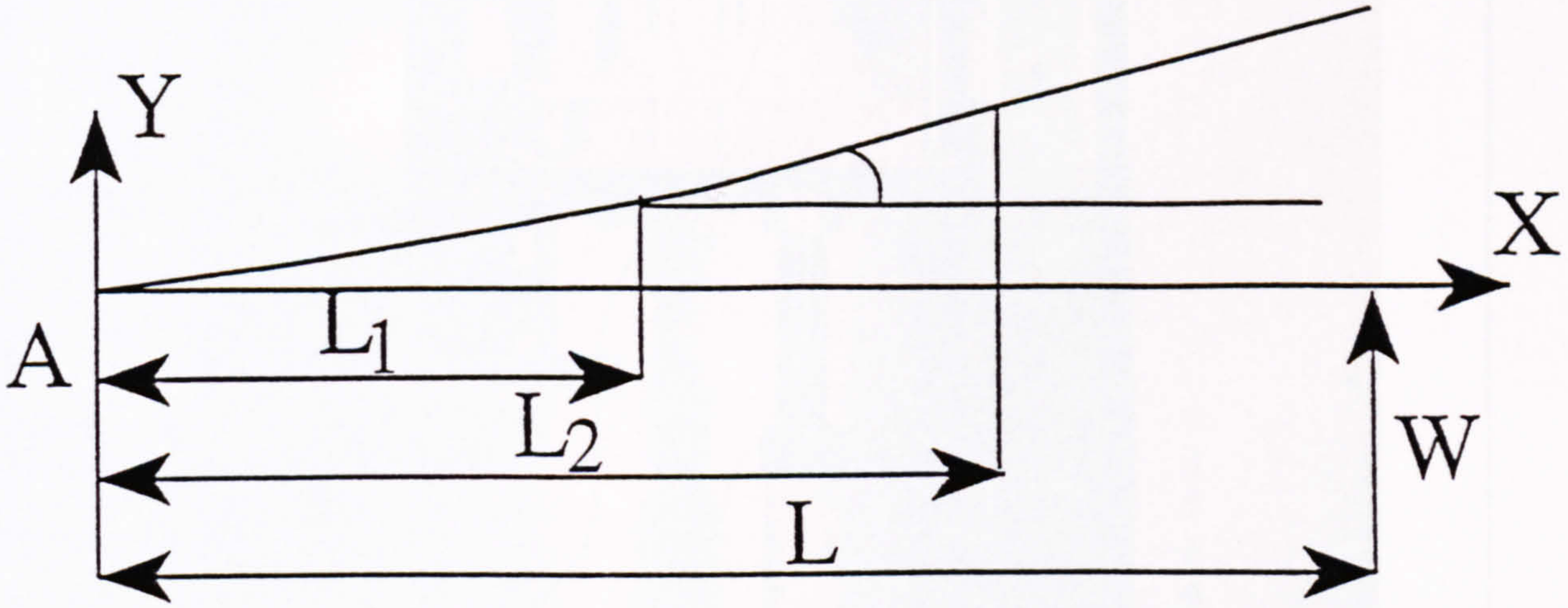

Figure 3.63 Differential rotation of two transducers attached to a cantilever under a concentrated load

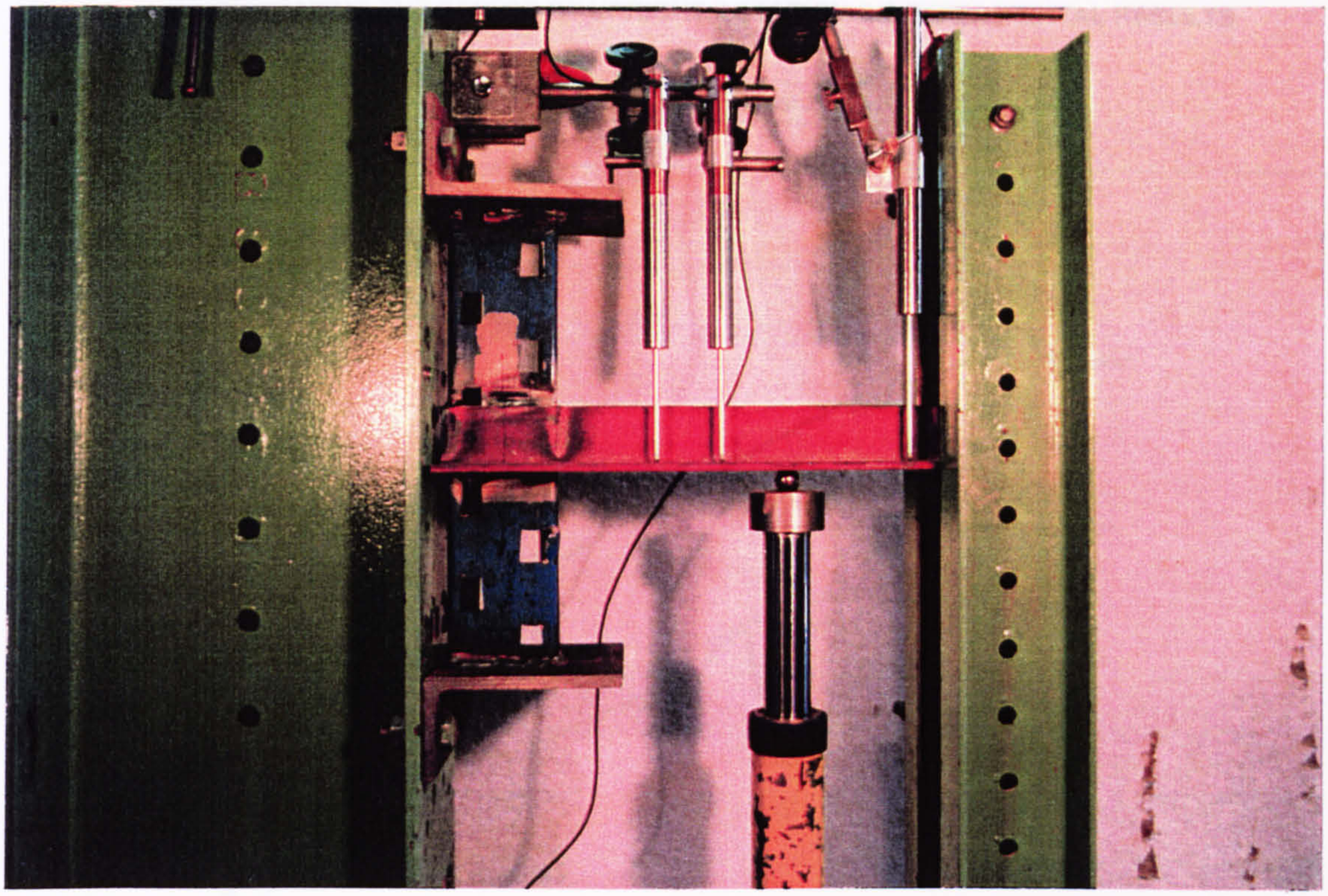

FIGURE 3.64

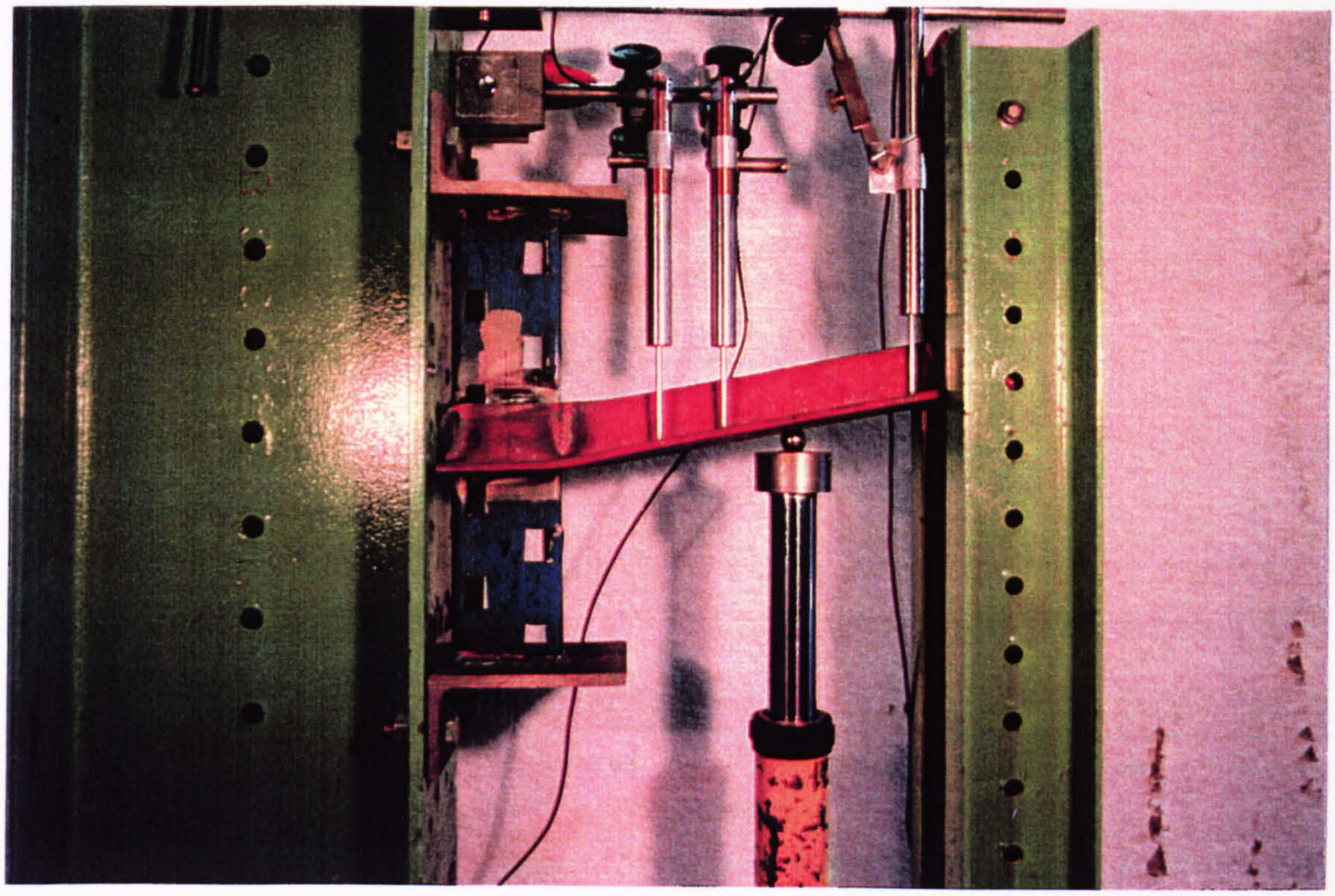

FIGURE 3.65

MOMENT- ROTATION CURVES
INVESTIGATING THE EFFECT OF UPRIGHT ROTATION ON EXPERIMENTAL RESULTS

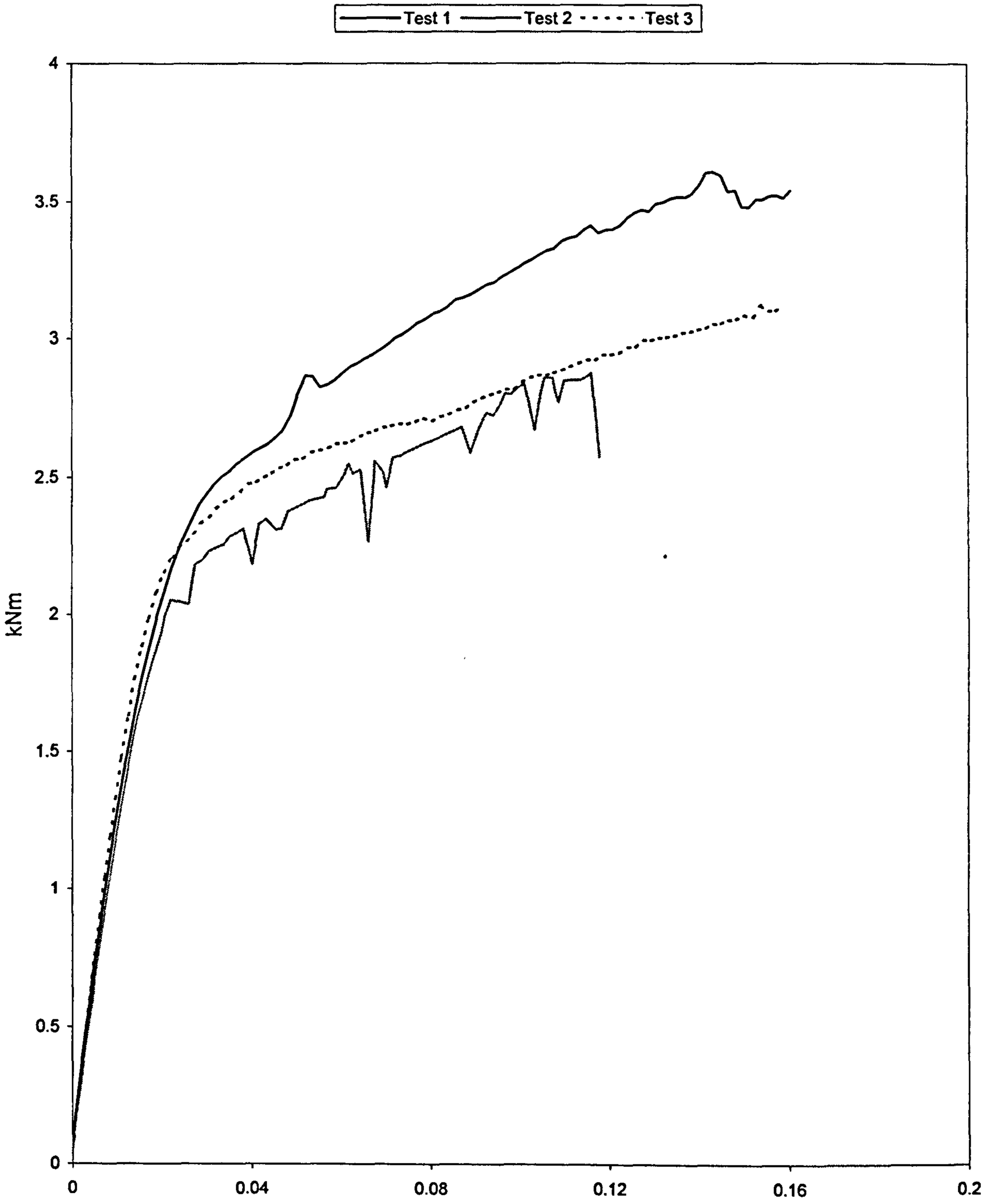

Figure 3.66

APPENDIX 3.1

Correction to Experimental Results

Derivation of stub beam rotation correction

The deflection profile of a cantilever under a point load is given by

$$y = \frac{Wx^2}{6EI}(3L - x)$$

Hence the difference in displacements between the two transducer positions at L_1 and L_2 is given by

$$\frac{W}{6EI}(3LL_2^2 - L_2^3 - 3LL_1^2 + L_1^3)$$

Apparent or theoretical rotation of the stub beam =

$$\frac{\text{difference in transducer displacements}}{L_2 - L_1}$$

Hence, if the experimental stiffness is k_E and the true stiffness is k_T we have:

$$\frac{1}{k_E} = \frac{1}{k_T} + \frac{1}{6EI} \frac{L_2^2(3L - L_2) - L_1^2(3L - L_1)}{L(L_2 - L_1)}$$

or

$$\frac{1}{k_T} = \frac{1}{k_E} - \frac{1}{6EI} \frac{L_2^2(3L - L_2) - L_1^2(3L - L_1)}{L(L_2 - L_1)}$$

APPENDIX 3.2

Correction to Experimental Results

Derivation of stub column rotation correction

The true beam end connector rotation is given by $\theta_T = \theta_E - \theta_B - \theta_U$

but $\theta_U = \theta_W - \theta_{BW}$

Where:

θ_E is the experimental beam end connector rotation

θ_B is the box beam rotation

θ_U is the stub column rotation

θ_W is the combined rotation of the stub column and angle stub beam section(rigid connection)

θ_{BW} is the angle-stub beam rotation

and hence

$$\frac{\theta_T}{M} = \frac{1}{k_E} - \frac{1}{k_B} - \frac{1}{k_W} + \frac{1}{k_{BW}} = \frac{1}{k_T}$$

Where k_T = true beam end connector stiffness.

CHAPTER 4

ELASTIC MODELLING OF BEAM END CONNECTOR

C H A P T E R 4

ELASTIC MODELLING OF BEAM END CONNECTOR

4.1 Introduction

As described in the previous chapters there are three types of structural connections, rigid, pinned and semi-rigid. The connection under consideration is semi-rigid, which derives its properties from an interlocking arrangement other than welds or bolts. In general, beam end connectors of this type are produced as the result of processes such as forming and punching. These methods produce "tabs" or "studs" which are the source of stiffness as they interlock with perforated uprights and engage against them under load, figures 4.1, 4.2 and 4.3.

The combination of a beam end connector, a beam and an accompanying upright form a joint whose strength and stiffness influence the value of the effective length factor for an upright being designed under sway conditions, MHR Godley[12].

Currently testing is the only way of determining the properties of such joints. As concluded in the preceding chapters a number of factors have been responsible for the absence of any modeling approaches which could either partially or completely predict the properties of boltless semi-rigid beam end connectors.

Amongst these were, as in conventional structural engineering, the historical trend that analyses of joints have always received secondary attention. Also, the fact that the structural analysis and design philosophy of rack structures have been until recently incoherent and isolated to individual nations with many gray and unresolved facets.

Consequently, only recently efforts have been made to try and homogenize the design approaches in Europe, Federation Europeenne De La Manutention[19], in the first instance, before any attention was paid to the analysis of the joints involved.

Furthermore, the experimental part of this work highlighted the complexities involved when determining the properties of a beam end connector. It showed that the behaviour of a beam end connector was sensitive to a large number of features and these features varied widely with different designs. So testing has always been regarded as the way to determine the properties of such joints, MHR Godley[12].

With no modeling approaches currently available, Finite Element techniques were used to model the behaviour of a typical beam end connector. The beam end connector in question was class A belonging to PSS Ltd., the original sponsor of the project, figures 4.1, 4.2 and 4.3.

To this end a number of modeling exercises were undertaken. The Finite Element program PAFEC-FE[25], was used.

The Finite Element modeling was carried out in two parts representing two distinct stages observed during loading of beam end connectors. Figure 4.5 shows the discretisation of the beam end connector. Figure 4.6 shows the discretisation of the stub beam and beam end connector assembly.

Figures 4.7 and 4.8 show the undeformed Finite Element model.

The first part related to the initial stages of loading when the end plate below the beam was free to move. This part of the end plate is referred to as the compression zone, figure 4.6. Figure 4.18 shows the model simulating this movement. The movement usually occurred between 0-40% of the total loading value on a test. The exact value of the load at which this occurred depended on the design of the beam end connector.

Figure 4.2 shows the force components responsible for the resistance to rotation at this stage. The directions of the forces were typical of all the beam end connectors with symmetrical welding arrangements.

The second part would simulate the stages during loading when the end plate below the beam came in contact with the side of the upright. Figure 4.9 shows the deformed structure.

The first part is referred to as free compression zone and the second part as restrained compression zone.

In both scenarios absolute restraints were applied to the tabs to simulate their interaction with upright's web, figure 4.2. Absolute restraints were also applied to the end plate below the beam to simulate the compression zone.

4.2 Aims

The aims were, using the parameters identified through the experimental part

a. to simulate the overall deformation shape

b. to establish the stress distribution involved

c. to estimate the initial stiffness values

d. to investigate various methods by which initial stiffness values can be determined and compared.

4.3 Finite Element modeling-global

The three possible welding positions as described in 3.4.1 are shown in figure 4.4. As the most common position of welding, the symmetrical welding arrangement was chosen for the purpose of this work. The term global modeling was used to imply the assessment of beam and beam end connector as an assembly.

The following assumptions were made when generating the global models,

1. Once the tabs are punched and formed they become thinner than the parent metal. They are also rounded due to the forming operation. This mainly applies to the bearing blocks 5, 6 and 7 shown in figure 4.5.
   For simplicity it was assumed that the gauges of these blocks remained the same and the radii associated with their curvature was ignored.

2. Usually the beam's width is smaller than the depth of the beam end connectors end plate, dimensions b1 and b, figure 3.20. The reason for this is to allow room for welding of the beam to the connector. As shown in figure 4.6 these two dimensions were taken to be equal.

3. The radius associated with the 90° bend in the beam end connector was represented using a corner block as shown in figure 4.5.

4. Tooling and drainage holes and slots usually associated with this type of connectors were not included. The tooling holes are produced during manufacture and are used for handling the component during multi stage operations. The drainage slots are required to allow water drainage after a beam and beam end connector assembly has been washed ready for paining.

5. The stiffening effect of the welds were ignored

4.3.1 Mesh generation

Initially the beam end connector was divided into twelve blocks, figure 4.5, with the stub beam treated as one solid block. This proved to be too rigid and resulted in negligible deformation in the rest of the structure, namely the beam end connector and in particular the plate containing the tabs. Later, it was decided to model the stub beam as a hollow section.

To simulate a hollow beam the core material of the solid beam was removed by reducing the value of its flexural rigidity. This idea was soon abandoned for a more direct approach to ensure better accuracy and quicker processing time.

Consequently it was decided to, actually model the stub arm as a hollow section using four blocks, figure 4.6. This meant increasing the number of blocks from thirteen to sixteen in total, with twelve of them dedicated to the beam end connector itself.

Initially a relatively coarse mesh for the overall beam end connector was considered. To refine the mesh in the areas of interest, namely the tabs and the plate containing the tabs, i.e. figure 4.5 blocks 1, 5, 6, 7, 8, 9, and 10, three available options were considered.

Firstly, to stay with the same type of block and directly refine the mesh by adopting finer spacings. Secondly to use a combination of a twenty and eight node isoparametric brick elements to account for the critical and less critical regions respectively. Thirdly, to consider using "transition blocks". These blocks allow gradual mesh refinement to extend to the critical regions, where they are required. This was done through generating fanned mesh patterns.

Due to the excessively large working files and the inability of the system to cope, the second option had to be abandoned. The third option however was thought to be too elaborate for this part of the work and was finally rejected in favour of the quicker, more straight forward approach, i.e. the first option. This was to model the structure using the eight node isoparametric brick element combined with progressive mesh refinement of the tabs and the plate containing them.

A convergence study showed that to ensure continuity in the regions of interest, the use of a " COUPLING" facility would be required. The function of this facility was to control the varying degrees of freedom resulting from two interfacing blocks with different mesh densities.

4.3.2 Anchorage-sources of resistance to rotation

Based on the experimental observations made, when a beam end connector was loaded, figure 3.24, there were two distinct sources of resistance to rotation that emerged at different stages.

Up to the first 4o% of loading, depending on the type of design, the only source of resistance to rotation was due to the bearing of the tabs on to the thickness of the upright's web within the perforation as the beam end connector engaged against it.

On further loading a hinge formed just below the beam where the stiffening effect of the beam terminated, figures 4.6 and 4.9. This then led to the lower end of the end plate bearing against the upright's flange and a compression zone began to form.

To simulate the initial stages of resistance to loading, absolute restraints were applied to the tabs only, allowing the part of the end plate below the beam to move. This was termed free compression zone, figure 4.18.

In a separate model absolute restraints were added to simulate the bearing of the end plate below the beam against the upright's flange. This was termed restrained compression zone, figure 4.9.

It was also decided that the two scenarios relating to the stages before and after compression zone formation be considered separately.

The latter scenario was considered first

4.3.2.1 Anchorage-simulating the sources of resistance to rotation-the restrained compression zone scenario (restraining tabs and end plate below stub beam)

Table 4.1 shows the top, middle and the bottom blocks responsible for the interaction with upright's web thickness. These are blocks 5, 6 and 7 extracted from either figure 4.5 or 4.6. Each block shows the relevant nodes where restraints were applied to simulate bearing against the upright's web.

To investigate the effects of number and directions of the restraints employed, six different cases were examined. These are tabulated as GM1A to GM6A, these two being the two extreme cases, table 4.2.

In each case the numbers 1, 2 and 3 denote restraints in X, Y and Z directions. As observed from numerous tests, for the symmetrical welding position, the directions of forces in the two top tabs were opposite to the one at the bottom. This has been taken account of accordingly and are shown on each tab, table 4.2.

To simulate the locking action in the compression zone the nodes in the bottom part of the end plate, below the beam's bottom flange were restrained in the X-direction only, figures 4.6 and 4.9.

4.3.2.2 Anchorage-simulating the initial sources of resistance to rotation-free compression zone-scenario (restraining tabs only)

Table 4.3 shows the six cases considered, the two extreme cases being GM1B and GM6B with the end plate free to move. Here also the number and the direction of the restraints

employed were investigated through the cases given in the table.

For each case a dedicated data file was prepared and run. All the structures contained 12315 nodes and 5467 elements but their degrees of freedom varied depending on the number of nodes restrained per tab, or whether or not the compression zone was restrained in the x-direction. Typically the number of degrees of freedom were 34356 in the analysis.

4.4 Results

4.4.1 Restrained compression zone

See section 4.3.2

4.4.1.1 Deformed shape

Figures 4.7 and 4.8 show two views of the beam end connector structure prior to loading. Figure 4.9 shows a typical deformed structure superimposed on the layout of the undeformed structure, case GM6A. Figures 4.10-4.12 show the deflections along the height of face A, block 1 in figure 4.5. This is the plate containing the tabs. These are shown for three cases of GM1A, GM3A and GM6A. The deflections are given for the horizontal, vertical as well as the out of plane directions. These are for the same load for all the cases. The resultant deflection is also included.

From the individual deflection graph it can be seen that the variation in the deflection band was quite large, so adopting a common scale for comparison purposes would have resulted in a loss of clarity.

4.4.1.2 Stress distribution

Figure 4.13 shows the stress distribution pattern in the plate containing the tabs. The stress distribution along the same plane, as described in 4.4.1.1, for the restrained compression zone models are shown in figures 4.14-4.16. The stress values are unaveraged, principal, Von Mises components.

4.4.1.3 Initial stiffness values

Figure 4.17 shows the various methods by which rotations were measured for various cases.

The rotational values were calculated, in the first instance, by determining the differential movements, in the horizontal direction of two central nodes on the top and the bottom flanges, δ_2 and δ_1, adjacent to the end plate as $\theta_v = (\delta_2 - \delta_1)/a$, where $a = 100mm$ and was the depth of the beam as shown in figure 4.17(a).

Secondly the differential movements of two central nodes, 50mm apart, on the top flange in the vertical direction both adjacent and remote from the end plate were evaluated, figures 4.17(b) and (c).

Thirdly the differential movements of two central nodes 50mm apart, on the bottom flange in the vertical direction were also evaluated, figures 4.17(d) and (e). The results were used to evaluate the initial stiffness values and are given in table 4.4.

These were compared with the initial stiffness values obtained experimentally. The experimental initial stiffness values were the slope of a straight line superimposed along

the straightest part of the moment-rotation curves given in chapter 3.

4.4.1.4 Discussion of results

Global Modeling-cases of Restraint At Tabs, Restrained Compression Zone

All the vertical dimensions are with respect to the global axes shown in figure 4.5.

Table 4.2 shows the various cases examined for this condition. Table 4.4 lists the extracted rotation and therefore the stiffness values obtained in the manner described in the previous section.

Considering cases of GM1A and GM2A, the tabs in these two models were restrained in three directions, X, Y and Z, table 4.2.

However, it was soon decided that restraining the movement of the tabs in the Z-direction, i.e. their out of plane movement, Figure 4.5, may not be a valid action. In practice, when load was applied to a beam end connector out of plane movement of the tabs, however small in magnitude could have occurred.

It was not possible to categorically detect the presence or the absence of such movement during initial loading stages when testing the beam end connectors.

The lowest stiffness values calculated for the two cases were 1070 and 1041 kNm/radian respectively. These were the results of rotation measurements carried out according to figure 4.17(e),θ_{br}. The highest stiffness values on the other hand were given by measurements taken as shown in

figure 4.17(a), θ_v, a difference of 30% to 40%. Figure 4.17(c) was the method used for the physical tests.

Table 4.4, eliminating restraints in the Z- direction and reducing the number of restraints in the x and y directions gave cases: GM3A, GM4A, GM5A and GM6A.

Considering cases: GM3A and GM6A the lowest stiffness values calculated for them were 837 and 586 kNm/radian, a difference of 35% on average. These stiffness values were the results of rotation measurements according to figure 4.17(c),θ_{tr}, table 4.4.

The highest stiffness values on the other hand were also given by θ_v, i.e. measurements taken according to figure 4.17(a). These were 1037 and 685 kNm/radian, a difference of 42% on average.

GM6A gave the lowest set of stiffness values with 586 kNm/radian being the lowest of the set, and obtained as the result of measurements carried out according to figure 4.17(c), θ_{tr}.

However, compared with the initial stiffness values given by the experimental results, figures 3.56 and 3.62 giving 300 to 500kNm/radian, there was on average 52% variation.

The reason for this variation is the fact that in these models the compression zones of the beam end connectors were restrained, aiming to simulate their interaction with the upright's flanges.

In practice, as observed during testing of the beam end connectors, the bearing of the lowest part of the beam end connector's end plate happened well after plastic

deformation had started and therefore was not a correct comparison.

Figures 3.56 and 3.62 represent the moment-rotation characteristics for products 16 and 22. The physical dimensions of these products matched those adopted in the make up of the global model, table 3.1.

The deflection graphs for cases GM1A, GM3A and GM6A are given in figures 4.10-4.12.

As described in section 4.4.1.1 the variation in the deflection band given by each case was quite large. This meant that adopting a common scale for comparison purposes would have resulted in a loss of clarity.

However, each graph shows a distinct, similar in shape deflection profile in the X-direction, represented by the most solid line. The graphs show that there is little movement up to a height of about 40mm in this direction, associated with the restrained compression zone.

The troughs and the peaks in the curves representing the X-direction movements are due to the stiffening effect of the stub beam coinciding with its bottom and top flanges, figure 4.6.

Figure 4.9 shows the deformed structure for GM6A, superimposed on the outline of the undeformed structure. The deformed shape is typical of this group of models.

Each table has been divided into three sections, top, relating to top block, middle, relating to middle block and bottom section representing the bottom block. Each section shows columns of node numbers representing the blocks which were restrained according to the diagrams in table 4.2,

global stresses, principal stresses, Von Mises and the angles of principal directions.

Referring to table 4.5 and examining the global/direct stresses for the restrained nodes only, initially σ_x, it was apparent that, with exception of nodes 45 and 41 the rest of the restrained nodes were in compression. Note that nodes 45 and 41 are on the left-hand side, vertical plane of the bottom tab. Considering σ_y, noting the restrained nodes, i.e. the four corners of the bottom plane of the blocks, with exception of node 35 of the middle block, the rest of the restrained nodes were in compression.

Table 4.5 also shows that some of the stresses at the nodes where restraints were applied are higher than the yield stress of the material. The stress intensity at these points is highest in models using the least number of restraints. The high stresses are the result of discontinuities caused due to the application of linear elastic theory and the point restraints at the supports. In linear elasticity these discontinuities can be infinitely large, (Dirac, Δ-function). Although such high stresses, due to presence of yielding, do not occur in practice, their very occurrence will explain the early non-linearity observed in the moment rotation curves during the bedding in stages, figure 3.60.

However, to ensure the accuracy of the models stress continuity across elements was checked. As an example, considering the stress values for the neighbouring nodes, 1.6mm apart, nodes 30 with 26 and 32 with 26 vary between 4 to 12% and less than the yield stress of the material proving the accuracy of the model.

Referring to table 4.6 and examining the global/direct stresses for the restrained nodes only, initially σ_x, it

was apparent that, all the restrained nodes were in compression. Considering σ_y, noting the restrained nodes, i.e. the front central node of the bottom plane of the blocks, all the restrained nodes were in compression.

The stress distribution, figure 4.13 was typical of the cases examined and agreed with the outcome of the stress lacquer exercise, figure 3.45.

4.4.2 Free compression zone

See section 4.3.2

4.4.2.1 Deformed shape

Two views of the unloaded beam end connector are shown in figures 4.7 and 4.8. Figure 4.18 shows a typical deformed structure superimposed on the layout of the undeformed structure, case GM6B.

Here also referring to figure 4.5, the deflection profiles along the height of block 1, face A are given for three cases of GM1B, GM3B and GM6B. These are shown in figures 4.19-4.21.

4.4.2.2 Stress distribution

Referring to figure 4.5, the stress distribution along the same plane as that described above are presented, figures 4.22-4.24. The stress values are unaveraged, principal, Von Mises components.

4.4.2.3 Initial stiffness values

Here, the initial stiffness values were also obtained according to figure 4.17.

A sample calculation was given in section 4.4.1.3 showing how the rotational values were calculated. The results were used to evaluate the initial stiffness values and are given in table 4.7.

4.4.2.4 Discussion of results

Global Modeling-cases of Restraint At Tabs, Free Compression Zone

Dimensions are with respect to the global axes shown in figure 4.5.

Table 4.3 shows the various cases examined for this condition. Table 4.7 lists the extracted rotation and therefore the stiffness values obtained in the manner described previously.

Table 4.3, GM1B and GM2B were two cases that included restraints in the Z-direction at their tabs.

However, as with their counterpart models discussed in section 4.4.1.4, restraining the tabs in this direction could not be justified. There, it was argued that out of plane movement of the tabs, namely movement in the z-direction, figure 4.5, during the initial stages of loading could well exist and therefore the validity of suppressing any movement in this direction was at dispute.

The stiffness values evaluated in such a way, however, are given in table 4.7. The lowest values calculated for the two cases were 735 and 694 kNm/radian and were the results of rotation measurements carried out according to figure 4.17(c), θ_{tr}. The highest stiffness value on the other hand was given by the method shown in figure 4.17(a), θ_v, a difference of about 20%.

Cases GM3B, GM4B, GM5B and GM6B have no restraints in the Z-direction. Table 4.3 shows the top, middle and the bottom tabs for each case.

As two extreme cases consideration is given to GM3B and GM6B.

The lowest stiffness values calculated for these two cases were 635 and 364 kNm/radian, a difference of 60% on average. These were the results of rotation measurements carried out as θ_{tr}, figure 4.17(c) and table 4.7.

As observed with the models that had restrained compression zones, GM1A and GM2A, section 4.4.1.4, here also the highest stiffness values were given by θ_v, figure 4.17(a) as 744 and 400 kNm/radian, a difference of 70% on average.

4.5 Conclusion

Absolute restraints provided a relatively simple means by which resistance to the rotation of the beam end connector could be simulated.

A number of global models were produced, with restrained and free compression zones. Each model incorporated a different number of restraints at their tabs.

The global models were used to evaluate the initial stiffness values of the beam end connector. The lower the number of the restraints at the tabs, the better was the correlation between the theoretical and the experimental results.

The best result, in terms of correlation with the experimental results, was obtained from the model that at

each of its tabs had a single restraint in the X and Y directions. The model was the case GM6B and its compression zone was free to move, this being the condition observed during the initial loading of a beam end connector.

Comparing the theoretically obtained initial stiffness value of 364kNm/rad with typical experimental results such as 375kNm/rad, showed that adopting appropriate anchorage systems could result in estimating the initial stiffness values accurately. This was done by using single restraints in the X and Y directions at the tabs.

Various methods of measuring rotations and hence the stiffness values were demonstrated, figure 4.17. In every case it was shown that measuring rotations by determining differential deflection of top and the bottom flanges adjacent to the beam end connector would result in the highest stiffness values, figure 4.17(a).

Deflection profile and the stress distribution along the height of face A of block 1 containing the tabs, figure 4.5, was examined. Doing so provided information on the deformed shape of the plate, stress distribution and the loading conditions at each tab.

The models simulated the deflected shape of the beam end connector. This matched the deformation modes observed during testing.

The stress distribution pattern in the critical regions was determined and matched those observed using stress lacquer.

BLOCK	Interfacing Blocks With Upright's Web These blocks are extracted from figure 4.5. They show the nodes used to apply restraints in x, y and z directions. A range of cases was produced depending on the number and directions of restraints employed. The cases considered are grouped in tables 4.2 and 4.3.
Block 5 and its nodes from top tab shown in figure 4.5	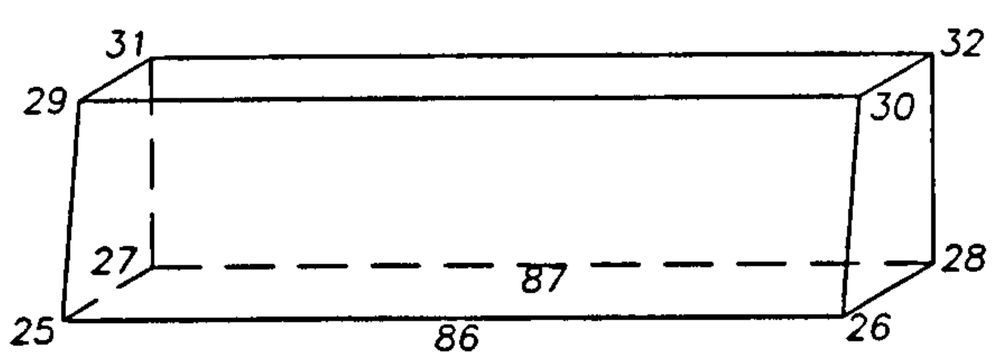 The nodes used to apply restraints in x, y and z directions as appropriate, figure 4.5.
Block 6 and its nodes from middle tab shown in figure 4.5	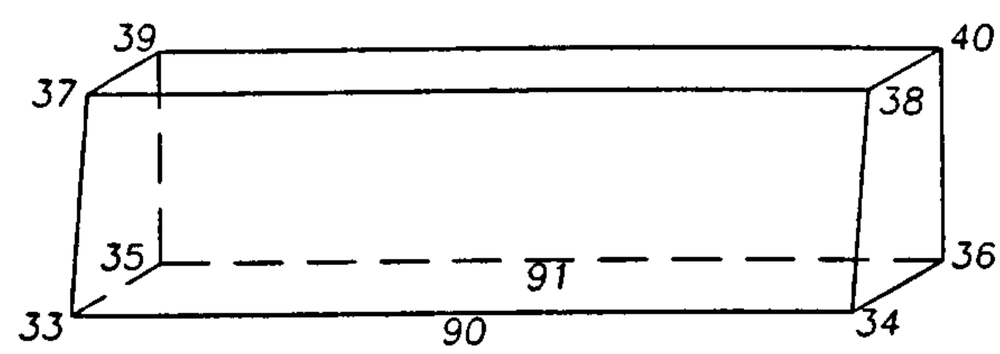 The nodes used to apply restraints in x, y and z directions as appropriate, figure 4.5.
Block 7 and its nodes from bottom tab shown in figure 4.5	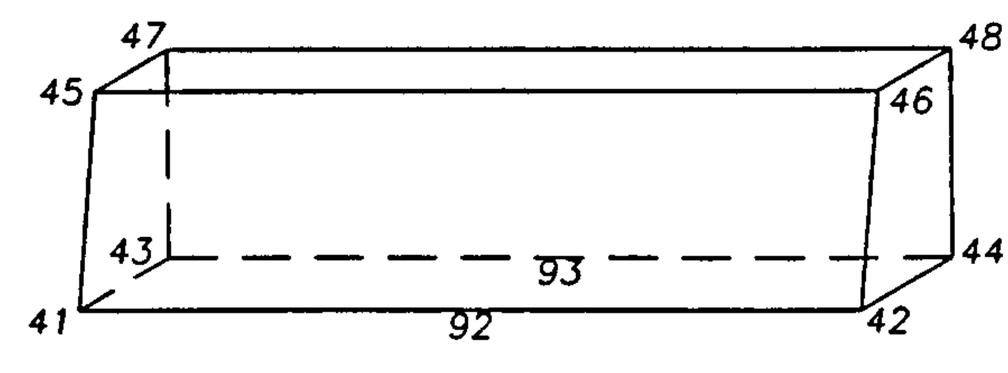 The nodes used to apply restraints in x, y and z directions as appropriate, figure 4.5.

Table 4.1
Interfacing blocks of top, middle and bottom tabs and their node numbers, applicable to all CASES

CASE No	TAB	CASE
GM1A	**Top** Block 5 from Figure 4.5	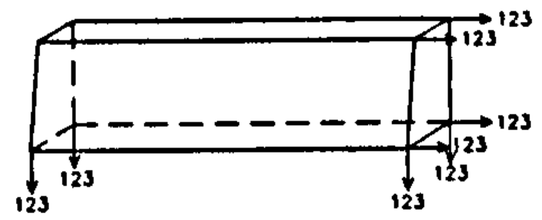 1, 2 and 3 denote restraints in x, y and z directions
	Middle Block 6 from figure 4.5	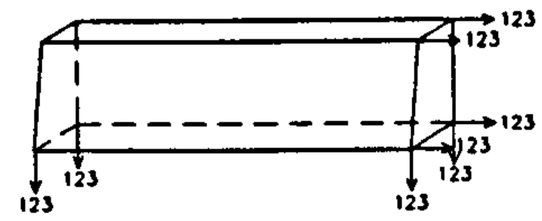 1, 2 and 3 denote restraints in x, y and z directions
	Bottom Block 7 from figure 4.5	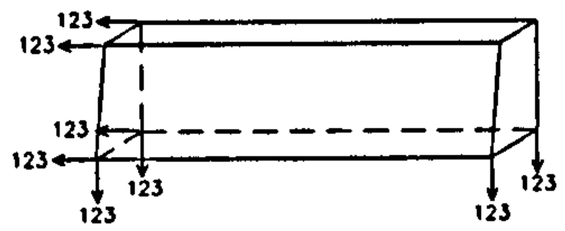 1, 2 and 3 denote restraints in x, y and z directions

CASE No	TAB	CASE
GM2A	**Top** Block 5 from Figure 4.5	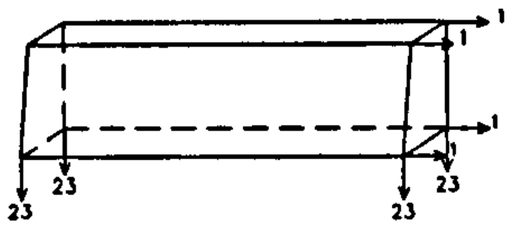 1, 2 and 3 denote restraints in x, y and z directions
	Middle Block 6 from figure 4.5	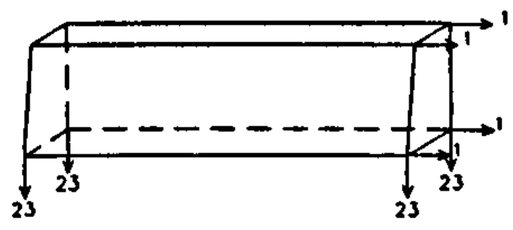 1, 2 and 3 denote restraints in x, y and z directions
	Bottom Block 7 from figure 4.5	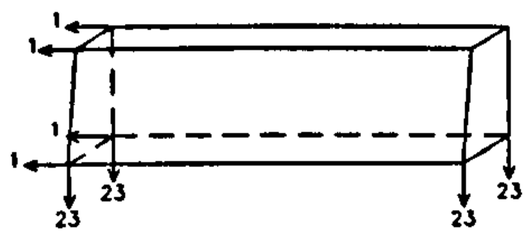 1, 2 and 3 denote restraints in x, y and z directions

CASE No	TAB	CASE
GM3A	**Top** Block 5 from Figure 4.5	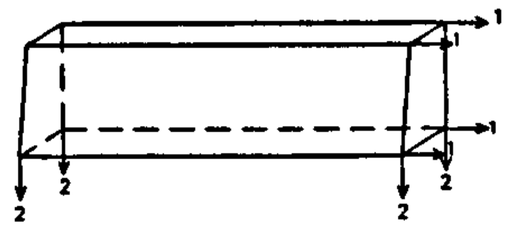 1 and 2 denote restraints in x and y directions
	Middle Block 6 from figure 4.5	1 and 2 denote restraints in x and y directions
	Bottom Block 7 from figure 4.5	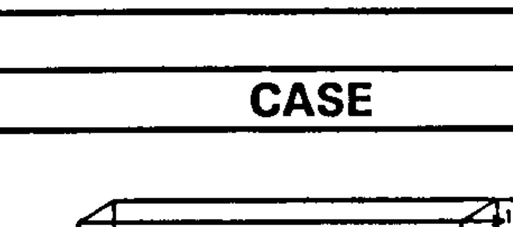 1 and 2 denote restraints in x and y directions

Table 4.2
CASES of Restraints At Tabs, Restrained Compression Zone Investigated, Cont/d...

CASE No	TAB	CASE
GM4A	**Top** Block 5 from Figure 4.5	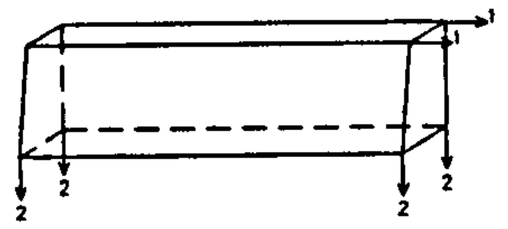 1 and 2 denote restraints in x and y directions
	Middle Block 6 from figure 4.5	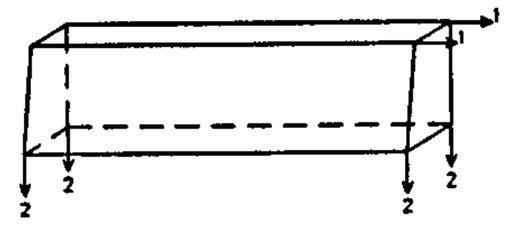 1 and 2 denote restraints in x and y directions
	Bottom Block 7 from figure 4.5	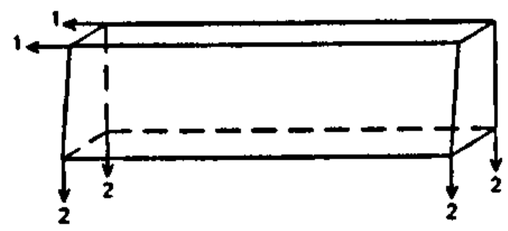 1 and 2 denote restraints in x and y directions

CASE No	TAB	CASE
GM5A	**Top** Block 5 from Figure 4.5	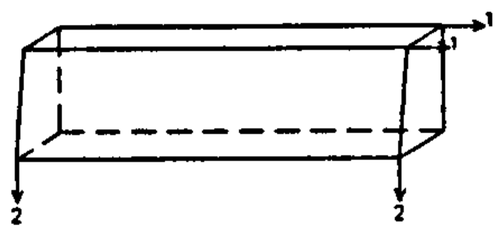 1 and 2 denote restraints in x and y directions
	Middle Block 6 from figure 4.5	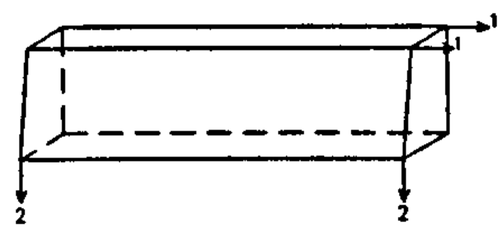 1 and 2 denote restraints in x and y directions
	Bottom Block 7 from figure 4.5	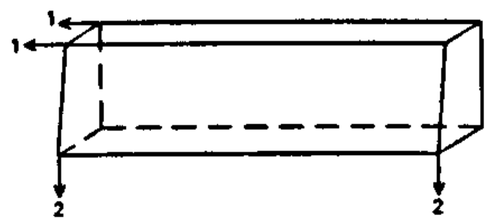 1 and 2 denote restraints in x and y directions

CASE No	TAB	CASE
GM6A	**Top** Block 5 from Figure 4.5	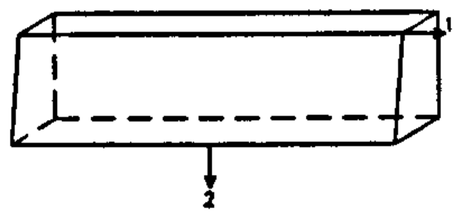 1 and 2 denote restraints in x and y directions
	Middle Block 6 from figure 4.5	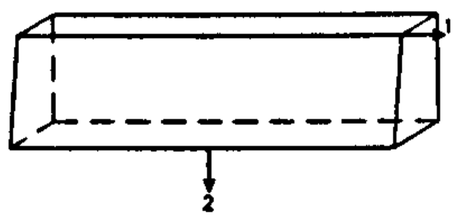 1 and 2 denote restraints in x and y directions
	Bottom Block 7 from figure 4.5	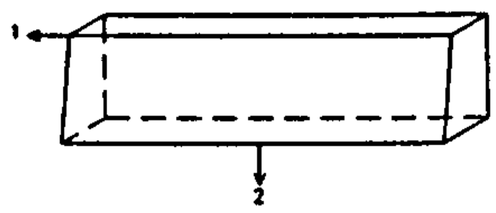 1 and 2 denote restraints in x and y directions

Table 4.2
CASES of Restraints At Tabs, Restrained Compression Zone Investigated, Concluded.

CASE No	TAB	CASE
GM1B	Top Block 5 from Figure 4.5	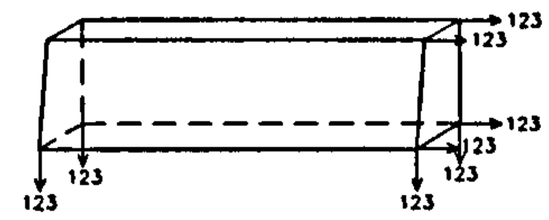 1, 2 and 3 denote restraints in x, y and z directions
	Middle Block 6 from figure 4.5	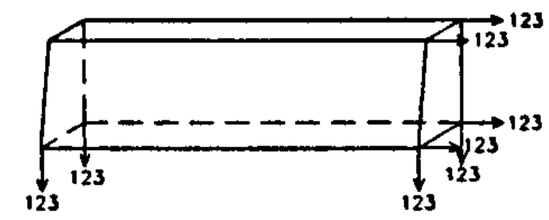 1, 2 and 3 denote restraints in x, y and z directions
	Bottom Block 7 from figure 4.5	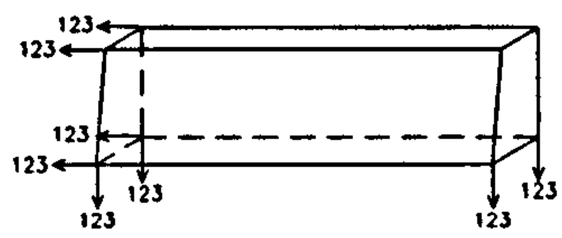 1, 2 and 3 denote restraints in x, y and z directions

CASE No	TAB	CASE
GM2B	Top Block 5 from Figure 4.5	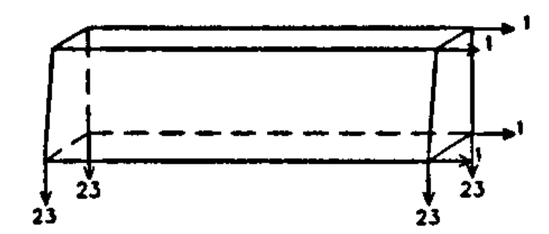 1, 2 and 3 denote restraints in x, y and z directions
	Middle Block 6 from figure 4.5	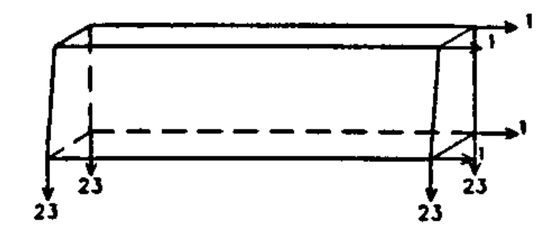 1, 2 and 3 denote restraints in x, y and z directions
	Bottom Block 7 from figure 4.5	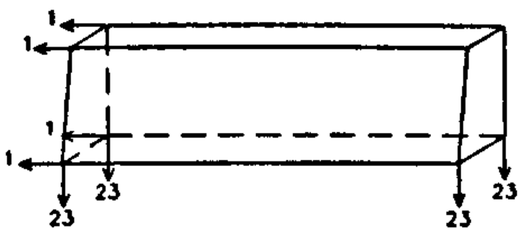 1, 2 and 3 denote restraints in x, y and z directions

CASE No	TAB	CASE
GM3B	Top Block 5 from Figure 4.5	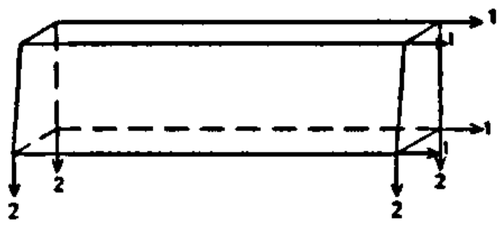 1 and 2 denote restraints in x and y directions
	Middle Block 6 from figure 4.5	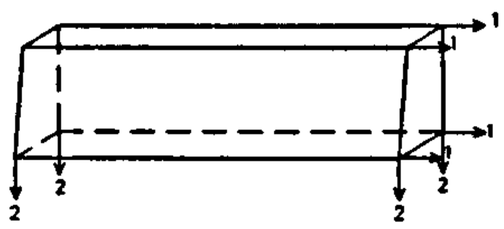 1 and 2 denote restraints in x and y directions
	Bottom Block 7 from figure 4.5	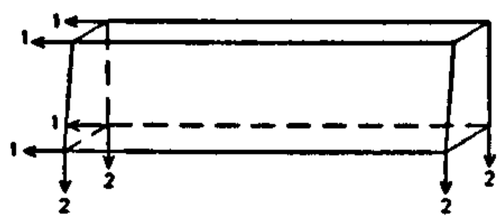 1 and 2 denote restraints in x and y directions

Table 4.3
CASES of Restraints At Tabs, Free Compression Zone investigated, Cont/d....

CASE No	TAB	CASE
GM4B	**Top** Block 5 from Figure 4.5	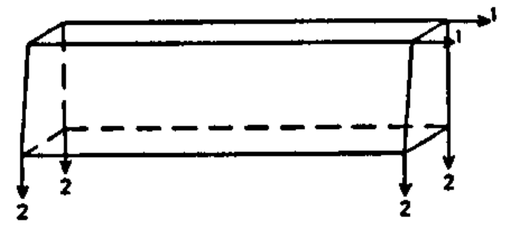 1 and 2 denote restraints in x and y directions
	Middle Block 6 from figure 4.5	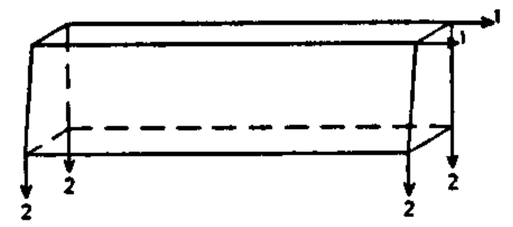 1 and 2 denote restraints in x and y directions
	Bottom Block 7 from figure 4.5	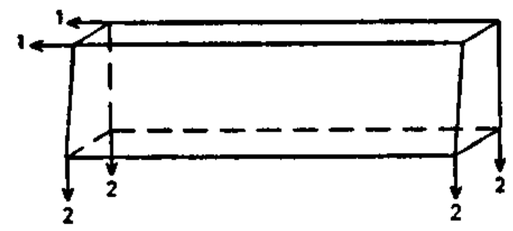 1 and 2 denote restraints in x and y directions

CASE No	TAB	CASE
GM5B	**Top** Block 5 from Figure 4.5	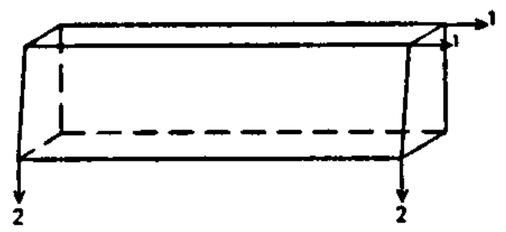 1 and 2 denote restraints in x and y directions
	Middle Block 6 from figure 4.5	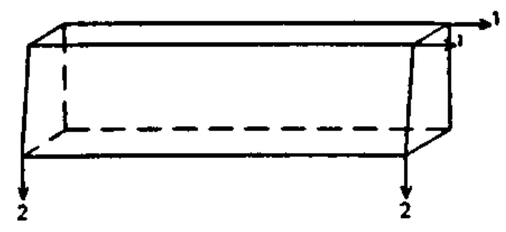 1 and 2 denote restraints in x and y directions
	Bottom Block 7 from figure 4.5	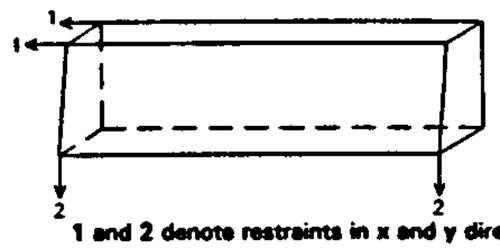 1 and 2 denote restraints in x and y directions

CASE No	TAB	CASE
GM6B	**Top** Block 5 from Figure 4.5	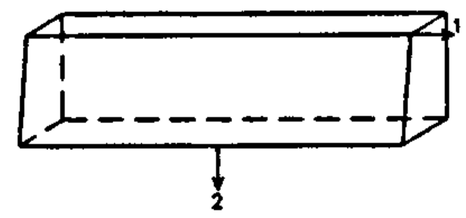 1 and 2 denote restraints in x and y directions
	Middle Block 6 from figure 4.5	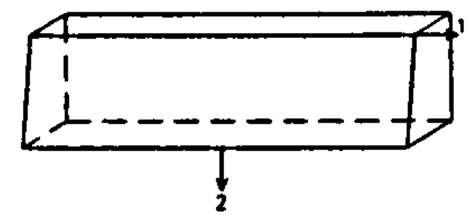 1 and 2 denote restraints in x and y directions
	Bottom Block 7 from figure 4.5	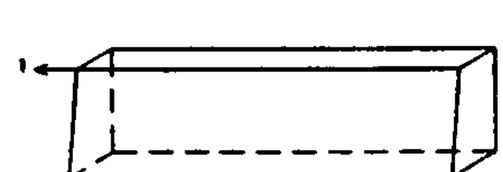 1 and 2 denote restraints in x and y directions

Table 4.3
CASES of Restraints At Tabs, Free Compression Zone investigated, Concluded.

Table 4.4

Rotation and stiffness values for various CASES, Symmetrical welding position, Restrained compression zone

CASE N°	CASE	θ_v (radian)	θ_{ta} (radian)	θ_{tr} (radian)	θ_{ba} (radian)	θ_{br} (radian)	k_v (kNm/rad)	k_{ta} (kNm/rad)	k_{tr} (kNm/rad)	k_{ba} (kNm/rad)	k_{br} (kNm/rad)
GM1A	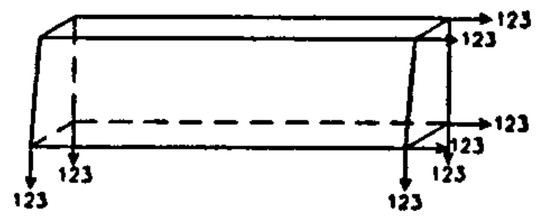	12931E-7	17441E-7	18558E-7	17002E-7	18824E-7	1558	1155	1085	1185	1070
GM2A	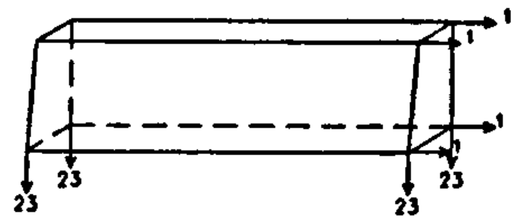	13459E-7	17966E-7	19102E-7	17540E-7	19342E-7	1497	1121	1054	1148	1041
GM3A	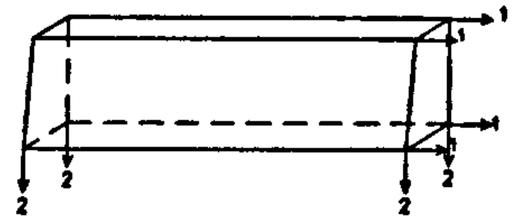	19427E-7	22396E-7	24052E-7	22360E-7	23832E-7	1037	899	837	901	845
GM4A	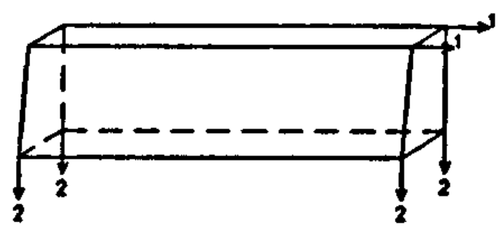	20590E-7	23576E-7	25198E-7	23514E-7	24978E-7	978	854	799	856	806
GM5A	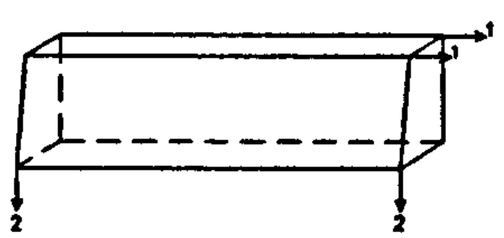	20672E-7	23680E-7	25304E-7	23563E-7	25092E-7	974	850	796	855	803
GM6A	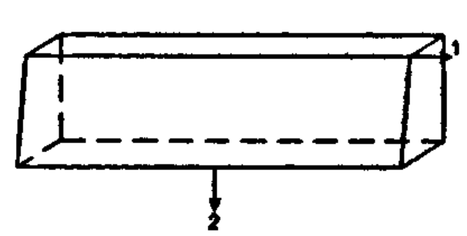	29413E-7	32644E-7	34358E-7	32660E-7	34052E-7	685	617	586	616	591

TABLE 4.5

REACTIONS AT TOP, BOTTOM AND MIDDLE TABS-SYMMETRICAL-RESTRAINED COMPRESSION ZONE-RESTRAINTS AT TABS

37100 8-NODE ISOPARAMETRIC BRICK ELEMENT

GLOBAL STRESSES - SIGMA-X, SIGMA-Y AND SIGMA-Z ARE THE STRESSES IN THE GLOBAL AXES
PRINCIPAL STRESSES - SIGMA-1 IS THE MOST POSITIVE PRINCIPAL STRESS
SIGMA-3 IS THE MOST NEGATIVE PRINCIPAL STRESS
ANGLES OF PRINCIPAL STRESSES - AX, AY AND AZ ARE THE ANGLES OF SIGMA-1 TO THE GLOBAL AXES
BX, BY AND BZ ARE THE ANGLES OF SIGMA-2 TO THE GLOBAL AXES
SIGMA-2 IS PERPENDICULAR TO SIGMA-1 AND SIGMA-3

NB:R DENOTES RESTRAINT AT NODE AND STRESS UNIT: N/m^2

LOAD CASE	NODE NO	.....GLOBAL.STRESSES..... SIGMA-X	SIGMA-Y	SIGMA-Z	.....PRINCIPAL.STRESSES..... SIGMA-1	SIGMA-2	SIGMA-3	VON.MISES STRESS	ANGS.OF.PRINCIPAL.DIRECTIONS AX	AY	AZ	BX	BY	BZ
1	R 30	-4.88E+08	7.36E+07	-7.52E+07	2.13E+08	-1.51E+08	-5.53E+08	6.64E+08	76	148	117	76	114	28
1	R 32	-9.67E+08	-4.77E+08	-3.84E+08	-4.09E+07	-4.30E+08	-1.36E+09	1.17E+09	60	141	112	72	105	23
1	R 26	-6.69E+08	-5.22E+08	-3.16E+08	-2.16E+08	-3.19E+08	-9.72E+08	7.10E+08	51	40	80	83	83	170
1	R 28	-1.12E+09	-1.09E+09	-6.20E+08	-3.77E+08	-6.22E+08	-1.82E+09	1.34E+09	45	44	95	85	86	5
1	R 25	9.57E+05	-6.01E+07	3.56E+07	1.72E+08	-5.63E+07	-1.39E+08	2.80E+08	48	91	138	81	167	80
1	R 27	-4.31E+08	-1.57E+08	-1.23E+08	-3.03E+06	-1.72E+08	-5.37E+08	4.72E+08	63	121	136	87	142	52
1	R 38	-5.86E+08	1.49E+08	-3.88E+07	3.13E+08	-1.14E+08	-6.76E+08	8.60E+08	78	149	117	72	113	29
1	R 40	-1.52E+09	-7.36E+08	-5.86E+08	-2.50E+08	-6.12E+08	-1.98E+09	1.58E+09	62	145	110	74	103	21
1	R 34	-8.75E+08	-7.22E+08	-5.08E+08	-2.66E+08	-5.59E+08	-1.28E+09	9.04E+08	54	45	65	72	72	154
1	R 36	-1.23E+09	-8.16E+08	-6.42E+08	-3.12E+08	-6.69E+08	-1.70E+09	1.25E+09	55	39	73	82	75	163
1	R 33	-4.72E+07	-8.89E+07	-2.21E+07	5.74E+07	-7.24E+07	-1.43E+08	1.76E+08	63	120	138	26	76	67
1	R 35	7.05E+07	3.04E+08	1.31E+08	3.89E+08	1.51E+08	-3.34E+07	3.67E+08	79	27	65	46	79	134
1	R 45	7.22E+07	3.02E+07	1.15E+08	2.70E+08	5.03E+07	-1.03E+08	3.25E+08	48	91	138	75	158	74
1	R 47	-4.36E+08	2.10E+06	-4.62E+07	1.79E+08	-1.05E+08	-5.54E+08	6.40E+08	66	42	122	89	54	35
1	R 41	2.38E+07	-5.86E+07	1.10E+08	2.59E+08	-1.85E+07	-1.65E+08	3.73E+08	52	86	141	63	147	73
1	R 43	-8.46E+08	-7.36E+08	-3.54E+08	-2.34E+08	-4.32E+08	-1.27E+09	9.51E+08	57	119	133	67	125	44
1	R 42	-3.61E+06	-1.60E+08	1.03E+08	1.32E+08	-3.79E+06	-1.89E+08	2.79E+08	68	76	153	29	76	64
1	R 44	-5.77E+07	-5.75E+08	-3.81E+07	4.86E+07	-1.17E+08	-6.03E+08	5.86E+08	44	82	134	47	79	44

TABLE 4.6

REACTIONS AT TOP, BOTTOM AND MIDDLE TABS-SYMMETRICAL-RESTRAINED COMPRESSION ZONE-RESTRAINTS AT TABS

37100 8-NODE ISOPARAMETRIC BRICK ELEMENT

GLOBAL STRESSES - SIGMA-X, SIGMA-Y AND SIGMA-Z ARE THE STRESSES IN THE GLOBAL AXES
PRINCIPAL STRESSES - SIGMA-1 IS THE MOST POSITIVE PRINCIPAL STRESS
SIGMA-3 IS THE MOST NEGATIVE PRINCIPAL STRESS
ANGLES OF PRINCIPAL STRESSES - AX, AY AND AZ ARE THE ANGLES OF SIGMA-1 TO THE GLOBAL AXES
BX, BY AND BZ ARE THE ANGLES OF SIGMA-2 TO THE GLOBAL AXES
SIGMA-2 IS PERPENDICULAR TO SIGMA-1 AND SIGMA-3

NB:R DENOTES RESTRAINT AT NODE AND STRESS UNIT: N/m^2

LOAD CASE		NODE NO	.....GLOBAL.STRESSES..... SIGMA-X	SIGMA-Y	SIGMA-Z	.....PRINCIPAL.STRESSES..... SIGMA-1	SIGMA-2	SIGMA-3	VON.MISES STRESS	ANGS.OF.PRINCIPAL.DIRECTIONS AX	AY	AZ	BX	BY	BZ
1	R	30	-1.24E+10	-4.14E+08	-3.77E+09	4.44E+09	-4.34E+09	-1.67E+10	1.84E+10	63	138	119	82	53	142
1		32	1.18E+09	1.66E+08	4.92E+08	6.72E+09	4.96E+08	-5.38E+09	1.05E+10	45	99	133	71	19	84
1		26	3.33E+08	6.79E+08	5.84E+08	1.06E+09	5.75E+08	-3.78E+07	9.52E+08	72	128	135	48	46	108
1		28	1.77E+09	1.20E+09	1.17E+09	2.51E+09	9.07E+08	7.39E+08	1.69E+09	42	119	118	47	57	59
1	R	86	-4.61E+08	-1.28E+09	-4.73E+08	-1.79E+08	-4.62E+08	-1.57E+09	1.28E+09	45	117	123	51	89	38
1		87	3.26E+08	2.77E+08	2.31E+08	5.92E+08	3.14E+08	-7.20E+07	5.77E+08	77	44	48	12	99	97
1		25	3.45E+07	1.15E+08	-6.85E+06	2.86E+08	3.97E+07	-1.84E+08	4.07E+08	64	48	127	40	129	98
1		27	-7.61E+08	-5.82E+08	-4.54E+08	-3.31E+08	-3.83E+08	-1.08E+09	7.28E+08	79	65	153	49	136	102
1	R	38	-8.48E+09	-2.52E+08	-2.55E+09	3.13E+09	-2.98E+09	-1.14E+10	1.27E+10	63	138	119	82	53	142
1		40	7.26E+08	-6.32E+07	2.66E+08	4.57E+09	2.30E+08	-3.87E+09	7.30E+09	45	99	134	70	20	83
1		34	2.94E+08	4.77E+08	4.92E+08	6.94E+08	3.30E+08	2.39E+08	4.17E+08	87	133	136	39	61	114
1		36	5.40E+08	3.78E+08	5.36E+08	8.98E+08	4.01E+08	1.56E+08	6.55E+08	57	120	132	32	70	65
1	R	90	-4.56E+08	-1.15E+09	-4.24E+08	-1.85E+08	-4.26E+08	-1.42E+09	1.14E+09	50	117	127	47	91	42
1		91	1.47E+08	2.14E+08	1.67E+08	4.99E+08	1.38E+08	-1.09E+08	5.30E+08	80	43	47	9	96	96
1		33	1.04E+07	6.45E+07	6.27E+07	9.63E+07	4.76E+07	-6.30E+06	8.89E+07	73	127	42	66	39	60
1		35	7.77E+07	1.39E+08	1.05E+08	1.95E+08	8.93E+07	3.83E+07	1.38E+08	60	38	67	77	71	157
1	R	45	-5.88E+08	-3.56E+07	-1.94E+08	2.14E+08	-2.34E+08	-7.98E+08	8.79E+08	63	42	59	83	127	37
1		47	2.10E+08	1.40E+08	9.87E+07	4.03E+08	1.74E+08	-1.28E+08	4.61E+08	38	91	51	79	160	106
1		41	1.63E+08	5.77E+07	4.21E+08	4.90E+08	1.58E+08	-6.36E+06	4.38E+08	79	109	157	14	77	84
1		43	1.53E+08	2.01E+08	4.61E+08	7.01E+08	1.48E+08	-3.38E+07	6.63E+08	83	55	34	6	95	93
1	R	92	-3.22E+08	-8.40E+08	-2.25E+08	-7.20E+07	-2.74E+08	-1.04E+09	8.86E+08	58	63	43	40	82	129
1		93	6.49E+07	1.28E+08	1.82E+08	4.63E+08	6.38E+07	-1.52E+08	5.40E+08	86	132	137	5	89	84
1		42	1.04E+08	7.90E+07	4.08E+08	4.79E+08	9.56E+07	1.60E+07	4.29E+08	66	93	156	63	28	81
1		44	6.39E+08	4.88E+08	6.91E+08	1.09E+09	4.22E+08	3.12E+08	7.25E+08	54	118	131	37	82	53

Table 4.7

Rotation and stiffness values for various CASES, Symmetrical welding position, Free compression zone

CASE N°	CASE	θ_v (radian)	θ_{ta} (radian)	θ_{tr} (radian)	θ_{ba} (radian)	θ_{br} (radian)	k_v (kNm/rad)	k_{ta} (kNm/rad)	k_{tr} (kNm/rad)	k_{ba} (kNm/rad)	k_{br} (kNm/rad)
GM1B	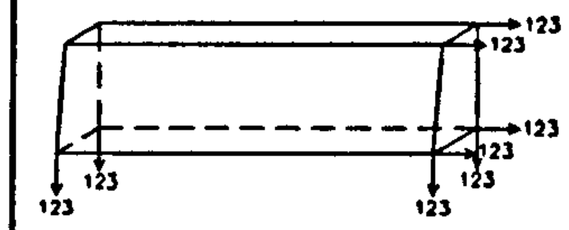	22819E-7	26033E-7	27414E-7	25933E-7	27303E-7	883	774	735	777	738
GM2B	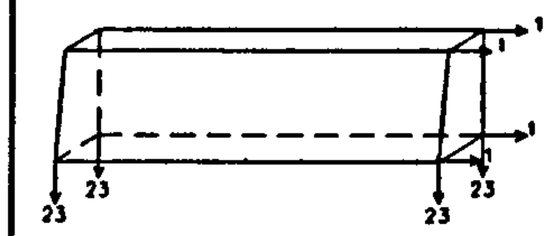	24423E-7	27628E-7	29020E-7	27532E-7	28866E-7	825	729	694	731	698
GM3B	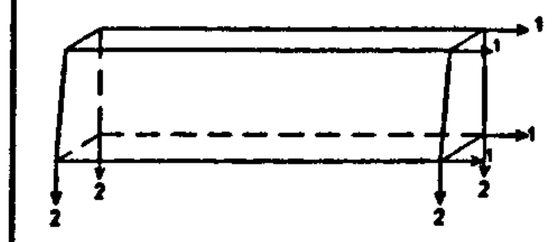	27073E-7	30147E-7	31728E-7	30177E-7	31508E-7	744	668	635	667	639
GM4B	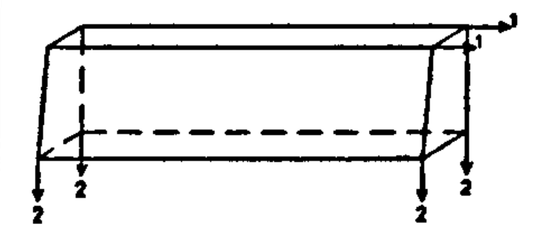	36246E-7	39623E-7	41030E-7	39196E-7	40694E-7	555	508	491	514	495
GM5B	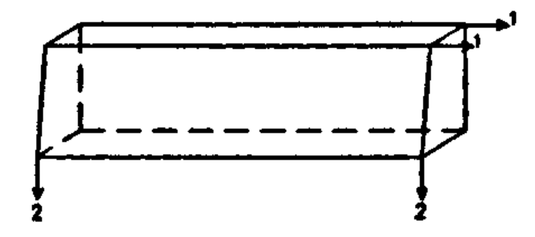	37119E-7	40525E-7	41946E-7	40035E-7	41612E-7	542	497	480	503	484
GM6B	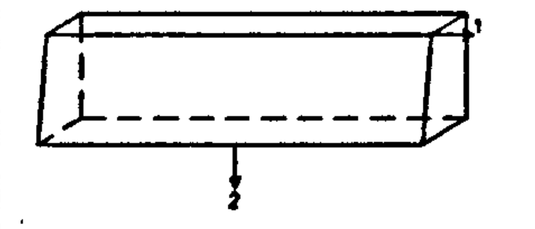	50297E-7	53780E-7	55240E-7	53260E-7	54944E-7	400	374	364	378	366

TABLE 4.8

REACTIONS AT TOP, BOTTOM AND MIDDLE TABS-SYMMETRICAL-FREE COMPRESSION ZONE-RESTRAINTS AT TABS

37100 8-NODE ISOPARAMETRIC BRICK ELEMENT

GLOBAL STRESSES - SIGMA-X, SIGMA-Y AND SIGMA-Z ARE THE STRESSES IN THE GLOBAL AXES
PRINCIPAL STRESSES - SIGMA-1 IS THE MOST POSITIVE PRINCIPAL STRESS
SIGMA-3 IS THE MOST NEGATIVE PRINCIPAL STRESS
ANGLES OF PRINCIPAL STRESSES - AX, AY AND AZ ARE THE ANGLES OF SIGMA-1 TO THE GLOBAL AXES
BX, BY AND BZ ARE THE ANGLES OF SIGMA-2 TO THE GLOBAL AXES
SIGMA-2 IS PERPENDICULAR TO SIGMA-1 AND SIGMA-3

NB:R DENOTES RESTRAINT AT NODE AND STRESS UNIT: N/m^2

LOAD CASE	NODE NO	.....GLOBAL.STRESSES..... SIGMA-X	SIGMA-Y	SIGMA-Z	.....PRINCIPAL.STRESSES..... SIGMA-1	SIGMA-2	SIGMA-3	VON.MISES STRESS	ANGS.OF.PRINCIPAL.DIRECTIONS AX	AY	AZ	BX	BY	BZ
1	R 30	-5.82E+08	8.82E+07	-8.80E+07	2.66E+08	-1.90E+08	-6.58E+08	8.00E+08	76	147	118	76	115	29
1	R 32	-1.16E+09	-5.94E+08	-4.65E+08	-5.92E+07	-5.32E+08	-1.63E+09	1.39E+09	61	140	114	71	106	25
1	R 26	-7.98E+08	-6.38E+08	-3.93E+08	-2.71E+08	-3.93E+08	-1.16E+09	8.38E+08	50	39	86	87	87	176
1	R 28	-1.33E+09	-1.39E+09	-7.76E+08	-4.91E+08	-7.83E+08	-2.22E+09	1.60E+09	44	46	98	82	84	8
1	R 25	1.43E+07	-6.95E+06	4.45E+07	2.04E+08	-6.49E+06	-1.45E+08	3.04E+08	47	88	137	85	175	88
1	R 27	-4.81E+08	-7.89E+07	-1.26E+08	3.76E+07	-1.31E+08	-5.93E+08	5.65E+08	65	131	128	83	43	133
1	R 38	-4.86E+08	6.94E+07	-2.94E+07	2.95E+08	-1.57E+08	-5.84E+08	7.61E+08	70	139	123	87	125	35
1	R 40	-6.27E+08	-3.97E+08	-2.11E+08	1.19E+07	-4.36E+08	-8.11E+08	7.14E+08	65	124	135	70	128	45
1	R 34	-7.75E+08	-7.09E+08	-4.65E+08	-3.02E+08	-4.30E+08	-1.22E+09	8.59E+08	45	47	103	89	109	160
1	R 36	-2.94E+08	-4.53E+08	-2.44E+08	-1.14E+08	-3.03E+08	-5.74E+08	4.01E+08	45	75	131	64	54	46
1	R 33	-1.99E+07	2.53E+07	1.11E+07	1.11E+08	-5.49E+06	-8.85E+07	1.73E+08	79	45	46	29	116	76
1	R 35	3.38E+08	6.11E+08	2.94E+08	7.66E+08	2.83E+08	1.95E+08	5.33E+08	64	31	72	48	94	138
1	R 45	-9.05E+08	2.24E+08	2.88E+08	7.42E+08	1.48E+08	-1.28E+09	1.80E+09	64	61	140	88	149	120
1	R 47	-3.05E+09	5.20E+07	-4.06E+08	9.99E+08	-6.97E+08	-3.70E+09	4.13E+09	68	35	116	86	62	27
1	R 41	-9.58E+08	-5.46E+07	-3.75E+08	3.23E+08	-1.68E+08	-1.54E+09	1.68E+09	57	130	122	79	44	132
1	R 43	-4.36E+09	-1.98E+09	-1.97E+09	-6.82E+08	-2.02E+09	-5.61E+09	4.42E+09	59	141	111	88	114	24
1	R 42	-4.45E+06	-9.35E+07	-5.97E+07	3.19E+08	-9.55E+07	-3.82E+08	6.11E+08	44	100	47	74	15	91
1	R 44	-1.11E+09	-1.15E+09	-7.08E+08	-3.87E+08	-1.02E+09	-1.56E+09	1.01E+09	55	72	40	69	40	123

TABLE 4.9

REACTIONS AT TOP, BOTTOM AND MIDDLE TABS-SYMMETRICAL-FREE COMPRESSION ZONE-RESTRAINTS AT TABS

37100 8-NODE ISOPARAMETRIC BRICK ELEMENT

GLOBAL STRESSES - SIGMA-X, SIGMA-Y AND SIGMA-Z ARE THE STRESSES IN THE GLOBAL AXES

PRINCIPAL STRESSES - SIGMA-1 IS THE MOST POSITIVE PRINCIPAL STRESS
SIGMA-3 IS THE MOST NEGATIVE PRINCIPAL STRESS

ANGLES OF PRINCIPAL STRESSES - AX, AY AND AZ ARE THE ANGLES OF SIGMA-1 TO THE GLOBAL AXES
BX, BY AND BZ ARE THE ANGLES OF SIGMA-2 TO THE GLOBAL AXES
SIGMA-2 IS PERPENDICULAR TO SIGMA-1 AND SIGMA-3

NB:R DENOTES RESTRAINT AT NODE AND STRESS UNIT: N/m^2

LOAD CASE		NODE NO	.....GLOBAL.STRESSES..... SIGMA-X	SIGMA-Y	SIGMA-Z	.....PRINCIPAL.STRESSES..... SIGMA-1	SIGMA-2	SIGMA-3	VON.MISES STRESS	ANGS.OF.PRINCIPAL.DIRECTIONS AX	AY	AZ	BX	BY	BZ
1	R	30	-1.50E+10	-5.06E+08	-4.57E+09	5.33E+09	-5.26E+09	-2.01E+10	2.22E+10	63	138	119	82	53	142
1		32	1.40E+09	1.80E+08	5.48E+08	8.06E+09	5.76E+08	-6.50E+09	1.26E+10	45	99	133	71	19	84
1		26	4.09E+08	8.22E+08	7.29E+08	1.30E+09	6.96E+08	-3.19E+07	1.15E+09	72	128	136	48	46	108
1		28	2.14E+09	1.47E+09	1.44E+09	3.05E+09	1.12E+09	8.95E+08	2.05E+09	43	119	118	46	59	58
1	R	86	-5.68E+08	-1.57E+09	-5.76E+08	-2.17E+08	-5.69E+08	-1.93E+09	1.57E+09	46	117	123	51	89	38
1		87	3.93E+08	3.39E+08	2.86E+08	7.27E+08	3.80E+08	-8.91E+07	7.10E+08	78	44	47	11	98	97
1		25	3.86E+07	1.33E+08	-2.33E+07	3.44E+08	4.52E+07	-2.41E+08	5.06E+08	62	48	126	42	130	98
1		27	-9.57E+08	-7.24E+08	-5.79E+08	-4.23E+08	-4.76E+08	-1.36E+09	9.13E+08	76	68	154	50	139	98
1	R	38	-1.85E+09	-1.01E+08	-7.58E+08	6.33E+08	-8.53E+08	-2.49E+09	2.71E+09	64	139	118	80	54	142
1		40	-3.81E+06	-2.46E+08	-2.46E+08	7.93E+08	-1.45E+08	-1.14E+09	1.68E+09	47	107	132	59	31	82
1		34	1.90E+08	9.20E+07	4.91E+08	5.58E+08	1.79E+08	3.54E+07	4.68E+08	77	72	21	17	105	97
1		36	1.26E+08	2.35E+08	5.15E+08	7.25E+08	1.20E+08	3.09E+07	6.54E+08	83	122	146	11	78	89
1	R	90	-4.91E+08	-1.15E+09	-4.23E+08	-1.79E+08	-4.68E+08	-1.41E+09	1.12E+09	52	117	130	45	93	45
1		91	1.21E+07	1.69E+08	1.23E+08	4.60E+08	1.52E+07	-1.72E+08	5.62E+08	87	42	47	8	86	97
1		33	4.37E+07	2.59E+07	2.02E+08	2.40E+08	4.41E+07	-1.20E+07	2.29E+08	69	79	22	47	137	96
1		35	3.86E+08	3.92E+08	4.15E+08	6.84E+08	2.73E+08	2.35E+08	4.31E+08	56	54	53	57	73	142
1	R	45	-1.86E+10	-1.17E+09	-6.73E+09	5.19E+09	-6.84E+09	-2.48E+10	2.62E+10	63	39	63	81	123	35
1		47	4.90E+09	2.06E+09	1.29E+09	1.04E+10	3.20E+09	-5.31E+09	1.36E+10	36	97	54	82	155	113
1		41	6.23E+08	1.42E+09	5.74E+08	1.62E+09	6.32E+08	3.66E+08	1.14E+09	88	156	113	11	84	99
1		43	3.32E+08	4.42E+08	1.94E+08	9.23E+08	3.23E+08	-2.78E+08	1.04E+09	81	39	51	10	93	99
1	R	92	-2.48E+08	-7.32E+08	-1.49E+08	-6.52E+07	-1.27E+08	-9.36E+08	8.42E+08	78	66	26	25	73	109
1		93	2.64E+08	2.36E+08	2.95E+08	5.44E+08	2.14E+08	3.73E+07	4.45E+08	63	123	135	32	58	82
1		42	-6.32E+07	1.27E+08	-2.09E+08	3.02E+08	2.80E+07	-4.75E+08	6.83E+08	61	133	56	47	46	74
1		44	-1.17E+09	-4.23E+08	-7.05E+08	-2.79E+08	-4.87E+08	-1.53E+09	1.16E+09	60	50	53	75	139	53

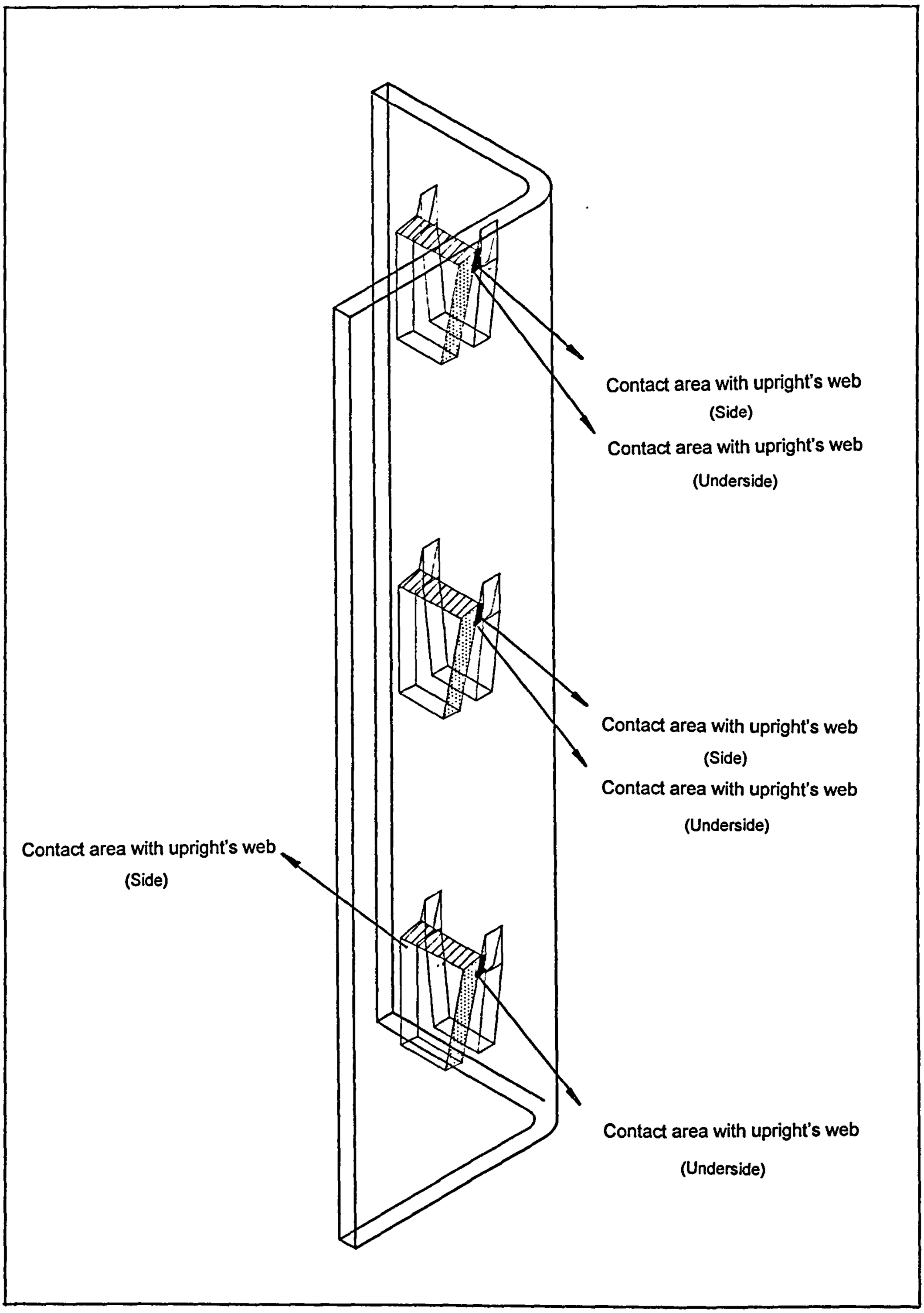

Figure 4.1 Typical beam end connector

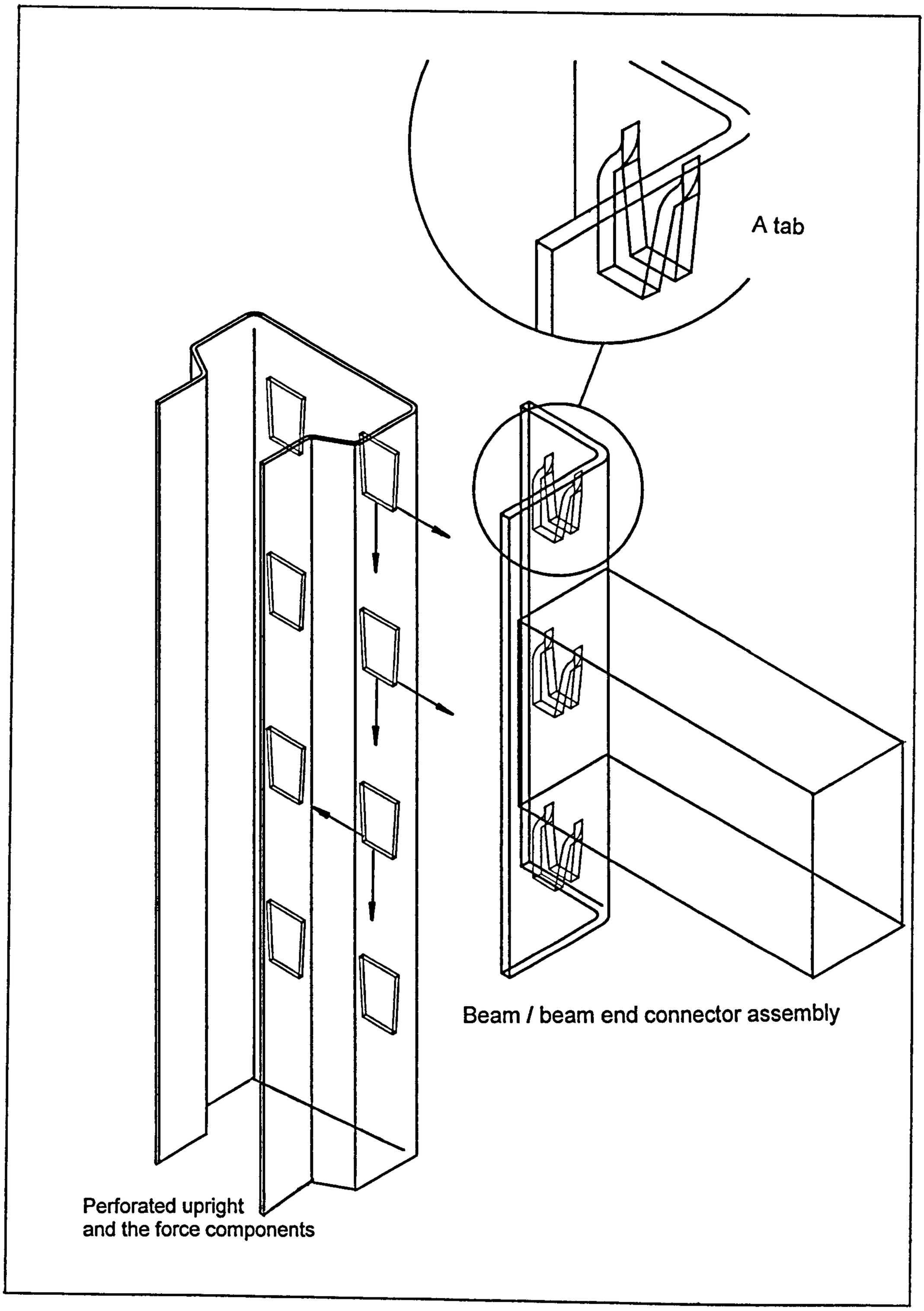

Figure 4.2 Beam end connector and upright

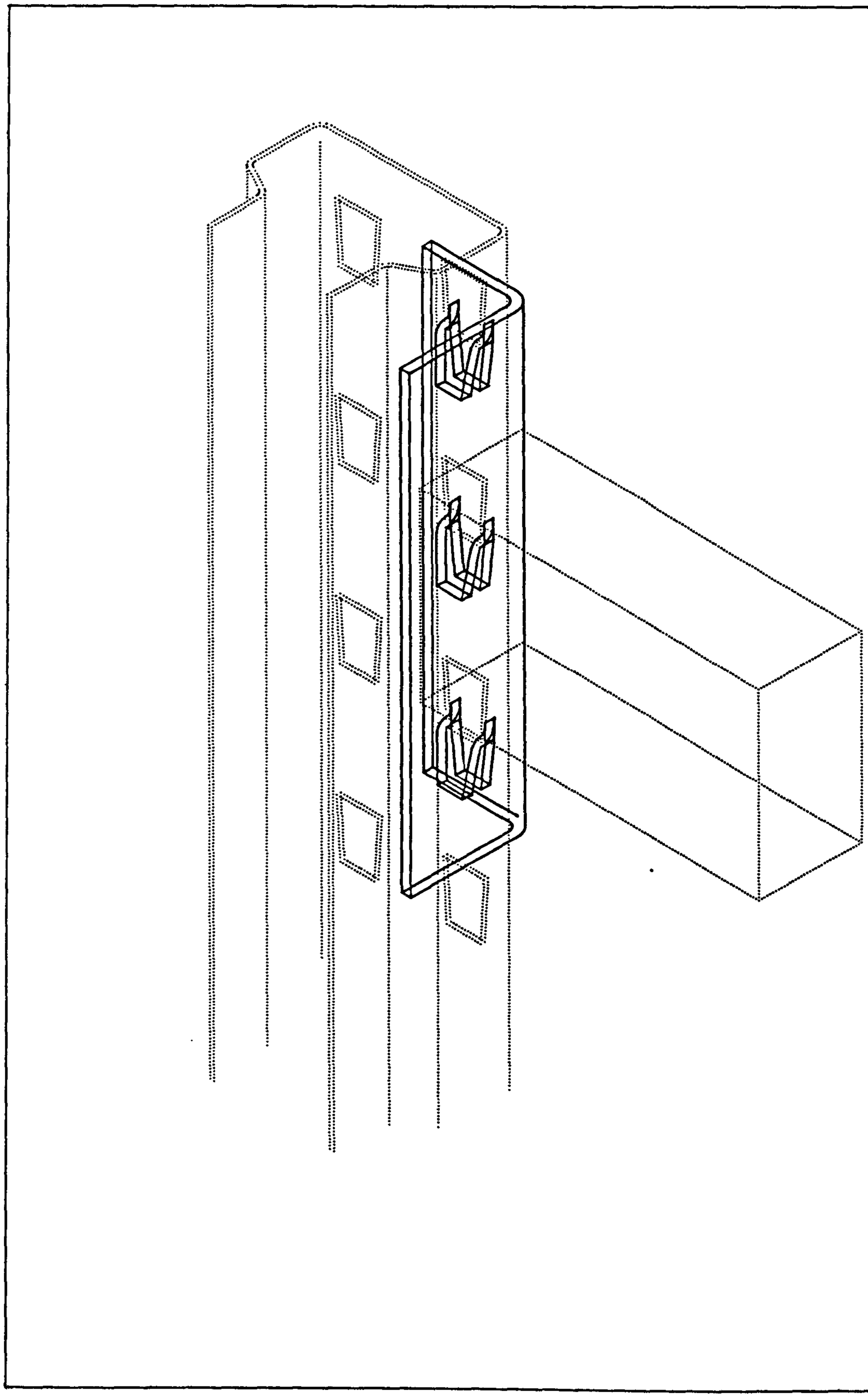

Figure 4.3 Beam end connector clipped to perforated upright

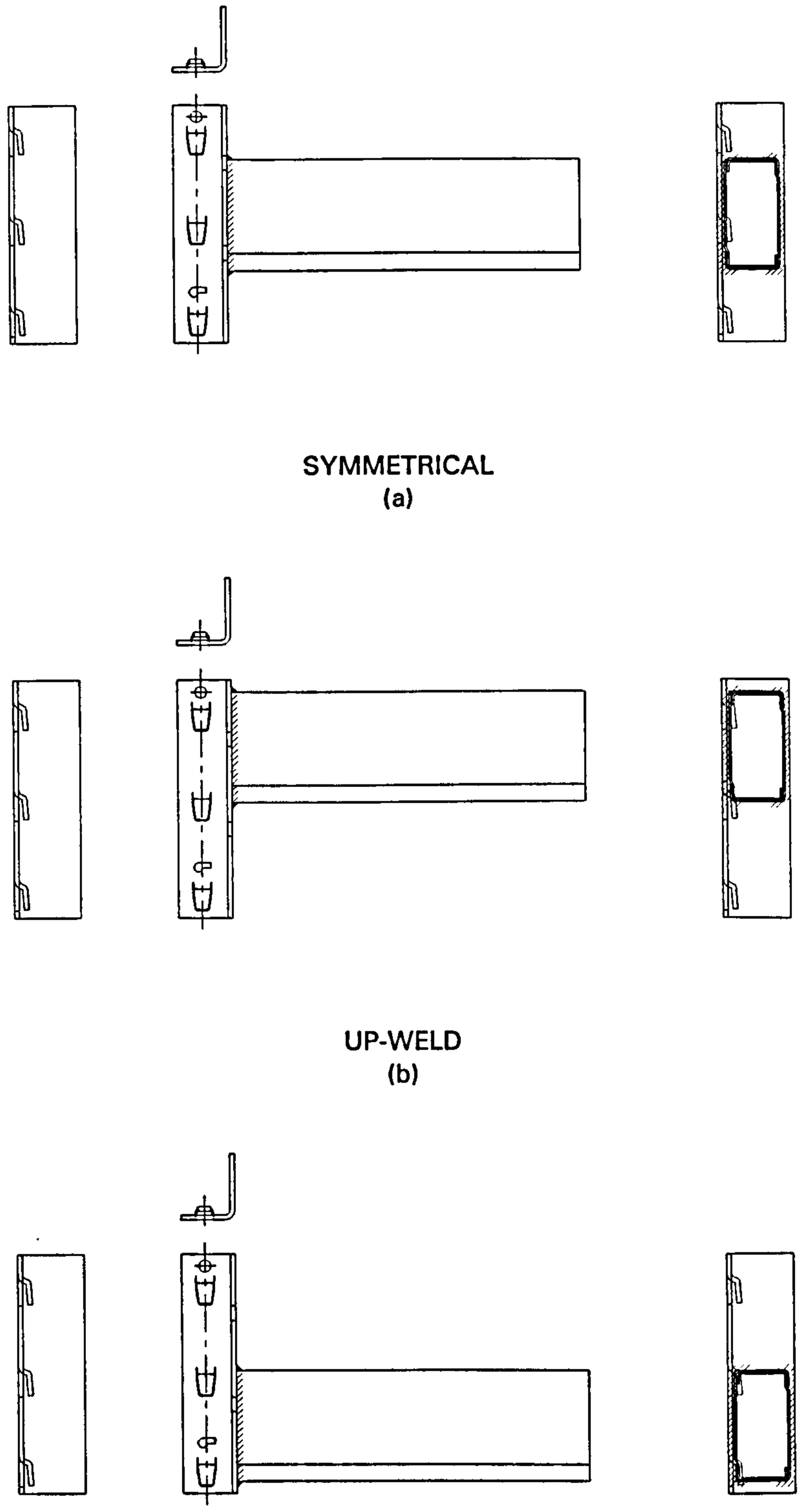

SYMMETRICAL
(a)

UP-WELD
(b)

DOWN-WELD
(c)

FIGURE 4.4 THREE WELDING POSITIONS OF BEAM TO BEAM END CONNECTOR

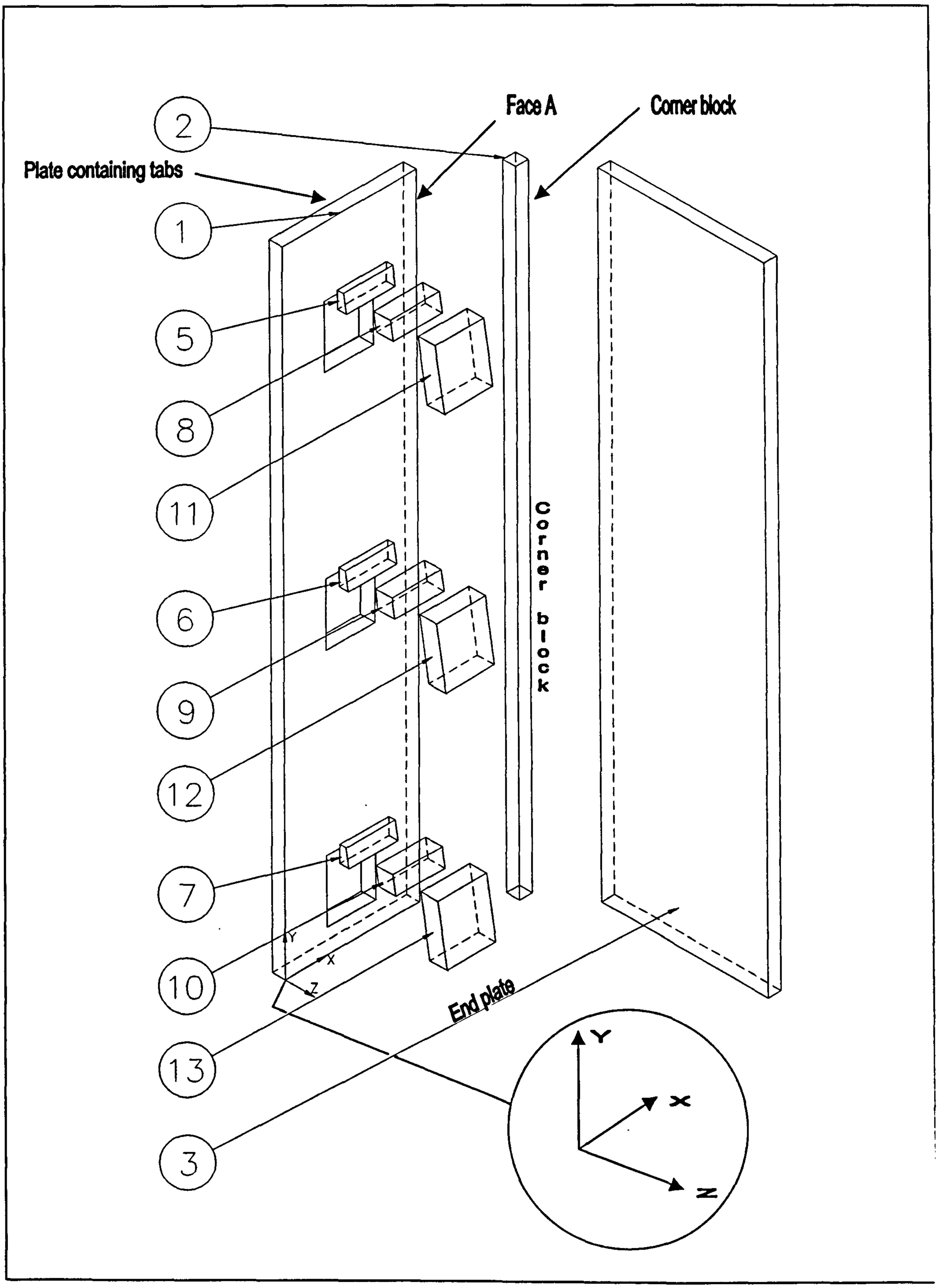

FIGURE 4.5 DISCRETISATION OF BEAM END CONNECTOR INTO TWELVE BLOCKS

FIGURE 4.6 DISCRETISATION OF STUB BEAM AND BEAM END CONNECTOR ASSEMBLY INTO SIXTEEN BLOCKS

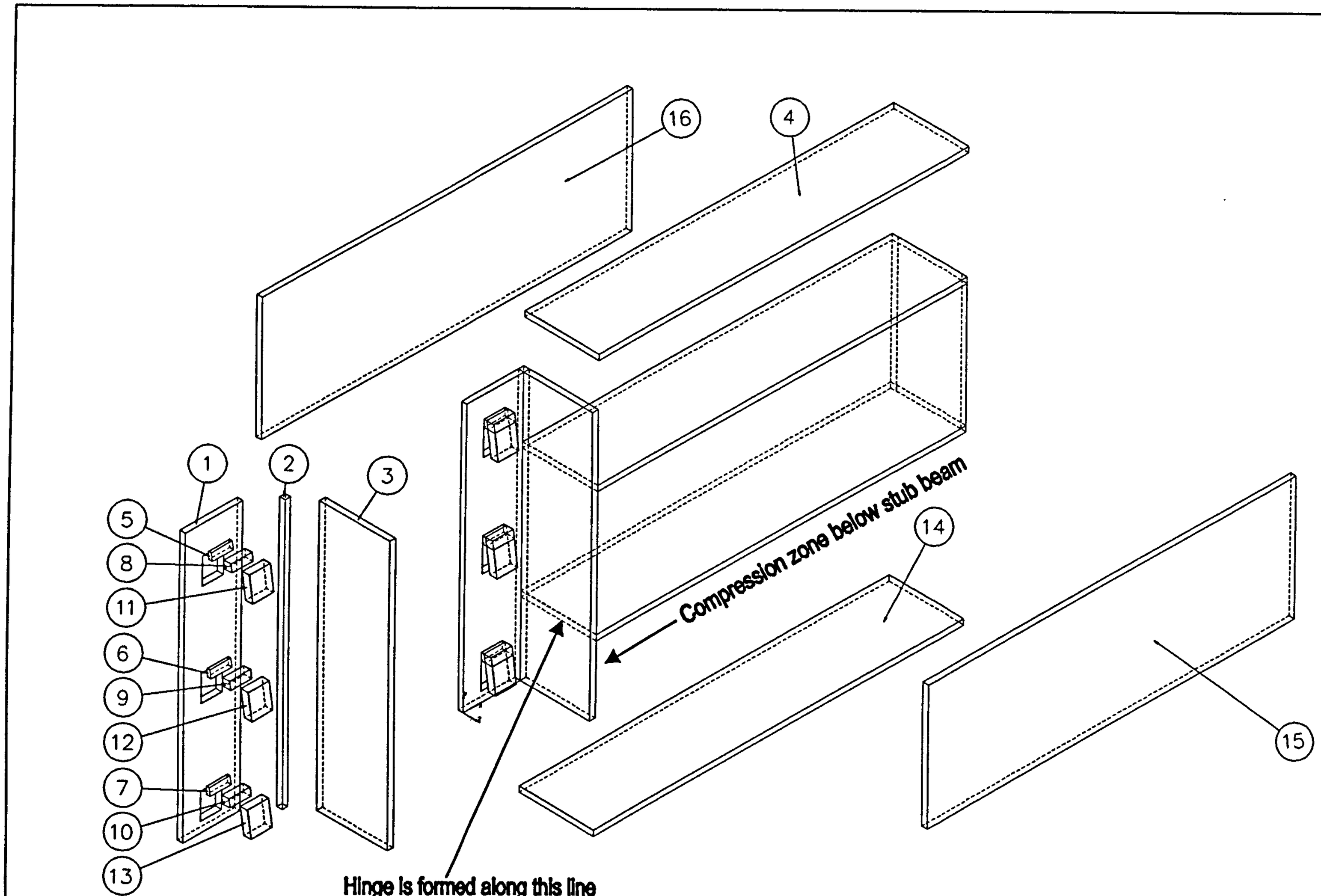

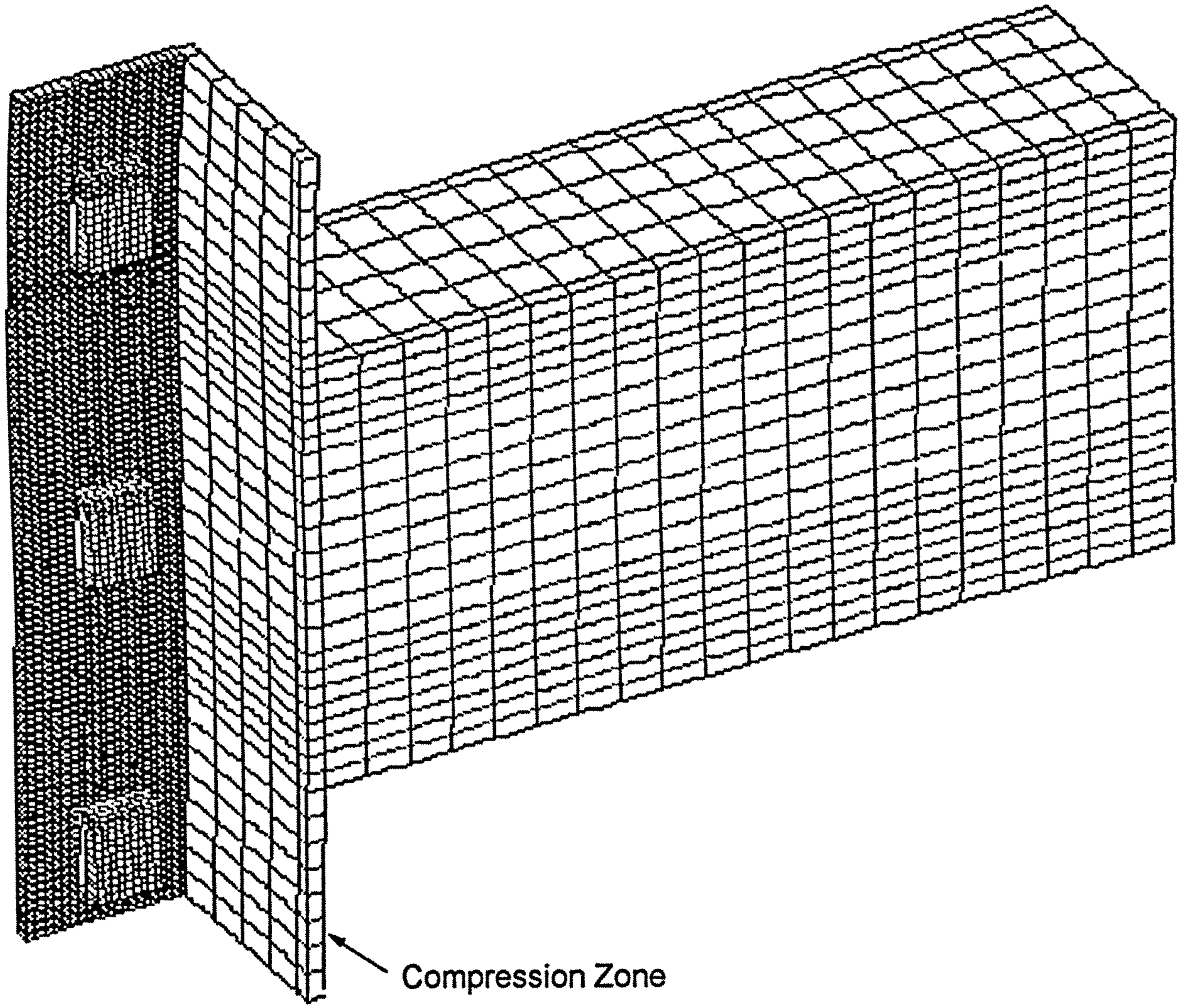

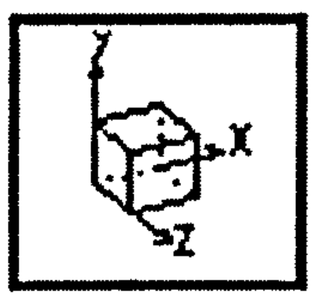

Figure 4.7 Undeformed Structure

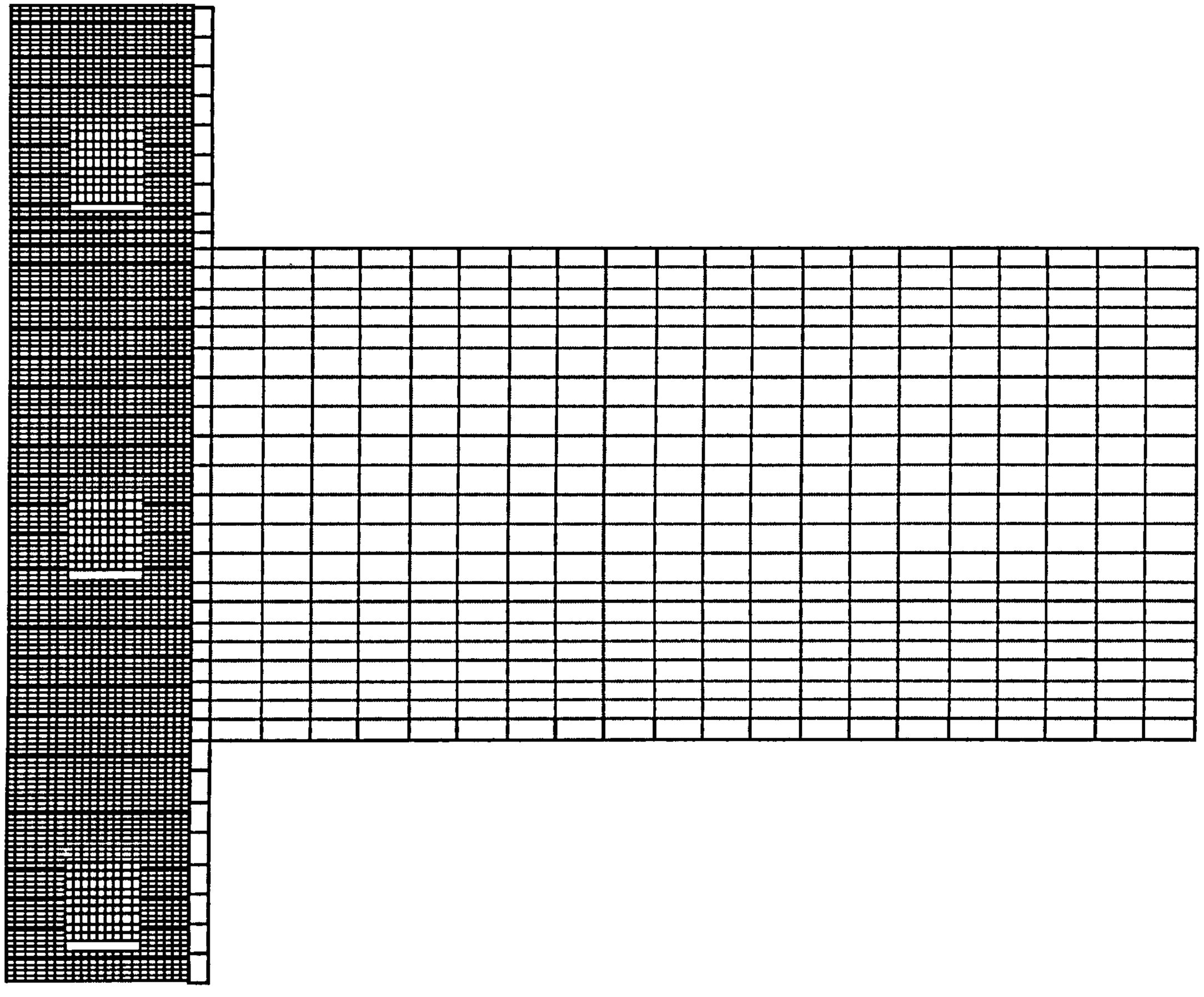

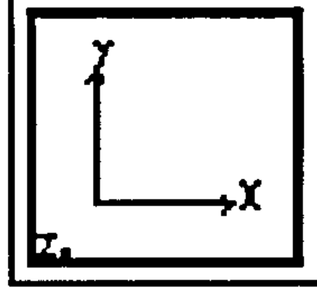

Figure 4.8 Undeformed Structure

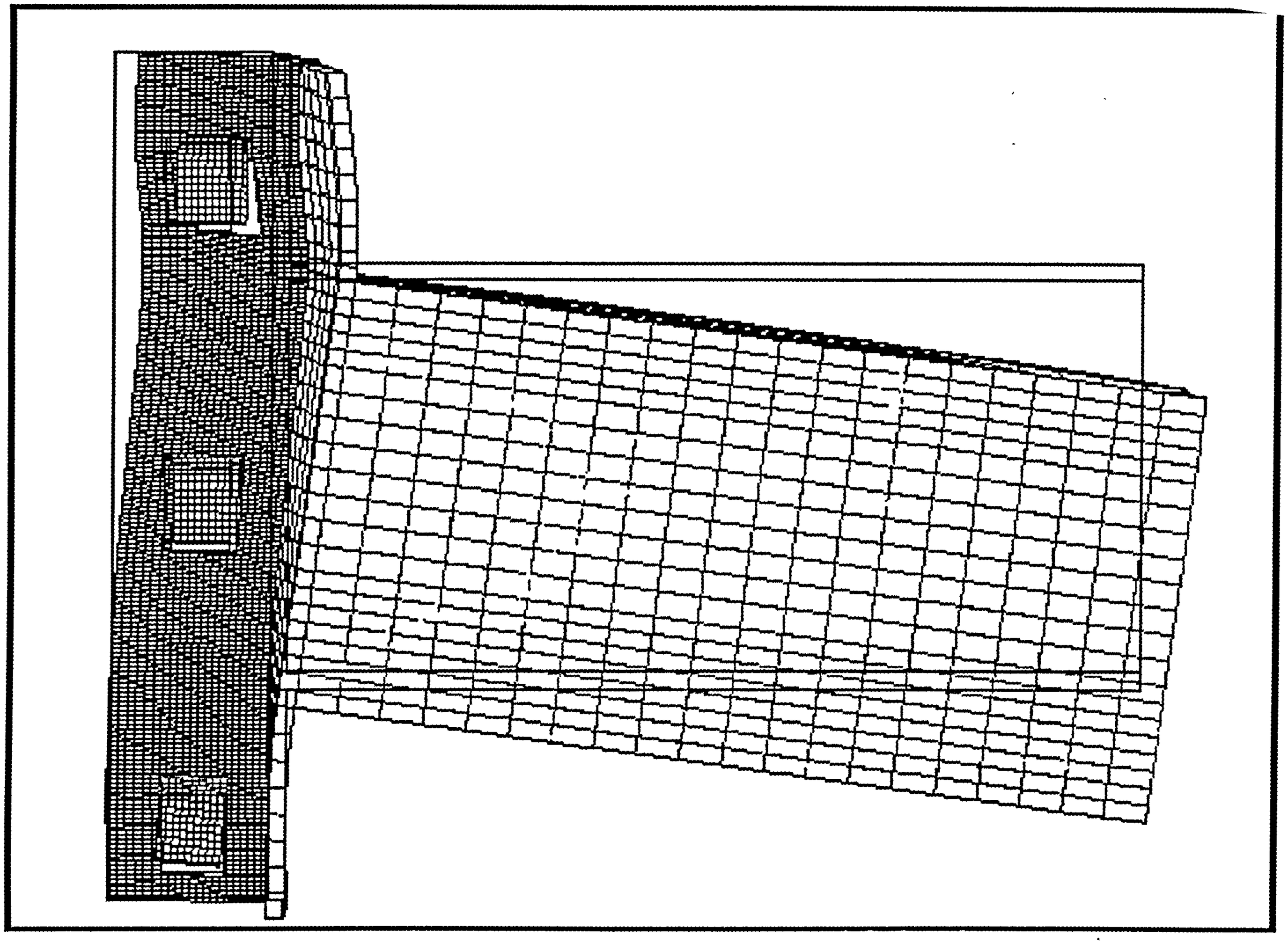

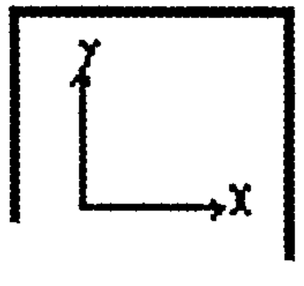

Figure 4.9 Deformed Structure Scale: 1/0.0253

Restraints At Tabs –Restrained Compression Zone-GM6A

FIGURE 4.10

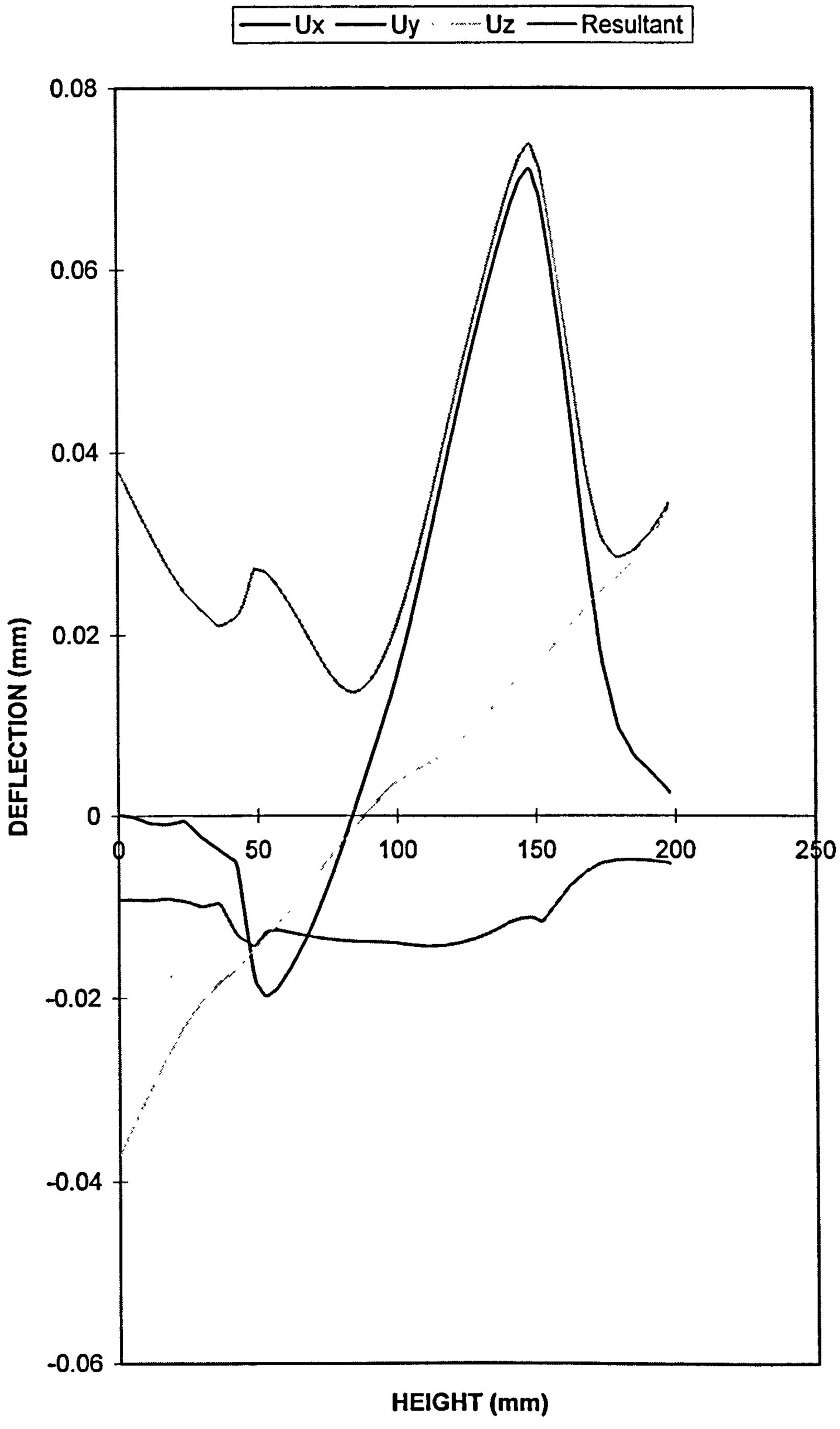
DEFLECTION V HEIGHT
GM1A
SYMMETRICAL-Restraints At Tabs-RESTRAINED
COMPRESSION ZONE
Ux
Uy
Uz
Resultant
0.08
0.06
0.04
0.02
0
-0.02
-0.04
-0.06
DEFLECTION (mm)
0
50
100
150
200
250
HEIGHT (mm)

FIGURE 4.11

DEFLECTION V HEIGHT
GM3A
SYMMETRICAL-Restraints At Tabs-RESTRAINED
COMPRESSION ZONE

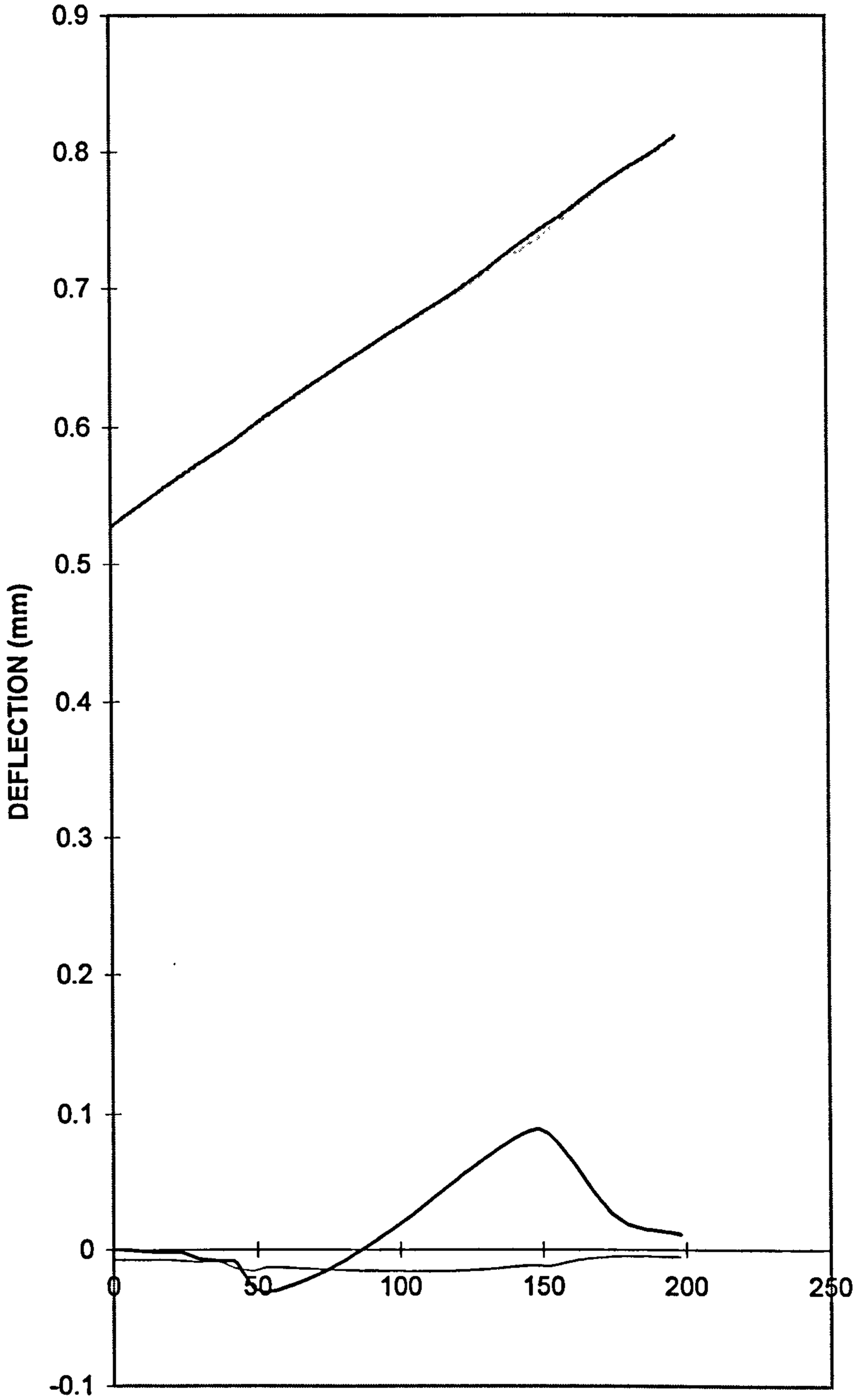

FIGURE 4.12

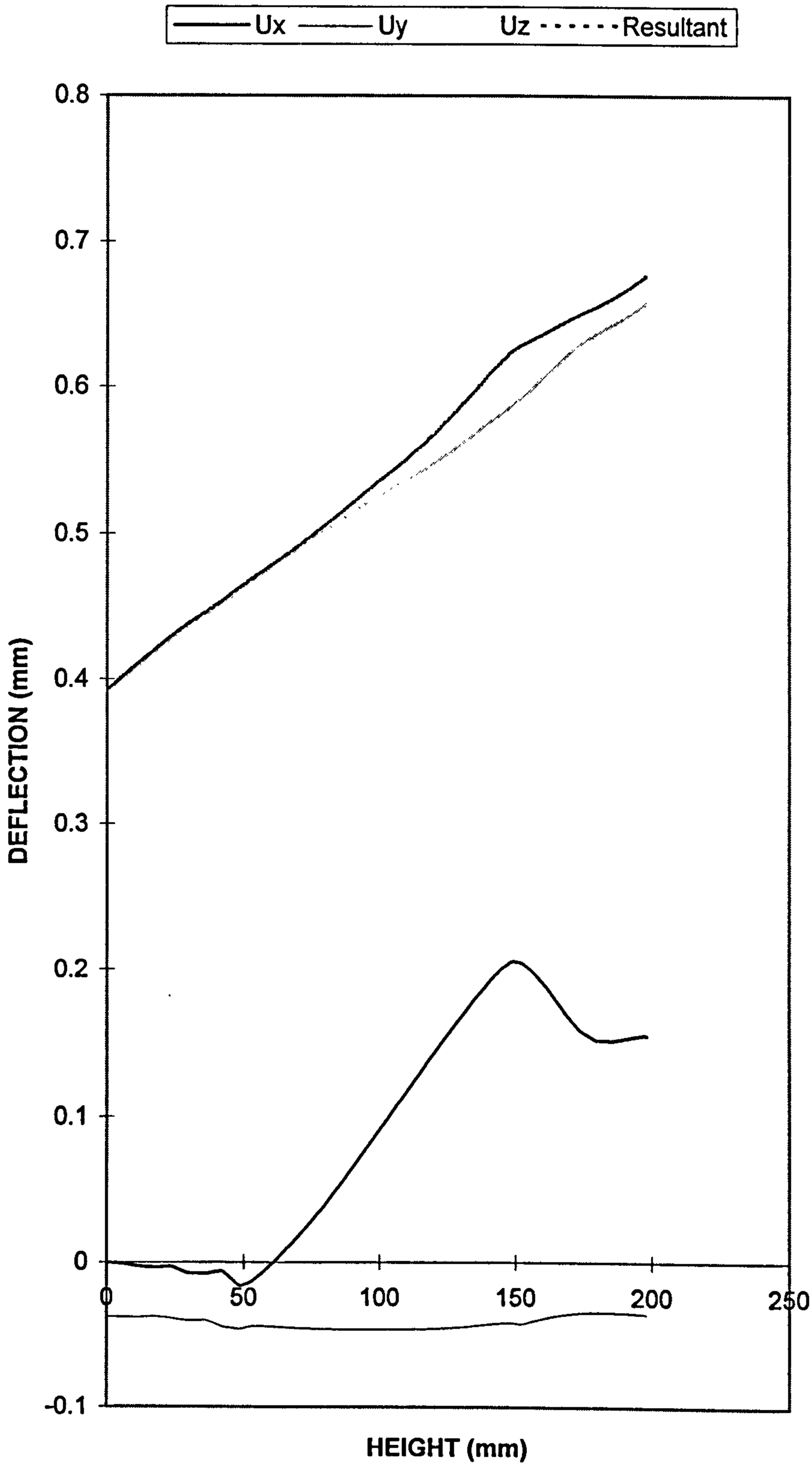
DEFLECTION V HEIGHT
GM6A
SYMMETRICAL-Restraints At Tabs-RESTRAINED
COMPRESSION ZONE
Ux
Uy
Uz
Resultant
DEFLECTION (mm)
0.8
0.7
0.6
0.5
0.4
0.3
0.2
0.1
0
-0.1
0
50
100
150
200
250
HEIGHT (mm)

FIGURE 4.13 Typical stress pattern in the tabs' plate

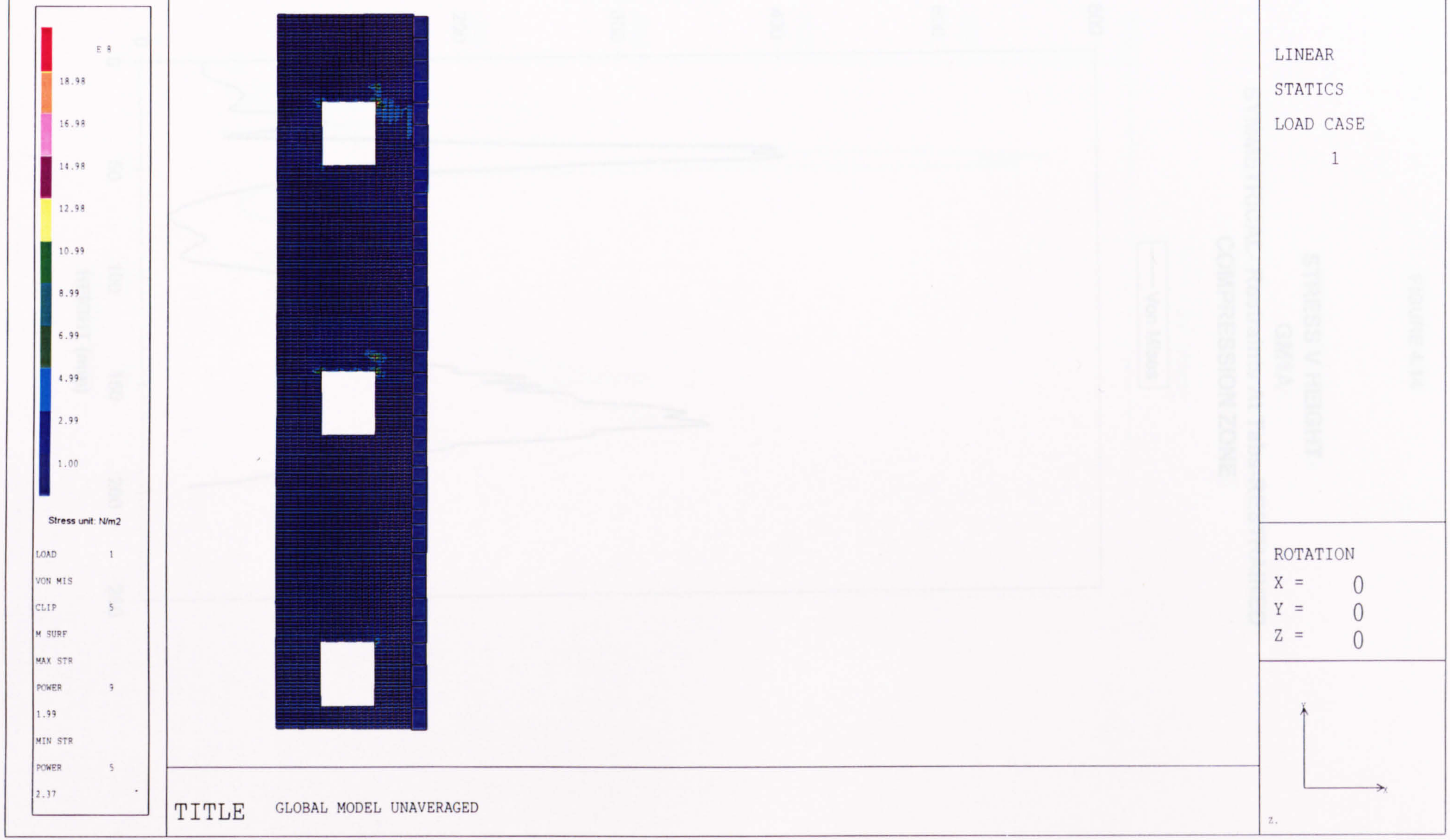

FIGURE 4.14

STRESS V HEIGHT
GM1A
SYMMETRICAL- Restraints At Tabs-RESTRAINED
COMPRESSION ZONE

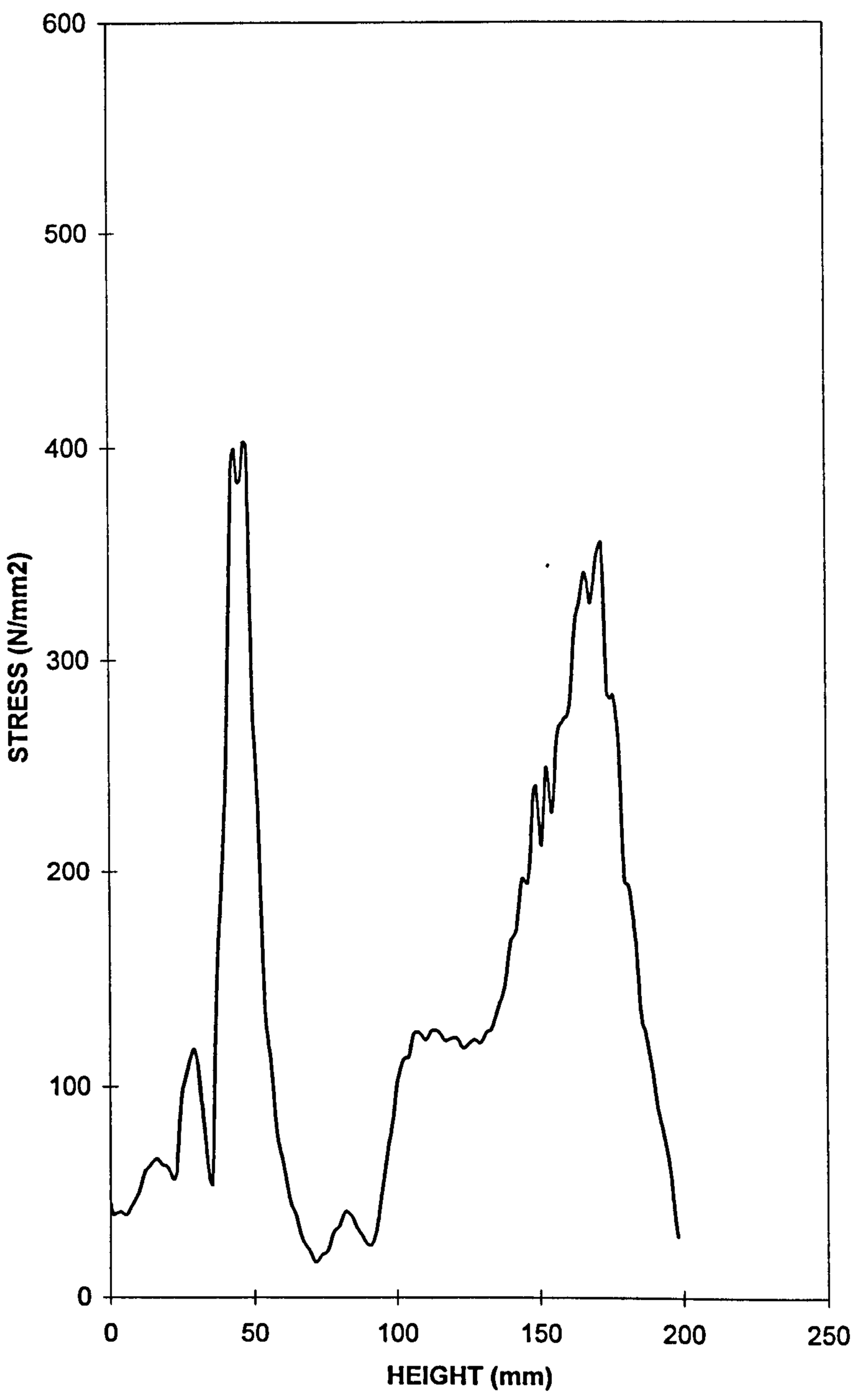

FIGURE 4.15

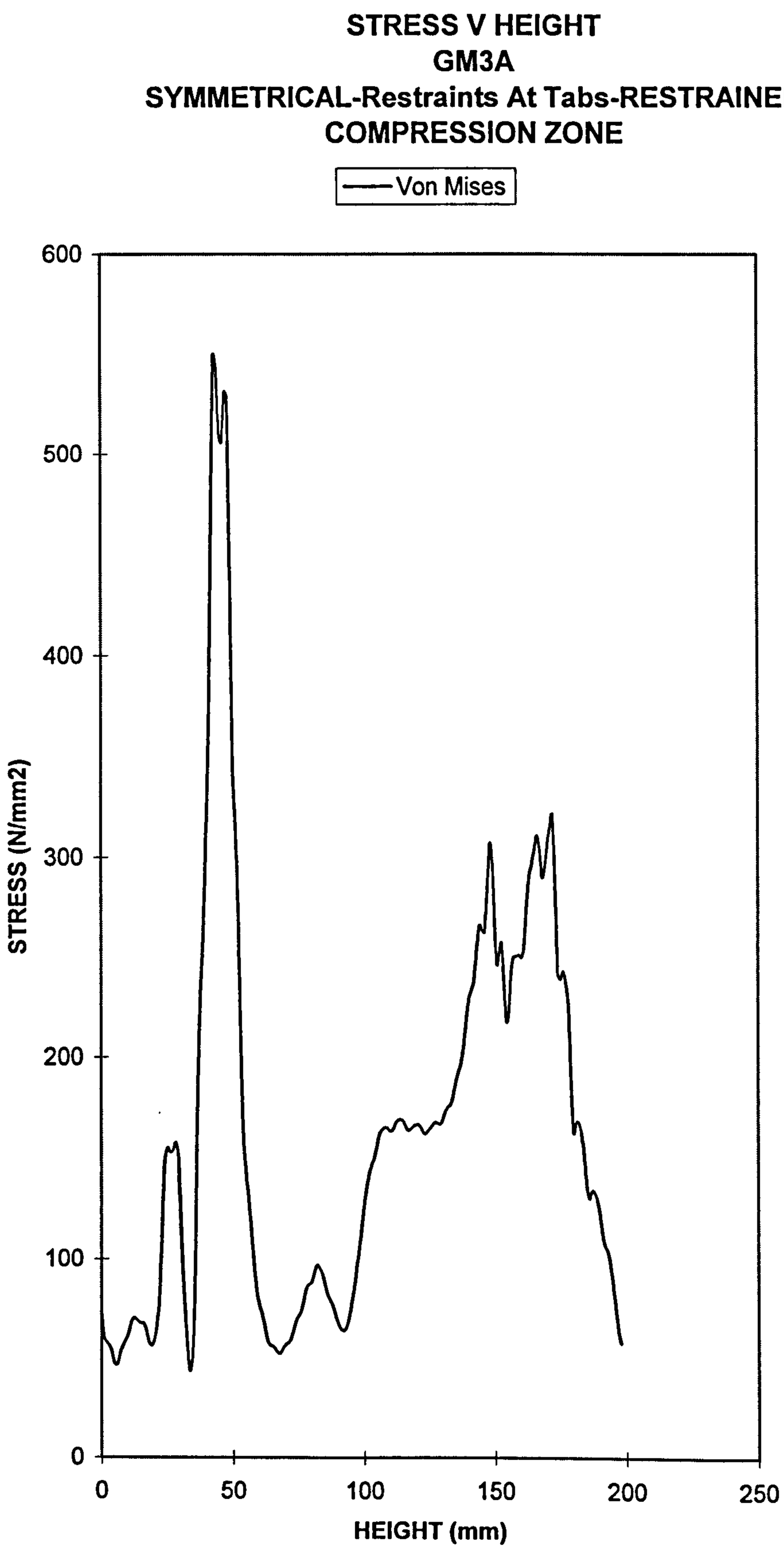
STRESS V HEIGHT
GM3A
SYMMETRICAL-Restraints At Tabs-RESTRAINED
COMPRESSION ZONE
Von Mises
STRESS (N/mm2)
600
500
400
300
200
100
0
0
50
100
150
200
250
HEIGHT (mm)

FIGURE 4.16

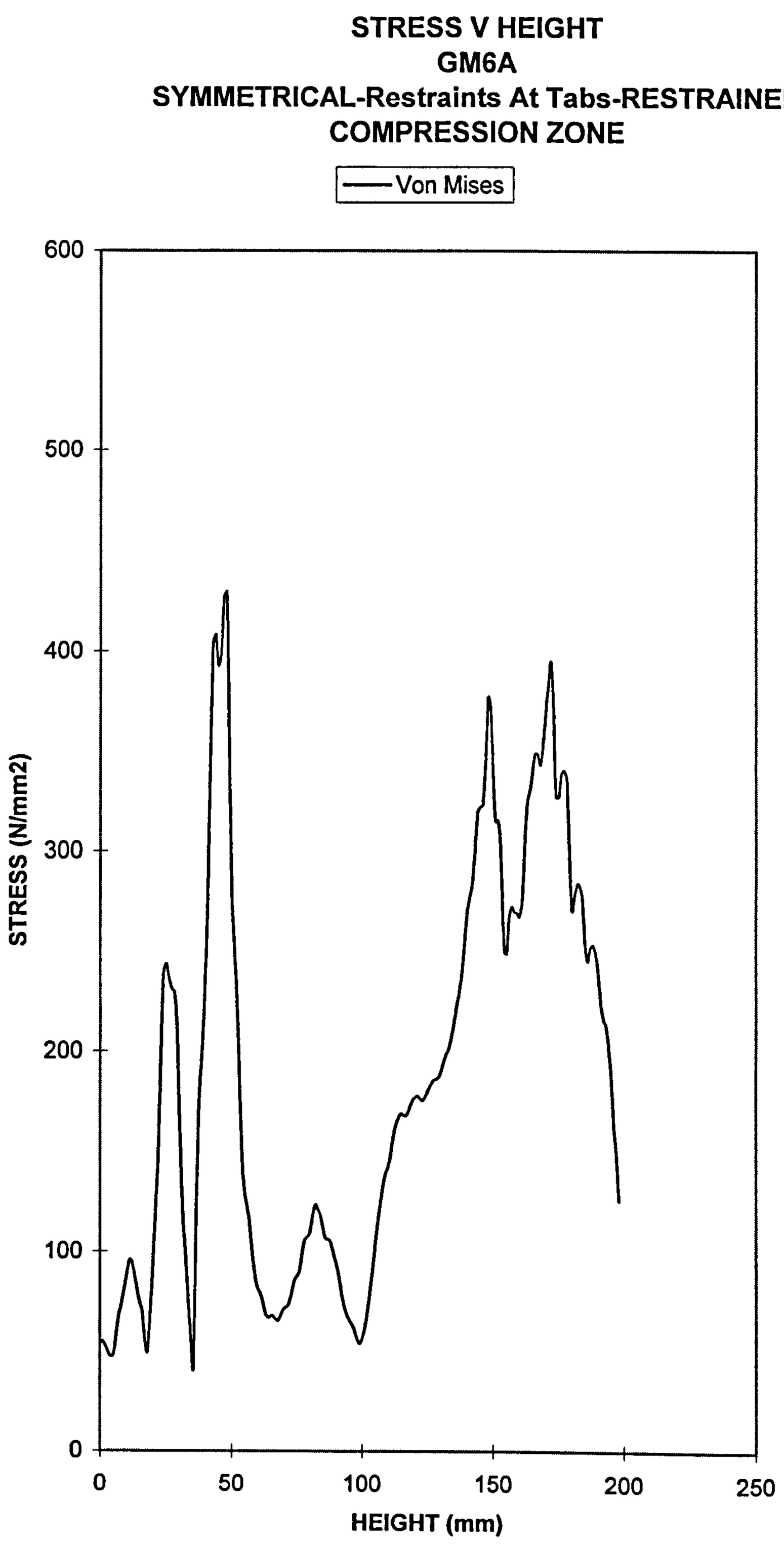
STRESS V HEIGHT
GM6A
SYMMETRICAL-Restraints At Tabs-RESTRAINED
COMPRESSION ZONE
Von Mises
STRESS (N/mm2)
600
500
400
300
200
100
0
0
50
100
150
200
250
HEIGHT (mm)

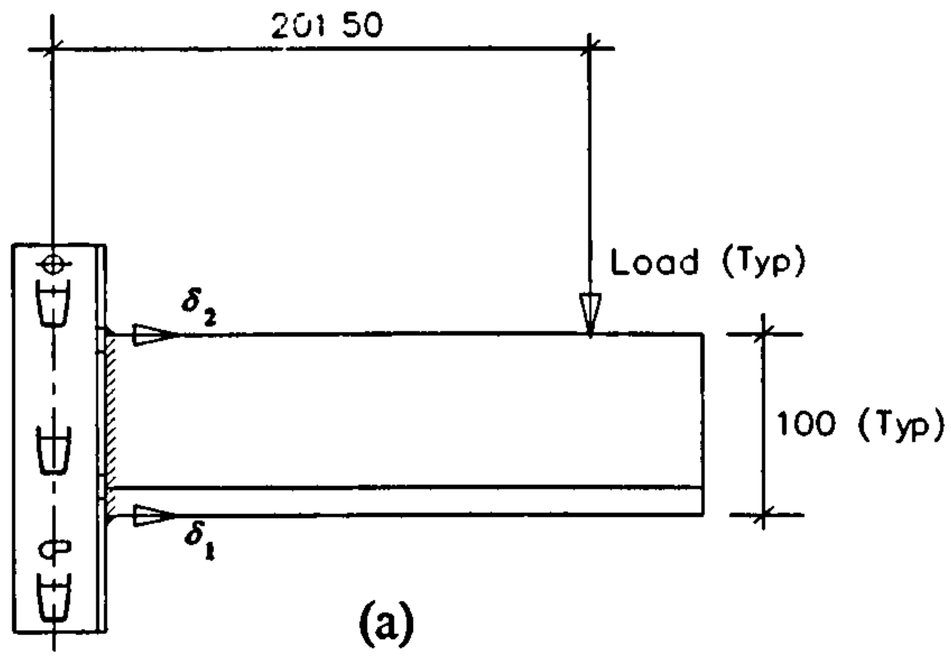

(a)

$\theta_{Vertical}=\theta_v$

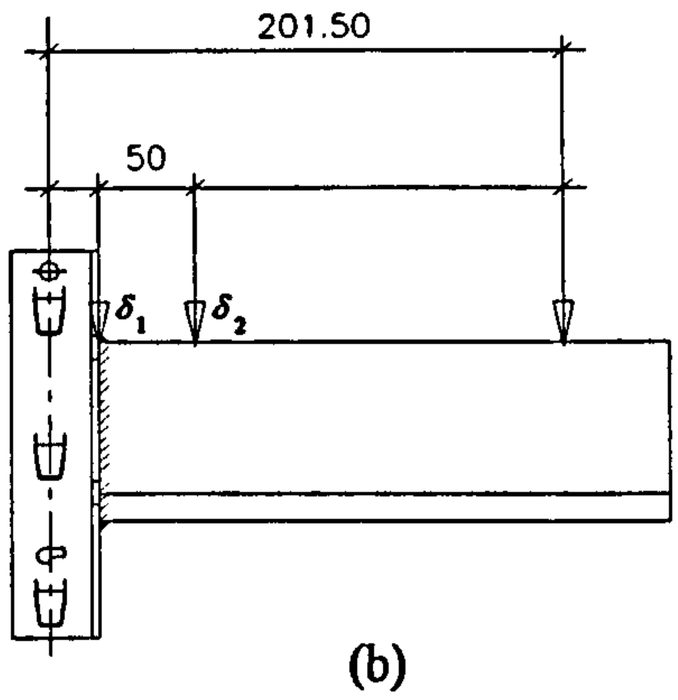

(b)

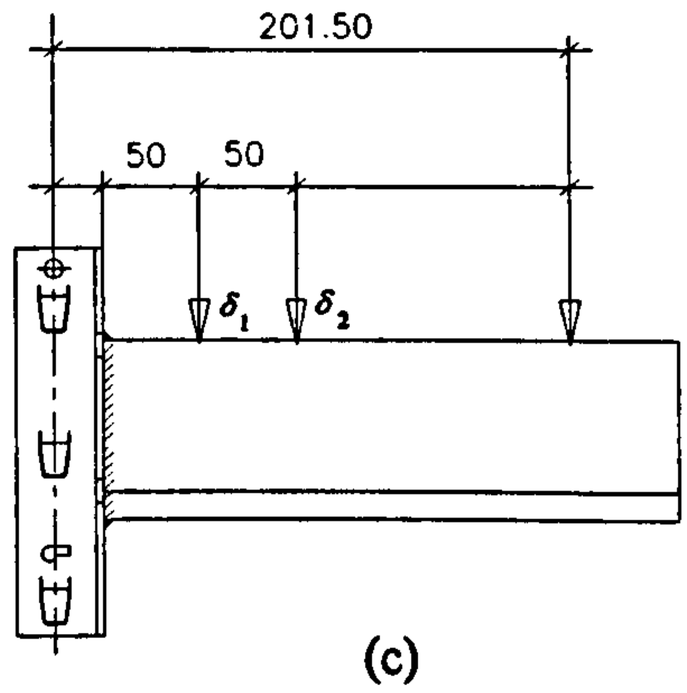

(c)

$\theta_{Top-Adjacent}=\theta_{ta}$

$\theta_{Top-Remote}=\theta_{tr}$

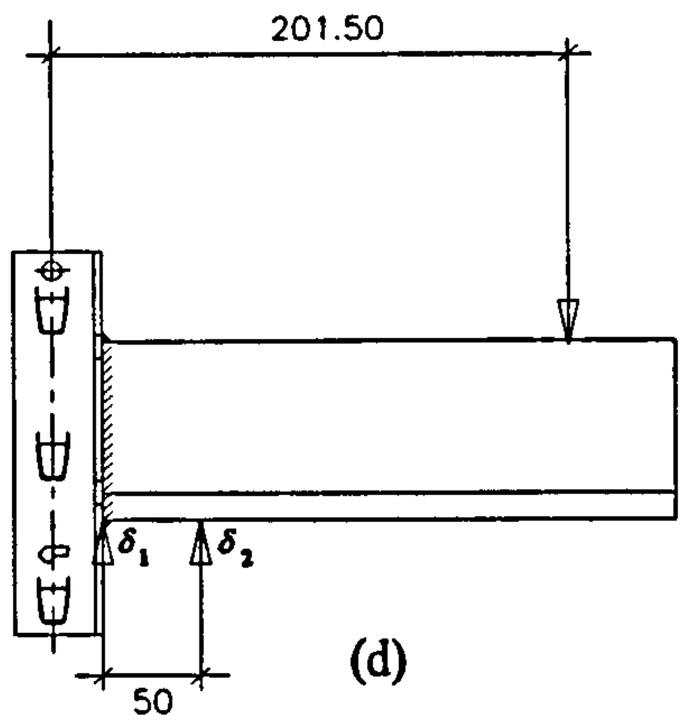

(d)

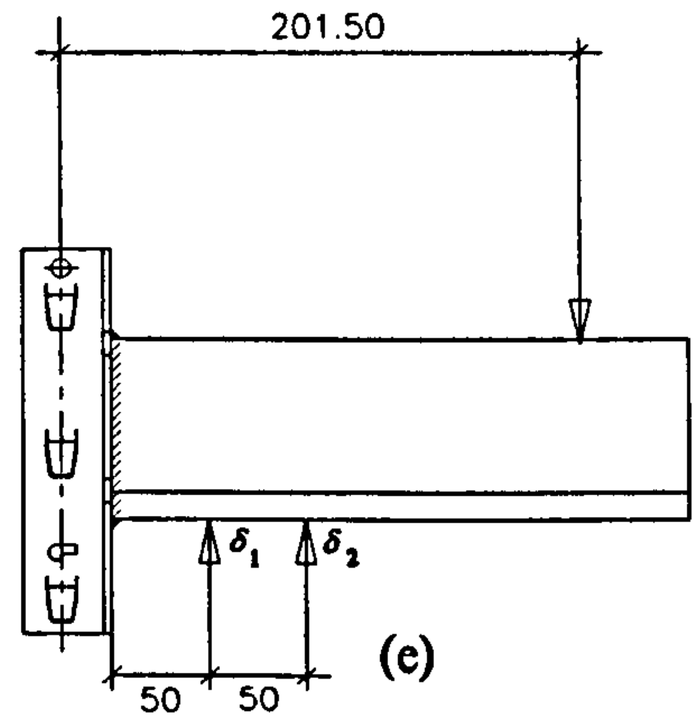

(e)

$\theta_{Bottom-Adjacent}=\theta_{ba}$

$\theta_{Bottom-Remote}=\theta_{br}$

FIGURE 4.17 ROTATION MEASUREMENT METHODS USING THE FE MODELS.

METHOD (c) WAS ADOPTED FOR TESTING THE BEAM END CONNECTORS.

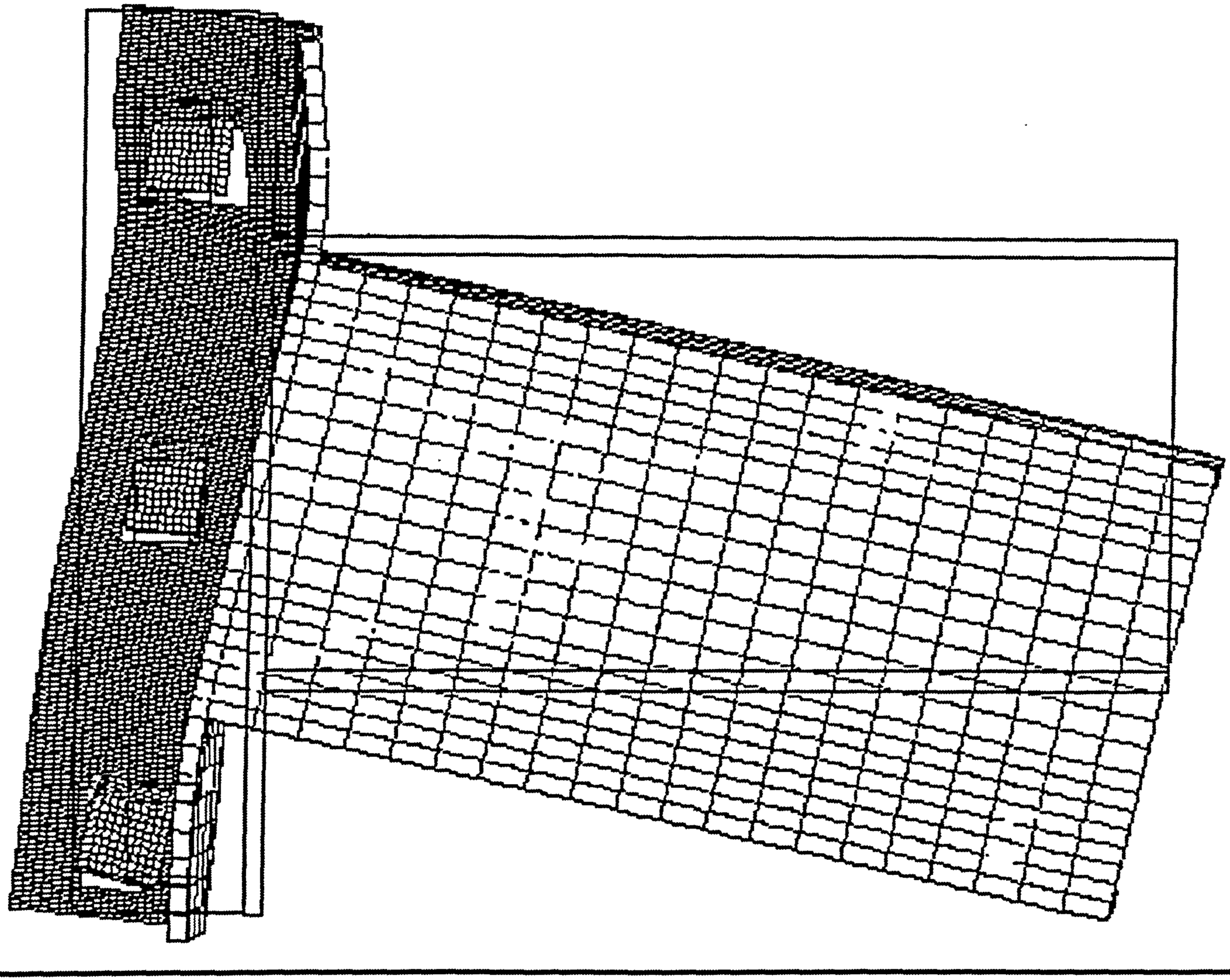

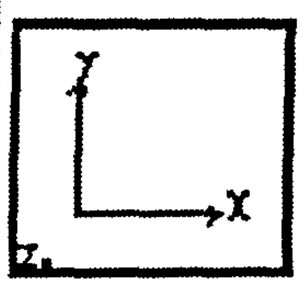

Figure 4.18 Deformed Structure Scale: 1/0.0253

Restraints At Tabs –Free Compression Zone-GM6B

FIGURE 4.19

DEFLECTION V HEIGHT
GM1B
SYMMETRICAL-Restraints At Tabs-FREE COMPRESSION ZONE

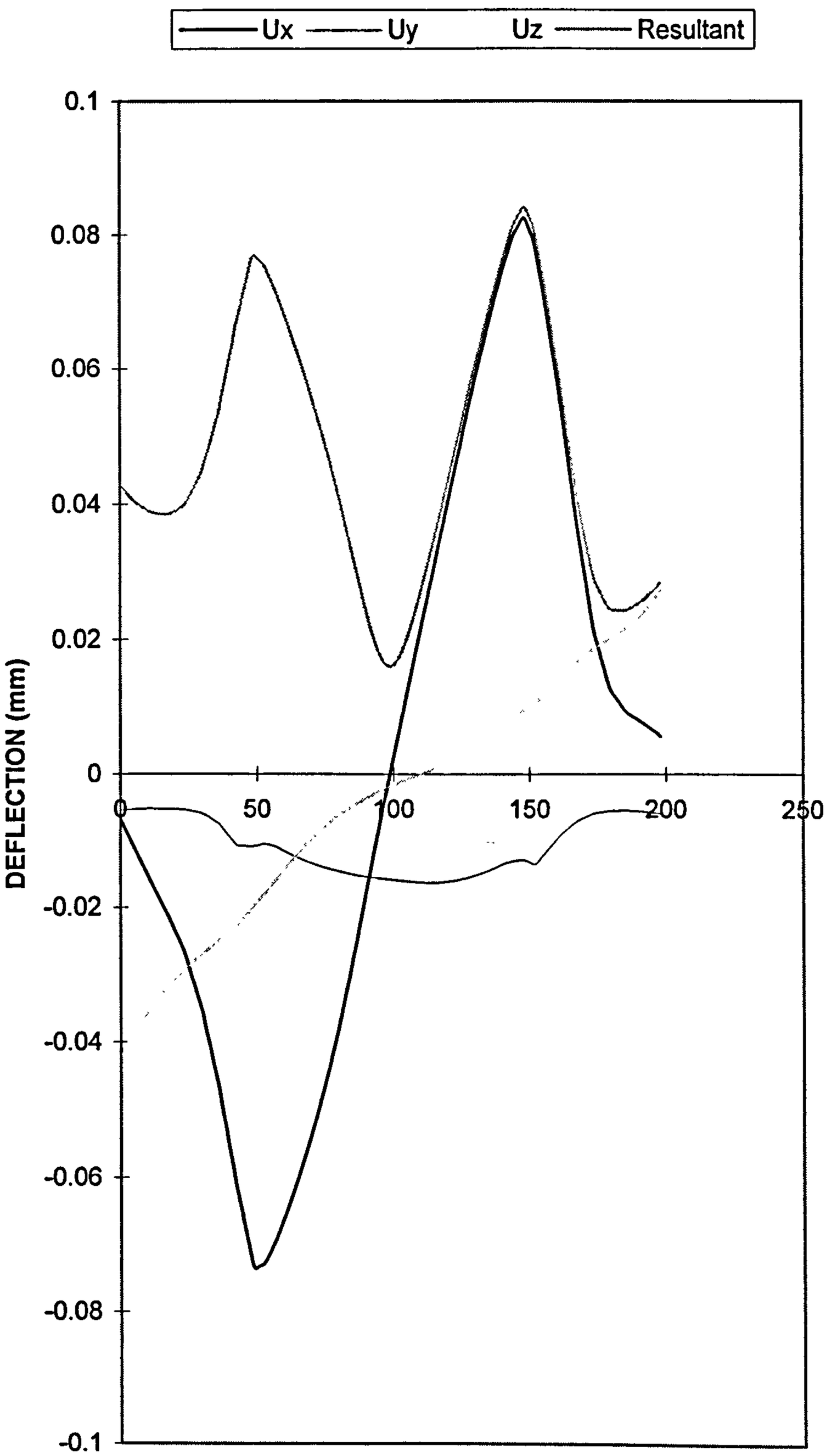

FIGURE 4.20

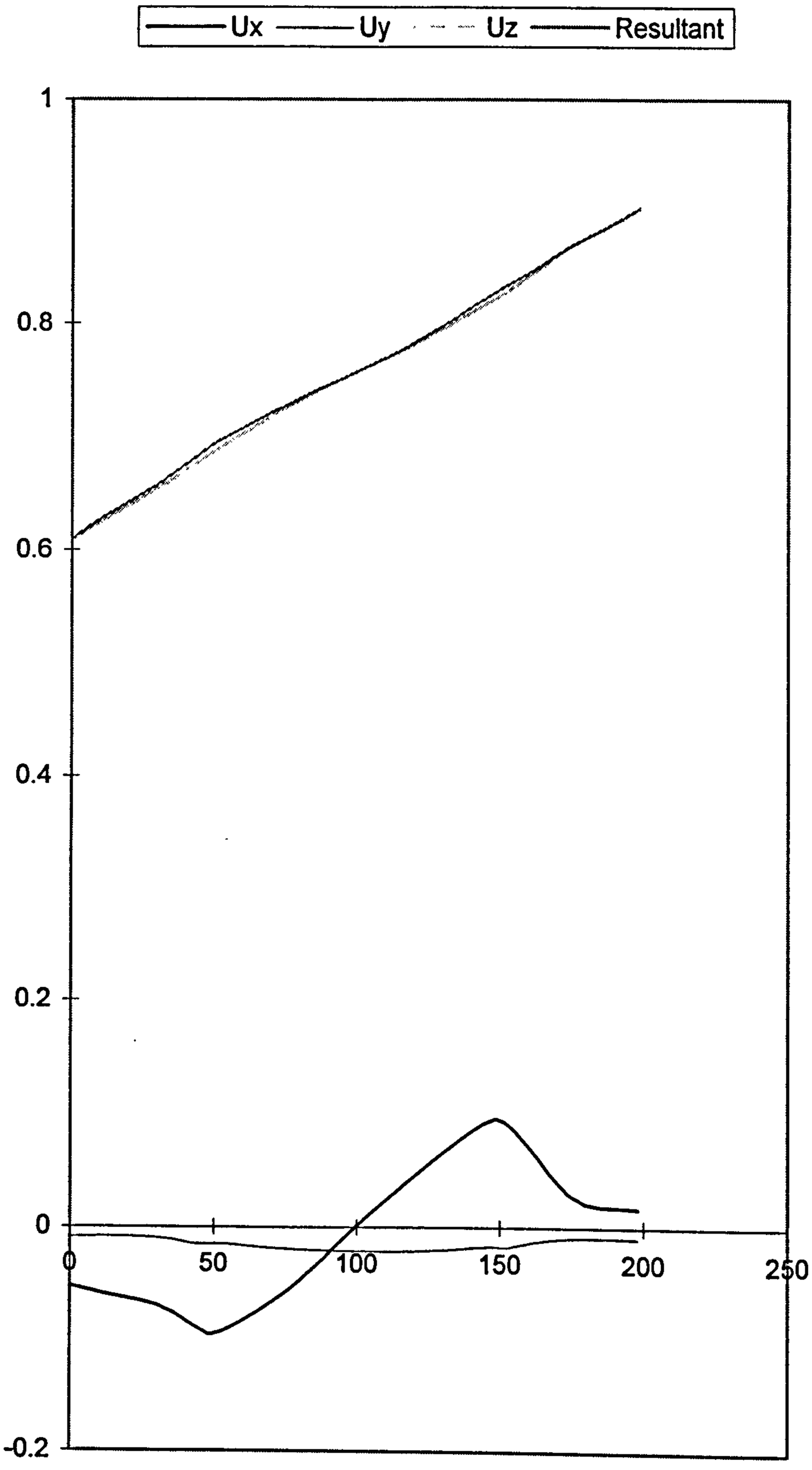
DEFLECTION V HEIGHT
GM3B
SYMMETRICAL-Restraints At Tabs-FREE COMPRESSION ZONE
Ux
Uy
Uz
Resultant
DEFLECTION (mm)
1
0.8
0.6
0.4
0.2
0
-0.2
0
50
100
150
200
250
HEIGHT (mm)

FIGURE 4.21

DEFLECTION V HEIGHT
GM6B
SYMMETRICAL-Restraints At Tabs-FREE COMPRESSION ZONE

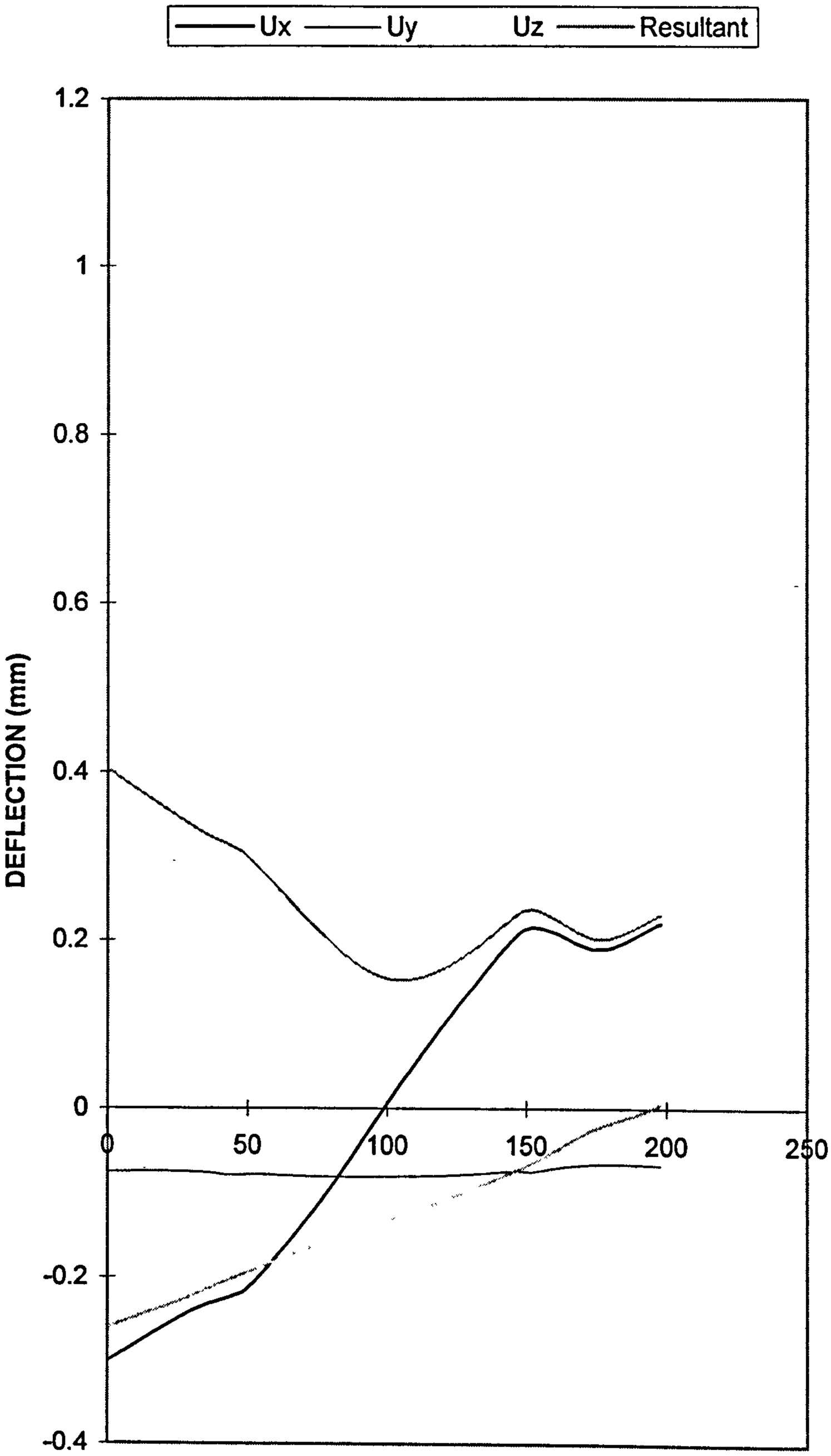

FIGURE 4.22

STRESS V HEIGHT
GM1B
SYMMETRICAL-Restraints At Tabs-FREE COMPRESSION ZONE

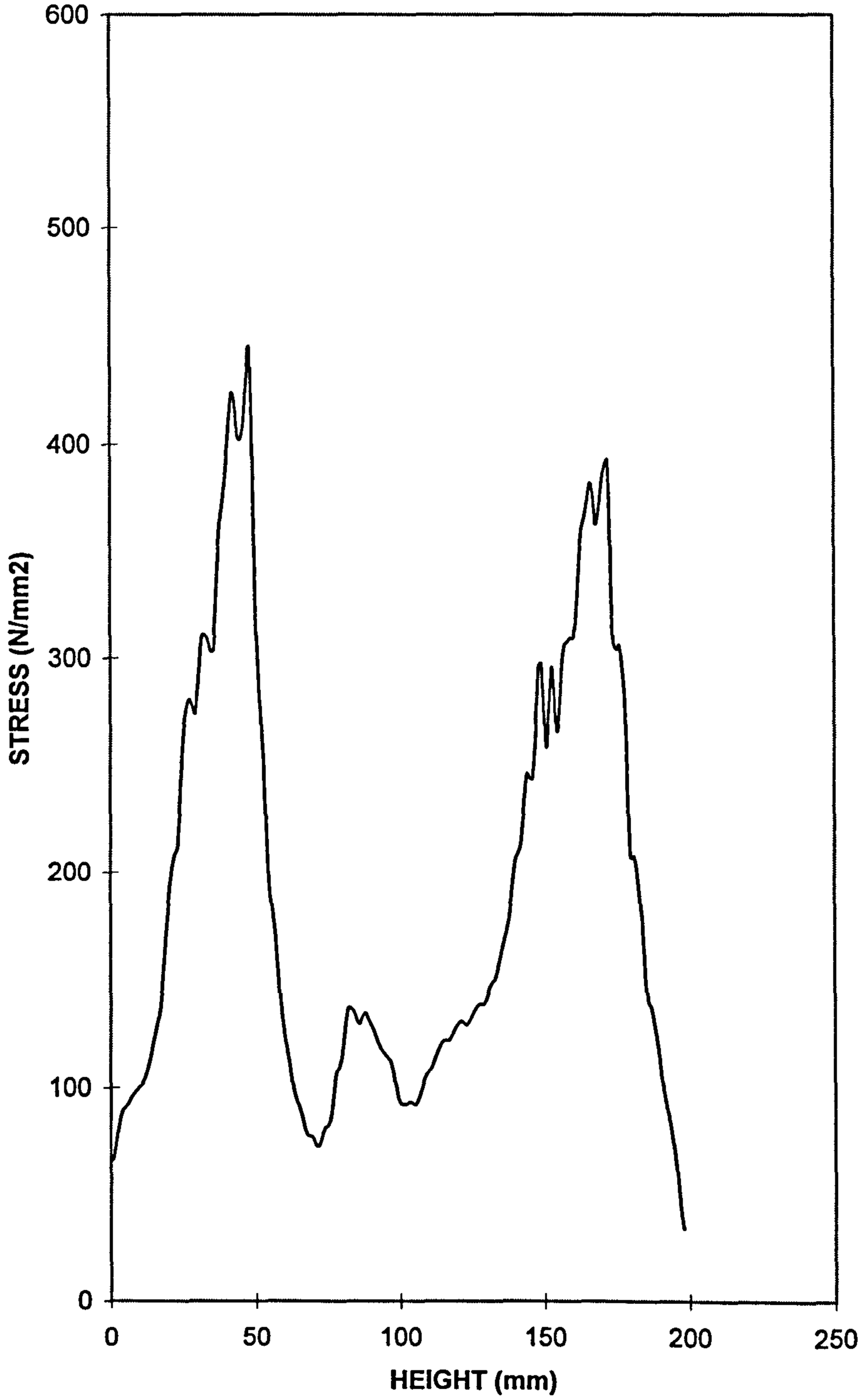

FIGURE 4.23

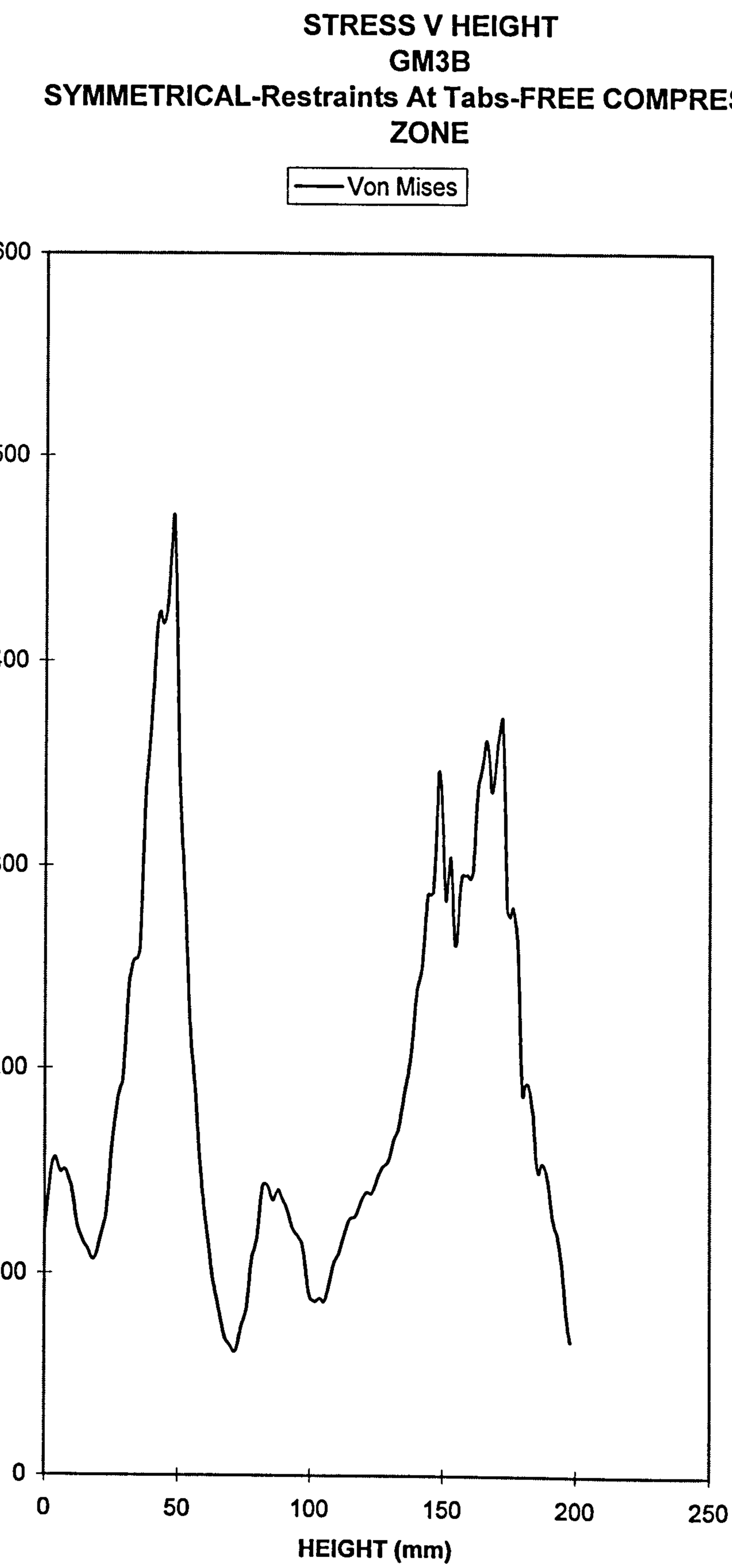
STRESS V HEIGHT
GM3B
SYMMETRICAL-Restraints At Tabs-FREE COMPRESSION ZONE
Von Mises
600
500
400
300
200
100
0
STRESS (N/mm2)
0
50
100
150
200
250
HEIGHT (mm)

FIGURE 4.24

STRESS V HEIGHT
GM6B
SYMMETRICAL-Restraints At Tabs-FREE COMPRESSION ZONE

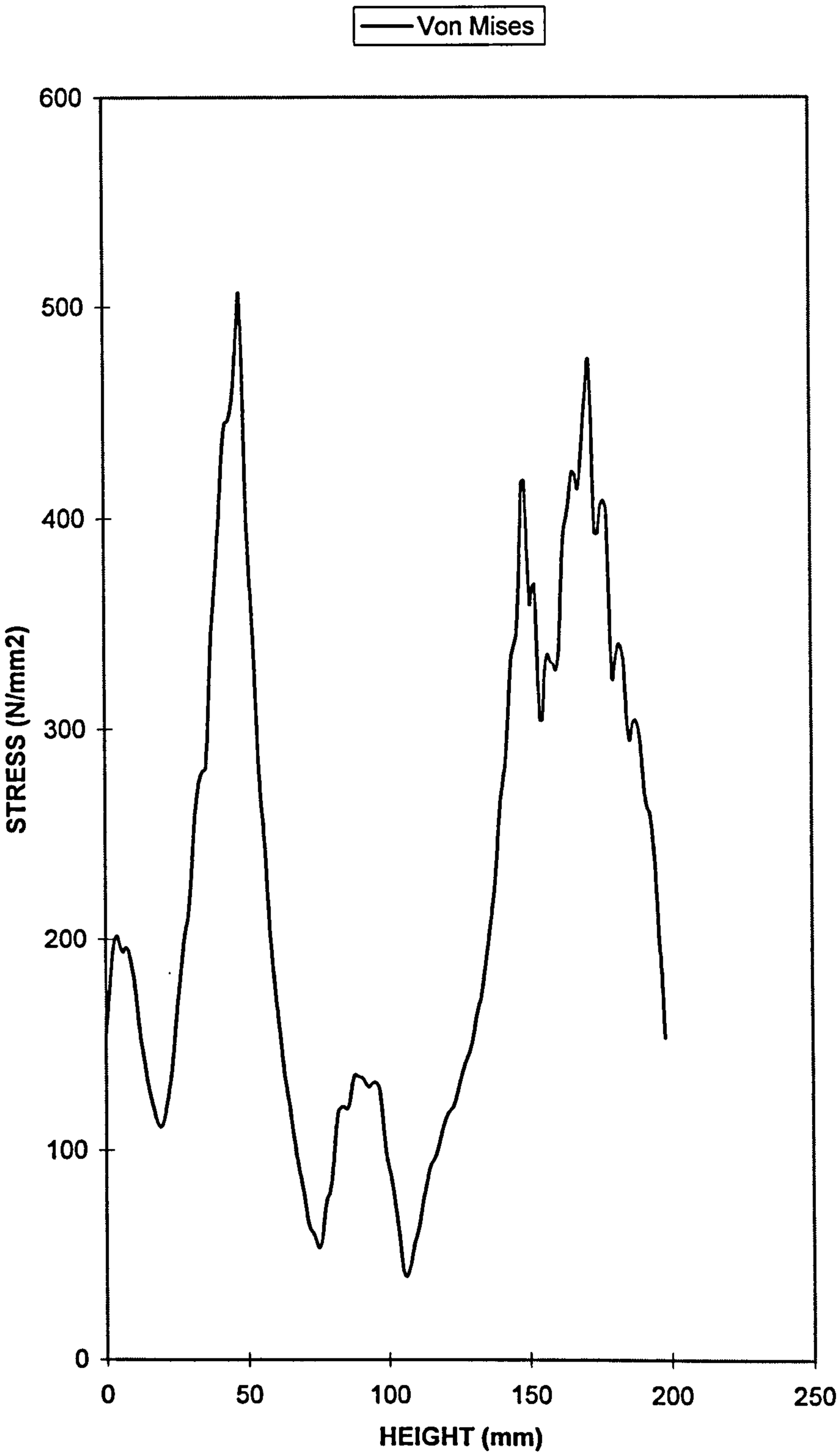

CHAPTER 5

ELASTO-PLASTIC SUB-MODEL OF UPRIGHT'S WEB

C H A P T E R 5

ELASTO-PLASTIC SUB-MODEL OF UPRIGHT'S WEB

5.1 Introduction

The previous chapter described the use of absolute restraints as the means of anchorage, providing the resistance to rotation required to generate the global models. They were used to restrain the tabs as well as to simulate the presence of the compression zone figure 4.6.

The work in the previous chapter provided useful information on the behaviour of the beam end connector but adopting absolute restraints meant that we had a rigid connection and as the result ignored the presence of an upright.

In practice as a beam end connector was loaded, the first resistance encountered was through the interaction of its tabs with the upright's web. Figure 4.2 shows the horizontal and vertical force components involved. These provided the elastic source of resistance to rotation before a hinge was formed resulting in a compression zone below the beam's bottom flange, figure 4.6.

During testing various beam end connector designs the tabs or the studs indented the upright's web as they were loaded. This happened during the initial stages of loading. At the same time, the tabs themselves remained intact until

the final stages of loading. This proved that the upright's web was the weak link.

The directions of the forces causing the indentations are shown in figure 4.2 and were due to the contact areas between the tabs and the upright's web, figure 4.1.

Therefore, it was decided that the magnitude of the resistance offered by the upright's web should be determined in these two directions, horizontal and vertical.

A sub-model was to be considered. The model would be a function of the web thickness, its width as well as the mechanical properties of the steel.

Two sub-models were generated. The first model determined the stiffness of the upright's web in the horizontal direction. The second model evaluated the stiffness of the upright's web in the vertical direction.

The results of the exercises were used to replace the absolute restraints at the tabs in the global model described in the previous chapter.

Once the global model was modified, as in the previous chapter, it was used to evaluate the initial stiffness values.

The two scenarios relating to before and after compression zone formation were considered here too. In each case the stress distribution and the variation in deflection along the face A, figure 4.5 was examined.

5.2 Sub-modeling upright's web to determine its strength in the horizontal direction-Mesh generation and results.

Figure 5.1 shows a mesh generated to model a section of the upright's web with a slot in the middle. The length, width and the thickness of the section were 45mm, 38mm and 1.8mm respectively. The dimensions of the slot were 25mm by 18mm. The selected dimensions were typical of the perforations of the upright used in the tests.

The perforation in the sub-structure is the location where the interlocking between the upright and the tabs of the beam end connector take place.

The aim was to carry out an elasto-plastic analysis of the side interaction between the tab and the upright, figures 4.1, 4.2 and 4.3, so that the stiffness offered by the upright's web horizontally could be evaluated.

To achieve this, initially a relatively coarse mesh was generated. The type of element used was an 8 noded flat isoparametric quadrilateral element suitable for plane stress applications. This is an element which carries load in its own plane only and has two degrees of freedom (u_x,u_y).

The load was applied as incremental displacements.

A series of models with increasing mesh densities in the vicinity of the load application area were generated so that a convergence check could be carried out. Each time plots of load versus deflection were produced and compared until either a drop in the load or a continuous plateau indicating attainment of convergence was observed.

Figure 5.2 shows a typical load versus deflection curve obtained giving a stiffness value of 2.84E8 N/m. Figures

5.3 and 5.4 show the deformed structure and the resulting stress pattern.

There were a number of options for restraining the sub-model and applying load to it. To ensure that such variations would not affect the results, various boundary conditions were investigated. Figure 5.6 shows the variations in boundary conditions considered. Figures 5.7-5.10 show the results obtained. No variation was observed.

For comparison purposes a second data file was produced, this time more loading increments were used in the elastic range. The difference in the outcome was negligible. Figure 5.5 shows a typical such curve.

5.3 Sub-modeling upright's web to determine its strength in the vertical direction- Mesh generation and results.

Figure 4.2 shows the resulting vertical force components when the tabs come into contact with the upright's web as a beam end connector is loaded.

An elasto-plastic analysis of this downward interaction was also considered and the stiffness offered by the upright's web vertically was evaluated.

Due to symmetry only one half of the structure was modeled. Figures 5.11 to 5.13 show the undeformed, deformed and the resulting stress pattern.

Here also, the effects of varying boundary conditions were investigated. There were none. Figure 5.14 shows the result obtained. From the curve a stiffness value of 8E8 N/m was evaluated.

5.4 Using the spring stiffness values obtained to modify the global models

The stiffness of the upright's web was determined as horizontal and vertical components as described above. They were used to replace the restraints at the tabs in the global models described in the previous chapter. The restraints were replaced with springs of appropriate number and magnitude ensuring that the total magnitude of resistance was maintained in X and Y directions.

The cases with spring elements are presented in tables 5.1 and 5.2 for the restrained and free compression zone scenarios respectively. Here, the first two cases were not applicable as the spring stiffness values were only measured horizontally and vertically.

As described in section 4.3.2, the two scenarios relating to stages before and after compression zone formation were considered and carried out separately.

The first scenario would simulate the 0%-40% loading stage, when the bottom part of the end plate was still moving towards the upright and as yet no contact had been made. In this case therefore the only source of resistance to rotation would be the bearing of the tabs against the upright's web, here simulated by the presence of the springs.

The second scenario, when the interaction between the lower part of the end plate of the beam end connector and the upright's flange has taken place and the compression zone had been formed. This scenario was considered first.

Table 4.1 shows the interfacing blocks and the node numbers involved. Table 5.1 shows the cases considered, GM3C to

GM6C are the cases for the restrained compression zone scenario. Table 5.2 shows the cases for the free compression zone scenario, GM3D to GM6D.

5.5 Simulating the sources of resistance to rotation using springs at tabs-the restrained compression zone scenario

Table 5.1 shows the top, middle and the bottom blocks responsible for the interaction with upright's web. These are blocks 5, 6 and 7 extracted from either figure 4.5 or 4.6. Each block shows the relevant nodes where springs were applied simulating their interaction with upright's web.

To investigate the effects of number and directions of the springs employed, four different cases were examined. These are tabulated as GM3C to GM6C, these two being the two extreme cases, table 5.1.

As observed from numerous tests, for the symmetrical welding position, the directions of forces in the two top tabs were opposite to the one at the bottom. The force directions are shown in figure 4.2. This was taken into account, table 5.1.

As in the previous chapter, the compression zone, figure 4.6, was simulated using absolute restraints in the X-direction at the nodes in the bottom part of the end plate, below the beam's bottom flange.

5.6 Simulating the sources of resistance to rotation using springs at tabs- the free compression zone scenario

Four cases were considered. These are shown in table 5.2. The two extreme cases being GM3D and GM6D with the end plate free to move. The same investigations as in section

5.5 were carried out here too, assessing the effect of the number and the directions of the springs employed, table 5.2.

5.7 Results

5.7.1 Restrained compression zone

This relates to simulating the intermediate and final stages of loading the beam end connector when the gap between the end plate of the beam end connector and the accompanying upright closes and a compression zone is formed.

5.7.1.1 Deformed shape

Figure 5.15 shows a typical deformed structure superimposed on the layout of the undeformed structure, case GM6C, Figures 5.16 and 5.17 show the deflections along the height of face A, block 1 in figure 4.5. These are shown for two cases of GM3C and GM6C. The deflections are given for the horizontal, vertical as well as the out of plane directions. The resultant deflection is also included.

5.7.1.2 Stress distribution

The stress distributions along the same face, A, block 1 containing the tabs, figure 4.5 are shown in figures 5.18 and 5.19. The stress values are unaveraged, principal, Von Mises components.

5.7.1.3 Initial stiffness values

Figure 4.17 shows the various methods by which rotations were measured for various cases. The same approach described in section 4.4.1.3 was used to calculate the rotational values. The results were used to evaluate the initial stiffness values and are given in table 5.3.

5.7.1.4 Discussion of results

Global Modeling-cases of Springs At Tabs, Restrained Compression Zone

All the vertical dimensions are with respect to the global axes shown in figure 4.5.

Table 5.1 shows the various cases examined for this condition. Table 5.3 lists the extracted rotation and therefore the stiffness values.

Cases of GM1C and GM2C were not applicable, as they would have included spring stiffness values in the Z-direction. The stiffness values were evaluated only in the X and Y directions. As two extreme cases, in terms of the number of spring elements employed, GM3C and GM6C were selected for discussion.

Considering table 5.3, the lowest stiffness values calculated in the two selected cases were 1336 and 1123 kNm/radian, a difference of 17%. These were the results of rotation measurement according to figure 4.17(c), θ_{tr}.
The highest stiffness values on the other hand were given by θ_v, figure 4.17(a), 1878 and 1492, a difference of about 23%.

However, comparing 1123 kNm/radian, the theoretical stiffness value, the lowest of the set, with the initial stiffness values given by the experimental results, figures 3.56 and 3.62, 300 to 500kNm/radian, the theoretical value, is greater by about 2.5 times.

The initial stiffness band was based on the slope of a straight line superimposed on different positions along the straightest part of the moment-rotation curve.
The reason for this was the fact that in this model the compression zone of the beam end connector was restrained simulating its interaction with the upright's flange. In practice this effect happened well after plastic deformation of upright's web had started and therefore was not a fair comparison.

Figures 3.56 and 3.62 represent the moment-rotation characteristics for products 16 and 22. The physical dimensions of these products matched those adopted in the make up of the global model, table 3.1.

The deflection graphs for cases: GM3C, and GM6C, are given in figures 5.16 and 5.17.

These are dramatically different in shape compared with their two counterpart models where absolute restraints at the tabs provided resistance to rotation, figures 4.11 and 4.12.

In the cases of GM3C, and GM6C the deflection formats in the X -direction are simple linear curves, with no indications of the presence of tabs with spring elements, reflecting the smoothing effect of the springs at the tabs.

The deflections given by figures 4.11 and 4.12 are greater in magnitude compared with those of figures 5.16 and 5.17. This was not expected.

The movement in the Y-direction is shown as a constant value.

The Z-direction deflections are shown as out of plane movements. The values of U_x, U_y and U_z increase with the reduction of the number of spring elements per tab.

Figure 5.15 shows the deformed structure for GM6C, superimposed on the outline of the undeformed structure. The deformed shape is typical of this group of models.

Figures 5.18 and 5.19 show the variation of Von Mises stress component along the face A. Each curve shows a relatively constant value of stress up to a height of 80mm associated with the compression zone, followed by two peaks.
The first peak is at about 104mm and attributed to the presence of the middle tab. The second peak occurs at 185mm associated with the top tab.

Blocks 5, 6 and 7 shown in figure 4.5 are the parts of the top, middle and bottom tabs that come into contact with the upright's web as a beam end connector is loaded. Tables 5.4 and 5.5 list the reactions at the spring elements inserted at the nodes of these blocks for GM3C and GM6C.

Each table has been divided into three sections, top relating to top block, middle, relating to middle block and bottom section representing the bottom block. Each section shows columns of node numbers representing the blocks 5, 6 and 7, global stresses, principal stresses, Von Misses and the angles of principal directions.

Adjacent to each node number, letter S denotes the presence of a spring element according to the diagrams in table 5.1.

Referring to table 5.4 and examining the global/direct stresses for the spring incorporated nodes only, initially σ_x, it is apparent that, with the exception of nodes 43 and

44 of the bottom block, the rest of the spring incorporated nodes are in compression.

Considering table 5.5 and examining the global/direct stresses for the spring-incorporated nodes only, initially σ_x, all the spring incorporated nodes are in compression.

Considering table 5.6, initially the forces in the X-direction, an algebraic sum of 7510N, 4008N, and -9N are extracted for the top, the middle and the bottom blocks respectively, i.e. blocks 5, 6 and 7, figure 4.5.

The low value of the force at the bottom block, block 7, was due to restraining the lowest part of the beam end connector's end plate, below the beam's bottom flange, figure 4.6. This was to simulate its bearing against the upright's flange, in doing so only a small amount of load was transmitted to the tab in question.

Considering the forces in the Y-direction an algebraic sum of -3158N, -3604N, and -3243N are recorded for the top, the middle and the bottom blocks respectively, being the total vertical shear force and almost exactly equating to the applied load of 10000N.

Considering table 5.7, initially the forces in the X-direction, single values of +5400N, +2990N, and +253N are extracted for the top, the middle and the bottom blocks respectively.

Note that the direction of the force in the bottom block is positive but on average the magnitude of it is only 5% of those of the top and the middle blocks.

Considering the forces in the Y-direction single values of -3570N, -3880N, and -2550N are recorded for the top, the

middle and the bottom blocks respectively and as the total shear force equate the applied load of 10000N.

5.7.2 Free compression zone

As described in section 5.4, this refers to the initial loading stages when the only source of resistance to rotation resulted from the bearing of the tabs against the upright's web, and the beam end connector's endplate below the beam, figure 4.6, was still free to move.

5.7.2.1 Deformed shape

Figure 5.20 shows a typical deformed structure superimposed on the layout of the undeformed structure, case GM6D, table 5.2. The deflection profiles along the height of block 1, face A, figure 4.5, are given in figures 5.21 and 5.22. These are for two cases of GM3D and GM6D. The deflection graphs give the horizontal, vertical as well as the out of plane displacements of face A in block 1, the block that contains the tabs, figure 4.5. The resultant deflection is also included.

5.7.2.2 Stress distribution

The stress distribution along the same plane, face A is shown in figures 5.23 and 5.24. The stress values are unaveraged, principal, Von Mises components.

5.7.2.3 Initial stiffness values

As in the previous chapter, the measurement methods shown in figure 4.17 were used here too to measure rotations for the various cases shown in table 5.2.

The rotational values were calculated by determining the differential movements of node positions. The nodes were

central and on the top and the bottom flanges of the beam. Their exact positions relative to the beam end connector are shown in figure 4.17.

A sample calculation was given in section 4.4.1.3 showing how the rotational values were calculated. The results were used to evaluate the initial stiffness values and are given in table 5.8.

5.7.2.4 Discussion of results

Global Modeling-cases of Springs At Tabs, Free Compression Zone

All the vertical dimensions are with respect to the global axes shown in figure 4.5.

Table 5.2 shows the various cases examined for this condition. Table 5.8 lists the extracted rotation and therefore the stiffness values obtained in the manner described above.

Cases: GM1D and GM2D were not applicable, as these were the models which would have included spring stiffness values in the Z-direction. The stiffness values were evaluated only in the X and Y directions.

As extreme cases GM3D and GM6D were selected for discussion.

The lowest stiffness value calculated in the two selected cases were 784 and 426 kNm/radian, different by a factor of two. This variation resulted from reducing the number of spring elements from 4 to 1 both in X and Y directions, in doing so the total value of the stiffness of the upright's web was maintained.

The stiffness values obtained from these models were the results of rotation measurements carried out as θ_{tr}, figure 4.17(c). The highest stiffness values on the other hand were given by θ_v, 1017 and 471, varying by a factor of two, figure 4.17(a).

The lowest value of the set from the case GM6D was 426 kNm/radian. This is within the band of the initial stiffness values given by the experimental results, figures 3.56 and 3.62, 300-500kNm/radian. The initial stiffness band was based on the slope of a straight line superimposed on different positions along the straightest part of the moment-rotation curve.

Figures 3.56 and 3.62 represent the moment-rotation characteristics for products 16 and 22. The physical dimensions of these products matched those adopted in the make up of the global model, table 3.1.

The deflection graphs for the cases: GM3D, and GM6D, are given in figures 5.21 and 5.22.

The deflection curves show the X -direction movements as being linear and symmetrical about 108mm height, just 4mm above the middle tab. The symmetry being the result of the free compression zone as well as the local deformation of the springs at the bottom tab.

There are no distinct effects or indications of the presence of the tabs, reflecting the smoothing effect of the springs at the tabs.

The movement in the Y-direction is shown as a constant value.

Deflection in the Z-direction for GM3D is shown as a positive out of plane movement, whereas for GM6D this movement is negative in value, maximum at zero height with a break off point to positive value at 170mm height associated with the top tab.

The values of U_x, U_y and U_z increased as the number of spring elements per tab was reduced.

Figure 5.20 shows the deformed structure for GM6D, superimposed on the outline of the undeformed structure. The deformed shape was typical of this group of models.

Comparing figure 5.20, free compression zone, with figure 5.15, restrained compression zone, a distinct difference in the deformed shape of the region is observed.

Figures 5.23 and 5.24 show the variation of Von Mises stress component along face A, figure 4.5.

Each curve shows two peaks, the first is at about 30mm height. This was due to the free compression zone which allowed movement resulting in the exposure of the bottom tab which in turn attracted load and caused the peak.

The second peak occurred at 185mm associated with the top tab reaction. This dropped almost to the same value of the first peak before attempting to rise again due to the stiffening effect of the corner block 2, figure 4.5. The abruptly ending of the curve related to the top of the beam end connector, which was a free edge.

A relatively constant value of stress between the two peaks was observed.

Tables 5.9 and 5.10, for GM3D and GM6D give the following information for the blocks that are in direct contact with the upright's web and primarily the source of resistance to rotation of the beam end connector. These are blocks 5, 6 and 7, figure 4.5, the top, the middle and the bottom blocks respectively.

Each table has been divided into three sections, top, relating to the top block, middle relating to the middle block, and the bottom section representing the bottom block. Each section shows columns of node numbers representing the blocks which incorporate springs according to the diagrams in table 5.2, global stresses, principal stresses, Von Mises and the angles of principal directions.

Referring to table 5.9 and examining the global/direct stresses for the spring incorporated nodes only, initially σ_x, all the spring-incorporated nodes of the top and bottom blocks are in compression. In the middle block only one out of the four spring incorporated nodes is in compression.

Considering σ_y, noting the spring incorporated nodes, i.e. the four corners of the bottom plane of the blocks, the top block has three nodes in compression and one node in tension, namely node 25. The middle tab has two nodes in compression and two in tension namely 33 and 35. The bottom block however has all its spring incorporated nodes in compression.

Referring to table 5.10 and examining the global/direct stresses for the spring-incorporated nodes only, initially σ_x, apart from node 38 of the middle block, the equivalent nodes in the top and bottom blocks are in compression.

Considering σ_y, noting the spring incorporated nodes, i.e. the front central node of the bottom plane of the blocks, all the nodes are in compression.

Considering table 5.11, initially the forces in the X-direction, an algebraic sum of 13610N, -1475N, and -12120N are extracted for the top, the middle and the bottom blocks respectively. This showed at early stages of loading during a physical test, here ensured through adopting a free compression zone, it was effectively the top and the bottom blocks which provided the resistance to rotation.

Considering the forces in the Y-direction an algebraic sum of -3037N, -3269N, and -3688N are recorded for the top, the middle and the bottom blocks respectively.

Considering table 5.12, initially the forces in the X-direction, single values of +13600N, -522N, and -13100N are extracted for the top, the middle and the bottom blocks respectively. As in the previous case adopting a free compression zone simulated the initial loading stages of a physical test. It can be seen that the force in the middle block is negligible in value compared with those of the top and the bottom blocks, implying that effectively the top and the bottom blocks provide the resistance to rotation.

Considering the forces in the Y-direction single values of -4340N, -4200N, and -1470N are recorded for the top, the middle and the bottom blocks respectively,

5.8 Conclusion

The sub-models determined the stiffness of the upright's web. The information obtained was converted into spring stiffness values and used in the global models as the

source of resistance to its rotation replacing the absolute restraints as used in the previous chapter.

A number of global models were produced, with restrained and free compression zones. Each model incorporated a different number of springs at their tabs, in doing so the total value of stiffness obtained from the sub-models was maintained.

The global models were used to evaluate the initial stiffness value of the beam end connector. The lower the number of the springs at the tabs, the better was the correlation between the theoretical and the experimental results.

The lowest value obtained was 426 kNm/radian. This was within the band of the initial stiffness values given by the experimental results, figures 3.56 and 3.62, 300-500kNm/radian and was obtained from the model that had a single spring element at its tabs in the X and Y directions.
The model was the case GM6D and its compression zone was free to move, this being the condition observed during the initial loading of a beam end connector.

Various methods of measuring rotations and hence the initial stiffness values were demonstrated, figure 4.17. In every case it was shown that measuring rotations by determining differential deflection of top and the bottom flanges adjacent to the beam end connector would result in the highest stiffness values, figure 4.17(a).

Figure 4.5, face A of block 1 containing the tabs, was selected to examine the deflection profile and the stress distribution along its height. Doing so provided information on the deformed shape of the plate, stress

distribution and more importantly a measure of load distribution into the tabs. This showed that for a symmetrical welding arrangement the middle tab is virtually redundant in terms of load carrying capacity.

The models simulated the deflected shape of the beam end connector. This matched the deformation modes observed during testing.

Generally the initial stiffness values obtained from the spring-incorporated models were higher than those of the models with absolute restraints, previous chapter. This was not expected and was attributed to the redistribution of forces at the tabs when springs were introduced.

CASE No	TAB	CASE
GM1C		**NOT APPLICABLE as:** In chapter 4 the model equivalent to this included restraints in the z-direction i.e. no out of plane movement of the tabs according to figure 4.5. Here the resistance to rotation evaluated as spring stiffness values was in the x and y directions only.

CASE No	TAB	CASE
GM2C		**NOT APPLICABLE as:** In chapter 4 the model equivalent to this included restraints in the z-direction i.e. no out of plane movement of the tabs according to figure 4.5. Here the resistance to rotation evaluated as spring stiffness values was in the x and y directions only.

CASE No	TAB	CASE
GM3C	Top Block 5 from figure 4.5	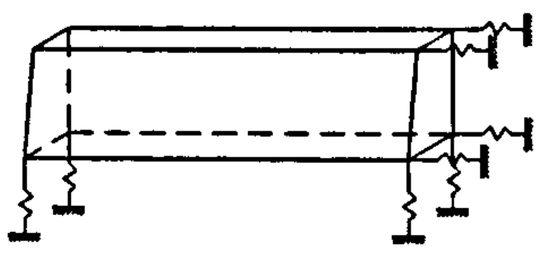
	Middle Block 6 from figure 4.5	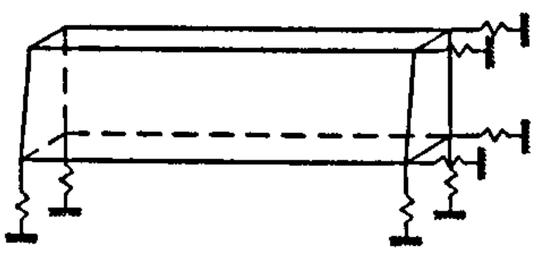
	Bottom Block 7 from figure 4.5	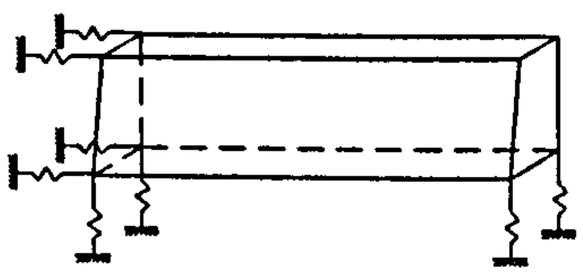

Table 5.1
CASES of Springs At Tabs, Restrained Compression Zone investigated, Cont/d....

CASE No	TAB	CASE
GM4C	Top Block 5 from figure 4.5	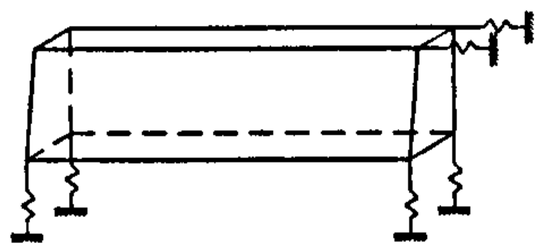
	Middle Block 6 from figure 4.5	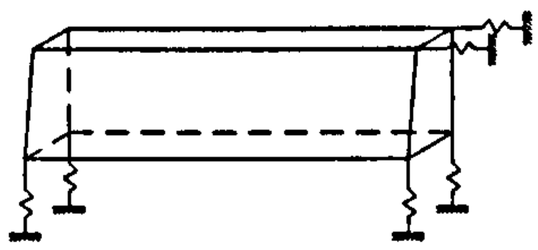
	Bottom Block 7 from figure 4.5	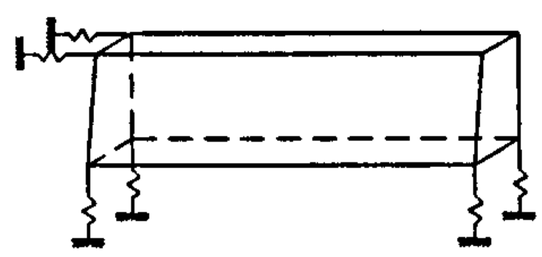

CASE No	TAB	CASE
GM5C	Top Block 5 from figure 4.5	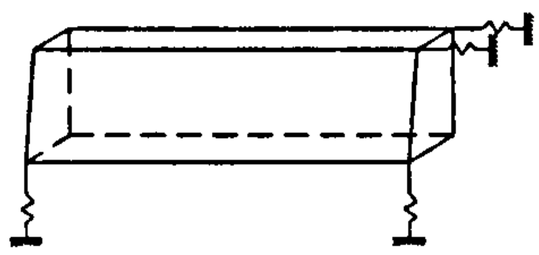
	Middle Block 6 from figure 4.5	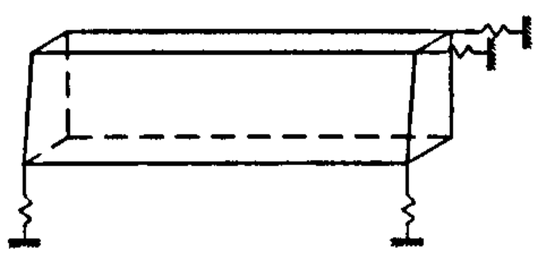
	Bottom Block 7 from figure 4.5	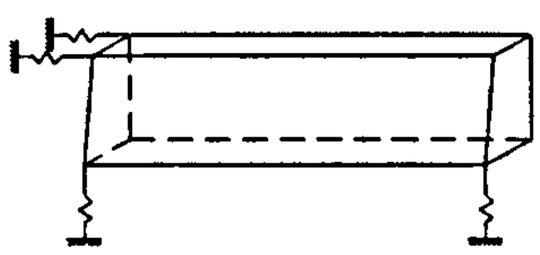

CASE No	TAB	CASE
GM6C	Top Block 5 from figure 4.5	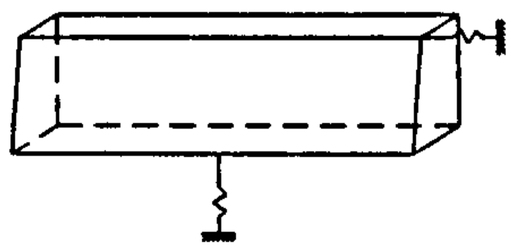
	Middle Block 6 from figure 4.5	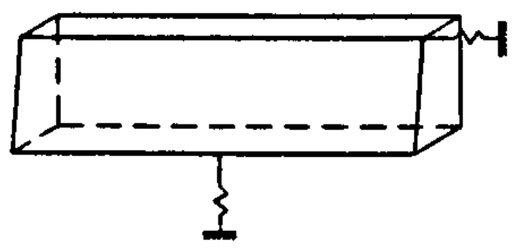
	Bottom Block 7 from figure 4.5	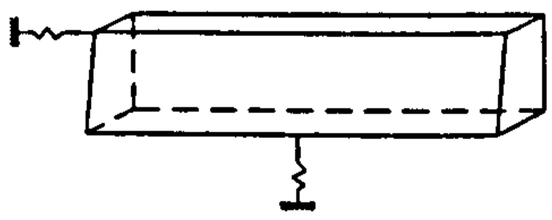

Table 5.1
CASES of Springs At Tabs, Restrained Compression Zone investigated, Concluded.

CASE No	TAB	CASE
GM1D		**NOT APPLICABLE as:** In chapter 4 the model equivalent to this included restraints in the z-direction i.e. no out of plane movement of the tabs according to figure 4.5. Here the resistance to rotation evaluated as spring stiffness values was in the x and y directions only.

CASE No	TAB	CASE
GM2D		**NOT APPLICABLE as:** In chapter 4 the model equivalent to this included restraints in the z-direction i.e. no out of plane movement of the tabs according to figure 4.5. Here the resistance to rotation evaluated as spring stiffness values was in the x and y directions only.

CASE No	TAB	CASE
GM3D	**Top** Block 5 from figure 4.5	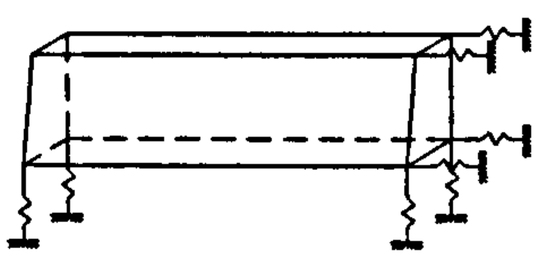
	Middle Block 6 from figure 4.5	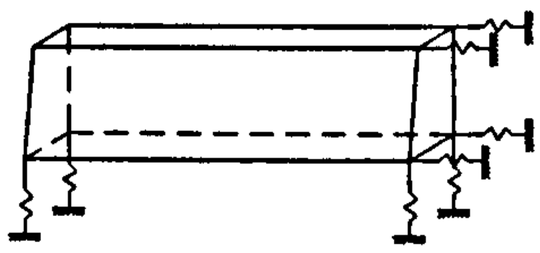
	Bottom Block 7 from figure 4.5	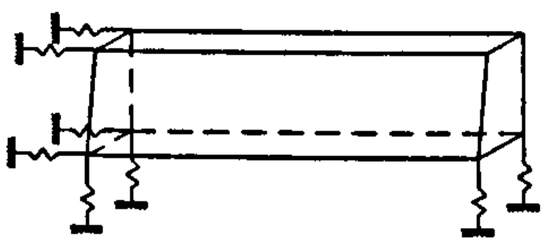

Table 5.2
CASES of Springs At Tabs, Free Compression Zone investigated, Cont/d....

CASE No	TAB	CASE
GM4D	**Top** Block 5 from figure 4.5	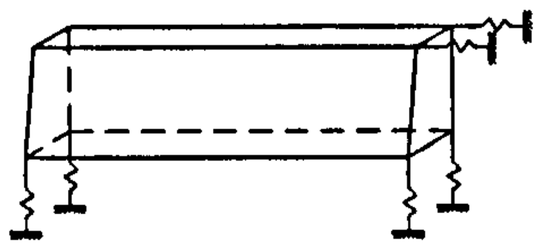
	Middle Block 6 from figure 4.5	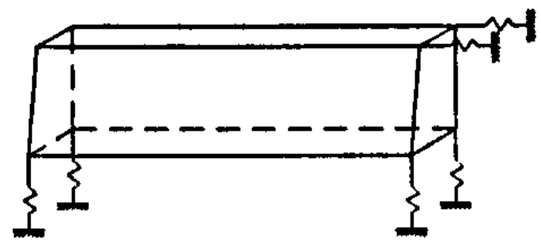
	Bottom Block 7 from figure 4.5	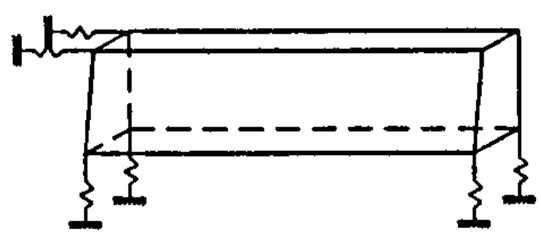

CASE No	TAB	CASE
GM5D	**Top** Block 5 from figure 4.5	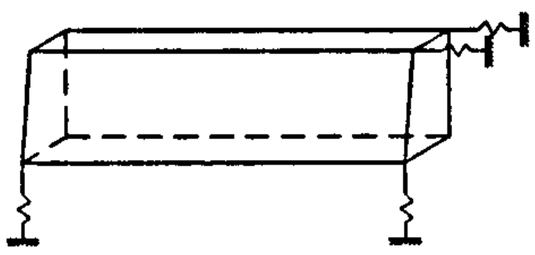
	Middle Block 6 from figure 4.5	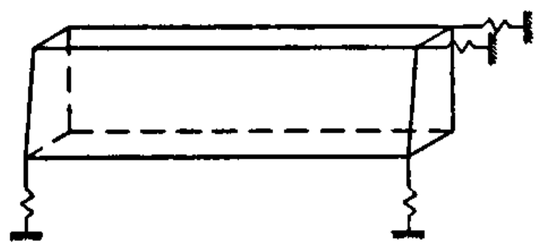
	Bottom Block 7 from figure 4.5	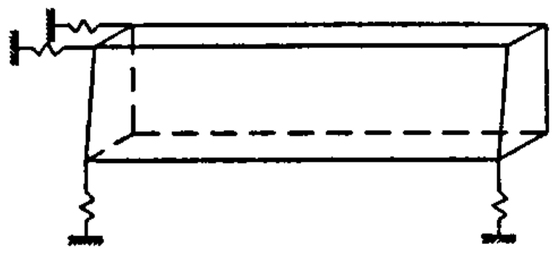

CASE No	TAB	CASE
GM6D	**Top** Block 5 from figure 4.5	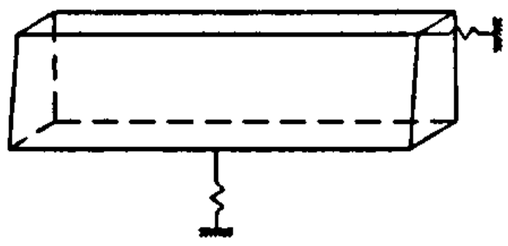
	Middle Block 6 from figure 4.5	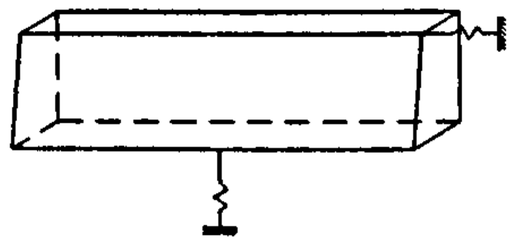
	Bottom Block 7 from figure 4.5	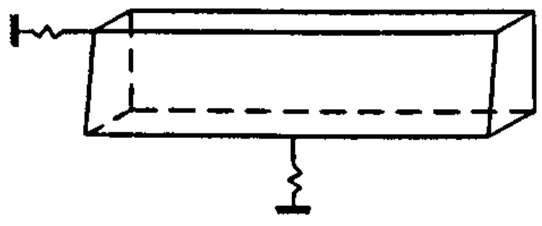

Table 5.2
CASES of Springs At Tabs, Free Compression Zone investigated, Concluded.

Table 5.3

Rotation and stiffness values for various CASES, Symmetrical welding position, Restrained compression zone

CASE N°	CASE	θ_v (radian)	θ_{ta} (radian)	θ_{tr} (radian)	θ_{ba} (radian)	θ_{br} (radian)	k_v (kNm/rad)	k_{ta} (kNm/rad)	k_{tr} (kNm/rad)	k_{ba} (kNm/rad)	k_{br} (kNm/rad)
GM1C	NOT APPLICABLE	----------	----------	----------	----------	----------	----------	----------	----------	----------	----------
GM2C	NOT APPLICABLE	----------	----------	----------	----------	----------	----------	----------	----------	----------	----------
GM3C	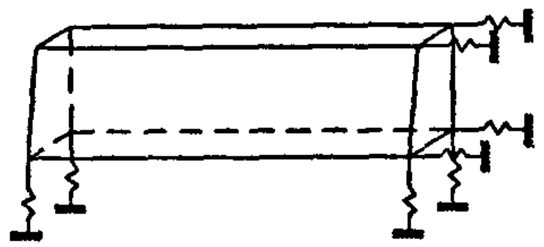	10728E-7	12832E-7	15074E-7	13077E-7	14816E-7	1878	1550	1336	1540	1360
GM4C	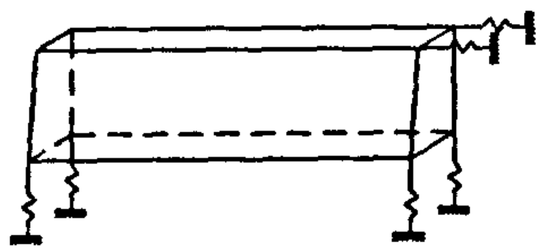	11194E-7	13444E-7	15506E-7	13506E-7	15258E-7	1800	1498	1299	1491	1320
GM5C	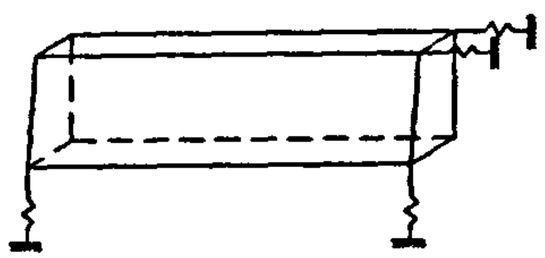	11143E-7	13440E-7	15482E-7	13450E-7	15228E-7	1808	1499	1301	1498	1323
GM6C	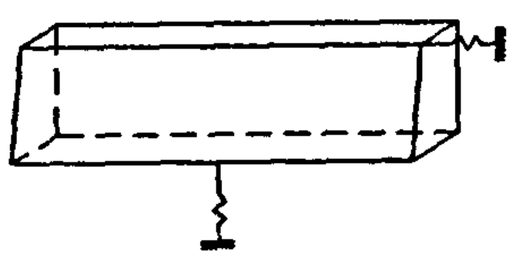	13496E-7	15898E-7	17934E-7	15834E-7	17664E-7	1492	1267	1123	1272	1140

TABLE 5.4

REACTIONS AT TOP, BOTTOM AND MIDDLE TABS-SYMMETRICAL-RESTRAINED COMPRESSION ZONE-SPRINGS AT TABS

37100 8-NODE ISOPARAMETRIC BRICK ELEMENT

GLOBAL STRESSES - SIGMA-X, SIGMA-Y AND SIGMA-Z ARE THE STRESSES IN THE GLOBAL AXES

PRINCIPAL STRESSES - SIGMA-1 IS THE MOST POSITIVE PRINCIPAL STRESS
SIGMA-3 IS THE MOST NEGATIVE PRINCIPAL STRESS

ANGLES OF PRINCIPAL STRESSES - AX, AY AND AZ ARE THE ANGLES OF SIGMA-1 TO THE GLOBAL AXES
BX, BY AND BZ ARE THE ANGLES OF SIGMA-2 TO THE GLOBAL AXES
SIGMA-2 IS PERPENDICULAR TO SIGMA-1 AND SIGMA-3

NB:S DENOTES SPRING AT NODE AND STRESS UNIT: N/m^2

LOAD CASE		NODE NO	.....GLOBAL.STRESSES..... SIGMA-X	SIGMA-Y	SIGMA-Z	.....PRINCIPAL.STRESSES..... SIGMA-1	SIGMA-2	SIGMA-3	VON.MISES STRESS	ANGS.OF.PRINCIPAL.DIRECTIONS AX	AY	AZ	BX	BY	BZ
1	S	30	-1.38E+09	2.88E+07	-3.38E+08	5.63E+08	-4.91E+08	-1.76E+09	2.02E+09	66	140	119	85	55	144
1	S	32	-4.87E+08	-3.42E+08	-1.81E+08	4.73E+08	-5.63E+08	-9.20E+08	1.25E+09	56	118	133	82	30	118
1	S	26	-9.84E+08	-8.17E+08	-4.86E+08	-3.15E+08	-4.26E+08	-1.55E+09	1.18E+09	47	46	105	89	111	158
1	S	28	-4.49E+08	-4.85E+08	-2.25E+08	-3.98E+07	-2.11E+08	-9.08E+08	7.97E+08	46	66	127	74	50	43
1	S	25	-5.29E+07	-1.50E+08	-5.29E+07	1.60E+07	-1.01E+08	-1.71E+08	1.63E+08	43	101	131	57	115	43
1	S	27	-1.97E+08	-1.95E+08	-1.10E+08	-5.29E+07	-1.65E+08	-2.84E+08	2.00E+08	56	109	139	68	136	54
1	S	38	-7.77E+08	-5.31E+06	-2.33E+08	3.15E+08	-3.39E+08	-9.91E+08	1.13E+09	66	139	120	84	54	143
1	S	40	-2.90E+08	-2.71E+08	-1.67E+08	2.57E+08	-4.36E+08	-5.48E+08	7.55E+08	56	119	132	67	29	108
1	S	34	-6.06E+08	-6.80E+08	-2.72E+08	-2.33E+08	-2.50E+08	-1.08E+09	8.34E+08	64	81	152	52	47	65
1	S	36	-2.49E+08	-4.26E+08	-8.92E+07	9.96E+06	-1.32E+08	-6.42E+08	5.94E+08	56	87	146	52	49	63
1	S	33	-6.46E+07	-2.32E+08	-1.90E+07	1.30E+07	-6.56E+07	-2.63E+08	2.46E+08	54	105	140	42	104	50
1	S	35	-9.82E+07	-1.89E+08	-1.62E+07	2.71E+06	-8.24E+07	-2.24E+08	1.98E+08	73	107	155	29	108	67
1	S	45	6.63E+07	-3.22E+06	2.35E+07	8.60E+07	2.00E+07	-1.94E+07	9.23E+07	26	108	108	79	111	24
1	S	47	1.09E+07	-9.32E+05	7.56E+06	2.82E+07	5.51E+05	-1.12E+07	3.51E+07	42	91	132	77	158	73
1	S	41	3.95E+05	-1.35E+08	1.09E+08	1.09E+08	2.37E+07	-1.58E+08	2.36E+08	89	90	179	20	110	89
1	S	43	-1.88E+07	-1.47E+08	9.97E+07	1.21E+08	7.31E+05	-1.88E+08	2.70E+08	77	79	16	25	113	97
1	S	42	-3.96E+07	-3.13E+08	1.11E+08	1.20E+08	1.18E+06	-3.63E+08	4.36E+08	82	80	11	21	71	99
1	S	44	2.12E+07	-3.26E+08	1.26E+08	1.87E+08	1.75E+07	-3.84E+08	5.07E+08	69	101	155	24	72	72

TABLE 5.5

REACTIONS AT TOP, BOTTOM AND MIDDLE TABS-SYMMETRICAL-RESTRAINED COMPRESSION ZONE-SPRINGS AT TABS

37100 8-NODE ISOPARAMETRIC BRICK ELEMENT

GLOBAL STRESSES - SIGMA-X, SIGMA-Y AND SIGMA-Z ARE THE STRESSES IN THE GLOBAL AXES

PRINCIPAL STRESSES - SIGMA-1 IS THE MOST POSITIVE PRINCIPAL STRESS
SIGMA-3 IS THE MOST NEGATIVE PRINCIPAL STRESS

ANGLES OF PRINCIPAL STRESSES - AX, AY AND AZ ARE THE ANGLES OF SIGMA-1 TO THE GLOBAL AXES
BX, BY AND BZ ARE THE ANGLES OF SIGMA-2 TO THE GLOBAL AXES
SIGMA-2 IS PERPENDICULAR TO SIGMA-1 AND SIGMA-3

NB:S DENOTES SPRING AT NODE AND STRESS UNIT: N/m^2

LOAD CASE	NODE NO	.....GLOBAL.STRESSES..... SIGMA-X	SIGMA-Y	SIGMA-Z	.....PRINCIPAL.STRESSES..... SIGMA-1	SIGMA-2	SIGMA-3	VON.MISES STRESS	ANGS.OF.PRINCIPAL.DIRECTIONS AX	AY	AZ	BX	BY	BZ
1	S 30	-6.45E+09	-2.30E+08	-2.05E+09	2.31E+09	-2.36E+09	-8.68E+09	9.56E+09	63	138	119	82	53	142
1	32	5.67E+08	-6.45E+07	1.09E+08	3.43E+09	1.36E+08	-2.96E+09	5.53E+09	45	100	133	69	21	83
1	26	2.41E+08	3.44E+08	4.93E+08	6.83E+08	3.02E+08	9.21E+07	5.19E+08	76	121	144	42	49	101
1	28	8.85E+08	6.11E+08	7.67E+08	1.37E+09	5.54E+08	3.42E+08	9.36E+08	50	119	126	39	69	57
1	S 86	-4.54E+08	-1.18E+09	-4.35E+08	-1.72E+08	-4.49E+08	-1.44E+09	1.16E+09	48	117	126	48	91	41
1	87	1.85E+08	2.17E+08	1.74E+08	5.10E+08	1.82E+08	-1.15E+08	5.42E+08	83	43	47	6	92	95
1	25	3.18E+07	5.73E+07	9.18E+07	1.24E+08	3.14E+07	2.58E+07	9.51E+07	86	55	145	7	86	83
1	27	-7.26E+07	-2.32E+07	3.64E+07	3.66E+07	-1.31E+07	-8.29E+07	1.04E+08	87	89	177	67	157	89
1	S 38	-3.60E+09	-1.67E+08	-1.28E+09	1.23E+09	-1.45E+09	-4.83E+09	5.27E+09	64	139	118	81	54	142
1	40	2.18E+08	-1.52E+08	-1.32E+08	1.77E+09	-3.96E+07	-1.79E+09	3.09E+09	45	103	132	65	24	84
1	34	1.90E+08	1.60E+08	4.66E+08	5.87E+08	1.94E+08	3.52E+07	4.92E+08	83	116	152	16	73	90
1	36	6.43E+08	5.39E+08	7.16E+08	1.17E+09	4.79E+08	2.50E+08	8.30E+08	60	123	132	30	77	63
1	S 90	-5.04E+08	-1.24E+09	-4.61E+08	-1.88E+08	-4.91E+08	-1.53E+09	1.22E+09	50	117	128	47	92	42
1	91	1.19E+08	2.07E+08	1.62E+08	5.21E+08	1.18E+08	-1.52E+08	5.87E+08	86	43	47	5	90	95
1	33	5.96E+07	5.21E+07	1.99E+08	2.04E+08	5.65E+07	5.06E+07	1.50E+08	81	95	10	9	84	97
1	35	8.63E+07	1.11E+08	2.25E+08	2.79E+08	7.91E+07	6.41E+07	2.07E+08	71	66	30	75	155	70
1	S 45	3.43E+08	2.19E+07	1.43E+08	4.49E+08	1.16E+08	-5.65E+07	4.45E+08	28	107	111	77	116	29
1	47	-4.53E+07	2.66E+07	2.81E+07	1.34E+08	8.84E+06	-1.33E+08	2.31E+08	55	61	131	86	145	123
1	41	1.15E+08	-2.27E+07	3.71E+08	4.17E+08	1.12E+08	-6.61E+07	4.23E+08	83	107	161	7	84	85
1	43	2.36E+08	2.64E+08	4.93E+08	7.33E+08	2.17E+08	4.21E+07	6.22E+08	78	55	36	12	92	102
1	S 92	-2.94E+08	-7.52E+08	-1.98E+08	-6.25E+07	-2.47E+08	-9.35E+08	7.96E+08	58	63	43	39	82	128
1	93	4.46E+07	1.11E+08	1.62E+08	4.17E+08	4.41E+07	-1.43E+08	4.93E+08	87	132	137	4	90	85
1	42	1.28E+08	8.86E+07	4.31E+08	4.48E+08	1.22E+08	7.78E+07	3.50E+08	77	93	167	30	61	80
1	44	3.64E+08	3.22E+08	5.72E+08	7.91E+08	2.78E+08	1.89E+08	5.63E+08	65	117	141	24	78	69

TABLE 5.6

Forces Applied To 30100 Spring Elements At Top, Bottom And Middle Tabs SYMMETRICAL-RESTRAINED COMPRESSION ZONE

FOR EACH SPRING ELEMENT THE FORCES AND MOMENTS FOR EACH NODE
ARE GIVEN. THE FORCES AND MOMENTS ARE GIVEN IN THE AXIS SET WHICH
WAS USED TO DEFINE THE SPRING ORIENTATION

F-X - FORCE IN THE SPRING X-DIRECTION
F-Y - FORCE IN THE SPRING Y-DIRECTION
F-Z - FORCE IN THE SPRING Z-DIRECTION

M-X - MOMENT ABOUT THE SPRING X-AXIS
M-Y - MOMENT ABOUT THE SPRING Y-AXIS
M-Z - MOMENT ABOUT THE SPRING Z-AXIS

NOTE- THE MOMENTS ARE GIVEN ACCORDING TO THE RIGHT HAND SCREW CONVENTION.

ELEMENT NUMBER	SPRING NUMBER	AXIS SET	LOAD CASE	NODE NUMBER	FORCES(N) AND MOMENTS(N.m) F-X	F-Y	F-Z	M-X	M-Y	M-Z
1	1	1	1	32	0.239E+04	0.000E+00	0.000E+00	0.000E+00	0.000E+00	0.000E+00
2	1	1	1	30	0.127E+04	0.000E+00	0.000E+00	0.000E+00	0.000E+00	0.000E+00
3	3	1	1	28	0.230E+04	-0.157E+04	0.000E+00	0.000E+00	0.000E+00	0.000E+00
4	3	1	1	26	0.155E+04	-984.	0.000E+00	0.000E+00	0.000E+00	0.000E+00
5	2	1	1	27	0.000E+00	-301.	0.000E+00	0.000E+00	0.000E+00	0.000E+00
6	2	1	1	25	0.000E+00	-303.	0.000E+00	0.000E+00	0.000E+00	0.000E+00
7	1	1	1	40	0.125E+04	0.000E+00	0.000E+00	0.000E+00	0.000E+00	0.000E+00
8	1	1	1	38	698.	0.000E+00	0.000E+00	0.000E+00	0.000E+00	0.000E+00
9	3	1	1	36	0.119E+04	-0.155E+04	0.000E+00	0.000E+00	0.000E+00	0.000E+00
10	3	1	1	34	870.	-988.	0.000E+00	0.000E+00	0.000E+00	0.000E+00
11	2	1	1	35	0.000E+00	-587.	0.000E+00	0.000E+00	0.000E+00	0.000E+00
12	2	1	1	33	0.000E+00	-479.	0.000E+00	0.000E+00	0.000E+00	0.000E+00
13	1	1	1	47	11.1	0.000E+00	0.000E+00	0.000E+00	0.000E+00	0.000E+00
14	1	1	1	45	56.5	0.000E+00	0.000E+00	0.000E+00	0.000E+00	0.000E+00
15	3	1	1	43	-88.7	-663.	0.000E+00	0.000E+00	0.000E+00	0.000E+00
16	3	1	1	41	12.1	-384.	0.000E+00	0.000E+00	0.000E+00	0.000E+00
17	2	1	1	44	0.000E+00	-0.146E+04	0.000E+00	0.000E+00	0.000E+00	0.000E+00
18	2	1	1	42	0.000E+00	-736.	0.000E+00	0.000E+00	0.000E+00	0.000E+00

TABLE 5.7

Forces Applied To 30100 Spring Elements At Top, Bottom And Middle Tabs SYMMETRICAL-RESTRAINED COMPRESSION ZONE

FOR EACH SPRING ELEMENT THE FORCES AND MOMENTS FOR EACH NODE
ARE GIVEN. THE FORCES AND MOMENTS ARE GIVEN IN THE AXIS SET WHICH
WAS USED TO DEFINE THE SPRING ORIENTATION

F-X - FORCE IN THE SPRING X-DIRECTION
F-Y - FORCE IN THE SPRING Y-DIRECTION
F-Z - FORCE IN THE SPRING Z-DIRECTION

M-X - MOMENT ABOUT THE SPRING X-AXIS
M-Y - MOMENT ABOUT THE SPRING Y-AXIS
M-Z - MOMENT ABOUT THE SPRING Z-AXIS

NOTE- THE MOMENTS ARE GIVEN ACCORDING TO THE RIGHT HAND SCREW CONVENTION.

ELEMENT NUMBER	SPRING NUMBER	AXIS SET	LOAD CASE	NODE NUMBER	FORCES(N) AND MOMENTS(N.m) F-X	F-Y	F-Z	M-X	M-Y	M-Z
1	1	1	1	30	0.540E+04	0.000E+00	0.000E+00	0.000E+00	0.000E+00	0.000E+00
2	2	1	1	86	0.000E+00	-0.357E+04	0.000E+00	0.000E+00	0.000E+00	0.000E+00
3	1	1	1	38	0.299E+04	0.000E+00	0.000E+00	0.000E+00	0.000E+00	0.000E+00
4	2	1	1	90	0.000E+00	-0.388E+04	0.000E+00	0.000E+00	0.000E+00	0.000E+00
5	1	1	1	45	253.	0.000E+00	0.000E+00	0.000E+00	0.000E+00	0.000E+00
6	2	1	1	92	0.000E+00	-0.255E+04	0.000E+00	0.000E+00	0.000E+00	0.000E+00

Table 5.8

Rotation and stiffness values for various CASES, Symmetrical welding position, Free compression zone

CASE N°	CASE	θ_v (radian)	θ_{ta} (radian)	θ_{tr} (radian)	θ_{ba} (radian)	θ_{br} (radian)	k_v (kNm/rad)	k_{ta} (kNm/rad)	k_{tr} (kNm/rad)	k_{ba} (kNm/rad)	k_{br} (kNm/rad)
GM1D	NOT APPLICABLE	----------	----------	----------	----------	----------	----------	----------	----------	----------	----------
GM2D	NOT APPLICABLE	----------	----------	----------	----------	----------	----------	----------	----------	----------	----------
GM3D	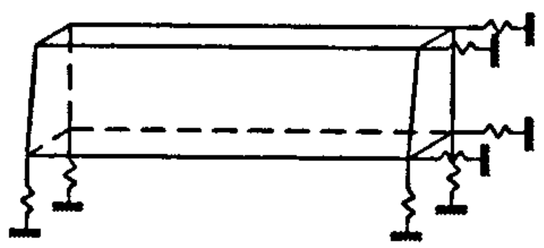	19800E-7	23582E-7	25672E-7	23692E-7	25438E-7	1017	854	784	850	792
GM4D	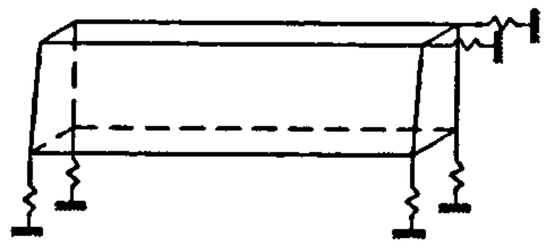	27681E-7	29921E-7	31982E-7	29979E-7	31748E-7	727	673	630	672	634
GM5D	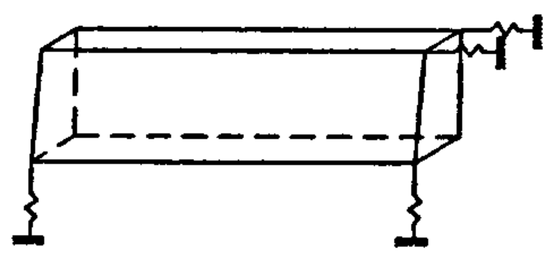	28183E-7	30496E-7	32524E-7	30465E-7	32284E-7	714	660	619	661	624
GM6D	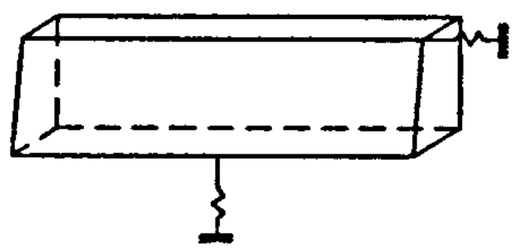	42699E-7	45234E-7	47212E-7	44968E-7	46958E-7	471	445	426	448	429

TABLE 5.9

REACTIONS AT TOP, BOTTOM AND MIDDLE TABS-SYMMETRICAL-FREE COMPRESSION ZONE-SPRINGS AT TABS

37100 8-NODE ISOPARAMETRIC BRICK ELEMENT

GLOBAL STRESSES - SIGMA-X, SIGMA-Y AND SIGMA-Z ARE THE STRESSES IN THE GLOBAL AXES
PRINCIPAL STRESSES - SIGMA-1 IS THE MOST POSITIVE PRINCIPAL STRESS
SIGMA-3 IS THE MOST NEGATIVE PRINCIPAL STRESS
ANGLES OF PRINCIPAL STRESSES - AX, AY AND AZ ARE THE ANGLES OF SIGMA-1 TO THE GLOBAL AXES
BX, BY AND BZ ARE THE ANGLES OF SIGMA-2 TO THE GLOBAL AXES
SIGMA-2 IS PERPENDICULAR TO SIGMA-1 AND SIGMA-3

NB:S DENOTES SPRING AT NODE AND STRESS UNIT: N/m^2

LOAD CASE		NODE NO	.....GLOBAL.STRESSES..... SIGMA-X	SIGMA-Y	SIGMA-Z	.....PRINCIPAL.STRESSES..... SIGMA-1	SIGMA-2	SIGMA-3	VON.MISES STRESS	ANGS.OF.PRINCIPAL.DIRECTIONS AX	AY	AZ	BX	BY	BZ
1	S	30	-2.63E+09	7.29E+07	-5.85E+08	1.10E+09	-8.67E+08	-3.38E+09	3.89E+09	66	139	120	85	54	144
1	S	32	-8.23E+08	-5.49E+08	-2.30E+08	9.59E+08	-8.91E+08	-1.67E+09	2.34E+09	55	116	134	81	27	115
1	S	26	-1.85E+09	-1.37E+09	-1.00E+09	-5.56E+08	-8.77E+08	-2.78E+09	2.09E+09	50	41	99	84	107	161
1	S	28	-8.64E+08	-8.35E+08	-5.46E+08	-1.35E+08	-5.11E+08	-1.60E+09	1.32E+09	45	57	118	83	55	35
1	S	25	-1.31E+07	8.01E+07	-8.42E+07	1.19E+08	7.42E+06	-1.44E+08	2.28E+08	63	35	111	43	124	112
1	S	27	-3.00E+08	-5.80E+07	-2.12E+08	-4.20E+07	-8.86E+07	-4.39E+08	3.75E+08	83	167	79	51	94	141
1	S	38	1.72E+07	-6.28E+07	-7.17E+07	7.89E+07	5.97E+06	-2.02E+08	2.53E+08	47	112	129	48	46	72
1	S	40	1.07E+08	-1.85E+08	-8.15E+07	1.45E+08	6.04E+07	-3.65E+08	4.73E+08	30	99	118	61	51	51
1	S	34	-1.14E+08	-6.14E+08	8.48E+06	2.41E+07	-5.78E+07	-6.86E+08	6.73E+08	84	79	11	18	73	98
1	S	36	1.87E+08	-4.70E+08	1.42E+08	3.09E+08	4.74E+07	-4.96E+08	7.12E+08	42	97	132	47	80	44
1	S	33	1.16E+07	1.96E+07	7.22E+07	1.12E+08	1.24E+07	-2.07E+07	1.19E+08	60	107	35	85	156	112
1	S	35	1.05E+08	1.01E+08	1.24E+08	1.92E+08	9.74E+07	4.07E+07	1.32E+08	49	73	45	88	22	112
1	S	45	-1.85E+09	3.01E+08	2.80E+08	9.14E+08	1.75E+08	-2.36E+09	2.97E+09	66	50	131	89	136	133
1	S	47	-4.54E+09	7.73E+07	-5.95E+08	1.42E+09	-1.01E+09	-5.47E+09	6.06E+09	68	34	115	86	63	26
1	S	41	-1.44E+09	-1.85E+08	-6.31E+08	1.66E+08	-6.02E+08	-1.82E+09	1.73E+09	65	155	92	80	88	9
1	S	43	-1.77E+09	-4.70E+08	-8.15E+08	-8.65E+07	-8.33E+08	-2.13E+09	1.79E+09	65	153	99	82	97	10
1	S	42	-9.59E+07	-4.82E+08	-7.45E+07	4.19E+08	-4.99E+08	-5.73E+08	9.57E+08	46	81	45	85	17	106
1	S	44	-1.25E+09	-1.02E+09	-5.82E+08	-1.21E+08	-1.14E+09	-1.59E+09	1.31E+09	61	64	39	80	35	123

TABLE 5.10

REACTIONS AT TOP, BOTTOM AND MIDDLE TABS-SYMMETRICAL-FREE COMPRESSION ZONE-SPRINGS AT TABS

37100 8-NODE ISOPARAMETRIC BRICK ELEMENT

GLOBAL STRESSES - SIGMA-X, SIGMA-Y AND SIGMA-Z ARE THE STRESSES IN THE GLOBAL AXES
PRINCIPAL STRESSES - SIGMA-1 IS THE MOST POSITIVE PRINCIPAL STRESS
SIGMA-3 IS THE MOST NEGATIVE PRINCIPAL STRESS
ANGLES OF PRINCIPAL STRESSES - AX, AY AND AZ ARE THE ANGLES OF SIGMA-1 TO THE GLOBAL AXES
BX, BY AND BZ ARE THE ANGLES OF SIGMA-2 TO THE GLOBAL AXES
SIGMA-2 IS PERPENDICULAR TO SIGMA-1 AND SIGMA-3

NB:S DENOTES SPRING AT NODE AND STRESS UNIT: N/m^2

LOAD CASE	NODE NO	.....GLOBAL.STRESSES..... SIGMA-X	SIGMA-Y	SIGMA-Z	.....PRINCIPAL.STRESSES..... SIGMA-1	SIGMA-2	SIGMA-3	VON.MISES STRESS	ANGS.OF.PRINCIPAL.DIRECTIONS AX	AY	AZ	BX	BY	BZ
1	S 30	-1.61E+10	-4.77E+08	-4.80E+09	5.91E+09	-5.58E+09	-2.17E+10	2.41E+10	63	138	119	82	53	142
1	32	1.58E+09	8.71E+07	6.87E+08	8.86E+09	5.86E+08	-7.09E+09	1.38E+10	45	98	133	71	19	83
1	26	4.58E+08	9.29E+08	7.07E+08	1.21E+09	7.52E+08	1.29E+08	9.43E+08	75	135	130	49	51	115
1	28	1.62E+09	9.27E+08	1.05E+09	2.22E+09	7.98E+08	5.80E+08	1.54E+09	40	114	120	49	57	57
1	S 86	-5.30E+08	-1.50E+09	-5.44E+08	-2.08E+08	-5.28E+08	-1.84E+09	1.49E+09	46	117	123	50	89	39
1	87	4.06E+08	3.32E+08	2.87E+08	7.09E+08	3.86E+08	-7.12E+07	6.79E+08	75	45	48	14	100	99
1	25	-2.89E+07	9.34E+07	-1.52E+08	1.73E+08	-2.68E+07	-2.34E+08	3.52E+08	76	30	115	20	109	97
1	27	-5.16E+08	-3.85E+08	-4.42E+08	-2.34E+08	-3.15E+08	-7.94E+08	5.24E+08	87	140	51	40	112	121
1	S 38	5.30E+08	-8.69E+07	-2.05E+08	7.56E+08	-1.18E+08	-4.00E+08	1.04E+09	26	70	72	83	144	55
1	40	-2.57E+08	-2.75E+08	-4.98E+08	7.54E+06	-1.81E+08	-8.57E+08	7.88E+08	36	87	53	75	157	106
1	34	1.37E+08	-7.99E+07	5.23E+08	5.86E+08	1.37E+08	-1.43E+08	6.37E+08	89	72	17	0	90	90
1	36	4.86E+08	5.49E+08	8.16E+08	1.21E+09	4.07E+08	2.29E+08	9.10E+08	70	124	138	22	88	67
1	S 90	-5.52E+08	-1.31E+09	-4.82E+08	-1.90E+08	-5.46E+08	-1.61E+09	1.28E+09	51	117	129	46	93	44
1	91	3.66E+07	1.89E+08	1.44E+08	5.29E+08	4.22E+07	-2.02E+08	6.44E+08	89	136	133	8	83	96
1	33	8.36E+07	2.34E+07	2.90E+08	2.98E+08	8.28E+07	1.67E+07	2.54E+08	83	82	9	11	100	95
1	35	2.29E+08	2.56E+08	4.03E+08	5.45E+08	1.80E+08	1.64E+08	3.73E+08	68	60	37	24	110	101
1	S 45	-1.72E+10	-1.09E+09	-6.24E+09	4.81E+09	-6.34E+09	-2.30E+10	2.43E+10	63	39	63	81	123	35
1	47	4.53E+09	1.90E+09	1.19E+09	9.58E+09	2.96E+09	-4.93E+09	1.26E+10	36	97	54	82	155	113
1	41	5.70E+08	1.31E+09	5.44E+08	1.50E+09	5.75E+08	3.50E+08	1.06E+09	88	156	113	8	85	97
1	43	3.92E+08	5.06E+08	2.48E+08	9.78E+08	3.69E+08	-2.01E+08	1.02E+09	77	39	53	14	95	103
1	S 92	-2.18E+08	-6.26E+08	-1.20E+08	-5.02E+07	-1.05E+08	-8.08E+08	7.32E+08	85	68	21	24	69	102
1	93	2.24E+08	2.12E+08	2.63E+08	4.76E+08	1.86E+08	3.70E+07	3.87E+08	63	122	135	35	55	85
1	42	-3.44E+07	1.31E+08	-1.60E+08	3.85E+08	6.70E+07	-5.15E+08	7.90E+08	53	121	52	58	34	78
1	44	-1.39E+09	-5.20E+08	-7.62E+08	-3.06E+08	-5.82E+08	-1.78E+09	1.36E+09	60	52	50	79	141	52

TABLE 5.11

Forces Applied To 30100 Spring Elements At Top, Bottom And Middle Tabs SYMMETRICAL-FREE COMPRESSION ZONE

FOR EACH SPRING ELEMENT THE FORCES AND MOMENTS FOR EACH NODE ARE GIVEN. THE FORCES AND MOMENTS ARE GIVEN IN THE AXIS SET WHICH WAS USED TO DEFINE THE SPRING ORIENTATION

F-X - FORCE IN THE SPRING X-DIRECTION
F-Y - FORCE IN THE SPRING Y-DIRECTION
F-Z - FORCE IN THE SPRING Z-DIRECTION

M-X - MOMENT ABOUT THE SPRING X-AXIS
M-Y - MOMENT ABOUT THE SPRING Y-AXIS
M-Z - MOMENT ABOUT THE SPRING Z-AXIS

NOTE- THE MOMENTS ARE GIVEN ACCORDING TO THE RIGHT HAND SCREW CONVENTION.

ELEMENT NUMBER	SPRING NUMBER	AXIS SET	LOAD CASE	NODE NUMBER	FORCES(N) AND MOMENTS(N.m) F-X	F-Y	F-Z	M-X	M-Y	M-Z
1	1	1	1	32	0.428E+04	0.000E+00	0.000E+00	0.000E+00	0.000E+00	0.000E+00
2	1	1	1	30	0.243E+04	0.000E+00	0.000E+00	0.000E+00	0.000E+00	0.000E+00
3	3	1	1	28	0.395E+04	-0.233E+04	0.000E+00	0.000E+00	0.000E+00	0.000E+00
4	3	1	1	26	0.295E+04	-0.142E+04	0.000E+00	0.000E+00	0.000E+00	0.000E+00
5	2	1	1	27	0.000E+00	581.	0.000E+00	0.000E+00	0.000E+00	0.000E+00
6	2	1	1	25	0.000E+00	132.	0.000E+00	0.000E+00	0.000E+00	0.000E+00
7	1	1	1	40	-580.	0.000E+00	0.000E+00	0.000E+00	0.000E+00	0.000E+00
8	1	1	1	38	-62.4	0.000E+00	0.000E+00	0.000E+00	0.000E+00	0.000E+00
9	3	1	1	36	-751.	-0.205E+04	0.000E+00	0.000E+00	0.000E+00	0.000E+00
10	3	1	1	34	-81.9	-0.118E+04	0.000E+00	0.000E+00	0.000E+00	0.000E+00
11	2	1	1	35	0.000E+00	40.0	0.000E+00	0.000E+00	0.000E+00	0.000E+00
12	2	1	1	33	0.000E+00	-78.9	0.000E+00	0.000E+00	0.000E+00	0.000E+00
13	1	1	1	47	-0.207E+04	0.000E+00	0.000E+00	0.000E+00	0.000E+00	0.000E+00
14	1	1	1	45	-0.223E+04	0.000E+00	0.000E+00	0.000E+00	0.000E+00	0.000E+00
15	3	1	1	43	-0.485E+04	-509.	0.000E+00	0.000E+00	0.000E+00	0.000E+00
16	3	1	1	41	-0.297E+04	66.2	0.000E+00	0.000E+00	0.000E+00	0.000E+00
17	2	1	1	44	0.000E+00	-0.227E+04	0.000E+00	0.000E+00	0.000E+00	0.000E+00
18	2	1	1	42	0.000E+00	-975.	0.000E+00	0.000E+00	0.000E+00	0.000E+00

TABLE 5.12

Forces Applied To 30100 Spring Elements At Top, Bottom And Middle Tabs SYMMETRICAL-FREE COMPRESSION ZONE

FOR EACH SPRING ELEMENT THE FORCES AND MOMENTS FOR EACH NODE
ARE GIVEN. THE FORCES AND MOMENTS ARE GIVEN IN THE AXIS SET WHICH
WAS USED TO DEFINE THE SPRING ORIENTATION

F-X - FORCE IN THE SPRING X-DIRECTION
F-Y - FORCE IN THE SPRING Y-DIRECTION
F-Z - FORCE IN THE SPRING Z-DIRECTION

M-X - MOMENT ABOUT THE SPRING X-AXIS
M-Y - MOMENT ABOUT THE SPRING Y-AXIS
M-Z - MOMENT ABOUT THE SPRING Z-AXIS

NOTE- THE MOMENTS ARE GIVEN ACCORDING TO THE RIGHT HAND SCREW CONVENTION.

ELEMENT NUMBER	SPRING NUMBER	AXIS SET	LOAD CASE	NODE NUMBER	FORCES(N) AND MOMENTS(N.m) F-X	F-Y	F-Z	M-X	M-Y	M-Z
1	1	1	1	30	0.136E+05	0.000E+00	0.000E+00	0.000E+00	0.000E+00	0.000E+00
2	2	1	1	86	0.000E+00	-0.434E+04	0.000E+00	0.000E+00	0.000E+00	0.000E+00
3	1	1	1	38	-522.	0.000E+00	0.000E+00	0.000E+00	0.000E+00	0.000E+00
4	2	1	1	90	0.000E+00	-0.420E+04	0.000E+00	0.000E+00	0.000E+00	0.000E+00
5	1	1	1	45	-0.131E+05	0.000E+00	0.000E+00	0.000E+00	0.000E+00	0.000E+00
6	2	1	1	92	0.000E+00	-0.147E+04	0.000E+00	0.000E+00	0.000E+00	0.000E+00

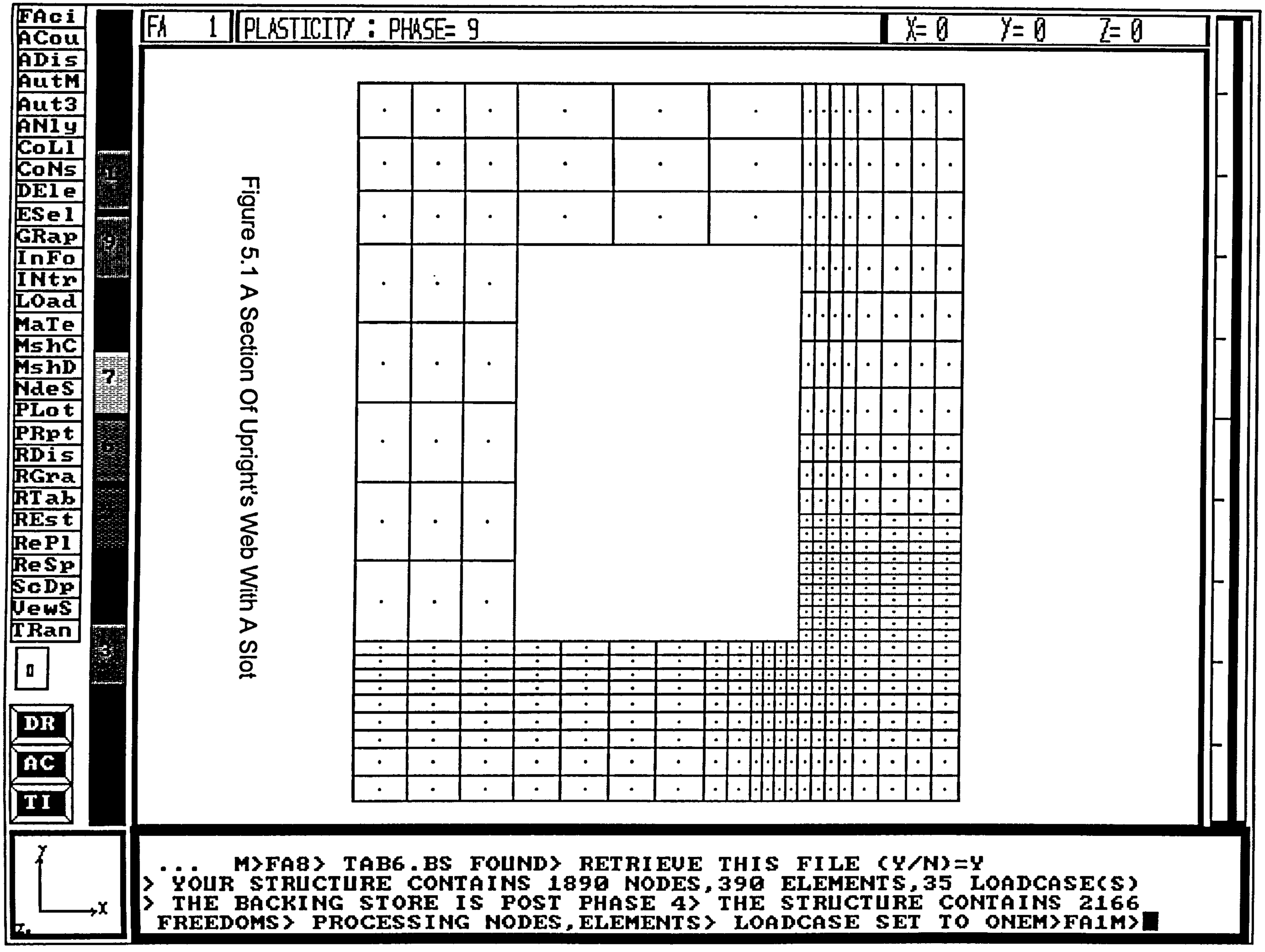

Figure 5.1 A Section Of Upright's Web With A Slot

FIGURE 5.2

UPRIGHT'S WEB STIFFNESS-HORIZONTALLY

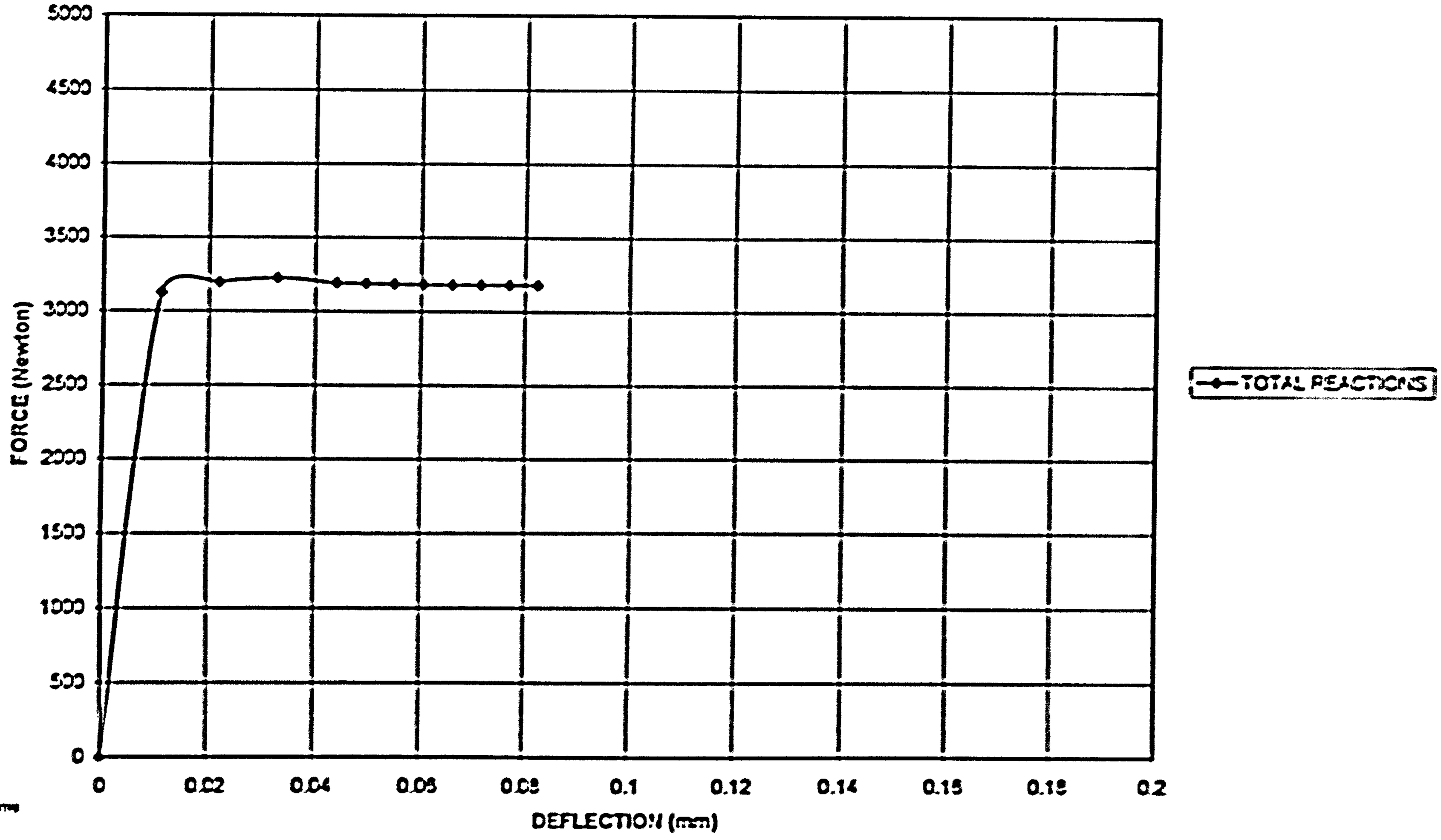

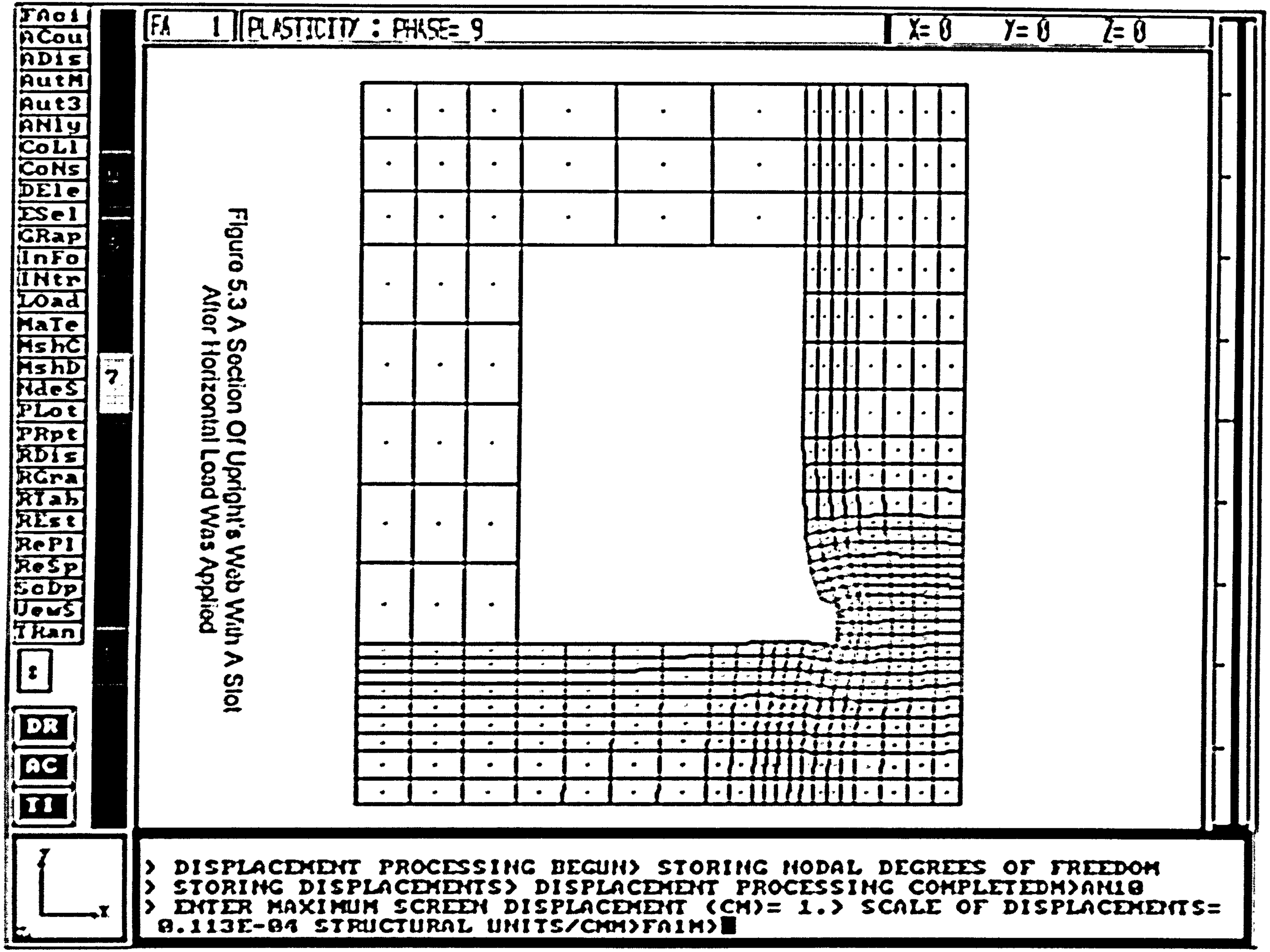

Figure 5.3 A Section Of Upright's Web Wuh A Slot
After Horizontal Load Was Applied

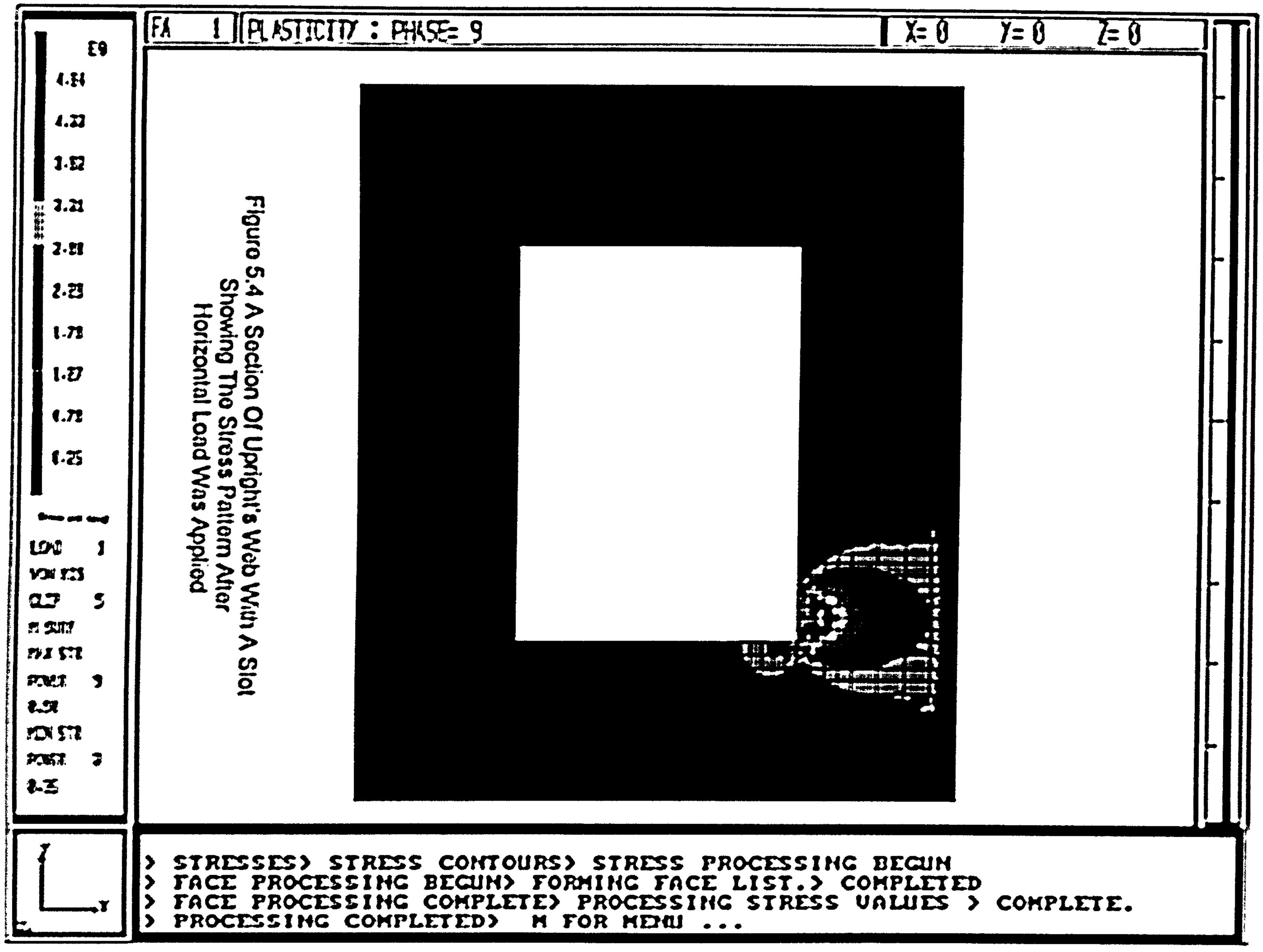

Figure 5.4 A Section Of Upright's Web With A Slot
Showing The Stress Pattern After
Horizontal Load Was Applied

FIGURE 5.5
UPRIGHT'S WEB STIFFNESS-HORIZONTALLY

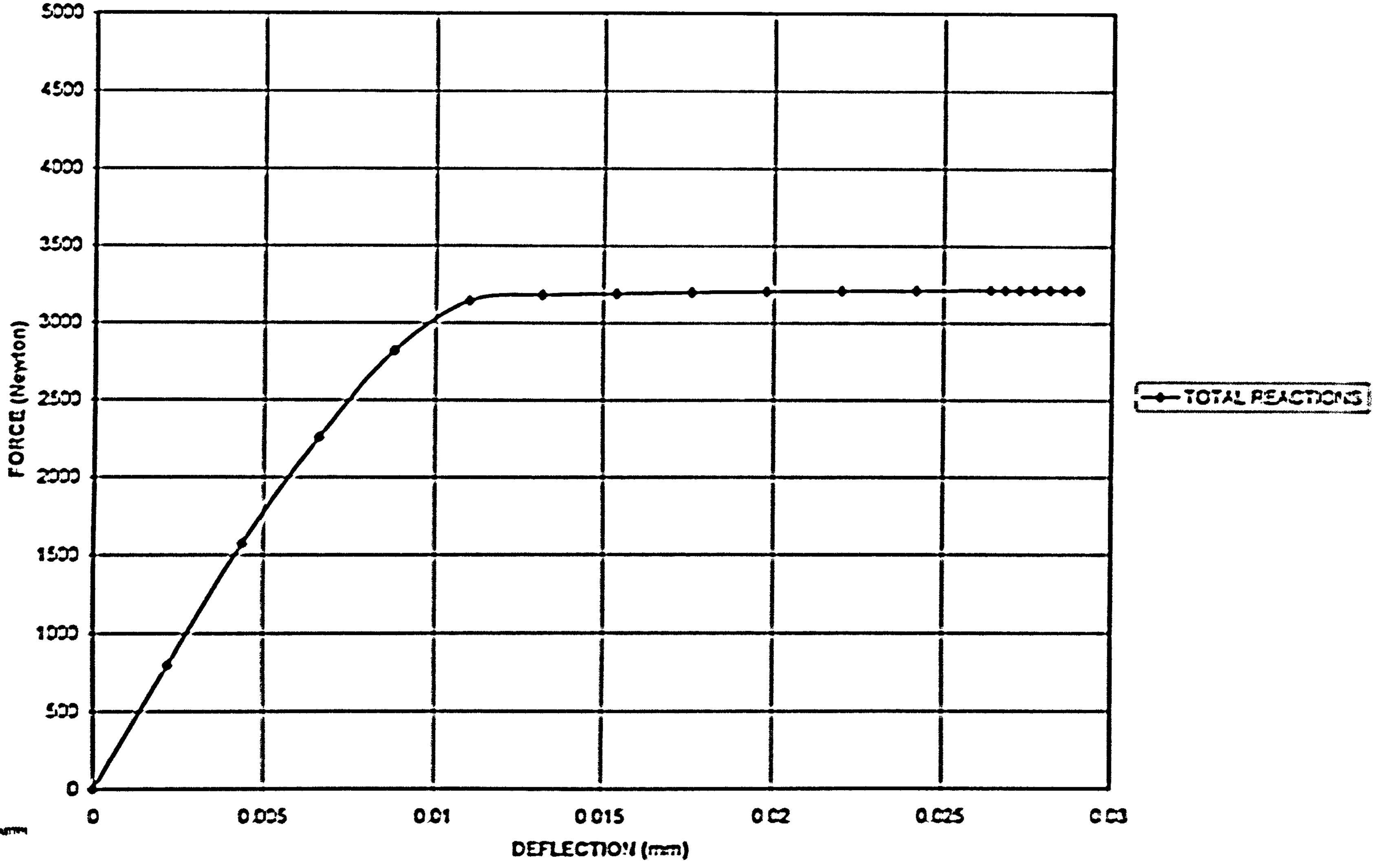

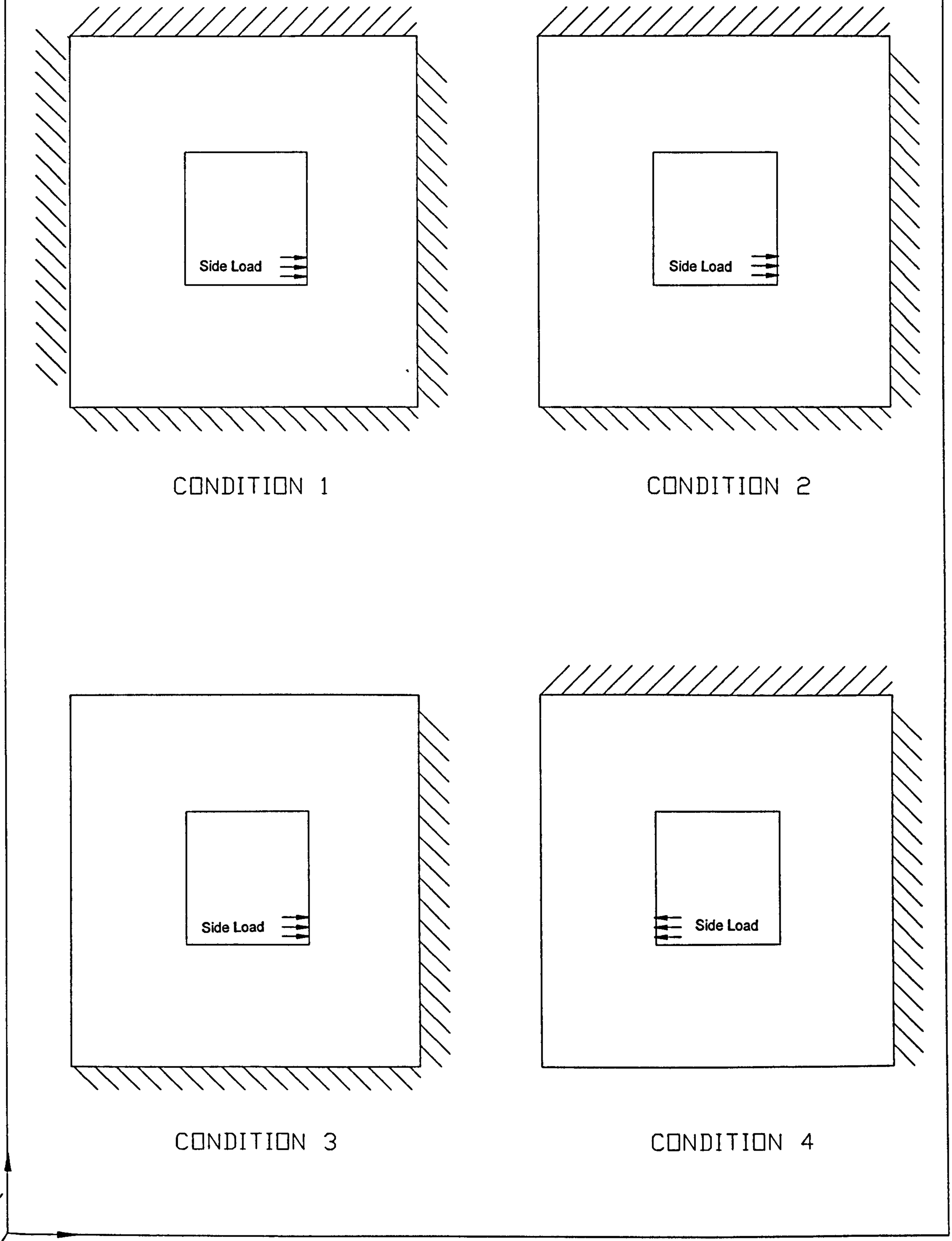

Figure 5.6 The boundary conditions examined

FIGURE 5.7

UPRIGHT STIFFNESS-boundary condition check-CONDITION 1

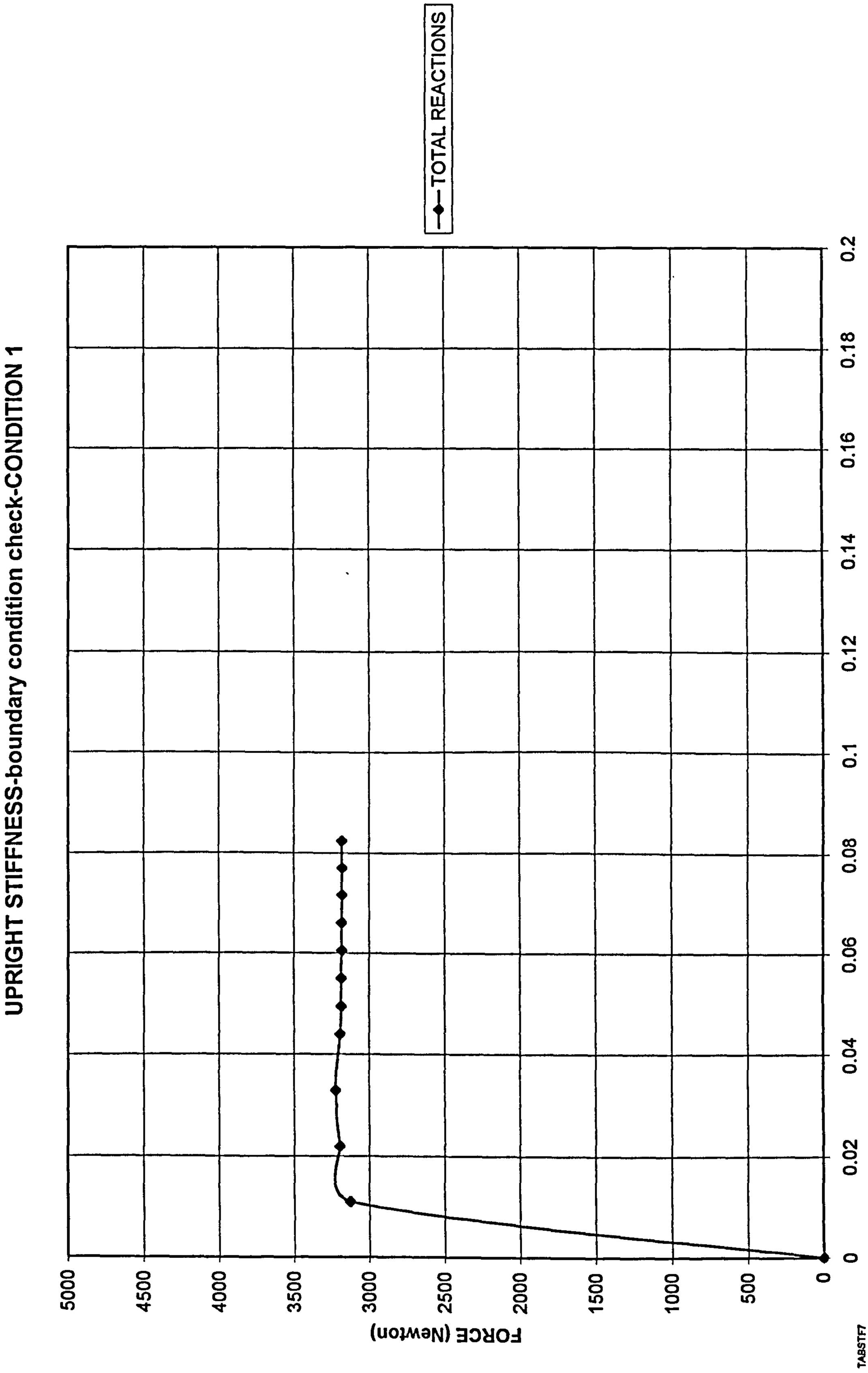

FIGURE 5.8
UPRIGHT STIFFNESS-boundary condition check-CONDITION 2

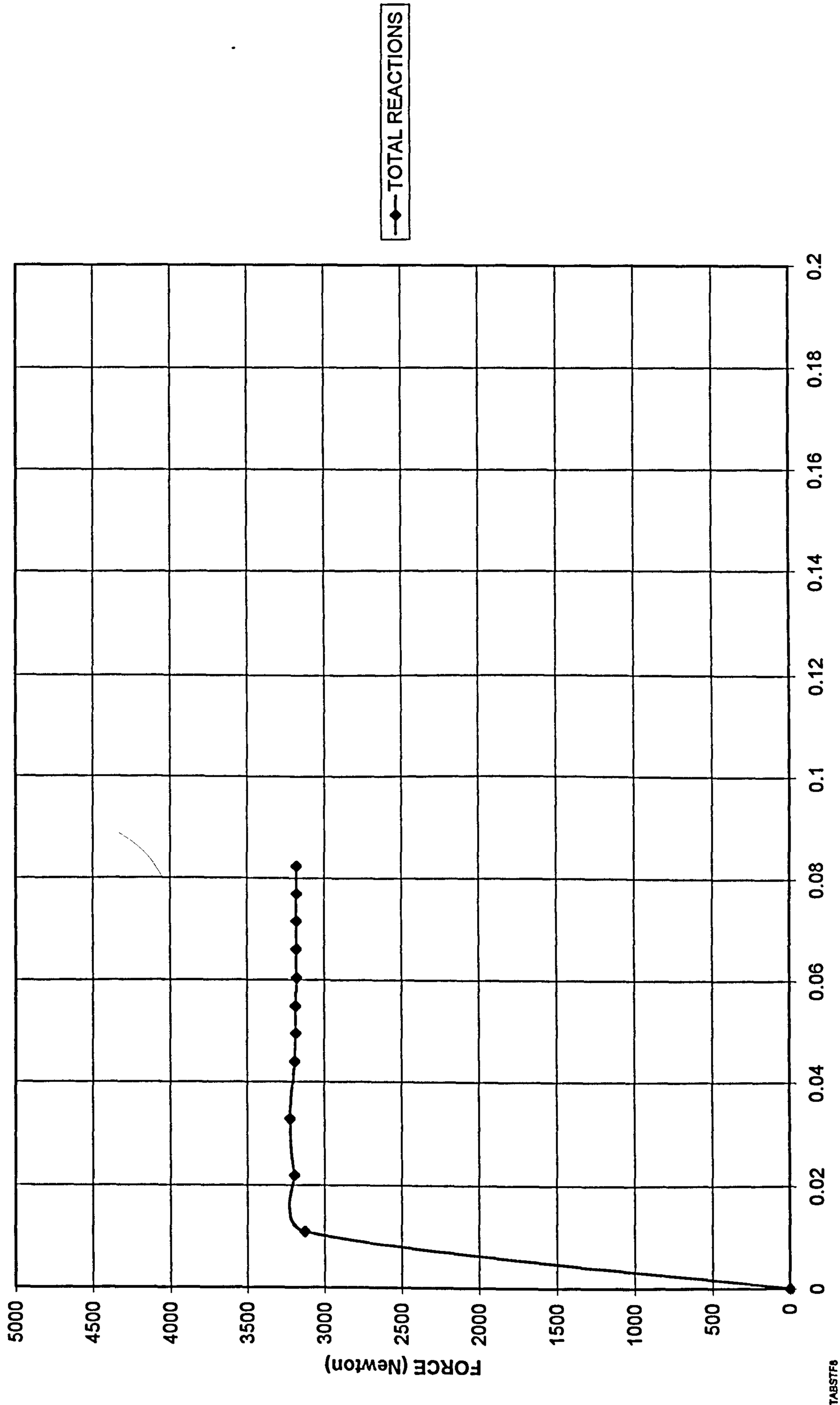

FIGURE 5.9
UPRIGHT STIFFNESS-boundary condition check-CONDITION 3

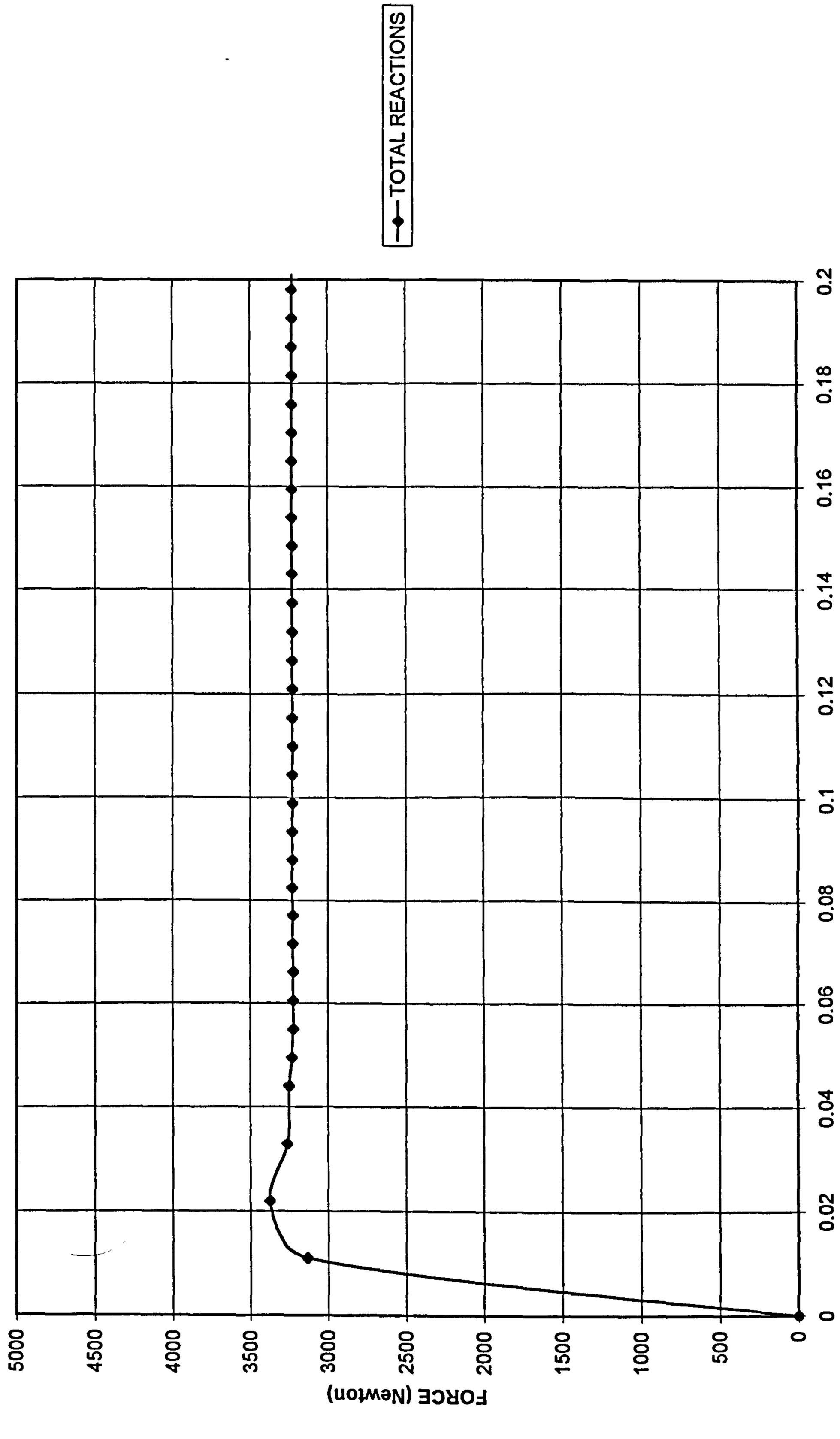

FIGURE 5.10
UPRIGHT STIFFNESS-boundary condition check-CONDITION 4

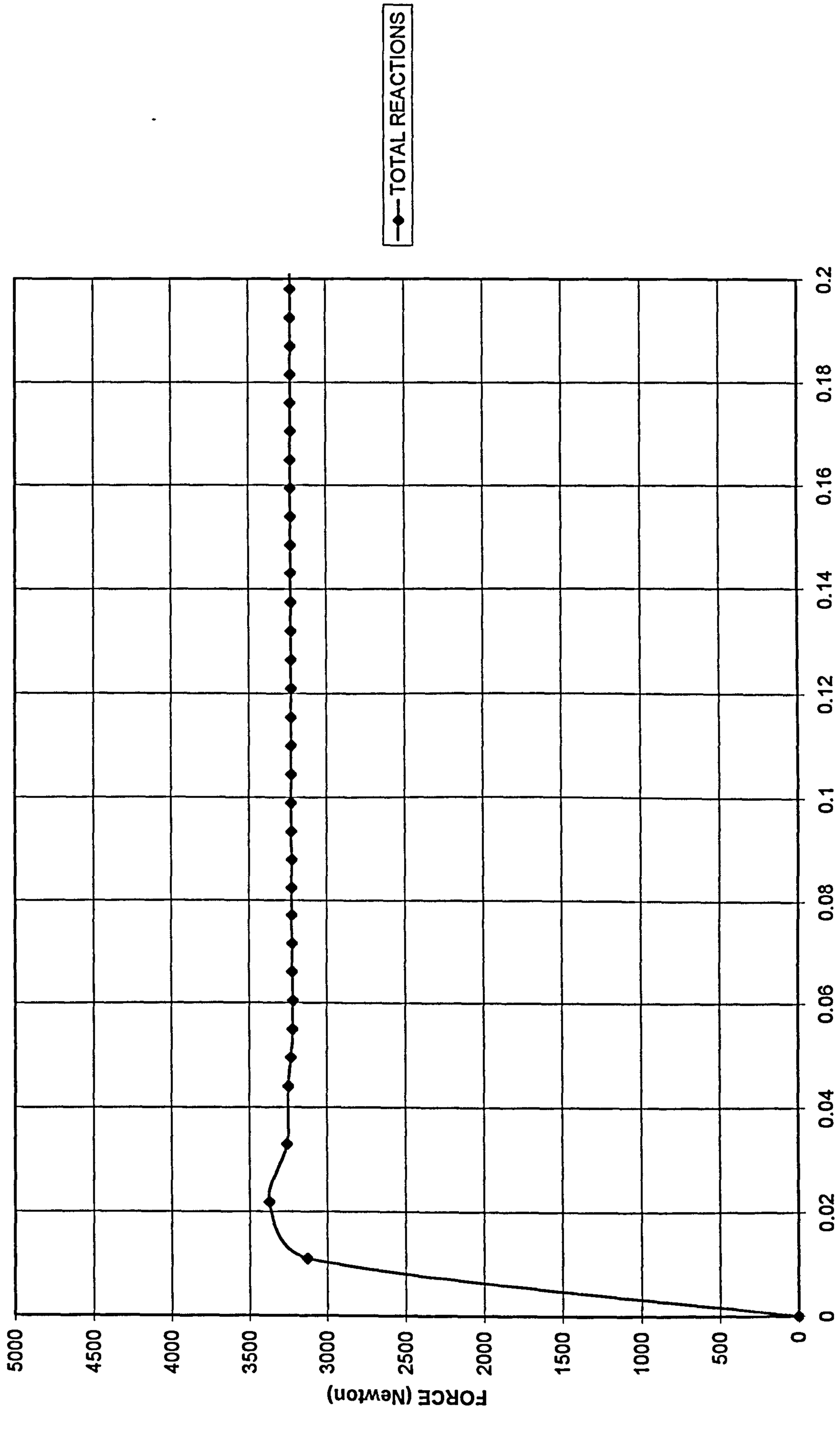

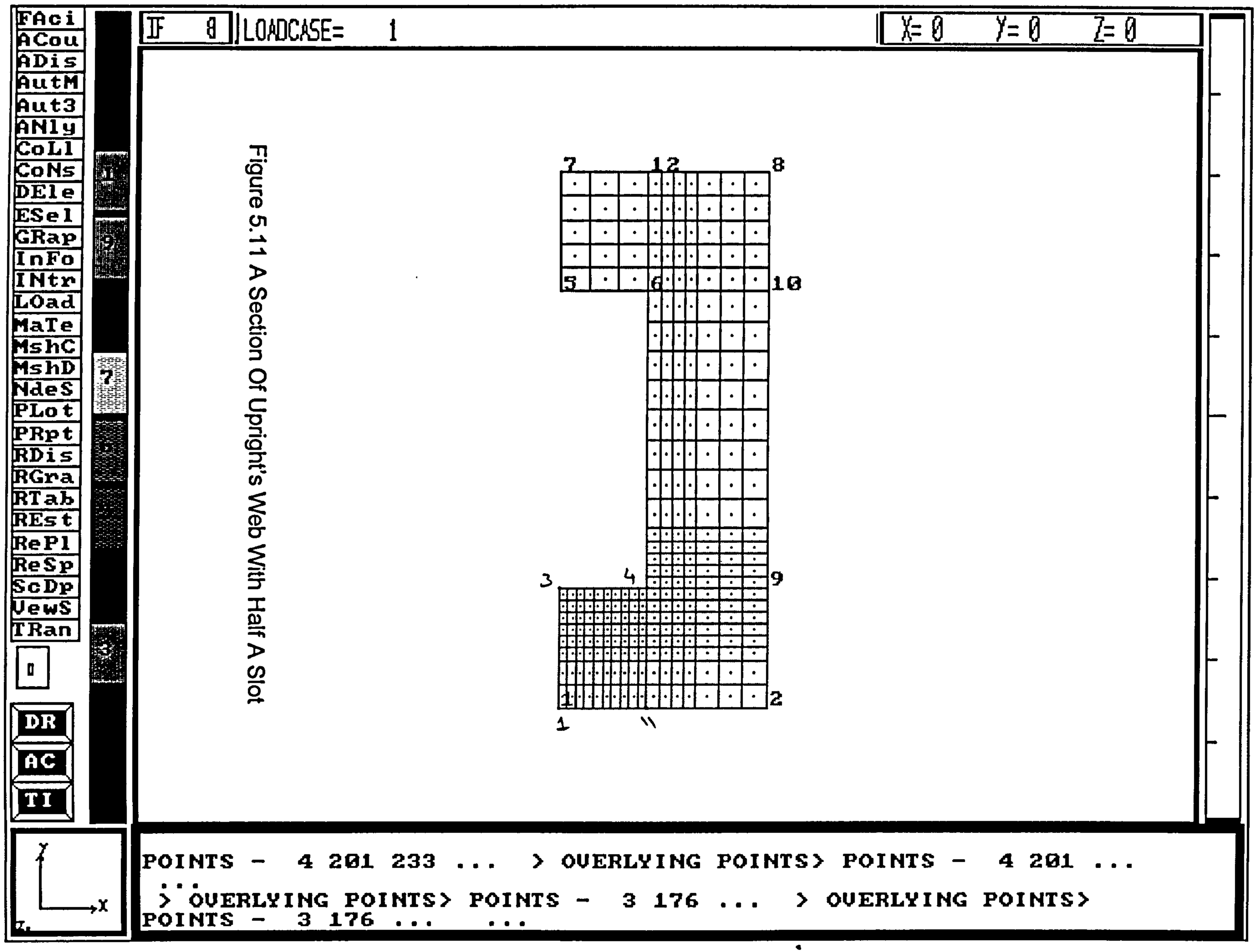

Figure 5.11 A Section Of Upright's Web With Half A Slot

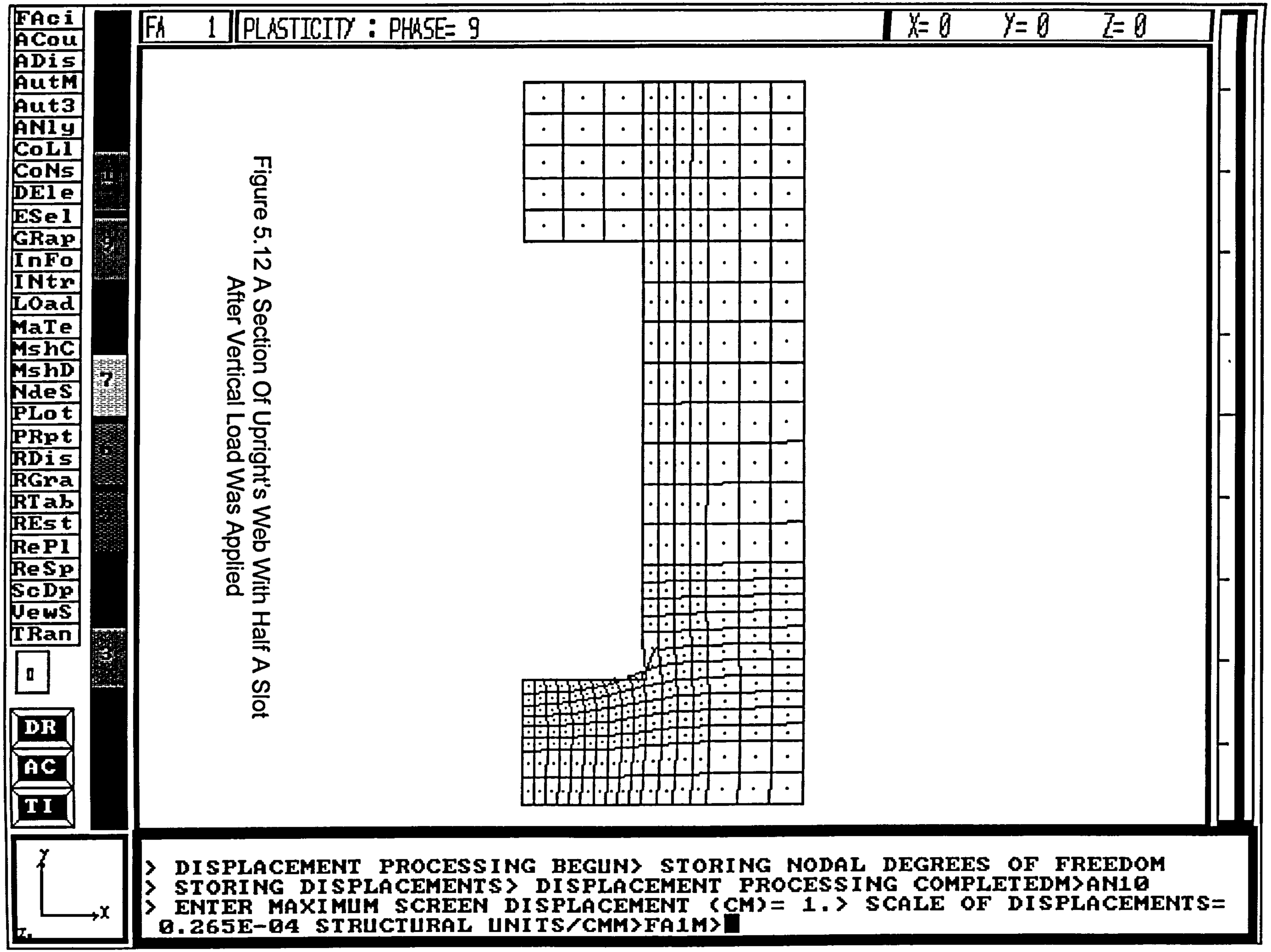

Figure 5.12 A Section Of Upright's Web With Half A Slot
After Vertical Load Was Applied

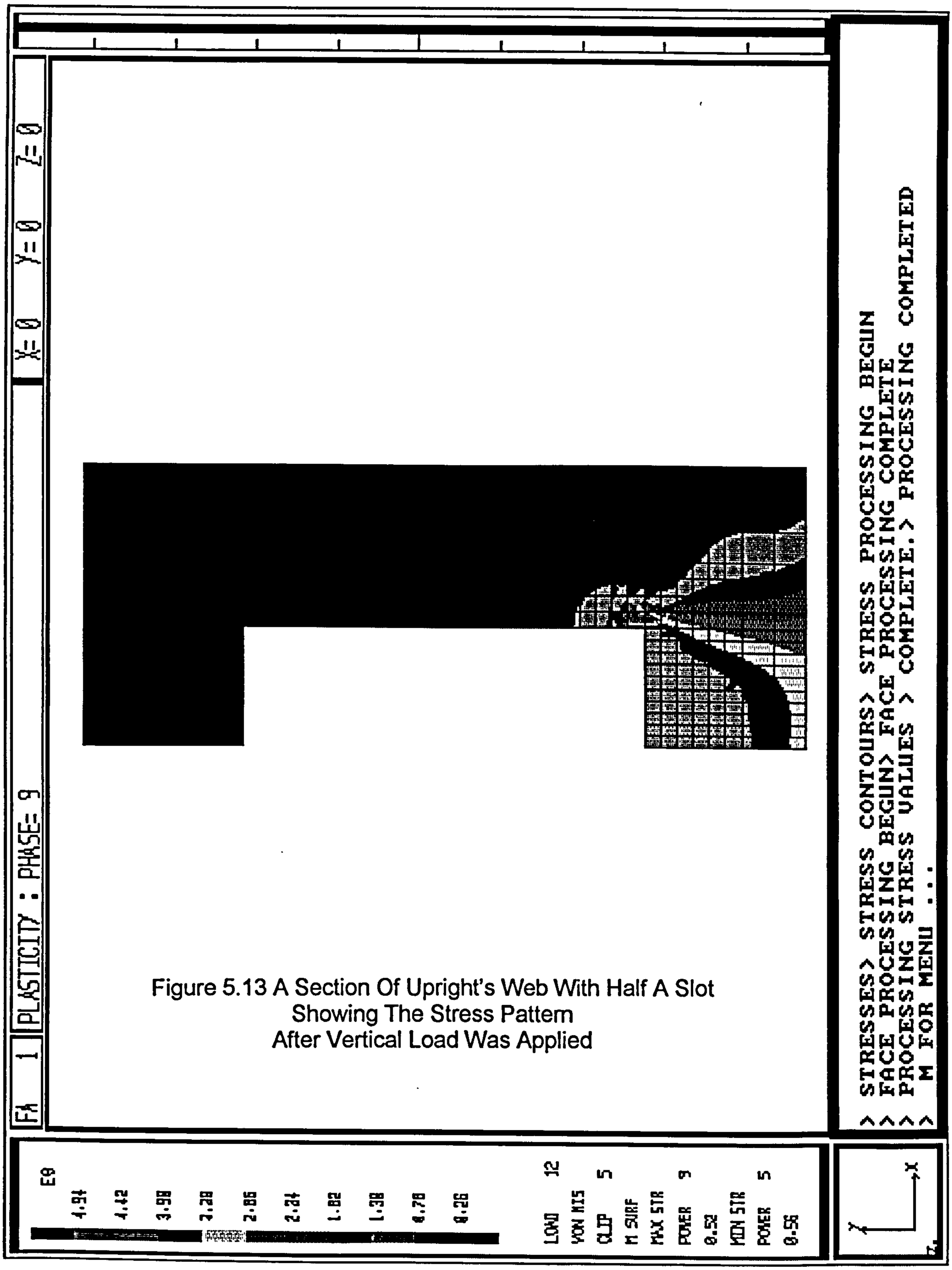

Figure 5.13 A Section Of Upright's Web With Half A Slot
Showing The Stress Pattern
After Vertical Load Was Applied

FIGURE 5.14
UPRIGHT'S WEB STIFFNESS-DOWNWARD

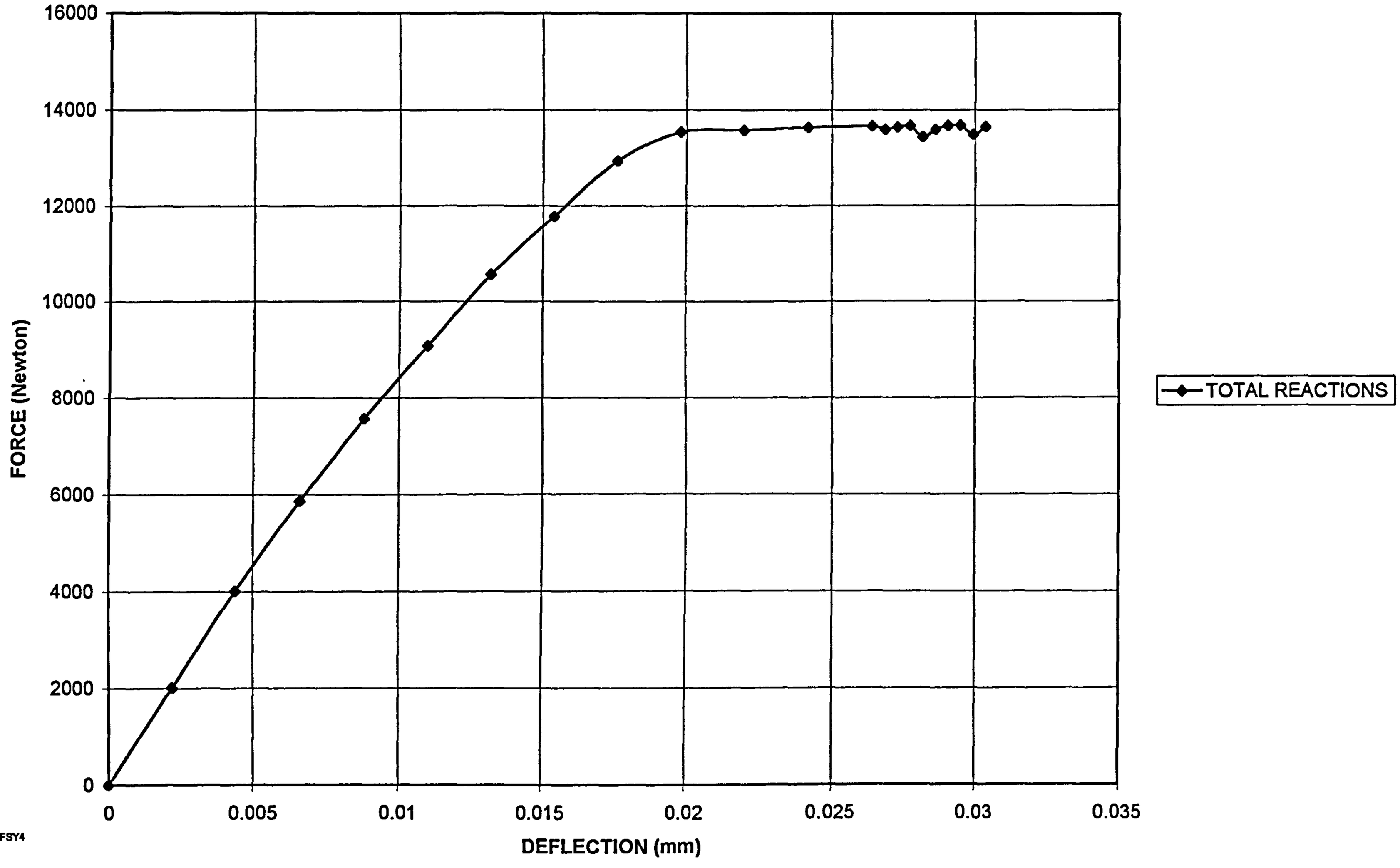

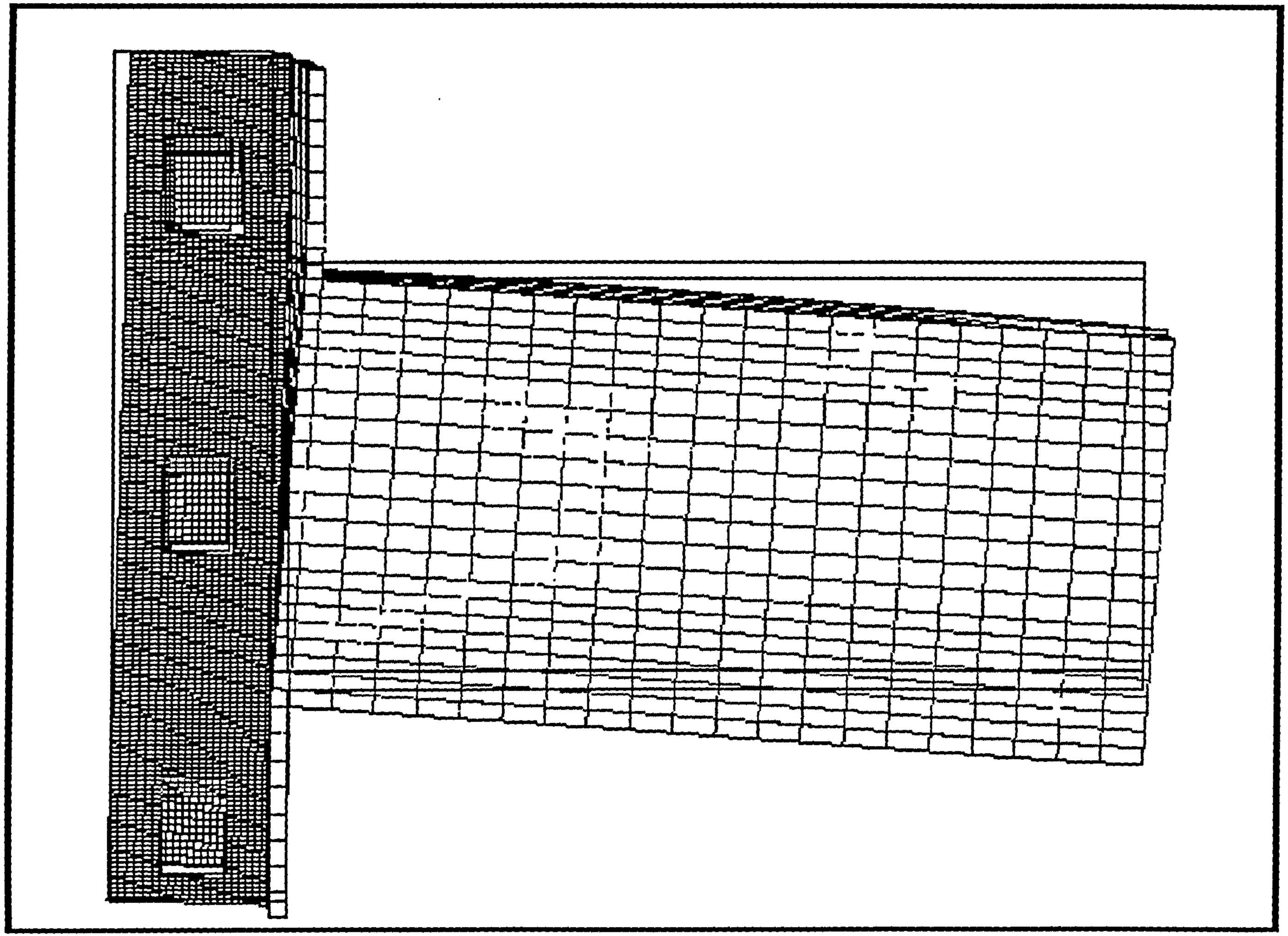

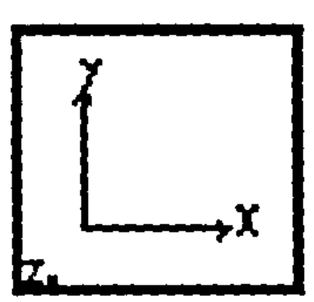

Figure 5.15 Deformed Structure Scale: 1/0.0253

Springs At Tabs–Restrainted Compression Zone-GM6C

FIGURE 5.16

DEFLECTION V HEIGHT
GM3C
SYMMETRICAL-Springs At Tabs-RESTRAINED
COMPRESSION ZONE

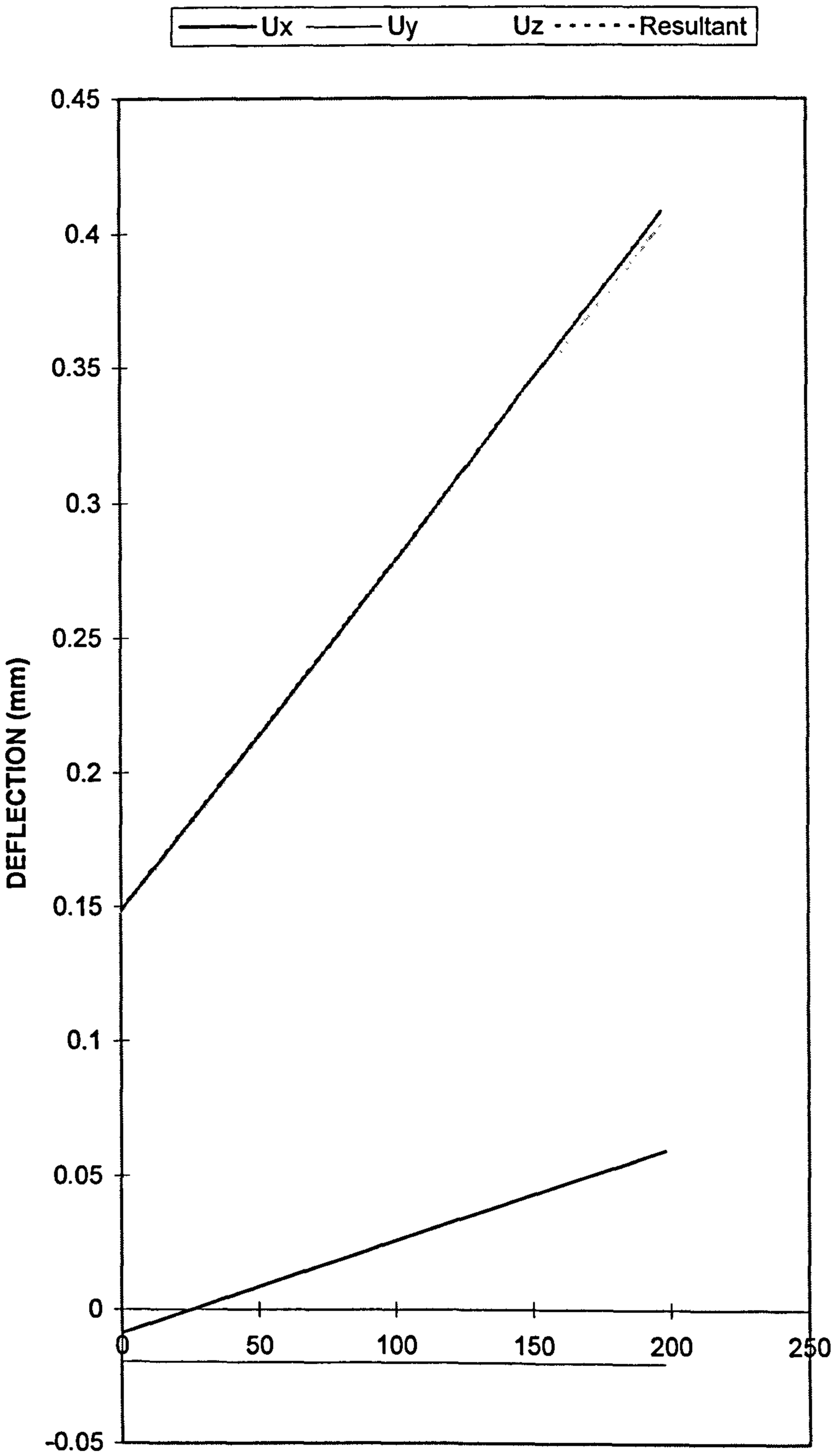

FIGURE 5.17

DEFLECTION V HEIGHT
GM6C
SYMMETRICAL-Springs At Tabs-RESTRAINED
COMPRESSION ZONE

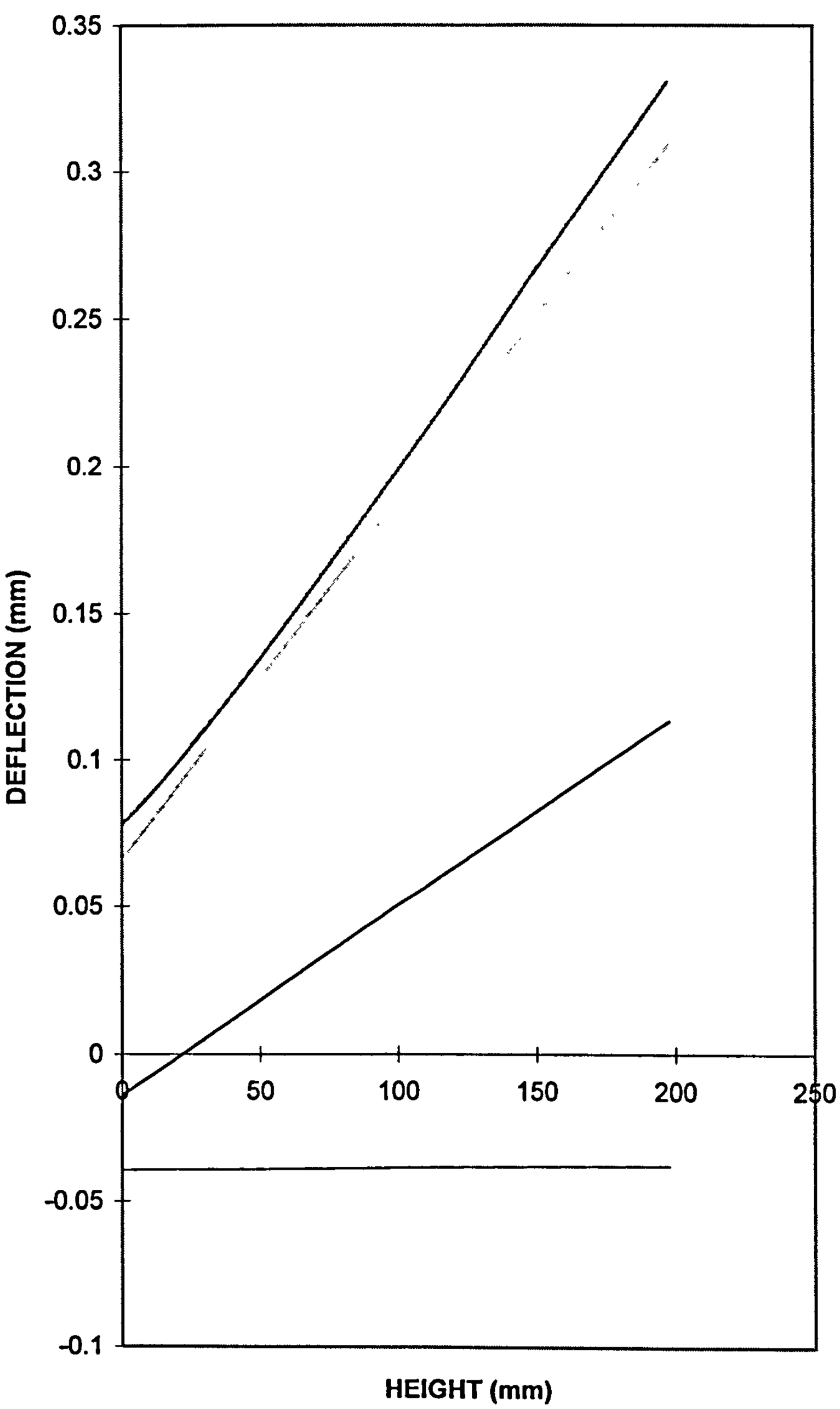

FIGURE 5.18

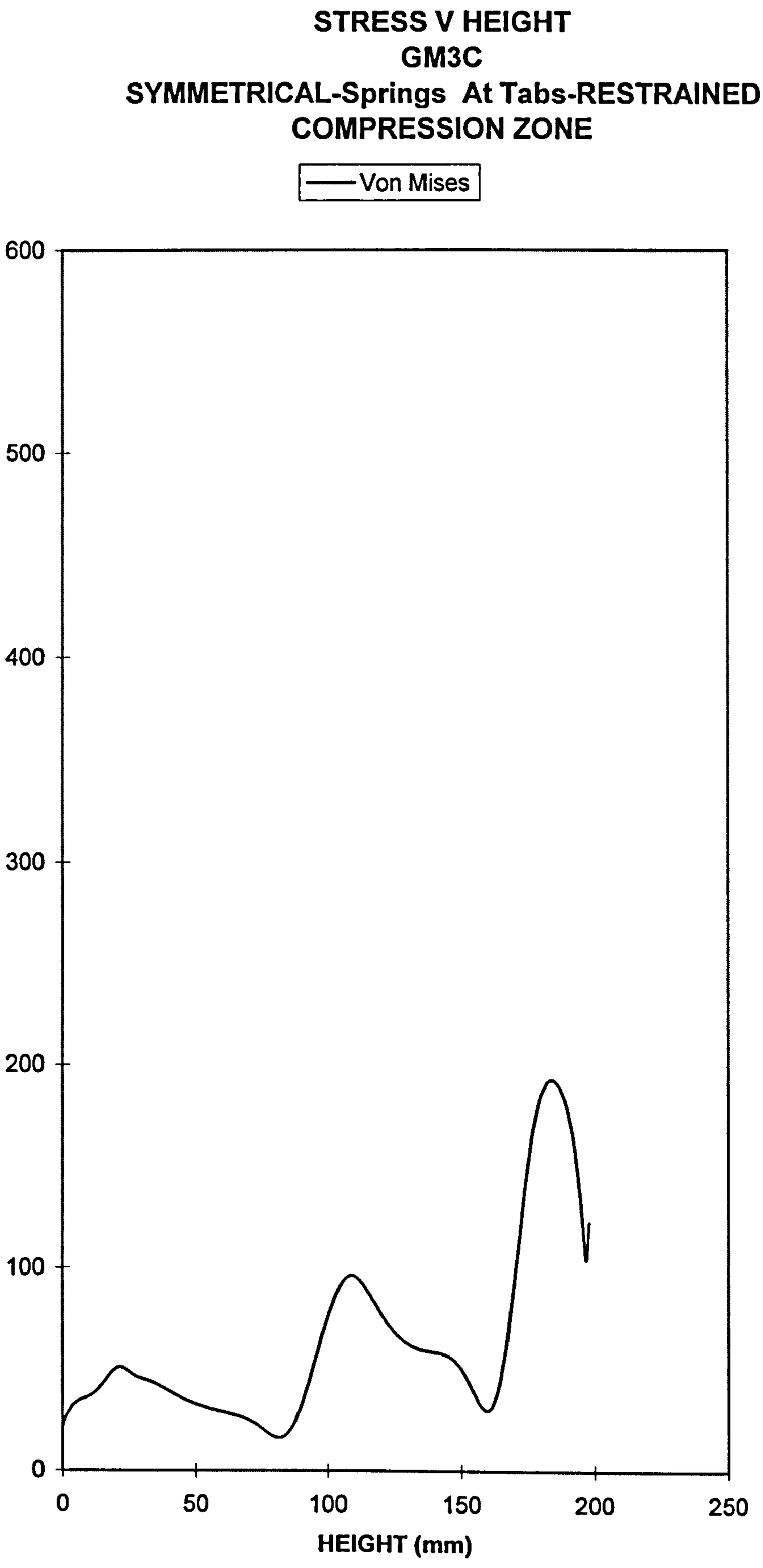
STRESS V HEIGHT
GM3C
SYMMETRICAL-Springs At Tabs-RESTRAINED
COMPRESSION ZONE
Von Mises
600
500
400
300
200
100
0
STRESS (N/mm2)
0
50
100
150
200
250
HEIGHT (mm)

FIGURE 5.19

STRESS V HEIGHT
GM6C
SYMMETRICAL-Springs At Tabs-RESTRAINED
COMPRESSION ZONE

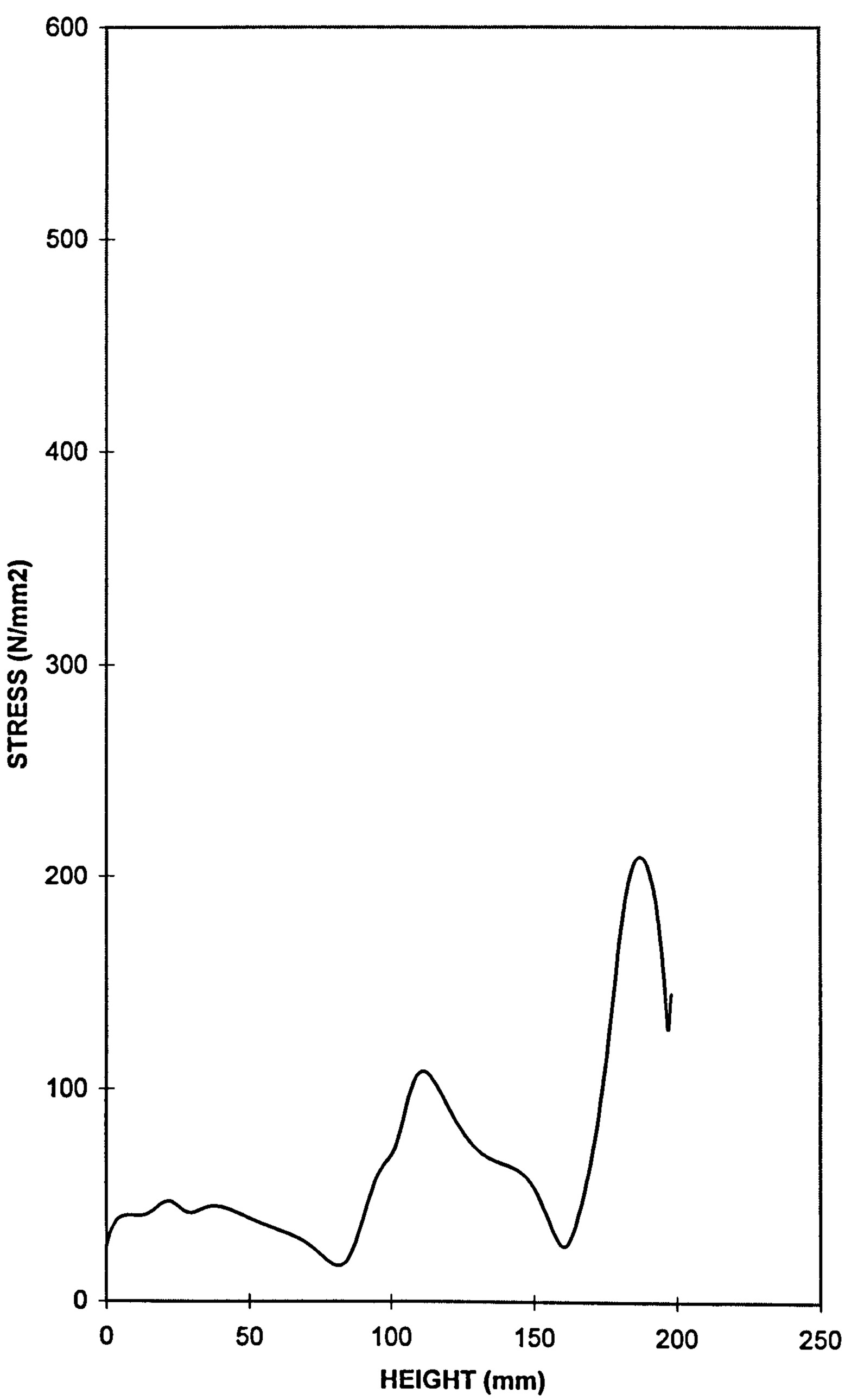

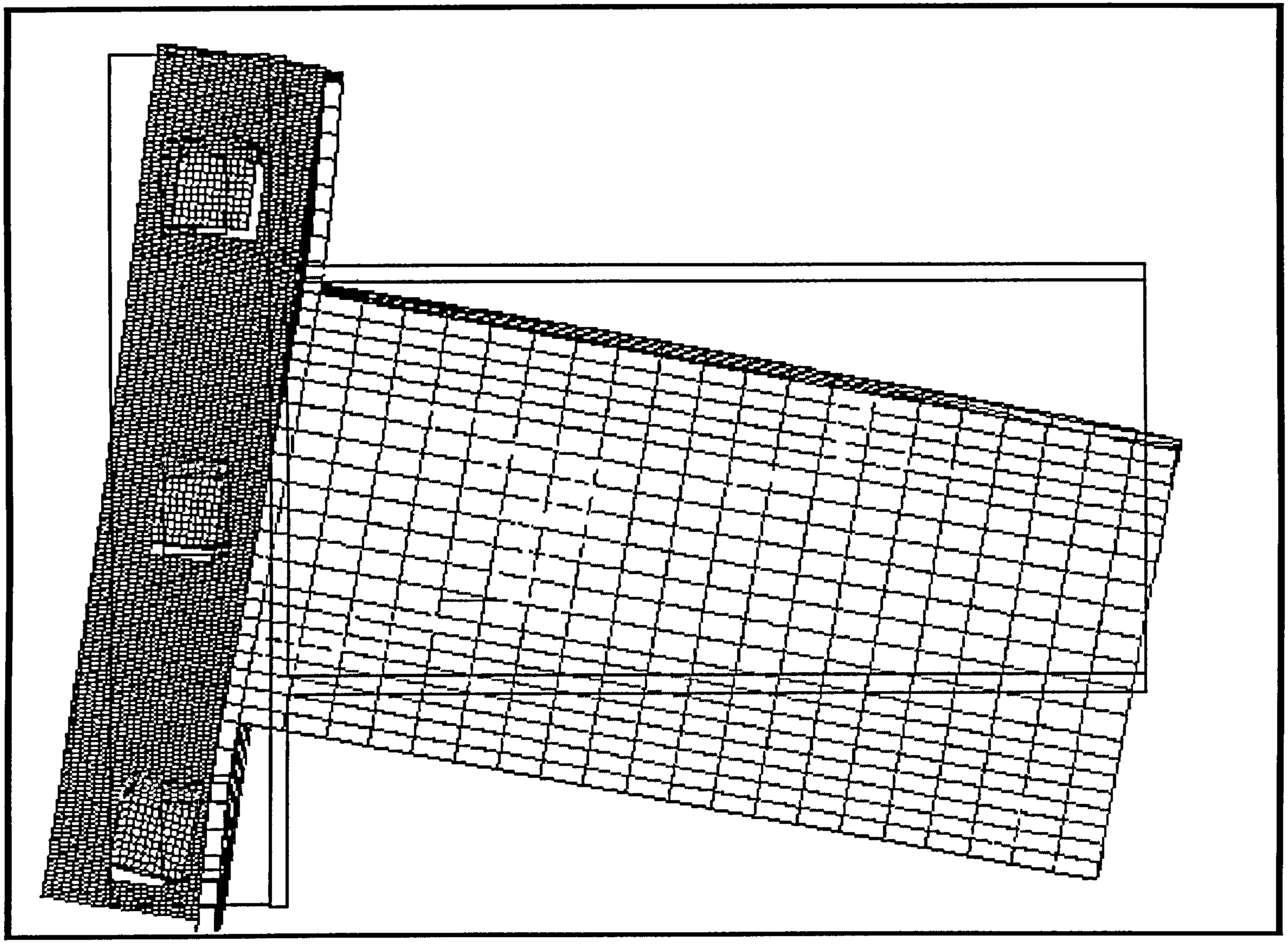

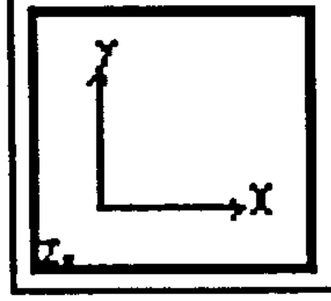

Figure 5.20 Deformed Structure Scale: 1/0.0253

Springs At Tabs–Free Compression Zone-GM6D

FIGURE 5.21

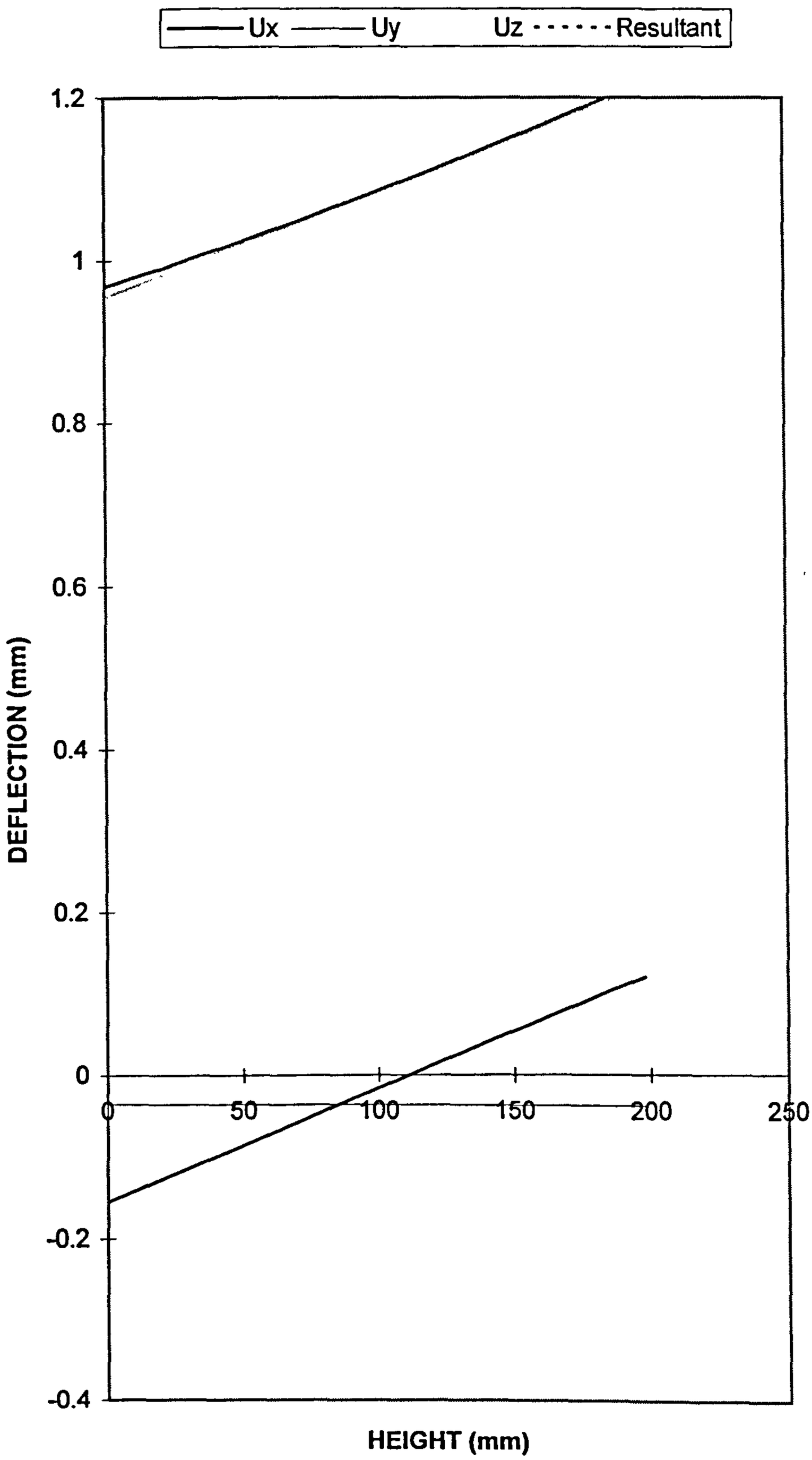

GM3DDS1

FIGURE 5.22

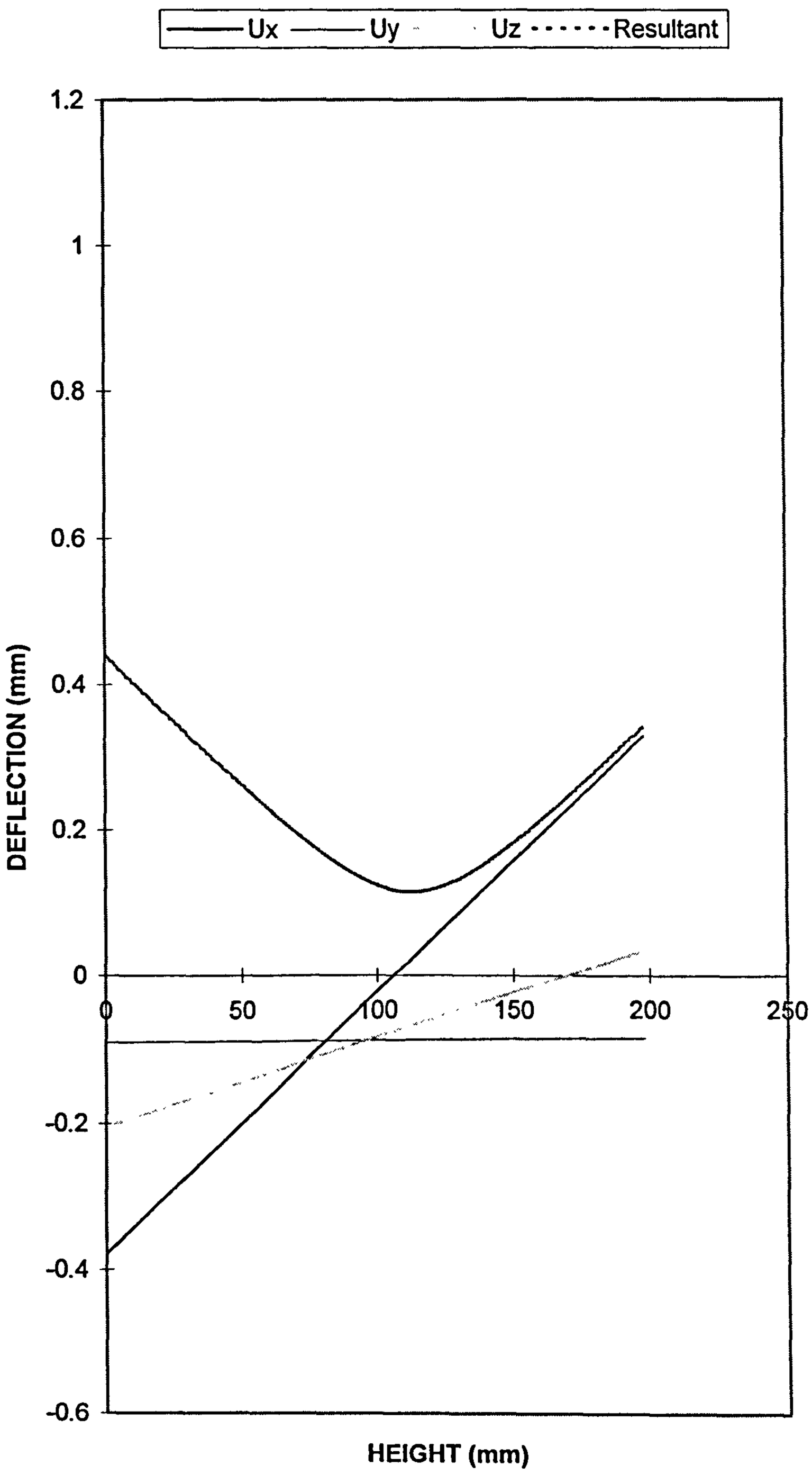

GM6DDS1

FIGURE 5.23

STRESS V HEIGHT
GM3D
SYMMETRICAL-Springs At Tabs-FREE COMPRESSION ZONE

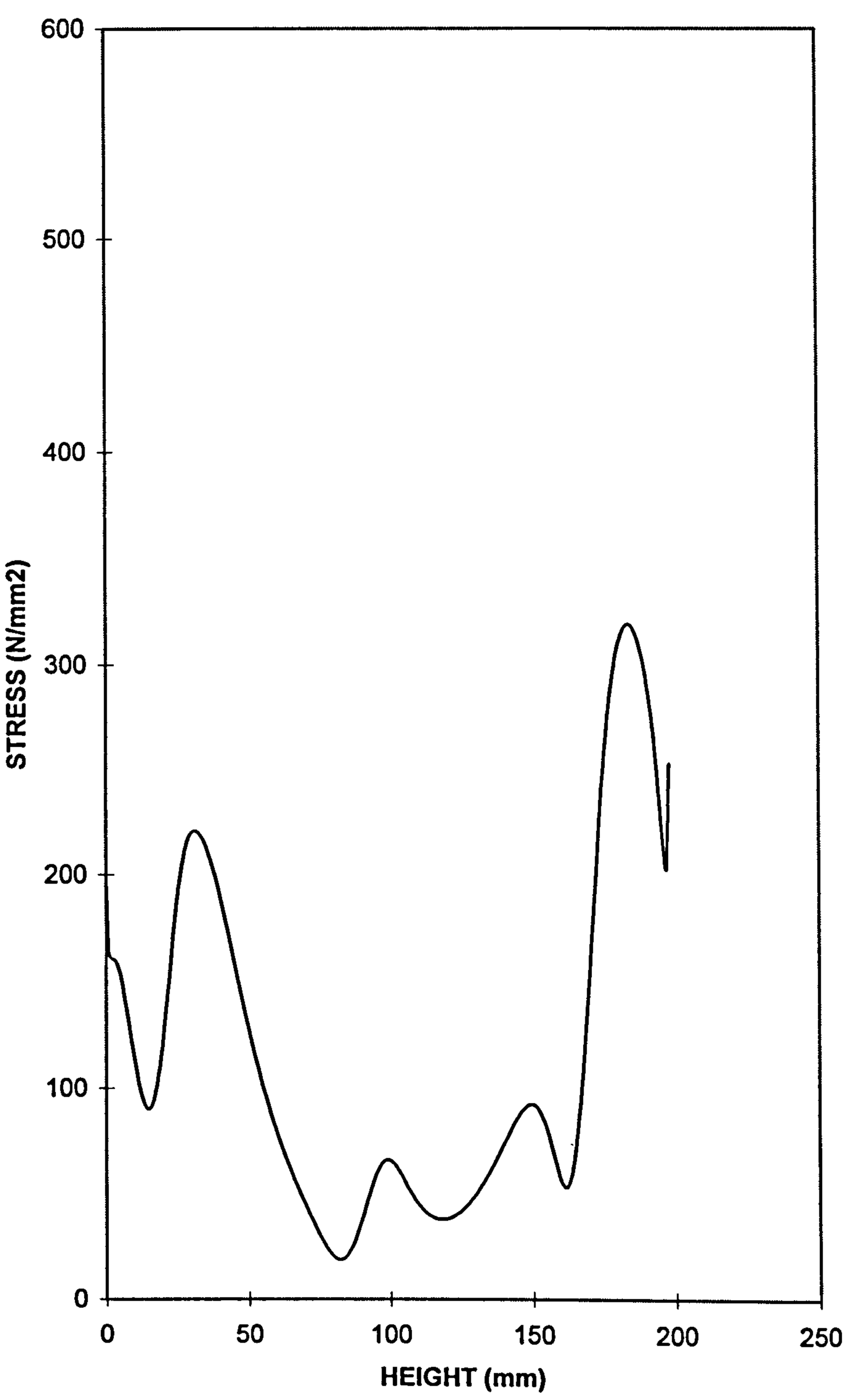

GM3DOS1

FIGURE 5.24

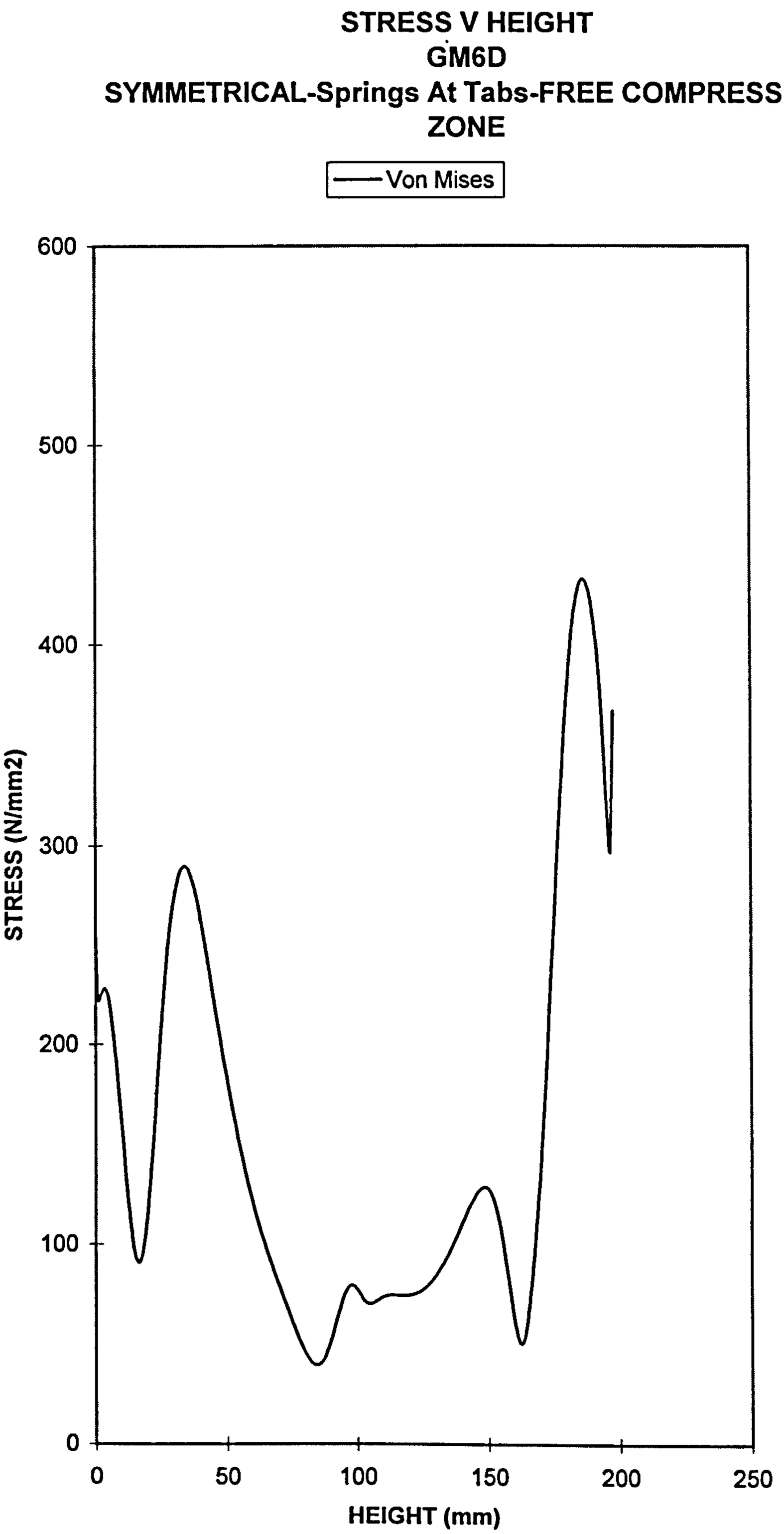
STRESS V HEIGHT
GM6D
SYMMETRICAL-Springs At Tabs-FREE COMPRESSION ZONE
Von Mises
600
500
400
300
200
100
0
STRESS (N/mm2)
0
50
100
150
200
250
HEIGHT (mm)

CHAPTER 6

GLOBAL MODELLING OF BEAM END CONNECTORS IN UP WELDED & DOWN WELDED ARRANGEMENTS

C H A P T E R 6

GLOBAL MODELLING OF BEAM END CONNECTORS IN UP WELDED & DOWN WELDED ARRANGEMENTS

6.1 Introduction

Chapter 5 described the details of a global model generated to simulate the behaviour of a beam end connector.

The model in chapter 5 used spring stiffness values as the means of resistance to rotation. These were used at the tabs. The spring stiffness values were determined from sub modeling of upright's web.

These were used in two models, the one, which had a free compression zone and a separate model with the compression zone restrained. Absolute restraints were used to suppress the movement of the compression zone.

The two models were used to investigate the beam end connector behaviour including determining the initial stiffness values of the connector. The exercises also provided information on how the load was distributed in the tabs.

It was decided that the work on the global modelling of the beam end connector, previously carried out for the symmetrical welding position should be extended to the up

welded and down welded arrangements, figure 4.4, (b) and (c).

The down welded arrangement, figure 4.4 (c) is rarely used in practice. This arrangement was not physically tested for the beam end connector being modelled.

Figure 3.49 however shows a different design tested with this configuration.

The inclusion of this welding arrangement variation here was merely to establish the load distribution in the tabs resulting from such extreme welding arrangement.

The degree of down weld adopted in the model represented the lowest possible position that the beam could take relative to the height of the beam end connector.

Initially Up weld and down weld modelling was confined to the case where springs were used at the tabs and compression zones were restrained. The models with restrained compression zones provided the load distribution in the tabs reflecting the final stages of loading. This was required for the next stage of the work.

Later the models were modified to free the compression zones. The models were used to determine the initial stiffness values.

The restrained compression zone cases were considered first.

Case GM6C, Table 5.1, having the lowest number of spring elements at the tabs was selected as the basis for generating up welded and down welded models.

6.2 Aims

The aims were, using the parameters identified through the experimental part

a. to determine the load distribution in the tabs associated with the middle to final stages of loading-i.e. Restrained compression zone, section 4.1.

b. to evaluate the stiffness values for the symmetrical, up welded and the down welded arrangements-Restrained compression zone

c. to determine the overall deformation shape for the three welding positions-Restrained compression zone

d. to determine the load distribution in the tabs associated with the initial stages of loading-i.e. free compression zone, section 4.1.

e. to determine the initial stiffness of the beam end connector in the up welded and down welded positions-i.e. free compression zone.

6.3 Mesh generation for up welded and down welded models

The mesh generated according to sections 4.3 and 4.3.1 was modified to produce the up welded and down welded cases. They were further modified according to sections 5.4 replacing the absolute restraints at the tabs with spring stiffness values.

Figures 6.1 and 6.2 show two views of the up welded condition before loading. Figure 6.3 shows the deformed structure. Two views of the undeformed structure of down

welded condition are shown in figures 6.4 and 6.5. Figure 6.6 shows the beam end connector after loading.

6.4 Results

Table 6.1 lists the forces applied to the springs at top, bottom and the middle tabs for the up welded condition. Considering, initially the forces in the X-direction, the top tab attracted a value of 5060N, the middle tab, 2000N, and the bottom tab, -561N the total of which equating to the sum of the reaction forces in the compression flange.

Considering the forces in the Y-direction values of -3840N, -3700N, and -2460N are recorded for the top, the middle and the bottom blocks respectively, the total of which equates to the applied load of 10000N.

Considering table 6.2 the forces applied to the springs horizontally at the top, middle and the bottom tabs are 8340N, 4790N, and 669N respectively and in equilibrium with the reaction forces in the compression zone.

In the Y direction the top, middle and the bottom tabs of the proportion -3350N, -3920N, -2730N respectively share the applied load of 10000N.

6.5 Investigating boundary conditions of the compression zone

As described in sections 4.1 and 4.3.2, beyond the initial stages of loading, 0%-40% of the total applied load, a hinge would form in the end plate just below the stub beam. This would then result in the endplate bearing against the upright's flange and therefore forming a tertiary source of resistance to rotation, figure 4.6.

The primary source of rotation was due to the bearing of the tabs against the upright's web, followed by the hinge formation, section 4.3.2.

In order to simulate this action absolute restraints were used. They were applied to a number of selected nodes in the lower part of the endplate below the stub beam. Figures 6.7, 6.8 and 6.9 show the restrained nodes for the symmetrical up welded and down welded arrangements.

It can be seen from figures 6.7, 6.8 and 6.9 the number of the restrained nodes varied to match the size of the compression zones for the different models.

The restrained nodes were adjacent to the plate containing the tabs and central to the end plate. The nodes along the free edge of the end plate were not restrained.

The selection of the nodes for restraining was based on the fact that the part of the compression zone nearest to the plate containing the tabs would come in contact with the side of the upright first. This was observed during the physical tests and was because of the stiffening effect of the plate that included the tabs.

GM6C is the spring-incorporated model with restrained compression zone, table 5.1. GM6D is the spring-incorporated model with free compression zone, table 5.2. Comparing the horizontal forces in their springs given in tables 5.7 and 5.12, it can be seen that there is marked difference in their magnitudes.

In fact the value of the force in the top tab of the model GM6D is 2.5 times greater than that of GM6C.

This was partly due to the fact that suppressing the movement in the compression zone prevented load from being transmitted into the tabs.

Added to this however was the fact that restraining nodes in the compression zone generated tension forces, which consequently reduced the load on the springs.

It was felt that the effect of this condition should be reduced or eliminated to allow freedom of the compression zone except in the -X direction figures 4.5 and 4.6.

Ideally the use of a gap facility would have overcome the problem, but the PAFEC program did not allow the use of a gap module in conjunction with a coupling facility.

As described in section 4.3.1, a coupling facility had to be used which automatically generated constraint equations so that displacement and stress continuity was ensured in the regions of varying mesh densities.

The problem was further investigated.

The nodes where tension forces had resulted were identified. These nodes were then released manually through an iterative process until no such forces existed in the system.

This work was limited to two of the models considered namely GM6C, the model with symmetrical welding arrangement and the model GM6C-UP representing the up welded arrangement. The model simulating the down welded arrangement, GM6C-DN did not generate any tension forces. The modified models were used to determine the stiffness values of the beam end connector. These as well as the

stiffness values obtained prior to releasing the tension nodes are given in tables 6.5 and 6.6 for GM6C and GM6C-UP.

Table 6.7 shows the stiffness values obtained from the model simulating the down welded arrangement, namely GM6C-DN.

Section 4.4.1.3 described the methods by which the rotational values and subsequently the stiffness values were arrived at.

Tables 6.3 and 6.4 show the applied forces to the springs for GM6C and GM6C-UP after tension forces were removed. The spring forces prior to the modification to the nodes are given in tables 5.7 and 6.1 for the same models respectively.

6.6 Free body diagrams

Figures 6.10, 6.11 and 6.12 show the free body diagrams for the three models after the iteration process.

They show the load distribution in the tabs as well as the resulting reaction forces in the compression zone.

Figures 6.7, 6.8 and 6.9 show the restrained nodes prior to the iteration process. As the result of this in the case of the symmetrical welding arrangement the number of restrained nodes was reduced from 8 to 2. In the case of the up welded arrangement 12 number restrained nodes were reduced to 5.

Only 2 nodes were restrained in the down welded model. The reaction forces in this case remained as compression.

Equilibrium was also checked for every model using the information in each figure, Appendix 6.1, 6.2 and 6.3.

6.7 Initial stiffness values up welded & down welded models with free compression zones

The two models representing the two extreme welding positions were modified so that the compression zones were free to move. They were then used to evaluate the initial stiffness values of the beam end connector. The stiffness values were obtained as described in section 4.4.1.3 and are given in table 6.11. For comparison purposes the initial stiffness values obtained for the symmetrical welding arrangement, free compression zone, model GM6D previously given in table 5.4 were included in this table. Tables 6.9 and 6.10 show the load distribution at the tabs for the two welding arrangements.

6.8 Discussion of results

6.8.1 Restrained compression zone

The deflected shapes of the beam end connectors shown in figures 6.3 and 6.6 were typical of the mode of failure observed during testing, figures 3.43 and 3.49.

Considering the results for the symmetrical model, GM6C, comparing tables 5.7 and 6.3 it can be seen that the effect of the tension forces having been eliminated resulted in the re-distribution of forces in the tabs.

A notable change was the increase of the horizontal force in the top tab increasing from 5400N, table 5.7 to 10100N.

Considering table 6.5 and 6.6, a further consequence of releasing the tension nodes was a reduction of about 30% in the stiffness values of the beam end connector.

Comparing the stiffness values obtained from the three models, table 6.8, the values obtained as the result of rotation measurement according to figure 4.17(c), θ_{tr} and consequently K_{tr}, the stiffness values obtained for the symmetrical welding arrangement were higher than those obtained for the up welded arrangement by 12%. This was confirmed by the experimental test results.

The stiffness values obtained for the down welded arrangement were higher than those for the symmetrical arrangement. The reason for this was the fact that the down welded beam coincided with the restrained compression zone, the lowest part of the end plate stiffening the beam end connector to a greater extend compared with other welding positions.

The beam end connector under consideration was not physically tested in this configuration.

As observed with all the cases with restrained compression zones, the bottom tab shielded by the formation of the compression zone was almost redundant in terms of load carrying capacity.

6.8.2 Free compression zone

Table 6.11 shows the initial stiffness values for the beam end connector with the three welding arrangements. The different methods of rotation measurements were explored and the same degrees of variations consistent with the findings in chapters 4 and 5 tables 4.7 and 5.8 were observed.

For example here also the highest value of stiffness was obtained when rotation measurements were carried out according to figure 4.17(a). This involved measuring rotations by determining differential deflection of top and the bottom flanges adjacent to the beam end connector.

The load distribution for the beam end connector, symmetrical welding arrangement, free compression zone was given in chapter 5, table 5.12. Considering table 5.12 and tables 6.9 and 6.10 it was noted that the load distributions into the tabs for these three welding positions GM6D, GM6D-UP, GM6D-DN were similar. In every case the horizontal forces formed a couple at the top and the bottom tab with the middle tab almost redundant in terms of load carrying capacity. The summation of the vertical components was 10000N equating to applied force.

6.9 Conclusion

The model for the symmetrical welding arrangement generated in Chapter 5 was modified to produce models simulating up welded and down welded arrangements.

These models had restrained compression zones achieved through the use of absolute restraints. Using absolute restraints resulted in tension forces being generated in the compression zones, which in turn reduced the forces in the spring elements.

The down welded model did not generate any tension forces. This could have been due to the fact the compression zone involved was a fraction of those of the symmetrical and the up welded arrangements.

The tension forces were eliminated through an iterative process. This resulted in an increase in the applied forces

to the tabs and a reduction of stiffness values by about 30%.

The models also determined the magnitude of the forces in the compression zone.

The main objective however was to determine the load distribution in the tabs for the various welding arrangements associated with the middle to final stages of loading of the beam end connector. This was loading beyond 40% of the total applied load which was facilitated by adoption of the restrained compression zone.

This was achieved. The outcome of this was that when the compression zone was formed, simulating the bearing of beam end connector against the upright's flange, the bottom tab became redundant in terms of load carrying.

Furthermore the up welded and the down welded models were modified to free their compression zones simulating the initial loading stages, 0% to 40%. This was carried out for the symmetrical arrangement in chapter 5, case GM6D.

The load distribution in the tabs for these conditions was also determined.

The models showed that during the initial loading stages the middle tab did not carry any load.

Using these models it was shown that an appreciable difference in the magnitude of stiffness values could be achieved depending on where on the beam end connector assembly measurements of rotations were taken.

TABLE 6.1

Forces Applied To 30100 Spring Elements At Top, Bottom And Middle Tabs UP WELD-RESTRAINED COMPRESSION ZONE

FOR EACH SPRING ELEMENT THE FORCES AND MOMENTS FOR EACH NODE
ARE GIVEN. THE FORCES AND MOMENTS ARE GIVEN IN THE AXIS SET WHICH
WAS USED TO DEFINE THE SPRING ORIENTATION

F-X - FORCE IN THE SPRING X-DIRECTION
F-Y - FORCE IN THE SPRING Y-DIRECTION
F-Z - FORCE IN THE SPRING Z-DIRECTION

M-X - MOMENT ABOUT THE SPRING X-AXIS
M-Y - MOMENT ABOUT THE SPRING Y-AXIS
M-Z - MOMENT ABOUT THE SPRING Z-AXIS

NOTE- THE MOMENTS ARE GIVEN ACCORDING TO THE RIGHT HAND SCREW CONVENTION.

ELEMENT NUMBER	SPRING NUMBER	AXIS SET	LOAD CASE	NODE NUMBER	FORCES(N) AND MOMENTS(N.m) F-X	F-Y	F-Z	M-X	M-Y	M-Z
1	1	1	1	30	0.506E+04	0.	0.	0.	0.	0.
2	2	1	1	86	0.	-0.384E+04	0.	0.	0.	0.
3	1	1	1	38	0.200E+04	0.	0.	0.	0.	0.
4	2	1	1	90	0.	-0.370E+04	0.	0.	0.	0.
5	1	1	1	45	-561.	0.	0.	0.	0.	0.
6	2	1	1	92	0.	-0.246E+04	0.	0.	0.	0.

TABLE 6.2

Forces Applied To 30100 Spring Elements At Top, Bottom And Middle Tabs DOWN WELD-RESTRAINED COMPRESSION ZONE

FOR EACH SPRING ELEMENT THE FORCES AND MOMENTS FOR EACH NODE
ARE GIVEN. THE FORCES AND MOMENTS ARE GIVEN IN THE AXIS SET WHICH
WAS USED TO DEFINE THE SPRING ORIENTATION

F-X - FORCE IN THE SPRING X-DIRECTION
F-Y - FORCE IN THE SPRING Y-DIRECTION
F-Z - FORCE IN THE SPRING Z-DIRECTION

M-X - MOMENT ABOUT THE SPRING X-AXIS
M-Y - MOMENT ABOUT THE SPRING Y-AXIS
M-Z - MOMENT ABOUT THE SPRING Z-AXIS

NOTE- THE MOMENTS ARE GIVEN ACCORDING TO THE RIGHT HAND SCREW CONVENTION.

ELEMENT NUMBER	SPRING NUMBER	AXIS SET	LOAD CASE	NODE NUMBER	FORCES(N) AND MOMENTS(N.m) F-X	F-Y	F-Z	M-X	M-Y	M-Z
1	1	1	1	30	0.834E+04	0.	0.	0.	0.	0.
2	2	1	1	86	0.	-0.335E+04	0.	0.	0.	0.
3	1	1	1	38	0.479E+04	0.	0.	0.	0.	0.
4	2	1	1	90	0.	-0.392E+04	0.	0.	0.	0.
5	1	1	1	45	669.	0.	0.	0.	0.	0.
6	2	1	1	92	0.	-0.273E+04	0.	0.	0.	0.

TABLE 6.3

Forces Applied To 30100 Spring Elements At Top, Bottom And Middle Tabs SYMMETRICAL-RESTRAINED COMPRESSION ZONE-Released tension nodes.

FOR EACH SPRING ELEMENT THE FORCES AND MOMENTS FOR EACH NODE
ARE GIVEN. THE FORCES AND MOMENTS ARE GIVEN IN THE AXIS SET WHICH
WAS USED TO DEFINE THE SPRING ORIENTATION

F-X - FORCE IN THE SPRING X-DIRECTION
F-Y - FORCE IN THE SPRING Y-DIRECTION
F-Z - FORCE IN THE SPRING Z-DIRECTION

M-X - MOMENT ABOUT THE SPRING X-AXIS
M-Y - MOMENT ABOUT THE SPRING Y-AXIS
M-Z - MOMENT ABOUT THE SPRING Z-AXIS

NOTE- THE MOMENTS ARE GIVEN ACCORDING TO THE RIGHT HAND SCREW CONVENTION.

ELEMENT NUMBER	SPRING NUMBER	AXIS SET	LOAD CASE	NODE NUMBER	FORCES(N) AND MOMENTS(N.m) F-X	F-Y	F-Z	M-X	M-Y	M-Z
1	1	1	1	30	0.101E+05	0.000E+00	0.000E+00	0.000E+00	0.000E+00	0.000E+00
2	2	1	1	86	0.000E+00	-0.378E+04	0.000E+00	0.000E+00	0.000E+00	0.000E+00
3	1	1	1	38	0.513E+04	0.000E+00	0.000E+00	0.000E+00	0.000E+00	0.000E+00
4	2	1	1	90	0.000E+00	-0.399E+04	0.000E+00	0.000E+00	0.000E+00	0.000E+00
5	1	1	1	45	-276.	0.000E+00	0.000E+00	0.000E+00	0.000E+00	0.000E+00
6	2	1	1	92	0.000E+00	-0.223E+04	0.000E+00	0.000E+00	0.000E+00	0.000E+00

TABLE 6.4

Forces Applied To 30100 Spring Elements At Top, Bottom And Middle Tabs UP WELD-RESTRAINED COMPRESSION ZONE-Released tension nodes.

FOR EACH SPRING ELEMENT THE FORCES AND MOMENTS FOR EACH NODE
ARE GIVEN. THE FORCES AND MOMENTS ARE GIVEN IN THE AXIS SET WHICH
WAS USED TO DEFINE THE SPRING ORIENTATION

F-X - FORCE IN THE SPRING X-DIRECTION
F-Y - FORCE IN THE SPRING Y-DIRECTION
F-Z - FORCE IN THE SPRING Z-DIRECTION

M-X - MOMENT ABOUT THE SPRING X-AXIS
M-Y - MOMENT ABOUT THE SPRING Y-AXIS
M-Z - MOMENT ABOUT THE SPRING Z-AXIS

NOTE- THE MOMENTS ARE GIVEN ACCORDING TO THE RIGHT HAND SCREW CONVENTION.

ELEMENT NUMBER	SPRING NUMBER	AXIS SET	LOAD CASE	NODE NUMBER	FORCES(N) AND MOMENTS(N.m) F-X	F-Y	F-Z	M-X	M-Y	M-Z
1	1	1	1	30	0.112E+05	0.	0.	0.	0.	0.
2	2	1	1	86	0.	-0.411E+04	0.	0.	0.	0.
3	1	1	1	38	0.505E+04	0.	0.	0.	0.	0.
4	2	1	1	90	0.	-0.385E+04	0.	0.	0.	0.
5	1	1	1	45	-424.	0.	0.	0.	0.	0.
6	2	1	1	92	0.	-0.204E+04	0.	0.	0.	0.

Table 6.5

Comparison between rotation and stiffness values obtained from the model simulating symmetrical welding arrangement before and after releasing the nodes that generated tension forces in the restrained compression zone

CASE N°	CASE, Spring Elements Arrangement At The Tabs	θ_v (radian)	θ_{ta} (radian)	θ_{tr} (radian)	θ_{ba} (radian)	θ_{br} (radian)	k_v (kNm/rad)	k_{ta} (kNm/rad)	k_{tr} (kNm/rad)	k_{ba} (kNm/rad)	k_{br} (kNm/rad)
GM6C Before releasing the nodes that generated tension forces in the compression zone	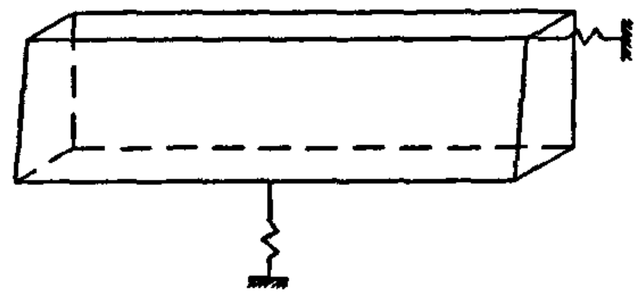	13496E-7	15898E-7	17934E-7	15834E-7	17664E-7	1492	1267	1123	1272	1140
GM6C After releasing the nodes that generated tension forces in the compression zone	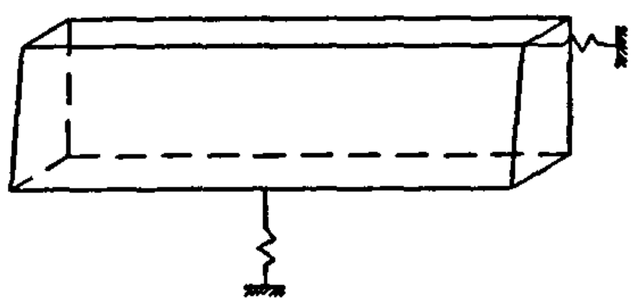	2.011E-3	2.260E-3	2.469E-3	2.253E-3	2.445E-3	1002	891	816	894	824

Table 6.6

Comparison between rotation and stiffness values obtained from the model simulating up welded arrangement before and after releasing the nodes that generated tension forces in the restrained compression zone

CASE N°	CASE, Spring Elements Arrangement At The Tabs	θ_v (radian)	θ_{ta} (radian)	θ_{tr} (radian)	θ_{ba} (radian)	θ_{br} (radian)	k_v (kNm/rad)	k_{ta} (kNm/rad)	k_{tr} (kNm/rad)	k_{ba} (kNm/rad)	k_{br} (kNm/rad)
GM6C-UP Before releasing the nodes that generated tension forces in the compression zone	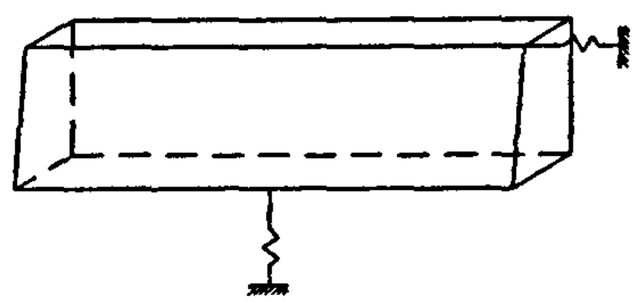	1.559E-3	1.743E-3	1.976E-3	1.811E-3	1.952E-3	1292	1155	1019	1112	1032
GM6C-UP After releasing the nodes that generated tension forces in the compression zone	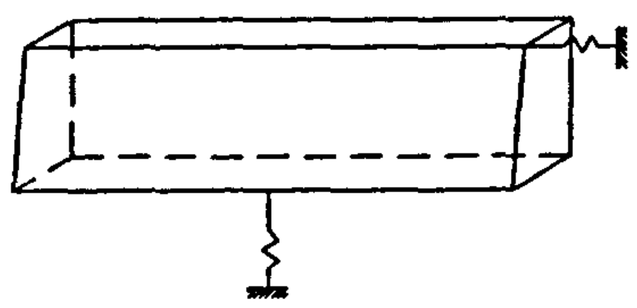	2.340E-3	2.528E-3	2.774E-3	2.608E-3	2.748E-3	861	797	726	772	733

Table 6.7

Rotation and stiffness values obtained from the model simulating down welded arrangement-Restrained compression zone

CASE N°	CASE, Spring Elements Arrangement At The Tabs	θ_v (radian)	θ_{ta} (radian)	θ_{tr} (radian)	θ_{ba} (radian)	θ_{br} (radian)	k_v (kNm/rad)	k_{ta} (kNm/rad)	k_{tr} (kNm/rad)	k_{ba} (kNm/rad)	k_{br} (kNm/rad)
GM6C-DN	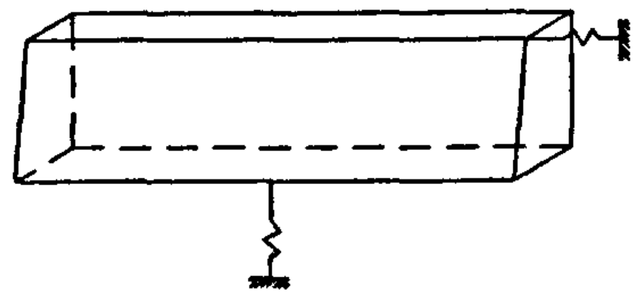	1.690E-3	1.968E-3	2.145E-3	1.907E-3	2.118E-3	1192	1023	939	1056	951
No tension forces in the compression zone were generated											

Table 6.8

Comparison between rotation and stiffness values obtained from the models simulating the three welding arrangements with restrained compression zones having released the nodes that generated tension forces

CASE N°	CASE, Spring Elements Arrangement At The Tabs	θ_v (radian)	θ_{ta} (radian)	θ_{tr} (radian)	θ_{ba} (radian)	θ_{br} (radian)	k_v (kNm/rad)	k_{ta} (kNm/rad)	k_{tr} (kNm/rad)	k_{ba} (kNm/rad)	k_{br} (kNm/rad)
SYMMETRICAL GM6C After releasing the nodes that generated tension forces in the compression zone	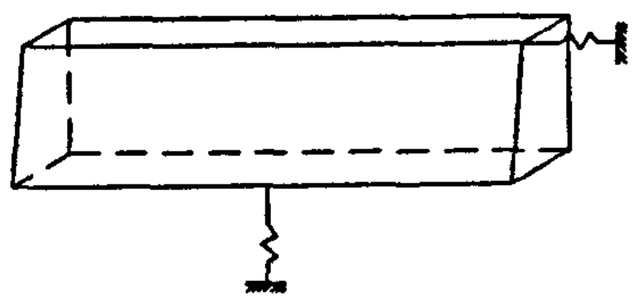	2.011E-3	2.260E-3	2.469E-3	2.253E-3	2.445E-3	1002	891	816	894	824
UP WELDED GM6C-UP After releasing the nodes that generated tension forces in the compression zone	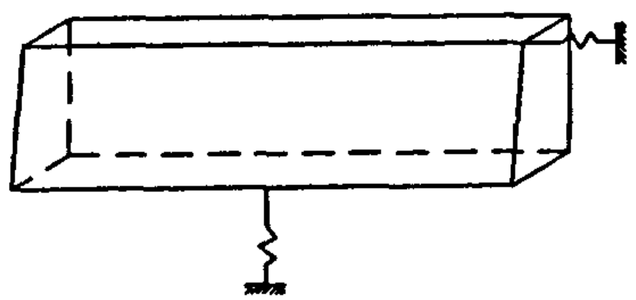	2.340E-3	2.528E-3	2.774E-3	2.608E-3	2.748E-3	861	797	726	772	733
DOWN WELDED GM6C-DN No tension forces were generated	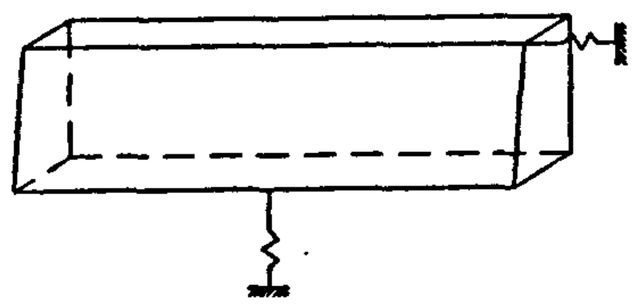	1.690E-3	1.968E-3	2.145E-3	1.907E-3	2.118E-3	1192	1023	939	1056	951

TABLE 6.9

Forces Applied To 30100 Spring Elements At Top, Bottom And Middle Tabs UP WELD-FREE COMPRESSION ZONE

FOR EACH SPRING ELEMENT THE FORCES AND MOMENTS FOR EACH NODE
ARE GIVEN. THE FORCES AND MOMENTS ARE GIVEN IN THE AXIS SET WHICH
WAS USED TO DEFINE THE SPRING ORIENTATION

F-X - FORCE IN THE SPRING X-DIRECTION
F-Y - FORCE IN THE SPRING Y-DIRECTION
F-Z - FORCE IN THE SPRING Z-DIRECTION

M-X - MOMENT ABOUT THE SPRING X-AXIS
M-Y - MOMENT ABOUT THE SPRING Y-AXIS
M-Z - MOMENT ABOUT THE SPRING Z-AXIS

NOTE- THE MOMENTS ARE GIVEN ACCORDING TO THE RIGHT HAND SCREW CONVENTION.

ELEMENT NUMBER	SPRING NUMBER	AXIS SET	LOAD CASE	NODE NUMBER	FORCES(N) AND MOMENTS(N.m) F-X	F-Y	F-Z	M-X	M-Y	M-Z
1	1	1	1	30	0.137E+05	0.	0.	0.	0.	0.
2	2	1	1	86	0.	-0.469E+04	0.	0.	0.	0.
3	1	1	1	38	-822	0.	0.	0.	0.	0.
4	2	1	1	90	0.	-0.406E+04	0.	0.	0.	0.
5	1	1	1	45	-0.129E+05	0.	0.	0.	0.	0.
6	2	1	1	92	0.	-0.125E+04	0.	0.	0.	0.

TABLE 6.10

Forces Applied To 30100 Spring Elements At Top, Bottom And Middle Tabs DOWN WELD-FREE COMPRESSION ZONE

FOR EACH SPRING ELEMENT THE FORCES AND MOMENTS FOR EACH NODE
ARE GIVEN. THE FORCES AND MOMENTS ARE GIVEN IN THE AXIS SET WHICH
WAS USED TO DEFINE THE SPRING ORIENTATION

F-X - FORCE IN THE SPRING X-DIRECTION
F-Y - FORCE IN THE SPRING Y-DIRECTION
F-Z - FORCE IN THE SPRING Z-DIRECTION

M-X - MOMENT ABOUT THE SPRING X-AXIS
M-Y - MOMENT ABOUT THE SPRING Y-AXIS
M-Z - MOMENT ABOUT THE SPRING Z-AXIS

NOTE- THE MOMENTS ARE GIVEN ACCORDING TO THE RIGHT HAND SCREW CONVENTION.

ELEMENT NUMBER	SPRING NUMBER	AXIS SET	LOAD CASE	NODE NUMBER	FORCES(N) AND MOMENTS(N.m) F-X	F-Y	F-Z	M-X	M-Y	M-Z
1	1	1	1	30	0.134E+05	0.	0.	0.	0.	0.
2	2	1	1	86	0.	-0.426E+04	0.	0.	0.	0.
3	1	1	1	38	-156	0.	0.	0.	0.	0.
4	2	1	1	90	0.	-0.429E+04	0.	0.	0.	0.
5	1	1	1	45	-0.132E+05	0.	0.	0.	0.	0.
6	2	1	1	92	0.	-0.145E+04	0.	0.	0.	0.

Table 6.11

Comparison between rotation and stiffness values obtained from the models simulating the three welding arrangements with free compression zones

CASE N°	CASE, Spring Elements Arrangement At The Tabs	θ_v (radian)	θ_{ta} (radian)	θ_{tr} (radian)	θ_{ba} (radian)	θ_{br} (radian)	k_v (kNm/rad)	k_{ta} (kNm/rad)	k_{tr} (kNm/rad)	k_{ba} (kNm/rad)	k_{br} (kNm/rad)
SYMMETRICAL GM6D	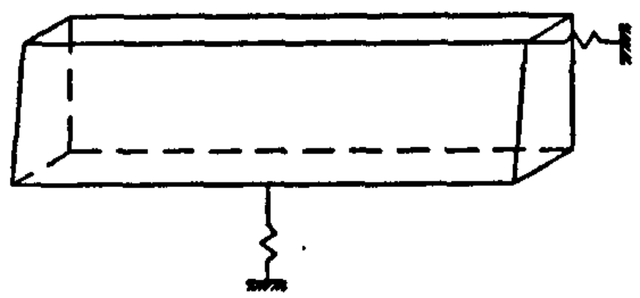	42699E-7	45234E-7	47212E-7	44968E-7	46958E-7	471	445	426	448	429
UP WELDED GM6D-UP	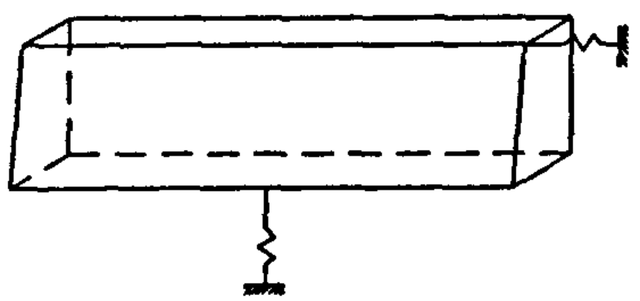	4.425E-3	4.620E-3	4.862E-3	4.684E-3	4.836E-3	455	436	414	430	416
DOWN WELDED GM6D-DN	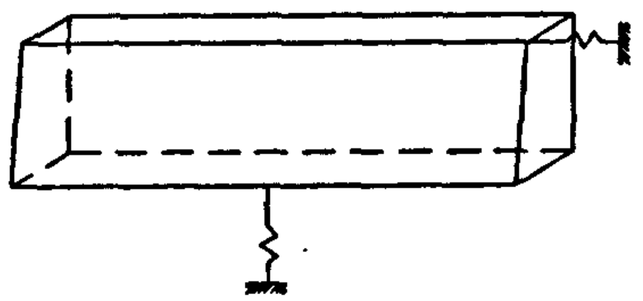	4.745E-3	5.032E-3	5.172E-3	4.918E-3	5.144E-3	424	400	389	410	392

Figure 6.1 Undeformed structure-Up welded, springs at tabs, restrained compression zone

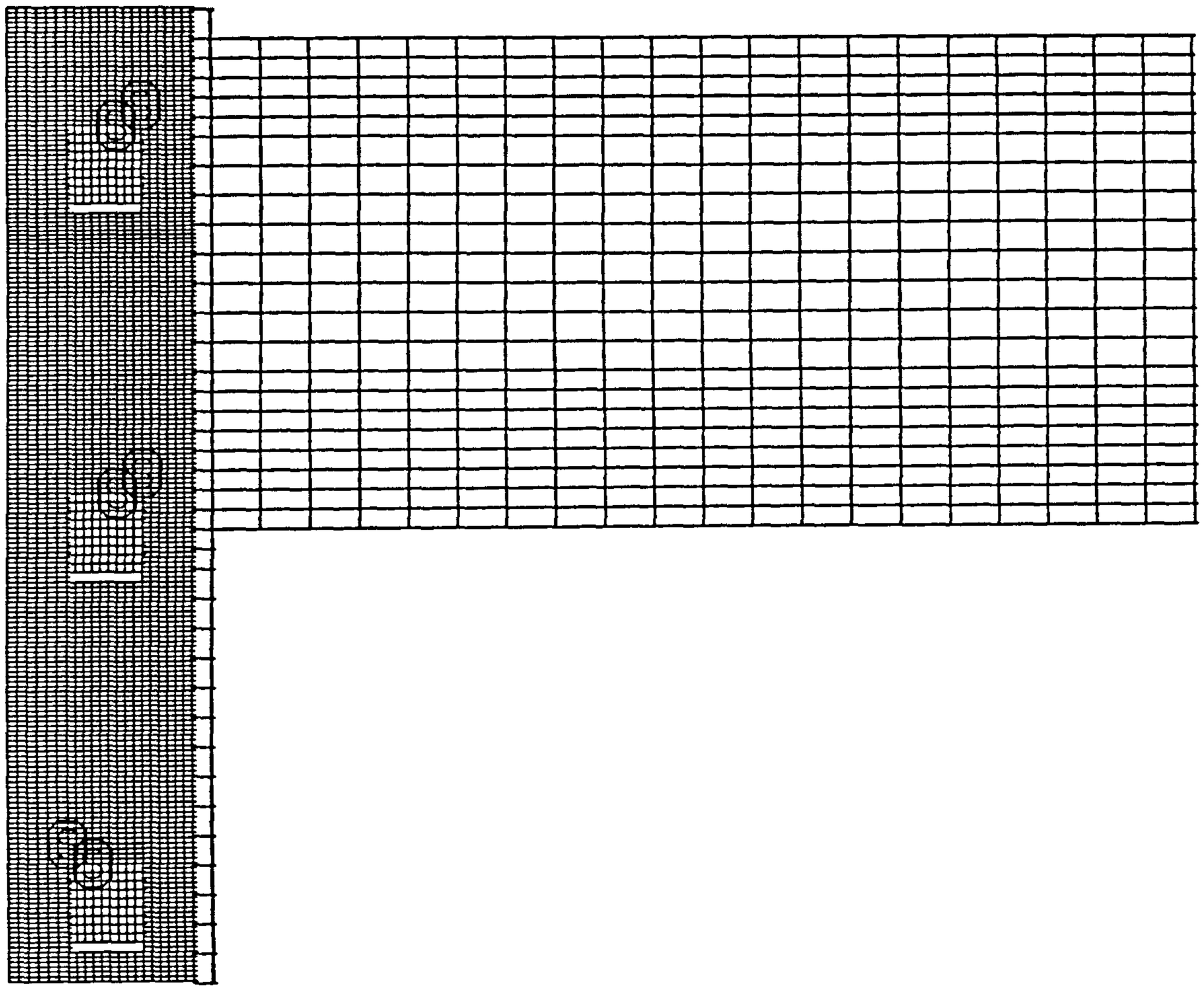

LINEAR
STATICS

ROTATION
X = 0
Y = 0
Z = 0

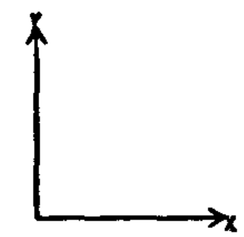

Figure 6.2 Undeformed structure-Up welded, springs at tabs, restrained compression zone

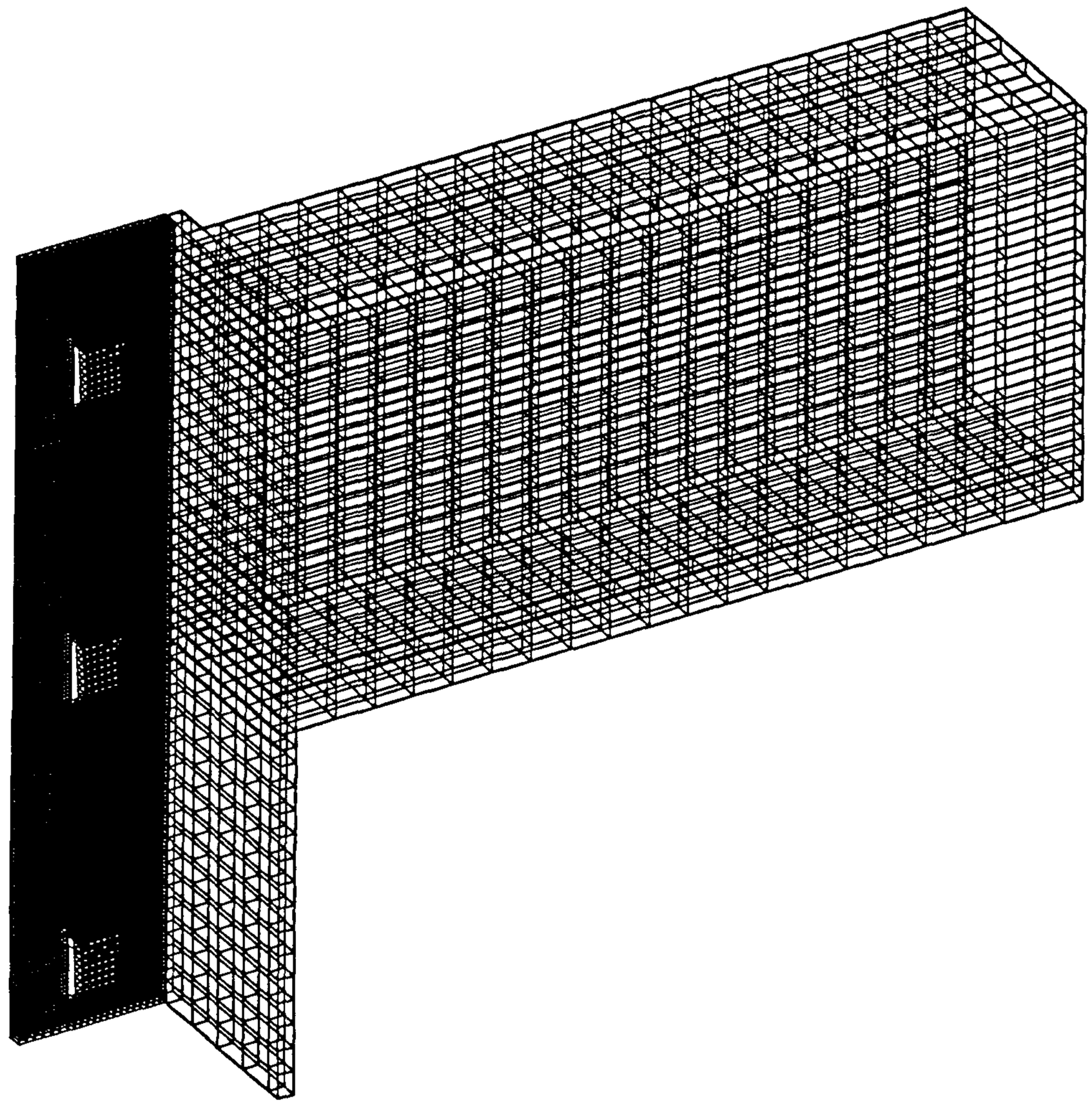

LINEAR

STATICS

ROTATION

X = 34

Y = 26

Z = 16

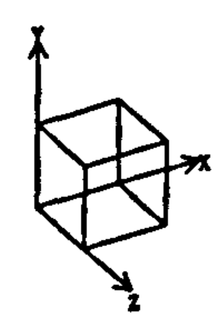

Figure 6.3 Deformed structure-Up welded, springs at tabs, restrained compression zone

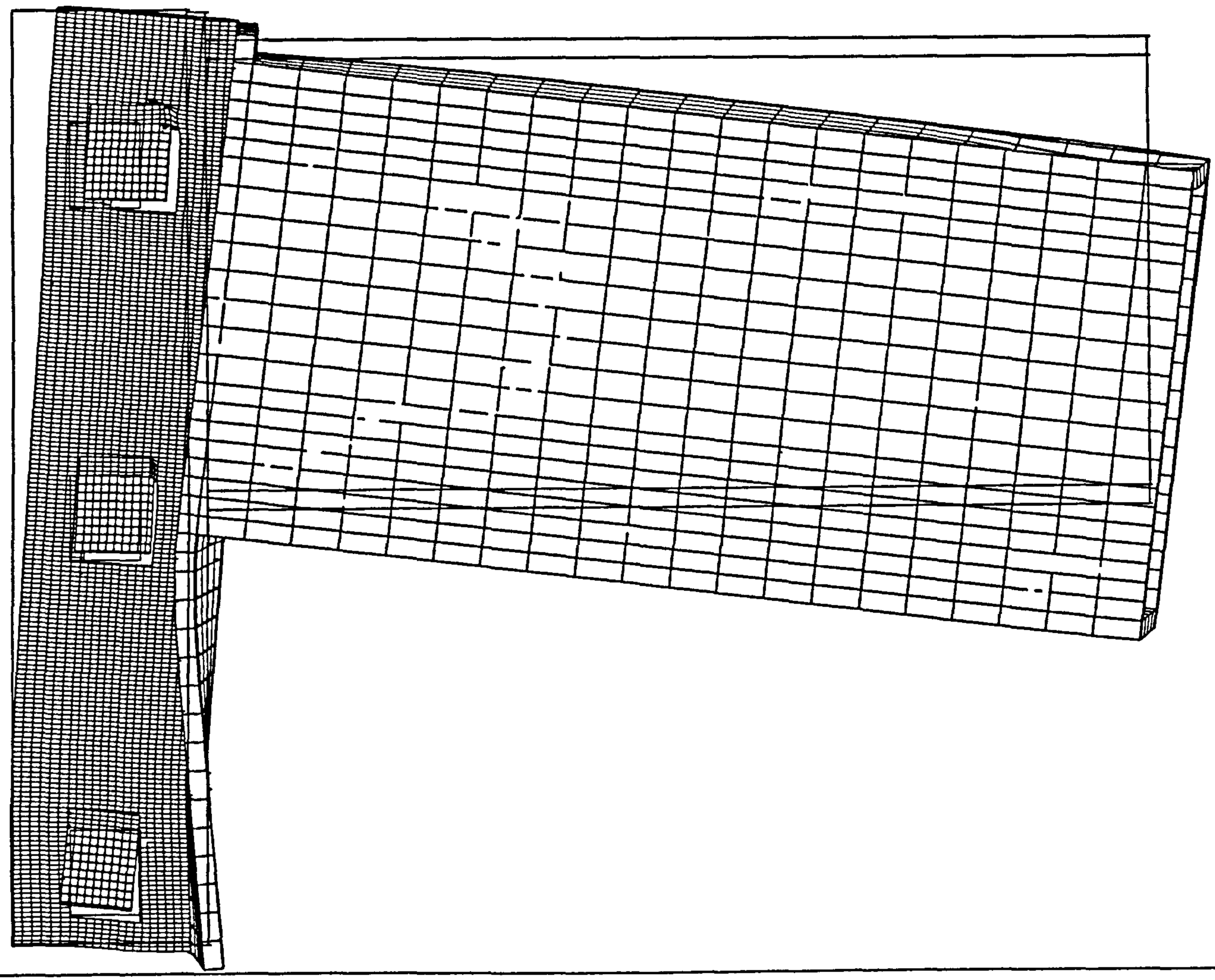

LINEAR

STATICS

ROTATION

X = 0

Y = 0

Z = 0

Figure 6.4 Undeformed structure-Down welded, springs at tabs, restrained compression zone

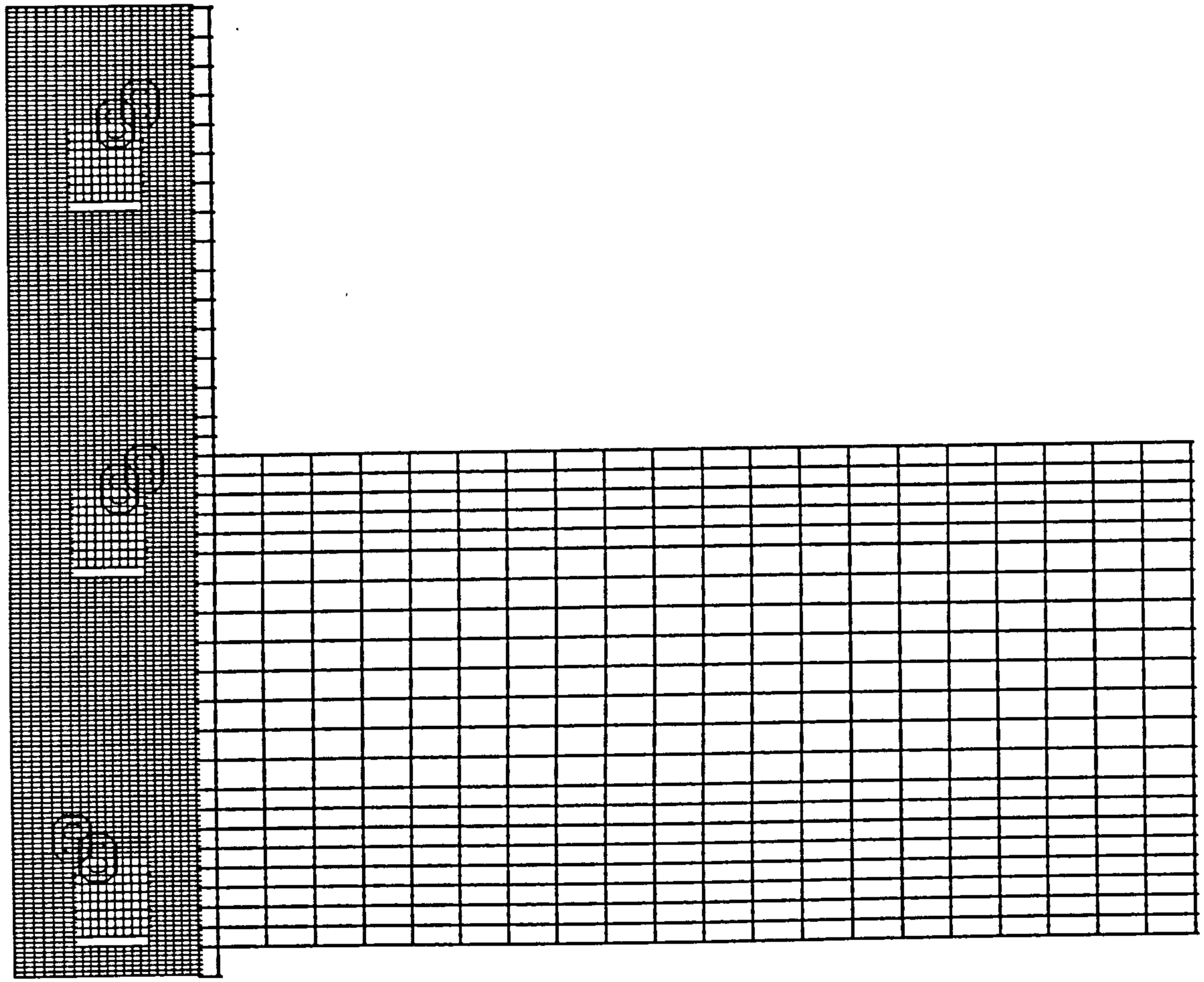

LINEAR

STATICS

ROTATION

X = 0

Y = 0

Z = 0

Figure 6.5 Undeformed structure-Down welded, springs at tabs, restrained compression zone

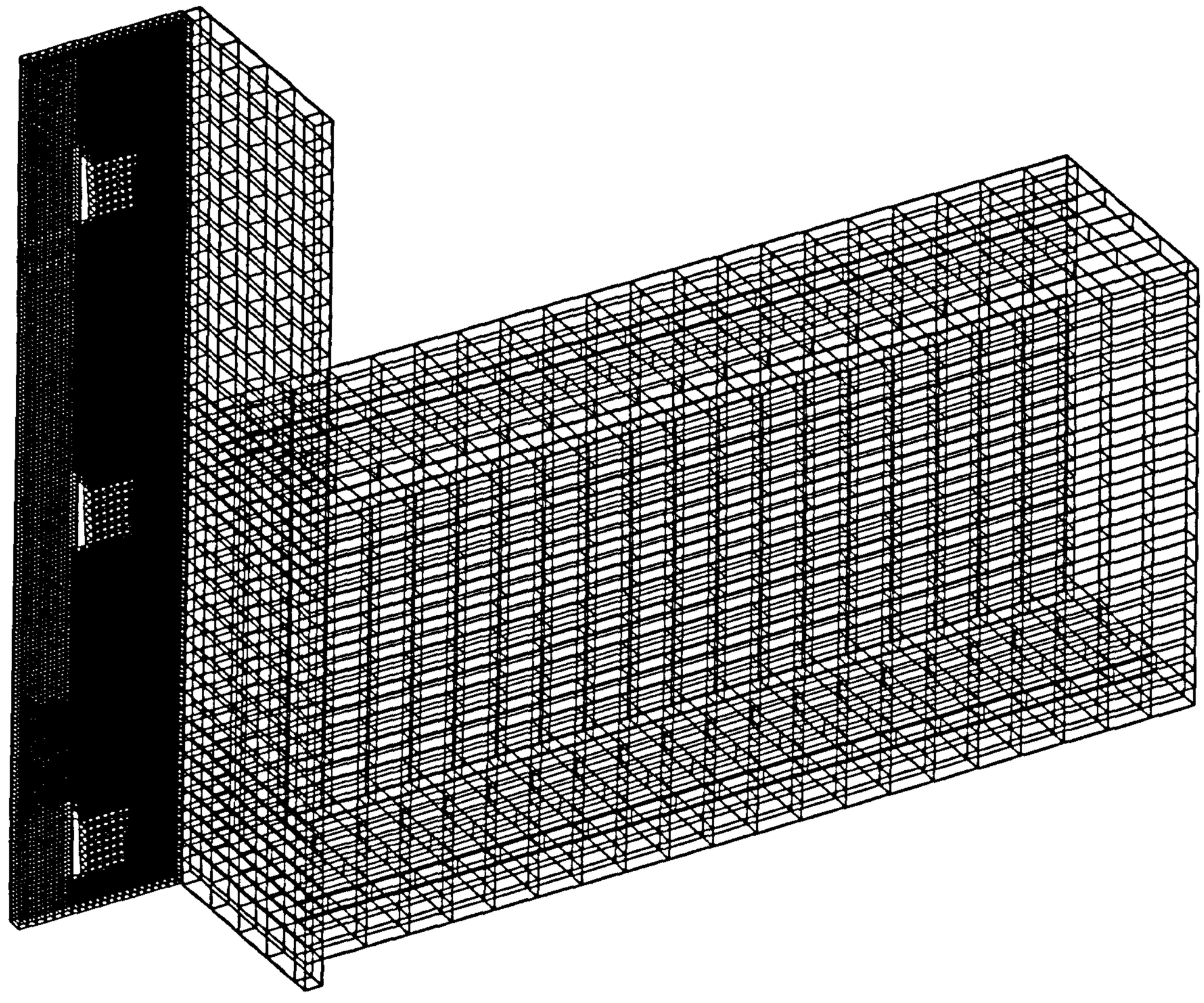

LINEAR

STATICS

ROTATION

X = 34

Y = 26

Z = 16

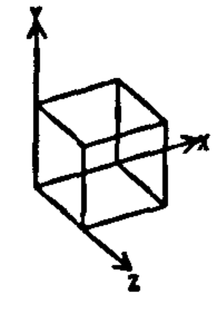

Figure 6.6 Deformed structure-Down welded, springs at tabs, restrained compression zone

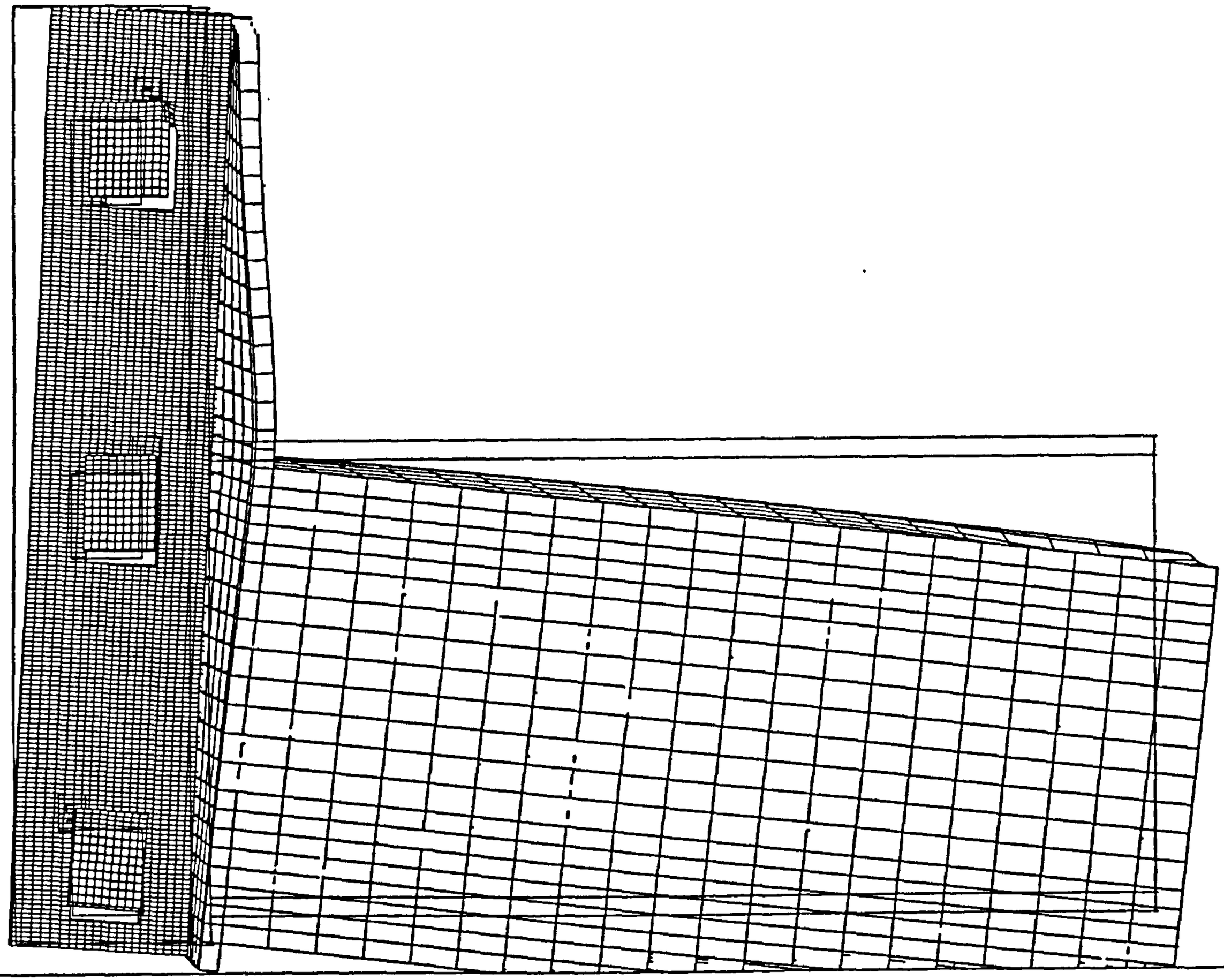

LINEAR

STATICS

ROTATION

X = 0

Y = 0

Z = 0

Figure 6.7 Restrained nodes in the compression zone-symmetrical

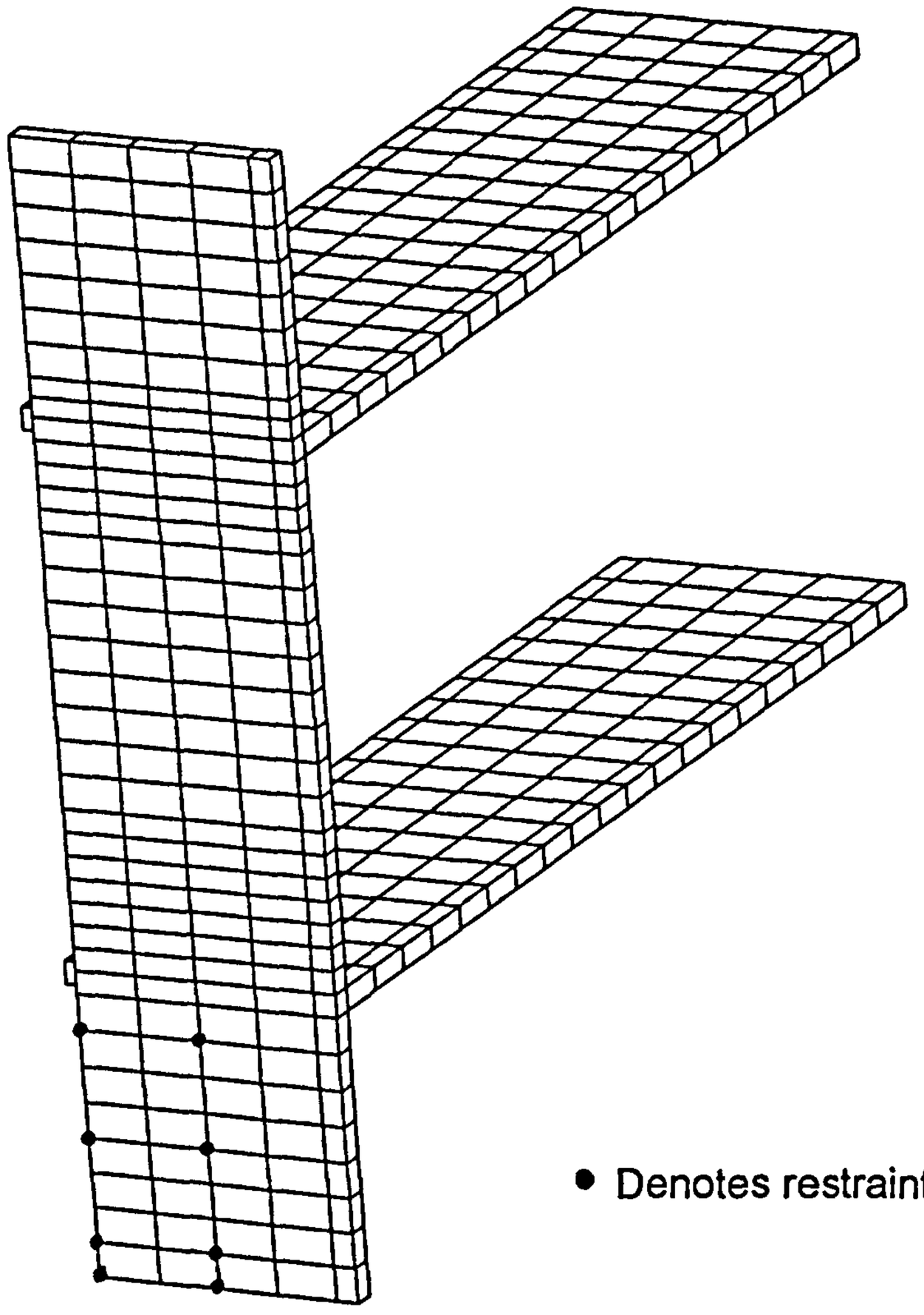

• Denotes restraint at node

LINEAR

STATICS

ROTATION

X = 36

Y = 56

Z = 36

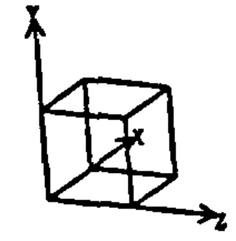

Figure 6.8 Restrained nodes in the compression zone-up welded

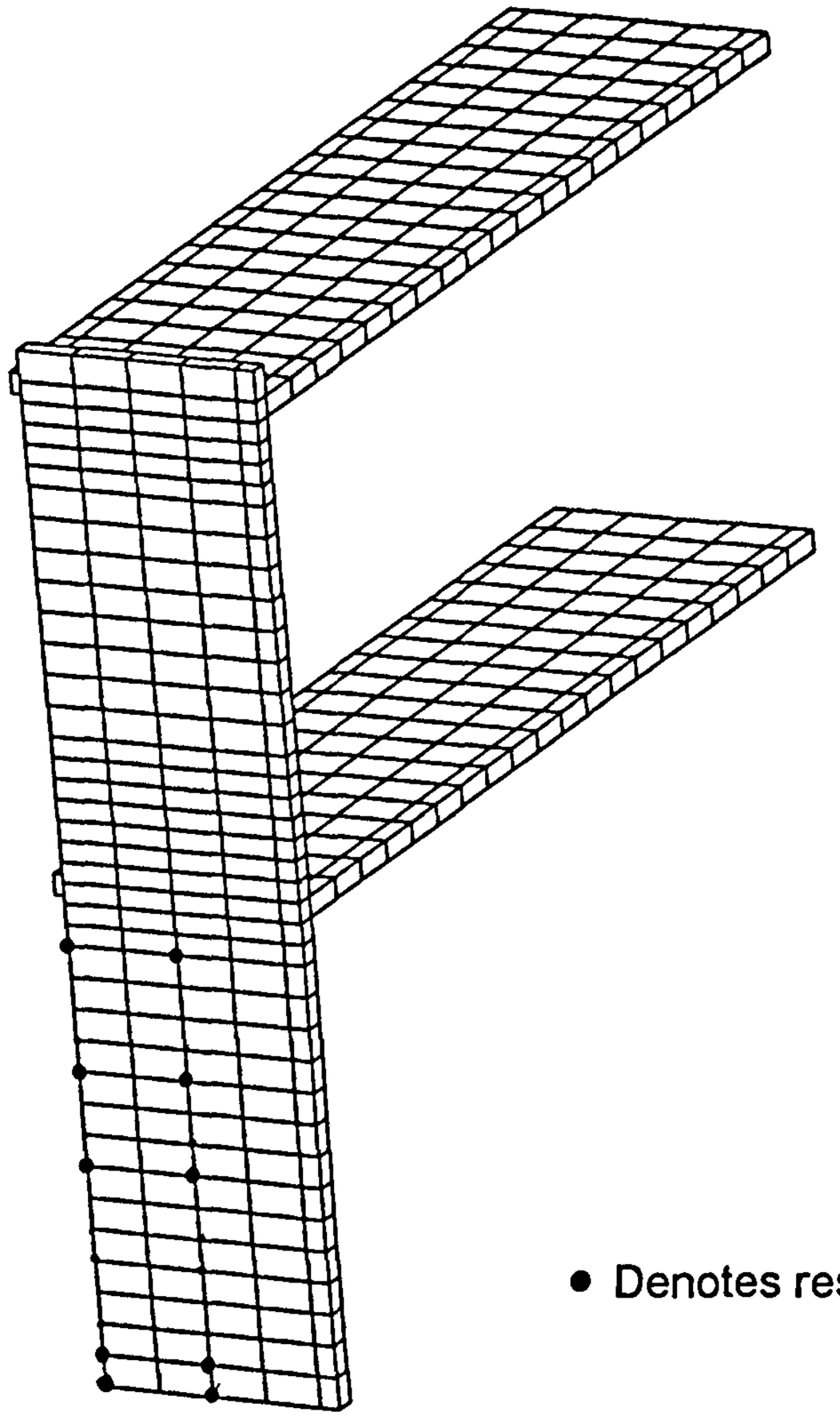

• Denotes restraint at node

LINEAR

STATICS

ROTATION

X = 36

Y = 56

Z = 36

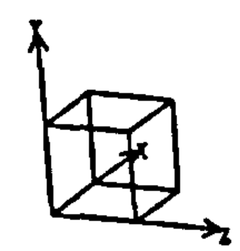

Figure 6.9 Restrained nodes in the compression zone-down welded

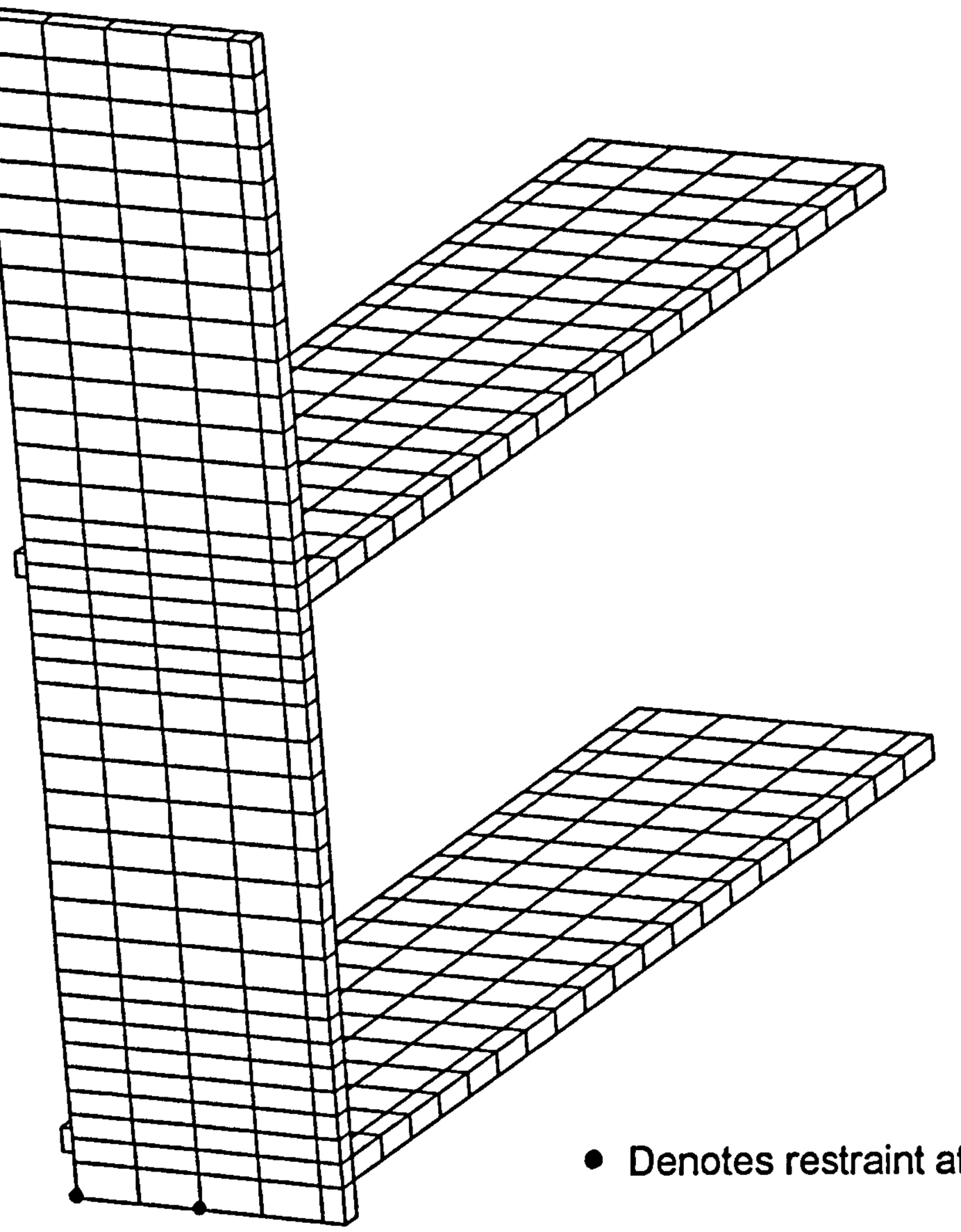

Free Body Diagram
Symmetrical Welding Position

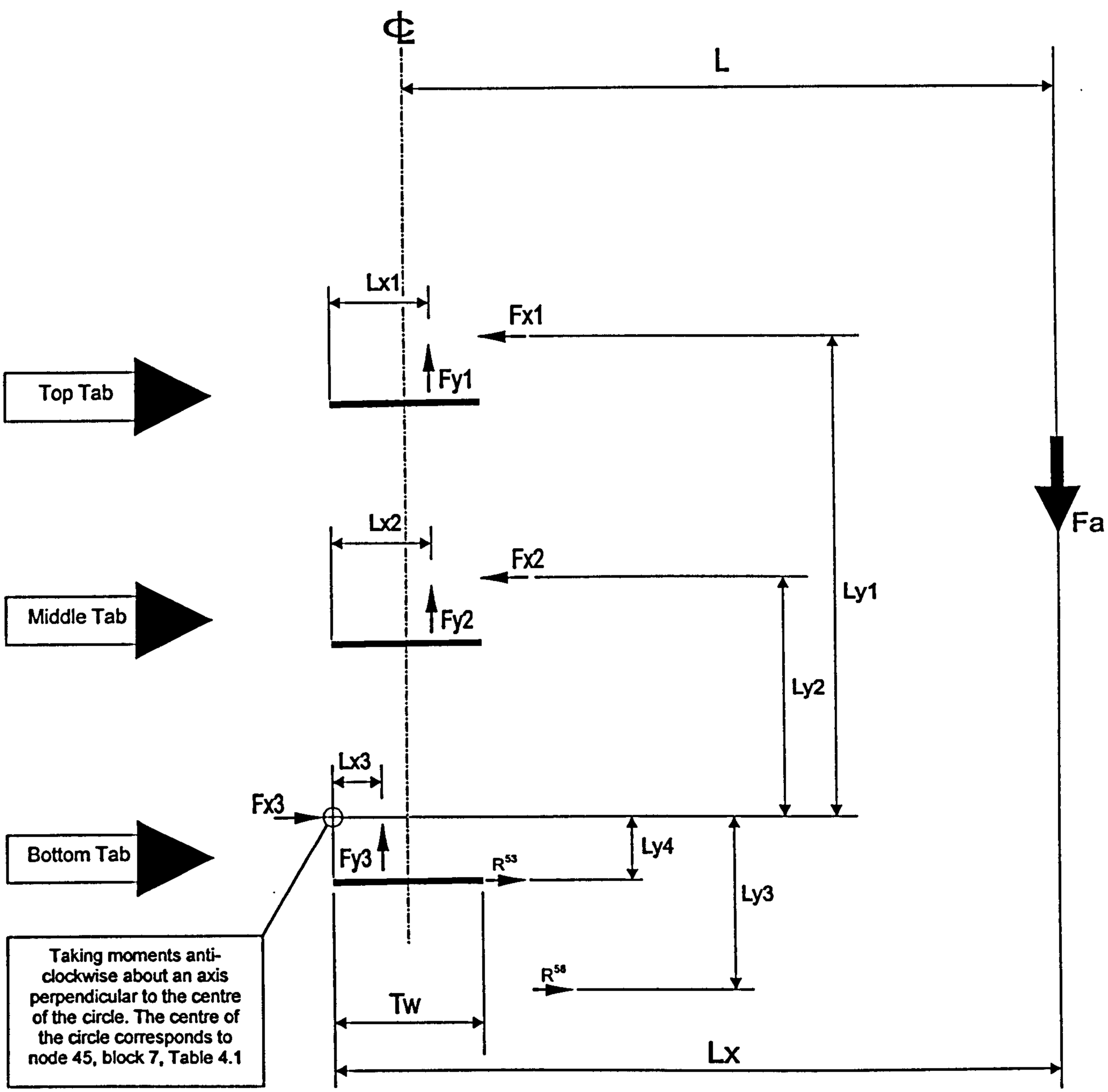

FIGURE 6.10

Free Body Diagram
Up Welded Position

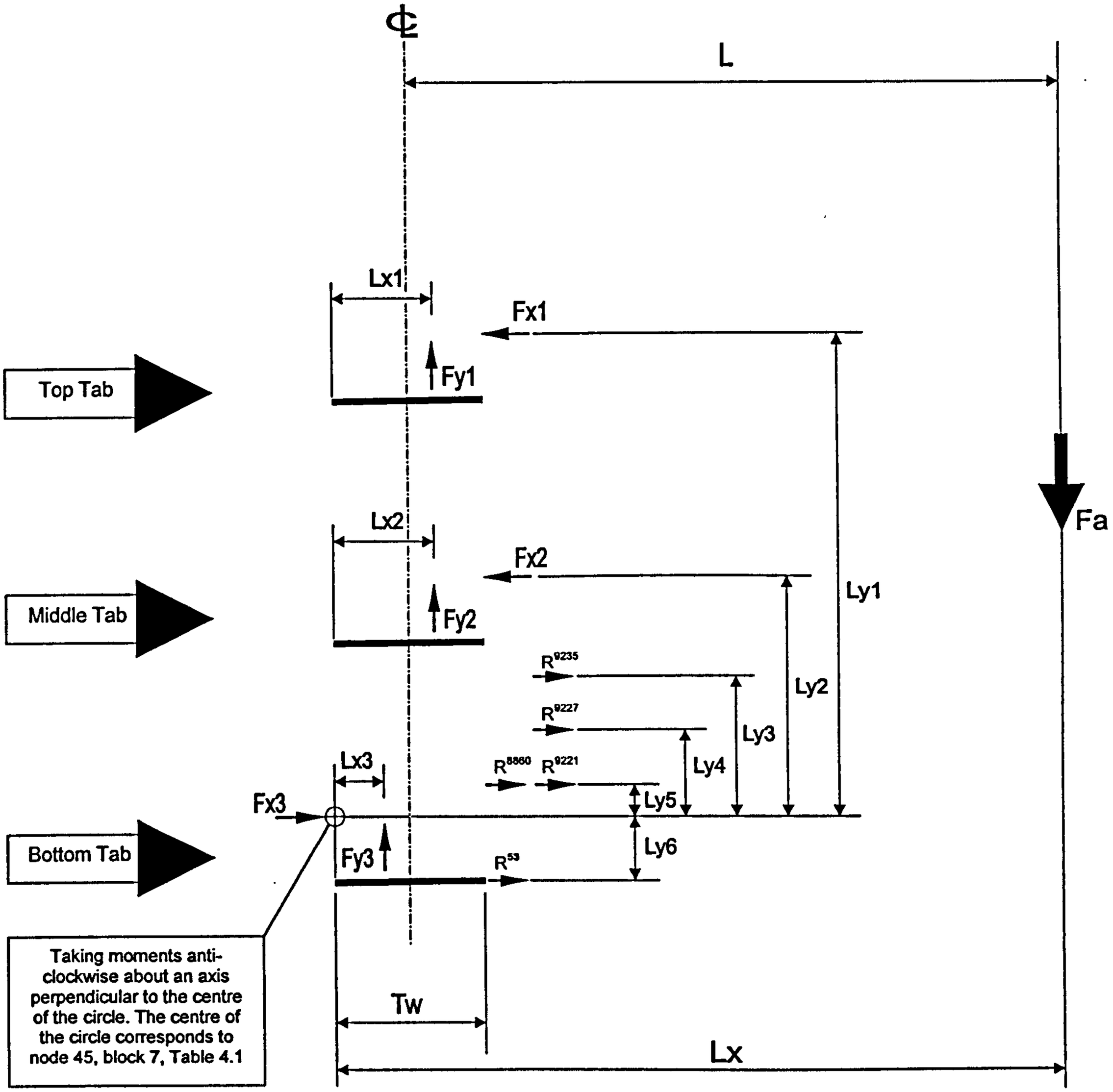

FIGURE 6.11

Free Body Diagram
Down Welded Position

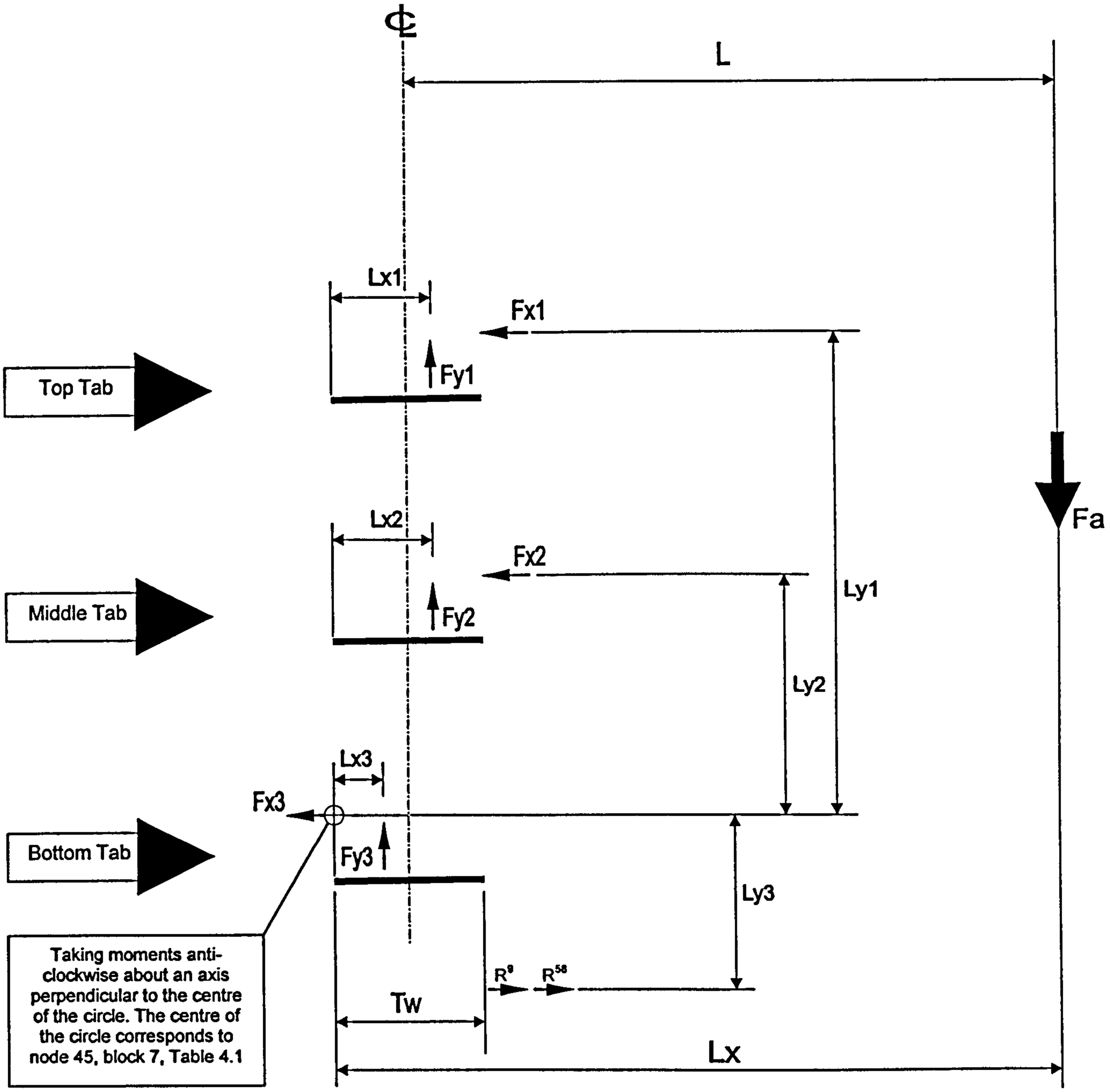

FIGURE 6.12

APPENDIX 6.1

To check for equilibrium, Symmetrical Welding Position & restrained compression zone after releasing nodes that generated tension forces
GM6C

Information obtained from plastic sub models gave the stiffness of the upright's web. The results were used as spring stiffness values in global models as the sources of resistance to rotation. The global models in turn gave the forces applied to the springs in horizontal and vertical directions. The horizontal forces are F_{x1}, F_{x2} and F_{x3}. The vertical forces are F_{y1}, F_{y2} and F_{y3}. These are given in Table 6.3 for the case GM6C.

For equilibrium applied moment versus the horizontal and vertical forces in the springs at the top, middle and the bottom tabs as well as the reactions in the compression zone are considered.

Width of the tab:

$$T_w = 15\,mm$$

Moment arm for vertical force, F_{y1} top tab, the Free Body diagram, figure 6.10:

$$L_{x1} = \left(\frac{T_w}{9} \times 6\right)$$

$$L_{x1} = 0.01\,m$$

Moment arm for vertical force, F_{y2} middle tab, the Free Body diagram, figure 6.10:

$$L_{x2} = L_{x1}$$

Moment arm for vertical force, F_{y3} bottom tab, the Free Body diagram, figure 6.10:

$$L_{x3} = \left(\frac{T_w}{9} \times 3\right)$$

$$L_{x3} = 0.005\, m$$

Beam end connector moment arm, figure 6.10:

$$L_x = 209\, mm$$

Applied load to the beam end connector:

$$f_a = 10000\, N$$

Applied bending moment:

$$M_a = f_a L_x$$

$$M_a = 2.09\, kNm$$

Moment arms for the horizontal forces F_{x1} and F_{x2} are $L_{y1} = 150\, mm$ and $L_{y2} = 75\, mm$.

Forces applied to the horizontal spring element-Horizontal forces-Table 6.3:

Top tab: $F_{x1} = 10100\, N$

Middle tab: $F_{x2} = 5130\, N$

Bottom tab: $F_{x3} = -276\, N$

Forces applied to the vertical spring elements-vertical forces-table 6.3:

Top tab: $F_{y1} = 3780\, N$

Middle tab: $F_{y2} = 3990\,N$

Bottom tab: $F_{y3} = 2230\,N$

$$M_{r1} = F_{x1}L_{y1} + F_{x2}L_{y2}$$

$$M_{r2} = F_{y1}L_{x1} + F_{y2}L_{x2} + F_{y3}L_{x3}$$

Lever arms for reaction forces in the compression zone:

$$L_{y3} = 28.5\,mm$$

$$L_{y4} = 4.5\,mm$$

Reaction forces in the compression zone: $R_{53} = 13875\,N$ and $R_{58} = 1125\,N$.

Moment expression for the reaction forces:

$$M_{r3} = R_{53}L_{y4} + R_{58}L_{y3}$$

$$M_{r1} + M_{r2} + M_{r3} = 2.08\,kNm$$

$$M_a = 2.09\,kNm$$

Moment of resistance equates to the applied moment.

Therefore we have equilibrium.

APPENDIX 6.2

To check for equilibrium, Up Welded Position & Restrained compression zone after releasing nodes that generated tension forces
GM6C-UP

Information obtained from plastic sub models gave the stiffness of the upright's web. The results were used as spring stiffness values in global models as the sources of resistance to rotation. The global models in turn gave the forces applied to the springs in horizontal and vertical directions. The horizontal forces are F_{x1}, F_{x2} and F_{x3}. The vertical forces are F_{y1}, F_{y2} and F_{y3}. These are given in Table 6.4 for the case GM6C-UP.

For equilibrium applied moment versus the horizontal and vertical forces in the springs at the top, middle and the bottom tabs as well as the reactions in the compression zone are considered.

Width of the tab:

$$T_w = 15\,mm$$

Moment arm for vertical force, F_{y1} top tab, the Free Body diagram, figure 6.11:

$$L_{x1} = \left(\frac{T_w}{9} \times 6\right)$$

$$L_{x1} = 0.01\,m$$

Moment arm for vertical force, F_{y2} middle tab, the Free Body diagram, figure 6.11:

$$L_{x2} = L_{x1}$$

Moment arm for vertical force, F_{y3} bottom tab, the Free Body diagram, figure 6.11:

$$L_{x3} = \left(\frac{T_w}{9} \times 3\right)$$

$$L_{x3} = 0.005\, m$$

Beam end connector moment arm, figure 6.11:

$$L_x = 209\, mm$$

Applied load to the beam end connector:

$$f_a = 10000\, N$$

Applied bending moment:

$$M_a = f_a L_x$$

$$M_a = 2.09\, kNm$$

Moment arms for the horizontal forces F_{x1} and F_{x2} are $L_{y1} = 150\, mm$ and $L_{y2} = 75\, mm$.

Forces applied to the horizontal spring element-Horizontal forces-Table 6.4:

Top tab: $F_{x1} = 11200\, N$

Middle tab: $F_{x2} = 5050\, N$

Bottom tab: $F_{x3} = -424\, N$

Forces applied to the vertical spring elements-vertical forces-table 6.4:

Top tab: $F_{y1} = 4110\, N$

Middle tab: $F_{y2} = 3850\, N$

Bottom tab: $F_{y3} = 2040\ N$

$$M_{r1} = F_{x1}L_{y1} + F_{x2}L_{y2}$$

$$M_{r2} = F_{y1}L_{x1} + F_{y2}L_{x2} + F_{y3}L_{x3}$$

Lever arms for reaction forces in the compression zone:

$L_{y3} = 55.5\ mm$ $L_{y4} = 31.5\ mm$

$L_{y5} = 13.5\ mm$ $L_{y6} = 4.5\ mm$

Reaction forces in the compression zone:

$R_{53} = 9763.40\ N$ $R_{8860} = 4844.90\ N$

$R_{9221} = 416.81\ N$ $R_{9227} = 679.04\ N$ $R_{9235} = 88.58\ N$

Moment expression for the reaction forces:

$$M_{r3} = R_{53}L_{y6} - R_{8860}L_{y5} - R_{9221}L_{y5} - R_{9227}L_{y4} - R_{9235}L_{y3}$$

$$M_{r1} + M_{r2} + M_{r3} = 2.08\ kNm$$

$$M_a = 2.09\ kNm$$

Moment of resistance equates to the applied moment.

Therefore we have equilibrium.

APPENDIX 6.3

To check for equilibrium, Down Welded Position & restrained compression zone, no tension forces generated GM6C-DN

Information obtained from plastic sub models gave the stiffness of the upright's web. The results were used as spring stiffness values in global models as the sources of resistance to rotation. The global models in turn gave the forces applied to the springs in horizontal and vertical directions. The horizontal forces are F_{x1}, F_{x2} and F_{x3}. The vertical forces are F_{y1}, F_{y2} and F_{y3}. These are given in Table 6.2 for the case GM6C-DN.

For equilibrium applied moment versus the horizontal and vertical forces in the springs at the top, middle and the bottom tabs as well as the reactions in the compression zone are considered.

Width of the tab:

$$T_w = 15\,mm$$

Moment arm for vertical force, F_{y1} top tab, the Free Body diagram, figure 6.12:

$$L_{x1} = \left(\frac{T_w}{9} \times 6\right)$$

$$L_{x1} = 0.01\,m$$

Moment arm for vertical force, F_{y2} middle tab, the Free Body diagram, figure 6.12:

$$L_{x2} = L_{x1}$$

Moment arm for vertical force, F_{y3} bottom tab, the Free Body diagram, figure 6.12:

$$L_{x3} = \left(\frac{T_w}{9} \times 3\right)$$

$$L_{x3} = 0.005\, m$$

Beam end connector moment arm, figure 6.12:

$$L_x = 209\, mm$$

Applied load to the beam end connector:

$$f_a = 10000\, N$$

Applied bending moment:

$$M_a = f_a L_x$$

$$M_a = 2.09\, kNm$$

Moment arms for the horizontal forces F_{x1} and F_{x2} are $L_{y1} = 150\, mm$ and $L_{y2} = 75\, mm$.

Forces applied to the horizontal spring element-Horizontal forces-Table 6.2:

Top tab: $F_{x1} = 8340\, N$

Middle tab: $F_{x2} = 4790\, N$

Bottom tab: $F_{x3} = 669\, N$

Forces applied to the vertical spring elements-vertical forces-table 6.2:

Top tab: $F_{y1} = 3350\, N$

Middle tab: $F_{y2} = 3920\, N$

Bottom tab: $F_{y3} = 2730\,N$

$$M_{r1} = F_{x1}L_{y1} + F_{x2}L_{y2}$$

$$M_{r2} = F_{y1}L_{x1} + F_{y2}L_{x2} + F_{y3}L_{x3}$$

Lever arms for reaction forces in the compression zone:

$$L_{y3} = 28\,mm$$

Reaction forces in the compression zone:

$$R_{58} = 12766\,N$$

$$R_9 = 1035\,N$$

Moment expression for the reaction forces:

$$M_{r3} = R_{58}L_{y3} + R_9L_{y3}$$

$$M_{r1} + M_{r2} + M_{r3} = 2.08\,kNm$$

$$M_a = 2.09\,kNm$$

Moment of resistance equates to the applied moment.

Therefore we have equilibrium.

C H A P T E R 7

ESTIMATING THE ULTIMATE BENDING CARRYING CAPACITY OF THE BEAM END CONNECTOR

C H A P T E R 7

ESTIMATING THE ULTIMATE BENDING CARRYING CAPACITY OF THE BEAM END CONNECTOR

7.1 Introduction

Chapter 5 described how the stiffness of the upright's web was evaluated. It established that this was the initial source of resistance to the rotation of the beam end connector.

This was based on the fact that as the beam end connector was loaded the bearing between the tabs and the upright's web took place first.

This interaction would then result in the failure of the web, as it was weaker than the tabs. Chapter 5 further described that the tabs would remain virtually intact throughout most of the loading sequence. Appreciable plastic deformation in the tabs would only be observed in the final stages of a physical test.

It was also described that cutting of the tabs into the upright's web, as they came into contact with each other would be followed closely with a hinge forming immediately below the stub beam's bottom flange.

Then, as the loading continued a compression zone would form in the lowest part of the end plate as shown figures 4.6 and 4.9.

On further loading, and towards the very end of a physical test, plastic deformation of the tab would commence resulting in some cases in its complete detachment from the rest of the beam end connector.

It was concluded that the following course of events was primarily responsible for the magnitude of the ultimate bending moment of a beam end connector. These are listed below in the order of significance.

- plastic deformation of the upright's web caused by the tabs as they bore onto it.

- formation of the hinge in the end plate below the beam.

- Formation of a compression zone in the end plate below the beam as it came into contact with the side of the upright.

- tensile failure in the free edge of the plate containing the tabs. This occurred more readily with the up welded arrangement.

- failure of the tabs

It was recognized that the above occurrences were collectively responsible for determining the magnitude of the ultimate bending capacity of the beam end connector.

However despite this it was decided to use the capacities of the tabs only, as the basis of a method capable of estimating the bending capacity of the beam end connector.

Initially it was intended that the method would achieve this in isolation from the influence of the upright and in fact the rest of the items listed above.

To do this the load distribution in the tabs after compression zone contact was used in conjunction with the shear strength of the tabs.

In the first instance the strength of the tab was simply estimated based on the product of the shear area and the yield stress of the steel. In a second attempt a sub model through an elasto-platic analysis determined the strength of the tab.

Finally the strength of the upright's web evaluated in chapter 5 was used to estimate the ultimate bending carrying capacity of the beam end connector.

The load distribution in the tabs was obtained for the three welding positions in chapter 6.

7.2 Aims

The aims were

a. to determine the strength of a tab

b. to estimate the ultimate bending carrying capacity of a beam end connector for the symmetrical, up welded and down welded arrangements using the load distributions into the tabs and

1. the strength of the tabs based on the product of the area and yield stress
2. the strength of the tab based on the outcome of sub model

3. the strength of the upright's web obtained in chapter 5

7.3 Failure modes of the tabs and the upright's web

The experimental work showed that the failure mechanism of the upright's web and the connector's tabs was complex. This was because many factors influenced their interrelated behaviour. Amongst these factors were:

- Welding position of the beam relative to the height of the beam end connector-this influenced the way tabs received load.

- Geometry of the beam end connector- this affected the degree to which the connector stiffened the tabs, i.e. whether or not tabs had been formed in the more rigid parts of the beam end connector.

- Geometry of the tabs and geometry of the uprights' slots-these determined the interaction details between the tab and the slots in the upright.

When the beam end connector was being loaded, initially, the tabs were subjected to a shearing action. As loading continued this changed to a torsional action under the combined influence of the force components in the horizontal and vertical directions shown in figure 4.2.

The change in the mode of failure depended on the way load was transmitted into the tabs governed primarily by the welding arrangement of the beam to the beam end connector.

Based on the observations made during the physical tests the horizontal force component shown in figure 4.2 precipitated the plastic failure of the upright's web, but this action was halted temporarily as loading continued.

This was due to the redistribution of load in the beam end connector.

These force components were ultimately responsible for the failure of the tabs themselves.

Depending on a number of design variables the magnitude of the load received by a tab changed continually. This was evident from the damage received by the upright's web at the tabs which changed from tab to tab due to redistribution of the load.

Redistribution of load took place from tab to tab, from tab to the compression zone and so on. This process was governed by the degree of resistance various parts of the beam end connector received from the upright. For example when the top tab tore the upright web, it came in contact with the upright's flange and encountered greater resistance. Consequently load was transferred to the neighboring tab where a lesser load was required to tear the upright's web. This process was repeated until excessive damage was done to the upright's slots and the surrounding area. This was associated with a drop in the applied load signalling a significant loss of joint stiffness.

Failure of the tabs took place after the maximum load had been reached. As described the maximum load was associated with excessive distortion of the upright's slots. As the slots became distorted they increased in size allowing free rotation of the beam end connector until the tabs locked against the upright's flange. This then led to the failure of the tabs under the applied load with relative ease.

Due to the load redistribution the tabs underwent different failure mode changes evident from the degree of distortion

they received during loading. The simplest form of tab failure however was a shear failure. This was determined by sub-modelling the tab.

7.4 Sub-model-shear capacity of tabs

An elasto-plastic sub-model was produced to determine the strength of the individual tabs.

7.4.1 Mesh generation and result

Figures 7.1 and 7.2 show two views of a mesh generated to model a section of the plate that contains the tabs figure 4.5, block 1.

The parts of the tabs that bear on to the upright's web are blocks 5, 6 and 7 shown in figure 4.5.

The sub-model has been set up to include a block representing one of these bearing blocks.

The rest of the blocks making up the tabs, namely 8, 9, 10, 11 and 12 shown in figure 4.5 do not play any role in offering horizontal or vertical support to the beam end connector.

The width and the thickness of the bearing block in the sub-model were taken as 15mm and 4mm respectively, compatible with the dimensions adopted in the global model. In general the same simplifying assumptions made and described in chapter 4 apply here too. Here however the selected dimensions were greater than the actual dimensions of the beam end connector used in the tests. The tab and in particular the bearing block reduced to 2.5mm to 3mm in thickness during production as the result of the forming and the punching operations.

An elasto-plastic analysis of the side interaction between the tab and the upright was carried out, figures 4.1, 4.2 and 4.3, and the shear strength offered by the tab horizontally was evaluated.

To achieve this, initially a relatively coarse mesh was generated.

The type of element used was the eight noded isoparametric brick element. This element has six faces, twelve straight sides and three translatory degrees of freedom at each node (u_x, u_y, u_z).

The load was applied as incremental displacements.

A series of models with increasing mesh densities in the vicinity of the load application area were generated so that a convergence check could be carried out. Each time plots of load versus deflection were produced and compared until either a drop in the load or a continuous plateau indicating attainment of convergence was observed.

Figure 7.3 shows a typical load versus deflection curve obtained giving a strength value of 30kN.

Figures 7.4 and 7.5 show the deformed structure and the resulting stress pattern.

7.4.2 Discussion of results

Figure 7.4 shows the deformed structure, the tab deflecting in the same way as was observed during the physical testing of the beam end connector.

Figure 7.5 shows the resultant stress pattern.

The actual area subject to shear was 38mm^2 and the yield stress was 350N/mm^2. The shear strength of the tab given by the sub-model was 30kN. This is greater by 2.28 times than the shear strength based on simple shear area consideration. This was reflective of the simplifying assumptions made when modelling the tab, i.e. ignoring the thinning of the bearing block that occurs during forming, and also ignoring the rounding effect that results when the tab is formed. These assumptions were given in chapter 4, section 4.3.

A more detailed finite element model of the tab is required to take account of its actual geometry.

7.5 Load distribution in the tabs

Chapter 6 established the load distribution into the tabs for the three welding positions. The load distributions were obtained for the cases when the compression zone was restrained from movement, simulating the final stages of loading. This was required for the determination of the ultimate bending carrying capacity.

One idea was to purely rely on the capacity of a single tab in conjunction with the load distribution for each welding arrangement.

A second idea would use the resistance from the upright's web alone.

These ideas were considered having acknowledged the complexities involved in the loading conditions and the deformation modes in sections 7.1 and 7.3.

In doing so however the assumption was made that the load distributions established through the global models were realistic and representative of the conditions associated with the ultimate failure of the beam end connector.

The load distribution given in chapter 6, figures 6.10, 6.11, and 6.12 were slightly modified to give the systems of forces for the three welding arrangements, figures 7.6, 7.8 and 7.10.

Figures 6.10, 6.11 and 6.12 show the vertical components Fy_1, Fy_2 and Fy_3 off centre of the tabs reflecting the positions of the spring elements in the global models. For the ease of computation these were taken to act along the centre line of the tabs in figures 7.6, 7.8 and 7.10.

To estimate the ultimate bending carrying capacity for each configuration the following simple criterion was explored. This assumed that at failure the maximum loaded tab has reached its ultimate load capacity. The forces in the other tabs were taken to be in the same proportion to the force in the maximum loaded tab as determined by the force distribution obtained from the elastic global models.

The sum of the loads attracted by each set of tabs depended on the welding position of the beam to the beam end connector. This was a reflection of the stiffening effect of the beam on the beam end connector relative to the height of the beam end connector. To account for this effect each expression was multiplied by a ratio of the applied load to the sum of the loads received by the three tabs.

7.5.1 Symmetrical

Figure 7.6 shows the system of forces involved.

Applying the criteria, Appendix 7.1, taking the shear capacity of the tab as area times stress, an ultimate bending carrying capacity of 2.58kN.m was obtained.

Repeating the same exercise with the strength of the tab at 30kN, the outcome of the sub-model, a value of bending carrying capacity of 5.82kNm was reached.

Appendix 7.1 was also used to derive the ultimate bending moment based on the capacity of the upright's web. The value obtained for the shear resistance of the web horizontally was 3.25kN, figure 5.2. This results in a value of 0.631kN.m as the ultimate bending carrying capacity of the beam end connector.

7.5.2 Up welded

Figure 7.7 is the system of forces for this arrangement. Appendix 7.2 shows the derivation of the ultimate bending carrying capacity based on the shear area approach. This gave a value of 2.52kN.m.

Using the shear strength of the tab from the sub model in Appendix 7.2, a bending carrying capacity of 5.294kNm was evaluated.

Using the horizontal shear resistance from the upright's web, figure 5.2, 3.25kN, and Appendix 7.2, gave a bending carrying capacity of 0.616kNm.

7.5.3 Down welded

The system of forces for this welding arrangement is given in figure 7.8. Appendix 7.3 gave the bending carrying capacities of 2.984kNm, 6.731kNm and 0.729kNm based on shear area approach, outcome of the sub-model and the upright's web capacity respectively.

7.6 Conclusion

Simple ideas were explored to estimate the ultimate bending carrying capacity of a beam end connector. This was despite acknowledging the complexities that surrounded the factors which were responsible for the determination of the maximum load carrying capacity.

From the approaches explored the simple shear area consideration gave the best result in terms of correlation with the experimental results. The carrying capacities obtained for the up welded, symmetrical and the down welded arrangements were 2.23, 2.6 and 3.36kNm respectively.

Table 3.2 shows the experimental bending carrying capacities obtained for the beam end connector that was modelled. For the up welded, product 15 and the symmetrical welding arrangements, product 22, the bending carrying capacities varied from 1.592 to 2.701kNm. This was not only because of the variation in welding arrangements, but also due to variations in the gauges of the accompanying uprights, 1.8mm to 2.3 as well as the difference in beam sizes.

In the theoretical models the uprights' gauges and the beam sizes were the same for the different welding arrangements.

The shear strength value of the tab obtained from the sub model was 30kN. This was high. The reason for such a high

value was due to the effects of the simplifying measures adopted in section 7.4.2. The high value of the shear strength was partly the reason for the large values of ultimate bending capacities that were obtained based on the outcome of the sub-model.

On the other hand, contrary to the assumption made, as explained in section 7.3 the failure of the tabs was not responsible for the determination of the ultimate bending carrying capacity.

Using the resistance from the upright's web gave low values. This was because in a physical test the applied load continued to increase after the tabs had cut into the upright's web, section 7.3.

Figure 7.1 Beam end connector's tab before load was applied

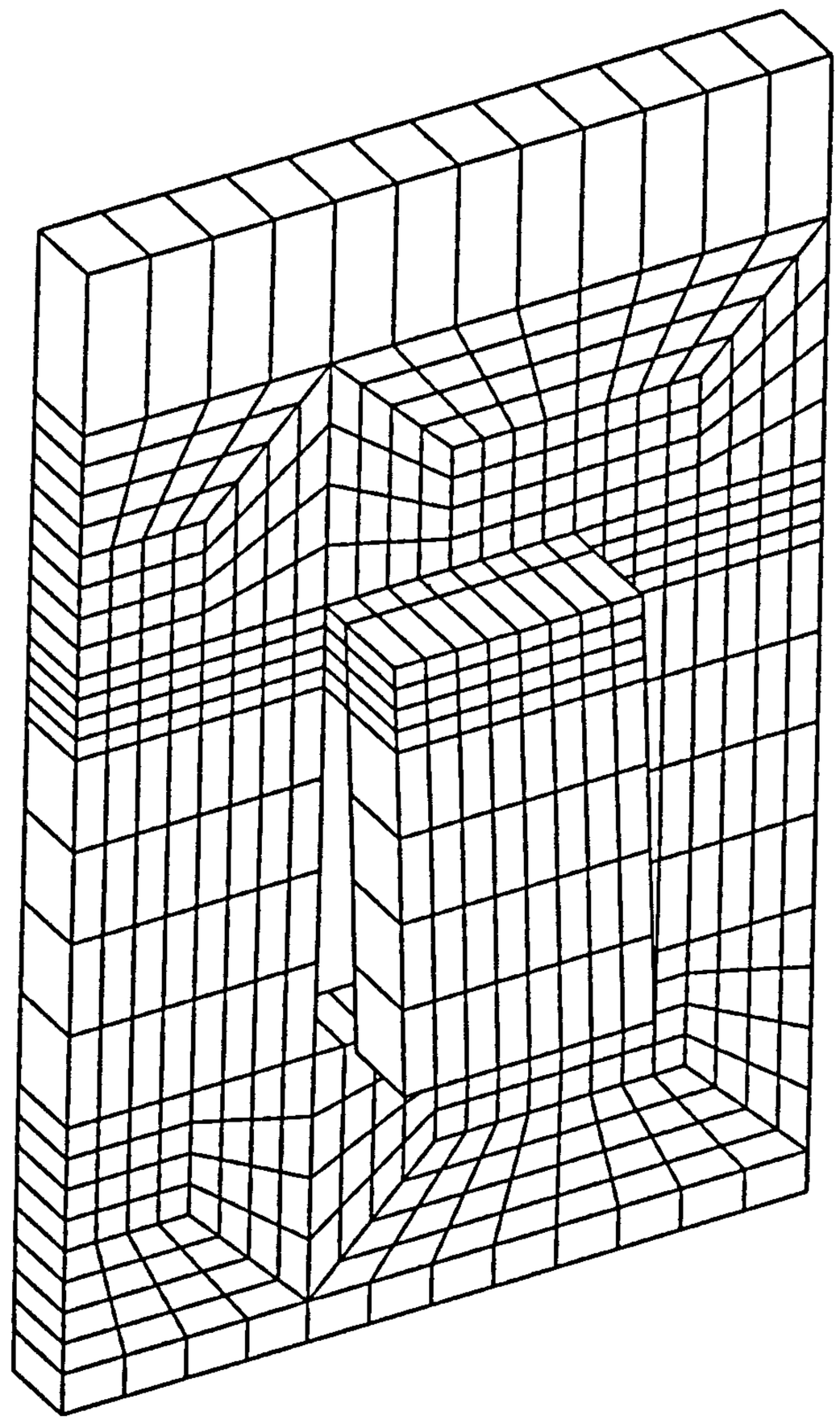

PLASTIC

ROTATION
X = 36
Y = 26
Z = 16

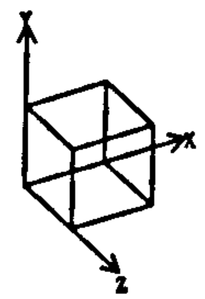

Figure 7.2 Beam end connector's tab before load was applied

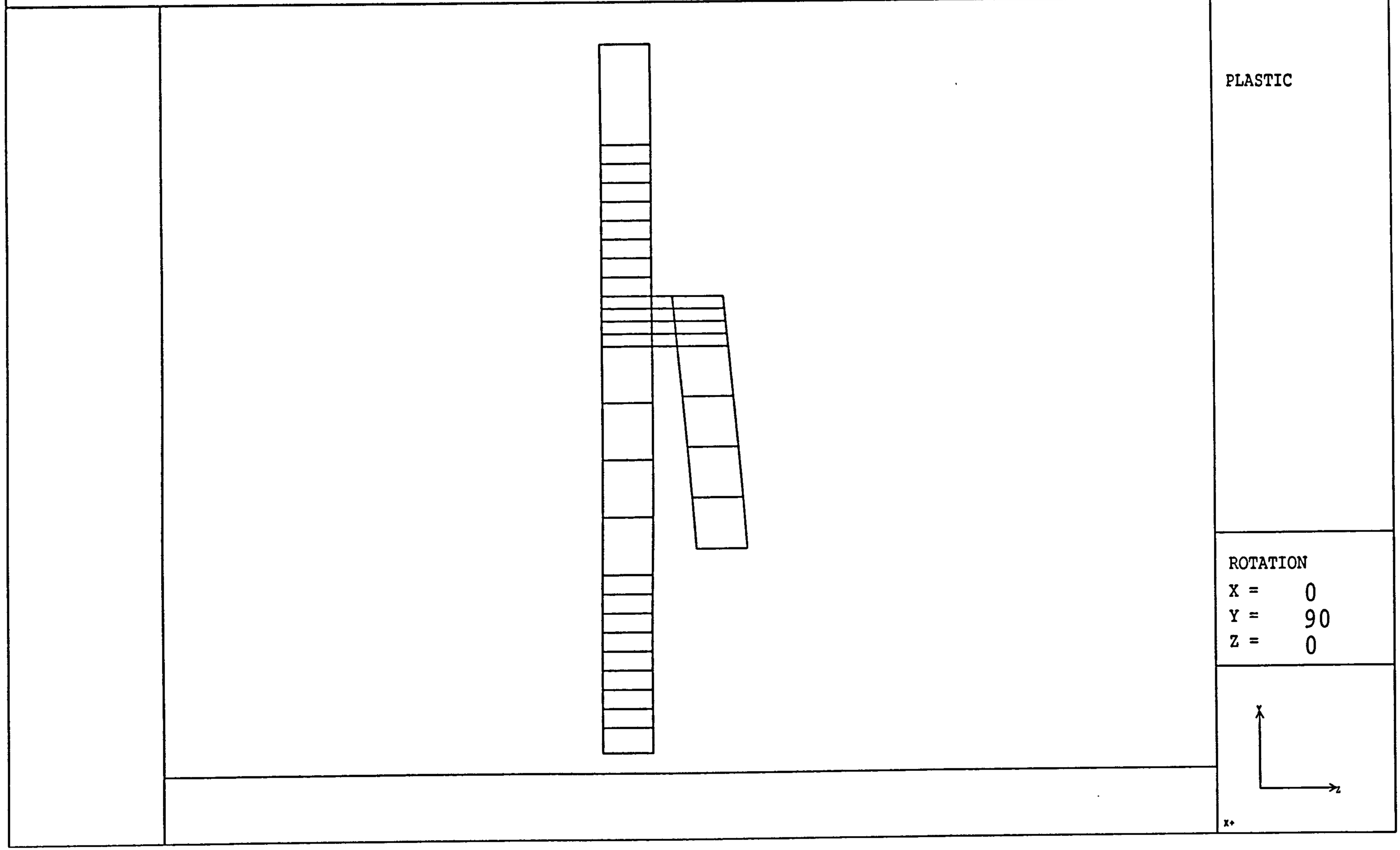

FIGURE 7.3
Stiffness and strength of a Tab

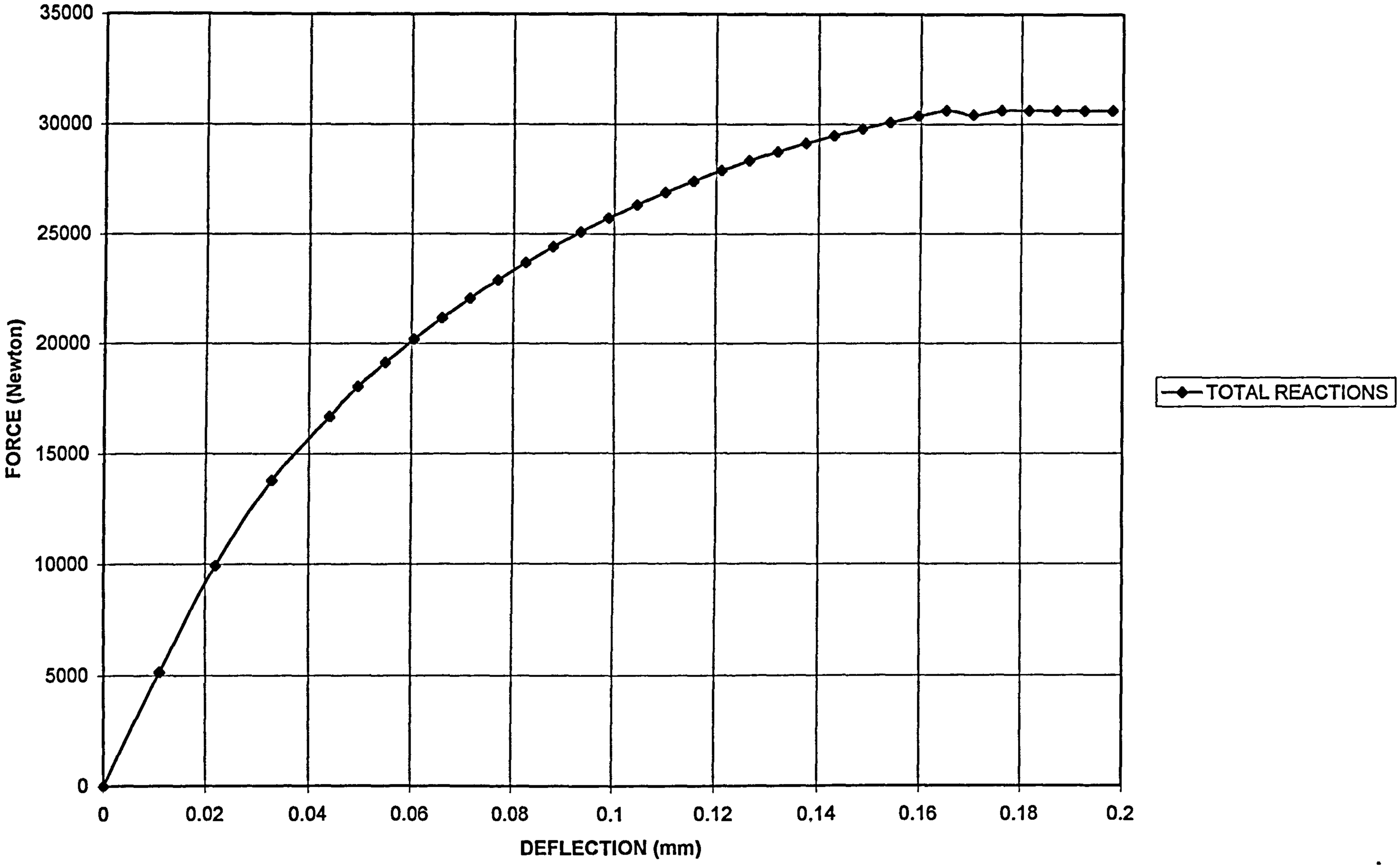

Figure 7.4 Beam end connector's tab after load was applied

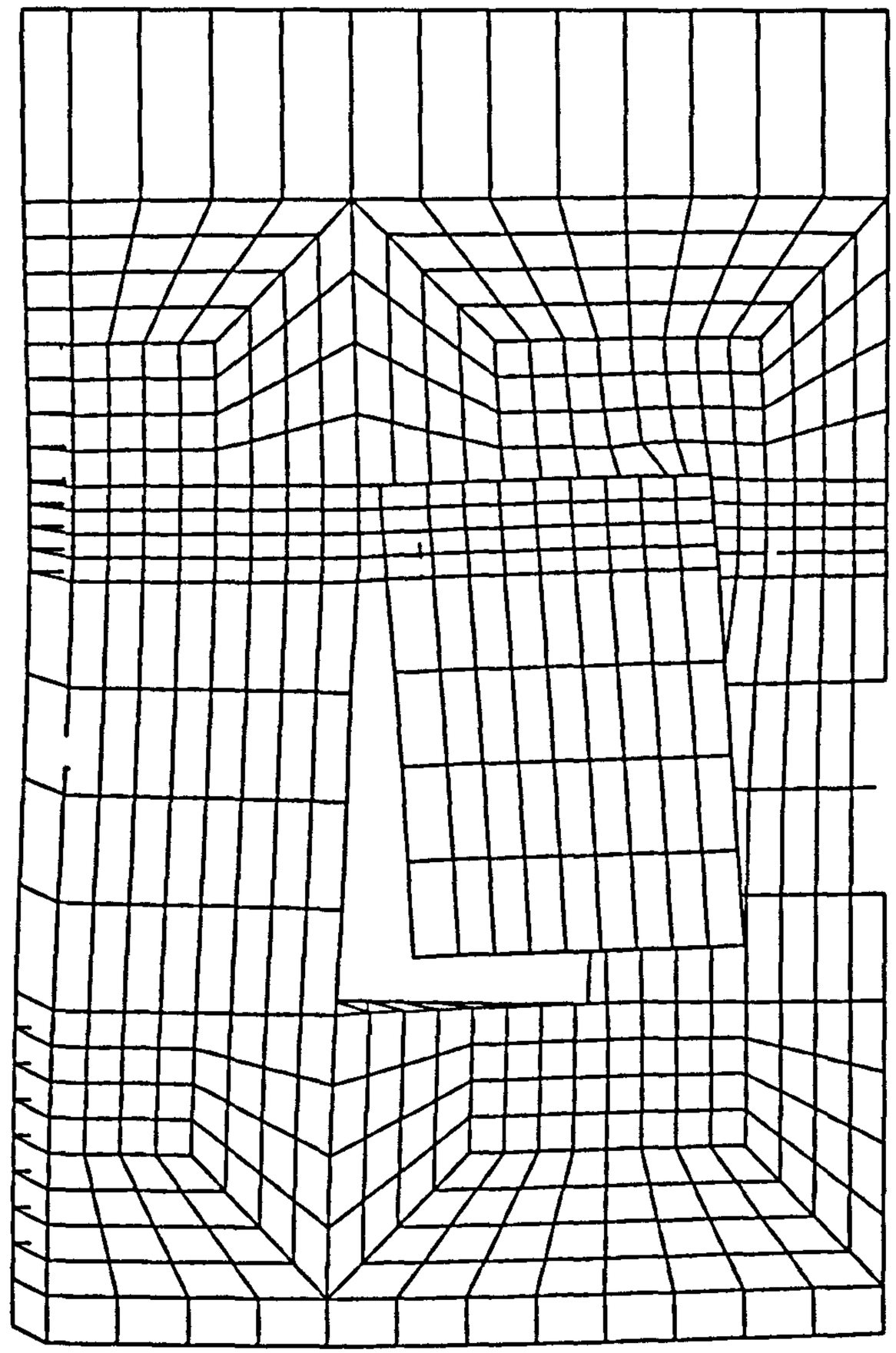

PLASTIC

ROTATION
X = 0
Y = 0
Z = 0

Figure 7.5 The stress pattern in the tab

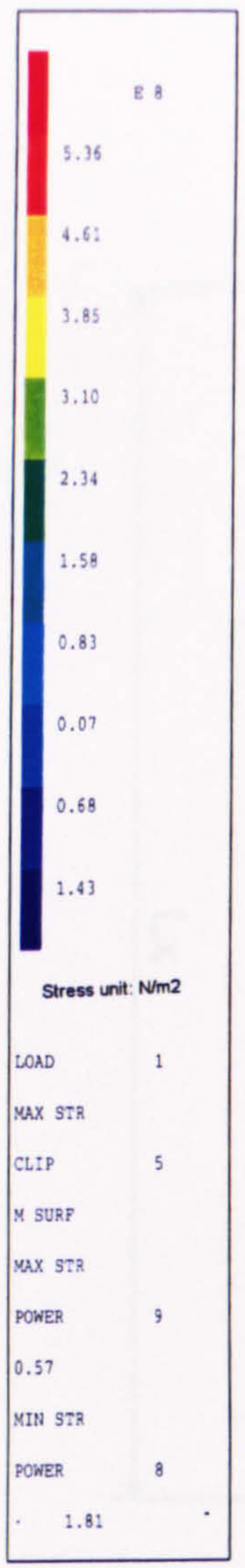

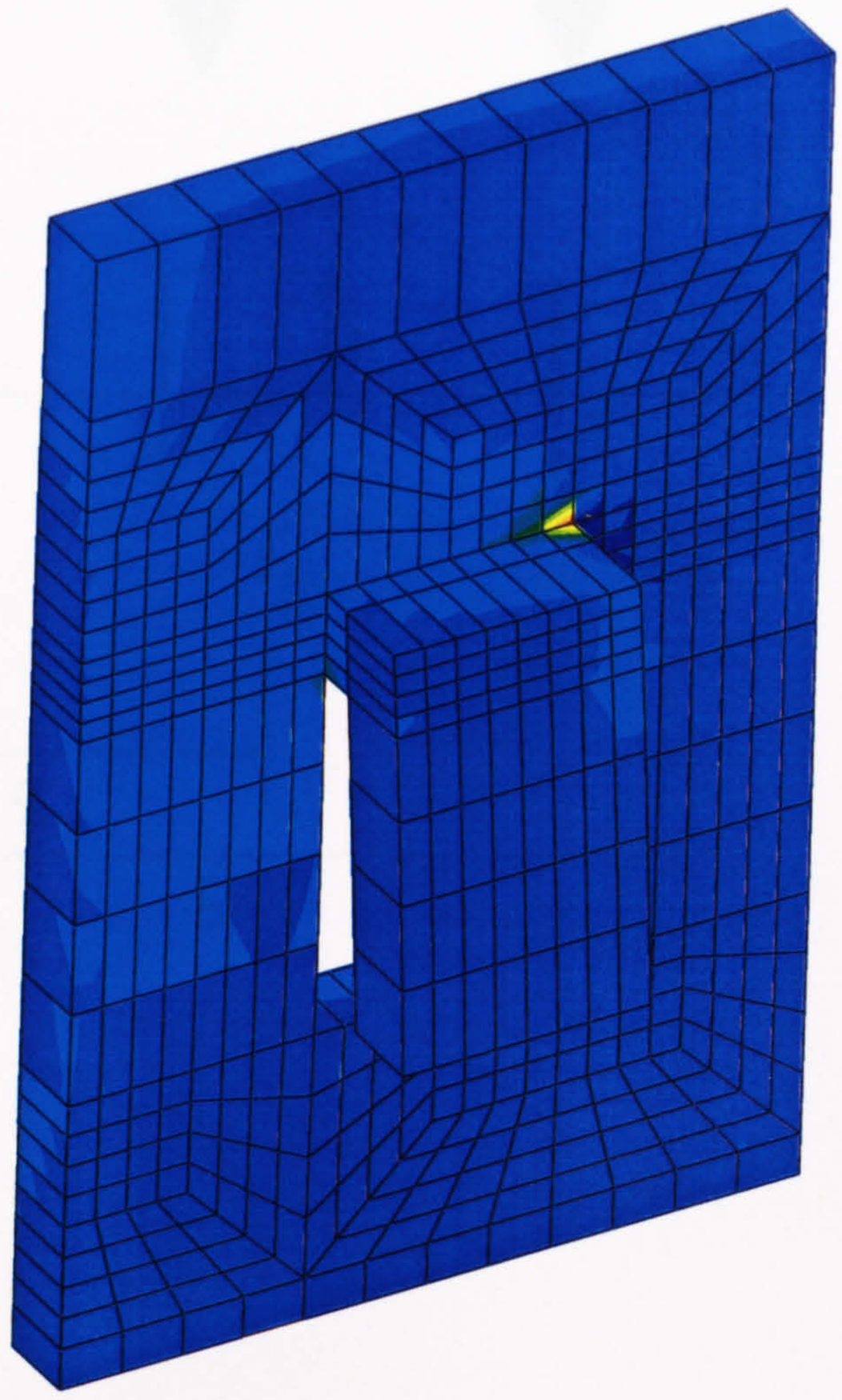

PLASTIC

ROTATION
X = 36
Y = 26
Z = 16

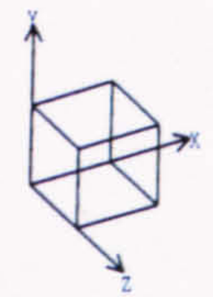

System Of Forces
Symmetrical Welding Position

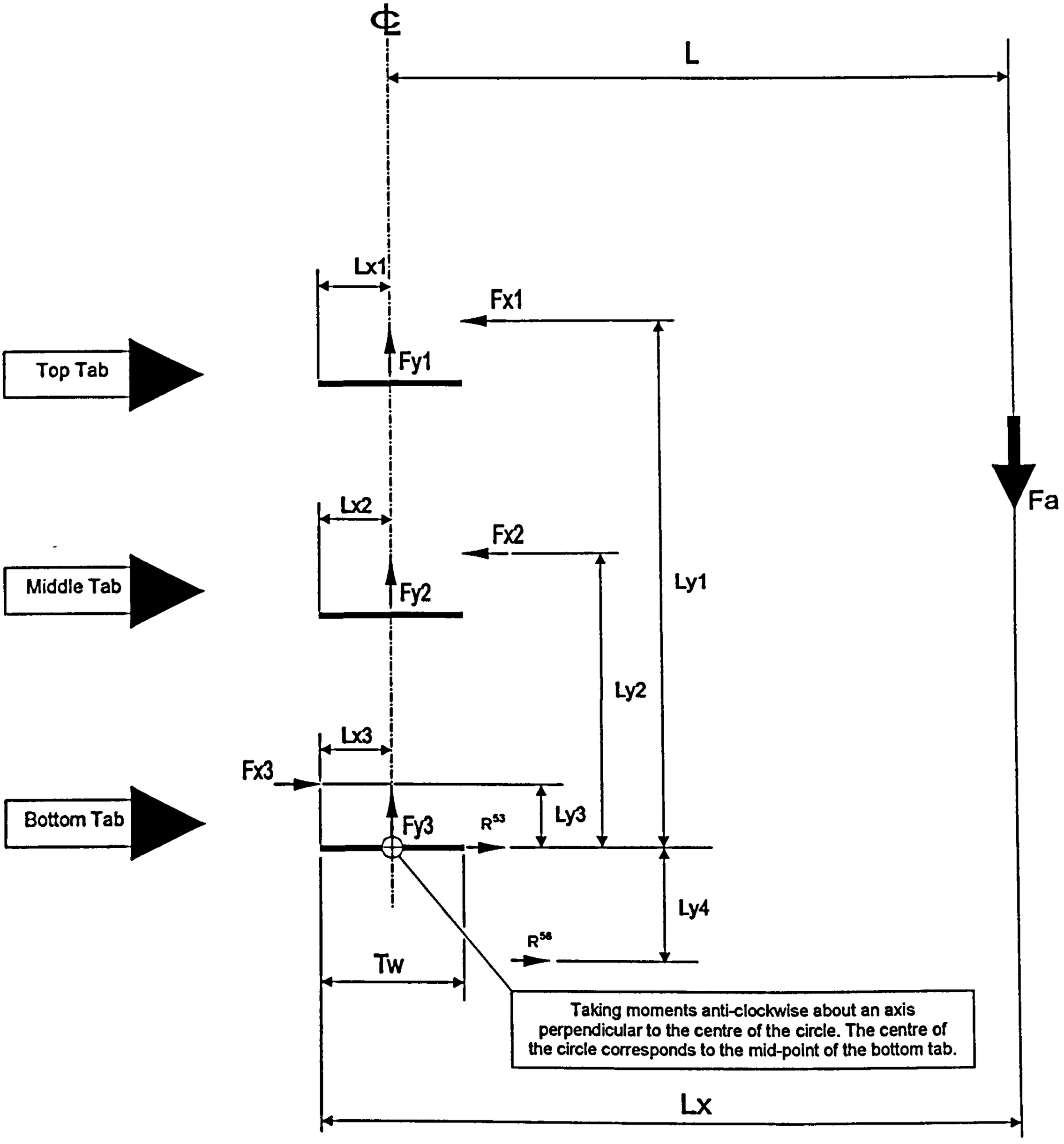

FIGURE 7.6

System Of Forces
Up Welded Position

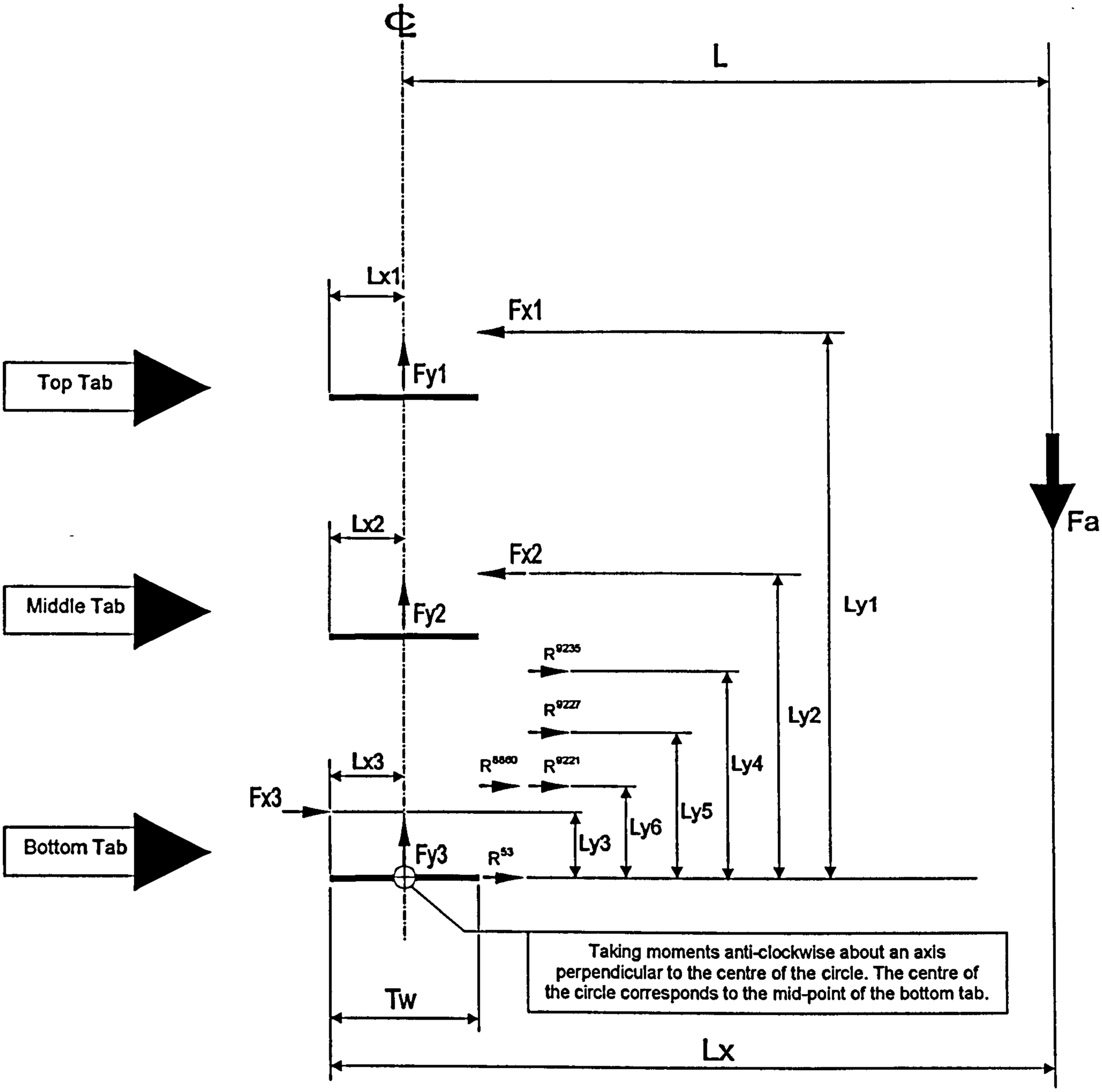

FIGURE 7.7

System Of Forces
Down Welded Position

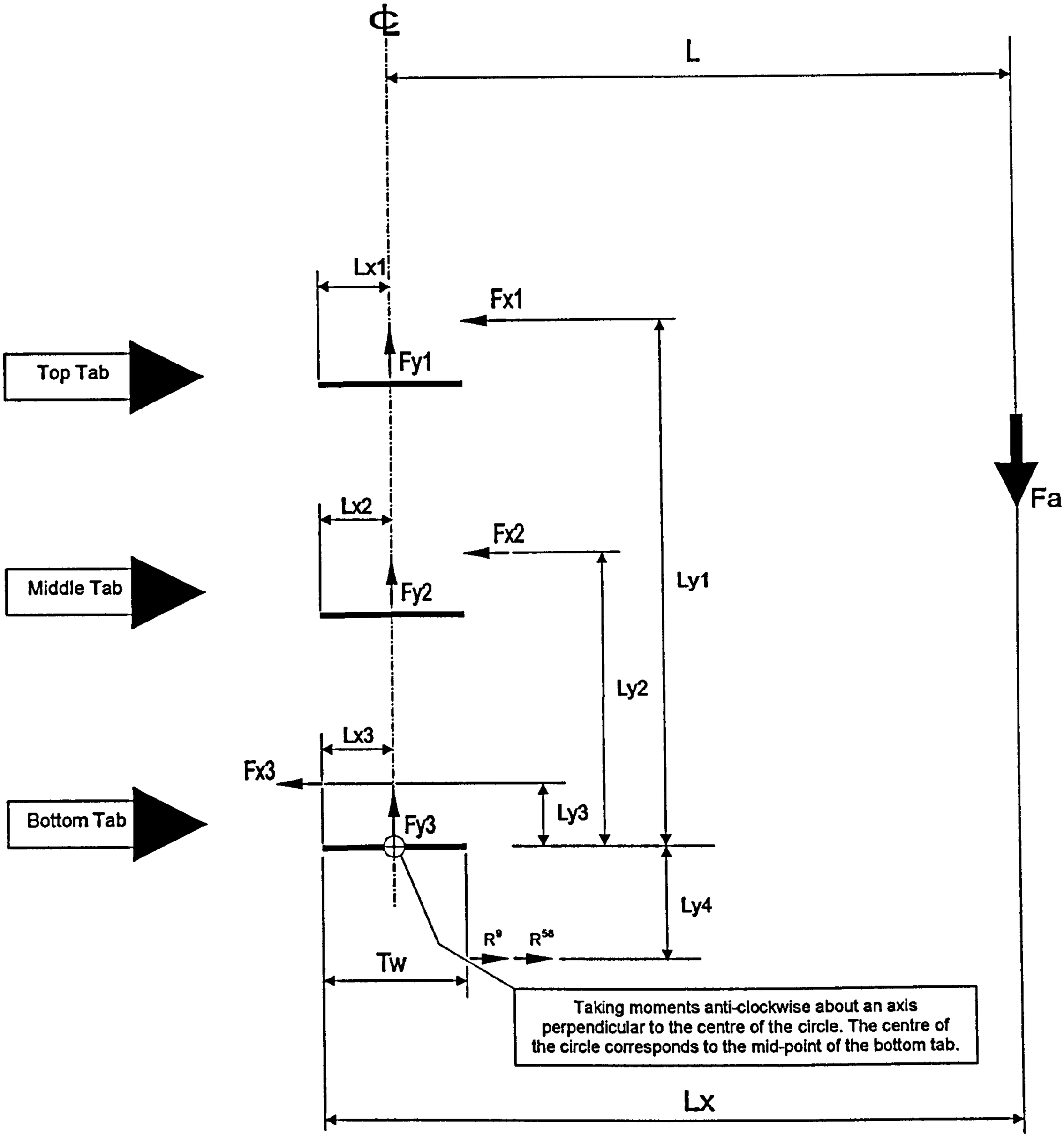

FIGURE 7.8

APPENDIX 7.1

SYMMETRICAL-Simple Rigid Plastic Analysis
Estimating the Ultimate Bending Moment Capacity

Information obtained from plastic sub models gave the stiffness of the upright's web. The results were used as spring stiffness values in global models as the sources of resistance to rotation. The global models in turn gave the forces applied to the springs in horizontal and vertical directions. The horizontal forces are F_{x1}, F_{x2} and F_{x3}. The vertical forces are F_{y1}, F_{y2} and F_{y3}. These are given in Table 6.3 for the case GM6C. This was the case where the compression zone was restrained and after eliminating the nodes that generated tension forces.

The sources of resistance to the rotation of beam end connectors were investigated experimentally. There we established that a number of occurrences were responsible for the carrying capacity of a beam end connector.

The following however is an attempt to relate the bending capacity of a connector to the physical geometry and the mechanical properties of its tabs and the upright's web. Initially the capacity of the single tab was worked out as the area times yield stress. As an alternative, a sub model was produced and using an elasto-plastic analysis the strength of a single tab in the horizontal direction equal to 30kN was evaluated. Alternatively the strength of the upright's web was considered as being responsible for determination of the ultimate bending carrying capacity of a beam end connector

The Free Body Diagram given in figure 6.10 was modified so that the vertical forces would be in line with the centre line of the tabs. A bending moment expression was written.

The system of forces for this configuration is given in figure 7.6.

Width of the tab:

$$T_w = 15\,mm$$

Beam end connector moment arm:

$$L_x = 201.5\,mm$$

Applied load to the beam end connector:

$$f_a = 10000\,N$$

Applied bending moment:

$$M_a = f_a L_x$$

$$M_a = 2.015\,kNm$$

Yield stress of the steel:

$$\sigma_{x1} = 400\,N/mm^2$$

Moment arms for the horizontal forces F_{x1}, F_{x2} and F_{x3} are $L_{y1} = 154\,mm$, $L_{y2} = 79\,mm$ and $L_{y3} = 4mm$; distances between the top plane of each bearing block and the lowest plane of the bottom bearing block, see figures 4.5 and 7.6.

Lever arm for reaction force in the compression zone is $L_{y4} = 24.5\,mm$.

Forces applied to the horizontal spring element-Horizontal forces-Table 6.3:

Top tab: $F_{x1} = 10100\,N$

Middle tab: $F_{x2} = 5130\,N$

Bottom tab: $F_{x3} = 276\,N$

Resistance to rotation from a single tab (shear capacity-area times yield stress): $R_1 = 13300\,N$

Resistance to rotation from a single tab (shear capacity-outcome of the sub model, elasto plastic exercise): $R_2 = 30000\,N$.

Resistance from the upright's web: $R_3 = 3250\,N$

Reaction forces in the compression zone: $R_{53} = 13875\,N$ and $R_{58} = 1125\,N$.

Percentage horizontal load attracted by each tab:

Top tab:

$$X_1 = \frac{F_{x1}}{F_{x1} + F_{x2} + F_{x3}} \qquad X_1 = 0.651$$

Middle tab:

$$X_2 = \frac{F_{x2}}{F_{x1} + F_{x2} + F_{x3}} \qquad X_2 = 0.331$$

Bottom tab:

$$X_3 = \frac{F_{x2}}{F_{x1} + F_{x2} + F_{x3}} \qquad X_3 = 0.018$$

The ratio of the applied load to the sum of the loads attracted by the three tabs, which varies with the different welding arrangements:

$$C_1 = \frac{f_a}{F_{x1} + F_{x2} + F_{x3}} \qquad C_1 = 0.645$$

Estimating the Ultimate Bending Moment of the beam end connector

1. Based on shear capacity of the tab-area times yield approach:

$$M_u = \left(\left(\frac{X_1}{X1}\right)R_1 L_{y1} + \left(\frac{X_2}{X_1}\right)R_1 L_{y2} - \left(\frac{X_3}{X_1}\right)R_1 L_{y3} + R_{58} L_{y4}\right)\left(\frac{C_1}{C_1}\right)$$

$$M_u = 2.60\ kNm$$

2. Based on shear capacity of the tab-the outcome of the elasto- plastic sub model:

$$M_u = \left(\left(\frac{X_1}{X1}\right)R_2 L_{y1} + \left(\frac{X_2}{X_1}\right)R_2 L_{y2} - \left(\frac{X_3}{X_1}\right)R_2 L_{y3} + R_{58} L_{y4}\right)\left(\frac{C_1}{C_1}\right)$$

$$M_u = 5.84\ kNm$$

3. Based on the resistance from the upright's web -(elasto plastic sub model):

$$M_u = \left(\left(\frac{X_1}{X1}\right)R_3 L_{y1} + \left(\frac{X_2}{X_1}\right)R_3 L_{y2} - \left(\frac{X_3}{X_1}\right)R_3 L_{y3} + R_{58} L_{y4}\right)\left(\frac{C_1}{C_1}\right)$$

$$M_u = 0.66\ kNm$$

APPENDIX 7.2

UP WELDED-Simple Rigid Plastic Analysis
Estimating the Ultimate Bending Moment Capacity

Information obtained from plastic sub models gave the stiffness of the upright's web. The results were used as spring stiffness values in global models as the sources of resistance to rotation. The global models in turn gave the forces applied to the springs in horizontal and vertical directions. The horizontal forces are F_{x1}, F_{x2} and F_{x3}. The vertical forces are F_{y1}, F_{y2} and F_{y3}. These are given in Table 6.4 for the case GM6C-UP. This was the case where the compression zone was restrained and after eliminating the nodes that generated tension forces.

The sources of resistance to the rotation of beam end connectors were investigated experimentally. We established that a number of occurrences were responsible for the carrying capacity of a beam end connector.

The following however is an attempt to relate the bending capacity of a connector to the physical geometry and the mechanical properties of its tabs and the upright's web. Initially the capacity of the single tab was worked out as the area times yield stress. As an alternative, a sub model was produced and using an elasto-plastic analysis the strength of a single tab in the horizontal direction equal to 30kN was evaluated. Alternatively the strength of the upright's web was considered as being responsible for determination of the ultimate bending carrying capacity of a beam end connector

The Free Body Diagram given in figure 6.11 was modified so that the vertical forces would be in line with the centre line of the tabs. A bending moment expression was written.

The system of forces for this configuration is given in figure 7.7.

Width of the tab:

$$T_w = 15\,mm$$

Beam end connector moment arm:

$$L_x = 201.5\,mm$$

Applied load to the beam end connector:

$$f_a = 10000\,N$$

Applied bending moment:

$$M_a = f_a L_x$$

$$M_a = 2.015\,kNm$$

Yield stress of the steel:

$$\sigma_{x1} = 400\,N/mm^2$$

Moment arms for the horizontal forces F_{x1}, F_{x2} and F_{x3} are $L_{y1} = 154\,mm$, $L_{y2} = 79\,mm$ and $L_{y3} = 4mm$; distances between the top plane of each bearing block and the lowest plane of the bottom bearing block, see figures 4.5 and 7.7.

Lever arms for reaction forces in the compression zone are $L_{y4} = 55.5\,mm$, $L_{y5} = 31.5\,mm$ and $L_{y6} = 18mm$.

Forces applied to the horizontal spring element-Horizontal forces-Table 6.4:

Top tab: $F_{x1} = 11200\,N$

Middle tab: $F_{x2} = 5050\,N$

Bottom tab: $F_{x3} = 424\,N$

Resistance to rotation from a single tab (shear capacity-area times yield stress): $R_1 = 13300\,N$

Resistance to rotation from a single tab (shear capacity-outcome of the sub model, elasto plastic exercise): $R_2 = 30000N$.

Resistance from the upright's web: $R_3 = 3250\,N$

Reaction forces in the compression zone: $R_{53} = 9763.4\,N$,

$R_{8860} = 4844.9\,N$, $R_{9221} = 416.81\,N$, $R_{9227} = 679.04\,N$ and $R_{9235} = 88.58\,N$.

Percentage horizontal load attracted by each tab:

Top tab:

$$X_1 = \frac{F_{x1}}{F_{x1} + F_{x2} + F_{x3}} \qquad X_1 = 0.672$$

Middle tab:

$$X_2 = \frac{F_{x2}}{F_{x1} + F_{x2} + F_{x3}} \qquad X_2 = 0.303$$

Bottom tab:

$$X_3 = \frac{F_{x2}}{F_{x1} + F_{x2} + F_{x3}} \qquad X_3 = 0.025$$

The ratio of the applied load to the sum of the loads attracted by the three tabs, which varies with the different welding arrangement:

$$C_2 = \frac{f_a}{F_{x1} + F_{x2} + F_{x3}}, \quad C_2 = 0.600 \text{ but from Appendix 7.1, } C_1 = 0.645$$

Estimating the Ultimate Bending Moment of the beam end connector

1. Based on shear capacity of the tab-area times yield approach:

$$M_u = \left(\left(\frac{X_1}{X1}\right)R_1 L_{y1} + \left(\frac{X_2}{X_1}\right)R_1 L_{y2} - \left(\frac{X_3}{X_1}\right)R_1 L_{y3} - R_{8860} L_{y6} - R_{9221} L_{y6} - R_{9227} L_{y5} - R_{9235} L_{y4}\right)\left(\frac{C_2}{C_1}\right)$$

$$M_u = 2.231\, kNm$$

2. Based on shear capacity of the tab-the outcome of the elasto-plastic sub model:

$$M_u = \left(\left(\frac{X_1}{X1}\right)R_2 L_{y1} + \left(\frac{X_2}{X_1}\right)R_2 L_{y2} - \left(\frac{X_3}{X_1}\right)R_2 L_{y3} - R_{8860} L_{y6} - R_{9221} L_{y6} - R_{9227} L_{y5} - R_{9235} L_{y4}\right)\left(\frac{C_2}{C_1}\right)$$

$$M_u = 5.173\, kNm$$

3. Based on the resistance from the upright's web -(elasto plastic sub model):

$$M_u = \left(\left(\frac{X_1}{X1}\right)R_3 L_{y1} + \left(\frac{X_2}{X_1}\right)R_3 L_{y2} - \left(\frac{X_3}{X_1}\right)R_3 L_{y3} - R_{8860} L_{y6} - R_{9221} L_{y6} - R_{9227} L_{y5} - R_{9235} L_{y4}\right)\left(\frac{C_2}{C_1}\right)$$

$$M_u = 0.46\, kNm$$

APPENDIX 7.3

DOWN WELDED-Simple Rigid Plastic Analysis
Estimating the Ultimate Bending Moment Capacity

Information obtained from plastic sub models gave the stiffness of the upright's web. The results were used as spring stiffness values in global models as the sources of resistance to rotation. The global models in turn gave the forces applied to the springs in horizontal and vertical directions. The horizontal forces are F_{x1}, F_{x2} and F_{x3}. The vertical forces are F_{y1}, F_{y2} and F_{y3}. These are given in Table 6.2 for the case GM6C-DN. This was the case where the compression zone was restrained but nodes did not generate tension forces.

The sources of resistance to the rotation of beam end connectors were investigated experimentally. We established that a number of occurrences were responsible for the carrying capacity of a beam end connector.

The following however is an attempt to relate the bending capacity of a connector to the physical geometry and the mechanical properties of its tabs and the upright's web. Initially the capacity of the single tab was worked out as the area times yield stress. As an alternative, a sub model was produced and using an elasto-plastic analysis the strength of a single tab in the horizontal direction equal to 30kN was evaluated. Alternatively the strength of the upright's web was considered as being responsible for determination of the ultimate bending carrying capacity of a beam end connector.

The Free Body Diagram given in figure 6.12 was modified so that the vertical forces would be in line with the centre line of the tabs. A bending moment expression was written.

The system of forces for this configuration is given in figure 7.8.

Width of the tab:

$T_w = 15\,mm$

Beam end connector moment arm:

$L_x = 201.5\,mm$

Applied load to the beam end connector:

$f_a = 10000\,N$

Applied bending moment:

$M_a = f_a L_x$

$M_a = 2.015\,kNm$

Yield stress of the steel:

$\sigma_{x1} = 400\,N/mm^2$

Moment arms for the horizontal forces F_{x1}, F_{x2} and F_{x3} are $L_{y1} = 154\,mm$, $L_{y2} = 79\,mm$ and $L_{y3} = 4mm$; distances between the top plane of each bearing block and the lowest plane of the bottom bearing block, see figures 4.5 and 7.8.

Lever arm for reaction forces in the compression zone is $L_{y4} = 24.5\,mm$.

Forces applied to the horizontal spring element-Horizontal forces-Table 6.2:

Top tab: $F_{x1} = 8340\,N$

Middle tab: $F_{x2} = 4790\,N$

Bottom tab: $F_{x3} = 669\,N$

Resistance to rotation from a single tab (shear capacity-area times yield stress): $R_1 = 13300N$

Resistance to rotation from a single tab (shear capacity-outcome of the sub model, elasto-plastic exercise) $R_2 = 30000\,N$

Resistance from the upright's web: $R_3 = 3250\,N$

Reaction forces in the compression zone: $R_{58} = 12766\,N$ and $R_9 = 1035\,N$.

Percentage horizontal load attracted by each tab:

Top tab:

$$X_1 = \frac{F_{x1}}{F_{x1} + F_{x2} + F_{x3}} \qquad X_1 = 0.604$$

Middle tab:

$$X_2 = \frac{F_{x2}}{F_{x1} + F_{x2} + F_{x3}} \qquad X_2 = 0.347$$

Bottom tab:

$$X_3 = \frac{F_{x2}}{F_{x1} + F_{x2} + F_{x3}} \qquad X_3 = 0.048$$

The ratio of the applied load to the sum of the loads attracted by the three tabs, which varies with the different welding arrangements:

$$C_3 = \frac{f_a}{F_{x1} + F_{x2} + F_{x3}}, \quad C_3 = 0.725 \text{ but from Appendix 7.1, } C_1 = 0.645$$

Estimating the Ultimate Bending Moment of the beam end connector

1. Based on shear capacity of the tab-area times yield approach:

$$M_u = \left(\left(\frac{X_1}{X1}\right)R_1 L_{y1} + \left(\frac{X_2}{X_1}\right)R_1 L_{y2} + \left(\frac{X_3}{X_1}\right)R_1 L_{y3} + R_9 L_{y4} + R_{58} L_{y4}\right)\left(\frac{C_3}{C_1}\right)$$

$$M_u = 3.364\, kNm$$

2. Based on shear capacity of the tab-the outcome of the elasto- plastic sub model:

$$M_u = \left(\left(\frac{X_1}{X1}\right)R_2 L_{y1} + \left(\frac{X_2}{X_1}\right)R_2 L_{y2} + \left(\frac{X_3}{X_1}\right)R_2 L_{y3} + R_9 L_{y4} + R_{58} L_{y4}\right)\left(\frac{C_3}{C_1}\right)$$

$$M_u = 7.11\, kNm$$

3. Based on the resistance from the upright's web -(elasto plastic sub model):

$$M_u = \left(\left(\frac{X_1}{X1}\right)R_3 L_{y1} + \left(\frac{X_2}{X_1}\right)R_3 L_{y2} + \left(\frac{X_3}{X_1}\right)R_3 L_{y3} + R_9 L_{y4} + R_{58} L_{y4}\right)\left(\frac{C_3}{C_1}\right)$$

$$M_u = 1.11\, kNm$$

C H A P T E R 8

CONCLUSIONS

8.1 Introduction

Despite a thorough research review no work was obtained that investigated the behaviour of semi-rigid boltless beam end connectors.

The majority of the work available related to the effect of using such connectors on the performance of rack structures.

A number of reasons were given for this, amongst them was the fact that beam end connectors varied in design greatly from one manufacturer to the next making it difficult to establish common characteristics.

It was noted that historically, detailed structural analysis of connection behaviour has been given a lower priority compared with the analysis of the whole structure.

These factors contributed towards a lack of work and information required for any theoretical work on the behaviour of such connectors.

The present work, however, may well be the first step towards attempts to try to identify, classify and document the governing parameters affecting the behaviour of

boltless semi-rigid beam end connectors, and to ultimately try and devise a modelling approach.

The following is a review of the structure used to carry out the work.

Chapter 1 defined the problem and outlined the objectives of the work.

Chapter 2 was a research review considering the work in the field of storage racks.

Chapter 3 covered the details of different beam end connectors and the experimental work carried out.

Chapter 4 contained the work on simulating the elastic behaviour of a beam end connector using finite element techniques.

Chapter 5 covered the work on elasto-plastic sub-models that determined the strength of the upright's web. The resulting spring stiffness values replaced the absolute restraints in the models presented in chapter 4.

Chapter 6 extended the work carried out in chapter 5 producing models that covered all the possible welding arrangements.

Chapter 7 presented the work to estimate the ultimate bending carrying capacity of the beam end connector.

8.2 The objectives achieved

1. Identification and classification of commercially available beam end connector designs.

Beam end connectors were classified based on their common features. Four different classifications were identified and presented in figure 3.9.

2. Testing of the various beam end connectors and comparing their performances.

Twelve products were tested. The results were used to investigate the effects of a number of variations that affected the performance of beam end connectors. The parameters responsible for the behaviour of beam end connectors were identified as follows:

- The effect of welding position of the beam relative to the height of the beam end connector: Welding symmetrically gave the best results. Up welded arrangement resulted in the weakest beam end connectors.

- The influence of beam depth on the beam end connector performance: The deeper the beam, the greater its stiffening effect on the connector and therefore the better the performance of the beam end connector.

- The effect of varying upright's gauges: The thicker the upright, the better were the moment rotation characteristics of the joint. For example with symmetrical welding, 28% gauge increase resulted in 28% and 18% increases in stiffness and strength respectively.

- The effect of increasing number of tabs in a beam end connector: Increasing beam end connector tabs from 3 to 4 resulted in 280% increase in stiffness value whereas the strength only increased by 20%.

These proved that the moment-rotation characteristic of a joint was determined by not only the design of the beam end connector, but also the efficiency of the accompanying members, in particular the upright.

It was also concluded that an efficient beam end connector is one whose bracket and tabs have been designed interactively so that they do not fail prematurely with respect to each other.

A qualitative assessment of the stress distribution in the beam end connector was carried out using brittle lacquer. This enabled the identification of the critical regions which were later confirmed theoretically using finite element techniques.

It was shown that different beam end connector designs would exhibit moment rotation characteristics of different shapes.

In general however the curves consisted of two parts. The first part, between 0 to 40% of the total load represented an apparently elastic behaviour. In some cases however it was difficult to make this distinction with certainty, as there were signs of non-linear behaviour.

The second part of the curve included the start of the material yielding followed by a peak associated with the Ultimate Failure Load of the connection.

Current work by M.T Abdel-Jaber[26], Oxford Brookes University, has shown that non-linear behaviour takes place right from the onset, as the beam end connector is loaded. This was established through tests that involved loading, unloading and reloading. On unloading the path taken was parallel to the original path. On reloading the same path was resumed. It was assumed that a combination of "bedding in" and plastic deformation may be responsible for this.

3. To determine the influence of upright's flexibility on experimental results.

A theoretical analysis of the influence of the flexibility of the upright on the experimental stiffness values was carried out. The experimental results were corrected for this and the stiffness values improved by 44%.

4. To determine the influence of stub beam flexibility on experimental results.

A theoretical analysis of the influence of the flexibility of the beam on the experimental stiffness values was carried out. The experimental results were corrected for this but only 3% increase in the stiffness values was observed.

5. To generate models to elastically determine the overall behaviour of a beam end connector.

Assuming a beam end connector to be a rigid joint linear elastic finite element models were produced to simulate its behaviour, chapter 4. The models were used to determine the deformation modes and the stress distribution in the critical regions of the beam end connector. The tabs and their vicinity proved to be the highest stressed regions.

These models were later enhanced to make allowances for the presence of the upright. The enhanced models were also used to establish the deformation modes of the connector.

6. To determine the initial stiffness of a beam end connector.

The initial stiffness of the beam end connector was determined using the two sets of models. The results from the models having used two different anchoring methods at tabs, absolute restraints (rigid) and spring stiffness values (elastic), were compared. The models using the springs at the tabs gave initial stiffness values similar in magnitude to those obtained experimentally.

7. To examine different methods of stiffness value measurement and to compare them with those recommended in the current and the forthcoming code of practice for the industry.

This was carried out. Appreciable differences in the initial stiffness values were observed depending on where deflection measurements were carried out. Figure 4.7 shows the deflection measurement methods.

It was shown that higher stiffness values would result if deflection measurements were taken closest to the line of action through the centre of tabs/slots in the upright.

Furthermore if measurements were carried out on the beam end connector itself, figure 4.17(a) the highest stiffness values would result.

The same differences in the stiffness values due to deflection measurement positions have recently been

confirmed experimentally by M.T Abdel-Jaber[26], Oxford Brookes University.

The existing codes of practice for the UK, its continental and American equivalents recommend guide positions for deflection measurements but do not acknowledge stiffness variations arising from different methods of deflection measurement.

8. To establish the load distribution in the "tabs".

This was achieved for three common welding arrangements of stub beam to the beam end connector, symmetrical, up welded and down welded. The load distribution was determined for two distinct stages during loading a beam end connector, 0-40% and beyond. It was shown that in the 0-40% stage the top and the bottom tabs were load carrying. It was also shown that beyond the 40% stage the top tab, the middle tab and the compression zone were load carrying.

9. To determine the shear strength of a tab using an elasto-plastic sub model.

This was carried out and the outcome of it was used as the source of resistance to the rotation of the beam end connector.

10. To estimate the ultimate moment carrying capacity of a beam end connector.

The load distribution in the tabs for the three welding positions formed the basis for this exercise. Prior to any such attempt the complexities surrounding the factors responsible for the ultimate failure of a joint were acknowledged.

Two simple ideas were then considered and in conjunction with the established load distributions estimates of the ultimate carrying capacities were made for the three popular welding positions.

The first idea assumed that the shear strength of the tabs in the beam end connector would determine the ultimate carrying capacity of a beam end connector. The shear strength of the tabs was determined by, initially the simple shear area consideration and later by the use of an elasto-plastic sub-model.

The second idea assumed that the resistance of the upright's web was responsible for the ultimate carrying capacity of the joint.

From the three attempts the shear area approach gave the best result in terms of correlation with the experimental results.

8.3 Author's comments

The work carried out provided a basic understanding of the behaviour of beam end connectors.

The findings of the work provided the information on the parameters that influenced efficient design of a beam end connector. The information was used to estimate the moment rotation characteristics of a beam end connector.

The work carried out will provide the information necessary for further work.

8.4 Suggestions for future work

The following are some recommendations for future work. More detailed finite element analysis should be carried out to:

1. Take account of the effects of gaps between the beam end connector and the upright. This will enable modelling of the beam end connector, upright and the beam as an assembly.

2. Take account of the $P\text{-}\Delta$ effects so that full non-linear behaviour of the joint can be investigated.

To avoid the inaccuracies associated with the simplifying assumptions made, techniques such as "scanning" should be adopted to take account of the actual geometry of the beam end connector's features.

Theoretical work and physical tests should be carried out to investigate the shear deflection effects of the upright and the beam on experimental test results.

APPENDIX 8.1

References

1. Jones S.W, Kirby P.A and Nethercot D.A, (1983), The Analysis of frames with Semi-Rigid connections, A state-of-the-art Report, *J. Construct. Steel Research* 2-13.

2. Rhodes J, (1991), Introduction to Cold Formed Steel Sections, Design Of Cold Formed Steel Members, Chapter 1, 1-48, Elsevier Applied Science.

3. Godley M.H.R, Beale R.G & Feng X, (1998), Rotational Stiffness of Semi-Rigid Baseplates, *14th Int Specialty Conf. Cold Formed Steel Structures*, 323-334, Ed LaBoube R.A & Yu W-W.

4. Stark, J.W.B and Tilburgs, C.J, (1979) Frame instability of unbraced pallet racks *Int. Conf. on Thin-Walled Structs, Univ of Strathclyde*, 160-185. Ed Rhodes J & Walker A.C.

5. Maxwell S.M, Jenkins W.M and Howlett J.H, (1981), A Theoretical Approach to the Analysis of Connection Behaviour, In *Proc. Conf. Joints in Steel work*, 249-269.

6. Jenkins W.M, (1989), Moment Transmitting Bolted End Plate Connection, In *Structural connections - Stability and Strength*, Chapter 7, 219-251, Ed Narayanan, R., Elsevier Applied Science.

7. Scholz H, (1990), Approximate P-Delta Method for Sway Frames with Semi-rigid Connections, *J. Construct. Steel Research:* 15, 215-231.

8. Davison J.B & Nethercot D.A, (1989), Overview of Connection Behaviour, Structural Connections, Stability & Strength, Chapter 1, 1-22, Ed R Narayanan, Elsevier Applied Science.

9. Cunningham R, (1990), Some aspects of semi-rigid connections in structural steelwork, *The Structural Engineer*, Volume 68, No.5.

10. SEMA, (1985), Code Of Practice For The Design of static Racking, The Storage Equipment Manufacturers' Association, UK Trade Association.

11. AISI, (1996), American Iron & Steel Institute, Cold Formed Steel Design Manual.

12. Godley M.H.R, (1991), Storage Racking, *Design of Cold Formed Steel Members*, Chapter 11, 361-399, Ed J.Rhodes, Elsevier Applied Science.

13. Godley M.H.R, Beale R.G, Feng X, (1997), Efficient Analysis and Design of Down-Aisle Pallet Rack Structures, Innovation in Civil and Structural Engineering, Civil Comp Press, Edinburgh, 249-257.

14. Cheng P.H., Effect of Semi-Rigid Connection to Steel Column of Cold Formed Perforated Singly Symmetric Section, Storage Products Division, Interlake, Inc., Chicago, Illinois.

15. Pekoz T, (1979),"Design of Cold-Formed Steel Storage Racks", *Int. Conference on Thin-Walled Structures*, Recent Technology Advance and Trends in Design, Research and Construction, Glasgow.

16. Pekoz T, (1978), Pallet Rack Design Criteria, Report, Cornell University, Ithaca, N.Y, U.S.A.

17. Pekoz T, (1978), Interpretation of Pallet Rack Test Results, Report, Cornell University, Ithaca, N.Y, U.S.A.

18. Pekoz T, (1978), Progress Report, a Rational Analysis for the Buckling Parallel to the aisle, Report, Cornell University, Ithaca, N.Y, U.S.A.

19. FEM, (1998), Section X, The Design of Steel Static Pallet Racking and Shelving, The Federation Europeene de la Manutention, European Trade Association.

20. Wood R.H, (1974), The Effective Lengths of Columns in Multi-Storey Buildings. *The Structural Engineer*, Vol. 52, No. 6, 235-244.

21. Lewis G.M., (1991), Stability of Rack Structures, *Thin-Walled Structures*, Vol. 12, 361-399, Ed J.Rhodes, Elsevier Applied Science.

22. Davies J.M, (1992), Down-Aisle Stability of Rack Structures, *Eleventh International Specialty Conference on Cold-Formed Steel Structures*, St. Louis, Missouri, U.S.A.

23. Horne M.R, (1975), An Approximate Method for Calculating the Elastic Critical Loads of Multi-Storey Frames, *The Structural Engineer*, Vol. 53, No.6, 242-248.

24. Lewis G.M., (1997), Imperfection Sensitivity of Structures with Semi-Rigid Joints, *Thin-Walled Structures*, Vol. 27, No 2, 361-399, Ed J.Rhodes, Elsevier Applied Science,.

25. PAFEC (1994), PAFEC-FE Level 8 Data Preparation Manual, PAFEC Ltd, Nottingham.

26. Abdel-Jaber M.T, (1999), Unpublished work, Oxford Brookes University.